DISSERTATION

SYNTHESIS AND EXPLORATION OF BIOLOGICALLY IMPORTANT, HYDROPHOBIC, REDOX-ACTIVE MOLECULES: INVESTIGATION OF PARTIAL SATURATION OF MYCOBACTERIAL ELECTRON TRANSPORT LIPIDS

Submitted by

Jordan T. Koehn

Department of Chemistry

In partial fulfillment of the requirements

For the Degree of Doctor of Philosophy

Colorado State University

Fort Collins, Colorado

Summer 2019

Doctoral Committee:

Advisor: Debbie C. Crans

Melissa M. Reynolds
Yian Shi
Dean C. Crick

Copyright by Jordan Tyler Koehn 2019

All Rights Reserved

ABSTRACT

SYNTHESIS AND EXPLORATION OF BIOLOGICALLY IMPORTANT, HYDROPHOBIC, REDOX-ACTIVE MOLECULES: INVESTIGATION OF PARTIAL SATURATION OF MYCOBACTERIAL ELECTRON TRANSPORT LIPIDS

There are many types of molecules that are biologically important because they either carry out crucial functions or exhibit exploitable biological activity. Some of the most interesting and challenging molecules to work with are those that are redox-active and hydrophobic or water insoluble. Herein, the synthesis and investigation of two classes of hydrophobic redox-active molecules are explored. Chapter one provides background on menaquinone (MK) and vanadium chemistry and primes the reader for the subsequent chapters. Chapter two describes the synthesis and characterization of truncated MK derivatives with varying isoprenyl side chain length and degrees of saturation. Chapter three explores the conformational flexibility of the isoprenyl side chain of MK and shows that a truncated MK analog, MK-2, can adopt folded conformations in hydrophobic environments and within a model membrane system. Chapter four isolates the conformational and chemical effect of saturation of the isoprenyl side chain on MK and shows that saturation minimally affects folded conformations of truncated MK derivatives but remarkably, a 20 mV redox potential difference was observed between unsaturated MK-1 and the saturated analog MK-1(H_2). Then in chapter five, hydrophobicity and steric bulk are explored as properties to enhance membrane affinity and anti-cancer properties of Schiff base vanadium(V) catecholate complexes, where the hydrophobic

[VO(Hshed)(ditertbutylcatechol)] complex was found to have enhanced hydrolytic stability and potent activity against a bone cancer cell line. Together, the findings of the studies presented herein help to further understand how the conformation and the degree of saturation in the isoprenyl side chain of MK affects the recognition, reactivity, and function of MK within the electron transport system of pathogenic bacteria. These studies are important because they begin to explain and provide a working model behind the chemical rationale as to why partially saturated MK-9 is observed in pathogenic *M. tuberculosis.* Furthermore, the studies with the hydrophobic vanadium(V) catecholate metallo-complexes underpin a drug design concept exploiting hydrolytic stability imparted by hydrophobicity and steric bulk of a non-innocent ligand.

ACKNOWLEDGEMENTS

“We do these things not because they are easy but because they are hard.”

– John F. Kennedy

“Don’t worry about what you miss, because the only thing that counts is what you find. And there is so very much to find.”

– K. Barry Sharpless

I would like to acknowledge family, friends, undergraduate researchers, and my committee for taking the time to work with me through the pleasant and not so pleasant times. Specifically, I would like to acknowledge my parents Ed Koehn and Donna Koehn, my brothers Ryan and Eric Koehn, the Crans group, and the Crick group for their support. I would like to give a special thanks to my amazing wife, Kimberly, who has provided support, guidance, and has been there with me through everything.

TABLE OF CONTENTS

ABSTRACT ii
ACKNOWLEDGEMENTS iv
TABLE OF CONTENTS v
Chapter 1: Hydrophobic Redox-Active Molecules of Biological Importance 1
1.1 Lipoquinones and The Electron Transport System 1
1.2 Hydrophobic Vanadium(V) Catecholates Containing Redox-Active Ligands- 10
1.3 Dealing and Working with Poorly Soluble and Hydrophobic Molecules 12
1.4 Studies of the Subsequent Chapters 15
References 16
Chapter 2: Synthesis and Characterization of Menaquinone Derivatives 21
2.1 Synthesis of Truncated Menaquinone Derivatives 21
2.2 Materials and Methods 25
2.2.1 Materials and Information 25
2.2.2 NMR Spectroscopic Studies 27
2.2.3 Mass Spectrometry and Elemental Analysis 28
2.2.4 Preparation of Menaquinone-1 29
2.2.5 Preparation of Menaquinone-1(H_2) 30
2.2.6 Preparation of Menaquinone-2 31
2.2.7 Preparation of Menaquinone-2(II-H_2) 32
2.2.8 Preparation of Menaquinone-2(I,II-H_4) 35
2.2.9 Preparation of Menaquinone-3 37
2.2.10 Preparation of Menaquinone-3(II-H_2) 38
2.2.11 Preparation of Menaquinone-3(I,II,III-H_6) 45
2.3 Results and Discussion 48
2.3.1 Synthesis and Characterization of Menaquinone-1 48
2.3.2 Synthesis and Characterization of Menaquinone-1(H_2) 49
2.3.3 Synthesis and Characterization of Menaquinone-2 50
2.3.4 Synthesis and Characterization of Menaquinone-2(II-H_2) 51
2.3.5 Synthesis and Characterization of Menaquinone-2(I,II-H_4) 55
2.3.6 Synthesis and Characterization of Menaquinone-3 56
2.3.7 Synthesis and Characterization of Menaquinone-3(II-H_2) 57
2.3.8 Synthesis and Characterization of Menaquinone-3(I,II,III-H_6) 60

2.4 Summary and Conclusions 62
References 65
Chapter 3:Investigation of the Conformational Flexibility of the Isoprenyl Side Chain on Menaquinone 68
3.1 Conformation of the Isoprenyl Side Chain of Mycobacterial Menaquinone 68
3.2 Materials and Methods 71
3.2.1 Materials 71
3.2.2 NMR Spectroscopic Studies 72
3.2.3 Solution 1D ^{1}H NMR Spectroscopic Studies 72
3.2.4 Sample Preparation for Solution ^{1}H-^{1}H 2D NOESY and ROESY NMR Spectroscopic Studies 72
3.2.5 ^{1}H-^{1}H 2D NOESY and ROESY NMR Spectroscopic Studies in Organic Solution 73
3.2.6 Molecular Mechanics Calculations 73
3.2.7 Sample Preparation for Reverse Micelle NMR Spectroscopic Studies 74
3.2.8 1D ^{1}H NMR Spectroscopic Studies of AOT/Isooctane that contain Menaquinone-2 74
3.2.9 Sample Preparation for Solution ^{1}H-^{1}H 2D NOESY and ROESY NMR Spectroscopic Studies in Reverse Micelles 74
3.2.10 ^{1}H-^{1}H 2D NOESY and ROESY NMR Spectroscopic Studies in AOT/isooctane w_0 12 Reverse Micelles 75
3.3 Results and Discussion 75
3.3.1 1D ^{1}H NMR Spectroscopic Studies of Menaquinone-2 in Different Organic Solvents 75
3.3.2 ^{1}H-^{1}H 2D NOESY and ^{1}H-^{1}H 2D ROESY NMR Spectroscopic Studies of Menaquinone-2 in d_6-DMSO and d_5-pyridine 78
3.3.3 Illustrating Menaquinone-2 Conformations using Molecular Mechanics 81
3.3.4 Electrochemistry of Menaquinone-2 in Different Organic Solvents 84
3.3.5 Interaction of Menaquinone-2 with Langmuir Phospholipid Monolayers 89
3.3.6 1D ^{1}H NMR Spectroscopic Studies of Menaquinone-2 in Reverse Micelles 93
3.3.7 ^{1}H-^{1}H 2D NOESY and ROESY NMR Spectroscopic Studies of Menaquinone-2 in a Reverse Micelle Model Membrane System 95
3.3.8 Implications of Folded Conformations for Menaquinone Derivatives 98
3.4 Summary and Conclusions 103
References 106
Chapter 4: Isolating the Influence of Saturation of the Isoprenyl Side Chain on Menaquinone on Conformation and Quinone Redox Potential 111
4.1 Role of Partial Saturation of the Isoprenyl Side Chain of Mycobacterial Menaquinone 111
4.2 Materials and Methods 116
4.2.1 Materials and General Information/Methods 116
4.2.2 NMR Spectroscopic Studies 117

4.2.3 Solution 1D ^{1}H NMR Spectroscopic Studies 118
4.2.4 Sample Preparation for ^{1}H-^{1}H 2D NOESY and ^{1}H-^{1}H 2D REOSY NMR Spectroscopic Studies 118
4.2.5 ^{1}H-^{1}H 2D NOESY and ^{1}H-^{1}H 2D ROESY NMR Spectroscopic Solution Studies 118
4.2.6 Molecular Mechanics Calculations 119
4.2.7 Sample Preparation for Reverse Micelle NMR Spectroscopic Studies 120
4.2.8 1D ^{1}H NMR Spectroscopic Studies of AOT/isooctane Reverse Micelles Containing Menaquinone-1 or Menaquinone-1(H_2) 120
4.2.9 Sample Preparation for ^{1}H-^{1}H 2D NOESY and ^{1}H-^{1}H 2D ROESY NMR Spectroscopic Studies in AOT/isooctane Reverse Micelles. 121
4.2.10 ^{1}H-^{1}H 2D NOESY and ^{1}H-^{1}H 2D ROESY NMR Spectroscopic Studies in a w_0 12 AOT/isooctane Reverse Micelles 122
4.2.11 Dynamic Light Scattering Studies 122
4.3 Results and Discussion 123
4.3.1 1D ^{1}H NMR Spectroscopic Studies of Menaquinone-1 in Organic Solvents 123
4.3.2 ^{1}H-^{1}H 2D NOESY and ^{1}H-^{1}H 2D ROESY NMR Spectroscopic Studies of Menaquinone-1 and Menaquinone-1(H_2) in d_5-pyridine, d_3-acetone, and d_6-DMSO. 124
4.3.3 Illustrating Menaquinone-1 and Menaquinone-1(H_2) Conformations using Molecular Mechanics 131
4.3.4 Reactivity of Menaquinone-1 and Menaquinone-1(H_2) in Different Organic Solvents: Electrochemistry 134
4.3.5 Interaction of Langmuir Phospholipid Monolayers with Menaquinone-1 and Menaquinone-1(H_2)……. 140
4.3.6 1D ^{1}H NMR Spectroscopic Studies of Menaquinone-1 and Menaquinone-1(H_2) in Reverse Micelles……. 145
4.3.7 ^{1}H-^{1}H 2D NOESY and ^{1}H-^{1}H 2D ROESY NMR Spectroscopic Studies of Menaquinone-1 and Menaquinone-1(H_2) in a Reverse Micelle Model Membrane System 147
4.4 Summary and Conclusions 152
References 157
Chapter 5: Hydrophobicity May Enhance Membrane Affinity and Anti-Cancer Effects of Schiff Base Vanadium(V) Catecholate Complexes 161
5.1 Hydrophobic and Redox-Active Vanadium(V) Catecholate Complexes 161
5.2 Materials and Methods 166
5.2.1 Chemicals, Biochemicals, and General Methods 166
5.2.2 Purification of NaAOT 167
5.2.3 Preparation of AOT/iso-octane Stock Solution and Reverse Micelle Samples 167
5.2.4 Stability of Probe in Aqueous Solution and Reverse Micelles 168
5.2.5 ^{1}H and ^{51}V NMR Spectroscopic Studies on Reverse Micelles 169
5.2.6 Reverse Micelle Sample Preparation for Dynamic Light Scattering (DLS) Studies 169

5.2.7 Dynamic Light Scattering (DLS) Measurements 170
5.2.8 Stability Studies by Electronic Absorption Spectroscopy 170
5.2.9 Cytotoxicity Experiments 170
5.3 Results and Discussion 171
5.3.1 Synthesis 171
5.3.2 Solubility of Free Ligands and V(V) Complexes and Stability of Free Ligand H_2shed and $[V(O)_2$(Hshed)] in Reverse Micelle Samples 172
5.3.3 ^{51}V NMR Spectra of the $[V(O)_2$(Hshed)] Complex 173
5.3.4 ^{1}H NMR Spectra of $[V(O)_2$(Hshed)] and H_2shed 174
5.3.5 NMR Spectra of [VO(Hshed)(dtb)] in Aqueous Solution and in Reverse Micelle Samples 177
5.3.6 NMR Spectra of [VO(Hshed)(cat)] in Aqueous Solution and in Reverse Micelle Samples 180
5.3.7 Examining the AOT/*iso*-octane Reverse Micelles Containing H_2shed, $[V(O)_2$(Hshed)], [VO(Hshed)(cat)], [VO(Hshed)(dtb)], using Dynamic Light Scattering 182
5.3.8 The Anti-Cancer Effects of V(V) Catecholate Complexes on Bone Cancer Cells (SW1353 cells)…… 182
5.3.9 Discussion 188
5.4 Summary and Conclusions 190
References 192
Chapter 6: Summary, Concluding Remarks, and Future Directions 199
6.1 Summary and Concluding Remarks 199
6.2 Future Directions 204
Appendix I: Contributions to Work 212
References 215
Appendix II: Supporting Information for Chapter 2 216
Appendix III: Supporting Information for Chapter 3 274
References 287
Appendix IV: Supporting Information for Chapter 4 288
References 322
Appendix V: Supporting Information for Chapter 5 323
References 326
Appendix VI: Synthesis and Characterization of Partially and Fully Saturated Menaquinone Derivatives 327
References 328
Appendix VII: A Synthetic Isoprenoid Lipoquinone, Menaquinone-2, Adopts a Folded Conformation in Solution and at a Model Membrane Interface 342
References 343

Appendix VIII: Investigating Substrate Analogs for Mycobacterial MenJ: Truncated and Partially Saturated Menaquinones.....358

References.....359

Appendix IX: Hydrophobicity May Enhance Membrane Affinity and Anti-Cancer Effects of Schiff Base Vanadium(V) Catecholate Complexes.....380

References.....381

Appendix X: Mycobacterial MenJ: An Oxidoreductase Involved in Menaquinone Biosynthesis.....396

References.....397

List of Abbreviations.....408

Chapter 1: Hydrophobic Redox-Active Molecules of Biological Importance

1.1 Lipoquinones and The Electron Transport System

The first class of redox-active and hydrophobic compounds explored in this dissertation are menaquinones (MK). Quinones are a unique type of α,β-unsaturated ketones existing as metabolites in numerous pathways where they have many functions in nature.[1-6] The importance of quinone chemistry has been recognized since the mid-1800s. Quinone containing compounds can be anti-oxidants, anti-tumoral or carcinogenic agents and are the inherent components of biological systems such as photosystem II.[1-6] Two major structural groups of lipoquinones (lipid containing a quinone moiety) are recognized; ubiquinones (or benzoquinones, UQ) typically found in eukaryotes and Gram-negative prokaryotes and MK (or naphthoquinones) typically found in Gram-positive prokaryotes, including many pathogens such as *Mycobacterium tuberculosis (M. tuberculosis)*. The roles and applications of lipoquinone derivatives are currently being explored where a range of different approaches are used for combatting human diseases.[7-19] MKs are essential components of the respiratory electron transport system (ETS), where they shuttle electrons and protons between protein complexes by acting as electron donors and acceptors (Figure 1.1.1).[6] The 1943 Nobel Prize in Physiology or Medicine was awarded to Henrik Dam and Edward Doisy for the discovery and characterization of vitamin K (a MK), a key cofactor in blood coagulation.[20] Interestingly, MKs role in humans as a blood coagulation factor (MK-4) is vastly different from its role as an electron transport lipid within bacteria (MK-9 or MK-9(II-H_2).

The structurally similar lipoquinone, UQ-10, is a component of the ETS in mammals and bacteria and participates in aerobic cellular respiration, which generates energy in the form of ATP within cellular membranes. The interest in and the importance of MK/vitamin K, its derivatives and vitamers (e.g., vitamins K_1, K_2 and K_3) has remained strong since the discovery of Vitamin K.

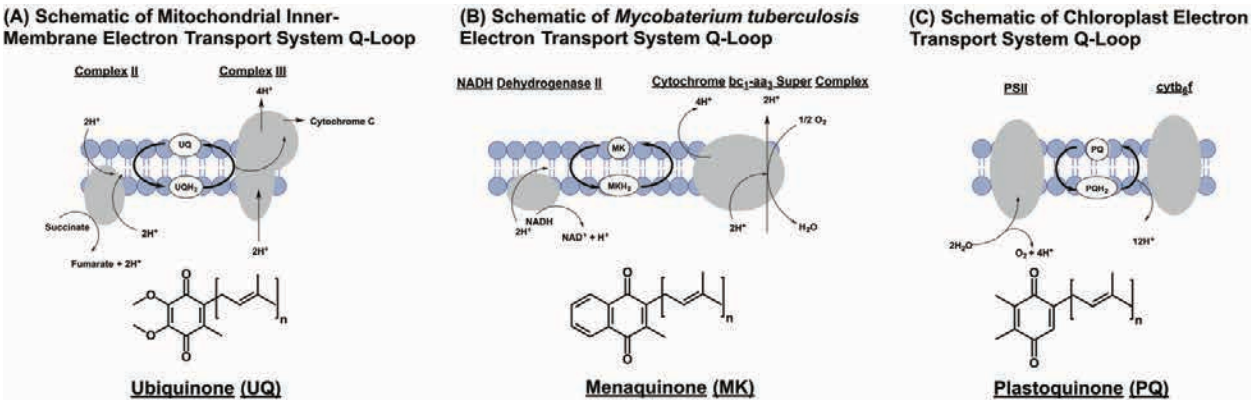

Figure 1.1.1 Partial schematic of the electron transport system of (A) mitochondria, (B) Gram positive bacteria, and (C) chloroplast. Schematic outlines the importance of each specific lipoquinone within each electron transport system. Figure was adapted from Kurosu *et al*, Rochaix, and Peters.[20-22]

MKs are structurally characterized by a naphthoquinone moiety and a repeating hydrophobic isoprenyl side chain of varying length and degree of saturation (Figure 1.1.1), where the latter is a characteristic that has long been used to assist taxonomic efforts.[23-24] It is important to know whether the evolutionarily conserved structural traits of lipoquinones are related solely to redox functioning properties, or related to recognition by respiratory enzymes in the ETS, or due to interactions with other lipids within the cellular membrane, or a combination. Textbooks often represent UQ and MK simply as "Q" or "MQ" in illustrations of the ETS and in primary literature they are generally shown in an extended conformation (Figure 1.1.2).[25-27] The extended conformation of these long hydrophobic MK molecules seems highly unlikely (Figure 1.1.2) in light of the one-step cyclization of squalene epoxide, a long isoprenoid compound containing six isoprene units, to form the protosterol cation, which contains the basic steroidal ring system with

eight chiral centers.[28-29] Woodward reported the cyclization of this polyisoprenoid squalene epoxide forming only one stereoisomer out of the possible 256 (2^8) in 1953.[28-29] The stereospecificity of this reaction requires preorganization of the epoxide before protonation in a specific conformation, and such a conformer is not the extended conformation commonly depicted in the literature. In addition, MK-9 and UQ-10 are too long to be accommodated within the hydrophobic region of the phospholipid bilayer unless the isoprenyl side chain is folded (Figure 1.1.2).

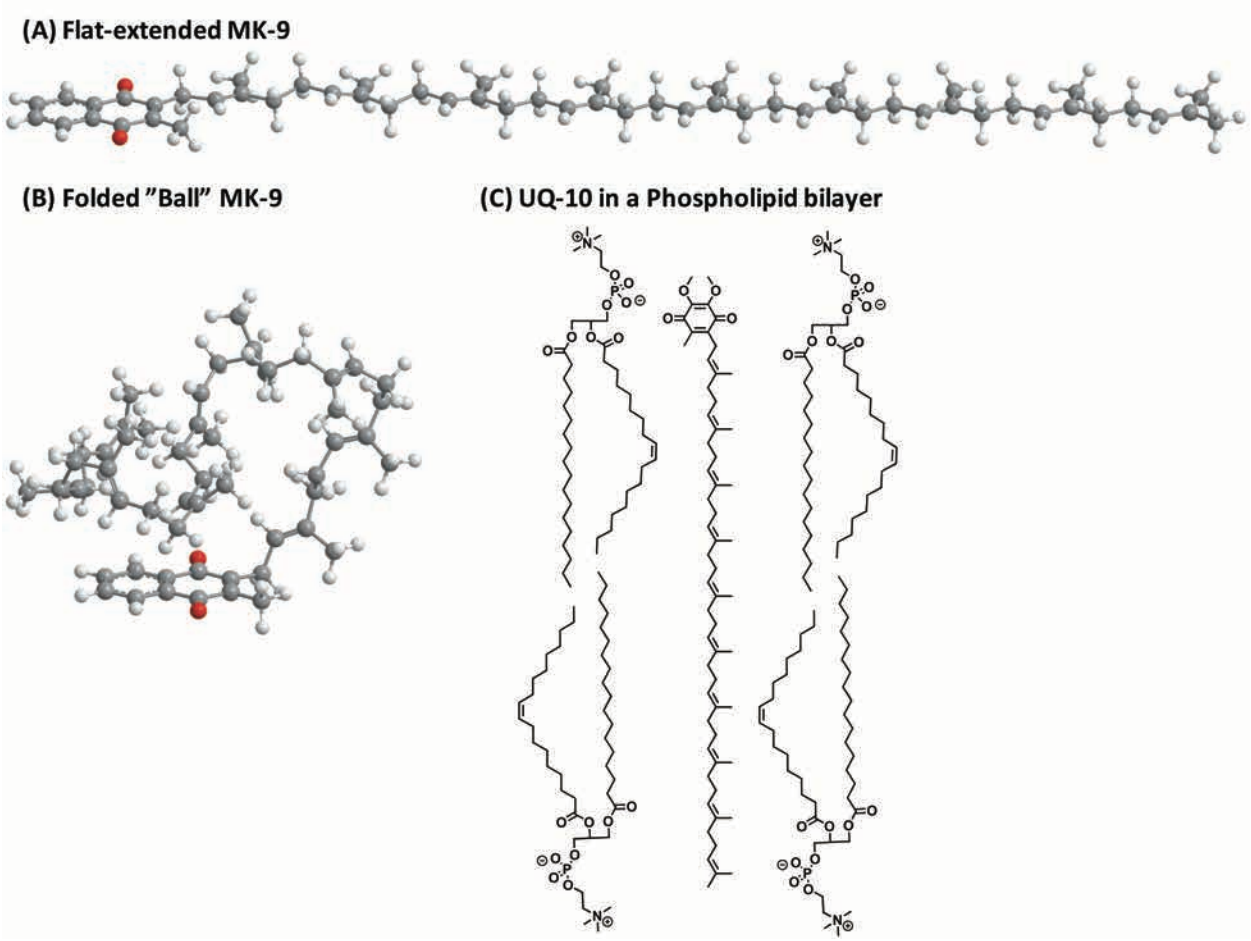

Figure 1.1.2 Illustration of (A) a flat-extended conformation of MK-9 (B) a folded ball conformation of MK-9 obtained from a simple molecular mechanics simulation followed by an energy optimization carried out on a flat-extended MK-9 conformation and (C) Ubiquinone-10 (UQ-10) in a phospholipid bilayer adapted from Trumpower.[30]

Currently, there are various MK compounds known with interesting biological activities. The most widely known MK compound is Vitamin K_2 (or MK-4), which as mentioned previously is essential for life in humans as it is a key cofactor in blood coagulation.[20] MK-4 was recently shown to be biosynthesized in humans[17] and as a part of the ETS in *Drosophila.*[16] MK-4 has been the subject of interesting reports demonstrating its biological roles and applications over the last ten years.[16-17, 31-32] The second most widely known MK compound is Vitamin K_1, also known as phylloquinone, which is found in green plants, contains four isoprene units with the terminal three saturated and functions as an electron acceptor during photosynthesis within photosystem I.[33] The simplest 1,4-naphthoquinone derivative known lacking the isoprenyl side chain is Vitamin K_3 (or menadione) and has been reported to have significant anti-tumoral properties.[2] N-alkylated MK derivatives have also been synthesized and characterized in literature with several exhibiting interesting biological properties.[34-37] In 2017, the potent cyclic peptide antibiotic, Lotilibcin, was demonstrated to be effective against Gram-positive bacteria including methicillin-resistant *Staphylococcus aureus* (MRSA).[38] Interestingly, the activity of Lotilibcin was attributed to lysis of the bacterial membrane, where its membrane disrupting effects depended on the presence of MK, and leaves the question if other MK derivatives produce the same membrane disrupting effect in the presence of Lotilibcin.[38] This report underlines the importance in understanding the relationship between MK structure, its biological role, and biological function.

MK analogs that contain partially and fully saturated isoprenyl side chains of various lengths are found in eubacteria and Archaea. These characteristics are evolutionarily conserved and have long been used in taxonomic classification efforts and phenotypic organization of bacteria.[23-24, 39] MK analogs with one or more saturated isoprene units are found in some members of Gram-

positive and Gram-negative bacteria.[23, 39-41] In contrast to partial saturation, the fully saturated MK-7(14H) has been observed in Archaea, which are single-celled microbes that typically live in extreme environments and were recently shown to comprise part of the human microbiota.[42-43] It is thought that the full saturation of the isoprenyl side chain observed in Archaea makes the cellular membrane more tolerant to extreme environments (e.g., high temperature, high salinity and low/high pH).[42] Thus, many MK homologs that contain various degrees of saturation in their isoprenyl side chains have been isolated but there is a limited understanding of the role or function of the partially saturated MK derivatives.[40, 44]

The conformation of the isoprenoid moiety in MK derivatives is likely important to its function as an electron transporter molecule and its other important biological roles. The shape, and thus the conformation of these molecules is relevant for molecular recognition motifs and the processing of these molecules within the membrane by respiratory enzymes. Currently, little information is available regarding the conformation of MKs in solution or within cell membranes and how partial saturation of the isoprenyl side chain on MK affects conformation and quinone reactivity, even though the structures and biological significance of lipoquinones and isoprenoids have been known for over 50 years.[6, 25, 39, 45-47] It is a well-known fact that evolutionary conserved structural differences in lipoquinone head group alter quinone redox potential[1] but it remains unknown how partial saturation of the isoprenyl side chain affects quinone redox potential. Partial saturation of the isoprenyl side chain may affect electron transfer efficiency within the membrane of *M. tuberculosis*. The conformation and electronic properties of a molecule can affect both the reactivity and function of a molecule in solution and within biological environments and it may be possible that the conformation of the isoprenyl side chain could

affect the quinone redox potential of MK. Alternatively, partial saturation could be solely responsible for recognition by respiratory enzymes and may have no influence on redox potential and electron transfer efficiency within the ETS.

Importantly, the longer partially saturated isoprenyl side chain MK analog, MK-9(II-H_2) (Figure 1.1.3) is an electron transporter within *M. tuberculosis* and the synthesis of MK-9(II-H_2) was found observed in pathogenic *M. tuberculosis*.[15, 48] MenJ is an oxidoreductase that selectively saturates the second isoprene unit of MK-9 (Figure 1.1.3) and mycobacterial electron transport efficiency was decreased 3-fold when MenJ expression was disrupted.[15, 48] Thus, the role of the partially saturated MKs should be determined, where partial saturation of the isoprenyl side chain may be essential for proper substrate recognition by respiratory enzymes, or may enhance electron transfer efficiency with the ETS or may be a novel virulence factor.[15, 48] Studies are ongoing to determine whether partially saturated MKs or MenJ are virulence factors for mycobacteria. MenJ is a contextually essential enzyme and may provide a realistic target for therapeutic drug development. Partial saturation of MK in these biological systems appears necessary for other organisms to survive as well.[15, 39, 48] In addition to mycobacteria, partially saturated MK analogs have been reported in other organisms such as members of the genera *Streptomyces* and *Actinomadura* to name a few.[39] These selected examples demonstrate a need to understand the role and necessity of partial saturation observed in the isoprenyl side chain of MK observed within different organisms.

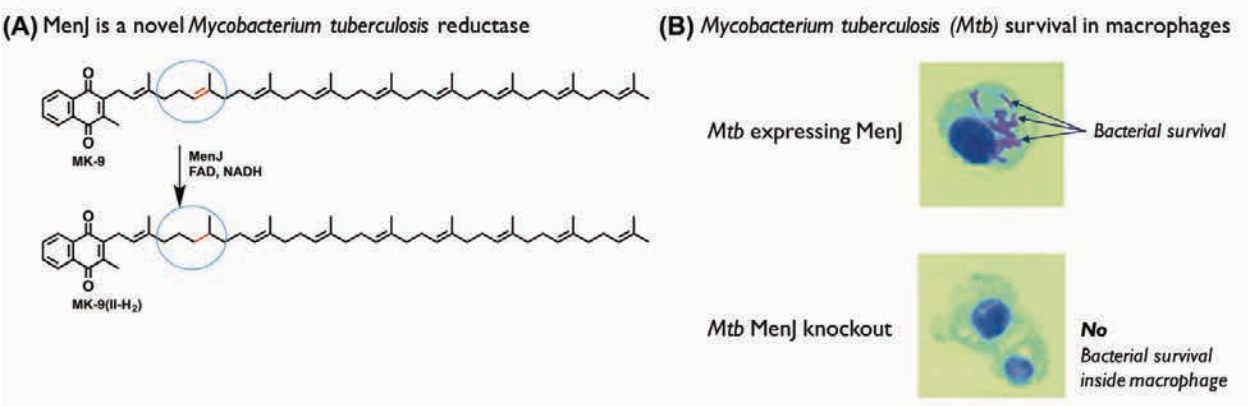

Figure 1.1.3 Illustration of (A) selective MenJ catalyzed reduction of MK-9 to MK-9(II-H_2) in the presence of FAD and NADH and (B) *Mycobacterium tuberculosis* survival inside macrophages expressing MenJ and with a MenJ knockout. Adapted from Upadhyay *et al*.[15]

Importantly, it is unclear whether hydrogenation of the double bond in specific isoprene units changes the reactivity of the quinone system found within MK. The double bonds present within the isoprenyl side chain are not conjugated to the quinone system within MK. Therefore, it would not be anticipated that a significant change in the quinone redox potential would occur upon reduction of an isoprenyl unit. However, it has been reported that even when there is no direct conjugation between the quinone system and a substituent group, electrochemical reduction of the quinone system is sensitive to the electronic perturbation of the substituents.[1] Thus, it is possible that partial saturation in the isoprenyl side chain could influence the quinone redox potential, where an indirect through bond effect could be a contributing factor and/or conformational effects of the substituent. This indirect through bond effect could explain saturation of the first isoprene unit that is only 4-5 carbons from the quinone moiety. However, it is unlikely that an indirect through bond effect could exist across 10 carbons as in the case when the second isoprene unit of MK-9 is saturated. It is more likely in this scenario that a conformation effect could be responsible or some other unrecognized mechanism. If a small change in redox potential was observed upon saturation of a double bond in the isoprenyl side

chain of MK, it could be biologically important and could reflect the biological function of these molecules.

Access to MK compounds that contain a varying number of isoprene units and degrees of saturation in the isoprenyl side chain is crucial for a fundamental understanding of the chemistry of MK. Unfortunately, most of these MK analogs are not commercially available but fortunately can be accessed through chemical synthesis. With these compounds in hand, the effects of conformation and saturation of the isoprenyl side chain can be isolated and their influence on quinone redox potential can be determined. Carrying out electrochemistry experiments to determine the quinone redox potential of these MK derivatives with varying number of isoprene units and degrees of saturation in the isoprenyl side chain will allow us to examine our hypothesis that saturation of the isoprenyl side chain can affect MK quinone redox potential. These results will shed light on the perplexing biological activity exhibited in MenJ knockout mutants of *M. tuberculosis* that can no longer survive inside macrophages and have reduced electron transport efficiency.[15, 48] Importantly, partial saturation of MK is observed in a pathogen that is responsible for the infection of ~1/3 of the global human population and the deaths of ~1.3 million people annually.[15, 48-49]

The physiologically relevant environment for MKs is in association with hydrophobic membranes; therefore, it is important to study the interaction and conformation of MKs within model membrane systems. Several membrane models exist including Langmuir monolayers, liposomes, micelles, and reverse micelles (RM) (Figure 1.1.4).[50-56] Each model system has advantages and disadvantages, and we have chosen herein to investigate mainly the RM system because RMs are well characterized, well behaved, and allow for determination of molecular

placement, orientation, and conformation of MK derivatives with regard to the membrane interface.[50-56]

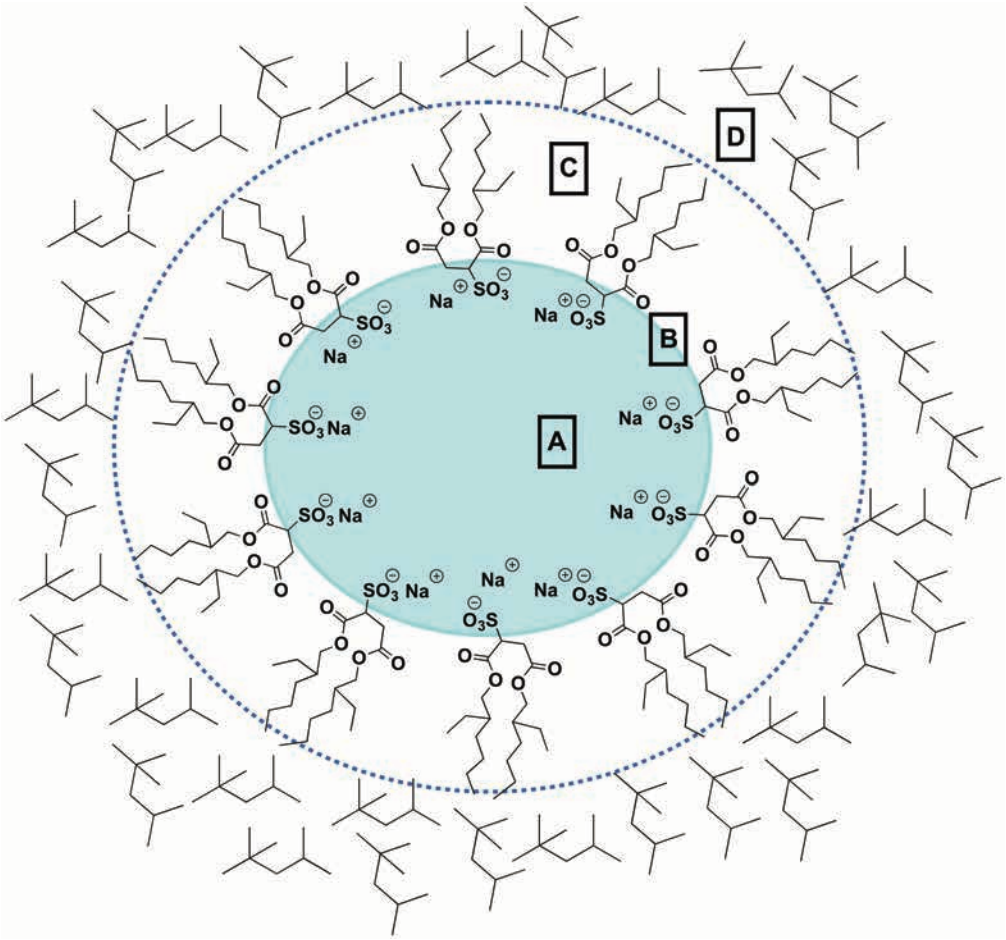

Figure 1.1.4 Schematic diagram of a reverse micelle present in a microemulsion. Labelling for the reverse micelle is as follows: (A) the water pool, (B) the Stern layer, (C) the hydrophobic surfactant tails, and (D) the organic solvent, isooctane. Figure adapted from Koehn *et al*.[57]

One major objective herein was to characterize the molecular details of MKs association with membrane-like interfaces. Therefore, we used a RM model membrane system to determine the location and conformation of MK derivatives (Figure 1.1.4).[55, 58-62] In a RM system, a ternary microemulsion system forms when a surfactant is dissolved in an organic solvent and the addition of water creates nanosized water droplets encased in surfactant (such as Aerosol-OT (AOT)).[51, 59, 61-64] This dynamic, yet simple, model can provide molecular detail on location and conformation

of MK at an interface using NMR spectroscopy.[62, 65-68] The use of phospholipids such as dipalmitoylphosphatidylcholine (DPPC) have overlapping hydrogen signals with key MK hydrogen signals making interpreting conformational information very complex by NMR spectroscopy unless expensive deuterated lipids are used. RM systems provide information regarding the location, conformation, and physical interactions of MK lipids with membrane-like interfaces, which allowed us to examine our hypothesis that MKs adopt folded conformations within membrane-like environments.

1.2 Hydrophobic Vanadium(V) Catecholates Containing Redox-Active Ligands-

The second class of redox-active and hydrophobic compounds explored in this dissertation are vanadium(V) catecholate complexes. Medicinal applications of metal complexes in the past has been dominated by the anti-cancer platinum drugs, as well as a range of complexes used for imaging diagnostics and nuclear medicinal applications.[69-75] However, several additional metal-based classes of complexes have been of interest for decades and are increasing in importance. Anti-cancer activities of vanadium compounds have generated recent interest because of a combination of desirable properties for chemotherapy, i.e., strong cytotoxicities, anti-metastatic activities and relatively low systemic toxicities. Certain hydrophobic vanadium(V) Schiff base/catecholate compounds display a range of interesting redox properties and, as shown herein, have increased stability in aqueous media and affinity for membrane interfaces (Figure 1.2.1). Depending on their hydrophobicity, the V-complexes may be able to enter cells intact due to increased hydrolytic stability imparted by the steric bulk and hydrophobic repulsion by an appropriately substituted catechol ligand (Figure 1.2.2).

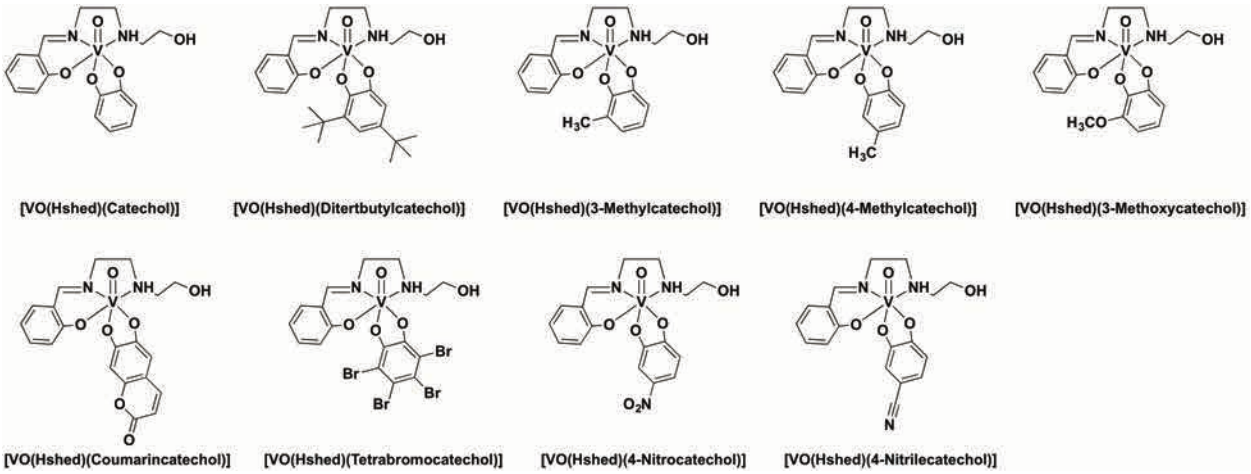

Figure 1.2.1 Structures of various mixed ligand Schiff base vanadium(V) catecholate complexes with different substituted catechol ligands.

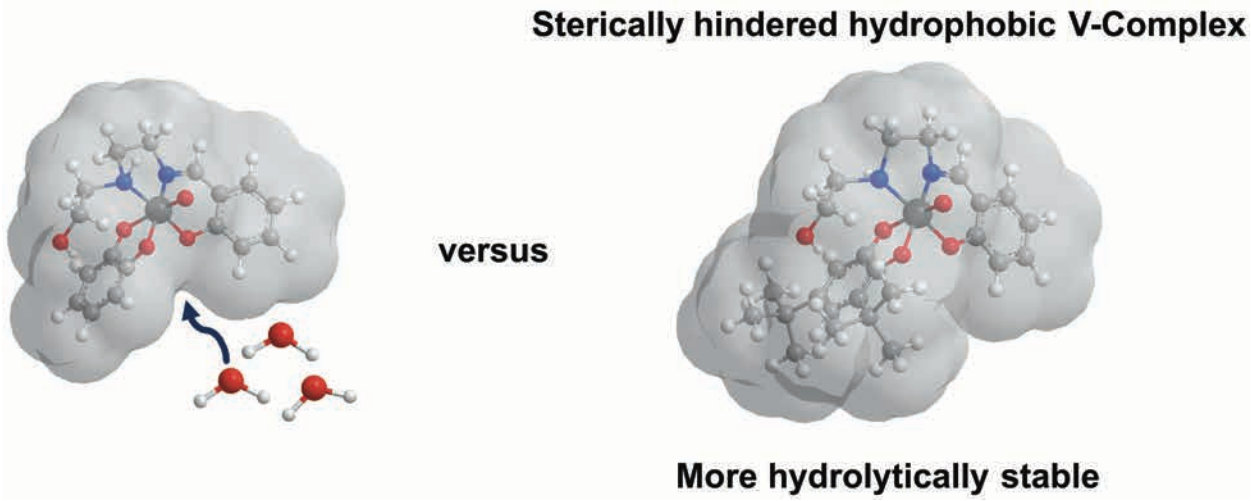

Figure 1.2.2 Illustration showing solvent accessible volume for the two V-complexes, [VO(Hshed)(catechol)] (left) and [VO(Hshed)(ditertbutylcatechol)] (right). Steric bulk imparted by the hydrophobic ditertbutylcatechol (dtb) ligand may increase hydrolytic stability allowing the V-complex to enter cancer cells intact and exhibit potent cytotoxicity toward the cancer cells.[76]

Vitamins and nutritional additives often include metal-ion containing supplements.[77-81] Some metal complexes can contain hydrophobic ligands, which can make solubility in biological systems challenging. However, the large number of different formulations for iron and vanadium are testament to the existence of a range of methodologies that can be applied to increase the efficacy of absorption.[82] Furthermore, Lipinski's rules[83] based on an empirical and statistical evaluation of efficacy suggest that statistically successful drugs are of certain size,

hydrophobicity, polarity, or reactivity, which thus limits the chemical space to search for available drugs. However, some of the more successful drugs do not follow these empirical rules, such as cisplatin; therefore, drug and supplement design continues to include the entire chemical space. For example, recent investigations have introduced promising hydrophobic titanium and vanadium drugs.[84-88] The water solubility of these compounds and other hydrophobic drugs is very limited, and as a result, the methods for *in vivo* studies with these compounds involve dissolving the compounds in methanol, ethanol, or DMSO or dissolution in assays containing surfactants and/or DMSO. Direct injection of the V-complex into the tumor via endoscopy would circumvent solubility and delivery issues of the drug. These hydrophobic V-complexes show promise as potential metallo-drug candidates. Therefore, the cytotoxicity in cancer cell lines and the stability/degradation of hydrophobic V-complexes in model membrane systems will be determined and discussed herein.

1.3 Dealing and Working with Poorly Soluble and Hydrophobic Molecules

Generally, most biologically relevant environments are aqueous based and are hydrophilic in nature. This presents certain challenges for studying molecules that are native to hydrophobic environments such as within a lipid bilayer as they are generally very hydrophobic molecules and sparingly soluble, if at all. Not only does this make solubilizing the hydrophobic compounds a challenge in aqueous systems, it is also imperative to study the hydrophobic compounds in environments that resemble their native environment as well, such as in systems that mimic biological environments. For example, carrying out electrochemical analysis in hydrophobic

environments such as in organic solvents or within model membrane systems like micelles, liposomes, or reverse micelles.

Problems and challenges faced can consist of solubility affecting interpretation of enzymatic assay results where the researcher is not able to test native substrates. This problem can usually be circumvented by using surfactants and/or DMSO (Figure 1.3.1) to assist in solubilization when the compound is not too hydrophobic. The interaction between a hydrophobic solid (insoluble drug) with the hydrophobic tails of dissolved surfactant decreases the energy required to wet and dissolve the solid, thereby increasing drug solubility.[89] Further enhancement of solubility can be achieved through subsequent partitioning of dissolved species into the hydrophobic core of surfactant micelles.[89] The naturally occurring lipoquinones discussed herein generally have longer isoprenyl side chains and very low water solubility, which causes problems for evaluation in biological assays; therefore, the use of truncated MK derivatives can circumvent solubility issues in aqueous assays and activity can then be measured. This trait allows rigorous characterization of truncated MKs in aqueous assays where the analysis of native substrates (e.g., MK-9 or UQ-8) was not possible due to the lack of solubility even with the use of detergents and DMSO.[48] The use of surfactants or DMSO can create problems such as denaturing proteins or slowing catalytic activity of enzymes or may even alter the conformation of some molecules and therefore, these problems should be taken into consideration. Poorly soluble and hydrophobic drugs can present difficulties in delivering the drug to the desired biological target. Drug formulation chemistry has made great strides in developing methods for effective drug delivery such as the use of liposomes or vesicles to deliver drugs. Drug formulation can be avoided all together if an alternative approach is used. For instance, direct injection of the drug to the

biological target would help circumvent formulation and stability issues. This method would be advantageous for compounds like the hydrophobic and unstable vanadium(V) catecholate complexes outlined in the previous section. One could envision preparing a fresh solution of intact V-complex right at the bedside of the patient and then direct injecting the cytotoxic solution into the tumor *via* endoscopy to exhibit a cytotoxic effect.

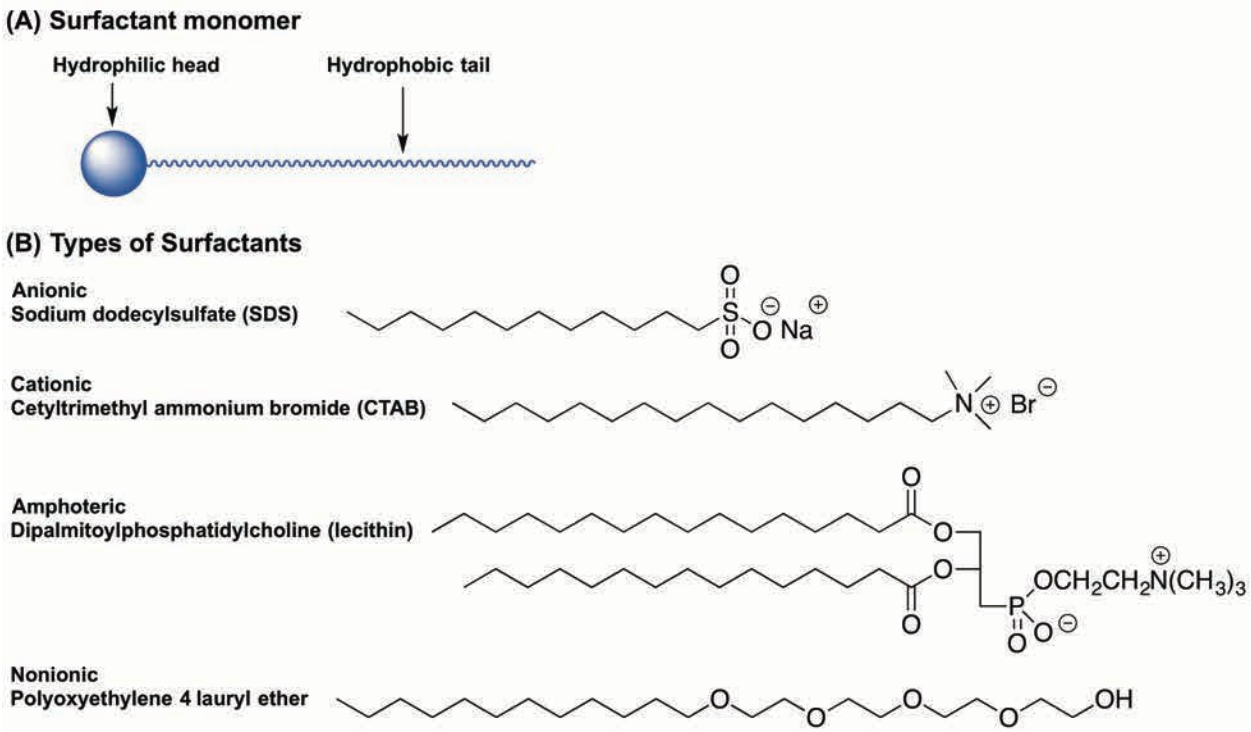

Figure 1.3.1 Illustration of (A) a surfactant monomer and (B) examples of different types of surfactant molecules. Figure adapted from *Poorly Soluble Drugs. Dissolution and Drug Release*.[89]

In summary, although organic compounds or metal complexes that are very hydrophobic and poorly soluble in aqueous systems present unique challenges, sufficient workarounds exist such as the use of surfactants or DMSO for solubilizing the compounds. These compounds should also be studied in their native environments such as in hydrophobic solvents or model membrane systems. However, care should be taken to make sure the use of such systems to aid in

solubilizing the compounds does not alter the experimental results and if they do, interpretations and conclusions should be made with such an understanding.

1.4 Studies of the Subsequent Chapters

Within these studies, the synthesis and investigation of two classes of biologically important, hydrophobic, redox-active molecules is explored. Chapter two describes the synthesis and characterization of truncated MK derivatives with varying isoprenyl side chain length and degrees of saturation. Chapter three explores the conformational flexibility of the isoprenyl side chain of MK and shows that a truncated MK analog, MK-2, can adopt folded conformations in hydrophobic environments and within a model membrane system. Chapter four isolates the conformational and chemical effect of saturation of the isoprenyl side chain on MK and shows that saturation minimally affects folded conformations of truncated MK derivatives but remarkably, a 20 mV redox potential difference was observed between unsaturated MK-1 and the saturated analog MK-1(H_2). Then in chapter five, hydrophobicity and steric bulk are explored as properties to enhance membrane affinity and anti-cancer properties of Schiff base vanadium(V) catecholate complexes, where the hydrophobic [VO(Hshed)(ditertbutylcatechol)] complex was found to have enhanced hydrolytic stability and potent activity against a bone cancer cell line. Finally, chapter six contains concluding remarks and future directions or studies that the author believes should be carried out.

References

1. Aguilar-Martínez, M.; Macías-Ruvalcaba, N. A.; Bautista-Martínez, J. A.; Gómez, M.; González, F. J.; González, I., Review: Hydrogen Bond and Protonation as Modifying Factors of the Quinone Reactivity. *Curr. Org. Chem.* **2004,** *8*, 1721-1738.
2. Astudillo-Sánchez, P. D.; Morales-Martínez, D.; Sánchez, A.; Rocha-Ortiz, G.; Salas-Reyes, M., Electrochemical Study of the Interactions Between Anionic Species of Menadione and Alkylated Nucleobases in Dimethylsulfoxide. *J. Electroanal. Chem.* **2017,** *801*, 104-113.
3. Gunner, M. R.; Madeo, J.; Zhu, Z., Modification of Quinone Electrochemistry by the Proteins in the Biological Electron Transfer Chains: Examples from Photosynthetic Reaction Centers. *J. Bioenerg. Biomembr.* **2008,** *40* (5), 509-519.
4. Monks, T. J.; Hanzlik, R. P.; Cohen, G. M.; Ross, D.; Graham, D. G., Quinone Chemistry and Toxicity. *Toxicol. Appl. Pharmacol* **1992,** *112* (1), 2-16.
5. Abraham, I.; Joshi, R.; Pardasani, P.; Pardasani, R. T., Recent Advances in 1,4-Benzoquinone Chemistry. *J. Braz. Chem. Soc.* **2011,** *22* (3), 385-421.
6. Nowicka, B.; Kruk, J., Occurrence, Biosynthesis and Function of Isoprenoid Quinones. *Biochim. Biophys. Acta* **2010,** *1797*, 1587-1605.
7. Caluwe, R.; Pyfferoen, L.; De Boeck, K.; De Vriese, A. S., The effects of vitamin K supplementation and vitamin K antagonists on progression of vascular calcification: ongoing randomized controlled trials. *Clin. Kidney J.* **2016,** *9* (2), 273-279.
8. Bergdoll, L.; ten Brink, F.; Nitschke, W.; Picot, D.; Baymann, F., From low- to high-potential bioenergetic chains: Thermodynamic constraints of Q-cycle function. *Biochim. Biophys. Acta, Bioenerg.* **2016,** *1857* (9), 1569-1579.
9. Epand, R. M.; Walker, C.; Epand, R. F.; Magarvey, N. A., Molecular mechanisms of membrane targeting antibiotics. *Biochim. Biophys. Acta, Biomembr.* **2016,** *1858* (5), 980-987.
10. Villaume, M. T.; Sella, E.; Saul, G.; Borzilleri, R. M.; Fargnoli, J.; Johnston, K. A.; Zhang, H.; Fereshteh, M. P.; Murali Dhar, T. G.; Baren, P. S., Antroquinonol A: Scalable Synthesis and Preclinical Biology of a Phase 2 Drug Candidate. *ACS Cent. Sci.* **2016,** *2*, 27-31.
11. Choi, S. R.; Larson, M. A.; Hinrichs, S. H.; Bartling, A. M.; Frandsen, J.; Narayanasamy, P., Discovery of bicyclic inhibitors against menaquinone biosynthesis. *Future Med. Chem.* **2016,** *8* (1), 11-16.
12. Matarlo, J. S.; Lu, Y.; Daryaee, F.; Daryaee, T.; Ruzsicska, B.; Walker, S. G.; Tonge, P. J., A Methyl 4-Oxo-4-phenylbut-2-enoate with in Vivo Activity against MRSA That Inhibits MenB in the Bacterial Menaquinone Biosynthesis Pathway. *ACS Infect. Dis.* **2016,** *2* (5), 329-340.
13. Szamosvari, D.; Bottcher, T., An Unsaturated Quinolone N-Oxide of Pseudomonas aeruginosa Modulates Growth and Virulence of Staphylococcus aureus. *Angew. Chem. Int. Ed.* **2017,** *56* (25), 7271-7275.
14. Vilcheze, C.; Hartman, T.; Weinrick, B.; Jain, P.; Weisbrod, T. R.; Leung, L. W.; Freundlich, J. S.; Jacobs, W. R., Enhanced respiration prevents drug tolerance and drug resistance in Mycobacterium tuberculosis. *Proc. Natl. Acad. Sci. U.S.A.* **2017,** *114* (17), 4495-4500.
15. Upadhyay, A.; Fontes, F. L.; Gonzalez-Juarrero, M.; McNeil, M. R.; Crans, D. C.; Jackson, M.; Crick, D. C., Partial Saturation of Menaquinone in *Mycobacterium tuberculosis*: Function and Essentiality of a Novel Reductase, MenJ. *ACS Cent. Sci.* **2015,** *1* (6), 292-302.

16. Vos, M.; Esposito, G.; Edirisinghe, J. N.; Vilain, S.; Haddad, D. M.; Slabbaert, J. R.; Van Meensel, S.; Schaap, O.; De Strooper, B.; Meganathan, R.; Morais, V. A.; Verstreken, P., Vitamin K_2 Is a Mitochondrial Electron Carrier That Rescues Pink1 Deficiency. *Science* **2012,** *336*, 1306-1310.
17. Nakagawa, K.; Hirota, Y.; Sawada, N.; Yuge, N.; Watanabe, M.; Uchino, Y.; Okuda, N.; Shimomura, Y.; Suhara, Y.; Okano, T., Identification of UBIAD1 as a Novel Human Menaquinone-4 Biosynthetic Enzyme. *Nature* **2010,** *468*, 117-121.
18. Hiratsuka, T.; Furihata, K.; Ishikawa, J.; Yamashita, H.; Itoh, N.; Seto, H.; Dairi, T., An Alternative Menaquinone Biosynthetic Pathway Operating in Microorganisms. *Science* **2008,** *321* (5896), 1670-1673.
19. Newman, D. K.; Kolter, R., A Role for Excreted Quinones in Extracellular Electron Transfer. *Nature* **2000,** *405*, 94-97.
20. Kurosu, M.; Begari, E., Vitamin K_2 in Electron Transport System: Are Enzymes Involved in Vitamin K_2 Biosynthesis Promising Drug Targets? *Molecules* **2010,** *15* (3), 1531-1553.
21. Rochaix, J. D., Regulation and Dynamics of the Light-Harvesting System. In *Annu. Rev Plant Biol.*, 2014; Vol. 65, pp 287-309.
22. Peters, B. J. Physical and Chemical Characteristics Behind Membrane Interactions of Small Molecules and Electron Transporters. Colorado State Univesity, 2018.
23. Collins, M. D.; Shah, H. N.; Minnikin, D. E., A Note on the Separation of Natural Mixtures of Bacterial Menaquinones Using Reverse-phase Thin-layer Chromatography. *J. Appl. Bacteriol.* **1980,** *48* (2), 277-282.
24. Thomson, R. H., *Naturally Occurring Quinones.* Academic Press Inc: 1971.
25. Meganathan, R., Biosynthesis of Menaquinone (Vitamin K_2) and Ubiquinone (Coenzyme Q): A Perspective on Enzymatic Mechanisms. In *Vitam. Horm.*, 2001; Vol. 61, pp 173-218.
26. Cooper, G. M.; Hausman, R. E., *The Cell A Molecular Approach.* 5th ed.; Sinauer Associates, INC.: Sunderland, Massachusetts, USA, 2009; p 820.
27. Nelson, D. L.; Cox, M. M., *Lehninger Principles of Biochemistry.* 5th ed.; W.H. Freeman and Company: New York, USA, 2008; p 1158.
28. Woodward, R. B.; Bloch, K., The Cyclization of Squalene in Cholesterol Synthesis. *J. Am. Chem. Soc.* **1953,** *75*, 2023-2024.
29. Hess Jr., B. A.; Smentek, L., The Concerted Nature of the Cyclization of Squalene Oxide to the Protosterol Cation. *Angew. Chem. Int. Ed.* **2013,** *52*, 11029-11033.
30. Trumpower, B. L., New Concepts on the Role of Ubiquinone in the Mitochondrial Respiratory Chain. *J. Bioenerg. Biomembr.* **1981,** *13*, 1-24.
31. Dragh, M. A.; Xu, Z.; Al-Allak, Z. S.; Hong, L., Vitamin K_2 Prevents Lymphoma in Drosophila. *Sci. Rep.* **2017,** *7*, 17047.
32. Okamoto, H.; Shidara, K.; Hoshi, D.; Kamatani, N., Anti-arthritis Effects of Vitamin K_2 (Menaquinone-4) - a New Potential Therapeutic Strategy for Rheumatoid Arthritis. *FEBS J.* **2007,** *274*, 4588-4594.
33. van der Est, A., Electron Transfer Involving Phylloquinone in Photosystem I. In *Photosystem I. Advances in Photosynthesis and Respiration*, Golbeck, J. H., Ed. Springer, Dordrecht: 2006; Vol. 24.
34. Josey, B. J.; Inks, E. S.; Wen, X.; Chou, C. J., Structure−Activity Relationship Study of Vitamin K Derivatives Yields Highly Potent Neuroprotective Agents. *J. Med. Chem.* **2013,** *56*, 1007-1022.
35. Rahn, J. J.; Bestman, J. E.; Josey, B. J.; Inks, E. S.; Stackley, K. D.; Rogers, C. E.; Chou, C. J.; Chan, S. S. L., Novel Vitamin K Analogs Suppress Seizures in Zebrafish and Mouse Models of Epilepsy. *Neuroscience* **2014,** *259*, 142-154.
36. Chadar, D.; Camilles, M.; Patil, R.; Khan, A.; Weyhermuller, T.; Salunke-Gawali, S., Synthesis and Characterization of *n*-alkylamino Derivatives of Vitamin K3: Molecular Structure of 2-propylamino-3-methyl-1,4-naphthoquinone and Antibacterial Activities. *J. Mol. Struct.* **2015,** *1086*, 179-189.

37. Kathawate, L.; Joshi, P. V.; Dash, T. K.; Pal, S.; Nikalje, M.; Weyhermuller, T.; Puranik, V. G.; Konkimalla, V. B.; Salunke-Gawali, S., Reaction Between Lawsone and Aminophenol Derivatives: Synthesis, Characterization, Molecular Structures and Antiproliferative Activity. *J. Mol. Struct.* **2014,** *1075*, 397-405.
38. Itoh, H.; Tokumoto, K.; Kaji, T.; Paudel, A.; Panthee, S.; Hamamoto, H.; Sekimizu, K.; Inoue, M., Total Synthesis and Biological Mode of Action of WAP-8294A2: A Menaquinone-Targeting Antibiotic. *J. Org. Chem.* **2018,** *83*, 6924-6935.
39. Collins, M. D.; Jones, D., Distribution of Isoprenoid Quinone Structural Types in Bacteria and Their Taxonomic Implications. *Microbiol. Rev.* **1981,** *45* (2), 316-354.
40. Dunphy, P. J.; Brodie, A. F., The Structure and Function of Quinones in Respiratory Metabolism. In *Methods in Enzymology*, 1971; Vol. 18, pp 407-461.
41. Dunphy, P. J.; Gutnick, D. L.; Phillips, P. G.; Brodie, A. F., A New Natural Naphthoquinone in *Mycobacterium phlei*. Cis-dihydromenaquinone-9, Structure and Function. *J. Biol. Chem.* **1968,** *243*, 398-407.
42. Ogawa, T.; Isobe, K.; Mori, T.; Asakawa, S.; Yoshimura, T.; Hemmi, H., A Novel Geranylgeranyl Reductase from the Methanogenic Archaeon *Methanosarcina acetivorans* Displays Unique Regiospecificity. *FEBS J.* **2014,** *281* (14), 3165-3176.
43. Bang, C.; Schmitz, R. A., Archaea Associated with Human Surfaces: Not To Be Underestimated. *FEMS Microbiol. Rev.* **2015,** *39* (5), 631-648.
44. Gale, P. H.; Arison, B. H.; Trenner, N. R.; Page, A. C.; Folkers, K.; Brodie, A. F., Characterization of Vitamin K9(H) from *Mycobacterium phlei. Biochemistry* **1963,** *2*, 200-203.
45. da Costa, M. S.; Albuquerque, L.; Nobre, M. F.; Wait, R., The Extraction and Identification of Respiratory Lipoquinones of Prokaryotes and Their Use in Taxonomy. In *Methods in Microbiology, Vol 38: Taxonomy of Prokaryotes*, Rainey, F.; Oren, A., Eds. Elsevier Academic Press Inc: San Diego, 2011; Vol. 38, pp 197-206.
46. Kroppenstedt, R. M.; Mannheim, W., Lipoquinones in Members of the Family Pasteurellaceae. *Int. J. Syst. Evol. Bacteriol.* **1989,** *39* (3), 304-308.
47. Jarchow-Choy, S. K.; Koppisch, A. T.; Fox, D. T., Synthetic Routes to Methylerythritol Phosphate Pathway Intermediates and Downstream Isoprenoids. *Curr. Org. Chem.* **2014,** *18*, 1050-1072.
48. Upadhyay, A.; Kumar, S.; Rooker, S. A.; Koehn, J. T.; Crans, D. C.; McNeil, M. R.; Lott, J. S.; Crick, D. C., Mycobacterial MenJ: An Oxidoreductase Involved in Menaquinone Biosynthesis. *ACS Chem. Biol.* **2018,** *13*, 2498-2507.
49. Glaziou, P.; Sismanidis, C.; Floyd, K.; Raviglione, M., Global Epidemiology of tuberculosis. *Cold Spring Harbor Perspect. Med.* **2015,** *5*, a017798.
50. Baruah, B.; Roden, J. M.; Sedgwick, M.; Correa, N. M.; Crans, D. C.; Levinger, N. E., When Is Water Not Water? Exploring Water Confined in Large Reverse Micelles Using a Highly Charged Inorganic Molecular Probe. *J. Am. Chem. Soc.* **2006,** *128*, 12758-12765.
51. Odella, E.; Falcone, R. D.; Silber, J. J.; Correa, N. M., Nanoscale Control Over Interfacial Properties in Mixed Reverse Micelles Formulated by Using Sodium 1,4-bis-2-ethylhexylsulfosuccinate and Tri-n-octyl Phosphine Oxide Surfactants. *ChemPhysChem* **2016,** *17* (15), 2407-2414.
52. Diaz-Fernandez, Y.; Foti, F.; Mangano, C.; Pallavicini, P.; Patroni, S.; Perez-Gramatges, A.; Rodriguez-Calvo, S., Micelles for the Self-Assembly of "Off–On–Off" Fluorescent Sensors for pH Windows. *Chem. Eur. J.* **2006,** *12*, 921-930.
53. Pallavicini, P.; Diaz-Fernandez, Y.; Pasotti, L., Micelles as Nanosized Containers for the Self-assembly of Multicomponent Fluorescent Sensors. *Coord. Chem. Rev.* **2009,** *253*, 2226-2240.
54. Stefaniu, C.; Brezesinski, G.; Mohwald, H., Langmuir Monolayers as Models to Study Processes at Membrane Surfaces. *Adv. Colloid Interface Sci.* **2014,** *208*, 197-213.

55. Sostarecz, A. G.; Gaidamauskas, E.; Distin, S.; Bonetti, S. J.; Levinger, N. E.; Crans, D. C., Correlation of Insulin-Enhancing Properties of Vanadium-Dipicolinate Complexes in Model Membrane Systems: Phospholipid Langmuir Monolayers and AOT Reverse Micelles. *Chem. Eur. J.* **2014,** *20* (17), 5149-5159.
56. Peters, B. J.; Groninger, A. S.; Fontes, F. L.; Crick, D. C.; Crans, D. C., Differences in Interactions of Benzoic Acid and Benzoate with Interfaces. *Langmuir* **2016,** *32* (37), 9451-9459.
57. Koehn, J. T.; Beuning, C. N.; Peters, B. J.; Dellinger, S. K.; Van Cleave, C.; Crick, D. C.; Crans, D. C., Investigating Substrate Analogues for Mycobacterial MenJ: Truncated and Partially Saturated Menaquinones. *Biochemistry* **2019,** *58* (12), 1596-1615.
58. Riter, R. E.; Kimmel, J. R.; Undiks, E. P.; Levinger, N. E., Novel Reverse Micelles Partitioning Nonaqueous Polar Solvents in a Hydrocarbon Continuous Phase. *J. Phys. Chem. B* **1997,** *101* (41), 8292-8297.
59. Maitra, A., Determination of Size Parameters of Water-aerosol-OT Oil Reverse Micelles From Their Nuclear Magnetic-resonance Data. *J. Phys. Chem.* **1984,** *88* (21), 5122-5125.
60. Durantini, A. M.; Falcone, R. D.; Silber, J. J.; Correa, N. M., Effect of Confinement on the Properties of Sequestered Mixed Polar Solvents: Enzymatic Catalysis in Nonaqueous 1,4-Bis-2-ethylhexylsulfosuccinate Reverse Micelles. *ChemPhysChem* **2016,** *17* (11), 1678-1685.
61. Lepori, C. M. O.; Correa, N. M.; Silber, J. J.; Falcone, R. D., How the Cation 1-butyl-3-methylimidazolium Impacts the Interaction Between the Entrapped Water and the Reverse Micelle Interface Created with an Ionic Liquid-like Surfactant. *Soft Matter* **2016,** *12* (3), 830-844.
62. De, T. K.; Maitra, A., Solution Behaviour of Aerosol OT in Non-polar Solvents. *Adv. Colloid Interface Sci.* **1995,** *59*, 95-193.
63. Sedgwick, M. A.; Trujillo, A. M.; Hendricks, N.; Levinger, N. E.; Crans, D. C., Coexisting Aggregates in Mixed Aerosol OT and Cholesterol Microemulsions. *Langmuir* **2011,** *27* (3), 948-954.
64. Zan, G. T.; Wu, Q. S., Biomimetic and Bioinspired Synthesis of Nanomaterials/Nanostructures. *Adv. Mater.* **2016,** *28* (11), 2099-2147.
65. Kuchler, A.; Yoshimoto, M.; Luginbuhl, S.; Mavelli, F.; Walde, P., Enzymatic Reactions in Confined Environments. *Nat. Nanotechnol.* **2016,** *11* (5), 409-420.
66. Dharaiya, N.; Bahadur, P., Phenol Induced Growth in Triton X-100 Micelles: Effect of pH and Phenols' Hydrophobicity. *Colloids Surf. A* **2012,** *410*, 81-90.
67. Dumas, C.; Meledandri, C. J., Insights into the Partitioning Behavior of Secondary Surfactants in a Microemulsion-Based Synthesis of Metal Nanoparticles: A DLS and 2D NMR Spectroscopic Investigation. *Langmuir* **2015,** *31* (26), 7193-7203.
68. Kaur, G.; Chiappisi, L.; Prevost, S.; Schweins, R.; Gradzielski, M.; Mehta, S. K., Probing the Microstructure of Nonionic Microemulsions with Ethyl Oleate by Viscosity, ROESY, DLS, SANS, and Cyclic Voltammetry. *Langmuir* **2012,** *28* (29), 10640-10652.
69. Sherman, S. E.; Lippard, S. J., Structural Aspects of Platinum Anticancer Drug-Interactions with DNA. *Chem. Rev.* **1987,** *87* (5), 1153-1181.
70. Evangelou, A. M., Vanadium in Cancer Treatment. *Crit. Rev. Oncol. Hematol.* **2002,** *42* (3), 249-265.
71. Farrell, N., Current Status of Structure-activity Relationships of Platinum Anticancer Drugs: Activation of the *trans*-geometry. *Met. Ions Biol. Syst.* **1996,** *32*, 603-639.
72. Pessoa, J. C.; Etcheverry, S.; Gambino, D., Vanadium Compounds in Medicine. *Coord. Chem. Rev.* **2015,** *301*, 24-48.
73. Yang, X.; Wang, K., Perspectives in Medicinal Chemistry - Focusing on the Link Between Diabetes, Alzheimer's Disease and Cancer for the Discovery of New Medicines. *Curr. Top. Med. Chem.* **2016,** *16* (7), 675-676.
74. Petanidis, S.; Kioseoglou, E.; Domvri, K.; Zarogoulidis, P.; Carthy, J. M.; Anestakis, D.; Moustakas, A.; Salifoglou, A., In vitro and ex vivo Vanadium Antitumor Activity in (TGF-β)-induced EMT. Synergistic

Activity with Carboplatin and Correlation with Tumor Metastasis in Cancer Patients. *Int. J. Biochem. Cell Biol.* **2016,** *74*, 121-134.
75. Vieira, A. P.; Wegermann, C. A.; Da Costa Ferreira, A. M., Comparative Studies of Schiff base-copper(II) and Zinc(II) Complexes Regarding their DNA Binding Ability and Cytotoxicity against Sarcoma Cells. *New J. Chem.* **2018,** *42*, 13169-13179.
76. Crans, D. C.; Koehn, J. T.; Petry, S. M.; Glover, C. M.; Wijetunga, A.; Kaur, R.; Levina, A.; Lay, P. A., Hydrophobicity May Enhance Membrane Affinity and Anti-Cancer Effects of Schiff Base Vanadium(V) Catecholate Complexes. *Dalton Trans.* **2019,** *48*, 6383-6395.
77. Gruzewska, K.; Michno, A.; Pawelczyk, T.; Bielarczyk, H., Essentiality and Toxicity of Vanadium Supplements in Health and Pathology. *J. Physiol. Pharmacol.* **2014,** *65* (5), 603-11.
78. Rehder, D.; Pessoa, J. C.; Geraldes, C.; Castro, M.; Kabanos, T.; Kiss, T.; Meier, B.; Micera, G.; Pettersson, L.; Rangel, M.; Salifoglou, A.; Turel, I.; Wang, D. R., In vitro Study of the Insulin-mimetic Behaviour of Vanadium(IV, V) Coordination Compounds. *J. Biol. Inorg. Chem.* **2002,** *7* (4-5), 384-396.
79. Thompson, K. H.; Lichter, J.; LeBel, C.; Scaife, M. C.; McNeill, J. H.; Orvig, C., Vanadium Treatment of Type 2 Diabetes: A View to the Future. *J. Inorg. Biochem.* **2009,** *103*, 554–558.
80. Willsky, G. R.; Halvorsen, K.; Godzala, M. E., III; Chi, L.-H.; Most, M. J.; Kaszynski, P.; Crans, D. C.; Goldfine, A. B.; Kostyniak, P. J., Coordination Chemistry May Explain Pharmacokinetics and Clinical Response of Vanadyl Sulfate in Type 2 Diabetic Patients. *Metallomics : integrated biometal science* **2013,** *5* (11), 1491-1502.
81. Crans, D. C.; Yang, L.; Haase, A. A.; Yang, X., Health Benefits of Vanadium and Its Potential as an Anticancer Agent. *Met. Ions Life Sci.* **2017,** *18* (1), 251-280.
82. Crans, D. C.; Woll, K. A.; Prusinskas, K.; Johnson, M. D.; Norkus, E., Metal Speciation in Health and Medicine Represented by Iron and Vanadium. *Inorg. Chem.* **2013,** *52* (21), 12262-12275.
83. Lipinski, C. A.; Lombardo, F.; Dominy, B. W.; Freeney, P. J., Experimental and Computational Approaches to Estimate Solubility and Permeability in Drug Discovery and Development Settings. *Adv. Drug Delivery Rev.* **2001,** *46*, 3-26.
84. Köpf-Maier, P., Antitumor Bis(cyclopentadienyl) Metal Complexes. *Met. Complexes Cancer Chemother.* **1993**, 259-296.
85. Ghosh, P.; D'Cruz, O. J.; Narla, R. K.; Uckun, F. M., Apoptosis-inducing Vanadocene Compounds Against Human Testicular Cancer. *Clin. Cancer Res.* **2000,** *6* (4), 1536-1545.
86. Kostova, I., Titanium and Vanadium Complexes as Anticancer Agents. *Anti-Cancer Agents Med. Chem.* **2009,** *9* (8), 827-842.
87. León, I.; Butenko, N.; Di Virgilio, A.; Muglia, C.; Baran, E.; Cavaco, I.; Etcheverry, S., Vanadium and Cancer Treatment: Antitumoral Mechanisms of Three Oxidovanadium (IV) Complexes on a Human Osteosarcoma Cell Line. *J. Inorg. Biochem.* **2014,** *134*, 106-117.
88. León, I.; Cadavid-Vargas, J.; Di Virgilio, A.; Etcheverry, S., Vanadium, Ruthenium and Copper Compounds: A New Class of Non-platinum Metallodrugs with Anticancer Activity. *Curr. Med. Chem.* **2017,** *24*, 112-148.
89. *Poorly Soluble Drugs. Dissolution and Drug Release*. Pan Stanford Publishing Pte. Ltd.: 2017; Vol. 1.

Chapter 2: Synthesis and Characterization of Menaquinone Derivatives[1]

2.1 Synthesis of Truncated Menaquinone Derivatives

Menaquinones (or naphthoquinones, MK) belong to the class of lipoquinones, which are a type of lipid-quinone containing isoprenoids that have a variety of biological roles.[1] These molecules contain both a redox active quinone moiety and a hydrophobic repeating isoprenyl side chain of varying length and degrees of saturation (Figure 2.1.1) depending on the organism. Although the naturally occurring lipoquinones generally have longer isoprenyl side chains, these MK analogs have very low water solubility, which causes problems for biological assays; therefore, the use of truncated MK derivatives can circumvent solubility issues in aqueous assays. The 1943 Nobel Prize in Physiology or Medicine was awarded to Henrik Dam and Edward Doisy for the discovery and characterization of vitamin K (a MK), a key cofactor in blood coagulation.[2] The interest in and the importance of MK/vitamin K, its derivatives and vitamers (e.g., vitamins K_1, K_2 and K_3) has remained strong. Vitamin K_1, also known as phylloquinone, is found in green plants, contains four isoprene units with the terminal three saturated and functions as an electron acceptor during photosynthesis within photosystem I.[3] Vitamin K_2, also known as menaquinone-4 (MK-4), has been the subject of interesting reports demonstrating its biological roles and applications over the last ten years.[4-7] Vitamin K_3 (or menadione) is the simplest 1,4-naphthoquinone derivative that lacks the isoprenyl side chain and non-naturally occurring N-alkylated MK derivatives have also shown interesting biological properties.[8-12] These examples of

[1]This chapter is published in part or in full in *ACS Omega*.[1]

different biological MK analogs underline the importance in understanding the relationship between MK structure, its biological role and biological function.

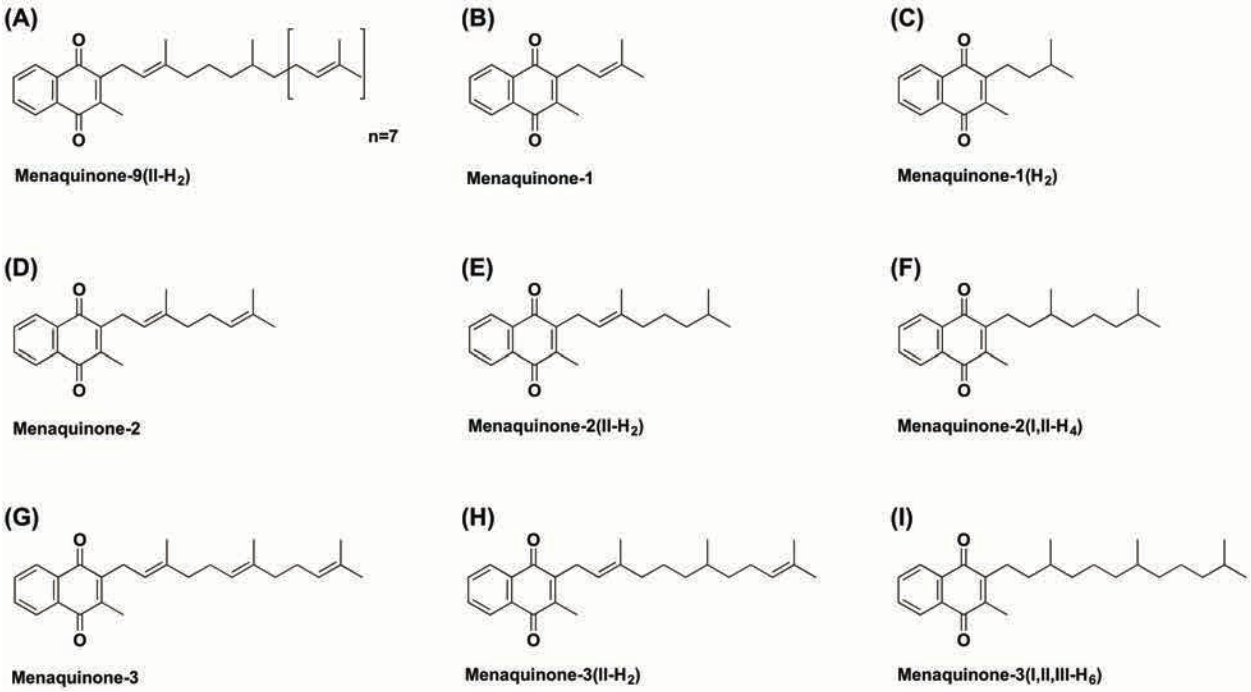

Figure 2.1.1 Structures of unsaturated and partially and fully saturated MK derivatives explored.

MK analogs that contain partially and fully saturated isoprenyl side chains of various lengths are found in eubacteria and Archaea. These characteristics are evolutionarily conserved and have long been used in taxonomic classification efforts and phenotypic organization of bacteria.[13-15] MK analogs with one or more saturated isoprene units are found in some members of Gram-positive and Gram-negative bacteria and therefore, the systematic preparation and characterization of a few selected truncated partially and fully saturated MK derivatives are described in this chapter.[14-17] In contrast to partial saturation, the fully saturated MK-7(14H) has been observed in Archaea, which are single-celled microbes that live in extreme environments and interestingly, comprise part of the human microbiota.[18-19] It is thought that the full saturation of the isoprenyl side chain observed in Archaea makes the cellular membrane more tolerant to

extreme environments (e.g., high temperature, high salinity and low/high pH).[18] Thus, many MK homologs that contain various degrees of saturation in their isoprenyl side chains have been isolated but there is a limited understanding of the role and function of the partially saturated MK derivatives.[16, 20] Menaquinone-9(II-H_2) (abbreviated as MK-9(II-H_2), Figure 2.1.1A), which is saturated at the second isoprene, has been observed in a number of bacteria including *Mycobacterium phlei* and pathogenic *M. tuberculosis.*[14, 16-17, 21-22] The biological significance of partial saturation of MK-9 has remained unclear 50 years after its first description.[20] Interestingly, the synthesis of MK-9(II-H_2) catalyzed by the enzyme MenJ was observed in *M. tuberculosis* and when MenJ was muted, *M. tuberculosis* survival in host macrophages was lost and electron transfer efficiency decreased 3-fold; therefore, the role of MenJ and MK-9(II-H_2) in tuberculosis disease progression should be investigated.[23]

Part of our ongoing studies includes why partial saturation of MK-9 is observed in pathogens such as *M. tuberculosis*.[23] Therefore, we needed access to MK analogs containing partially and fully saturated isoprenyl side chains. However, they are generally not commercially available nor sold as a mixture of geometric isomers as in the case of vitamin K_1. The potential for formation of *cis* and *trans* MK isomers and the separation and characterization of these geometric isomers is sometimes overlooked in literature but it is critical for their applications in biological systems. The use of *cis*/*trans* MK mixtures in biological systems would lead to inaccurate biological activities. Recently, the separation and NMR analysis of *cis*/*trans* mixtures of the dietary supplement menaquinone-7 (MK-7) was reported demonstrating the importance in understanding the different chemical, biochemical, conformational, and physical properties exhibited between *cis* and *trans* MK isomers.[24-25] Truncated MK analogs (i.e., 1-3 isoprene units)

have the advantage of being less hydrophobic, which can improve their biological activity compared to longer isoprenyl MK analogs (e.g., MK-7 and MK-9) and can be prepared using similar methodology described in this chapter and reports elsewhere.[26-27]

In this chapter, we present the synthesis and characterization of eight truncated isoprenyl side chain MK derivatives of varying chain length and degrees of saturation (Figure 2.1.1), as well as separated and characterized geometric isomers formed in the reactions. We have adopted the simple naming system where menaquinone-2 with a saturated double bond at the second isoprene unit is denoted as menaquinone-2(II-H_2) and abbreviated as MK-2(II-H_2), where II denotes the second isoprene unit and H_2 denotes saturation of one double bond (Figure 2.1.1E).[23, 28] This naming system follows for higher degrees of saturation such as menaquinone-2(I,II-H_4) that is saturated at isoprene's I and II and menaquinone-3(I,II,III-H_6) that is saturated at isoprene's I, II, and III (Figure 2.1.1F,I). Although MK-2(II-H_2) and menaquinone-3(II-H_2) (abbreviated as MK-3(II-H_2)) are known in literature reports mostly in the 1950s[29-34] and MK-2(II-H_2) was considered in a computational model study,[35] there are no modern syntheses reported and these analogs have not been extensively characterized nor have their geometric isomers been resolved and characterized in literature. Evidence supports the *trans* MK isomer as the only biologically active isomer.[27] Therefore, the separation and isolation of geometric isomers of MK derivatives is critical when testing these compounds in biological assays.

The synthesis and characterization of truncated isoprenyl MK analogs such as the two novel fully saturated MK derivatives described in this work is important for understanding their requirement in biological systems, as little is known about their physical properties, reactivity nor 3D-conformation within solution or cell membranes. Access to these truncated MK analogs in

pure geometric form is critical considering the recent discovery and timeliness for understanding why partially saturated MKs (e.g., MK-9(II-H_2), Figure 2.1.1A) are observed in pathogenic *M. tuberculosis,* when currently around one-third of the world's population is infected with Tuberculosis (TB) and over 1.3 million people worldwide die annually from TB.[36]

2.2 Materials and Methods

2.2.1 Materials and Information

Menadione (crystalline), sodium hydrosulfite (85.0%), 1,4 dioxane (anhydrous, 99.9%), BF_3 etherate (≥46.5%), Luperox A98 benzoyl peroxide (≥98%), methanol (99.9%), magnesium (powder, ≥99%), polyene carbonate (anhydrous, 99.7%), *n*-heptane (anhydrous, 99%), ethyl acetoacetate (≥99%), tert-Butanol (ACS reagent, ≥99%), Red-Al® sodium bis(2-methoxyethoxy)aluminium hydride solution (vitride reagent, ≥60 wt. % in toluene), sodium iodide (anhydrous, free-flowing, Redi-Dri™, ACS reagent, ≥99.5%), potassium permanganate (ACS reagent, ≥99.0%, low in mercury), potassium tert-butoxide (reagent grade, ≥98%), sodium bicarbonate (ACS grade), potassium hydroxide (ACS reagent, ≥85%, pellots), sodium methoxide (purum, ≥97%), aluminum oxide (activated neutral, Brockman I, standard grade, ~150 mesh, 58 Å), potassium carbonate (ACS reagent, anhydrous, ≥99.0%), farnesol (95%), 3,7-dimethyl-1-octanol (≥98%), (±)β-citronellol (95%), methanesulfonyl chloride (≥99.7%), ammonium formate (97%), celite® 545 filter agent, Pd/C (10% Pd basis), trimethylamine (≥99%), GC grade *n*-pentane, benzene, and triethyl phosphonoacetate (98%) were purchased from Sigma-Aldrich and were used as received unless otherwise noted. 3,7-Dimethyl-1-octen-3-ol (isophytol) was purchased from Santa Cruz Biotechnology. Ultra-high purity argon gas (99.9%) was acquired from Airgas. SiliCycle®SiliaFlash® F60, 43-60 μm 60 Å silica gel was purchased from SilliCycle. Anhydrous

sodium sulfate (Certified ACS, Granular), HPLC grade ethyl acetate (EtOAc) and HPLC grade dichloromethane (DCM) stabilized with 50 ppm amylene (unstabilized DCM can degrade menaquinones) was purchased from Fisher Chemical. Merck TLC Silica gel 60 F_{254} TLC plates and GC grade acetone were purchased from Merck. Washed sea sand was purchased from Fisher Scientific. Hydrofluoric (HF) solution (48 wt. %) was purchased from Mallinckrodt Pharmaceuticals. Deuterated NMR solvents of $CDCl_3$ (chloroform-d, 99.8% atom % D), dimethylsulfoxide (DMSO) (D 99.9%, + 0.05% V/V tetramethylsilane), and C_6D_6 (benzene-d_6, 99.6% atom % D) were acquired from Sigma-Aldrich. Distilled Deionized Water (DDI H_2O) was purified with a Barnstead E-pure system (18.2 MΩ-cm). Absolute ethanol was acquired from Pharmco-Aaper.

All non-aqueous reactions were carried out under an atmosphere of argon in flame-dried glassware and were stirred on a magnetic stir plate using anhydrous solvent unless otherwise noted. All solvents were purchased from commercial sources and either used directly or after drying. Solvents were dried either by passing through an alumina drying column (Solv-Tek Inc.) under argon pressure (i.e. benzene, methanol, and trimethylamine), or by passing through a column packed with activated neutral alumina under argon pressure (i.e. *n*-pentane), or dried over activated 3 Å molecular sieves for 48-72 h under argon atmosphere (i.e. tertbutanol, 10 g sieves / 100 mL solvent).[37] Reactions were monitored by thin layer chromatography (TLC) on Whatman Partisil® K6F TLC plates (silica gel 60 Å, 0.250 mm thickness) or Merck TLC Silica gel 60 F_{254} plates and visualized using a UV lamp (366 or 254 nm), Seebachs stain (and heated to visualize), or $KMnO_4$ stain (and heated to visualize) and preparative TLC was carried out using full size 20 X 20 cm Merck TLC Silica gel 60 F_{254} plates and visualized using a UV lamp. Products were

purified by flash chromatography (SiliCycle®SiliaFlash® F60, 43-60 μm 60 Å). Yields refer to dried, chromatographically and spectroscopically (^{1}H NMR) homogenous materials unless otherwise noted. All chemicals were used without purification unless otherwise noted. ^{1}H and ^{13}C spectra were recorded on a 400 MHz Varian Model MR400 or a Bruker Model Avance Neo400 equipped with BBFO smart probe operating at 400 MHz or 101 MHz, respectively. Chemical shift values (δ) are reported in ppm and referenced against the internal solvent peaks in ^{1}H NMR ($CDCl_3$, δ at 7.26 ppm; benzene-d_6, δ at 7.16 ppm) and in ^{13}C NMR ($CDCl_3$, δ at 77.16 ppm; benzene-d_6, δ at 128.06 ppm). All NMR spectra were acquired either at 25 or 26 °C. Integral values were determined using standard, uncalibrated NMR experiments and should be viewed accordingly. ^{1}H NMR spectra are reported as follows: chemical shift (multiplicity, coupling constant, integration). The following abbreviations are used to indicate multiplicities: s, singlet; d, doublet; t, triplet; q, quartet; m, multiplet; br, broad. NMR spectra were processed using MestReNova version 10.0.1. or 12.0.2. Details of NMR experiments are provided in representative experimental sections and captions of figures.

2.2.2 NMR Spectroscopic Studies

Synthesized compounds were dried under vacuum for ~2-4 days (~150-200 mTorr) unless otherwise noted to ensure as much residual solvent from purification was removed as possible. Samples for NMR studies were prepared immediately prior to running the samples using deuterated solvents sealed under inert atmosphere in glass ampules. The NMR sample solutions were placed under an argon atmosphere immediately, capped, and then spectra were acquired unless otherwise noted. NMR samples of MKs were protected from light by wrapping the samples in aluminum foil while not in the NMR instrument due to potential degradation; however, we

have not observed degradation due to light exposure. ^{1}H and ^{13}C spectra were recorded using a Varian Model MR400 or a Bruker Model Avance Neo400 equipped with BBFO smart probe and automated tuning module (ATM) operating at 400 MHz or 101 MHz, respectively. ^{1}H and ^{13}C spectra were recorded using a Varian Model MR400 or Model Inova400 operating at 400 MHz and 100 MHz, respectively. Chemical shift values (δ) are reported in ppm and referenced against the internal solvent peaks in ^{1}H NMR (d_6-DMSO, δ at 2.50 ppm, $CDCl_3$, δ at 7.26 ppm; benzene-d_6, δ at 7.16 ppm) and in ^{13}C NMR (d_6-DMSO, δ at 39.52 ppm, $CDCl_3$, δ at 77.16 ppm; benzene-d_6, δ at 128.06 ppm). All NMR spectra were recorded at either 25 or 26 °C. NMR spectra were processed using MestReNova version 10.0.1. or 12.0.2. See Supporting Information for 1D & 2D NMR spectra and NMR experimental details.

2.2.3 Mass Spectrometry and Elemental Analysis

High resolution mass spectrometry (HRMS) experiments were conducted either on an Agilent 6224 TOF LC/MS (O-TOF) interfaced with Direct Analysis in Real Time (DART) source (IonSense DART-100) or were conducted on a Bruker MaXis TOF MS (Q-TOF) interfaced with DART source (IonSense DART-SVP) or were conducted on an Agilent 6220 TOF LC/MS ("OTOF") interfaced to an Agilent 1200 HPLC with electrospray (ESI) mode. Low resolution mass spectrometry (LRMS) experiments were conducted by Electron Spray Ionization Mass Spectrometry (ESI) on an Agilent technologies 6130 Quadrupole LCMS. A standard of Jeffamine was used as an internal standard calibration for HRMS DART experiments carried out in positive mode. Combustion elemental analysis was carried out by ALS Environmental located in Tucson, AZ.

2.2.4 Preparation of Menaquinone-1

2-methyl-3-(3-methylbut-2-en-1-yl)naphthalene-1,4-dione, MK-1 (2.4). Menadiol (2.2) was synthesized as previously described[26] from menadione (2.1) and MK-1 (2.4) was synthesized previously.[38] However, here the reaction to form MK-1 (2.4) was scaled up and characterization reported data in $CDCl_3$. To a 100 mL Schlenk flask was added a stir bar, EtOAc (16 mL), and 1,4 dioxane (16 mL), which was then purged/evacuated with argon repeatedly. Then, crude menadiol (2.2) (2.50 g, 4:1 menadiol:menadione by NMR integration, note that menadiol is prone to auto-oxidation in $CDCl_3$, 11.48 mmol) was added followed by 3-methyl-2-buten-1-ol (2.3) (1.08 g, 12.52 mmol) and then dropwise addition of distilled BF_3 etherate (0.8 mL). The reaction solution turned dark orange and was refluxed at 70 °C for 3 h under argon. The reaction was quenched with ice-H_2O (100 mL) and then extracted with diethyl ether (3 x 100 mL). The yellow organic extracts were washed with sat. $NaHCO_3$ (100 mL), washed with brine (100 mL), dried with anhydrous Na_2SO_4, and then concentrated under reduced pressure at ambient temperature to yield 3.50 g of crude red oil. The crude oil was purified by flash column chromatography (1000 mL of 230-400 mesh SiO_2, 70 mm column, 20:1 *n*-pentane/EtOAc). The red oil obtained was dried under reduced pressure (~125 mTorr) overnight to yield 0.628 g (2.61 mmol, 22.7% yield) as a deep red oil. ^{1}H NMR (400 MHz, $CDCl_3$) δ: 8.06-8.08 (m, 2H), 7.67-7.69 (m, 2H), 5.02 (t, J = 7.0 Hz, 1H), 3.36 (d, 2H, J = 7.0 Hz), 2.19 (s, 3H), 1.79 (s, 3H), 1.69 (s, 3H). ^{13}C NMR (101 MHz, $CDCl_3$) δ: 185.6, 184.7, 146.2, 143.4, 134.1, 133.47, 133.42, 132.33, 132.30, 126.4, 126.3, 119.3, 26.3, 25.9, 18.2, 12.8. HRMS (DART) m/z: [$(M+H)^+$] Calcd for $C_{16}H_{17}O_2$ 241.1223; Found 241.1222.

2.2.5 Preparation of Menaquinone-1(H_2)

2-isopentyl-3-methylnaphthalene-1,4-dione, MK-1(H_2) (2.6). To a dry 100 mL round bottom Schlenk flask was added a stir bar and dry and degassed benzene (30 mL) followed by 1-Iodo-3-methylbutane (2.5) (1.98 g, 10.0 mmol, 1 equiv.), which was then purged/evacuated with argon repeatedly. To a dry 20 mL vial was added dry benzene (15 mL), which was then degassed *via* argon needle purge, followed by addition of menadione (2.1) (1.72 g, 10.0 mmol), and benzoyl peroxide (2.42 g, 10.0 mmol, 1 equiv.). This solution was sonicated until dissolution occurred under argon. The naphthoquinone-benzoyl peroxide solution was added dropwise over 2 h 15 min to the refluxing prenyl iodide solution, which was under argon atmosphere during the reaction. After the addition was complete, the solution refluxed for an additional 1 h. The solution was then diluted with sat. $NaHCO_3$ (100 mL) and diethyl ether (100 mL) and then the two phases were separated. The aqueous layer was extracted with diethyl ether (3 x 100 mL) and the combined organic extracts were washed with sat. $NaHCO_3$ (100 mL), washed with brine (100 mL), dried with anhydrous Na_2SO_4, and then concentrated under reduced pressure at ambient temperature to yield a crude yellow powder. The crude powder was purified by flash column chromatography (10:1.5 *n*-pentane/EtOAc) to yield 0.493 g as a yellow solid (2.03 mmol, 20.3 % yield). ^{1}H NMR (400 MHz, C_6D_6) δ: 8.05-8.07 (m, 2H), 7.04-7.06 (m, 2H), 2.41-2.45 (m, 2H), 1.92 (s, 3H), 1.45-1.55 (m, 1 H), 1.16-1.21 (m, 2H), 0.89 (d, J = 6.6 Hz, 2H). ^{13}C NMR (101 MHz, C_6D_6) δ: 184.9, 184.3, 147.5, 142.7, 133.09, 133.08, 132.74, 132.71, 126.26, 126.21, 37.8, 28.9, 25.2, 22.5, 12.3. HRMS (DART) m/z: [$(M+H)^+$] Calcd for $C_{16}H_{19}O_2$ 243.1380; Found 243.1378.

2.2.6 Preparation of Menaquinone-2

(E)-2-(3,7-dimethylocta-2,6-dien-1-yl)-3-methylnaphthalene-1,4-dione, MK-2 (2.8). Here we report an improvement on our previously reported method[26] for synthesizing menadiol where thorough and extensive stirring while triturating in *n*-pentane leads to practically pure menadiol with very residual menadione (mendione:menadione >30:1 by NMR integration). To a 500 mL round bottom Schlenk flask was added a stir bar, diethyl ether (100 mL), and menadione (5.00 g, 29.0 mmol). Then, 10% aq. $Na_2S_2O_4$ (100 mL, 57.4 mmol) was added and the solution immediately turned dark red. After 30 min. of stirring at ambient temperature, the solution was clear yellow. The aqueous layer was separated and extracted with diethyl ether (3 x 100 mL). The combined organic extracts were washed with sat. $NaHCO_3$ (100 mL), followed by DDI H_2O (100 mL), and lastly with brine (100 mL). The combined organic extracts were dried with anhydrous Na_2SO_4 and then concentrated under reduced pressure at room temperature. The crude powder was triturated thoroughly in *n*-pentane (50 mL), vacuum filtered, and washed with *n*-pentane (100 mL) to yield a pale purple solid (~quantitative). Menadiol formation is indicative by ^{1}H NMR ($CDCl_3$) by the presence of a peak at 6.65 ppm and is consistent with literature.[39]

To a 100 mL round bottom Schlenk flask was added ethyl acetate (16 mL) and 1,4-dioxane (16 mL), which was purged/evacuated with argon repeatedly. Then, crude menadiol (2.2) (2.50 g, 4:1 menadiol:menadione by NMR integration, 11.5 mmol, residual menadione is likely due to not triturating in pentane thoroughly enough) was added followed by geraniol (2.7) (1.92 g, 12.5 mmol) and then drop wise addition of fresh BF_3 etherate (0.8 mL). The solution was allowed to reflux at 70-72 °C for 3 hrs. under argon. The dark orange colored reaction mixture was quenched with ice-H_2O (100 mL) and then extracted with diethyl ether (3 x 100 mL). The yellow organic

extracts were washed with sat. $NaHCO_3$ (100 mL), washed with DDI H_2O (100 mL), washed with brine (100 mL), dried with anhydrous Na_2SO_4, and then concentrated under reduced pressure at room temperature to yield 3.71 g of crude red oil. The crude oil was purified by flash column chromatography (1000 mL of 230-400 mesh SiO_2, 70 mm column, 20:1 *n*-pentane/ethyl acetate). The yellow oil obtained was dried under reduced pressure (~125 mTorr) overnight to yield 0.713 g (2.31 mmol, 20.1% yield) as a yellow solid. The scale of this reaction was ~14 times larger than the previously reported synthesis with the deuterated MK-2 analog.[40] ^{1}H NMR (400 MHz, d_6-DMSO) δ: 7.96-8.01 (m, 2H), 7.80-7.84 (m, 2H), 4.96-5.00 (m,2H), 3.30 (d, 2H, J=4 Hz), 2.10 (s, 3H), 1.92-2.04 (m, 4H), 1.73 (s, 3H), 1.53 (s, 3H), 1.49 (s, 3H). ^{13}C NMR (100 MHz, d_6-DMSO) δ: 184.7, 183.6, 145.3, 142.9, 136.4, 133.9, 131.5, 130.7, 125.9, 125.8, 123.9, 119.4, 26.0, 25.4, 25.4, 17.5, 16.1, 12.4. LRMS (ESI 70 eV, EtOAc) m/z: [$(M+H)^+$] Calcd for $C_{21}H_{25}O_2$ 309.2; found 309.2. HRMS (ESI, OTOF) m/z: [$(M+H)^+$] Calcd for $C_{21}H_{25}O_2$ 309.1849; found 309.1851.

2.2.7 Preparation of Menaquinone-2(II-H_2)

2-(3,7-dimethyloct-2-en-1-yl)-3-methylnaphthalene-1,4-dione, Menaquinone-2(II-H_2) (2.10). To a dry 150 mL round-bottom thick-walled pressure flask was added a dry stir bar, dry heptane (21 mL) and polyene carbonate (21 mL). The solution was bubbled with argon for several min. Then, menadiol (2.2) (1.22 g, 7.00 mmol) was added and stirred until dissolution occurred under argon bubbling. Then, isophytol (2.9) (1.09 g, 7.00 mmol) was added followed by MgF_2-48 (350 mg). The biphasic reaction mixture was bubbled with argon for ~1 min and then sealed tightly with a Teflon screw cap. The sealed reaction mixture was covered in aluminum foil to minimize light exposure and was stirred for 5 h at 100 °C under argon atmosphere. The yellow biphasic suspension was then cooled to ambient temperature. The ^{1}H NMR spectrum of the crude product

confirmed product formation by the presence of a doublet at 3.37 ppm ($CDCl_3$). The layers were separated and the polyene carbonate layer (bottom layer) was extracted with *n*-pentane (3 x 100 mL). The combined yellow organic extracts were washed with DDI H_2O (100 mL), washed with sat. $NaHCO_3$ (100 mL), washed with brine (100 mL), dried over anhydrous Na_2SO_4, and concentrated under reduced pressure at ambient temperature. The crude oil was dried overnight under reduced pressure to yield 1.31 g crude red oil. The crude red oil was purified by flash column chromatography (300 mL of 230-400 mesh SiO_2, 20:1 *n*-pentane/EtOAc, 40 mm column) to yield 0.235 g (0.757 mmol, 10.8% yield) as a yellow/red oil after drying under vacuum (200 mTorr). The C2 isomeric side product was readily separated by flash column chromatography eluting after the C3 desired product. The product was obtained as a mixture of *trans*:*cis* isomers (ratio of *trans*:*cis* = 2.7:1 by NMR integration of alkene peaks) as has similarly been reported for vitamin K_1 analogs[41] and various MK analogs.[27] ^{1}H NMR (400 MHz, C_6D_6) δ: 8.00-8.06 (m, 2H), 7.0-7.06 (m, 2H), 5.12 (t, J = 7.0 Hz, 1H, *trans* isomer), 5.06 (t, J = 7.0 Hz, 1H, *cis* isomer), 3.28 (d, J = 7.7 Hz, 2H, *cis* isomer), 3.26 (d, J = 7.1 Hz, 2H, *trans* isomer), 2.19 (t, J = 7.8 Hz, 2H, *cis* isomer), 1.98 (s, 3H), 1.92 (t, J = 7.5 Hz, 2H, *trans* isomer), 1.72 (s, 3H, *trans* isomer), 1.63 (s, 3H, *cis* isomer), 1.50-1.58 (m, 1H, *cis* isomer),1.40-1.49 (m, 1H, *trans* isomer), 1.40-1.48 (m, 2H, *cis* isomer), 1.31-1.39 (m, 2H, *trans* isomer), 1.21-1.27 (q, 2H, *cis* isomer), 1.06-1.11 (q, 2H, *trans* isomer), 0.93 (d, J = 6.6 Hz, 6H, *cis* isomer), 0.83 (d, J = 6.6 Hz, 6H, *trans* isomer). ^{13}C NMR (101 MHz, C_6D_6) δ: 184.99, 184.97, 184.24, 184.16, 145.97, 145.95, 143.21, 143.18, 137.93, 137.62, 133.09, 133.06, 132.68, 132.66, 126.31, 126.22, 120.31, 119.82, 40.36, 39.34, 38.95, 32.56, 28.35, 28.20, 26.25, 26.15, 26.08, 25.98, 23.54, 22.87, 22.81, 16.32, 12.62, 12.58. HRMS (DART, Q-TOF) calcd for $C_{21}H_{27}O_2$ [$(M+H)^+$] 311.2006, found 311.2018.

A sample for analytical characterization of *trans*-MK-2(II-H_2) was purified by normal phase preparative TLC (see experimental below) on silica gel using (30:1) *n*-pentane/EtOAc as the eluting solvent; R_f *cis*: 0.37, R_f *trans* 0.32; ratio of *trans*:*cis* before separation was 2.7:1 (the ratio was measured from the NMR integration of alkene peaks). Although we isolated the pure *trans* isomer, the *cis* isomer co-eluted with the *trans* isomer and efforts to obtain a sample of the pure *cis* isomer were not successful. The *cis* and the *trans* isomers have different NMR spectra in C_6D_6 for the hydrogens and carbons within the isoprenyl side chain. Data for *trans*-MK-2(II-H_2): ^{1}H NMR (400 MHz, C_6D_6) δ: 8.00-8.07 (m, 2H), 7.00-7.05 (m, 2H), 5.12 (t, J = 7.0 Hz, 1H), 3.26 (d, J = 7.0 Hz, 2H), 1.98 (s, 3H), 1.92 (t, J = 7.5 Hz, 2H), 1.72 (s, 3H), 1.40-1.49 (m, 1H), 1.31-1.39 (m, 2H), 1.06-1.11 (q, 2H), 0.83 (d, J = 6.6 Hz, 6H). ^{13}C NMR (101 MHz, C_6D_6) δ: 184.98, 184.24, 145.97, 143.21, 137.62, 133.09, 133.05, 132.69, 132.66, 126.31, 126.22, 119.82, 40.36, 38.95, 28.20, 26.25, 26.08, 22.81, 16.32, 12.58. HRMS (DART, Q-TOF) calcd for $C_{21}H_{27}O_2$ [$(M+H)^+$] 311.2006, found 311.1991. NMR data for the *cis* isomer (obtained from spectra with both *cis* and *trans* isomers present): ^{1}H NMR (400 MHz, C_6D_6) δ: 8.00-8.06 (m, 2H), 7.00-7.06 (m, 2H), 5.06 (t, J = 7.0 Hz, 1H), 3.28 (d, J = 7.7 Hz, 2H), 2.19 (t, J = 7.8 Hz, 2H), 1.98 (s, 3H), 1.63 (s, 3H), 1.50-1.58 (m, 1H), 1.40-1.48 (m, 2H), 1.21-1.27 (q, 2H), 0.93 (d, J = 6.6 Hz, 6H).

A sample for analytical characterization of *trans*-MK-2(II-H_2) was prepared by using normal phase preparative TLC. First, 8.0 mg of *cis*/*trans*-MK-2(II-H_2) (dissolved in a minimal amount of DCM) was loaded onto a preparative TLC plate *via* capillary tube, then eluted once using 30:1 *n*-pentane/EtOAc and an elution time of 45 min. The TLC plate was briefly air dried and then eluted a second time under the same conditions. The yellow band was illuminated under UV light and while illuminated, the band was divided into a top two-thirds and a bottom one-third. The bottom

one-third was carefully removed with a razor blade, extracted with DCM, filtered through a disposable Pasteur pipette filled with glass wool (pre-rinsed with DCM) and concentrated under reduced pressure at ambient temperature and dried for 4 days at reduced pressure (200 mTorr) to provide 2.5 mg *trans*-MK-2(II-H_2) as a yellow oil (31.3% recovery).

2.2.8 Preparation of Menaquinone-2(I,II-H_4)

Menaquinone-2(I,II-H_4) (2.13) was accessed through compound (2.12) from commercially available compound (2.11).

1-Iodo-3,7-dimethyloctane (2.12). To a dry 250 mL round-bottom Schlenk flask was added a dry stir bar, 3,7-dimethyl-1-octanol (2.11) (8.61 g, 54.4 mmol), dry DCM (100 mL) and then purged/evacuated with argon, repeatedly. The solution was cooled to 0 °C in an ice-H_2O bath. Then, methanesulfonyl chloride (2.16 mL, 3.20 g, 27.9 mmol, 1.2 equiv) was added under argon atmosphere followed by drop-wise addition of dry triethylamine (11.39 mL, 8.26 g, 81.6 mmol, 1.5 equiv) over 5 min at 0° C. The resulting solution was stirred at ambient temperature for 1.5 h under argon. The reaction was quenched with sat. $NaHCO_3$ (100 mL) and then the phases were separated. The aqueous layer was extracted with diethyl ether (3 x 100 mL). The combined organic extracts were washed with sat. $NaHCO_3$ (100 mL), washed with brine (100 mL), dried over anhydrous Na_2SO_4, and then concentrated under reduced pressure at ambient temperature (residual triethylamine can be removed by vacuum pumping for ~1 h) to yield 9.65 g crude yellow oil. The crude mesylate was dissolved in dry and degassed acetone (100 mL, dried over anhydrous K_2CO_3 immediately prior for ~10 min) in a dry 250 mL round-bottom Schlenk flask. Then, NaI (16.50 g, 110.0 mmol, 2.0 equiv) was added and the solution was refluxed for 2 h under argon. The white reaction mixture was diluted with ice-DDI H_2O (100 mL) and diethyl ether (100 mL) and

then the phases were separated. The aqueous layer was extracted with diethyl ether (3 x 100 mL). The combined organic extracts were washed with sat. $NaHCO_3$ (100 mL), washed with brine (100 mL), dried over anhydrous Na_2SO_4, and then concentrated under reduced pressure at ambient temperature to yield 9.83 g crude clear and yellow oil. The crude product was purified by flash column chromatography (800 mL of 230-400 mesh SiO_2, 10:1 *n*-pentane/EtOAc, 70 mm column) to yield 6.91 g (25.8 mmol, 47.4% yield) as a clear and colorless oil after drying under vacuum (150 mTorr). ^{1}H NMR (400 MHz, $CDCl_3$) δ: 3.14-3.28 (m, 2H), 1.83-1.92 (m, 1H), 1.60-1.69 (m, 1H), 1.48-1.58 (m, 2H), 1.21-1.35 (m, 3H), 1.06-1.21 (m, 3H), 0.87 (d, J = 6.6 Hz, 9H). ^{13}C NMR (101 MHz, $CDCl_3$) δ: 41.13, 39.33, 34.04, 28.10, 24.68, 22.85, 22.75, 18.89, 5.58. Anal. Calcd for $C_{10}H_{21}I$: C, 44.79; H, 7.89. Found: C, 44.81; H, 7.72.

2-(3,7-dimethyloctyl)-3-methylnaphthalene-1,4-dione MK-2(I,II-H$_4$) (2.13). To a dry 100 mL round-bottom Schlenk flask was added a dry stir bar and dry and degassed benzene (30 mL) followed by 1-Iodo-3,7-dimethyloctane (2.12) (2.68 g, 10.0 mmol, 1 equiv). To a dry 20 mL vial was added dry and degassed benzene (15 mL) followed by menadione (2.1) (1.72 g, 10.0 mmol) and benzoyl peroxide (2.42 g, 10.0 mmol, 1 equiv) and then sonicated until dissolution occurred under argon. The naphthoquinone-benzoyl peroxide solution was added drop-wise over 2 h 15 min to the refluxing prenyl iodide solution, which was under argon atmosphere during the reaction. After the addition was complete, the solution was refluxed for an additional 1 h. The solution was diluted with sat. $NaHCO_3$ (100 mL) and diethyl ether (100 mL) and then the phases were separated. The aqueous layer was extracted with diethyl ether (3 x 100 mL). The combined organic extracts were washed with sat. $NaHCO_3$ (100 mL), washed with brine (100 mL), dried over anhydrous Na_2SO_4, and then concentrated under reduced pressure at ambient temperature to

yield a crude yellow powder. The crude powder was purified by flash column chromatography (10:1.5 *n*-pentane/EtOAc) to yield 0.539 g (1.73 mmol, 17.3% yield) after drying under vacuum (150 mTorr) as a yellow oil. ^{1}H NMR (400 MHz, $CDCl_3$) δ: 8.05-8.09 (m, 2H), 7.66-7.70 (m, 2H), 2.55-2.68 (m, 2H), 2.18 (s, 3H), 1.12-1.58 (m, 10H), 0.98 (d, J = 6.6 Hz, 3H), 0.87 (d, J = 6.6 Hz, 6H). ^{13}C NMR (101 MHz, $CDCl_3$) δ: 185.51, 184.81, 148.13, 143.02, 133.44, 133.40, 132.40, 132.34, 126.38, 126.32, 39.45, 37.08, 35.90, 33.58, 28.11. HRMS (DART, O-TOF) calcd for $C_{21}H_{29}O_2$ $[(M+H)^+]$ 313.2162, found 313.2158.

2.2.9 Preparation of Menaquinone-3

2-methyl-3-((2E,6E)-3,7,11-trimethyldodeca-2,6,10-trien-1-yl)naphthalene-1,4-dione, MK-3 (2.15). To a dry 100 mL round bottom Schlenk flask were added a dry stir bar, ethyl acetate (16 mL) and 1, 4-dioxane (16 mL), which was then evacuated/purged with argon, repeatedly. Then, crude menadiol (2.2) (2.20 g, 10:1 menadiol:menadione, 11.5 mmol accounting for residual menadione) and *trans*-*trans*-farnesol (2.14) (2.78 g, 12.5 mmol, 1.09 equiv.) was added followed by drop wise addition of distilled BF_3 etherate (0.8 mL). The reaction mixture was refluxed at 75-80 °C for 3 h under argon. The red/orange reaction mixture was quenched with ice DDI-H_2O (100 mL) and extracted with diethyl ether (3 x 100 mL). The combined yellow organic extracts were then washed with saturated $NaHCO_3$ (100 mL), DDI H_2O (100 mL), and saturated NaCl (100 mL), dried over anhydrous Na_2SO_4, and then concentrated at reduced pressure at ambient temperature to yield 4.67 g of crude red oil after drying under vacuum overnight. The crude red oil was purified by flash column chromatography (1000 mL of 230-400 mesh SiO_2, 70 mm column, 20:1 *n*-pentane:EtOAc). The red/yellow oil was dried under reduced pressure (~100 mTorr) for 4

days to yield 0.930 g (2.47 mmol, 21.5% yield) as an orange oil. ^{1}H NMR (400 MHz, $CDCl_3$) δ: 8.05-8.10 (m, 2H), 7.66-7.71 (m, 2H), 5.00-5.06 (m, 3H), 3.37 (d, J = 7.0 Hz, 2H), 2.19 (s, 3H), 1.88-2.09 (m, 8H), 1.79 (s, 3H), 1.65 (s, 3H), 1.56 (s, 6H). ^{13}C NMR (101 MHz, $CDCl_3$) δ: 185.62, 184.68, 146.31, 143.51, 137.69, 135.34, 133.48, 133.42, 132.34, 132.31, 131.40, 126.46, 126.34, 124.45, 124.00, 119.25, 39.85, 39.82, 26.87, 26.61, 26.17, 25.83, 17.79, 16.57, 16.16, 12.83.

2.2.10 Preparation of Menaquinone-3(II-H_2)

Menaquinone-3(II-H_2) (2.21) was accessed through compounds (2.17), (2.18), (2.19), and (2.20) starting from commercially available compound (2.16).

8-iodo-2,6-dimethyloct-2-ene (2.17). To a dry 500 mL round-bottom Schlenk flask was added a dry stir bar, (±)β-citronellol (2.16) (17.00 g, 108.8 mmol), dry dichloromethane (200 mL), and dry trimethylamine (22.8 mL, 16.52 g, 163.2 mmol, 1.5 equiv), which was then purged/evacuated with argon, repeatedly. Then, methanesulfonyl chloride (10.4 mL, 15.33 g, 133.8 mmol, 1.23 equiv) was added drop-wise over 5 min at 0° C under argon. The resulting solution was stirred at ambient temperature for 1.5 h under argon. The reaction was quenched with sat. $NaHCO_3$ (200 mL) and then the phases were separated. The aqueous layer was extracted with diethyl ether (3 x 100 mL). The combined organic extracts were washed with sat. $NaHCO_3$ (100 mL), washed with brine (100 mL), dried over anhydrous Na_2SO_4, and concentrated under reduced pressure at ambient temperature (residual triethylamine can be removed by vacuum pumping for ~1 h) to yield a crude orange oil. The crude mesylate was dissolved in dry acetone (200 mL) in a dry 500 mL round-bottom Schlenk flask. Then, NaI (33.00 g, 220.2 mmol, 2.02 equiv) was added and the solution was refluxed for 3 h under argon. The resulting white reaction mixture was diluted with ice-DDI H_2O (200 mL) and diethyl ether (100 mL) and then the phases were separated. The

aqueous layer was extracted with diethyl ether (3 x 100 mL). The combined organic extracts were washed with sat. $NaHCO_3$ (100 mL), washed with brine (100 mL), dried over anhydrous Na_2SO_4, and then concentrated under reduced pressure at ambient temperature to yield 22.56 g crude yellow oil. The crude yellow oil was purified by flash column chromatography (800 mL of 230-400 mesh SiO_2, 10:1 *n*-pentane/EtOAc, 70 mm column) to yield 19.10 g (71.8 mmol, 66.0% yield) after vacuum pumping (150 mTorr) overnight as a clear and colorless oil. ^{1}H NMR (400 MHz, $CDCl_3$) δ:, 5.09 (t, J = 7.0 Hz, 1H), 3.13-3.28 (m, 2H), 1.92-2.02 (m, 2H), 1.84-1.92 (m, 1H), 1.69 (s, 3H), 1.62-1.67 (m, 1H), 1.61 (s, 3H), 1.51-1.59 (m, 1H), 1.29-1.39 (m, 1H), 1.13-1.22 (m, 1H), 0.89 (d, J = 6.6 Hz, 3H). ^{13}C NMR (101 MHz, $CDCl_3$) δ: 131.63, 124.60, 41.06, 36.47, 33.73, 25.87, 25.47, 18.81, 17.84, 5.32. HRMS (DART, Q-TOF) calcd for $C_{10}H_{20}I$ [$(M+H)^+$] 267.0604, found 267.0613.

6,10-dimethylundec-9-en-2-one (2.18). To a dry 250 mL round-bottom Schlenk flask was added a dry stir bar and dry tert-Butanol (60 mL, dried over activated 3 Å molecular sieves 10 g sieves / 100 mL solvent) followed by t-BuOK (4.92 g, 40.3 mmol, 1.2 equiv) and the solution was refluxed for 30 min under argon to dissolve the t-BuOK and then cooled to 60 °C. Then, ethyl acetoacetate (4.81 g, 36.9 mmol, 1.1 equiv) was added drop-wise and the reaction mixture was stirred for 30 min at 60 °C under argon. Then, 8-iodo-2,6-dimethyloct-2-ene (2.17) (8.94 g, 33.6 mmol) was added drop-wise. The reaction mixture was refluxed for 25 h under argon. The reaction mixture was then vacuum filtered and washed with diethyl ether (50 mL). The filtrate solvent was removed under reduced pressure at ambient temperature. To the crude residue was added 2 N KOH (128 mL) and the reaction mixture was stirred for 3 h at 80 °C under argon. The reaction mixture was cooled to ambient temperature and then the alkaline solution was acidified with acetic acid (20 mL). The acidified solution was extracted with diethyl ether (3 x 100 mL). The

combined organic extracts were washed with sat. $NaHCO_3$ (100 mL), washed with brine (100 mL), dried over anhydrous Na_2SO_4, and then concentrated under reduced pressure at ambient temperature to yield 6.37 g crude clear and colorless oil. The crude oil was purified by vacuum distillation (bp: 108-111 °C / 4 mmHg)[42] to yield 5.82 g (29.6 mmol, 88.1% yield) as a clear and colorless oil after drying under vacuum (150 mTorr). ^{1}H NMR (400 MHz, $CDCl_3$) δ: 5.09 (t, J = 7.2 Hz, 1H), 2.40 (t, J = 7.5 Hz, 2H), 2.13 (s, 3H), 1.87-2.03 (m, 2H), 1.68 (s, 3H), 1.60 (s, 3H), 1.49-1.63 (m, 2H), 1.34-1.43 (m, 1H), 1.23-1.34 (m, 2H), 1.05-1.17 (m, 2H), 0.87 (d, J = 6.5 Hz, 3H). ^{13}C NMR (101 MHz, $CDCl_3$) δ: 209.43, 131.26, 125.00, 44.26, 37.09, 36.58, 32.42, 30.01, 25.87, 25.66, 21.54, 19.58, 17.79. HRMS (DART, O-TOF) calcd for $C_{13}H_{25}O$ [$(M+H)^+$] 197.1905, found 197.1894.

Methyl 3,7,11-trimethyldodeca-2,10-dienoate (2.19). To a 50 mL dry round-bottom Schlenk flask that was purged/evacuated with argon was added NaOMe (4.87 g, 90.2 mmol, 1.36 equiv to triethyl phosphonoacetate) followed by MeOH (12.51 g) and this solution was stirred for 5 min under argon. To this solution was added triethyl phosphonoacetate (14.86 g, 66.3 mmol, 1.54 equiv) drop-wise and allowed to stir at ambient temperature for 30 min under argon. To a dry 250 mL round-bottom Schlenk flask was added dry pentane (80 mL, dried by passing through an activated neutral alumina column under argon immediately prior) followed by 6,10-dimethylundec-9-en-2-one (2.18) (8.45 g, 43.0 mmol). Then, the phosphonium ylide solution was added drop-wise over 10 min under argon. The reaction mixture was stirred for 4 h at ambient temperature under argon. Then, DDI H_2O (100 mL) was added to terminate the reaction. The reaction mixture was extracted with pentane (3 x 100 mL). The combined organic extracts were washed with sat. $NaHCO_3$ (100 mL), washed with DDI H_2O (100 mL), washed with brine (100 mL), dried over anhydrous Na_2SO_4, and then concentrated under reduced pressure at ambient

temperature to yield 9.60 g crude oil after vacuum pumping overnight. The crude oil was purified by flash column chromatography (95:5 *n*-pentane/EtOAc) to yield 6.71 g (26.6 mmol, 61.9% yield) as a clear and colorless oil after drying under vacuum (150 mTorr). ^{1}H NMR (400 MHz, $CDCl_3$) δ: 5.66 (s, 1H), 5.09 (t, J = 7.1 Hz, 1H), 3.68 (s, 3H), 2.15 (s, 3H), 2.11 (t, J = 7.6 Hz, 2H), 1.90-2.00 (m, 2H), 1.68 (s, 3H), 1.60 (s, 3H), 1.37-1.57 (m, 3H), 1.24-1.33 (m, 2H), 1.08-1.17 (m, 2H), 0.87 (d, J = 6.6 Hz, 3H). ^{13}C NMR (101 MHz, $CDCl_3$) δ: 167.44, 160.87, 131.27, 125.01, 115.16, 50.91, 41.37, 37.14, 36.57, 32.38, 25.87, 25.68, 24.97, 19.64, 18.88, 17.78. HRMS (DART, O-TOF) calcd for $C_{15}H_{32}NO$ [$(M+NH_4)^+$] 242.2478, found 242.2484.

3,7,11-trimethyldodeca-2,10-dien-1-ol (2.20). To a dry 250 mL round-bottom Schlenk flask was added a dry stir bar, dry pentane (85 mL, dried over an activated alumina column under argon immediately prior), and methyl 3,7,11-trimethyldodeca-2,10-dienoate (2.19) (8.31 g, 32.9 mmol). The flask was purged/evacuated with argon, repeatedly. Then, Vitride reagent (Red-Al® sodium bis(2-methoxyethoxy)aluminum hydride solution, 32.1 mL of ≥60 wt. % solution in toluene, 98.7 mmol, 3.0 equiv) was added drop-wise *via* a dry glass syringe. The reaction mixture turned milky white upon addition of Vitride reagent. The reaction mixture was stirred for 1.75 h at ambient temperature under argon and was complete by TLC analysis (10:1 *n*-pentane/EtOAc, stain with $KMnO_4$ to visualize) and by ^{1}H NMR analysis. A Fieser method quench was used as follows.[43] The reaction solution was cooled to -78 °C (dry ice/acetone) and then DDI H_2O (20 mL) was slowly added (drop-wise) under argon purge to quench the reaction. The reaction solution was removed from the -78 °C (dry ice/acetone) bath and then 15% aq. NaOH (20 mL) was added slowly followed by DDI H_2O (60 mL) and *n*-pentane (100 mL). The solution was stirred at ambient temperature for 30 min. The solution was filtered through a pad of Celite, washed with *n*-pentane

(200 mL), and then the phases were separated. The aqueous layer was extracted with *n*-pentane (3 x 100 mL). The combined organic extracts were washed with sat. $NaHCO_3$ (100 mL), washed with DDI H_2O (100 mL), washed with brine (100 mL), dried over anhydrous Na_2SO_4, and then concentrated under reduced pressure at ambient temperature. The crude oil was vacuum pumped over night to yield 6.34 g as a crude opaque colorless oil. The crude oil was purified *via* flash column chromatography (1000 mL of 230-400 mesh SiO_2, 5:1 *n*-pentane/EtOAc, 70 mm column) to yield 6.09 g (27.2 mmol, 82.7% yield) as an opaque colorless oil after drying under vacuum (150 mTorr). ^{1}H NMR (400 MHz, $CDCl_3$) δ: 5.41 (t, J = 7.5 Hz, 1H), 5.10 (t, J = 7.1 Hz, 1H), 4.15 (d, J = 7.0 Hz, 2H), 1.90-2.07 (m, 4H), 1.73 (s, 3H, *cis* isomer*), 1.68 (s, 3H), 1.67 (s, 3H, *trans* isomer*), 1.60 (s, 3H), 1.33-1.47 (m, 3H), 1.23-1.32 (m, 2H), 1.06-1.17 (m, 2H), 0.87 (d, J = 6.6 Hz, 3H). ^{13}C NMR (101 MHz, $CDCl_3$) δ 140.40, 131.18, 125.14, 123.28, 59.58, 40.01, 37.23, 36.74, 32.47, 25.87, 25.70, 25.25, 19.72, 17.78, 16.33. HRMS (DART, Q-TOF) calcd for $C_{15}H_{32}NO$ $[(M+NH_4)^+]$ 242.2478, found 242.2473. *Determined from the ^{1}H-^{13}C 2D HSQC and ^{1}H-^{1}H 2D COSY NMR spectra (data not shown).

2-methyl-3-(3,7,11-trimethyldodeca-2,10-dien-1-yl)naphthalene-1,4-dione, MK-3(II-H_2) (2.21). To a 100 mL round-bottom Schlenk flask was added a stir bar, EtOAc (16 mL) and 1,4 dioxane (16 mL) and then the flask was purged/evacuated with argon, repeatedly. Then, menadiol (2.2) (2.50 g, 11.5 mmol, 4:1 menadiol:menadione by NMR integration in $CDCl_3$, menadiol is unstable in $CDCl_3$ and requires trituration in *n*-pentane for purification) and 3,7,11-trimethyldodeca-2,10-dien-1-ol (2.20) (2.81 g, 12.5 mmol, 1.09 equiv) were added followed by drop-wise addition of distilled BF_3 etherate (0.8 mL, fresh bottle) under argon. The reaction mixture refluxed at 70 °C for 3 h under argon. The reaction mixture turned dark orange and was

quenched with ice-DDI H_2O (100 mL) and then extracted with diethyl ether (3 x 100 mL). The combined yellow organic extracts were washed with sat. $NaHCO_3$ (100 mL), washed with DDI H_2O (100 mL), washed with brine (100 mL), dried with anhydrous Na_2SO_4, and then concentrated under reduced pressure at ambient temperature to yield 5.06 g crude red solid. The crude solid was purified by flash column chromatography (1000 mL of 230-400 mesh SiO_2, 20:1 *n*-pentane/EtOAc) to yield 1.28 g (yield at this stage = 29.4%, 3.38 mmol) as a red oil but further purification was needed as evidenced by ^{1}H NMR analysis. The C2 isomeric side product was readily separated by flash column chromatography eluting after the C3 desired product. The red oil was subjected to a second column chromatography purification using the same conditions as the first purification and then the material was dried under reduced pressure (150 mTorr) overnight to yield 0.501 g (1.32 mmol, 11.5 % yield) as a yellow oil. Similar to vitamin K_1 analogs,[41] various MK analogs[27] and MK-2(II-H_2) (2.10), the product was obtained as a mixture of *trans*:*cis* isomers (ratio of *trans*:*cis* = 2.7:1 by NMR integration of alkene peaks). ^{1}H NMR (400 MHz, C_6D_6) δ: 8.00-8.07 (m, 2H), 7.01-7.06 (m, 2H), 5.27 (t, J = 7.1 Hz, 1H, *cis* isomer), 5.19 (t, J = 7.1 Hz, 1H, *trans* isomer), 5.13 (t, J = 7.0 Hz, 1H, *trans* isomer), 5.07 (t, J = 7.0 Hz, 1H, *cis* isomer), 3.29 (d, J = 7.2 Hz, 2H, *cis* isomer), 3.26 (d, J = 7.1 Hz, 2H, *trans* isomer), 2.21 (t, J = 7.5 Hz, 2H, *cis* isomer), 1.98 (s, 3H), 1.94 (t, J = 7.5 Hz, 2H, *trans* isomer), 1.73 (s, 3H, *trans* isomer), 1.71 (s, 3H, *cis* isomer), 1.67 (s, 3H, *trans* isomer), 1.64 (s, 3H, *cis* isomer), 1.61 (s, 3H, *cis* isomer), 1.56 (s, 3H, *trans* isomer), 1.01-1.51 (m, 9H), 0.95 (d, J = 6.6 Hz, 3H, *cis* isomer), 0.86 (d, J = 6.5 Hz, 3H, *trans* isomer). ^{13}C NMR (101 MHz, C_6D_6) δ: 184.99, 184.96, 184.23, 184.15, 145.96, 143.20, 143.18, 137.93, 137.59, 133.08, 133.05, 132.68, 132.66, 130.97, 130.89, 126.31, 126.22, 125.58, 125.51, 120.32, 119.87, 40.40, 37.60, 37.58, 37.39, 36.92, 32.80, 32.66, 32.60, 26.27, 26.12, 26.06, 25.99, 25.95,

25.91, 25.80, 25.67, 23.55, 19.86, 19.81, 17.79, 17.73, 16.33, 12.63, 12.59. HRMS (DART, Q-TOF) calcd for $C_{26}H_{35}O_2$ [$(M+H)^+$] 379.2632, found 379.2643.

A sample for analytical characterization of *trans*-MK-3(II-H_2) was prepared similarly as described (see experimental below) for *trans*-MK-2(II-H_2) above by normal phase preparative TLC on silica gel using (30:1) *n*-pentane/EtOAc as the eluting solvent; R_f *cis*: 0.35, R_f *trans* 0.30; ratio of *trans:cis* before separation was 2.7:1 (ratio by NMR integration of alkene peaks). Importantly, the bottom one-half of the band was isolated, instead of isolating the bottom one-third of the band as was done to obtain *trans*-MK-2(II-H_2). This purification provided 3.7 mg *trans*-MK-3(II-H_2) as a yellow oil (43.5% recovery) from the initial 8.5 mg *cis*/*trans* mixture loaded onto the TLC plate after drying under vacuum (200 mTorr) for 4 days. Similar to MK-2(II-H_2) (2.10), we isolated the pure *trans* isomer; however, the *cis* isomer co-eluted with the *trans* isomer and efforts to obtain a sample of the pure *cis* isomer were not successful. Similar to MK-2(II-H_2) (2.10), the *cis* and *trans* isomers of MK-3(II-H_2) have different NMR spectra in C_6D_6 for the hydrogens and carbons that belong to the isoprenyl side chain. Data for *trans*-MK-3(II-H_2): ^{1}H NMR (400 MHz, C_6D_6) δ: 8.00-8.07 (m, 2H), 7.00-7.06 (m, 2H), 5.19 (t, J = 7.1 Hz, 1H), 5.13 (t, J = 7.0 Hz, 1H), 3.27 (d, J = 7.1 Hz, 2H), 1.98 (s, 3H), 1.94 (t, J = 7.5 Hz, 2H), 1.73 (s, 3H), 1.67 (s, 3H), 1.56 (s, 3H), 1.01-1.47 (m, 9H), 0.86 (d, J = 6.5 Hz, 3H). ^{13}C NMR (101 MHz, C_6D_6) δ: 184.97, 184.24, 145.96, 143.21, 137.59, 133.08, 133.05, 132.69, 132.67, 130.89, 126.31, 126.22, 125.51, 119.87, 40.40, 37.58, 36.91, 32.60, 26.27, 26.06, 25.91, 25.67, 19.81, 17.73, 16.33, 12.59. HRMS (DART, Q-TOF) calcd for $C_{26}H_{35}O_2$ [$(M+H)^+$] 379.2632, found 379.2639. NMR data for the *cis* isomer (obtained from spectra with both *cis* and *trans* isomers present): ^{1}H NMR (400 MHz, C_6D_6) δ: 8.00-8.06 (m, 2H), 7.01-7.06 (m, 2H), 5.27 (t, J = 7.1 Hz, 1H), 5.07 (t, J = 7.0 Hz, 1H), 3.29 (d, J = 7.2 Hz, 2H), 2.21 (t, J

= 7.5 Hz, 2H), 1.98 (s, 3H), 1.71 (s, 3H), 1.64 (s, 3H), 1.61 (s, 3H), 1.01-1.51 (m, 9H), 0.95 (d, J = 6.6 Hz, 3H).

2.2.11 Preparation of Menaquinone-3(I,II,III-H_6)

Menaquinone-3(I,II,III-H_6) (2.25) was accessed through compounds (2.23) and (2.24) starting from commercially available compound (2.22).

3,7,11-trimethyldodecan-1-ol (2.23). To a dry 500 mL round-bottom Schlenk flask was added a dry stir bar, dry methanol (200 mL), ammonium formate (29.15 g, 462.3 mmol, 9.28 equiv), and farnesol (2.22) (11.08 g, 49.83 mmol) followed by careful addition by funnel of palladium catalyst on carbon (2.14 g, 20.1 mmol, 0.4 equiv). The reaction mixture was stirred at ambient temperature for 5 days under positive pressure from an argon balloon and ^{1}H NMR analysis showed only residual alkene present. The reaction mixture was filtered through a pad of Celite and washed with MeOH (600 mL). The MeOH was remove under reduced pressure at ambient temperature. The crude product was then filtered through a silica plug (4:1 *n*-pentane/EtOAc, 500 mL eluent) and washed with EtOAc (300 mL). The organic filtrate was concentrated under reduced pressure at ambient temperature to yield a crude clear and colorless oil. The crude oil was suspended in diethyl ether (200 mL), washed with sat. $NaHCO_3$ (200 mL), washed with brine (100 mL), dried over anhydrous Na_2SO_4, and then concentrated under reduced pressure at ambient temperature to yield a crude clear and colorless oil. The crude oil was purified by flash column chromatography (1000 mL of 230-400 mesh SiO_2, 4:1 *n*-pentane/EtOAc, 70 mm column) to yield 9.99 g (43.7 mmol, 87.8% yield) as a clear and colorless oil after drying under vacuum (150 mTorr). ^{1}H NMR (400 MHz, $CDCl_3$) δ: 3.63-3.73 (m, 2H), 1.49-1.63 (m, 3H), 1.01-1.42 (m, 14H), 0.89 (d, J = 6.5 Hz, 3H), 0.86 (d, J = 6.6 Hz, 6H), 0.84 (d, J = 6.8 Hz, 3H). ^{13}C NMR (101 MHz,

$CDCl_3$) δ: 61.43, 40.21, 40.12, 39.51, 37.64, 37.60, 37.51, 37.47, 37.41, 32.94, 29.67, 29.65, 28.13, 24.97, 24.94, 24.52, 22.87, 22.78, 19.89, 19.84, 19.82, 19.77. HRMS (DART, Q-TOF) calcd for $C_{15}H_{36}NO$ [$(M+NH_4)^+$] 246.2791, found 246.2796.

1-Iodo-3,7,11-trimethyldodecane (2.24). To a dry 250 mL round-bottom Schlenk flask was added a dry stir bar, 3,7,11-trimethyldodecan-1-ol (2.23) (9.41 g, 41.2 mmol) and dry DCM (125 mL). The flask was purged/evacuated with argon, repeatedly. The solution was cooled to 0 °C in an ice-H_2O bath. Then, dry triethylamine (8.61 mL, 6.25 g, 61.8 mmol, 1.5 equiv) was added to the flask followed by drop-wise addition of methanesulfonyl chloride (3.82 mL, 5.66 grams, 49.4 mmol, 1.2 equiv) at 0 °C over five min while stirring under argon. The reaction mixture was stirred at ambient temperature for 40 min under argon. The off-white reaction mixture was quenched with sat. $NaHCO_3$ (100 mL) and then the phases were separated. The aqueous layer was extracted with diethyl ether (3 x 100 mL). The combined organic extracts were washed with sat. $NaHCO_3$ (100 mL), washed with brine (100 mL), dried over anhydrous $MgSO_4$, vacuum filtered, and then concentrated under reduced pressure at ambient temperature (residual triethylamine can be removed by vacuum pumping for ~1 h) to yield 12.98 g crude clear and light-yellow oil. To another dry 250 mL round-bottom Schlenk flask was added dry and degassed acetone (100 mL, dried over anhydrous K_2CO_3 for ~10 min immediately prior) and the crude mesylate followed by NaI (15.44 g, 103.0 mmol, 2.5 equiv). The reaction mixture turned bright yellow upon addition of NaI and was refluxed for 1 h and 40 min under argon. The yellow reaction mixture was diluted with diethyl ether (100 mL) and DDI H_2O (100 mL) and then the phases were separated. The aqueous layer was extracted with diethyl ether (3 x 100 mL). The combined organic extracts were washed with sat. $NaHCO_3$ (100 mL), washed with brine (100 mL), dried over anhydrous $MgSO_4$, vacuum

filtered, and then concentrated under reduced pressure at ambient temperature to yield a crude yellow murky oil. To remove the salt impurities, the crude oil was suspended in *n*-pentane (100 mL), washed with DDI H_2O (100 mL) and then the phases were separated. The aqueous layer was extracted with *n*-pentane (3 x 100 mL). The combined organic extracts were washed with sat. $NaHCO_3$ (100 mL), washed with brine (100 mL), dried over anhydrous $MgSO_4$, vacuum filtered, and then concentrated under reduced pressure at ambient temperature to yield 13.19 g crude clear and light-yellow oil. The crude oil was purified by flash column chromatography (1000 mL of 230-400 mesh SiO_2, 100% *n*-pentane, R_f = 0.71, 70 mm column) to yield 6.52 g (19.3 mmol, 46.8% yield) after drying under vacuum (200 mTorr) as a clear and colorless oil. ^{1}H NMR (400 MHz, $CDCl_3$) δ: 3.14-3.28 (m, 2H), 1.83-1.92 (m, 1H), 1.60-1.69 (m, 1H), 1.47-1.57 (m, 2H), 1.01-1.41 (m, 13H), 0.84-0.88 (m, 12H).^{13}C NMR (101 MHz, $CDCl_3$) δ: 41.19, 41.12, 39.52, 37.52, 37.46, 37.42, 37.40, 36.76, 36.70, 34.07, 34.04, 32.93, 32.91, 28.15, 24.98, 24.96, 24.38, 24.37, 22.89, 22.79, 19.90, 19.83, 18.95, 18.89, 5.55. Anal. Calcd for $C_{15}H_{31}I$: C, 53.25; H, 9.24. Found: C, 53.78; H, 9.38.

2-methyl-3-(3,7,11-trimethyldodecyl)naphthalene-1,4-dione, MK-3(I,II,III,H$_6$) (2.25). To a dry 100 mL round-bottom Schlenk flask was added under argon, a dry stir bar, dry and degassed benzene (30 mL) and 1-iodo-3,7,11-trimethyldodecane (2.24) (3.38 g, 10.0 mmol, 1.00 equiv). To a dry 20 mL vial was added benzene (15 mL), which was degassed *via* argon needle purge, followed by menadione (2.1) (1.72 g, 10.0 mmol, 1.00 equiv) and benzoyl peroxide (2.42 g, 10.0 mmol, 1.00 equiv) and then sonicated until dissolution occurred under argon. The naphthoquinone-benzoyl peroxide solution was added drop-wise to the refluxing prenyl iodide solution over 2 h and 15 min while the reaction mixture was refluxing under argon. The solution

was then refluxed for an additional 1 h. The reaction mixture was diluted with sat. $NaHCO_3$ (100 mL) and DDI H_2O (100 mL) and then the phases were separated. The aqueous layer was extracted with diethyl ether (3 x 100 mL). The combined yellow organic extracts were washed with sat. $NaHCO_3$ (100 mL), washed with brine (100 mL), dried over anhydrous $MgSO_4$, and concentrated under reduced pressure at ambient temperature to yield 6.63 g crude yellow powder. The crude product was purified by flash column chromatography (1000 mL of 230-400 mesh SiO_2, 10:1 *n*-pentane/EtOAc, 70 mm column) to yield 0.555 g (1.45 mmol, 14.5% yield) after drying under vacuum (200 mTorr) as a yellow oil. ^{1}H NMR (400 MHz, $CDCl_3$) δ: 8.05-8.09 (m, 2H), 7.66-7.70 (m, 2H), 2.55-2.68 (m, 2H), 2.18 (s, 3H), 1.02-1.57 (m, 17H), 0.98 (d, J = 6.6 Hz, 3H), 0.84-0.87 (m, 9H).^{13}C NMR (101 MHz, $CDCl_3$) δ: 185.53, 184.82, 148.14, 143.03, 133.45, 133.42, 132.41, 132.34, 126.40, 126.33, 39.52, 37.55, 37.52, 37.44, 37.20, 37.17, 35.95, 35.86, 33.59, 32.94, 28.14, 24.98, 24.95, 24.57, 22.88, 22.79, 19.90, 19.85, 19.69, 19.62, 12.65. HRMS (DART, Q-TOF) calcd for $C_{26}H_{39}O_2$ [$(M+H)^+$] 383.2945, found 383.2935.

2.3 Results and Discussion

2.3.1 Synthesis and Characterization of Menaquinone-1

We have previously synthesized MK-1[38] and it has been synthesized by other reported routes;[27, 44-47] however, here we present a scaled-up version and NMR spectral characterization in chloroform-d (Scheme 2.3.1). Menadiol (2.2**)** was synthesized as previously described from menadione (2.1).[26, 40, 48] To introduce the isoprenyl side chain, menadiol (2.2) was treated with 3-methyl-2-buten-1-ol (2.3) in the presence of the Lewis acid catalyst, boron trifluoride.[26, 40] MK-1

(2.4) was obtained as a red oil in a 23% yield (Scheme 2.3.1). See Supporting Information for NMR spectra.

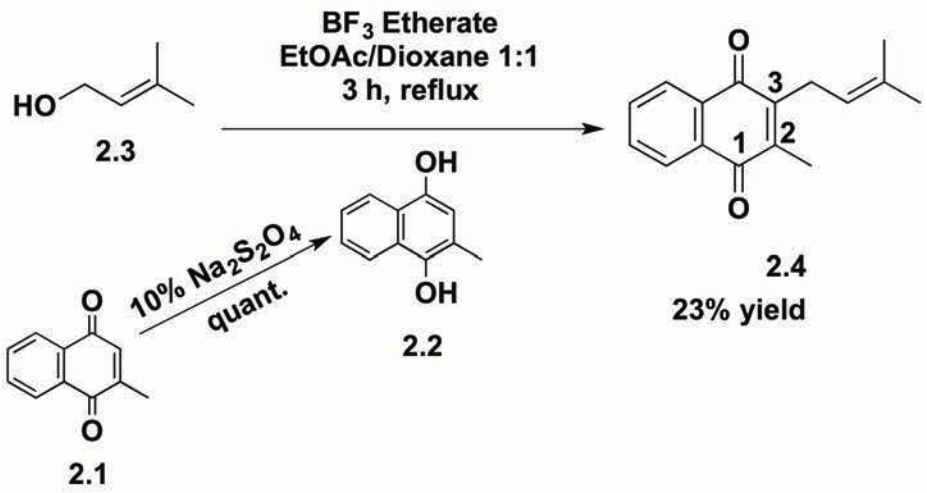

Scheme 2.3.1. Synthetic scheme for the allylic alcohol coupling reaction to obtain MK-1 (2.4).[26, 40]

2.3.2 Synthesis and Characterization of Menaquinone-1(H_2)

Although the route to obtain MK-1(H_2) has been reported in literature[49] (Scheme 2.3.2), the product was not isolated in pure form or characterized by NMR spectroscopy. We modified and optimized the reported route to increase the yield and scaled the reaction up to a preparatory scale using similar methodology we recently reported.[1] MK-1(H_2) (2.6) was synthesized by a one-step radical alkylation reaction where menadione (2.1) and 1-iodo-3,7-dimethylbutane (2.5) were coupled using benzoyl peroxide as the radical initiator.[1, 49] MK-1(H_2) (2.6) was obtained as a yellow powder in a 20% yield (Scheme 2.3.2). The menadione-benzoyl peroxide solution was added drop wise over ~2 h to the refluxing prenyl iodide solution to keep the stationary menadione (2.1) concentration sufficiently low in the reaction to ensure good selectivity of alkylation, favoring alkylation at C3 over C2 (Scheme 2.3.2).[1, 49] See Supporting Information for NMR spectra.

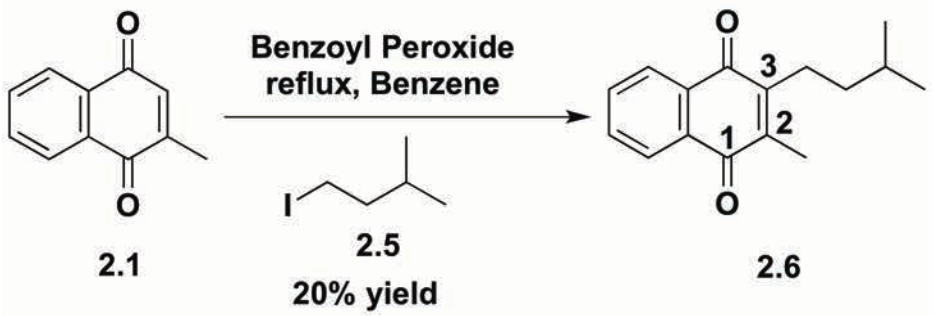

Scheme 2.3.2. Synthetic scheme for the radical alkylation of menadione (2.1) and 1-iodo-3-methylbutane (2.5) to form MK-1(H_2) (2.6).[1, 49]

2.3.3 Synthesis and Characterization of Menaquinone-2

MK-2 was synthesized using an adapted procedure from literature (Scheme 2.3.3).[40, 48] First, menadione (2.1) was reduced to menadiol (2.2) using aqueous sodium dithionite.[26, 40, 48] Geraniol (2.7) was coupled to menadiol (2.2) using the Lewis acid catalyst, boron trifluoride. This preparation produced MK-2 (2.8) in a yield of 20%, which is lower than the reported MK-2 preparation with the deuterated analog in literature.[40] The lower yield appears to be due to extensive alkylation at the C2 position instead of the desired C3 position; however, this side product is readily separated using column chromatography. Highly pure material yields a yellow solid upon crystallization at -20 °C and retains this state when warmed to room temperature, while material with impurities does not crystallize and remains a red oil. See Supporting Information for NMR spectra.

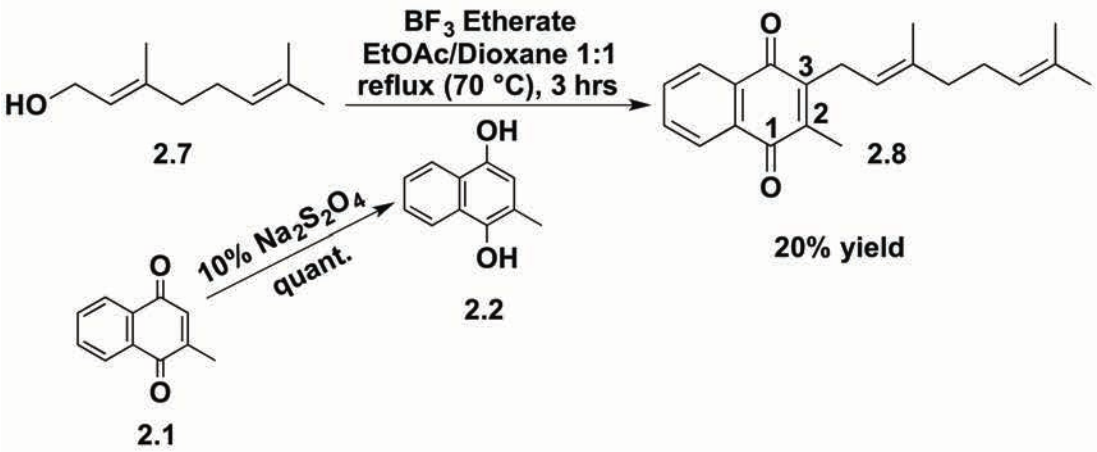

Scheme 2.3.3. Synthetic route to prepare MK-2 (2.8), from menadiol (2.2) and geraniol (2.7) using Lewis acid catalyst conditions.[40]

2.3.4 Synthesis and Characterization of Menaquinone-2(II-H_2)

The partially saturated MK analog, MK-2(II-H_2) (2.10) was synthesized in a single step using a Friedel-Crafts coupling between menadiol (2.2) and isophytol (2.9) (Scheme 2.3.4). The precursor menadiol (2.2) was synthesized as previously described from menadione.[26, 40] The partly hydroxylated heterogeneous Lewis–Brønsted acid catalyst, MgF_2-48, was synthesized as previously described.[50-52] We chose MgF_2-48 over other catalysts because it was readily prepared from inexpensive methanol and Mg^0 powder as well as commonly available 48% aqueous Hydrofluoric acid.[50-52] Furthermore, the partly hydroxylated MgF_2 catalyst was recently used with a biphasic *n*-heptane:polyene carbonate solvent system to synthesize vitamin K_1 and K_1-chromanol.[51] Therefore, we thought this catalyst would be an excellent choice to synthesize the partially saturated MK-2(II-H_2), which has an analogous (but truncated) structure of vitamin K_1 (or MK-4(II,III,IV-H_6)).

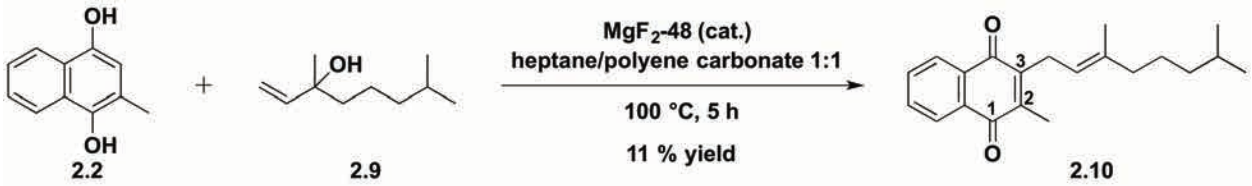

Scheme 2.3.4. Synthetic scheme for the coupling reaction using a MgF_2-48 catalyst to obtain MK-2(II-H_2) (2.10) from menadiol (2.2) and isophytol (2.9).[51]

The Friedel-Crafts alkylation of (2.2) and (2.9) (Scheme 2.3.4) followed by *in situ* oxidation of dihydro-MK-2(II-H_2) formed the desired product (2.10) in an 11% yield. The low yield may be attributed to the formation of the undesired C2 isomeric side product (see Scheme 2.3.4), which was readily separated using column chromatography. The inherent instability of menadiol, which is prone to auto-oxidation even when purified immediately before use may also contribute to the low yield. MK-2(II-H_2) (2.10) was obtained a yellow/red oil. The reaction was carried out in the dark and the product was exposed minimally to light as previous studies have shown that interconversion to undesirable geometric isomers can occur through photo-oxidation if exposed to light; however, we did not observe isomerization or decomposition due to light exposure.[16, 53-54]

We considered other possible catalysts to carry out the transformation shown in Scheme 2.3.4. For instance, we also explored a commercially available strong Brønsted acid catalyst (Nafion perfluorinated powdered resin and Nafion perfluorinated ion-exchange resin in 10 wt. % dispersion in water); however, the yields were significantly lower with an increased formation of the C2 prenylated isomeric side-product (see Scheme 2.3.4). Furthermore, we were concerned about the Nafion catalyst (containing super acidic sites) dehydrating isophytol to form undesirable phytadienes,[51] which presumably contributes to it being a less desirable catalyst for this purpose.

An interesting feature of MKs is the possibility of geometric isomer formation (Figure 2.3.1A-B). The biologically active *trans* isomer of vitamin K_1 is the natural biological form of vitamin K_1.[27] Evidence also demonstrates that biological MKs have an all-*trans* configuration of the double bonds within the isoprenyl side chain.[27] The geometric isomers of vitamin K_1, MK-7 and MK-9(II-H_2) (isolated from *Mycobacterium phlei*, Figure 2.1.1A) have been successfully separated; therefore, efforts to isolate the *trans* isomer of MK-2(II-H_2) from its *cis* isomer byproduct (Figure 2.3.1B) were carried out.[16, 24, 27] MK-2(II-H_2) (2.10) was initially isolated as a 2.7:1 mixture of *trans*/*cis* isomers (by NMR integration of alkene peaks in benzene-d_6) after column chromatography. The *trans* isomer of MK-2(II-H_2) (2.10) can be isolated using preparative thin layer chromatography (TLC), similar to reports for vitamin K_1 analogs[41] and MK analogs.[16]

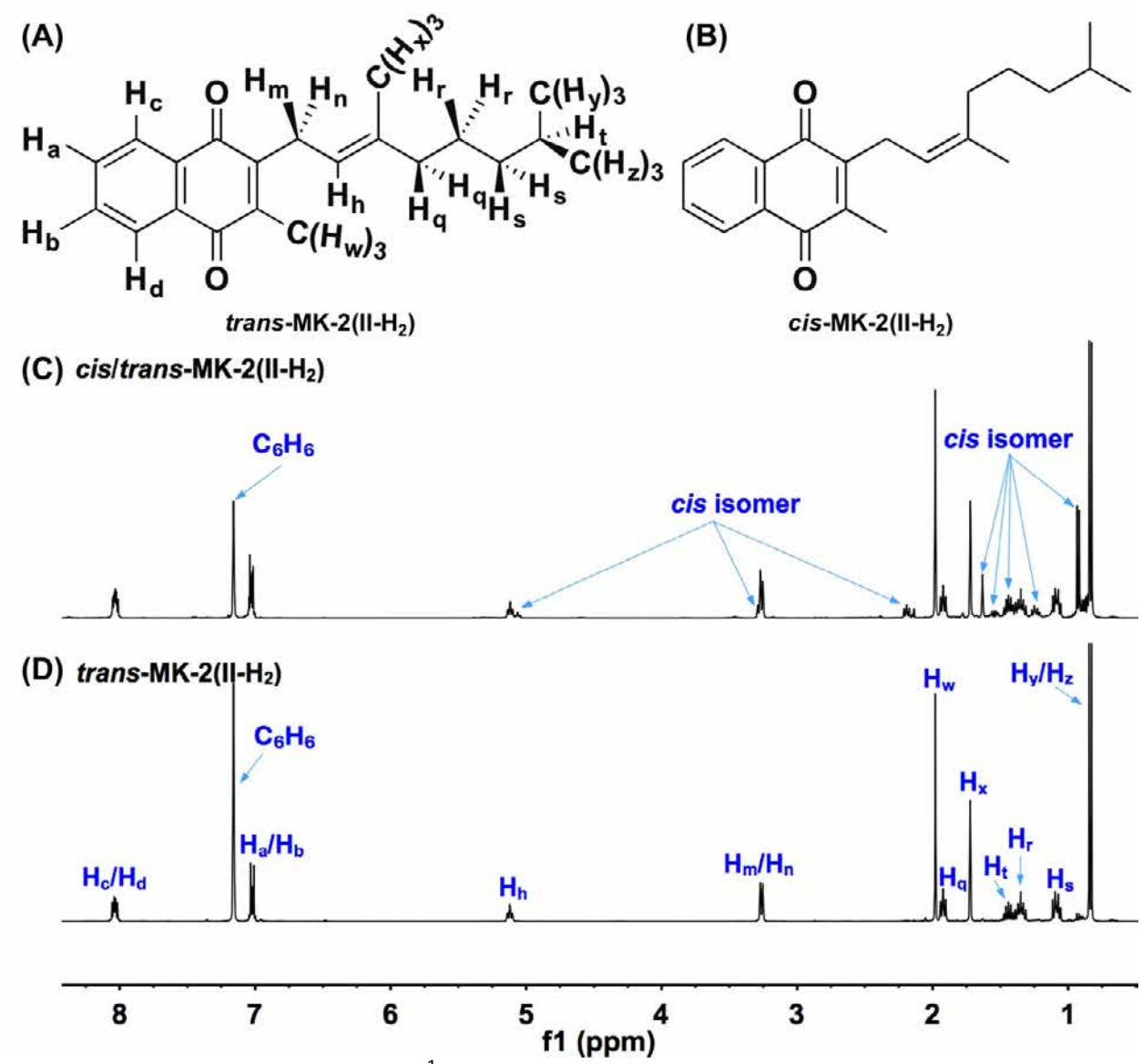

Figure 2.3.1. Comparison of the 1D ^{1}H NMR (400 MHz) spectra for the mixture of *cis*/*trans*-MK-2(II-H_2) and *trans*-MK-2(II-H_2) in C_6D_6 at 25 °C. (A) Structure of *trans*-MK-2(II-H_2) with hydrogen labeling scheme key, (B) Structure of *cis*-MK-2(II-H_2), (C) 1D ^{1}H NMR spectrum of the *cis*/*trans* mixture of MK-2(II-H_2) in C_6D_6 and (D) 1D ^{1}H NMR spectrum of *trans*-MK-2(II-H_2) in C_6D_6.

The successful separation of the *trans* isomer of (2.10) by preparative TLC allowed for characterization of a single pure geometric isomer of MK-2(II-H_2), Figure 2.3.1. The structural assignment of *trans*-MK-2(II-H_2) (Figure 2.3.1) was elucidated using 2D NMR spectroscopic methods (^{1}H-^{1}H COSY, and ^{1}H-^{13}C HSQC, see Supporting Information for spectra, Figures A2.7-

10.1 and A2.13-14.1). Spectra obtained in benzene-d_6 (C_6D_6) results in less overlap of the NMR signals for the *cis*/*trans* isomer mixture (Figure 2.3.1C-D), compared to $CDCl_3$ where some of the geometric isomer peaks overlap (e.g., *cis*/*trans* alkene hydrogens coalesce in $CDCl_3$) and the formation of isomers is not obvious. Therefore, the use of C_6D_6 as a diagnostic NMR solvent for the evaluation of *cis*/*trans* mixtures for MK analogs was critical and is in line with a recently reported NMR analysis of *cis*/*trans* isomer mixtures of MK-7[24] (see Supporting Information for spectra in $CDCl_3$ vs. C_6D_6, Figure A2.50).

2.3.5 Synthesis and Characterization of Menaquinone-2(I,II-H_4)

The fully saturated isoprenyl MK analog, MK-2(I,II-H_4) (2.13), was synthesized in three steps from commercially available 3,7-dimethyloctan-1-ol (2.11) (Scheme 2.3.5). The first step converted the aliphatic alcohol (2.11) to the mesylate, which was then subjected to an S_N2 reaction using NaI to yield 1-Iodo-3,7-dimethyloctane (2.12) in 47% yield over two steps.[40] The alkyl iodide (2.12) was then coupled to menadione (2.1) *via* a radical alkylation using benzoyl peroxide[49] as a radical initiator to yield MK-2(I,II-H_4) 7 in 17% yield. The yield for the coupling reaction is close in the range with that reported in literature for other coupling reactions for the synthesis of MK analogs.[26-27, 40] The unreacted alkyl iodide (2.12) can be recovered during column chromatography. In an effort to ensure selectivity of prenylation at C3 vs C2 (Scheme 2.3.5), the slow addition of the napthoquinone (2.1) during the reaction was carried out so that the naphthoquinone stationary concentration in the reaction mixture is low compared to the prenyl iodide concentration.[49] MK-2(I,II-H_4) (2.13) was obtained as a yellow oil. This is the first report of the synthesis and characteriation of MK-2(I,II-H_4) (2.13) (see Supporting Information for 2D NMR spectra, Figures A2.19-20.1), the fully saturated analog of MK-2 (2.8).

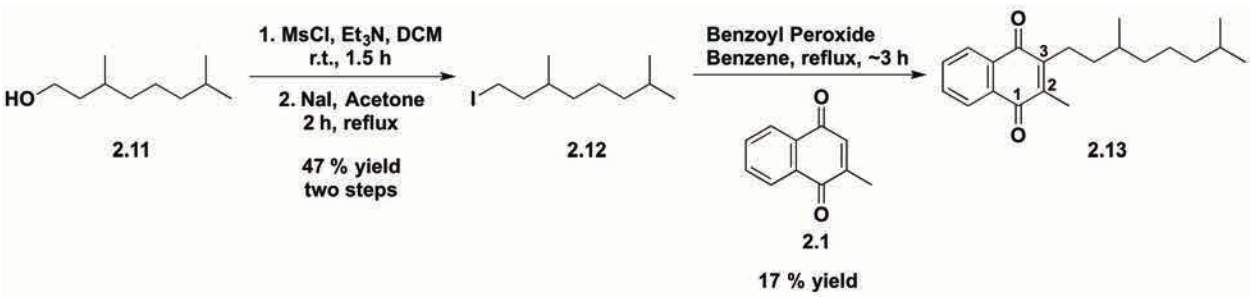

Scheme 2.3.5 Synthetic scheme for the 3-step synthesis to obtain MK-2(I,II-H_4) (2.13). The first step forms the mesylate from (2.12). The second step forms the aliphatic iodide (2.12) *via* a S_N2 reaction. The final step couples menadione (2.1) and the aliphatic iodide (2.12) using a radical alkylation initiated by benzoyl peroxide.

2.3.6 Synthesis and Characterization of Menaquinone-3

MK-3 (2.15) was synthesized using an adapted procedure from literature (Scheme 2.3.3).[40, 48] First, menadione (2.1) was reduced to menadiol (2.2) using aqueous sodium dithionite as previously described in this dissertation and elsewhere.[26, 40, 48] *Trans,trans*-Farnesol (2.14) was coupled to menadiol (2.2) using the Lewis acid catalyst, boron trifluoride. This preparation produced MK-3 (2.15) as a red oil in a yield of 22%, which is lower than the reported MK-3 preparation with the deuterated analog in literature.[40] The lower yield appears to be due to extensive alkylation at the C2 position instead of the desired C3 position (see Scheme 2.3.6); however, this side product is readily separated using column chromatography. Importantly, we tried this reaction using commercially available farnesol (purity of 95%), which would always give rise to erroneous NMR peaks and off integrations in the aliphatic region. We suspected this might be due to *cis*-farnesol impurity present in the commercially available material. Therefore, we sought out and were able to purchase *trans,trans*-farnesol, which we used in the synthesis and yielded a clean NMR spectrum with accurate integrations. See Supporting Information for 1D and 2D NMR spectra, Figures A2.21-24.1.

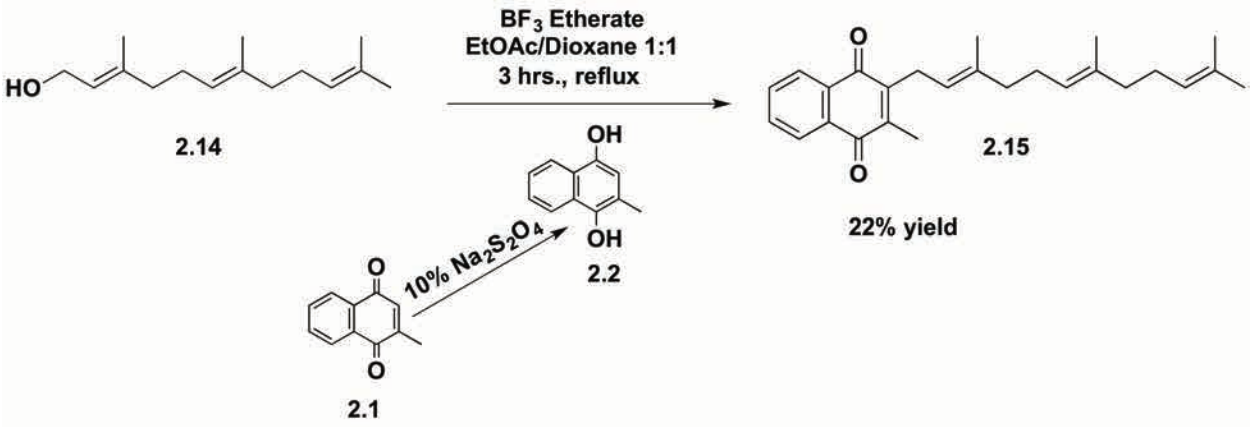

Scheme 2.3.6 Synthetic route to prepare MK-3 (2.15) from menadiol (2.2) and *trans,trans*-farnesol (2.15) using Lewis acid catalyst conditions.[1, 26, 40]

2.3.7 Synthesis and Characterization of Menaquinone-3(II-H_2)

The partially saturated isoprenyl MK analog, MK-3(II-H_2) (2.21), was synthesized in seven steps from commercially available β-citronellol (2.16) (Scheme 2.3.7) *via* a modified adaptation of a combination of a reported synthesis of menaquinone-4(II-H_2)[40] and a less recent 1965 synthesis of MK-3(II-H_2).[33] First, the hydroxyl group of β-citronellol (2.16) was converted into the iodide (2.17) through the methane sulfonate in 66% yield over two steps.[40] The introduction of a carbonyl group to produce citronellylacetone (2.18) was accomplished under basic conditions in 88% yield over two steps.[42] This was followed by a Horner–Wadsworth–Emmons (HWE) reaction to give the methyl ester (2.19) in 62% yield.[40] Reduction of (2.19) with Vitride reagent produced 6,7-dihydrofarnesol (2.20) in 83% yield.[40, 43] Finally, MK-3(II-H_2) (2.21) was obtained from the BF_3 catalyzed coupling between the partially saturated allylic alcohol (2.20) and menadiol (2.2) (prepared from menadione)[26, 40] in 12% yield.[40] The low yield may be attributed to the formation of the undesired C2 isomeric side product (see Scheme 2.3.7), which was readily separated using column chromatography and the requirement of multiple column chromatography purifications

due to purity concerns. MK-3(II-H_2) (2.21) was obtained as a yellow oil. Scheme 2.3.7 Synthetic scheme for the 7-step synthesis to obtain MK-3(II-H_2) (2.21) from β-citronellol (2.16).

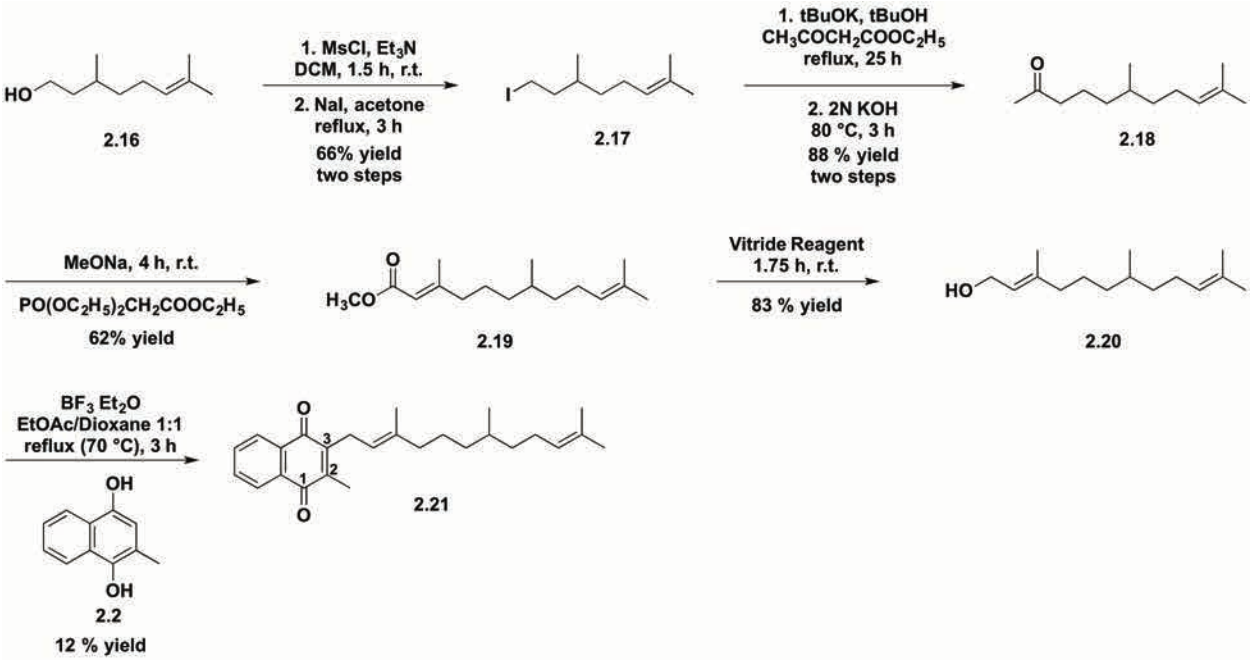

Scheme 2.3.7. Synthetic scheme for the 7-step synthesis to obtain MK-3(II-H_2) (2.21) from β-citronellol (2.16).[33, 40]

Similar to MK-2(II-H_2) (2.10), MK-3(II-H_2) (2.21) was initially isolated as a 2.7:1 mixture (by NMR integration of alkene peaks in C_6D_6) of *trans*/*cis* isomers. However, the *trans* isomer (Figure 2.3.2A) can be isolated from the *cis* isomer byproduct (Figure 2.3.2B) using preparative TLC, similar to a report on *cis*/*trans* vitamin K_1 analogs.[41] MK analogs can be very sensitive, for example, during purification we observed degradation of *trans*-MK-3(II-H_2) (Figure 2.3.2A) within a solution of dichloromethane (DCM) that was not stabilized with amylene. This was evidenced by a decreased integration value for the alkene at 5.19 ppm and the appearance of two extra peaks ~1.3 ppm and a peak at 1.12 ppm in C_6D_6. Amylene is a radical scavenger and it is likely that the alkene is undergoing a radical reaction with chloride radicals present in the unstabilized

DCM. Similar to MK-2(II-H_2) (2.10), the use of benzene-d_6 as a diagnostic NMR solvent for the evaluation of *cis*/*trans* mixtures of MK-3(II-H_2) (2.21) (Figure 2.3.2C-D) was essential because the presence of the *cis* isomer was not well observed in $CDCl_3$ (see Supporting Information for spectra in $CDCl_3$ vs. benzene-d_6, Figure A2.50).

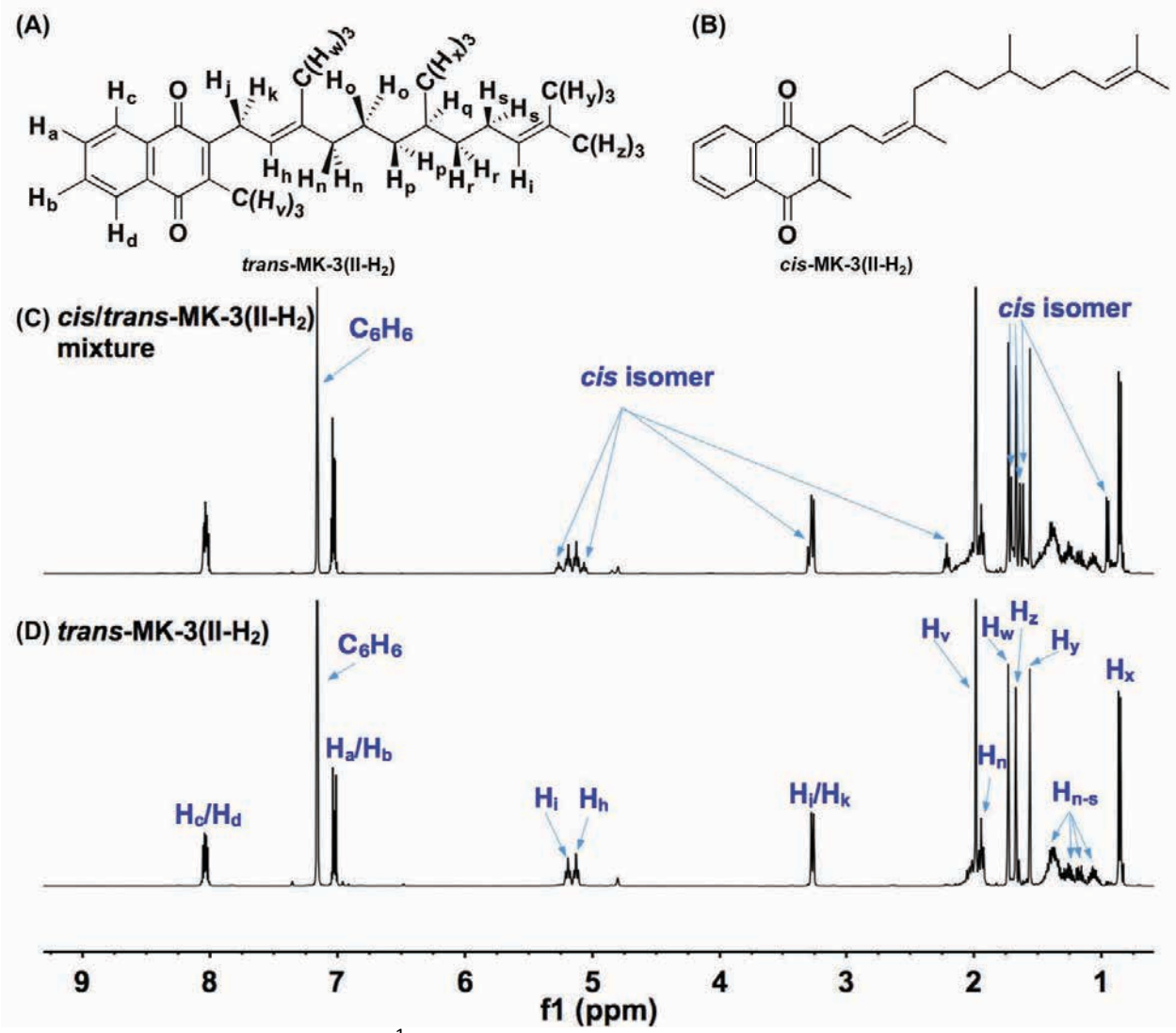

Figure 2.3.2. Comparison of the 1D ^{1}H NMR (400 MHz) spectra for the mixture of *cis*/*trans*-MK-3(II-H_2) and *trans*-MK-3(II-H_2) in C_6D_6 at 25 °C. (A) Structure of *trans*-MK-3(II-H_2) with hydrogen labeling scheme key, (B) Structure of *cis*-MK-3(II-H_2), (C) 1D ^{1}H NMR spectrum of *cis*/*trans* mixture of MK-3(II-H_2) in C_6D_6, and (D) 1D ^{1}H NMR spectrum of *trans*-MK-3(II-H_2) in C_6D_6. Overlapping *cis*/*trans* peaks have been left unlabeled.

The structural assignment of *trans*-MK-3(II-H_2) (Figure 2.3.2) was elucidated using 2D NMR spectroscopic methods (^{1}H-^{1}H COSY, ^{1}H-^{13}C HSQC, and ^{1}H-^{1}H ROESY, see Supporting Information for spectra, Figures A2.35-36.1 and A2.39-40.1). The assignment of the alkene hydrogen H_h at 5.13 ppm was determined by the following: the observation of a cross peak in the COSY spectrum at 5.13 ppm and 1.73 ppm (assignment H_w, Figure 2.3.2), the observation of a cross peak at 5.13 ppm and 1.94 ppm (assignment H_n, Figure 2.3.2), and the lack of an observed cross peak at 5.19 ppm and 1.73 ppm (H_w). The assignment of alkene hydrogen H_i at 5.19 ppm was determined by the observation of a cross peak at 5.19 ppm and 1.67 ppm and the lack of a cross peak at 5.19 ppm and 1.73 ppm (H_w). ^{1}H-^{1}H 2D ROESY NMR spectroscopy (see Supporting Information) also supported the alkene assignment by the observation of a ROE cross peak at 5.19 ppm and 1.67 ppm (H_i - H_z interaction) and the lack of a ROE cross peak at 5.19 ppm and 1.56 ppm. The assignment of the terminal methyl groups, H_y and H_z, was also determined by ^{1}H-^{1}H 2D ROESY NMR spectroscopy. It is anticipated that a ROE cross peak would be observed between the alkene hydrogen H_i and the methyl group that is *cis* to H_i due to the close spatial proximity and a ROE cross peak is observed, as expected, at 5.19 ppm and 1.67 ppm (H_i – H_z interaction) (see Supporting Information). Although H_y and H_i are within the spatial limits of an expected ROE cross peak observation, an ROE cross peak is not observed at 5.19 ppm and 1.56 ppm. This supports the structural assignment of H_y as *trans* to alkene hydrogen H_i as H_y is further away, spatially, from H_i compared to H_z.

2.3.8 Synthesis and Characterization of Menaquinone-3(I,II,III-H_6)

The fully saturated isoprenyl MK analog, MK-3(I,II,III-H_6) (2.25), was synthesized in four steps (Scheme 2.3.8) from the commercially available allylic alcohol, farnesol (2.22). The first step was

the Pd catalyzed transfer hydrogenation of farnesol to yield the fully saturated alcohol (2.23) in 88% yield.[55] Subsequent mesylation of the alcohol of product (2.23) followed by substitution with NaI gave the aliphatic iodide (2.24) in 47% yield over two steps.[40, 56] The final step was the radical coupling of menadione (2.1) and the aliphatic iodide (2.24) using benzoyl peroxide[49] as the radical initiator to yield the desired final product, MK-3(I,II,III-H_6) (2.25) in 15% yield. This yield is similar to that attained for the coupling reaction to obtain MK-2(I,II-H_4) (2.13). The unreacted aliphatic iodide (2.24) can be recovered during purification. Similar to MK-2(I,II-H_4) (2.13), in an attempt to ensure good selectivity of prenylation (C3 over C2, Scheme 2.3.8), slow addition of the napthoquinone (2.1) to the prenyl iodide solution during the course of the reaction was carried out.[49] Similar to the synthesis of MK-2(I,II-H_4) (2.25) above, this is the second report of this type of primary alkyl radical coupling reaction to access MK and the first report at a preparatory scale. MK-3(I,II,III-H_6) (2.25) was obtained as a yellow oil. This is the first report of the synthesis and characteriation of MK-3(I,II,III-H_6) (2.25) (see Supporting Information for 2D NMR spectra, Figures A2.48-49.1), the fully saturated analog of MK-3 (2.15).

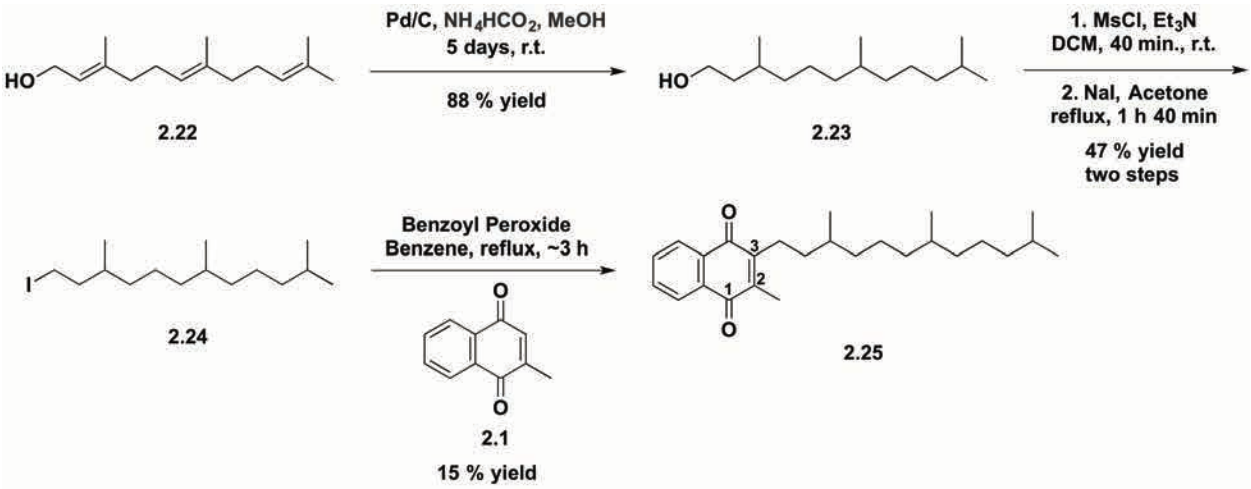

Scheme 2.3.8. Synthetic scheme for the 4-step synthesis to obtain MK-3(I,II,III-H_6) (2.25). The first step is a transfer hydrogenation to produce the fully saturated alcohol (2.23) from farnesol (2.22). The second step forms the mesylate from (2.23). The third step forms the aliphatic iodide (2.24) *via* a SN_2 reaction. The final step couples menadione (2.1) and the aliphatic iodide (2.24) using a radical alkylation initiated by benzoyl peroxide.

2.4 Summary and Conclusions

The results of these studies will allow for the synthesis of various MK analogs and gives access to previously unexplored compounds with unknown biological activity. In summary, this chapter described the synthesis and characterization of eight truncated MK analogs with varying isoprenyl side chain length and degrees of saturation, as well as separated and characterized geometric isomers formed in the reactions. The fully unsaturated MK derivatives, MK-1, MK-2, and MK-3 were successfully from menadione in two steps using a Lewis acid catalyst and respective corresponding allylic alcohol isoprenoid. MK-1(H_2) was successfully synthesized in single step from 1-iodo-3-methylbutane utilizing a key radical alkylation reaction. The partially saturated MK-2(II-H_2) was successfully synthesized in a single step from menadiol and isophytol, and the *trans* isomer was separated from the *cis* isomer byproduct by preparative TLC, followed by characterization. The novel fully saturated MK-2(I,II-H_4) was successfully synthesized in three steps from 3,7-dimethyloctan-1-ol. The partially saturated MK-3(II-H_2) was successfully

synthesized in seven steps from β-citronellol, and the *trans* isomer was readily separated from the *cis* isomer byproduct by preparative TLC, followed by characterization. Finally, the novel fully saturated MK-3(I,II,III-H_6) was successfully synthesized in four steps from farnesol. The use of benzene-d_6 as a diagnostic NMR solvent for the rapid evaluation of *cis*/*trans* mixtures for MK/vitamin K analogs was essential as *cis*/*trans* peaks often coalesce in chloroform-d.

The separation and characterization of an MK analog's *trans* isomer is essential for use of these compounds in biological systems or understanding biological systems that use MK, since evidence shows the *cis* isomer is not biologically active. The MK analogs synthesized in this chapter are substrate analogs for enzymes involved in MK/vitamin K metabolism and are essential for understanding structure-activity relationships of these biological systems. They are also critical for understanding the function, reactivity, and conformation of partially saturated MK analogs as little is currently known. These MK analogs are also of interest from a therapeutic and medicinal standpoint. For instance, MK-4 (vitamin K_2) was recently shown to be a potential new therapeutic strategy to treat rheumatoid arthritis, is a proposed drug for the effective treatment of osteoporosis and has anticancer properties. Nevertheless, the synthesis of partially saturated MK analogs remains a challenge as there is currently not a suitable catalyst to selectively saturate an individual isoprene unit on an MK analog while leaving the other double bonds unaffected. Importantly, the synthesis and characterization of these MK substrate analogs containing varying isoprenyl side chain length and degrees of saturation is essential for understanding why they are necessary for various organisms to survive. These studies are important for understanding the reason MK-9(II-H_2) (i.e., saturated at the second isoprene unit)

is observed in pathogenic *M. tuberculosis*, which is responsible for the deaths of ~1.3 million people annually.

References

1. Koehn, J. T.; Crick, D. C.; Crans, D. C., Synthesis and Characterization of Partially and Fully Saturated Menaquinone Derivatives. *ACS Omega* **2018,** *3*, 14889-14901.
2. Kurosu, M.; Begari, E., Vitamin K_2 in Electron Transport System: Are Enzymes Involved in Vitamin K_2 Biosynthesis Promising Drug Targets? *Molecules* **2010,** *15* (3), 1531-1553.
3. van der Est, A., Electron Transfer Involving Phylloquinone in Photosystem I. In *Photosystem I. Advances in Photosynthesis and Respiration*, Golbeck, J. H., Ed. Springer, Dordrecht: 2006; Vol. 24.
4. Nakagawa, K.; Hirota, Y.; Sawada, N.; Yuge, N.; Watanabe, M.; Uchino, Y.; Okuda, N.; Shimomura, Y.; Suhara, Y.; Okano, T., Identification of UBIAD1 as a Novel Human Menaquinone-4 Biosynthetic Enzyme. *Nature* **2010,** *468*, 117-121.
5. Vos, M.; Esposito, G.; Edirisinghe, J. N.; Vilain, S.; Haddad, D. M.; Slabbaert, J. R.; Van Meensel, S.; Schaap, O.; De Strooper, B.; Meganathan, R.; Morais, V. A.; Verstreken, P., Vitamin K_2 Is a Mitochondrial Electron Carrier That Rescues Pink1 Deficiency. *Science* **2012,** *336*, 1306-1310.
6. Dragh, M. A.; Xu, Z.; Al-Allak, Z. S.; Hong, L., Vitamin K_2 Prevents Lymphoma in Drosophila. *Sci. Rep.* **2017,** *7*, 17047.
7. Okamoto, H.; Shidara, K.; Hoshi, D.; Kamatani, N., Anti-arthritis Effects of Vitamin K_2 (Menaquinone-4) - a New Potential Therapeutic Strategy for Rheumatoid Arthritis. *FEBS J.* **2007,** *274*, 4588-4594.
8. Astudillo-Sánchez, P. D.; Morales-Martínez, D.; Sánchez, A.; Rocha-Ortiz, G.; Salas-Reyes, M., Electrochemical Study of the Interactions Between Anionic Species of Menadione and Alkylated Nucleobases in Dimethylsulfoxide. *J. Electroanal. Chem.* **2017,** *801*, 104-113.
9. Josey, B. J.; Inks, E. S.; Wen, X.; Chou, C. J., Structure−Activity Relationship Study of Vitamin K Derivatives Yields Highly Potent Neuroprotective Agents. *J. Med. Chem.* **2013,** *56*, 1007-1022.
10. Rahn, J. J.; Bestman, J. E.; Josey, B. J.; Inks, E. S.; Stackley, K. D.; Rogers, C. E.; Chou, C. J.; Chan, S. S. L., Novel Vitamin K Analogs Suppress Seizures in Zebrafish and Mouse Models of Epilepsy. *Neuroscience* **2014,** *259*, 142-154.
11. Chadar, D.; Camilles, M.; Patil, R.; Khan, A.; Weyhermuller, T.; Salunke-Gawali, S., Synthesis and Characterization of *n*-alkylamino Derivatives of Vitamin K3: Molecular Structure of 2-propylamino-3-methyl-1,4-naphthoquinone and Antibacterial Activities. *J. Mol. Struct.* **2015,** *1086*, 179-189.
12. Kathawate, L.; Joshi, P. V.; Dash, T. K.; Pal, S.; Nikalje, M.; Weyhermuller, T.; Puranik, V. G.; Konkimalla, V. B.; Salunke-Gawali, S., Reaction Between Lawsone and Aminophenol Derivatives: Synthesis, Characterization, Molecular Structures and Antiproliferative Activity. *J. Mol. Struct.* **2014,** *1075*, 397-405.
13. Thomson, R. H., *Naturally Occurring Quinones.* Academic Press Inc: 1971.
14. Collins, M. D.; Jones, D., Distribution of Isoprenoid Quinone Structural Types in Bacteria and Their Taxonomic Implications. *Microbiol. Rev.* **1981,** *45* (2), 316-354.
15. Collins, M. D.; Shah, H. N.; Minnikin, D. E., A Note on the Separation of Natural Mixtures of Bacterial Menaquinones Using Reverse-phase Thin-layer Chromatography. *J. Appl. Bacteriol.* **1980,** *48* (2), 277-282.
16. Dunphy, P. J.; Brodie, A. F., The Structure and Function of Quinones in Respiratory Metabolism. In *Methods in Enzymology*, 1971; Vol. 18, pp 407-461.
17. Dunphy, P. J.; Gutnick, D. L.; Phillips, P. G.; Brodie, A. F., A New Natural Naphthoquinone in *Mycobacterium phlei*. Cis-dihydromenaquinone-9, Structure and Function. *J. Biol. Chem.* **1968,** *243*, 398-407.

18. Ogawa, T.; Isobe, K.; Mori, T.; Asakawa, S.; Yoshimura, T.; Hemmi, H., A Novel Geranylgeranyl Reductase from the Methanogenic Archaeon *Methanosarcina acetivorans* Displays Unique Regiospecificity. *FEBS J.* **2014,** *281* (14), 3165-3176.
19. Bang, C.; Schmitz, R. A., Archaea Associated with Human Surfaces: Not To Be Underestimated. *FEMS Microbiol. Rev.* **2015,** *39* (5), 631-648.
20. Gale, P. H.; Arison, B. H.; Trenner, N. R.; Page, A. C.; Folkers, K.; Brodie, A. F., Characterization of Vitamin K9(H) from *Mycobacterium phlei. Biochemistry* **1963,** *2*, 200-203.
21. Azerad, R.; Cyrot, M. O.; Lederer, E. L., Structure of the Dihydromenaquinone-9 of *Mycobacterium phlei*. *Biochem. Biophys. Res. Commun.* **1967,** *27* (2), 249-252.
22. Azerad, R.; Cyrot-Pelletier, M.-O., Structure and Configuration of the Polyprenoid Side Chain of Dihydromenaquinones from *Myco*- and *Corynebacteria*. *Biochimie* **1973,** *55*, 591-603.
23. Upadhyay, A.; Fontes, F. L.; Gonzalez-Juarrero, M.; McNeil, M. R.; Crans, D. C.; Jackson, M.; Crick, D. C., Partial Saturation of Menaquinone in *Mycobacterium tuberculosis*: Function and Essentiality of a Novel Reductase, MenJ. *ACS Cent. Sci.* **2015,** *1* (6), 292-302.
24. Sitkowski, J.; Bocian, W.; Szterk, A., The Application of Multidimensional NMR Analysis to *cis*/*trans* Isomers Study of Menaquinone-7 (Vitamine K2MK-7), Identification of the (E,Z3,E2,u)-menaquinone-7 Isomer in Dietary Supplements. *J. Mol. Struct.* **2018,** *1171*, 449-457.
25. Szterk, A.; Zmyslowski, A.; Bus, K., Identification of *cis*/*trans* Isomers of Menaquinone-7 in Food as Exemplified by Dietary Supplements. *Food Chem.* **2018,** *243*, 403-409.
26. Koehn, J. T.; Magallanes, E. S.; Peters, B. J.; Beuning, C. N.; Haase, A. A.; Zhu, M. J.; Rithner, C. D.; Crick, D. C.; Crans, D. C., A Synthetic Isoprenoid Lipoquinone, Menaquinone-2, Adopts a Folded Conformation in Solution and at a Model Membrane Interface. *J. Org. Chem.* **2018,** *83*, 275-288.
27. Daines, A. M.; Payne, R. J.; Humphries, M. E.; Abell, A. D., The Synthesis of Naturally Occurring Vitamin K and Vitamin K Analogues. *Curr. Org. Chem.* **2003,** *7*, 1-15.
28. IUPAC-IUB, Nomenclature of Quinones with Isoprenoid Side-chains. *Pure Appl. Chem.* **1974,** *38* (3), 439-447.
29. Phoenix, J.; Edwards, R. H. T.; Jackson, M., The Effect of Vitamin E Analogues and Long Hydrocarbon Chain Compounds on Calcium-induced Muscle Damage. A Novel Role For a-tocopherol? *Biochim. Biophys. Acta, Mol. Basis Dis.* **1991,** *1097* (3), 212-218.
30. Wiss, O.; Weber, F.; Ruegg, R.; Isler, O., The Biological Activity of Vitamins K_1 and K_2 and their Isoprenologs. *Hoppe-Seyler's Z. Physiol. Chem.* **1959,** *314*, 245-249.
31. Noll, H., Physicochemical Characterization of Vitamin K Homologs. I. Identification by a Novel Method of Quantitative Infrared Spectrophotometry. *J. Biol. Chem.* **1960,** *235* (8), 2207-2216.
32. Isler, O.; Ruegg, R.; Studer, A.; Jurgens, R., Specificity of the Vitamin K_1 Constitution and its Analogs Toward Coumarin Linkages. *Hoppe-Seyler's Z. Physiol. Chem.* **1953,** *295*, 290-309.
33. Azerad, R.; Cyrot, M. O., Synthesis of Two Dihydrofarnesylnaphthoquinones Related to Vitamin K2(45)H from *Mycobacterium phlei*. *Bull. Soc. Chim. Fr.* **1965,** *12*, 3740-3745.
34. Karrer, P.; Yap, K. S., Über ein weiteres niederes Homologe des α-Tocopherols. *Helv. Chim. Acta* **1940,** *23* (1), 581.
35. Zakharov, A.; Vogt, N., Conformational Analysis of Vitamin K_1 Model Molecule: A Theoretical Study. *Struct. Chem.* **2011,** *22* (2), 305-311.
36. Glaziou, P.; Sismanidis, C.; Floyd, K.; Raviglione, M., Global Epidemiology of tuberculosis. *Cold Spring Harbor Perspect. Med.* **2015,** *5*, a017798.
37. Williams, D. B. G.; Lawton, M., Drying of Organic Solvents: Quantitative Evaluation of the Efficiency of Several Desiccants. *J. Org. Chem.* **2010,** *75*, 8351-8354.
38. Upadhyay, A.; Kumar, S.; Rooker, S. A.; Koehn, J. T.; Crans, D. C.; McNeil, M. R.; Lott, J. S.; Crick, D. C., Mycobacterial MenJ: An Oxidoreductase Involved in Menaquinone Biosynthesis. *ACS Chem. Biol.* **2018,** *13*, 2498-2507.

39. Dobrinescu, C.; Iorgulescu, E. E.; Mihailciuc, C.; Macovei, D.; Wuttke, S.; Kemnitz, E.; Parvulescu, V. I.; Coman, S. M., One-Pot Hydroacetylation of Menadione (Vitamin K_3) to Menadiol Diacetate (Vitamin K_4) by Heterogeneous Catalysis. *Adv. Synth. Catal.* **2012,** *354* (7), 1301-1306.
40. Suhara, Y.; Wada, A.; Tachibana, Y.; Watanabe, M.; Nakamura, K.; Nakagawa, K.; Okano, T., Structure-activity Relationships in the Conversion of Vitamin K Analogues into Menaquinone-4. Substrates Essential to the Synthesis of Menaquinone-4 in Cultured Human Cell Lines. *Bioorg. Med. Chem.* **2010,** *18* (9), 3116-3124.
41. Lowenthal, J.; Chowdhury, M. N. R., Synthesis of Vitamin K_1 analogs. A New Class of Vitamin K_1 Antagonists. *Can. J. Chem.* **1970,** *48*, 3957-3958.
42. Kim, J.; Matsuyama, S.; Suzuki, T., Deuterated Analogues of 4,8-dimethyldecanal, the Aggregation Pheromone of *Tribolium castaneum*: Synthesis and Pheromonal Activity. *J. Labelled Compd. Radiopharm.* **2004,** *47* (13), 921-934.
43. Fieser, L. F.; Fieser, M., In *Reagents for Organic Synthesis*, Wiley, New York, 1967; Vol. 1, pp 581-595.
44. Hagiwara, E.; Hatanaka, Y.; Gohda, K.-i.; Hiyama, T., Allylation of Quinones with Allyl(trifluoro)silanes: Direct Synthesis of Isoprenoid Quinones. *Tetrahedron Lett.* **1995,** *36* (16), 2773-2776.
45. Mal, D.; Ghosh, K.; Jana, S., Synthesis of Vitamin K and Related Naphthoquinones via Demethoxycarbonylative Annulations and a Retro-Wittig Rearrangement. *Org. Lett.* **2015,** *17*, 5800-5803.
46. Teitelbaum, A. M.; Scian, M.; Nelson, W. L.; Rettie, A. E., Efficient Syntheses of Vitamin K Chain-Shortened Acid Metabolites. *Synthesis* **2015,** *47*, 944-948.
47. Yamago, S.; Hashidume, M.; Yoshida, J.-i., A New Synthetic Route to Substituted Quinones by Radical-mediated Coupling of Organotellurium Compounds with Quinones. *Tetrahedron* **2002,** *58*, 6805-6813.
48. Payne, R. J.; Daines, A. M.; Clark, B. M.; Abell, A. D., Synthesis and Protein Conjugation Studies of Vitamin K Analogues. *Bioorg. Med. Chem.* **2004,** *12* (22), 5785-5791.
49. Coppa, F.; Fontana, F.; Minisci, F.; Nogueira Barbosa, M. C.; Vismara, E., Homolytic Alkylation of Naphthoquinone and Methyl-naphthoquinone. Enthalpic, Steric and Polar Effects. *Tetrahedron* **1991,** *47* (35), 7343-7352.
50. Wuttke, S.; Coman, S. M.; Scholz, G.; Kirmse, H.; Vimont, A.; Daturi, M.; Schroeder, S. L. M.; Kemnitz, E., Novel Sol–Gel Synthesis of Acidic $MgF_{2-x}(OH)_x$ Materials. *Chem. Eur. J.* **2008,** *14* (36), 11488-11499.
51. Coman, S. M.; Parvulescu, V. I.; Wuttke, S.; Kemnitz, E., Synthesis of Vitamin K_1 and K_1-Chromanol by Friedel–Crafts Alkylation in Heterogeneous Catalysis. *ChemCatChem* **2010,** *2* (1), 92-97.
52. Coman, S. M.; Patil, P.; Wuttke, S.; Kemnitz, E., Cyclisation of Citronellal Over Heterogeneous Inorganic Fluorides—Highly Chemo- and Diastereoselective Catalysts for (±)-isopulegol. *Chem. Commun.* **2009**, 460-462.
53. DiMari, S. J.; Rapoport, H., The Reconstitution of Oxidative Phosphorylation in *Mycobacterium phlei* with *cis*- and *trans*-Phylloquinone. Evidence against Isomerization. *Biochemistry* **1968,** *7* (7), 2650-2652.
54. Creed, D.; Werbin, H.; Daniel, T., The Mechanism of Photooxidation of the Menaquinones. *Tetrahedron Lett.* **1981,** *22* (22), 2039-2042.
55. Lerman, L.; Weinstock-Rosin, M.; Nudelman, A., An Improved Synthesis of Hydroxyindoles. *Synthesis* **2004,** *18*, 3043-3046.
56. Bennett, C. J.; Caldwell, S. T.; McPhail, D. B.; Morrice, P. C.; Duthie, G. G.; Hartley, R. C., Potential Therapeutic Antioxidants that Combine the Radical Scavenging Ability of Myricetin and the Lipophilic Chain of Vitamin E to Effectively Inhibit Microsomal Lipid Peroxidation. *Bioorg. Med. Chem.* **2004,** *12* (9), 2079-2098.

Chapter 3: Investigation of the Conformational Flexibility of the Isoprenyl Side Chain on Menaquinone[1]

3.1 Conformation of the Isoprenyl Side Chain of Mycobacterial Menaquinone

Isoprenoids are among the most numerous and diverse compounds found in nature.[1-4] It was reported that 55,000 of these naturally occurring compounds had been identified by 2007[4]; an estimate that increased to 70,000 in 2015.[2] Classes of isoprenoids include lipoquinones, sterols, carotenoids, prenylated proteins, dolichols, monoterpenes, and sesquiterpenes. These compounds are involved in diverse functions such as electron transport, hormone function, membrane structure and fluidity, vision, photoprotection, insect reproduction, fragrance and defense. The solution structures of many of these compounds, such as the sterols, are well studied. However, the conformations of long linear polymers of isoprene units such as those found in the side chains of lipoquinones involved in bacterial and eukaryotic electron transport systems (ETS) have not been characterized.[5-8] Lipoquinones are small hydrophobic molecules that shuttle electrons between the membrane-bound protein complexes acting as electron acceptors and donors in the respiratory ETS. Two major structural groups of lipoquinones are recognized; ubiquinones (or benzoquinones, UQ) typically found in eukaryotes and Gram-negative prokaryotes and menaquinones (or naphthoquinones, MK) typically found in Gram-positive prokaryotes, including many pathogens such as *M. tuberculosis*. The roles and applications of lipoquinone derivatives are currently being explored where a range of different

[1]This chapter is published in part or in full in *The Journal of Organic Chemistry*.[1]

approaches are used for combatting human diseases.[9-21] This chapter aims to characterize the conformation of a synthetic truncated MK analog in organic solution and within a model membrane interface, as well as document the redox potential of these systems accompanying the conformational studies.

Here, we use an abbreviation system where MK with two isoprene units is MK-2 and with nine isoprene units is MK-9, Figure 3.1.1. Naturally occurring lipoquinones are characterized by the presence of an isoprenyl side chain of varying length from 1-14 isoprene units[22-23] depending on the species of origin; a characteristic long used to assist taxonomic efforts. Textbooks often represent UQ and MK as "Q" or "MQ" in illustrations of the ETS and in primary literature they are generally shown in an extended conformation, which is not a realistic conformation as the lipoquinone would have to fold to be confined within the hydrophobic region of the phospholipid bilayer (Figure 3.1.1).[8, 24-25]

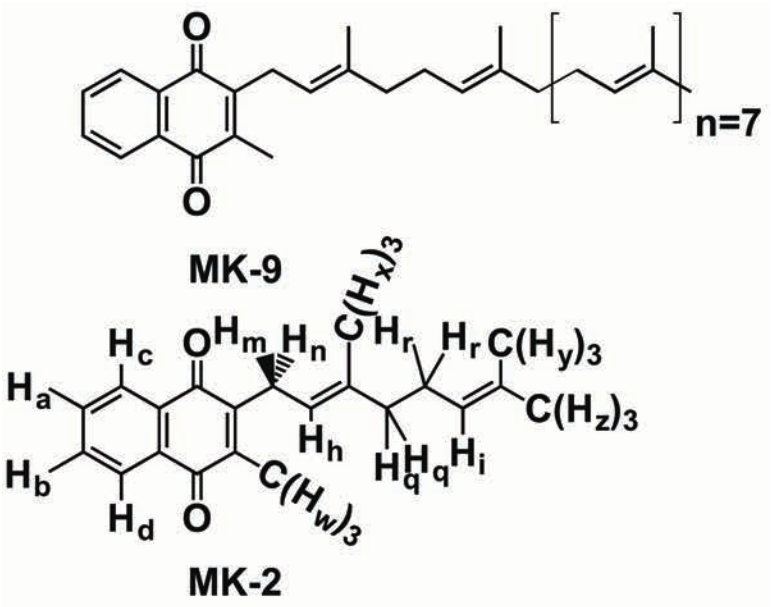

Figure 3.1.1. Structure of menaquinone-9 (MK-9), present in small quantities in *Mycobacterium tuberculosis* (top) and MK-2, a simplified MK analog (bottom), is also shown. Hydrogens are labelled on MK-2 for spectral interpretation.

Small angle X-ray diffraction experiments with the isoprenoid dolichol, an alcohol with 18-20 isoprene units, indicated that the molecule adopted a helical structure in organic solvent.[26] The conformation of the isoprenoid moiety in MK derivatives is likely important to its function as an electron transfer agent and other biological roles. Although nothing is known about the conformation of MK derivatives, limited conformational analysis is available on different classes of compounds including alkanes, alkenes, and fatty acids with much simpler structures.[27-41] The all-*trans* conformations of alkanes are generally considered the most stable and therefore, it is expected that the most prevalent conformation of an alkane is the fully extended alkyl chain.[27] A few studies have been reported with simple alkanes and a range of other, more complex compounds with large alkane-components such as in polyenes and fatty acids.[28,29] The U-shape in fatty acids were described when bound to a fatty acid binding protein (FABP), where the alkyl chain region of two fatty acids, palmitic and oleic acids, folds over in the shape of a U.[38-39] In 2008, X-ray crystal structure analysis, as well as NMR spectroscopy, also supported the U-shaped conformation of amphiphilic alkyl chains bound to a synthetic receptor where the folded C_8, C_{10}, and C_{12} conformations have anticlinal as well as *gauche* arrangements.[38-39]Based on these few examples, we hypothesized that MKs will adopt folded conformations depending on specific environmental conditions.

In this chapter, we describe the characterization of a truncated MK derivative with two isoprene units. MK-2 (Figure 3.1.1) can be characterized in detail and serves as a representative MK reference compound as it is the simplest MK containing a naphthoquinone and repeating isoprenyl side chain allowing comparison to more complex MK-derivatives found in various microorganisms.[7, 42-43] First, the conformation of MK-2 was investigated in organic solvents (polar

and hydrophobic). Next, because we are ultimately interested in the function of these derivatives, we measured the electrochemical potential of MK-2 in the organic solvents where the conformations were determined. Finally, the location and conformation of MK-2 in simple membrane model systems was examined. Combined, our results show that MK-2 folds into a U-shaped conformation in solution contrary to common perception, and that a folded, slightly different U-shaped conformation also exists in the presence of a simple model lipid membrane interface.

3.2 Materials and Methods

3.2.1 Materials

Bis(2-ethylhexyl) sulfosuccinate sodium salt (AOT, 97.0%), isooctane (2,2,4-trimethylpentane, ≥99.0%), chloroform (99.8%), methanol (99.9%), disodium phosphate (anhydrous), trisodium phosphate (96.0%), tetrabutylammonium perchlorate (TBAP, ≥ 99.0%), ferrocene (Fc, anhydrous), silver nitrate ($AgNO_3$, ≥ 99.0%), and activated charcoal were purchased from Sigma Aldrich. Absolute ethanol and ultra-high purity argon gas (99.9%) were acquired from Pharmco-Aaper and Airgas, respectively. Deuterated solvents of acetonitrile (CH_3CN) (D 99.8%), dimethylsulfoxide (DMSO) (D 99.9%, + 0.05% V/V tetramethylsilane), and deuterium oxide (D_2O, 99.9%) were acquired from Cambridge Isotope Laboratories, Inc. Deuterated pyridine (D 99.8%) was purchased from Arcos Organics. DPPC (1,2-dipalmitoyl-sn-glycero-3-phosphocholine, ≥ 99.0%) and DPPE (1,2-dipalmitoyl-sn-glycero-3-phosphoethanolamine, ≥ 99.0%) were purchased from Avanti Polar Lipids Inc. Distilled Deionized Water (DDI H_2O) was purified with a Barnstead

E-pure system (18.2 MΩ-cm). All chemicals were used without purification except AOT, and the organic solvents where AOT was purified by using previously reported methods.[44]

3.2.2 NMR Spectroscopic Studies

1D and 2D ^{1}H studies were carried out both in organic solvents and more complex media (see below for RM studies). ^{1}H and ^{13}C spectra were recorded using a Varian Model MR400 or Model Inova400 operating at 400 MHz and 100 MHz, respectively. Chemical shift values (δ) are reported in ppm and referenced against the internal solvent peaks in ^{1}H NMR (d_6-DMSO, δ at 2.50 ppm; $CDCl_3$, δ at 7.26 ppm; d_5-pyridine, δ at 8.74 ppm; d_3-acetonitrile δ at 1.94 ppm; D_2O, δ at 4.79 ppm; C_6D_6, δ at 7.16 ppm) and in ^{13}C NMR (d_6-DMSO, δ at 39.52 ppm). All NMR spectra were recorded either at 22 °C or 26 °C.

3.2.3 Solution 1D ^{1}H NMR Spectroscopic Studies

Samples were prepared by dissolving ~5 mg of MK-2 in either 0.5 mL of isooctane, d_5-pyridine, C_6D_6, d_3-acetonitirle, d_6-DMSO, or D_2O. The MK-2 sample in D_2O was vortexed for ~1 hr. to dissolve maximum amount of MK-2. The NMR spectrum was collected by running 32 scans and was locked onto the deuterated solvent except for isooctane, which was ran unlocked using $CDCl_3$ as a spectral window reference.

3.2.4 Sample Preparation for Solution ^{1}H-^{1}H 2D NOESY and ROESY NMR Spectroscopic Studies

To prepare the samples in d_6-DMSO and d_5-pyridine, 0.0031 g of MK-2 was dissolved in 0.5 mL of solvent to yield a 20 mM solution of MK-2. The NMR tubes containing the MK-2 solution were purged with argon prior to data collection.

3.2.5 ^{1}H-^{1}H 2D NOESY and ROESY NMR Spectroscopic Studies in Organic Solution

2D NMR spectroscopic studies in organic solution were carried out on a Varian model MR400 400 MHz magnet at 26 °C. A standard NOESY pulse sequence was used consisting of either 200 or 256 transients with 16 scans in the f1 domain using a 500 ms mixing time, 45° pulse angle, and a 1.5 sec. relaxation delay. A standard ROESYAD pulse sequence was used consisting of either 200 or 256 transients with 16 scans in the f1 domain using a 400 ms mixing time, 45° pulse angle, and a 2.0 sec. relaxation delay. The NMR was locked onto either d_6-DMSO or d_5-pyridine and referenced to the internal solvent peak. The resulting spectrum was processed using MestReNova NMR software version 10.0.1.

3.2.6 Molecular Mechanics Calculations

To obtain visual aids of MK-2 conformations, Merck Molecular Force Field 94 (MMFF94) Molecular Mechanics gas phase simulations were conducted using ChemBio3D Ultra 12.0 at 25°C. Starting conformations were obtained from ChemDraw structures or by rotating desired bonds and then either had simulations run or simply an energy minimized to achieve the desired conformation. Conformations A-B in Figure 3.3.3 were generated and then energy minimized with a root mean square (RMS) gradient of 0.1 and up to 50 iterations to obtain conformations that agreed with our interpretation of the cross peak observations in the ^{1}H-^{1}H 2D NOESY and ROESY NMR spectral data. One simulation was run for 10,000 iterations and then energy minimized using an MMFF994 energy minimization calculation using 500 iterations with a RMS gradient of 0.001 to achieve conformation C in Figure A3.10C. Conformations D-H in Figure A3.10 were generated by rotating bonds to achieve the desired conformation followed by an energy minimization using 20-50 iterations and an RMS gradient of 0.1. For a table of structural

parameters such as selected distances between hydrogen atoms within the conformations and energies calculated for the 3D conformations can be found in the Supporting Information section.

3.2.7 Sample Preparation for Reverse Micelle NMR Spectroscopic Studies

A 0.50 M AOT stock solution was made by dissolving AOT (5.56 g, 12.5 mmol) in isooctane (25.0 mL). RMs were prepared by mixing the 0.50 M AOT stock solution with D_2O (pH 7.0, pD 7.4), and then vortexed until clear. MK-2 RMs were made in a similar manner except an 11.2 mM MK-2 stock solution was prepared by directly dissolving MK-2 in the 0.50 M AOT/isooctane solution. Then, the MK-2-AOT-isooctane stock solution along with D_2O (pH 7.0, pD 7.4) were used to make RMs.

3.2.8 1D ^{1}H NMR Spectroscopic Studies of AOT/Isooctane that contain Menaquinone-2

1D ^{1}H NMR spectroscopic experiments were carried out using a Varian Inova 400 MHz instrument using routine parameters (pulse angle: 45°, relaxation delay of 1 sec.) at 22 °C. The RM spectra were internally referenced using the isooctane methyl peak set to 0.904 ppm.[45] Data analysis and spectrum workup was done using the NMR software, MestReNova version 10.0.1.

3.2.9 Sample Preparation for Solution ^{1}H-^{1}H 2D NOESY and ROESY NMR Spectroscopic Studies in Reverse Micelles

To prepare the AOT/isooctane stock solution, 0.22 g AOT (0.50 mmol) was dissolved into isooctane (1.0 mL) for a final 0.50 M AOT stock solution. Then 0.035 g (1.10 mmol) of MK-2 was dissolved into the 0.50 M AOT stock solution for a final concentration of 110 mM MK-2. Then, 892.6 μL of MK-2 AOT/isooctane stock solution was mixed with 107.3 μL of D_2O (pH = 7, pD = 7.4) and then vortexed until clear. This final mixture results in a w_0 12 RM microemulsion with an overall concentration of MK-2 being 100 mM (~29 molecules per RM).

3.2.10 ^{1}H-^{1}H 2D NOESY and ROESY NMR Spectroscopic Studies in AOT/isooctane w_0 12 Reverse Micelles

2D NMR samples were ran using similar conditions used previously[46] using a Varian model MR400 400 MHz magnet at 26 °C similar to conditions used previously. A standard NOESY pulse sequence was used, 256 transients with 16 scans in the f1 direction using a 200 ms mixing time, 45° pulse angle, and a relaxation delay of 1.5 sec. A standard ROESY pulse sequence was used, 256 transients with 16 scans in the f1 direction using a 200 ms mixing time, 45° pulse angle, and a relaxation delay of 2.0 sec. The NMR was locked onto 10% D_2O and the spectrum was referenced to the isooctane methyl peak at 0.904 ppm as previously reported.[45] The resulting spectrum was processed using MestReNova NMR software version 10.0.1. The 3D structure illustration within a RM was drawn using ChemBioD Ultra 12.0 and ChemBio3D Ultra 12.0 based on spectral parameters described under results.

3.3 Results and Discussion

3.3.1 1D ^{1}H NMR Spectroscopic Studies of Menaquinone-2 in Different Organic Solvents

MK-2 was first characterized using 1D ^{1}H NMR spectroscopy. Figure 3.3.2 shows ^{1}H NMR spectra of MK-2 in isooctane (2,2,4-trimethylpentane), d_5-pyridine, d_6-benzene, d_3-acetonitrile, d_6-DMSO, and D_2O. The observed chemical shifts of MK-2 vary dramatically in the different solvents shown. Hydrophobic solvent environments including aliphatic (isooctane) and aromatic (d_5-pyridine and d_6-benzene) as well as hydrophilic (d_3-acetonitrile, d_6-DMSO, and H_2O/D_2O) solvent environments generate very different spectroscopic signatures. For example, the pairs of aromatic hydrogens, H_a/H_b and H_c/H_d, are significantly different in the two different classes of

solvents. This observed variation in chemical shift could be attributed to conformational changes of MK-2 in the various solvent environments investigated, alterations of the electronic state due to interaction with the solvent, or most likely, a combination of both. Focusing on the ^{1}H NMR spectra of MK-2 in the three hydrophilic solvents, d_3-acetonitrile, d_6-DMSO, and D_2O, some differences and similarities are observed (Figure 3.3.2). The MK-2 spectrum in D_2O required significantly more scans to produce a reasonable spectrum because of the poor solubility in D_2O. The hydrogen chemical shifts generally are observed further up field in D_2O, presumably indicative of more aggregation in this solvent. The alkene H_h and H_i hydrogen signals are not observed in the D_2O spectrum because of overlap with the HOD peak. However, the HOD signal in the d_6-DMSO spectrum is observed at 3.3 ppm, which allows for observation of the alkene hydrogens, H_h and H_i, at 4.9 ppm. The spectrum of MK-2 in d_6-DMSO is very similar to that in d_3-acetonitrile and both also have some similarities to the MK-2 spectrum in D_2O. The aromatic hydrogens, H_a/H_b, shifted about 0.2 ppm from the H_c/H_d signals in both solvents. This suggests that these hydrogens remain in similar chemical environments in these two solvent environments. Combined, these three spectra provide a representation of the properties of the MK-2 in a hydrophilic solvent environment.

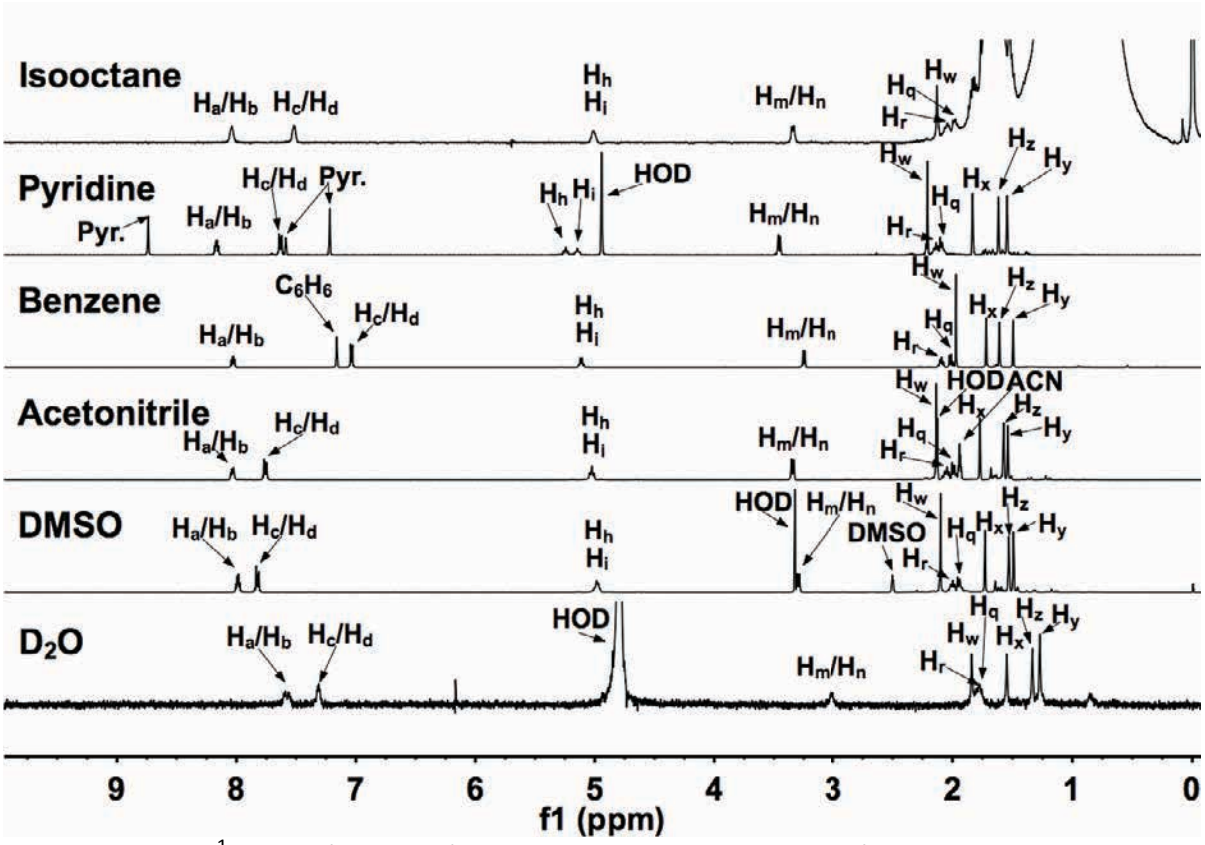

Figure 3.3.1. 1D ^{1}H NMR (400 MHz) spectra of MK-2 in hydrophilic (d_6-DMSO, d_3-acetonitrile, and D_2O) and hydrophobic [isooctane (2,2,4-trimethtylpentane), d_5-pyridine, and d_6-benzene] solvents. Hydrogen peak text labelling corresponds to MK-2 structure in Figure 3.1.2.

Next, the aromatic and alkene protons were examined in the hydrophobic solvents, isooctane, d_5-pyridine, and d_6-benzene (Figure 3.3.1). Here, protons H_a, H_b, H_c, H_d, H_h, and H_i are observed and readily identified. The signals from alkene hydrogens, H_h and H_i, are both further downfield compared to the signals in hydrophilic solvents and most interestingly, the two alkene hydrogens become non-chemical shift equivalent in d_5-pyridine. This contrasts with the aliphatic hydrogens in the spectrum in d_6-benzene, which are like those in d_6-DMSO except for H_q, H_r, H_w, and H_z. The changes in the chemical shifts are most distinctive in the aromatic and alkene hydrogens, suggesting that there are some major differences in their respective environments. Together, these differences strongly indicate that MK-2 is sensitive to the solvent environment.

However, information from 2D NMR techniques is needed to elucidate if this change in chemical shift is due to conformational variations or solvent effect.

3.3.2 ^{1}H-^{1}H 2D NOESY and ^{1}H-^{1}H 2D ROESY NMR Spectroscopic Studies of Menaquinone-2 in d_6-DMSO and d_5-pyridine

Differences between the conformations observed in d_6-DMSO vs. d_5-pyridine are likely manifested by the conformation minimizing the unfavorable interactions with the solvent environment and maximizing favorable intramolecular interactions with the isoprenyl side chain. To investigate the conformation of MK-2 in organic solvents, we utilized two different but complementary 2D NMR methods, ^{1}H-^{1}H 2D NOESY and ^{1}H-^{1}H 2D ROESY. Figure 3.3.2 shows the ^{1}H-^{1}H 2D NOESY and ROESY NMR spectra of MK-2 in d_6-DMSO and portions of the spectrum in d_5-pyridine. Figure 3.3.2A shows the complete ^{1}H-^{1}H 2D NOESY spectrum of MK-2 in d_6-DMSO and Figure 3.3.2B-C shows zoomed in regions of interest in the NOESY and ROESY spectra collected in d_6-DMSO, respectively (See Figure A3.1-2 for full spectra). Figure 3.3.2D-F shows zoomed in regions of interest in the NOESY and ROESY spectra collected in d_5-pyridine, respectively (see Figures A3.4-5 for full spectra). Figure 3.3.2B and Figure 3.3.2D illustrates that alkene hydrogens, H_h and H_i, are in similar environments in d_5-pyridine and d_6-DMSO due to the observance of similar NOE cross peaks. In both solvents, Figure 3.3.2B and Figure 3.3.2D show NOE cross peaks illustrating that H_h and H_i interact with H_n/H_m, H_q, H_r and H_z. Figure 3.3.2B and Figure 3.3.2D show NOE cross peaks demonstrating hydrogen H_w interacts with hydrogens H_h/H_i and H_m/H_n in both d_6-DMSO and d_5-pyridine. Figure 3.3.2C and Figure 3.3.2E shows partial ^{1}H-^{1}H 2D ROESY NMR spectra where the focus is on hydrogen H_w in d_6-DMSO and d_5-pyridine (see Figure A3.2 & A3.5 for full spectra and Figure A3.7 for NOE/ROE correlation traces (slices)). Figure

3.3.2B-C for MK-2 in d_6-DMSO, NOE and ROE cross peaks indicate the H_w hydrogen interacts with H_q, H_r, H_y, and H_z. However, the lack of ROE cross peaks in Figure 3.3.2E shows H_w does not interact with H_y or H_z in d_5-pyridine (observed cross peaks between H_w and H_y or H_z in d_5-pyridine are likely due to TOCSY exchange). The observation of cross peaks show that there are similar interactions between the aromatic and alkene hydrogens in the two solvents; however, there is a twist around the C-C bond leading to closer proximity of the H_w with the H_q, H_r, H_x, and H_y hydrogens in d_6-DMSO. The NOE and ROE cross peaks in the d_6-DMSO spectrum in Figure 3.3.2 clearly supports a folded, U-shaped conformation for MK-2 in d_6-DMSO. However, evidence of a folded conformation for MK-2 is not as definitive in d_5-pyridine due to the lack of NOE and ROE cross peaks between H_w and H_y or H_z. If MK-2 did adopt a U-shaped conformation in d_5-pyridine, it would have a conformation as shown in Figure 3.3.3B, where the distance between H_w and H_y/H_z is beyond observation in the ^{1}H-^{1}H 2D NOESY and ROESY NMR experiment. This conformation for MK-2 in d_5-pyridine is based on other NOE/ROE cross peaks observed (i.e. H_w to H_h, H_w to H_q or H_r, H_w to H_x) Figure 3.3.2F illustrates π-π stacking between pyridine and part of the naphthoquinone ring, which could possibly explain the cross peak phase or lack of interaction between H_w and H_y or H_z.

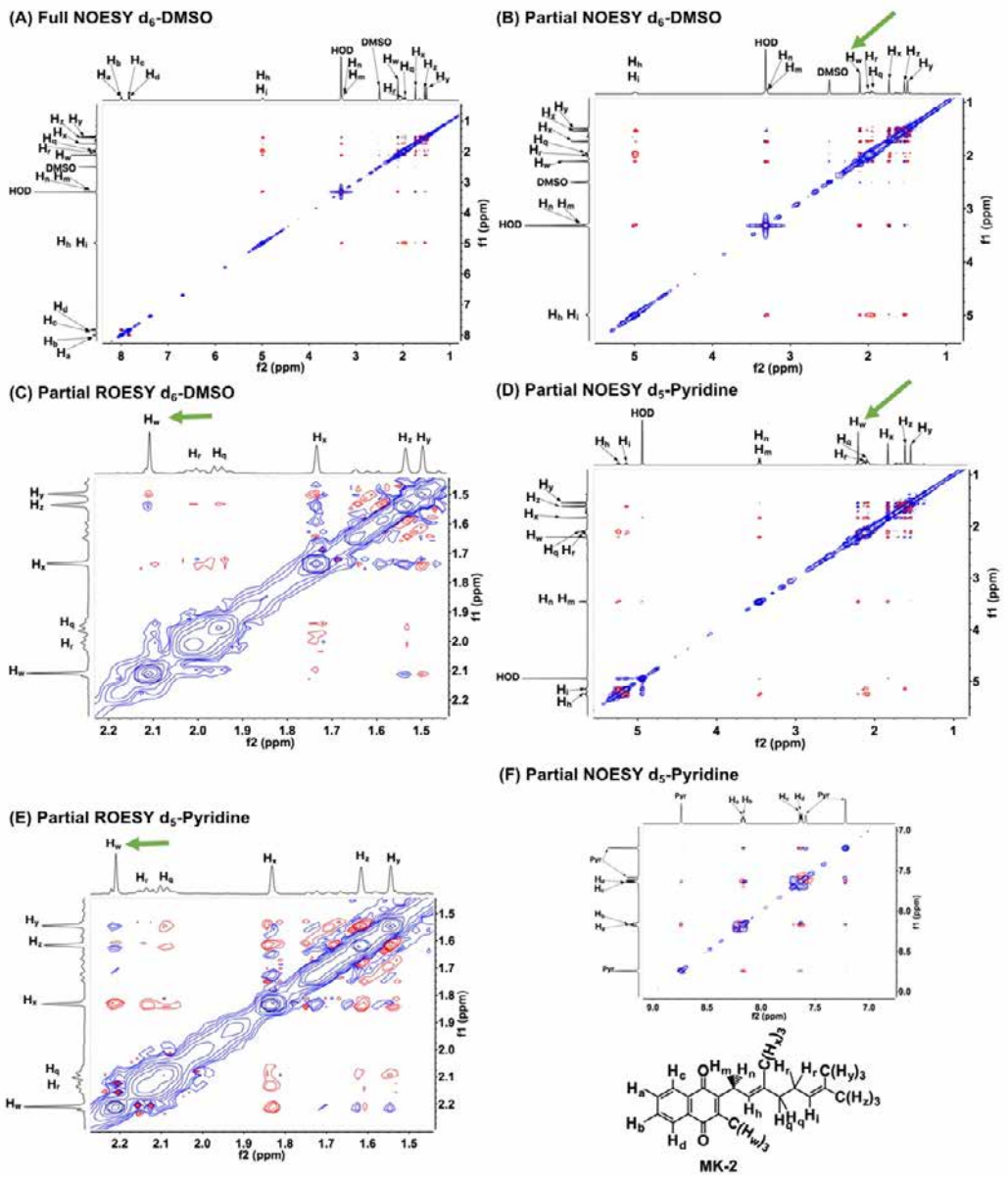

Figure 3.3.2. ^{1}H-^{1}H 2D NOESY and ^{1}H-^{1}H 2D ROESY NMR (400 MHz) spectra of 20 mM MK-2 in d_6-DMSO and d_5-pyridine at 26 °C. (A) Full ^{1}H-^{1}H 2D NOESY NMR spectrum of MK-2 in d_6-DMSO, (B) Partial ^{1}H-^{1}H 2D NOESY NMR spectrum of MK-2 in d_6-DMSO, (C) Partial ^{1}H-^{1}H 2D ROESY NMR spectrum of MK-2 in d_6-DMSO, (D) Partial ^{1}H-^{1}H 2D NOESY NMR spectrum of MK-2 in d_5-pyrdine, (E) Partial ^{1}H-^{1}H 2D ROESY NMR spectrum of MK-2 in d_5-pyrdine (F) Partial ^{1}H-^{1}H 2D ROESY NMR spectrum of MK-2 in d_5-pyridine illustrating stacking interactions. Blue intensity contours represent negative NOE's or ROE's and red intensity contours represent positive NOE's or ROE's. A standard NOESY pulse sequence was used consisting of 200 or 256 transients with 16 scans in the f1 domain using a 500 ms mixing time and 1.5 sec. relaxation delay. A standard ROESY pulse sequence was used consisting of 200 or 256 transients with 16 scans in the f1 domain using a 400 ms mixing time and 2.0 sec. relaxation delay. The structure of MK-2 is shown with a hydrogen labelling scheme key. Green arrows indicate hydrogen H_w, where the observed cross peaks differed the most between the two solvents studied.

3.3.3 Illustrating Menaquinone-2 Conformations using Molecular Mechanics

MK-2 has a short repeating isoprenyl chain (C_{10}) but enough carbons with numerous degrees of rotational freedom; therefore, even the truncated version of MK, MK-2, can assume many different conformations. Using molecular mechanics calculations, we explored the energy surface and visualized specific conformations defined by the ^{1}H-^{1}H 2D NOESY and ROESY NMR experiments of MK-2 in d_6-DMSO and d_5-pyridine. Specific conformations were generated based on distances imposed by the NMR spectral data and then energy optimized to produce realistic bond lengths and angles for these conformations. Finally, an energy was calculated to assure that the conformation was at a reasonable energy. Longer molecular mechanics calculations generally lead to rotations around bonds and conformations not exactly as those suggested from the NMR data (see below and Supporting Information). The intent with the molecular mechanics calculations was to illustrate conformations corresponding to the ^{1}H-^{1}H 2D NOESY and ROESY NMR spectral data in d_6-DMSO and d_5-pyridine constrained by all cross peak interactions observed as well as to provide visual aids (Figure 3.3.3). One of the low energy conformations generated for MK-2 has a conformation (Figure 3.3.3A, 66.8 kcal/mol, H_w-H_y: 2.6 Å) consistent with the NOESY and ROESY spectral parameters observed in d_6-DMSO. Figure 3.3.3B illustrates a potential conformation of MK-2 that is consistent with NOESY and ROESY spectral parameters observed in d_5-pyridine (66.7 kcal/mol, H_w-H_y: 6.1 Å). See Table A3.1 for selected hydrogen to hydrogen distances for conformations seen in Figure 3.3.3A-B consistent with 2D NOESY and ROESY NMR spectral parameters. The MK-2 conformation determined in d_6-DMSO adopts a folded, U-shaped conformation.

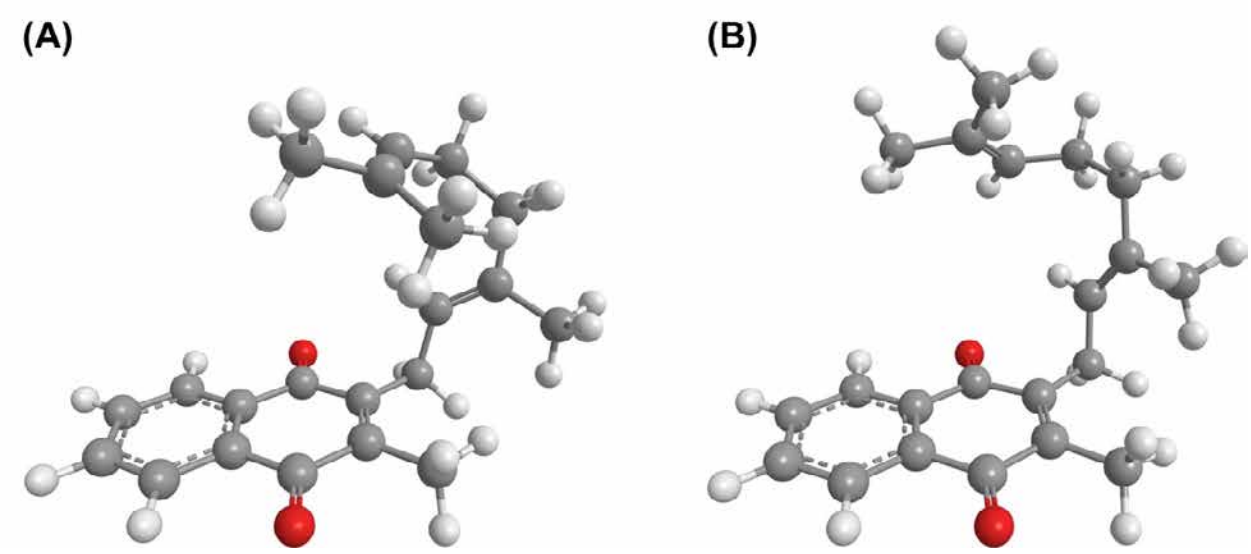

Figure 3.3.3. MK-2 conformations generated using MMFF94 calculations to illustrate the conformations elucidated by the NMR studies. (A) Illustrates the MK-2 conformation in d_6-DMSO determined from ^{1}H-^{1}H 2D NOESY and ROESY NMR spectral data cross peak interactions (66.8 kcal/mol, and internuclear distance H_w-H_y: 2.6 Å), (B) Illustrates a potential U-shaped MK-2 conformation in d_5-pyridine consistent with the ^{1}H-^{1}H 2D NOESY and ROESY NMR spectral data cross peak interactions (66.7 kcal/mol, and internuclear distance H_w-H_y: 6.1 Å). See Supporting Information for a table of selected hydrogen to hydrogen distances for conformations A and B.

Fewer NOE and ROE cross peaks were observed in d_5-pyridine that would indicate a folded conformation and although this does not preclude a U-shaped conformation, it does suggest that the H_w-H_y internuclear distance is longer and outside the observable range using the ^{1}H-^{1}H 2D NOESY and ROESY NMR experiment. We based this folded conformation off other NOE and ROE cross peaks observed, which were suggestive of folding (see Figure 3.3.2 and related discussion). However, a U-shaped conformation has been observed by NMR analysis in another aromatic solvent, d_6-benzene, for *n*-dodecane.[33] The U-shaped conformations shown in Figure 3.3.3 are representative of many possible stable conformations MK-2 could adopt. For comparison, Figure A3.10C shows another favorable conformation for MK-2 that has a characteristic U-shape. The energy of the conformation shown in Figure A3.10C was the lowest energy we found. This conformation was obtained by subjecting an extended MK-2 conformation to 10,000 iterations

followed by an energy minimization, illustrating that non-extended conformations are readily reached and energetically favorable.

Combined, the stability of the U-shaped conformations shown by these simple calculations are in line with work reported that showed ^{1}H NMR spectra of *n*-pentane and *n*-hexane measured in polar and spherical solvents such as DMSO favor *gauche* conformations as well as the reported U-shaped conformations of alkyl chains bound to synthetic receptors.[38-39, 47] The folded conformations demonstrated herein from experiment for MK-2 align with reported computationally determined conformations for MK analogs.[48] However, it is contrary to the general expectation that the all-*trans* conformations of alkanes or alkyl components are most stable.[8, 24-25, 27]

In addition to the U-shaped conformations seen in conformations A and B in Figure 3.3.3, a series of alternative conformations of MK-2 (Figure A3.10D-E) were also generated from the structures most often depicted by representations in the literature and then were energy optimized. Conformations D-H in Figure A3.10 were generated to compare these conformations energetically to the two U-shaped conformations shown in Figure 3.3.3A-B. The energies of conformations D-H in Figure A3.10 were all higher (~11 to ~23 kcal/mol) than the conformations found in d_6-DMSO, d_5-pyridine, and conformation C. Additional analysis of conformations and a table of selected internuclear distances of MK-2 conformations from Figure 3.3.3 and Figure A3.10 are given in Table A3.1.

Selected simple alkanes and a few other, more complex compounds with long alkyl-segments such as in polyenes and fatty acids report that the extended and folded forms are comparable in energy to the all-*trans* form.[28,29] The "pentane effect" for longer chains destabilizes the *trans*

conformations because of unfavorable g^+g^- arrangements, which increases the energy by ~0.55 kcal/mol with each kink in the chain.[28,29] In contrast, *gauche* arrangements are often energetically favored because of entropic contributions.[30-31] This is in part due to the spatial requirements that all molecules exert and can be justified using limited sphere-considerations.[32] *Gauche* arrangements tend to favor folded conformations where the degree of folding of *n*-alkanes (C_5-C_{32}) in solution depends on the strength of the dispersion force of the solvent[34] and the degree of folding increases with increasing chain length of the solute.[33, 35] Other molecules that contain alkyl chains such as fatty acids and polyethylene derivatives have also been reported as either extended chains or in folded conformations depending on physical and environmental conditions.[30-31, 36-37] Conformational analysis of long chain allylic polyunsaturated fatty acid chains using Hartree-Fock calculations showed that conformational differences between the all-*trans* and helical folded structures are only a few kcal/mol.[36] Ultimately, there are a few but strongly convincing examples[29, 38-41] that folded and/or U-shaped conformations are likely to become much more important than have been recognized previously. The studies presented herein represent a new class of compounds that adopt a U-shaped conformation, illustrating that these folded conformations are likely to be important and may impact the biological function of these lipoquinone systems. It is very important to recognize the molecular plasticity, which allows the alkyl chain to assume shapes depending on the complementary structures or influences of the immediately surrounding environment.

3.3.4 Electrochemistry of Menaquinone-2 in Different Organic Solvents

Our interest in these systems relates to the fact that the redox potential of MK is important in shuttling electrons between protein complexes. Although the focus of this chapter thus far has

been on the conformations of these compounds, we are particularly interested in redox properties because we are aiming to investigate the function and reactivity of these systems as well. For MKs to carry out this process, MKs must associate with the transmembrane proteins involved in the electron transfer processes.[49] The electron transfer processes all take place within or near the membrane interface with two one electron reduction processes sequentially forming the radical anion (semiquinone) and then the dianion.[50-52] Even though there has been many reports in literature on the redox potentials of MK derivatives, the origin of these changes are not well understood.[50-52] These processes are particularly poorly understood when the quinones are present in a hydrophobic molecule that is entirely or partly located in the membrane of a biological system. Although, it is premature to correlate conformation with redox potential, we are seeking systematic information where redox potentials and conformations are known (i.e. within different organic solvents) and the electrochemical data on this system becomes an important frame of reference because the conformational analysis has been carried out. We hypothesized that the redox potential of MK-2 will vary based on organic solvent environment. Although this hypothesis would be anticipated to be confirmed, it is important to measure how and if the magnitude of the redox potential changes as the solvent environment changes because the function of MK-2 is tied to the redox potentials. Initially, redox studies were planned to be carried out in DMSO, acetonitrile, and benzene; however, because of low solubility of all of the electrolytes examined in benzene, benzene was replaced with pyridine as a representative aromatic solvent.[53] The electrolyte tetrabutylammonium perchlorate (TBAP) was chosen because 1D ^{1}H NMR studies showed that the addition of TBAP to MK-2 solutions (solvents: d_6-DMSO, d_5-pyridine, d_3-acetonitrile) did not affect the observed chemical shifts of the MK-2 hydrogens and

thus no evidence for artifacts due to ion pairing would be observed (see Supporting Information for further description of the electrochemical analysis, and for MK-2/TBAP NMR studies).

MK-2's first electrochemical potential is the one electron reduction of the quinone to semiquinone ($Q/Q^{\bullet -}$) and the second is the one electron reduction of the semiquinone to the dianion ($Q^{\bullet -}/Q^{2-}$), (see Supporting Information).[50-52] The cyclic voltammogram's (CVs) of MK-2 and an internal standard of ferrocene (Fc^{+}/Fc) in the three solvents are shown in Figure 3.3.4. The $Q/Q^{\bullet -}$ $E_{1/2}$ vs Fc^{+}/Fc for MK-2 in DMSO, CH_3CN, and pyridine were measured to be -1.155 (±0.001) V, -1.230 (±0.003) V, and -1.331 (±0.001) V, respectively. As shown in Figure 3.3.4, we included the Fc^{+}/Fc reference in the data presented. These results are consistent with $Q/Q^{\bullet -}$ $E_{1/2}$ vs Fc^{+}/Fc values given for 1,4-naphthoquinone.[50, 54] The values determined experimentally for $Q^{\bullet -}/Q^{2-}$ $E_{1/2}$ vs. Fc^{+}/Fc for MK-2 in DMSO, CH_3CN, and pyridine were measured to be -1.863 (±0.008) V, -1.902 (±0.012) V, and -2.075 (±0.003) V, respectively (see Supporting Information). In Figure 3.3.5, the half-wave potentials are plotted showing the trend that both redox processes are more readily reduced in DMSO than CH_3CN or pyridine similar to the trend observed in literature for 1,4-napthoquinone potentials.[54]

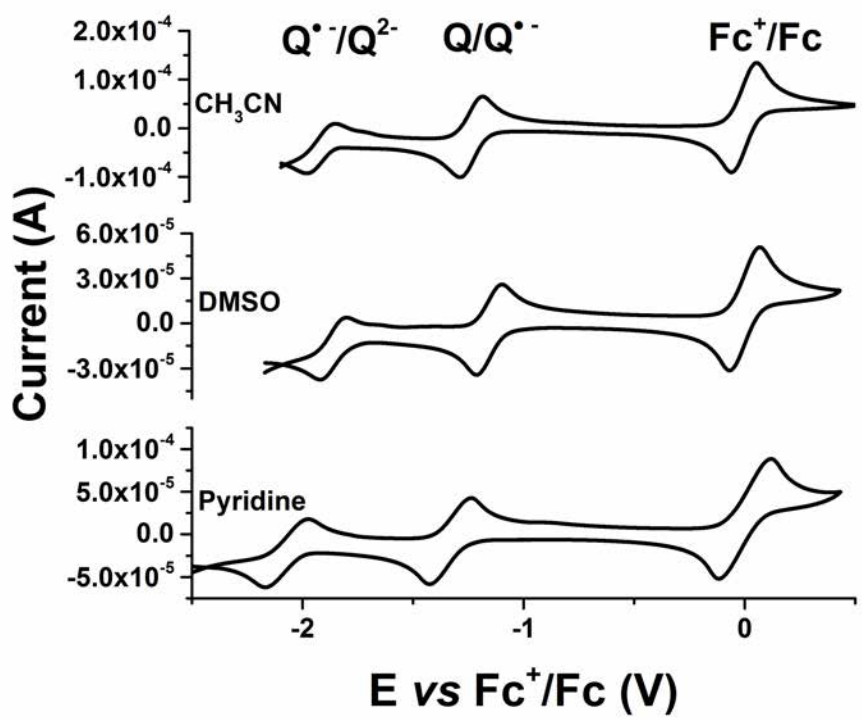

Figure 3.3.4. Three representative cyclic voltammogram's (CVs) of 2 mM MK-2 in CH_3CN, DMSO, and pyridine. The potentials are referenced to the Fc^+/Fc couple (2 mM) determined in each solvent. From left to right, redox processes are $Q^{\bullet-}/Q^{2-}$, $Q/Q^{\bullet-}$, and Fc^+/Fc. Each sample has 0.1 M TBAP and was degassed with argon gas for 10 minutes at ambient room temperature before spectra were recorded. Current sweeps are in the anodic direction from -2V to 1V and back to -2V. A 100 mV scan rate was used.

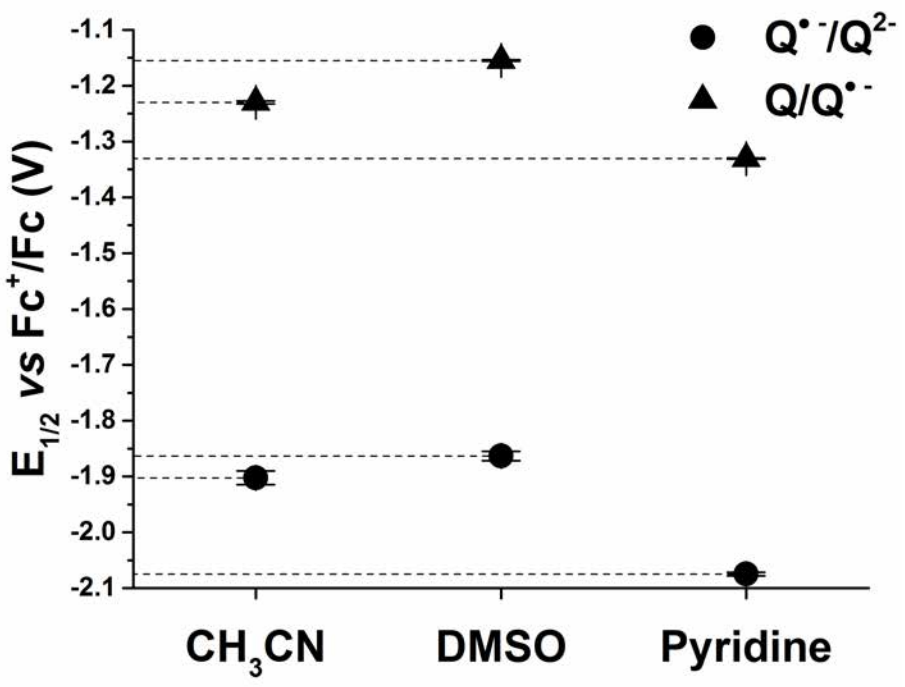

Figure 3.3.5. Measured $E_{1/2}$ (*vs* Fc^+/Fc in V) of MK-2 $Q/Q^{\bullet-}$ and $Q^{\bullet-}/Q^{2-}$ redox processes versus solvent. Added lines show the distinction between each solvent for each redox process. Each solvent was run in triplicate with error bars shown as standard deviations. Statistics were performed using a Student's *t* test that indicated the half wave potentials of each redox process are significantly different in each solvent ($p<0.01$ for $Q^{\bullet-}/Q^{2-}$ CH_3CN-DMSO and $p<0.0001$ for all other comparisons). See Supporting Information for details.

In summary, during the first electrochemical process producing the semiquinone, MK-2 has the most positive potential in DMSO and the most negative potential in pyridine, showing MK-2 is slightly more reducible in DMSO than pyridine or CH_3CN. The observation of differing redox potentials between organic solvents supports the second hypothesis that the redox potential of MK-2 is influenced by the specific organic solvent, where a contributing factor to the observed changes is due to the differences between the dielectric constant of each solvent. The different organic solvents influence the observed redox potential of MK-2 and from the 2D NMR studies on the conformation of MK-2, slight differences in conformation were observed, which may suggest that a combination of solvent effect and conformational differences of MK-2 may affect redox potential.

3.3.5 Interaction of Menaquinone-2 with Langmuir Phospholipid Monolayers

The physiologically relevant environment for MKs is in association with membranes; therefore, we also studied the interaction of MK-2 with a more direct model membrane interface, a phospholipid monolayer. Several membrane models exist including Langmuir monolayers, liposomes, micelles, and reverse micelles (RM) (Figure 3.3.6).[46, 55-60] Each model system has advantages and disadvantages, and we have chosen to investigate the phospholipid monolayer because of their direct association with a cellular membrane and the RM system because RMs allow for molecular placement of MK-2 with regard to the interface.[46, 55-60]

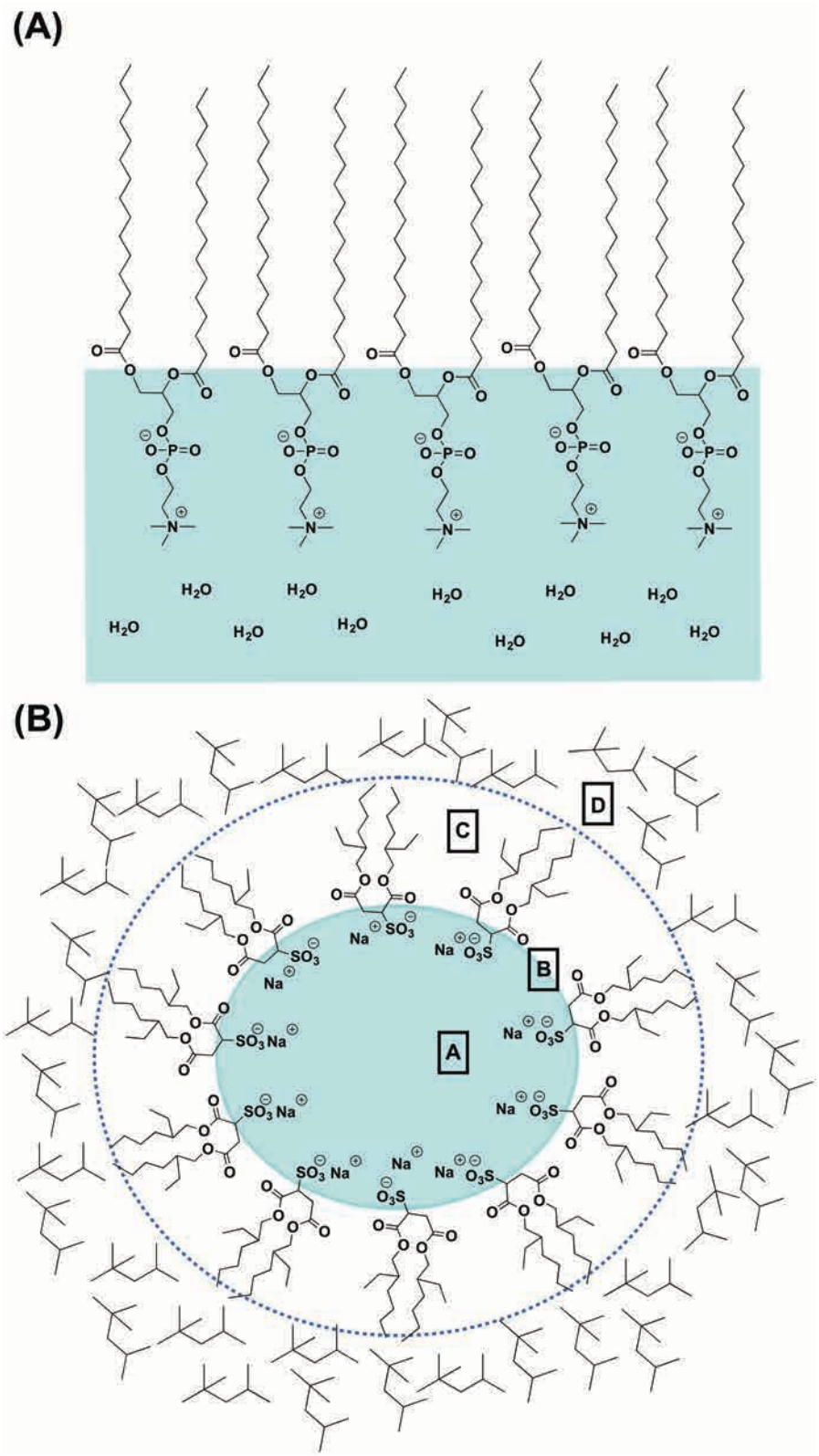

Figure 3.3.6. Schematic diagram of (A) a Langmuir phospholipid monolayer and (B) a RM present in a microemulsion. Labelling for the RM is as follows: (A) the water pool, (B) the Stern layer, (C) the hydrophobic surfactant tails, and (D) the organic solvent, isooctane.

First, we describe our studies with Langmuir monolayers[46, 60] consisting of phospholipids to gain insight into the interactions between two classes of phospholipids (dipalmitoylphosphatidylcholine (DPPC) or dipalmitoylphosphatidylethanolamine (DPPE)) and MK derivatives. These studies will demonstrate how the phospholipid packing is affected by the presence of MK derivatives as it interacts with the phospholipid interface (Figure 3.3.7A).[60-64] Due to the low solubility of MK-2 in aqueous environments, the Langmuir monolayer studies involve experimental protocols used for other materials with low solubility in water, such as UQ.[65-66] Figure 3.3.7 shows the change in surface pressure as a function of area per molecule of DPPC or DPPE in the presence of various amounts of MK-2. The resulting compression moduli as functions of surface pressure are shown in the Supporting Information.

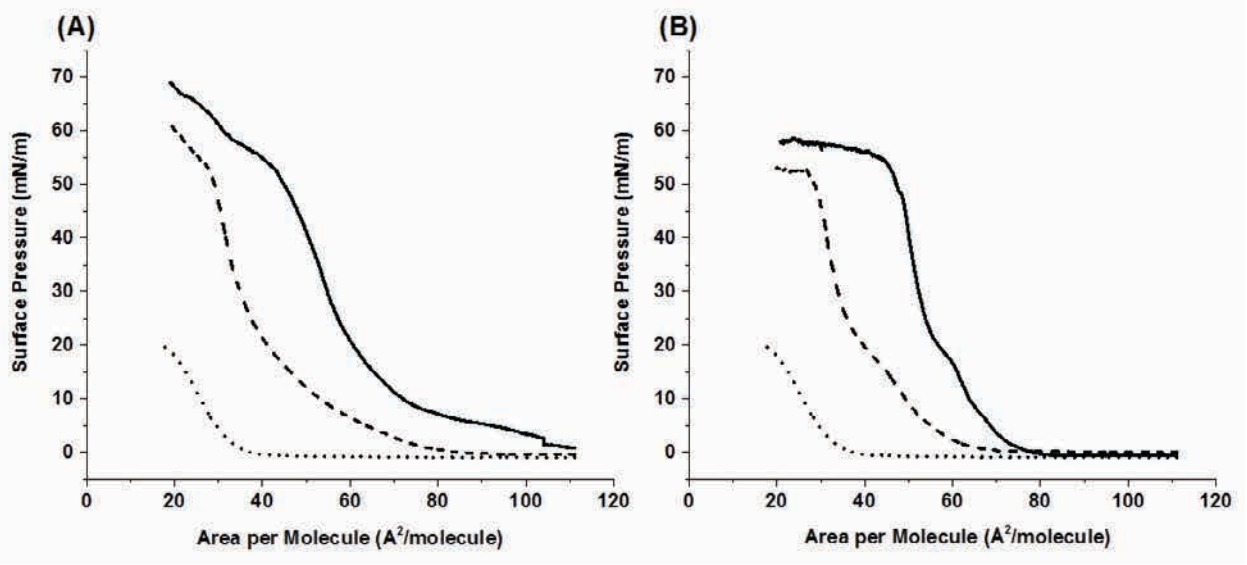

Figure 3.3.7. Compression isotherms of MK-2 films (dotted lines), DPPC or DPPE phospholipid films (solid lines), or a 50:50 mixture of MK-2 and phospholipid (dashed line). On the left (A) are the resulting compression isotherms of MK-2 and DPPC, while on the right (B) are the resulting compression isotherms of MK-2 and DPPE.

The compression isotherm of DPPC shows a transition at ~8 mN/m and both DPPC and DPPE collapse at ~55 mN/m similar to findings reported in literature.[67] The compression isotherm of

the 1:1 mixture of DPPC and MK-2 shows a disappearance of the gas to liquid phase transition at 8 mN/m, suggesting there is a condensing effect of MK-2 with DPPC at a high area per molecule/low surface pressure. Moving to DPPE, the 1:1 mixture of MK-2 with DPPE reduces the collapse pressure of the film to 50 mN/m showing destabilization of the DPPE film. The pure MK-2 films had limited stability shown by a maximum surface pressure of ~20 mN/m. This result suggests MK-2 forms a less stable film than the phospholipids.[65-67] To understand the interactions of MK-2 with DPPE and DPPC further, the compression moduli were calculated using eq. (4) (see Supporting Information) where the compression modulus is the measure of the compressibility of the film.

Our results are interpreted as MK-2 having a condensing effect on DPPC phospholipid films at high area per molecule/low pressure and destabilization of DPPE phospholipid films. The resulting mixed films (DPPC/MK-2 or DPPE/MK-2) were also consistent with reported UQ suggesting similar trends where UQ was shown to be "squeezed" out of the phospholipid interface.[65-66, 68] In summary, MK-2 has a condensing effect on DPPC phospholipid films, a destabilization of DPPE phospholipid films, and is most likely compressed out of the phospholipid film similar to UQ.[65-66, 68] Unfortunately, these studies do not directly show whether a folded or extended conformation of MK-2 exists. A folded conformation occupies a larger volume than the extended conformation, which would affect packing within the phospholipid interface. Our studies do demonstrate that MK-2 interacts with the phospholipid model membrane interfaces of DPPC and DPPE even above physiologically relevant pressures. It is possible that the observation of the destabilization of the DPPE phospholipid films (not observed for DPPC) by the

presence of the MK may suggest a folded MK-2 conformation that does not fit in the organization of the DPPE film (possibly related to packing of the phospholipid).

3.3.6 1D ^{1}H NMR Spectroscopic Studies of Menaquinone-2 in Reverse Micelles

One of our ultimate objectives was to characterize the molecular details of MK-2's association with membrane-like interfaces. This characterization includes determining the location and conformation of MK-2; therefore, the RM model system was investigated (Figure 3.3.6B).[60-64, 69] In the RM, a ternary microemulsion system forms when a surfactant is dissolved in an organic solvent and the addition of water creates nano-sized water droplets encased in surfactant.[56, 62, 64, 69-71] This dynamic, yet simple, model can provide molecular detail on location and conformation of MK at an interface using NMR spectroscopy, whereas the use of phospholipids such as DPPC have overlapping hydrogen signals with key MK hydrogen signals making interpreting conformational information very complex.[69, 72-75] RM systems provide information regarding the location, conformation, and physical interactions of MK with lipid films and potentially membranes, which allowed us to examine our third hypothesis that the membrane interface influences the conformation of the MK derivative.

To explore the location of MK-2 at a lipid/water interface further, studies were conducted using a simple microemulsion interfacial system, which allows for identification of molecular placement. Figure 3.3.8 shows a stack plot of 1D ^{1}H NMR spectra for the aromatic hydrogens (H_a/H_b and H_c/H_d) of MK-2 in solutions of D_2O, isooctane, or isooctane solutions of MK-2 containing RMs (D_2O/AOT/isooctane microemulsions) of various sizes (w_0: 4, 8, 12, 16, and 20 where w_0=[D_2O]/[AOT]) and for comparison with an empty AOT/isooctane RM. The aromatic MK-2 hydrogens in the AOT/isooctane RMs are similar to the signals observed in isooctane but very

different from the signals observed in D_2O. The distance between H_a/H_b and H_c/H_d is 0.52 ppm in isooctane, 0.47 ppm in the RM, and 0.27 ppm in D_2O. This suggests that the environment of the MK-2 hydrogens in the AOT/isooctane RMs is more like an environment in isooctane than D_2O, where MK-2 is no longer in isooctane but associating with the AOT molecules. The signals from the H_c/H_d hydrogens in the AOT/isooctane RMs do change slightly as the RM size increase or decreases. This observation is also consistent with MK-2 penetrating and residing in the interface.

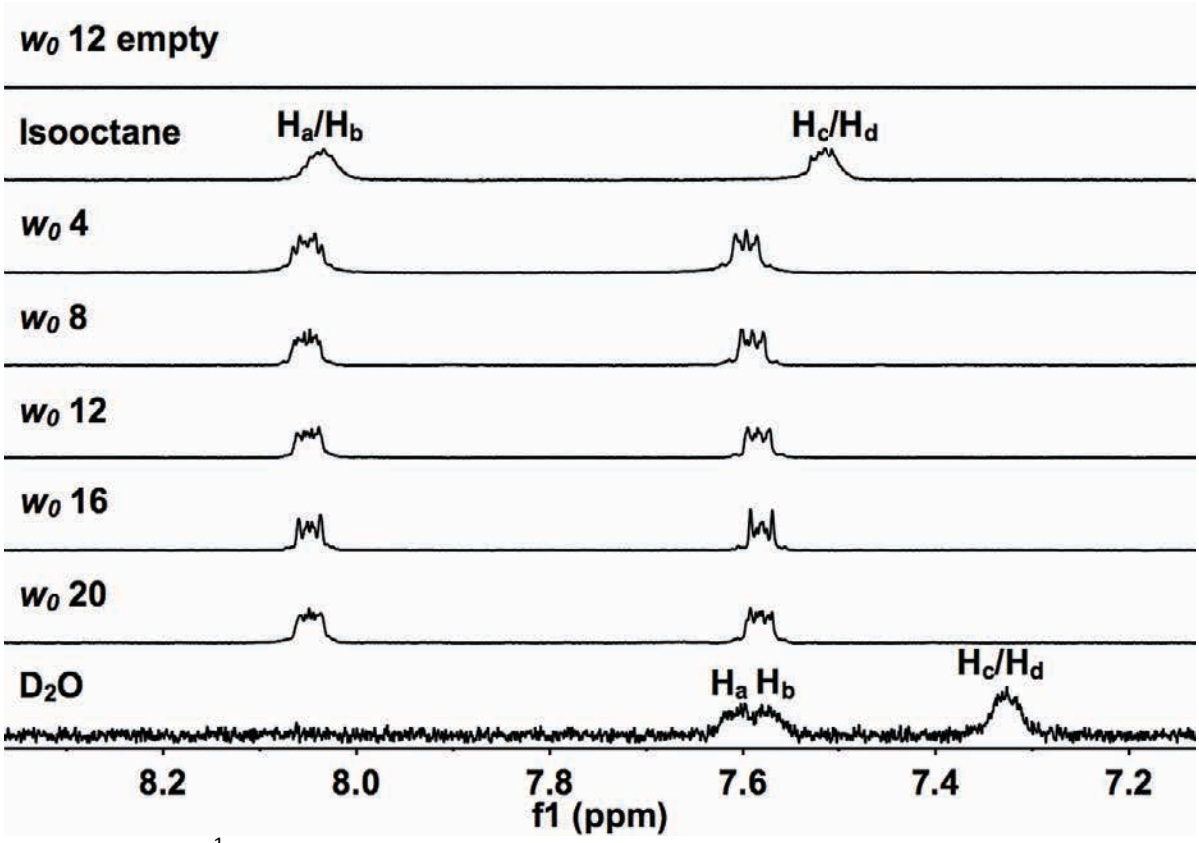

Figure 3.3.8. 1D ^{1}H NMR (400 MHz) spectra of MK-2's aromatic hydrogens, H_a, H_b, H_c, and H_d in D_2O, isooctane and different sized RMs. Hydrogen peak text labelling corresponds to MK-2 hydrogen labelling scheme key found in Figure 3.3.2 H_a, H_b, H_c, and H_d hydrogens undergo a chemical shift upon inclusion inside RMs.

To verify that the RMs formed in the samples used and that the properties of the samples are consistent with previous studies[46, 62, 69, 76-77], Dynamic Light Scattering (DLS) experiments were carried out. These studies confirmed the formation of RMs, and that the RM did not change

significantly upon the addition of MK-2. This was carried out by measuring the sizes in the presence and absence of MK-2 and confirming that the size was as those reported previously (data not shown).[62] Overall, these results are consistent with MK-2 penetrating the RM model membrane interface; however, 2D studies are described below to get more information regarding the placement and conformation of MK-2 within the RM system.

3.3.7 ^{1}H-^{1}H 2D NOESY and ROESY NMR Spectroscopic Studies of Menaquinone-2 in a Reverse Micelle Model Membrane System

To provide further evidence regarding the location, orientation, and conformation of MK-2 within RMs, we obtained the ^{1}H-^{1}H 2D NOESY NMR spectrum and the ^{1}H-^{1}H 2D ROESY NMR spectrum of MK-2 in a w_0 12 RM, Figure 3.3.9 and Figure 3.3.10. Figure 3.3.9 shows a partial ^{1}H-^{1}H 2D NOESY and ROESY NMR spectra indicating both AOT and MK-2 hydrogens, whereas Figure 3.3.10 focused in on selected hydrogen interactions specifically in the NOESY spectrum (see Figure A3.8-9 for full spectra). Figure 3.3.10A shows cross peaks between the aromatic H_a/H_b and H_c/H_d and parts of the AOT CH_2 and CH_3 tail groups (i.e. H8′ and H10′ hydrogens, see Figure 3.3.11 for AOT hydrogen labeling key). Figure 3.3.10B shows cross peaks between alkene hydrogens, H_i and H_h, with HOD and AOT's H1, H1', H3, and H3' hydrogens and only evidence of a weak interaction between MK-2 and isooctane. These interactions are consistent with placement of MK-2 between the AOT tails as shown using a depth perception drawing in Figure 3.3.11.

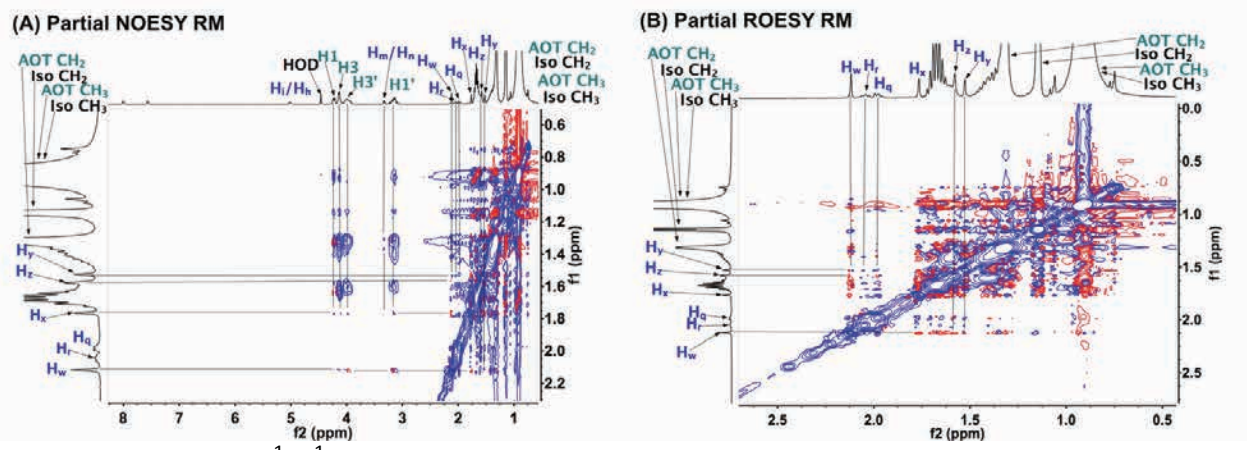

Figure 3.3.9. Partial ^{1}H-^{1}H 2D NOESY and ROESY NMR (400 MHz) spectra of MK-2 inside w_0 12 RM at 26 °C. (A) Partial ^{1}H-^{1}H 2D NOESY NMR spectrum in w_0 12 RM and (B) Partial ^{1}H-^{1}H 2D ROESY NMR spectrum in w_0 12 RM. Blue to blue hydrogen text labelling shows MK-2 to MK-2 interactions, teal to teal hydrogen text labelling shows AOT to AOT interactions, and blue to teal hydrogen text labelling shows MK-2 to AOT interactions. Blue intensity contours represent negative NOE's or ROE's and red intensity contours represent positive NOE's or ROE's. A standard NOESY pulse sequence was used consisting of 256 transients with 16 scans in the f1 domain using a 200 ms mixing time and 1.5 sec. relaxation delay. A standard ROESY pulse sequence was used consisting of 256 transients with 16 scans in the f1 domain using a 200 ms mixing time and 2.0 sec. relaxation delay. See Figure 3.3.2 for MK-2 hydrogen labelling scheme key and Figure 3.3.11 for AOT hydrogen labelling scheme key.

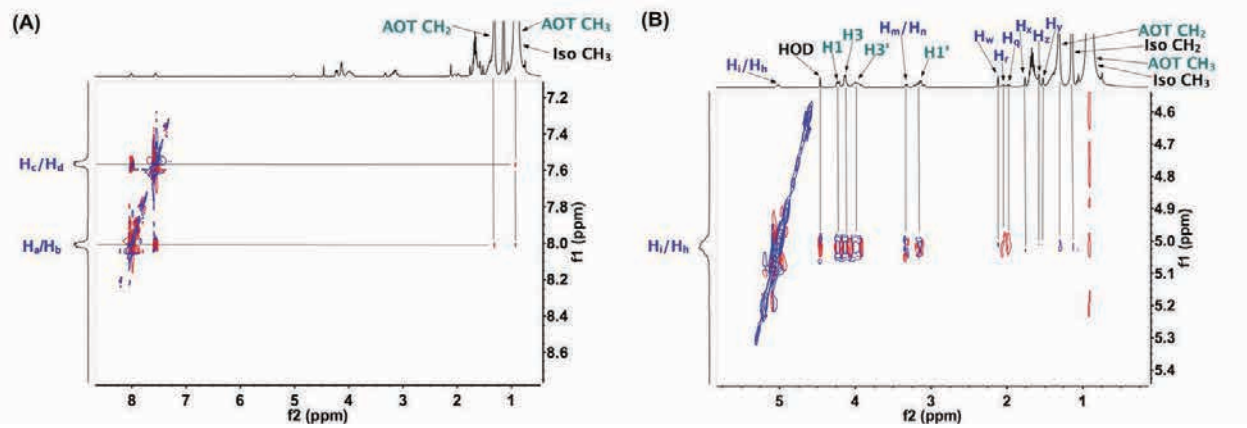

Figure 3.3.10. Partial ^{1}H-^{1}H 2D NOESY NMR (400 MHz) spectra of MK-2 inside w_0 12 RM at 26 °C illustrating interactions of MK-2 with the AOT surfactant tails. (A) Interactions between MK-2's aromatic hydrogens and AOT. (B) Interactions between MK-2 alkene hydrogens and AOT. The blue hydrogen text labelling shows MK-2 to MK-2 interactions, teal hydrogen text labelling shows AOT to AOT interactions and blue to teal hydrogen text labelling shows MK-2 to AOT interactions. Blue intensity contours represent negative NOE's and red intensity contours represent positive NOE's. A standard NOESY pulse sequence was used consisting of 256 transients with 16 scans in the f1 domain using a 200 ms mixing time and 1.5 sec. relaxation delay. See Figure 3.3.2 for MK-2 hydrogen labelling scheme key and Figure 3.3.11 for AOT hydrogen labelling scheme key.

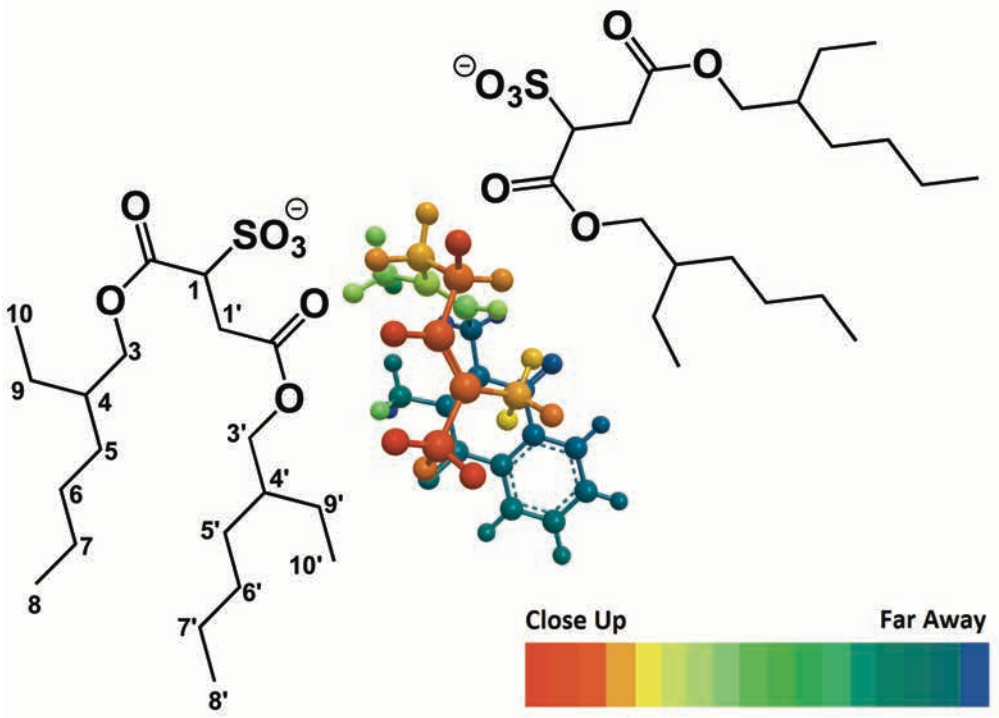

Figure 3.3.11. Illustration of MK-2's proposed folded, U-shaped conformation and placement in the RM interface. This arrangement is consistent with ^{1}H-^{1}H 2D NOESY and ROESY NMR spectral data obtained in w_0 12 RM; however, MK-2 likely tumbles freely within the interface but maintains interactions with the region of AOT shown in the illustration. Color depth fading legend shows dark red as closer in distance and dark blue as farther in distance from the reader. AOT hydrogen labelling scheme key is shown.

Regarding the conformation of MK-2 associated with the RM water-interface, the NOE and ROE cross peaks in Figure 3.3.9 show interactions between H_w and H_z/H_y and between H_w and the alkene hydrogens, H_h/H_i, which is consistent with a folded, U-shaped conformation. In the proposed conformation, the C2-C6 atom to atom distance in MK-2's isoprenyl side chain was found to be 3.6 Å, which is consistent with a U-shape (g^+g^- conformation, Figure 3.3.12) for MK-2 placed at the RM interface (see Supporting Information for further discussion and internuclear distances of different MK-2 conformations). An illustration of an MK-2 conformation consistent with these observations is shown in Figure 3.3.12. This U-shaped conformation observed when MK-2 is associated with the RMs changed slightly from that observed in d_6-DMSO regarding

where the double bond overlaps with the naphthoquinone moiety. The overlap of the alkene and naphthoquinone functionalities in the conformation associated with the interface is best illustrated by the top view in Figure 3.3.12B. Importantly, the U-shape fold remains, but slight rotation around the C-C bond facilitates the conformational changes in the U-shape.

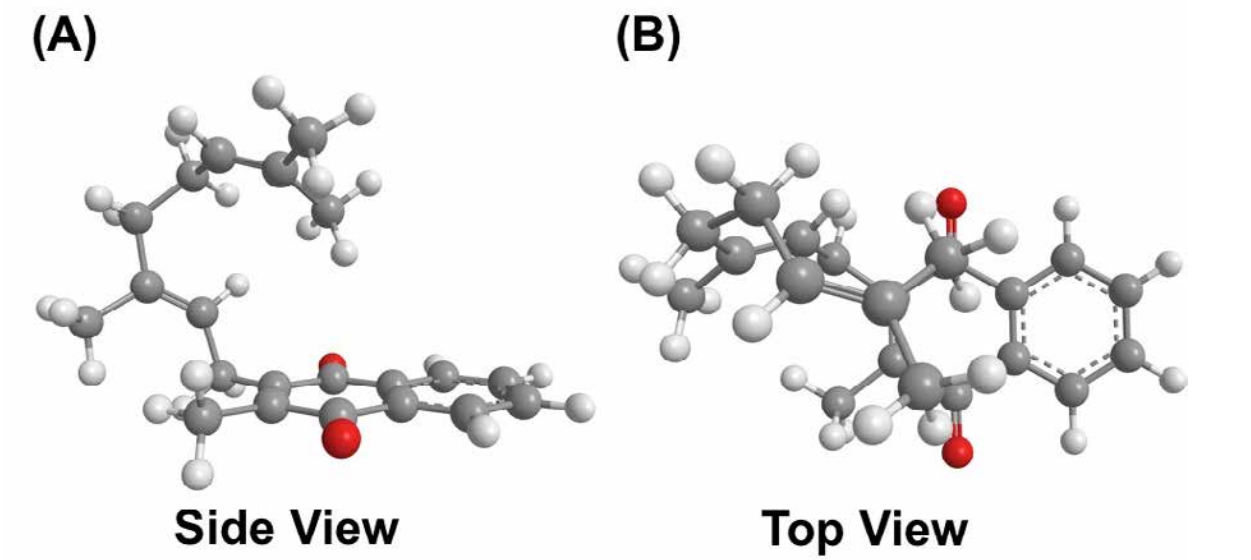

Figure 3.3.12. MK-2 conformation at an interface visualized using Merck Molecular Force Field 94 (MMFF94) calculations. Molecular mechanics simulations generating the 3D conformation of MK-2 in a RM that is consistent with ^{1}H-^{1}H 2D NOESY and ROESY NMR spectral data. (A) Side view of energy minimized conformation (63.5 kcal/mol, and internuclear distance H_w-H_z: 4.0 Å) showing MK-2's isoprene chain adopting a hook-like shape also known as a folded, U-shaped conformation. (B) Top view of energy minimized conformation showing the terminal isoprene methyl-groups overlapping the carbonyl groups on the naphthoquinone.

3.3.8 Implications of Folded Conformations for Menaquinone Derivatives

Natural MKs contain a naphthoquinone and an isoprenyl side chain with some variable number of repeating isoprene units, where MKs support the electron transfer reactions in a range of systems.[7, 42] MK-2 was synthesized allowing for detailed characterization of the molecule. The results presented here for MK-2 suggests that other important MK derivatives in biology will

adopt folded conformations as well and demonstrates the need to prepare and study such derivatives both experimentally and computationally.

The extended conformations of long chain biological molecules such as fatty acids and polyenes are generally shown in the literature if the structure is presented.[8, 24-25] However, a few studies of isoprene conformers and 1,3 acyclic dienes show the extended *trans* alkane conformations compare in energy with folded or helical conformations.[78-79] Although the folded conformations in those studies may be slightly higher in energy than unfolded conformations, the difference is surprisingly small. The C-C single bond lengths reported for stearic acid decreases under high pressure.[41] These bond shrinkages cause conformational and shape changes in stearic acid favoring folded conformations.[41] Previous studies using high temperature UV-absorption spectroscopy, molecular orbital calculations, and gas-phase electron diffraction found that isoprene and chloroprene conformations did, in fact, favor folded conformations.[80-81] Although these conditions are non-physiological, they do demonstrate that changes in a physical parameter can affect the preferred conformation. Previous work has been carried out with fatty acids where the experimental studies showed that the conformations of the alkane portion of the fatty acids can and do change similar to conformations of MK-2 as shown in this work.[36] Our studies confirm the first hypothesis that MKs have different conformations depending on specific environmental conditions, which was achieved by first synthesizing MK-2 and then demonstrating that a U-shaped, folded conformation was adopted in d_6-DMSO, which was different from the conformation in d_5-pyridine.

Conformations can affect reactivity, and as in this case, the electron transfer reactions facilitated by MK. MK forms complexes with several enzymes during the electron transfer

processes, and although kinetic characterization of these systems have been reported,[82-84] less is known structurally. The redox potentials of MK-2 depicted in Figure 3.3.4-5 illustrate the trend where the most positive potential is in DMSO and the most negative potential is in pyridine, which agrees with literature reports on menadione.[50, 54] These results have identified that the redox potential of MK-2 changes as a function of solvent, and the origin of this change (presumably in part due to a change in dielectric constant between solvents) and whether these observed solvent effects can be associated with changes in conformation should be investigated in the future using both suitable high level computational methods as well as electrochemistry. Indeed, the change in redox potential is likely to be important, and since there is no conjugation between the isoprenyl side chain and naphthoquinone, these effects are very interesting and may reflect that the energy required for the reduction is determined by the energy difference of the HOMO-LUMO gap in the two different conformations.[85] Orbital analysis of the HOMO-LUMO gap could potentially be informative and describe the origin of the observed varied biological effects of a series of N-alkyl MK derivatives that have been reported.[86-87] For example, replacement of a CH_2 group with a N-atom modifies the parent system creating a class of compounds with a nitrogen bound directly to the "naphthoquinone group." These molecules have dramatically different biological properties than the parent MK derivatives[86-87] and it is possible that these activities could be related to the change in fundamental physical and chemical properties that occurs with N-alkyl isoprenoid substitution of the naphthoquinone ring. Combined, these results confirm the second hypothesis that the redox potential of MK-2 is influenced by organic solvent environment, which is likely to be important for understanding the mechanistic details in MK metabolism.

The third hypothesis involved determining if the association of MK with the membrane interface influences the conformation of the MK derivative. We investigated the interaction of MK-2 with a phospholipid Langmuir monolayer, which is a simple 2D model of a single leaflet of a cell membrane.[59, 88-89] The fact that MK-2 interacts with the phospholipid monolayer is consistent with the expected MK affinity for the hydrophobic phospholipids that make up the cell membrane. Langmuir monolayer studies support interaction of MK-2 with the phospholipid monolayer interface; however, the lipoquinone is likely pushed out of the interfacial portion of the phospholipid monolayer into the more hydrophobic alkyl tail groups on the top of the monolayer as the pressure increases. Unfortunately, Langmuir phospholipid monolayer studies could not determine the conformation of MK-2; however, the RM surfactant interface complements studies with the phospholipid monolayer interface. The question of folding was further investigated by combining ^{1}H NMR spectroscopic studies of MK-2 in organic solution and in a simple model membrane system, RMs. The conformation of MK-2 was characterized in organic solvents and was found to differ slightly from the conformation when it was associated with the surfactant interface within RMs. It is to be expected that MK-2 would have an affinity for the interface because of its hydrophobicity, which agrees with results observed in the RM system. The RM interface is known to be penetrated by water molecules and thus less packed than a biological membrane, and therefore has a lower interface pressure meaning MK-2 is unlikely to be squeezed out once inside.[62, 69, 90] The ^{1}H NMR spectroscopic studies in RMs allowed us to observe the association of MK-2 with the interface molecules as well as with itself in its folded state. The ^{1}H-^{1}H 2D NOESY and ROESY NMR spectral data indicates that the U-shaped conformation of MK-2 (Figure 3.3.12) remained intact while associating with the RM model

membrane interface; however, the overlap between the alkene and the naphthoquinone varies with the specific environment. The small changes in the U-shaped conformation document the environmental influence on the conformational folding of MK-2. These results are very important because they document the possibility that MK derivatives in the cell membrane environment may be folded and if so, such folds will impact the interaction with proteins in the ETS and affect reactivity and function.

Naturally occurring lipoquinones are characterized by the presence of an isoprenyl side chain of varying length and degree of saturation depending on the species of origin. MK-2's isoprenyl side chain is shorter than most lipoquinones involved in electron transport; therefore, it may not fully mimic the interactions generated by MK derivatives with longer isoprene chains with the membrane or the enzyme systems. However, these results show that the folding of MK-2 is very important and may suggest that MK derivatives with the longer isoprenyl side chains may adopt folded conformations as well. Understanding how MK-2 and other MK derivatives fold in a hydrophobic environment is critical to gauge how these molecules will behave within a biological membrane associated with the ETS. Folded MK conformations may be important for substrate recognition by respiratory enzymes within the ETS.

Investigation of the conformation of a particular MK derivative's location and conformation will also allow for a more realistic interpretation of data obtained with the novel fluorogenic probe, a vitamin K analog, reported to fluoresce after reduction to the quinol.[91] Studies with this new probe may help provide information on the role that vitamin K plays in key redox processes. Accurate information obtained from the use of this probe would provide better quality data regarding photosynthesis and cellular respiration and future consideration of MK derivatives

location and conformation will be important for proper interpretation of the results obtained from the use of this probe.[91]

3.4 Summary and Conclusions

Conformations exhibited by alkanes and alkenes are essential for explaining trends in reactivity and manifestation of physical properties but little is understood regarding biological systems with hydrophobic small components containing alkyl-segments. The studies presented in this chapter describes the chemical and biochemical properties of MK, which is an essential component of the ETS in many Gram-positive bacteria, including pathogens such as *M. tuberculosis*, *Mycobacterium leprae*, and *Staphylococcus aureus,* to name a few. We report for the first time in this class of molecules that MK-2 adopts a folded, U-shaped conformation in organic solution. The specific nature of the conformation varied within different organic solvents and thus confirmed our first hypothesis that MK-2 conformations are very sensitive to their environment. These findings contrast with the simple, extended conformation represented in textbooks and the literature that is shown for MK derivatives as well as the more common "Q", belonging to the UQ family of lipoquinones.

The change in the observed redox potentials of MK-2 with different organic solvents confirmed our second hypothesis. This is important for future studies probing the function of the substrate and potential correlation between conformation and redox potential of MK derivatives and although most of the studies in this chapter are of a structural nature, it is important to recognize that the function is likely related to the conformation of the MK-derivative. The discovery that MK-2 adopts a folded conformation may suggest that other MK derivatives will have similar conformations, which ultimately will impact all the biological systems in which MKs

have a role such as within the ETS in specific Gram-positive bacterial pathogens. The result of a stable U-shape conformation in solution and within an interface is important as little information is available on these essential hydrophobic biological components.

Although the NMR spectral data illustrated using molecular mechanics allowed for the conclusion that MK-2's conformation is environment dependent, it was important to investigate if this U-shaped conformation remained at a membrane like interface. We used two membrane model systems to investigate this question. The more physiologically relevant DPPC/DPPE phospholipid monolayers confirmed that MK-2 interacted with the phospholipid interface similar to UQs; however, the conformation of MK-2 remained unspecified. Complementary studies using the AOT-RM model membrane system allowed determination of the molecular location of MK-2 as penetrating the water-surfactant interface as well as the conformation of MK-2 within the RM interface. We found that the folded, U-shaped conformations observed in organic solution remained upon association with the AOT-RM interface but the U-shaped conformation differed slightly indicating the interface's environmental influence on conformation. Together, these results support the interpretation that the MKs conformation remains folded in a U-shape even in contact with a model membrane interface, which agrees with our third hypothesis.

More broadly, the results of this study will also enhance our understanding of folded conformations for chemically and biologically important hydrophobic small molecules in solutions and confined hydrophobic environments. The shape, and thus the conformation of these molecules, are relevant for molecular recognition motifs and the processing of these molecules within the membrane. This chapter represents the first attempt to characterize the conformation as well as the chemical and biochemical properties manifested by the

conformation of any electron transferring lipoquinone derivative. Although many studies have been carried out with these systems kinetically, the conformation and how this impacts the biological chemistry has not yet been addressed.

References

1. Koehn, J. T.; Magallanes, E. S.; Peters, B. J.; Beuning, C. N.; Haase, A. A.; Zhu, M. J.; Rithner, C. D.; Crick, D. C.; Crans, D. C., A Synthetic Isoprenoid Lipoquinone, Menaquinone-2, Adopts a Folded Conformation in Solution and at a Model Membrane Interface. *J. Org. Chem.* **2018,** *83*, 275-288.
2. Beller, H. R.; Soon Lee, T.; Katz, L., Natural Products as Biofuels and Bio-based Chemicals: Fatty Acids and Isoprenoids. *Nat. Prod. Rep.* **2015,** *32*, 1508-1526.
3. Frank, A.; Groll, M., The Methylerythritol Phosphate Pathway to Isoprenoids. *Chem. Rev.* **2017,** *117*, 5675-5703.
4. Thulasiram, H. V.; Erickson, H. K.; Poulter, C. D., Chimeras of Two Isoprenoid Synthases Catalyze All Four Coupling Reactions in Isoprenoid Biosynthesis. *Science* **2007,** *316* (5821), 73-76.
5. da Costa, M. S.; Albuquerque, L.; Nobre, M. F.; Wait, R., The Extraction and Identification of Respiratory Lipoquinones of Prokaryotes and Their Use in Taxonomy. In *Methods in Microbiology, Vol 38: Taxonomy of Prokaryotes*, Rainey, F.; Oren, A., Eds. Elsevier Academic Press Inc: San Diego, 2011; Vol. 38, pp 197-206.
6. Kroppenstedt, R. M.; Mannheim, W., Lipoquinones in Members of the Family Pasteurellaceae. *Int. J. Syst. Evol. Bacteriol.* **1989,** *39* (3), 304-308.
7. Collins, M. D.; Jones, D., Distribution of Isoprenoid Quinone Structural Types in Bacteria and Their Taxonomic Implications. *Microbiol. Rev.* **1981,** *45* (2), 316-354.
8. Meganathan, R., Biosynthesis of Menaquinone (Vitamin K_2) and Ubiquinone (Coenzyme Q): A Perspective on Enzymatic Mechanisms. In *Vitam. Horm.*, 2001; Vol. 61, pp 173-218.
9. Caluwe, R.; Pyfferoen, L.; De Boeck, K.; De Vriese, A. S., The effects of vitamin K supplementation and vitamin K antagonists on progression of vascular calcification: ongoing randomized controlled trials. *Clin. Kidney J.* **2016,** *9* (2), 273-279.
10. Bergdoll, L.; ten Brink, F.; Nitschke, W.; Picot, D.; Baymann, F., From low- to high-potential bioenergetic chains: Thermodynamic constraints of Q-cycle function. *Biochim. Biophys. Acta, Bioenerg.* **2016,** *1857* (9), 1569-1579.
11. Epand, R. M.; Walker, C.; Epand, R. F.; Magarvey, N. A., Molecular mechanisms of membrane targeting antibiotics. *Biochim. Biophys. Acta, Biomembr.* **2016,** *1858* (5), 980-987.
12. Villaume, M. T.; Sella, E.; Saul, G.; Borzilleri, R. M.; Fargnoli, J.; Johnston, K. A.; Zhang, H.; Fereshteh, M. P.; Murali Dhar, T. G.; Baren, P. S., Antroquinonol A: Scalable Synthesis and Preclinical Biology of a Phase 2 Drug Candidate. *ACS Cent. Sci.* **2016,** *2*, 27-31.
13. Choi, S. R.; Larson, M. A.; Hinrichs, S. H.; Bartling, A. M.; Frandsen, J.; Narayanasamy, P., Discovery of bicyclic inhibitors against menaquinone biosynthesis. *Future Med. Chem.* **2016,** *8* (1), 11-16.
14. Matarlo, J. S.; Lu, Y.; Daryaee, F.; Daryaee, T.; Ruzsicska, B.; Walker, S. G.; Tonge, P. J., A Methyl 4-Oxo-4-phenylbut-2-enoate with in Vivo Activity against MRSA That Inhibits MenB in the Bacterial Menaquinone Biosynthesis Pathway. *ACS Infect. Dis.* **2016,** *2* (5), 329-340.
15. Szamosvari, D.; Bottcher, T., An Unsaturated Quinolone N-Oxide of Pseudomonas aeruginosa Modulates Growth and Virulence of Staphylococcus aureus. *Angew. Chem. Int. Ed.* **2017,** *56* (25), 7271-7275.
16. Vilcheze, C.; Hartman, T.; Weinrick, B.; Jain, P.; Weisbrod, T. R.; Leung, L. W.; Freundlich, J. S.; Jacobs, W. R., Enhanced respiration prevents drug tolerance and drug resistance in Mycobacterium tuberculosis. *Proc. Natl. Acad. Sci. U.S.A.* **2017,** *114* (17), 4495-4500.

17. Upadhyay, A.; Fontes, F. L.; Gonzalez-Juarrero, M.; McNeil, M. R.; Crans, D. C.; Jackson, M.; Crick, D. C., Partial Saturation of Menaquinone in *Mycobacterium tuberculosis*: Function and Essentiality of a Novel Reductase, MenJ. *ACS Cent. Sci.* **2015,** *1* (6), 292-302.
18. Vos, M.; Esposito, G.; Edirisinghe, J. N.; Vilain, S.; Haddad, D. M.; Slabbaert, J. R.; Van Meensel, S.; Schaap, O.; De Strooper, B.; Meganathan, R.; Morais, V. A.; Verstreken, P., Vitamin K_2 Is a Mitochondrial Electron Carrier That Rescues Pink1 Deficiency. *Science* **2012,** *336*, 1306-1310.
19. Nakagawa, K.; Hirota, Y.; Sawada, N.; Yuge, N.; Watanabe, M.; Uchino, Y.; Okuda, N.; Shimomura, Y.; Suhara, Y.; Okano, T., Identification of UBIAD1 as a Novel Human Menaquinone-4 Biosynthetic Enzyme. *Nature* **2010,** *468*, 117-121.
20. Hiratsuka, T.; Furihata, K.; Ishikawa, J.; Yamashita, H.; Itoh, N.; Seto, H.; Dairi, T., An Alternative Menaquinone Biosynthetic Pathway Operating in Microorganisms. *Science* **2008,** *321* (5896), 1670-1673.
21. Newman, D. K.; Kolter, R., A Role for Excreted Quinones in Extracellular Electron Transfer. *Nature* **2000,** *405*, 94-97.
22. Collins, M. D.; Shah, H. N.; Minnikin, D. E., A Note on the Separation of Natural Mixtures of Bacterial Menaquinones Using Reverse-phase Thin-layer Chromatography. *J. Appl. Bacteriol.* **1980,** *48* (2), 277-282.
23. Thomson, R. H., *Naturally Occurring Quinones.* Academic Press Inc: 1971.
24. Cooper, G. M.; Hausman, R. E., *The Cell A Molecular Approach.* 5th ed.; Sinauer Associates, INC.: Sunderland, Massachusetts, USA, 2009; p 820.
25. Nelson, D. L.; Cox, M. M., *Lehninger Principles of Biochemistry.* 5th ed.; W.H. Freeman and Company: New York, USA, 2008; p 1158.
26. Murgolo, N. J.; Patel, A.; Stivala, S. S.; Wong, T. K., The Conformation of Dolichol. *Biochemistry* **1989,** *28*, 253-260.
27. Lowry, T. H.; Richardson, K. S., *Mechanism and Theory in Organic Chemistry.* 3rd ed.; Harper & Row, Publishers New York, USA, 1987; p 1090.
28. Klauda, J. B.; Brooks, B. R., An Ab Initio Study on the Torsional Surface of Alkanes and Its Effect on Molecular Simulations of Alkanes and a DPPC Bilayer. *J. Phys. Chem. B* **2005,** *109*, 5300-5311.
29. Choudhury, R.; Barman, A.; Prabhakar, R.; Ramamurthy, V., Hydrocarbons Depending on the Chain Length and Head Group Adopt Different Conformations within a Water-Soluble Nanocapsule: 1H NMR and Molecular Dynamics Studies. *J. Phys. Chem. B* **2013,** *117*, 398-407.
30. Chum, S. P.; Knight, G. W.; Ruiz, J. M., Computer Modeling of {110} Adjacent Reentry of Polyethylene Molecules. *Macromolecules* **1994,** *27*, 656-659.
31. Robertson, M. B.; Klein, P. G.; Ward, I. M.; Packer, K. J., NMR Study of the Energy Difference and Population of the *gauche* and *trans* Conformations in Solid Polyethylene. *Polymer* **2001,** *42*, 1261-1264.
32. Cao, M.; Monson, P. A., Solid-Fluid and Solid-Solid Equilibrium in Hard Sphere United Atom Models of
n-Alkanes: Rotator Phase Stability. *J. Phys. Chem. B* **2009,** *113* (42), 13866-13873.
33. Nikki, K.; Inakura, H.; Wu-Le; Suzuki, N.; Endo, T., Remarkable Changes in Conformations of *n*-alkanes with thier Carbon Numbers and Aromatic Solvents. *J. Chem. Soc., Perkin Trans. 2* **2001,** (2370-2373).
34. Nikki, K.; Nakagawa, N., Elucidation of the Structure of Alkane Chains in Solution by Means of 1H NMR. *Org. Magn. Reson.* **1983,** *21* (9), 552-554.
35. Nikki, K., 1H and 13C NMR Aromatic Solvent-induced Shifts of *n*-alkanes. *Magn. Reson. Chem.* **1990,** *28* (5), 385-388.
36. Law, J. M. S.; Setiadi, D. H.; Chass, G. A.; Csizmadia, I. G.; Viskolcz, B., Flexibility of "Polyunsaturated Fatty Acid Chains" and Peptide Backbones: A Comparative Ab Initio Study. *J. Phys. Chem. A* **2005,** *109* (3), 520-533.

37. Kanicky, J. R.; Shah, D. O., Effect of Degree, Type, and Position of Unsaturation on the pKa of Long-Chain Fatty Acids. *J. Colloid Interface Sci.* **2002,** *256*, 201-207.
38. Ho Ko, Y.; Kim, Y.; Kim, H.; Kim, K., U-Shaped Conformation of Alkyl Chains Bound to a Synthetic Receptor Cucurbit[8]uril. *Chem. Asian J.* **2011,** *6*, 652-657.
39. Ho Ko, Y.; Kim, H.; Kim, Y.; Kim, K., U-Shaped Conformation of Alkyl Chain Bound to a Synthetic Host. *Angew. Chem. Int. Ed.* **2008,** *47*, 4106-4109.
40. Schramm, M. P.; Rebek Jr., J., Moving Targets: Recognition of Alkyl Groups. *Chem. Eur. J.* **2006,** *12*, 5924-5933.
41. de Sousa, F. F.; Freire, P. T. C.; Saraiva, G. D.; Lima, J. A.; Alcantara, P.; Melo, F. E. A.; Mendes, J., Pressure-induced Phase Transitions in Stearic Acid C Form. *Vib. Spectrosc.* **2010,** *54* (2), 118-122.
42. Collins, M. D.; Kroppenstedt, R. M., Structures of the Partially Saturated Menaquinones of *Glycomyces rutgersensis*. . *FEMS Microbiol. Lett.* **1987,** *44* (2), 215-219.
43. Bentley, R., Biosynthesis of Vitamin-K and Other Natural Naphthoquinones. *Pure Appl. Chem.* **1975,** *41* (1-2), 47-68.
44. Stahla, M. L.; Baruah, B.; James, D. M.; Johnson, M. D.; Levinger, N. E.; Crans, D. C., 1H NMR Studies of Aerosol-OT Reverse Micelles with Alkali and Magnesium Counterions: Preparation and Analysis of MAOTs. *Langmuir* **2008,** *24* (12), 6027-6035.
45. Samart, N.; Beuning, C. N.; Haller, K. J.; Rithner, C. D.; Crans, D. C., Interaction of a Biguanide Compound with Membrane Model Interface Systems: Probing the Properties of Antimalaria and Antidiabetic Compounds. *Langmuir* **2014,** *30* (29), 8697-8706.
46. Peters, B. J.; Groninger, A. S.; Fontes, F. L.; Crick, D. C.; Crans, D. C., Differences in Interactions of Benzoic Acid and Benzoate with Interfaces. *Langmuir* **2016,** *32* (37), 9451-9459.
47. Tynkkynen, T.; Hassinen, T.; Tiainen, M.; Soininen, P.; Laatikainen, R., 1H NMR Spectral Analysis and Conformational Behavior of *n*-alkanes in Different Chemical Environments. *Magn. Reson. Chem.* **2012,** *50*, 598-607.
48. Ishihara, M.; Sakagami, H., QSAR of Molecular Structure and Cytotoxic Activity of Vitamin K_2 Derivatives with Concept of Absolute Hardness. *Anticancer Res.* **2007,** *27*, 4059-4063.
49. Lancaster, C. R. D.; Haas, A. H.; Madej, M. G.; Mileni, M., Recent Progress on Obtaining Theoretical and Experimental Support for the "E-Pathway Hypothesis" of Coupled Transmembrane Electron and Proton Transfer in Dihaem-containing Quinol: Fumarate Reductase. *Biochim. Biophys. Acta, Bioenerg.* **2006,** *1757* (8), 988-995.
50. Prince, R. C.; Leslie Dutton, P.; Malcolm Bruce, J., Electrochemistry of Ubiquinones. *FEBS Lett.* **1983,** *160* (1), 273-276.
51. Guin, P. S.; Das, S.; Mandal, P. C., Electrochemical Reduction of Quinones in Different Media: A Review. *Int. J. Electrochem.* **2011,** *2011*, 22.
52. Dryhurst, G., Kadish, K. M., Scheller, F., Renneberg, R. , *Biological Eletrochemistry.* Academic Press: New York, 1982.
53. Luder, W. F.; Kraus, P. B.; Kraus, C. A.; Fuoss, R. M., Properties of Electrolytic Solutions. XVII. The Conductance of Some Salts in Benzene and Dioxane. *J. Am. Chem. Soc.* **1936,** *58* (2), 255-258.
54. Jaworski, J. S.; Leniewska, E.; Kalinowski, M. K., Solvent Effect on the Redox Potential of Quinone-semiquinone Systems. *J. Electroanal. Chem.* **1979,** *105* (2), 329-334.
55. Baruah, B.; Roden, J. M.; Sedgwick, M.; Correa, N. M.; Crans, D. C.; Levinger, N. E., When Is Water Not Water? Exploring Water Confined in Large Reverse Micelles Using a Highly Charged Inorganic Molecular Probe. *J. Am. Chem. Soc.* **2006,** *128*, 12758-12765.
56. Odella, E.; Falcone, R. D.; Silber, J. J.; Correa, N. M., Nanoscale Control Over Interfacial Properties in Mixed Reverse Micelles Formulated by Using Sodium 1,4-bis-2-ethylhexylsulfosuccinate and Tri-n-octyl Phosphine Oxide Surfactants. *ChemPhysChem* **2016,** *17* (15), 2407-2414.

57. Diaz-Fernandez, Y.; Foti, F.; Mangano, C.; Pallavicini, P.; Patroni, S.; Perez-Gramatges, A.; Rodriguez-Calvo, S., Micelles for the Self-Assembly of "Off–On–Off" Fluorescent Sensors for pH Windows. *Chem. Eur. J.* **2006,** *12*, 921-930.
58. Pallavicini, P.; Diaz-Fernandez, Y.; Pasotti, L., Micelles as Nanosized Containers for the Self-assembly of Multicomponent Fluorescent Sensors. *Coord. Chem. Rev.* **2009,** *253*, 2226-2240.
59. Stefaniu, C.; Brezesinski, G.; Mohwald, H., Langmuir Monolayers as Models to Study Processes at Membrane Surfaces. *Adv. Colloid Interface Sci.* **2014,** *208*, 197-213.
60. Sostarecz, A. G.; Gaidamauskas, E.; Distin, S.; Bonetti, S. J.; Levinger, N. E.; Crans, D. C., Correlation of Insulin-Enhancing Properties of Vanadium-Dipicolinate Complexes in Model Membrane Systems: Phospholipid Langmuir Monolayers and AOT Reverse Micelles. *Chem. Eur. J.* **2014,** *20* (17), 5149-5159.
61. Riter, R. E.; Kimmel, J. R.; Undiks, E. P.; Levinger, N. E., Novel Reverse Micelles Partitioning Nonaqueous Polar Solvents in a Hydrocarbon Continuous Phase. *J. Phys. Chem. B* **1997,** *101* (41), 8292-8297.
62. Maitra, A., Determination of Size Parameters of Water-aerosol-OT Oil Reverse Micelles From Their Nuclear Magnetic-resonance Data. *J. Phys. Chem.* **1984,** *88* (21), 5122-5125.
63. Durantini, A. M.; Falcone, R. D.; Silber, J. J.; Correa, N. M., Effect of Confinement on the Properties of Sequestered Mixed Polar Solvents: Enzymatic Catalysis in Nonaqueous 1,4-Bis-2-ethylhexylsulfosuccinate Reverse Micelles. *ChemPhysChem* **2016,** *17* (11), 1678-1685.
64. Lepori, C. M. O.; Correa, N. M.; Silber, J. J.; Falcone, R. D., How the Cation 1-butyl-3-methylimidazolium Impacts the Interaction Between the Entrapped Water and the Reverse Micelle Interface Created with an Ionic Liquid-like Surfactant. *Soft Matter* **2016,** *12* (3), 830-844.
65. Hoyo, J.; Torrent-Burgues, J.; Guas, E., Biomimetic Monolayer Films of Monogalactosyldiacylglycerol Incorporating Ubiquinone. *J. of Colloid and Interface Sci.* **2012,** *384*, 189-197.
66. Quinn, P. J.; Esfahani, M. A., Ubiquinones have Surface-Active Properties Suited to Transport Electrons and Protons Across Membranes. *Biochem. J.* **1980,** *185*, 715-722.
67. Patterson, M.; Vogel, H. J.; Prenner, E. J., Biophysical Characterization of Monofilm Model Systems Composed of Selected Tear Film Phospholipids. *Biochim. Biophys. Acta, Biomembr.* **2016,** *1858* (2), 403-414.
68. Roche, Y.; Peretti, P.; Bernard, S., The Redox State Influences the Interaction of Ubiquinones with Phospholipid Bilayers a DSC Study. *J. Therm. Anal. Calorim.* **2007,** *89* (3), 867-873.
69. De, T. K.; Maitra, A., Solution Behaviour of Aerosol OT in Non-polar Solvents. *Adv. Colloid Interface Sci.* **1995,** *59*, 95-193.
70. Sedgwick, M. A.; Trujillo, A. M.; Hendricks, N.; Levinger, N. E.; Crans, D. C., Coexisting Aggregates in Mixed Aerosol OT and Cholesterol Microemulsions. *Langmuir* **2011,** *27* (3), 948-954.
71. Zan, G. T.; Wu, Q. S., Biomimetic and Bioinspired Synthesis of Nanomaterials/Nanostructures. *Adv. Mater.* **2016,** *28* (11), 2099-2147.
72. Kuchler, A.; Yoshimoto, M.; Luginbuhl, S.; Mavelli, F.; Walde, P., Enzymatic Reactions in Confined Environments. *Nat. Nanotechnol.* **2016,** *11* (5), 409-420.
73. Dharaiya, N.; Bahadur, P., Phenol Induced Growth in Triton X-100 Micelles: Effect of pH and Phenols' Hydrophobicity. *Colloids Surf. A* **2012,** *410*, 81-90.
74. Dumas, C.; Meledandri, C. J., Insights into the Partitioning Behavior of Secondary Surfactants in a Microemulsion-Based Synthesis of Metal Nanoparticles: A DLS and 2D NMR Spectroscopic Investigation. *Langmuir* **2015,** *31* (26), 7193-7203.
75. Kaur, G.; Chiappisi, L.; Prevost, S.; Schweins, R.; Gradzielski, M.; Mehta, S. K., Probing the Microstructure of Nonionic Microemulsions with Ethyl Oleate by Viscosity, ROESY, DLS, SANS, and Cyclic Voltammetry. *Langmuir* **2012,** *28* (29), 10640-10652.

76. Sanchez-Lombardo, I.; Baruah, B.; Alvarez, S.; Werst, K. R.; Segaline, N. A.; Levinger, N. E.; Crans, D. C., Size and Shape Trump Charge in Interactions of Oxovanadates with Self-assembled Interfaces: Application of Continuous Shape Measure Analysis to the Decavanadate Anion. *New J. Chem.* **2016,** *40*, 962-975.
77. Crans, D. C.; Levinger, N. E., The Conundrum of pH in Water Nanodroplets: Sensing pH in Reverse Micelle Water Pools. *Acc. Chem. Res.* **2012,** *45* (10), 1637-1645.
78. Bock, C. W.; Panchenko, Y. N.; Krasnoshchiokov, S. V.; Aroca, R., Abinitio Structures and Vibrational Analysis of the Isoprene Conformers. *J. Mol. Struct.* **1987,** *160* (3-4), 337-346.
79. Squillacote, M. E.; Semple, T. C.; Mui, P. W., The Geometries of the s-cis Conformers of Some Acyclic 1,3-dienes - Planar or Twisted. *J. Am. Chem. Soc.* **1985,** *107* (24), 6842-6846.
80. Mui, P. W.; Grunwald, E., Enthalpy Change for the s-trans and s-cis Conformational Equilibrium in 2-methyl-1,3-butadiene (Isoprene), as Studied by High-temperature Ultraviolet Absorption Spectroscopy. . *J. Phys. Chem.* **1984,** *88* (25), 6340-6344.
81. Gundersen, G.; Thomassen, H. G., The Molecular-structure and Conformational Behavior of 2-chloro-1,3-butadiene (Chloroprene) Studied by Gas-phase Electron-diffraction and Ab-initio MO Calculations. *J. Mol. Struct.* **1991,** *243* (3-4), 385-409.
82. Fujimoto, N.; Kosaka, T.; Yamada, M., *Menaquinone as Well as Ubiquinone as a Crucial Component in the Escherichia coli Respiratory Chain.* InTech: 2012; p 444.
83. Lai, C.-T.; Li, H.-J.; Yu, W.; Shah, S.; Bommineni, G. R.; Perrone, V.; Garcia-Diaz, M.; Tonge, P. J.; Simmerling, C., Rational Modulation of the Induced-Fit Conformational Change for Slow-Onset Inhibition in *Mycobacterium tuberculosis* InhA. *Biochemistry* **2015,** *54*, 4683-4691.
84. Yano, T.; Rahimian, M.; Aneja, K. K.; Schechter, N. M.; Rubin, H.; Scott, C. P., *Mycobacterium tuberculosis* Type II NADH-Menaquinone Oxidoreductase Catalyzes Electron Transfer through a Two-Site Ping- Pong Mechanism and Has Two Quinone-Binding Sites. *Biochemistry* **2014,** *53*, 1179-1190.
85. Peover, M. E., A Polarographic Investigation into the Redox Behaviour of Quinones: The Roles of Electron Affinity and Solvent. *J. Chem. Soc.* **1962**, 4540-4549.
86. Chadar, D.; Camilles, M.; Patil, R.; Khan, A.; Weyhermuller, T.; Salunke-Gawali, S., Synthesis and Characterization of *n*-alkylamino Derivatives of Vitamin K3: Molecular Structure of 2-propylamino-3-methyl-1,4-naphthoquinone and Antibacterial Activities. *J. Mol. Struct.* **2015,** *1086*, 179-189.
87. Kathawate, L.; Joshi, P. V.; Dash, T. K.; Pal, S.; Nikalje, M.; Weyhermuller, T.; Puranik, V. G.; Konkimalla, V. B.; Salunke-Gawali, S., Reaction Between Lawsone and Aminophenol Derivatives: Synthesis, Characterization, Molecular Structures and Antiproliferative Activity. *J. Mol. Struct.* **2014,** *1075*, 397-405.
88. McQuaw, C. M.; Sostarecz, A. G.; Zheng, L.; Ewing, A. G.; Winograd, N., Lateral Heterogeneity of Dipalmitoylphosphatidylethanolamine-Cholesterol
Langmuir-Blodgett Films Investigated with Imaging Time-of-Flight Secondary Ion Mass Spectrometry and Atomic Force Microscopy. *Langmuir* **2005,** *21*, 807-813.
89. Demel, R. A.; Geurts Van Kessel, W. S. M.; Zwaal, R. F. A.; Roelofsen, B.; Van Deenen, L. M., Relation Between Various Phospholipase Actions on Human Red Cell Membranes and the Interfacial Phospholipid Pressure in Monolayers. *Biochim. Biophys. Acta* **1975,** *406*, 97-107.
90. Choi, Y.; Attwood, S. J.; Hoopes, M. I.; Drolle, E.; Karttunen, M.; Leonenko, Z., Melatonin Directly Interacts with Cholesterol and Alleviates Cholesterol Effects in Dipalmitoylphosphatidylcholine Monolayers. *Soft Matter* **2014,** *10*, 206-213.
91. Belzile, M.-N.; Godin, R.; Durantini, A.; Cosa, G., Monitoring Chemical and Biological Electron Transfer Reactions with a Fluorogenic Vitamin K Analogue Probe. *J. Am. Chem. Soc.* **2016,** *138*, 16388-16397.

Chapter 4: Isolating the Influence of Saturation of the Isoprenyl Side Chain on Menaquinone on Conformation and Quinone Redox Potential[1]

4.1 Role of Partial Saturation of the Isoprenyl Side Chain of Mycobacterial Menaquinone

Quinones are a unique type of unsaturated α,β-ketones existing as metabolites in numerous pathways where they have many functions in nature.[1-7] The importance of quinone chemistry has been recognized since the mid-1800s. Quinone containing compounds can be anti-oxidants, anti-tumoral, or carcinogenic agents and are the inherent components of biological systems such as photosystem II.[2-7] Menaquinones (or naphthoquinones, MK) are a member of the lipoquinone (lipid-quinone) class of molecules and are essential components of the respiratory electron transport system (ETS), where they shuttle electrons and protons between protein complexes by acting as electron donors and acceptors.[7] Partial saturation of the isoprenyl side chain of MK has been known for a long time but recently MenJ was shown to selectively reduce MK-9 at the second isoprene unit demonstrating the origin of partially saturated MKs within mycobacteria.[8-9] Currently, little is known regarding the conformation of MKs in solution or within cell membranes and how partial saturation of the isoprenyl side chain affects conformation and quinone reactivity, even though the structures and biological significance of lipoquinones and isoprenoids have been known for over 50 years.[7, 10-14] Partial saturation may affect substrate recognition by respiratory enzymes within the ETS or it may be able to affect quinone redox

[1]This chapter is published in part or in full in *Biochemistry*.[1]

potential, or a combination of both. Interestingly, disruption of expression of MenJ reduces mycobacterial electron transfer efficiency by 3-fold but the mycobacteria were able to maintain ATP levels by increasing the total levels of the total menaquinone in the membrane.[8] It is a well-known fact that evolutionary conserved structural differences in lipoquinone head group alter quinone redox potential[2] but it remains uncertain how partial saturation of the isoprenyl side chain affects quinone redox potential. Therefore, this chapter aims to characterize the conformation of the most fundamental MKs containing one isoprene unit (unsaturated vs saturated side chain) in organic solution and a model membrane interface as well as determine the quinone redox potentials of unsaturated MK-1 and saturated MK-1(H_2) in organic solution.

MKs are structurally characterized by a naphthoquinone moiety and a repeating isoprenyl side chain of varying length (Figure 4.1.1), where the latter is a characteristic that has long been used to assist taxonomic efforts.[15-16] The most widely known MK analog is Vitamin K_2 (or MK-4), which is essential for life in humans as it is a key cofactor in blood coagulation.[17] MK-4 was recently shown to be biosynthesized in humans[18] and as a part of the ETS in *Drosophila.*[19] Vitamin K_3 (or menadione), the simplest 1,4-naphthoquinone derivative lacking the isoprenyl side chain, has been reported to have significant anti-tumoral properties.[3] N-alkylated MK derivatives have also been synthesized and characterized in literature with several exhibiting interesting biological properties.[20-23] The truncated MK analogs, menaquinone-1 (MK-1) and menaquinone-1(H_2) [MK-1(H_2)], are vital to study as they are the simplest, most fundamental MKs, where they retain the core requirements (i.e., a naphthoquinone moiety and a one unit isoprenyl side chain). MK-1(H_2) is crucial to study as it lacks the double bond in the isoprenyl side chain and importantly, biologically isolated MK analogs containing partial saturation (reduced double bond) in the

isoprenyl side chain have been reported (Figure 4.1.1).[7-9] Truncated MK analogs are more soluble than the natural MK substrate, thus allowing rigorous characterization in aqueous assays.[9] Furthermore, MK-9 contains eighty hydrogens with significant spectral overlap making conformational analysis non-trivial. Therefore, the conformational analysis of these two truncated MK-1 analogs is essential as the conformation of the first isoprene unit will influence the conformation of the rest of the isoprenyl side chain in naturally occurring longer MK analogs (e.g., MK-4, MK-9 or MK-9(II-H_2), Figure 4.1.1).

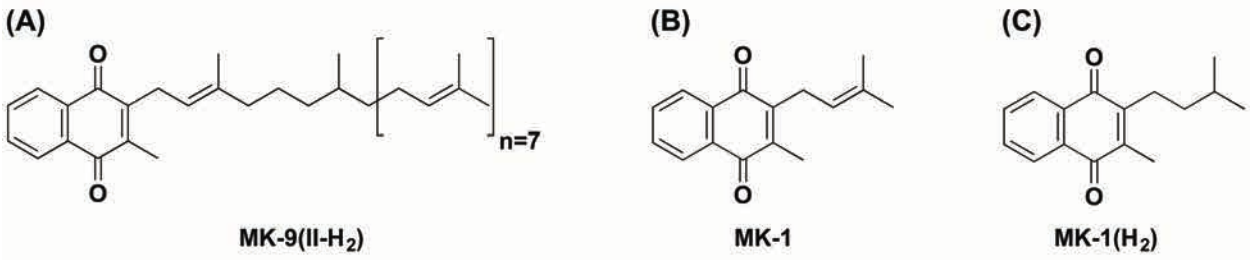

Figure 4.1.1. Structures of (A) MK-9(II-H_2), present within *Mycobacterium tuberculosis*, (B) the unsaturated MK analog, MK-1, and (C) the saturated MK analog, MK-1(H_2).

The synthesis of truncated MK analogs is necessary as it allows experimental conformational analysis to be carried out. Molecular conformations are significant for manifesting physical and chemical reactivity, as well as recognition in biological systems. MKs contain an alkyl side chain of varying lengths and conformations have been reported for various alkanes, alkenes, and fatty acids, which all contain alkyl chains of varying length.[24-36] For example, the degree of folding of C_5-C_{32} *n*-alkanes in solution depends on the strength of the dispersion force of the solvent and increases with increasing chain length.[28-30] Furthermore, studies on *n*-hexane and *n*-pentane in various solvents suggested that the solvent environment had only minor effects on the conformational equilibrium.[36] Interestingly, conformations observed in polar and spherical solvents such as DMSO favored *gauche* conformations.[36] Computational studies have been

carried out on MK analogs where folded conformations were found to be favorable.[35, 37] Importantly, we demonstrated in chapter three that menaquinone-2 (MK-2) adopts a folded, U-shaped conformation in solution and within a model membrane interface.[38] However, MK-1 contains only one isoprene unit and presents the best opportunity for a flat-extended conformation to exist, and therefore it is important to determine if a flat-extended (i.e., trans or extended configuration of the side chain and isoprene planar), folded-extended (i.e., isoprene folded upwards), or u-shaped conformation (i.e., isoprene folded up and back towards the naphthoquinone in a u-shape) is preferred (see Figure 4.1.2). Based on these selected examples, we hypothesized that MK-1 analogs adopt folded conformations regardless of the degree of saturation in their isoprenyl side chain.

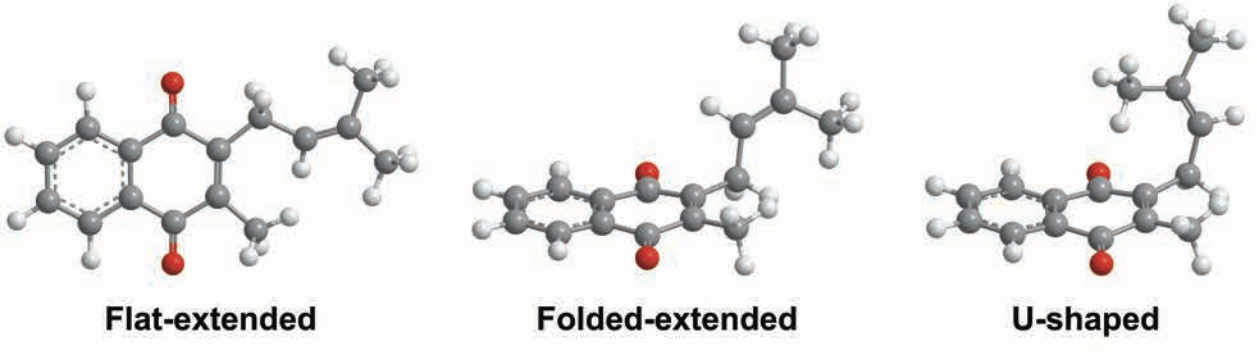

Figure 4.1.2. Illustration showing MK-1 conformations for flat-extended (i.e., trans or extended configuration of the side chain and isoprene planar), folded-extended (i.e., isoprene folded upwards), or u-shaped conformation (i.e., isoprene folded up and back towards the naphthoquinone in a u-shape).

The conformation and electronic properties of a molecule can affect both the reactivity and function of a molecule in solution and within biological environments. The longer partially saturated isoprenyl side chain MK analog, MK-9(II-H_2) (Figure 4.1.1A) is an electron transporter within *Mycobacterium tuberculosis* (*M. tuberculosis*) and the synthesis of MK-9(II-H_2) was

observed in pathogenic *M. tuberculosis*.[8-9] In addition, partially saturated MK analogs have been reported in other organisms such as members of the genera *Streptomyces* and *Actinomadura.*[12] It is unclear whether hydrogenation of the double bond in specific isoprene units changes the reactivity of the quinone system. The double bonds present within the isoprenyl side chain are not conjugated to the quinone system within MK. Therefore, it would not be anticipated that a significant change in the quinone redox potential would occur upon reduction of an isoprenyl unit. However, it has been reported that even when there is no direct conjugation between the quinone system and a substituent group, electrochemical reduction of the quinone system is sensitive to the electronic perturbation of the substituents.[2] Thus, it is possible that partial saturation in the isoprenyl side chain could influence the quinone redox potential, where an indirect through bond effect could be a contributing factor and/or conformational effects of the substituent. Therefore, we hypothesized that the quinone redox potential of MK-1 is influenced by the degree of saturation in the isoprenyl side chain.

In this chapter, the conformations of MK-1 and MK-1(H_2) (Figure 4.1.1) within organic solvents were elucidated by 1D and 2D ^{1}H NMR spectroscopy. MK-1 and MK-1(H_2) adopted similar folded-extended conformations in each solvent but the preferred folded-extended conformations differed slightly between solvent environments. The quinone redox potentials of MK and MK-1(H_2) were measured in three organic solvents, where a solvent effect (presumably due to a change in dielectric constant) was observed and most interestingly, a ~20 mV difference in semiquinone redox potential was observed between MK-1 and MK-1(H_2). The interaction of MK-1 and MK-1(H_2) with phospholipid monolayers was characterized using Langmuir monolayers and the two MK-1 analogs were found to interact with the phospholipid interface. Finally, using

a complementary study, the location, orientation, and conformation of MK-1 and MK-1(H_2) within a reverse micelle (RM) model membrane interface was determined using 1D and 2D NMR spectroscopy. The two MK-1 analogs interacted similarly with the RM model membrane interface and MK-1 adopted a slightly different folded conformation within the RM interface compared to that observed in organic solution.

4.2 Materials and Methods

4.2.1 Materials and General Information/Methods

Most reagents were used without further purification. Dioctyl sulfosuccinate sodium salt (AOT, 97.0%), isooctane (2,2,4-trimethylpentane, ≥99.0%), chloroform (99.8%), methanol (99.9%), sodium phosphate monobasic monohydrate (NaH_2PO_4, 98%) tetrabutylammonium perchlorate (TBAP, ≥99.0%), ferrocene (Fc, anhydrous), silver nitrate ($AgNO_3$, ≥99.0%), and activated charcoal were purchased from Sigma Aldrich and used as received unless otherwise noted. Absolute ethanol and ultra-high purity argon gas (99.9%) were acquired from Pharmco-Aaper and Airgas, respectively. Deuterated solvents of acetonitrile (d_3-ACN, CD_3CN) (D 99.8%), dimethylsulfoxide (d_6-DMSO) (D 99.9%, + 0.05% V/V tetramethylsilane, and d_6-benzene ($\geq$99.6%) were acquired from Sigma-Aldrich. Deuterium oxide (D_2O, 99.9%), d_2-dichloromethane (99.9%), d_4-methanol (99.8%) were acquired from Cambridge Isotope Laboratories, Inc. Deuterated pyridine (D 99.8%) was purchased from Arcos Organics. DPPC (1,2-dipalmitoyl-sn-glycero-3-phosphocholine, ≥99.0%) and DPPE (1,2-dipalmitoyl-sn-glycero-3-phosphoethanolamine, ≥99.0%) were purchased from Avanti Polar Lipids Inc. Monosodium phosphate (96.0%) and

sodium phosphate dibasic anhydrous (Na_2HPO_4) was purchased from Fisher Scientific and Distilled Deionized Water (DDI H_2O) was purified with a Barnstead E-pure system (~18 MΩ-cm).

All chemicals were used without purification except AOT and the organic solvents. AOT was purified using activated charcoal and methanol to remove acidic impurities using previously reported methods.[39] Organic solvents dimethylsulfoxide (DMSO), acetonitrile (CH_3CN, ACN) and pyridine were purified by distillation and then dried over activated 3 Å molecular sieves (40 g / 200 mL solvent) for three days. When preparing samples for RM NMR experiments, deuterium oxide was used instead of H_2O and the pH was adjusted to consider the presence of deuterium (pD = 0.4 + pH).[40] ^1H and ^{13}C spectra were recorded on a 400 MHz Varian Model MR400, 400 MHz Varian iNova400 or a 500 MHz Varian iNova500. Chemical shift values (δ) are reported in ppm and referenced against the internal solvent peaks in ^1H NMR ($CDCl_3$, δ at 7.26 ppm; d_3-acetonitrile δ at 1.94 ppm; d_6-DMSO, δ at 2.50 ppm; d_4-methanol, δ at 4.87 ppm; d_2-methylene chloride, δ at 5.32 ppm; d_6-benzene, δ at 7.16 ppm; d_5-pyridine, δ at 8.74 ppm; D_2O, δ at 4.79 ppm;) and in ^{13}C NMR ($CDCl_3$, δ at 77.16 ppm; d_6-benzene, δ at 128.06 ppm).

4.2.2 NMR Spectroscopic Studies

1D and 2D ^1H NMR spectroscopic studies were carried out both in organic solvents and a RM model membrane system. ^1H and ^{13}C spectra were recorded using either a Varian Model MR400, Model Inova400, or Model Inova500 operating at either 400 MHz or 500 MHz and 101 MHz, respectively. Chemical shift values (δ) are reported in ppm and referenced against the internal solvent peaks in ^1H NMR ($CDCl_3$, δ at 7.26 ppm; d_3-ACN δ at 1.94 ppm; d_6-DMSO, δ at 2.50 ppm; d_4-methanol, δ at 4.87 ppm; d_2-methylene chloride, δ at 5.32 ppm; d_6-benzene, δ at 7.16 ppm; d_5-pyridine, δ at 8.74 ppm; D_2O, δ at 4.79 ppm;) and in ^{13}C NMR ($CDCl_3$, δ at 77.16 ppm; d_6-

benzene, δ at 128.06 ppm). All NMR spectra were recorded at either 22 °C, 25 °C, or 26 °C. See figure captions and Supporting Information for more details.

4.2.3 Solution 1D ^{1}H NMR Spectroscopic Studies

Samples were prepared by dissolving ~5.0 milligrams of MK-1 in 0.5 mL of either d_1-chloroform, d_2-methylene chloride, d_4-methanol, d_6-DMSO, d_5-pyridine, d_3-ACN, and d_6-benzene, respectively. The NMR instrument was locked onto the respective deuterium signal in the deuterated solvent used. NMR spectra were then collected using 32 scans for each sample. The data was processed using MestReNova NMR processing software version 10.0.1. The spectra were manually phased and then the baseline was corrected using a Bernstein Polynomial Fit (polynomial order 3). The obtained spectra were referenced to the proper internal solvent peak.

4.2.4 Sample Preparation for ^{1}H-^{1}H 2D NOESY and ^{1}H-^{1}H 2D REOSY NMR Spectroscopic Studies

To prepare the solutions of MK-1 or MK-1(H_2) in d_5-pyridine, d_3-ACN, and d_6-DMSO, 0.0024 g of MK-1 or 0.0024 g of MK-1(H_2) was dissolved in 0.5 mL of deuterated solvent to produce a 20 mM solution of MK-1 or MK-1(H_2). The NMR samples containing either MK-1 or MK-1(H_2) solution were purged with argon and capped prior to data collection.

4.2.5 ^{1}H-^{1}H 2D NOESY and ^{1}H-^{1}H 2D ROESY NMR Spectroscopic Solution Studies

^{1}H-^{1}H 2D NOESY NMR and ^{1}H-^{1}H 2D ROESY NMR spectroscopic experiments were conducted using a 400 MHz Varian MR400 NMR operating at 26 °C. A standard NOESY pulse sequence was used consisting of 256 transients with 16 scans in the f1 domain using a 500 ms mixing time, 45° pulse angle, and a 1.5 sec. relaxation delay. A standard ROESYAD pulse sequence was used consisting of 256 transients with 16 scans in the f1 domain using a 400 ms mixing time, 45° pulse

angle, and a 2.0 sec. relaxation delay. The NMR was locked onto either d_5-pyridine, d_3-ACN, or d_6-DMSO. The resulting spectrum was processed using MestReNova NMR software version 10.0.1 (see Supporting Information for further details). The spectra were referenced to the proper internal solvent peak.

4.2.6 Molecular Mechanics Calculations

To illustrate conformations for MK-1 and MK-1(H_2), Merck Molecular Force Field 94 (MMFF94) molecular mechanics gas phase simulations were conducted using ChemBio3D Ultra 12.0 at 25 °C. Starting conformations were obtained by building ChemDraw structures, rotating desired bonds, and then either had simulations run followed by energy optimization or simply an energy minimization to achieve the desired conformation. Conformations A-A1, B-B1, and C-C1 in Figure 4.3.4 were constructed and then energy minimized with a root mean square (RMS) gradient of 0.1 and up to 50 iterations to obtain MK-1 and MK-1(H_2) conformations that agreed with our interpretation of the cross peak observations and intensities in the ^{1}H-^{1}H 2D NOESY and ROESY NMR spectral data. Two simulations were run for 10,000 iterations and then energy minimized using an MMFF94 energy minimization calculation using 500 iterations with a RMS gradient of 0.001 to achieve conformations D-D1 in Figure A4.23. Conformations E-E1 and F-F1 in Figure A4.23 were generated by rotating bonds to achieve the desired conformation followed by an energy minimization using 20-50 iterations and an RMS gradient of 0.1. For a table of structural parameters such as selected distances between hydrogens within the conformations in Figure 4.3.4 and Figure A4.23 and energies calculated for the 3D conformations can be found in the Supporting Information. Tables of Cartesian coordinates for the MK-1 analog conformations can be found in the Supporting Information.

4.2.7 Sample Preparation for Reverse Micelle NMR Spectroscopic Studies

A 0.50 M AOT stock solution was prepared by dissolving AOT (5.56 g, 12.5 mmol) in isooctane (25.0 mL). Empty RMs were prepared by mixing 0.50 M AOT stock solution with a D_2O water pool, and then vortexed. MK-1 and MK-1(H_2) RMs were made in a similar matter. The only difference being a 14.3 mM stock solution for MK-1 and MK-1(H_2) was prepared by dissolving MK-1 or MK-1(H_2) in a 0.50 M AOT/isooctane solution. The RM's were then prepared using the MK-1 or MK-1(H_2) AOT/isooctane stock solution. First, 2.0 mL samples were made using specific amounts of MK-1 or MK-1(H_2) AOT/isooctane stock solution and then diluting the sample to 2.0 mL with the 0.50 M AOT/isooctane solution. From the 2.0 mL solutions, 1.0 mL RM samples were prepared using designated amounts of the 2.0 mL sample and then adding the proper amount of D_2O with pH 6.65 (see General Methods for pH measurements) for MK-1 (D_2O pH was 6.71 for the MK-1(H_2) samples) to form the desired size RM. The samples were then vortexed until the solution was clear. The overall concentrations for the 1.0 mL MK-1 RM samples are as follows: w_0 4, 13.8 mM; w_0 8, 6.5 mM; w_0 12, 3.5 mM; w_0 16, 1.9 mM; and w_0 20, 1.3 mM. The overall concentrations for the 1.0 mL MK-1(H_2) RM samples are as follows: w_0 4, 13.8 mM; w_0 8, 6.4 mM; w_0 12, 3.5 mM; w_0 16, 2.0 mM; and w_0 20, 1.4 mM.

4.2.8 1D ^{1}H NMR Spectroscopic Studies of AOT/isooctane Reverse Micelles Containing Menaquinone-1 or Menaquinone-1(H_2)

NMR spectra of MK-1 and MK-1(H_2) in various size RMs, isooctane and D_2O were obtained using a Varian Inova 400 MHz instrument operating at 22 °C using routine parameters (pulse angle: 45°, relaxation delay of 1 sec.) and 64 scans. The NMR instrument was locked onto 10% D_2O signal for the RM samples and locked onto 100% D_2O for the sample in D_2O. The 1D ^{1}H

spectra of MK-1 or MK-1(H_2) in isooctane were doped with ~5% d_6-benzene for the NMR instrument to lock onto and to achieve properly shimmed spectra. The spectral data was processed using MestReNova NMR processing software version 10.0.1. The spectra were manually phased and then the baseline was corrected using a multipoint baseline correction (cubic splines). The spectrum in D_2O was referenced to the internal D_2O peak and the spectra in isooctane and RMs were referenced to the isooctane methyl peak (0.904 ppm) as previously reported.[40]

4.2.9 Sample Preparation for ^{1}H-^{1}H 2D NOESY and ^{1}H-^{1}H 2D ROESY NMR Spectroscopic Studies in AOT/isooctane Reverse Micelles.

RM samples of MK-1 and MK-1(H_2) were prepared in the following manner. A 0.50 M AOT stock solution was first prepared by dissolving AOT (5.56 g, 12.5 mmol) in isooctane (25.0 mL). A 1.0 mL stock solution of 112 mM MK-1 in AOT/isooctane was prepared by dissolving 27.7 mg of MK-1 in 1.0 mL of 0.50 M AOT/isooctane stock solution. To prepare a w_0 12 RM, 894.68 μL of 112 mM MK-1 AOT/isooctane stock solution and 105.32 μL of D_2O at pH 7.03 were mixed together and then vortexed until the solution was clear. The MK-1(H_2) w_0 12 RM sample was prepared similarly to MK-1 using a 112 mM stock solution and D_2O (pH of 7.01). This final mixture results in a w_0 12 RM microemulsion with an overall concentration of MK-1 or MK-1(H_2) ~100 mM (~29 molecules per RM). The NMR samples containing the MK-1 or MK-1(H_2) RM solution were purged with argon and capped prior to data collection.

4.2.10 ^{1}H-^{1}H 2D NOESY and ^{1}H-^{1}H 2D ROESY NMR Spectroscopic Studies in a w_0 12 AOT/isooctane Reverse Micelles

2D NMR spectra of MK-1 and MK-1(H_2) in RMs were obtained using similar conditions and methods used previously[38, 41-42] using a 400 MHz Varian MR400 NMR operating at 26 °C for MK-1 and were obtained using a 500 MHz Varian Inova 500 operating at 25 °C for MK-1(H_2). A standard NOESY pulse sequence was used consisting of 200 or 256 transients with either 16 or 32 scans in the f1 direction using a 200 ms mixing time, 45° pulse angle, and a relaxation delay of 1.5 sec. A standard ROESYAD pulse sequence was used consisting of 256 transients with 16 scans in the f1 direction using a 200 ms mixing time, 45° pulse angle, and a relaxation delay of 2.0 sec. The NMR instrument was locked onto 10% D_2O signal. The resulting spectrum was processed using MestReNova NMR software version 10.0.1 (see Supporting Information for further details). The spectrum was referenced to the isooctane methyl peak at 0.904 ppm on both axes as previously reported.[40] The 3D conformation illustration within a RM interface was constructed using ChemDraw Professional 15.0 and ChemBio3D Ultra 12.0 based on spectral parameters described under results.

4.2.11 Dynamic Light Scattering Studies

RMs for DLS studies were prepared as described for the NMR spectroscopic studies except that distilled deionized (DDI) H_2O was used as the water pool instead of D_2O and the 0.50 M AOT was diluted with isooctane after the RM had formed to a final concentration of 0.1 M AOT. The hydrodynamic radius of the RMs was determined by DLS measurements performed on a Malvern Zetasizer Nano ZS instrument (Malvern Instruments, Malvern, UK). The DLS cuvette (1 cm X 1 cm, glass) was washed three times with isooctane followed by three washes with the RM sample.

Then, the cuvette was filled with 1 mL of the RM sample and closed with a Teflon cap. Each experiment was conducted at 25 °C and consisted of a 700 sec. sample equilibration period followed by 10 measurements consisting of 15 scans each.[41] Each sample was measured in triplicate and the radius and polydispersity (PDI) were recorded. The data were analyzed using Malvern Zetasizer Software Version 7.11 and compared to values reported in literature.[43] See Supporting Information for data and interpretation.

4.3 Results and Discussion

4.3.1 1D ^{1}H NMR Spectroscopic Studies of Menaquinone-1 in Organic Solvents

The synthesis of MK-1 and MK-1(H_2) provided material to investigate if the solvent environment induced chemical shift changes. NMR spectra of MK-1 were collected in various organic solvents ranging from aromatic to non-aromatic and of differing polarity (Figure 4.3.1). The most drastic chemical shift change observed for MK-1 was in the aromatic solvents, d_6-benzene and d_5-pyridine, compared to the other solvents in Figure 4.3.1. This is seen by focusing on the chemical shift differences observed between the MK-1 aromatic hydrogens, H_a/H_b and H_c/H_d. The chemical shift difference is nearly one ppm in d_6-benzene compared to 0.2-0.4 ppm differences in the other solvents. The methylene hydrogens, H_r/H_s, and the naphthoquinone methyl, H_x, also shifts in d_6-benzene compared to the other solvents. It is clear by examining the chemical shift differences in the spectra in Figure 4.3.1 that MK-1 is influenced by solvent environment but it remains unclear whether MK-1 adopts different conformations in these organic solvent environments.

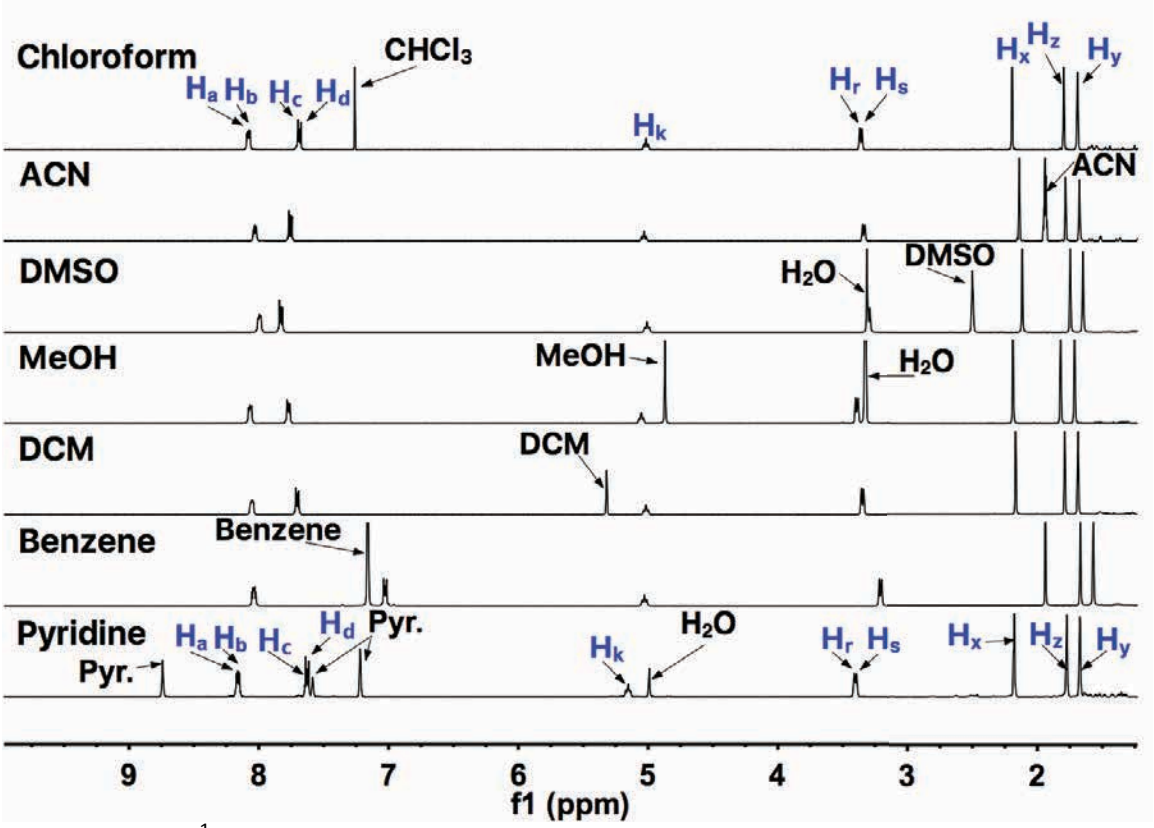

Figure 4.3.1. 1D ^{1}H NMR (400 MHz) spectra illustrating chemical shift differences of MK-1 hydrogens between various organic solvent environments. Abbreviations are as follows: ACN = d_3-acetonitrile, DMSO = d_6-dimethyl sulfoxide, MeOH = d_4-methanol, DCM = d_2-dichloromethane, Pyr = d_5-pyridine. A structure of MK-1 with a hydrogen labeling scheme key in shown in Figure 4.3.2

4.3.2 ^{1}H-^{1}H 2D NOESY and ^{1}H-^{1}H 2D ROESY NMR Spectroscopic Studies of Menaquinone-1 and Menaquinone-1(H_2) in d_5-pyridine, d_3-acetone, and d_6-DMSO.

The 1D ^{1}H NMR experiments demonstrated that the solvent environment impacts the chemical environment surrounding MK-1 enough to change the observed chemical shift. However, whether the conformation of MK-1 and MK-1(H_2) changes depending on the solvent environment remained unclear. Therefore, we used two different complementary 2D NMR spectroscopic techniques (^{1}H-^{1}H 2D NOESY and ^{1}H-^{1}H 2D ROESY NMR) to elucidate the MK analogs conformation in organic solution. We present the 2D NMR data for MK-1 in Figure 4.3.2,

the 2D NMR data for MK-1(H_2) in Figure 4.3.3, and the 3D conformations for MK-1 and MK-1(H_2) are shown in Figure 4.3.4. We used a semi-quantitative approach for the 2D NMR conformational analysis where NOE/ROE distance intensities are as follows: a strong cross peak is ~2-3 Å, a medium cross peak is ~3-4 Å, and a weak cross peak is >4 Å distance.[44] We standardized the signal intensities on the basis of the intensity of the H_a-H_c cross peak of MK-1 or MK-1(H_2), which was used as the internal intensity calibrant (the actual distance is 2.5 Å, which indicates a strong cross peak). Figure 4.3.2 shows ^{1}H-^{1}H 2D NOESY and ^{1}H-^{1}H 2D ROESY NMR spectra of MK-1 in d_5-pyridine, d_3-acetonitrile (d_3-ACN), and d_6-DMSO (see Figures A4.1-9 and Figures A4.12-20 for full 2D NMR spectra and Figure A4.22 for ROE/NOE correlation traces). These organic solvents were chosen because they differed sufficiently regarding shape, polarity, aromatic vs non-aromatic, and are well behaved in electrochemical studies.

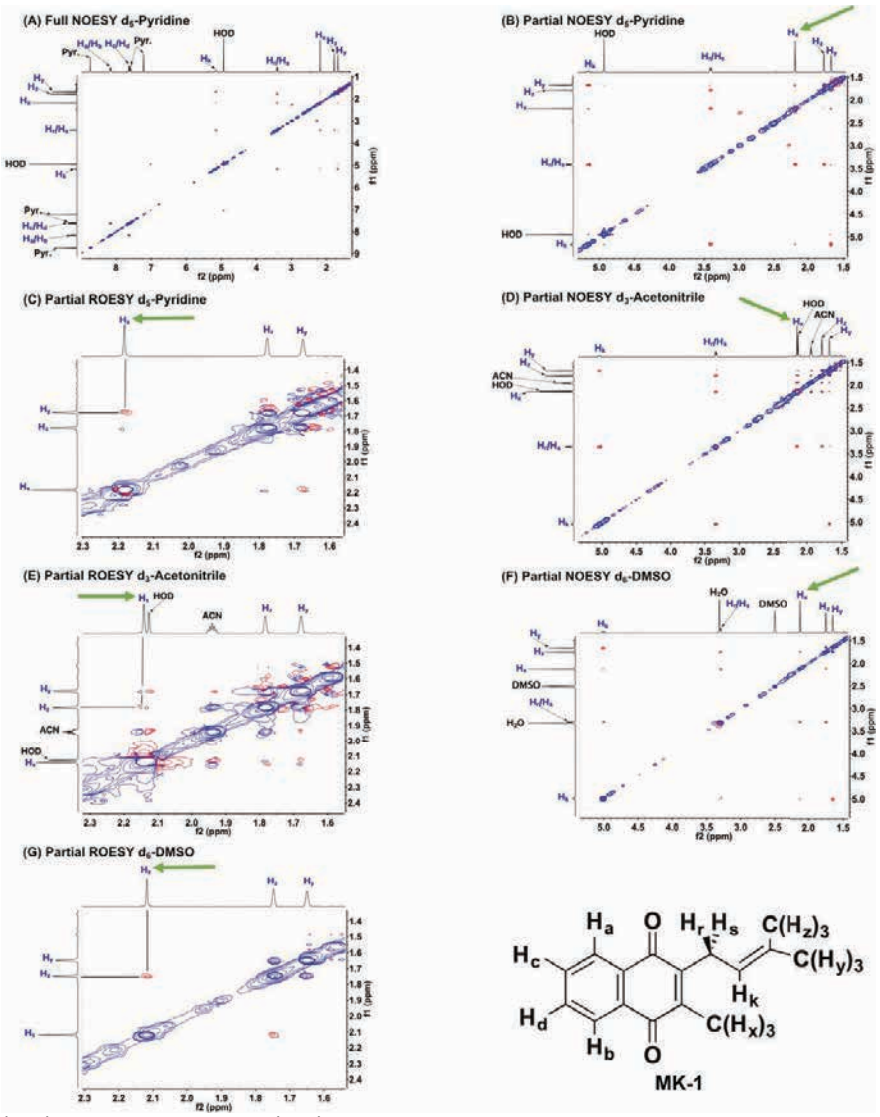

Figure 4.3.2. ^{1}H-^{1}H 2D NOESY and ^{1}H-^{1}H 2D ROESY NMR (400 MHz) spectra of 20 mM MK-1 in d_5-pyridine, d_3-acetonitrile (d_3-ACN), and d_6-DMSO and at 26 °C. (A) Full ^{1}H-^{1}H 2D NOESY NMR spectrum of MK-1 in d_5-pyridine, (B) Partial ^{1}H-^{1}H 2D NOESY NMR spectrum of MK-1 in d_5-pyridine, (C) Partial ^{1}H-^{1}H 2D ROESY NMR spectrum of MK-1 in d_5-pyridine, (D) Partial ^{1}H-^{1}H 2D NOESY NMR spectrum of MK-1 in d_3-ACN, (E) Partial ^{1}H-^{1}H 2D ROESY NMR spectrum of MK-1 in d_3-ACN (F) Partial ^{1}H-^{1}H 2D NOESY NMR spectrum of MK-1 in d_6-DMSO, (G) Partial ^{1}H-^{1}H 2D ROESY NMR spectrum of MK-1 in d_6-DMSO. Blue intensity contours represent negative NOE's or ROE's and red intensity contours represent positive NOE's or ROE's. A standard NOESY pulse sequence was used consisting of 256 transients with 16 scans in the f1 domain using a 500 ms mixing time and a 1.5 sec. relaxation delay. A standard ROESYAD pulse sequence was used consisting of 256 transients with 16 scans in the f1 domain using a 400 ms mixing time and a 2.0 sec. relaxation delay. The structure of MK-1 is shown with a hydrogen labelling scheme key. Green arrows indicate hydrogen H_x, where the observed cross peaks differed the most between the three solvents studied.

The conformation of MK-1 in d_5-pyridine was determined by analyzing the ^{1}H-^{1}H 2D NOESY and ROESY NMR spectra (Figure 4.3.2A-C, Figures A4.1-2). Figure 4.3.2B shows a strong NOE cross peak observed between hydrogens $H_{r/s}$ and H_z and a weak NOE cross peak between $H_{r/s}$ and H_y (see Supporting Information for hydrogen peak assignments of H_z and H_y). Weak NOE/ROE cross peaks are also observed between H_x and H_y (Figure 4.3.2B-C), which supports a folded-extended conformation where the terminal methyl groups orient themselves in a manner to fold upward (C-C bond rotation allows the methyl groups to rotate upwards) positioning H_y close enough to H_x to observe a NOE/ROE cross peak. The weak cross peak (same phase as diagonal) observed between H_x and H_z is likely due to TOCSY or chemical exchange. The weak NOE cross peak in Figure 3B between H_x-H_k has a similar intensity as the NOE cross peak observed between H_x-H_y, which is not explained by a flat-extended conformation (see Figure A4.23E and Table A4.1 for structure and internuclear distances of MK-1 flat-extended conformation). Together, the above observations provide evidence that MK-1 adopts a conformation in d_5-pyridine where the isoprenyl side chain folds upwards.

Regarding the conformation of MK-1 in d_3-ACN, Figure 4.3.2D-E (Figure A4.4-5) shows a weak NOE/ROE cross peak observed between H_x and H_z and no cross peak observed between H_x and H_y (the cross peak observed is opposite in phase to the diagonal and likely due to chemical exchange or TOCSY exchange where the latter is more reasonable). There is a weak NOE cross peak between H_x and H_k that is only visible in the spectrum upon zooming in to lower floors, which is not consistent with an extended-flat conformation and is different from that observed in d_5-pyridine, indicating slightly different conformations adopted between solvent environments. However, the cross peak intensity between $H_{r/s}$ and H_z or H_y is similar to that in

d_5-pyridine. There is also a NOE/ROE cross peak observed between H_y and HOD and between H_y and the solvent, d_3-ACN, and interactions between MK and solvent were not observed in the 2D NMR spectra of MK-1 in d_5-pyridine or d_6-DMSO. Based on the above observations, MK-1 likely adopts a folded-extended conformation in d_3-ACN that differs slightly from the folded-extended conformation in d_5-pyridine.

Finally, the conformation of MK-1 in d_6-DMSO was determined. Figure 4.3.2F-G (Figure A4.7-8) shows a weak NOE cross peak between H_x and H_k and a medium NOE/ROE cross peak between H_x and H_z, with no NOE/ROE cross peak observed between H_x and H_y. This is similar to the cross peaks observed in d_3-ACN, but the H_x to H_z cross peak is stronger in d_6-DMSO, indicating slightly different conformations. The above observations would not be explained by a flat-extended conformation and MK-1 likely adopts a folded-extended conformation in d_6-DMSO more similar to that in d_3-ACN than in d_5-pyridine.

To investigate whether saturation of the alkene in the isoprenyl side chain influences the conformation of MK-1(H_2), ^{1}H-^{1}H 2D NOESY and ^{1}H-^{1}H 2D ROESY NMR spectra were collected in d_5-pyridine, d_3-ACN, and d_6-DMSO (Figure 4.3.3). Similar NOE/ROE cross peaks were observed for MK-1(H_2) in d_5-pyridine compared to MK-1 in d_5-pyridine (Figure 4.3.3A-C, Figure A4.12-13). Specifically, a weak NOE/ROE cross peak between H_x and H_z/H_y, a medium NOE/ROE cross peak between H_x and $H_{r/s}$, and a medium NOE/ROE cross peak between $H_{r/s}$ and H_y was observed. There is also no NOE/ROE cross peak observed between H_x and H_l, which further supports a folded-extended conformation. This is suggestive of a similar conformation for MK-1(H_2) and MK-1 in d_5-pyridine, where both adopt a similar folded-extended conformation. Similar NOE/ROE cross peaks were observed for MK-1(H_2) in d_3-ACN compared to MK-1 in d_3-ACN (Figure 4.3.3D-E,

Figure A4.15-16). Specifically, the lack of an observable cross peak between H_x and H_z/H_y (compared to a weak NOE/ROE cross peak in the case of MK-1), a medium NOE/ROE cross peak between H_x and $H_{r/s}$, a medium NOE/ROE cross peak between $H_{r/s}$ and H_y, and a very weak NOE/ROE cross peak between H_x and H_k was observed. There is also no NOE/ROE cross peak observed between H_x and H_l. This is suggestive of a similar conformation for MK-1(H_2) and MK-1 in d_3-ACN, where both adopt a similar folded-extended conformation. Comparable NOE/ROE cross peaks were observed for MK-1(H_2) in d_6-DMSO compared to MK-1 in d_6-DMSO (Figure 4.3.3F-G, Figure A4.18-19). For instance, a medium NOE/ROE cross peak between H_x and H_z/H_y, a medium NOE/ROE cross peak between H_x to $H_r/_s$, a medium NOE/ROE cross peak between $H_r/_s$ to H_y/H_z, a medium NOE/ROE cross peak between H_x and H_k was observed. There was also no NOE/ROE cross peak observed between H_x and H_l. This is suggestive of a comparable conformation for MK-1(H_2) and MK-1 in d_6-DMSO, where both adopt a similar folded-extended conformation.

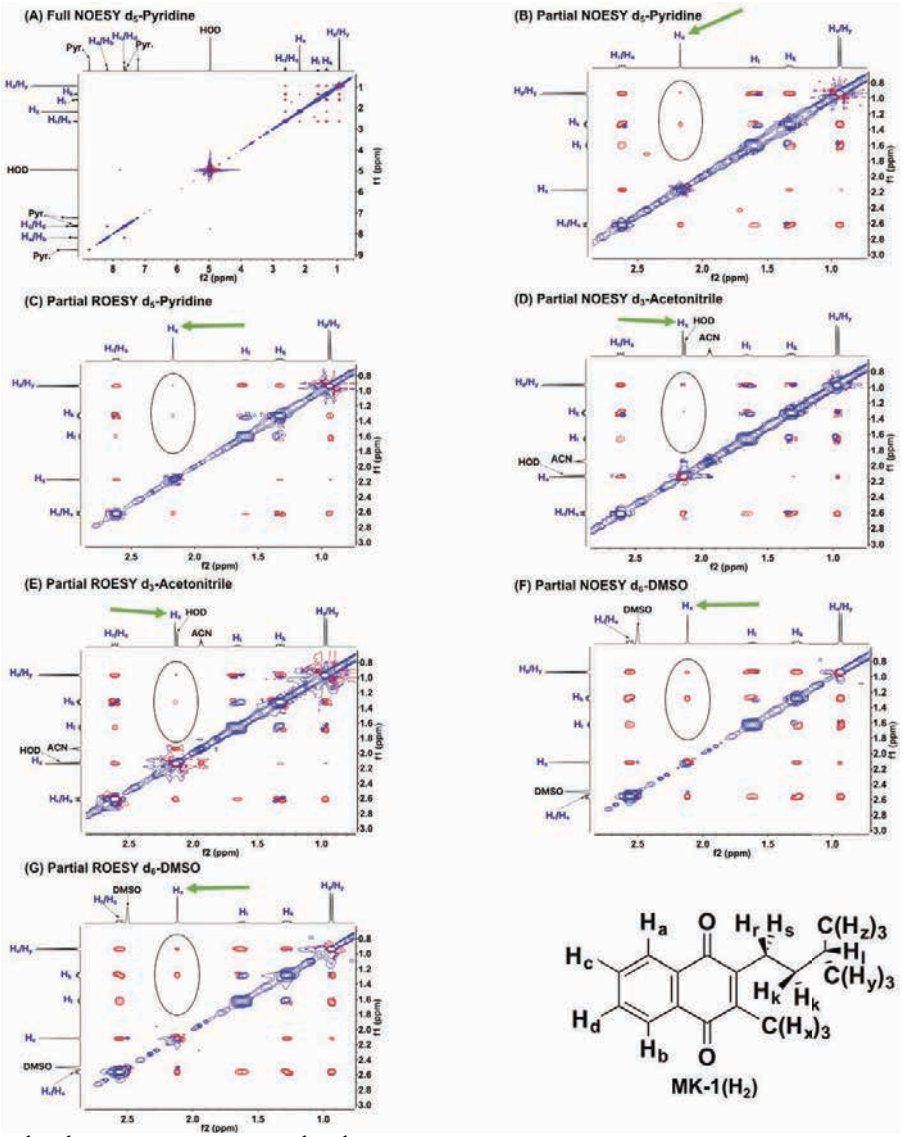

Figure 4.3.3. ^{1}H-^{1}H 2D NOESY and ^{1}H-^{1}H 2D ROESY NMR (400 MHz) spectra of 20 mM MK-1(H_2) in d_5-pyridine, d_3-acetonitrile (d_3-ACN), and d_6-DMSO and at 26 °C. (A) Full ^{1}H-^{1}H 2D NOESY NMR spectrum of MK-1(H_2) in d_5-pyridine, (B) Partial ^{1}H-^{1}H 2D NOESY NMR spectrum of MK-1(H_2) in d_5-pyridine, (C) Partial ^{1}H-^{1}H 2D ROESY NMR spectrum of MK-1(H_2) in d_5-pyridine, (D) Partial ^{1}H-^{1}H 2D NOESY NMR spectrum of MK-1(H_2) in d_3-ACN, (E) Partial ^{1}H-^{1}H 2D ROESY NMR spectrum of MK-1(H_2) in d_3-ACN (F) Partial ^{1}H-^{1}H 2D NOESY NMR spectrum of MK-1(H_2) in d_6-DMSO, (G) Partial ^{1}H-^{1}H 2D ROESY NMR spectrum of MK-1(H_2) in d_6-DMSO. Blue intensity contours represent negative NOE's or ROE's and red intensity contours represent positive NOE's or ROE's. A standard NOESY pulse sequence was used consisting of 256 transients with 16 scans in the f1 domain using a 500 ms mixing time and a 1.5 sec. relaxation delay. A standard ROESYAD pulse sequence was used consisting of 256 transients with 16 scans in the f1 domain using a 400 ms mixing time and a 2.0 sec. relaxation delay. The structure of MK-1(H_2) is shown with a hydrogen labelling scheme key. Green arrows indicate hydrogen H_x, where the observed cross peaks differed the most between the two solvents studied and black circles highlight the region that changes the most between spectra.

Considering the similar trends in cross peaks and intensities observed for MK-1 and MK-1(H_2) in d_5-pyridine, d_3-ACN, and d_6-DMSO, it appears that saturation does not affect the conformation significantly. The subtle differences observed for MK-1 and MK-1(H_2) in the different organic solvents suggests that slightly different folded-extended conformations are adopted between each of the organic solvents, but MK-1 and MK-1(H_2) have very similar conformations in each solvent. This suggests that there could be a correlation between a preferred conformation in each solvent environment and that a simple change such as saturation of a double bond only slightly influences this preferred conformation. Overall, these truncated MK analogs appear to adopt folded-extended conformations in organic solution based on the 2D NMR data and the folded-extended conformations differ slightly between solvent environments. However, it is possible that an equilibrium population exists between multiple conformations (e.g., folded and/or non-folded conformations). The observations from the 2D NMR spectroscopic studies support our first hypothesis that the most fundamental MK-1 analogs adopt folded conformations regardless of the degree of saturation in their isoprenyl side chain.

4.3.3 Illustrating Menaquinone-1 and Menaquinone-1(H_2) Conformations using Molecular Mechanics

To clearly show illustrations of MK-1 and MK-1(H_2), conformations were generated based on our interpretation of observed cross peak intensities in the ^{1}H-^{1}H 2D NOESY and ROESY NMR spectral data using a semi-quantitative approach. We used molecular mechanics calculations (MM) to illustrate and model these conformations. This allowed us to explore the energy surface of conformations corresponding to MK-1 or MK-1(H_2) in either d_5-pyridine, d_3-ACN, or d_6-DMSO

determined from the spectral data and provided a means for a visual comparison between conformations (Figure 4.3.4). Specific conformations were generated by constraining internuclear distances consistent with the 2D NMR spectral data observations, then energy optimized to calculate an energy value as well as produce realistic bond lengths and angles.

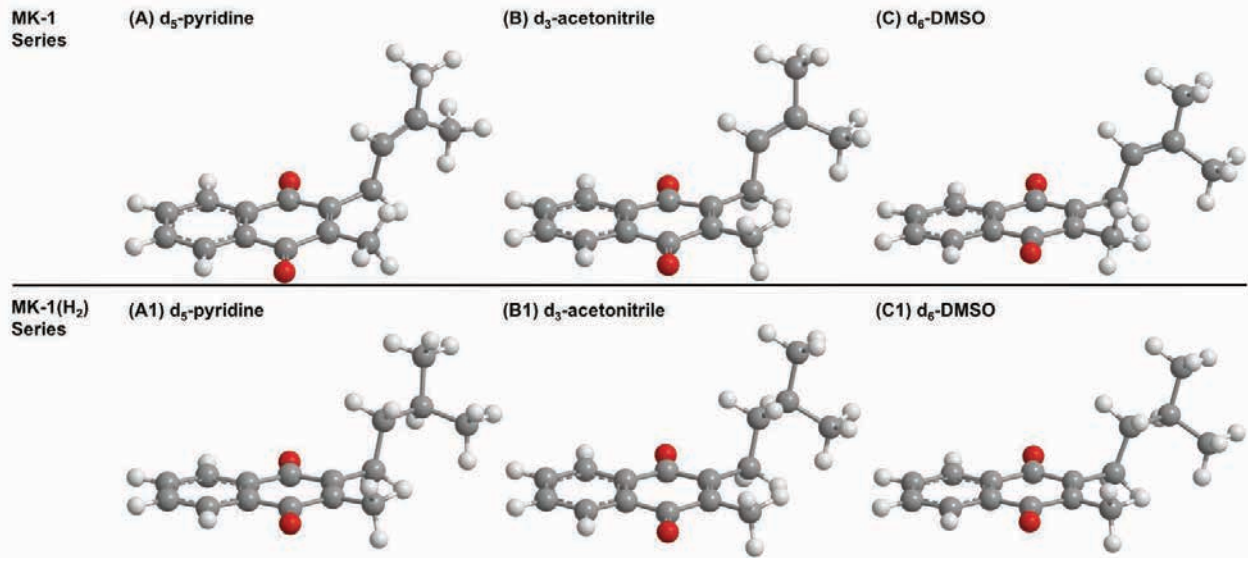

Figure 4.3.4. MK-1 and MK-1(H_2) conformations generated using MMFF94 calculations to illustrate the possible conformations consistent with the ^{1}H-^{1}H 2D NOESY and ROESY NMR spectral studies where conformations agree with observed cross peak interactions and intensities. MK-1 Series: (A) Illustrates proposed MK-1 conformation in d_5-pyridine determined from ^{1}H-^{1}H 2D NOESY and ROESY NMR spectral data cross peak interactions (51.8 kcal/mol, H_x-H_y: 4.3 Å), (B) Illustrates proposed MK-1 conformation in d_3-ACN determined from ^{1}H-^{1}H 2D NOESY and ROESY NMR spectral data cross peak interactions (48.6 kcal/mol, H_x-H_z: 3.9 Å). (C) Illustrates proposed MK-1 conformation in d_6-DMSO determined from ^{1}H-^{1}H 2D NOESY and ROESY NMR spectral data cross peak interactions (47.3 kcal/mol, H_x-H_z: 3.2 Å). MK-1(H_2) Series: (A1) Illustrates proposed MK-1(H_2) conformation in d_5-pyridine determined from ^{1}H-^{1}H 2D NOESY and ROESY NMR spectral data cross peak interactions (42.1 kcal/mol, H_x-H_z: 3.6 Å), (B1) Illustrates proposed MK-1(H_2) conformation in d_3-ACN determined from ^{1}H-^{1}H 2D NOESY and ROESY NMR spectral data cross peak interactions (43.0 kcal/mol, H_x-H_z: 4.0 Å). (C1) Illustrates proposed MK-1(H_2) conformation in d_6-DMSO determined from ^{1}H-^{1}H 2D NOESY and ROESY NMR spectral data cross peak interactions (41.9 kcal/mol, H_x-H_z: 3.4 Å).

One of the low energy conformations generated for MK-1 has a conformation (Figure 4.3.4A, 51.8 kcal/mol, H_x-H_y: 4.3 Å) consistent with the 2D NOESY/ROESY spectral parameters in d_5-pyridine. A lower energy conformation for MK-1 (Figure 4.3.4B, 48.6 kcal/mol, H_x-H_z: 3.9 Å) is

consistent with the 2D NOESY/ROESY spectral parameters in d_3-ACN. A slightly lower energy conformation for MK-1 (Figure 4.3.4C, 47.3 kcal/mol, H_x-H_z: 3.2 Å) is consistent with the 2D NOESY/ROESY spectral parameters in d_6-DMSO. One of the low energy conformations generated for MK-1(H_2) has a conformation (Figure 4.3.4A1, 42.1 kcal/mol, H_x-H_z: 3.6 Å) consistent with the NOESY/ROESY spectral parameters in d_5-pyridine. A conformation with slightly higher energy for MK-1(H_2) (Figure 4.3.4B1, 43.0 kcal/mol, H_x-H_z: 4.0 Å) is consistent with the 2D NOESY/ROESY spectral parameters in d_3-ACN. A lower energy conformation for MK-1(H_2) (Figure 4.3.4C1, 41.9 kcal/mol, H_x-H_z: 3.4 Å) is consistent with the 2D NOESY/ROESY spectral parameters in d_6-DMSO. All six of these conformations exhibit folding of the isoprenyl side chain upward out of the quinone plane (Figure 4.3.4) and can be described as a folded-extended conformation. Conformations for MK-1(H_2) are very similar to that of MK-1 in each organic solvent environment examined based on 2D NMR studies.

For comparison, conformations seen in Figure A4.23D-D1 are the lowest energy conformations we found for MK-1 or MK-1(H_2), where a flat-extended conformation was subjected to a MM simulation using 10,000 iterations followed by an energy minimization, which illustrates that folded conformations are easily reached and energetically favorable. In addition to the folded conformations shown in Figure 4.3.4, a series of alternative flat conformations for MK-1 and MK-1(H_2) (Figure A4.23E-E1 & F-F1) were also generated based on what is commonly seen in life science textbooks and literature and then subjected to energy optimization.[13, 45-46] These flat-extended conformations are ~11-20 kcal/mol higher than the lowest energy conformations of MK-1 and MK-1(H_2). A table of selected internuclear distances for conformations seen in Figure 4.3.4 and Figure A4.23 is shown in the Supporting Information.

Importantly, the folded-extended conformations for MK-1 determined in organic solution closely resemble the folded conformation of the first isoprene unit of MK-2 (containing two isoprene units), which we determined previously in the same organic solvent environments.[38]

4.3.4 Reactivity of Menaquinone-1 and Menaquinone-1(H_2) in Different Organic Solvents: Electrochemistry

To determine the effect of saturation of the MK isoprenyl side chain on the quinone redox potential, we used cyclic voltammetry to measure the redox potentials of MK-1 and MK-1(H_2). Both MK-1 and MK-1(H_2) have two reversible single electron redox processes, the first is the quinone to semiquinone ($Q/Q^{\bullet-}$) and the second is the semiquinone to the dianion ($Q^{\bullet-}/Q^{2-}$) (Scheme 4.3.1). The half-wave potentials for each redox process $Q/Q^{\bullet-}$ and $Q^{\bullet-}/Q^{2-}$ in each solvent for MK-1 and MK-1(H_2) are listed in the Supporting Information and cyclic voltammograms (CVs) are shown in Figure 4.3.5. The electrolyte, tetrabutylammonium perchlorate (TBAP), was chosen because of the excellent solubility in all organic solvents. Furthermore, the addition of TBAP to MK-1 solutions in each solvent did not affect the observed chemical shifts of the MK-1 hydrogens and thus no evidence for ion pairing was found (see Supporting Information). The water content of the solvents can affect the semiquinone $Q^{\bullet-}/Q^{2-}$ process as acidic protons influence hydroquinone production, which results in potentials that approach the quinone $Q/Q^{\bullet-}$ half-wave potentials and therefore, we only compared the first redox process, $Q/Q^{\bullet-}$ in our analyses.[47-48] Thus, it was important that we carried out our electrochemical experiments in anhydrous aprotic organic solvents as this issue is then avoided and organic solvents more closely resemble the native MK environment within a cellular membrane compared to aqueous solutions.

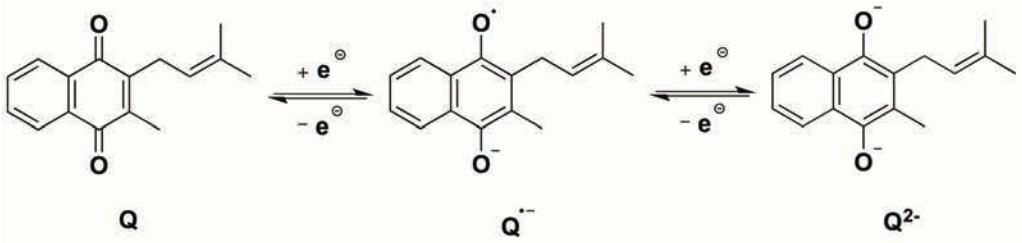

Scheme 4.3.1. Illustration of the one electron reduction of the quinone (Q) of MK-1 to the semiquinone radical anion ($Q^{\bullet-}$) and the second one electron reduction to the dianion (Q^{2-}).

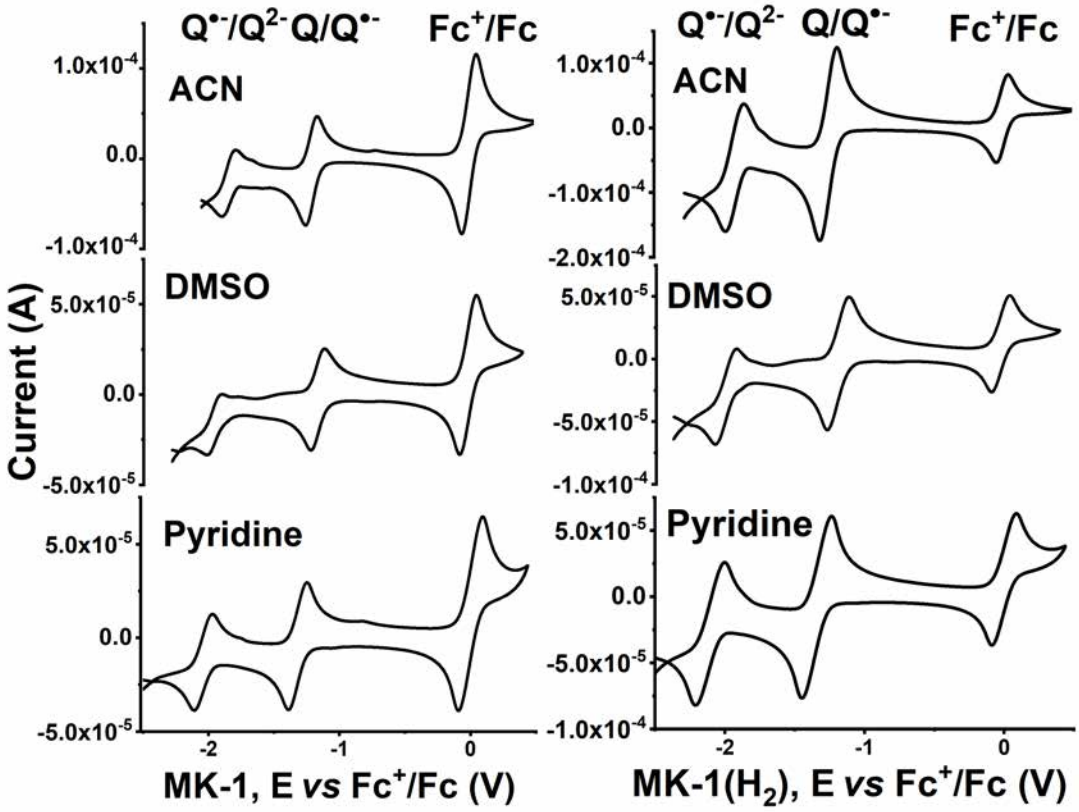

Figure 4.3.5. Six cyclic voltammogram's (CVs) of 2 mM MK-1 and MK-1(H_2) in ACN, DMSO, and pyridine. The potentials are referenced to the Fc^+/Fc couple internal standard (2 mM) determined in each solvent. From left to right, redox processes are $Q^{\bullet-}/Q^{2-}$, $Q/Q^{\bullet-}$, and Fc^+/Fc. Each sample has 0.1 M TBAP and was degassed with argon gas for 10 min at ambient temperature before spectra were recorded. Current sweeps are in the anodic direction from -2V to 1V and back to -2V *vs* Ag/AgCl. A 100 mV/s scan rate was used.

As shown in Figure 4.3.5, the ferrocene couple, Fc^+/Fc, was used as an internal reference standard so that the half-wave potentials are set to 0 V *vs* Fc^+/Fc. The $Q/Q^{\bullet-}$ $E_{1/2}$ *vs* Fc^+/Fc for MK-1 in ACN, DMSO, and pyridine were measured to be -1.227 (± 0.002) V, -1.158 (± 0.002) V, and -

1.319 (± 0.001) V, respectively. The $Q/Q^{\bullet-}$ $E_{1/2}$ *vs* Fc^{+}/Fc for MK-1(H_2) in ACN, DMSO, and pyridine were measured to be -1.247 (± 0.007) V, -1.179 (± 0.002) V, and -1.343 (± 0.001) V, respectively. The results for the $Q/Q^{\bullet-}$ $E_{1/2}$ vs Fc^{+}/Fc values are near those reported for 1,4-naphthoquinone and those previously reported by our group for MK-2.[38, 49-50] The $Q^{\bullet-}/Q^{2-}$ $E_{1/2}$ *vs* Fc^{+}/Fc for MK-1 in ACN, DMSO, and pyridine were measured to be -1.882 (± 0.014) V, -1.949 (± 0.006) V, and -2.037 (± 0.005) V, respectively. The $Q^{\bullet-}/Q^{2-}$ $E_{1/2}$ *vs* Fc^{+}/Fc for MK-1(H_2) in ACN, DMSO, and pyridine were measured to be -1.912 (± 0.009) V, -1.9947 (± 0.0008) V, and -2.109 (± 0.005) V, respectively. The measured quinone half-wave redox potential differences in these solvents are statistically significant as they are distinctly different from each other at high confidence intervals (see Figure 4.3.6 caption and Supporting Information).

The difference in mV between the unsaturated MK-1 vs. the saturated MK-1(H_2) quinone redox potential in each solvent of the less variable $Q/Q^{\bullet-}$ process are of the same magnitude of ~20 mV with specific values of 20.033 (± 0.007) mV, 21.333 (± 0.002) mV, and 23.917 (± 0.001) mV for ACN, DMSO, and pyridine, respectively (Figure 4.3.6). The $Q/Q^{\bullet-}$ process potentials are less variable as the presence of acidic protons and/or water can create the hydroquinone species, which results in the $Q^{\bullet-}/Q^{2-}$ process coalesced onto the first redox potential. Our previous work on MK-2 demonstrated that the isoprenyl side chain folds over toward the naphthoquinone moiety and that the solvent environment can influence the preferred conformation.[38] The mixing of molecular orbitals (MOs) on the naphthoquinone moiety with the isoprenyl side chain may potentially result in different energies of the electrochemical band gap (or HOMO to LUMO gap) needed to reduce the quinone carbonyl oxygen to an anionic oxygen radical. The electrochemical band gap is suggestive of the potential observed or the energy required to reduce or oxidize an

electrochemical process. This difference in the band gap results in unique half-wave potentials as energy (E) and potential difference (V) are directly proportional as evident by the electrostatic equation E = V*Q where Q is charge. The saturation or unsaturation of the isoprenyl side chain can therefore potentially influence these MOs and may alter the quinone redox potential in this manner. The semiquinone redox potential difference of ~20 mV between MK-1 and MK-1(H_2) could indicate the band gap energy difference between the saturated and unsaturated double bond in the one unit isoprenyl side chain. However, the difference of ~20 mV is most likely due to an indirect effect manifested by a through bond electronic change by the isoprenyl substituent on the quinone. An indirect substituent effect was used to explain a redox potential change for an N-aromatic substituent on a quinone.[2] The conformational differences of MK-1 between solvents were small and the short isoprenyl side chain has limited spatial reach toward the naphthoquinone. If such an effect existed between conformation and redox potential, it may not be evident in the one isoprene unit system. However, suitable high level computational calculations should be carried out to characterize the HOMO-LUMO gap of this system and determine the exact contributions to the observed ~20 mV difference.

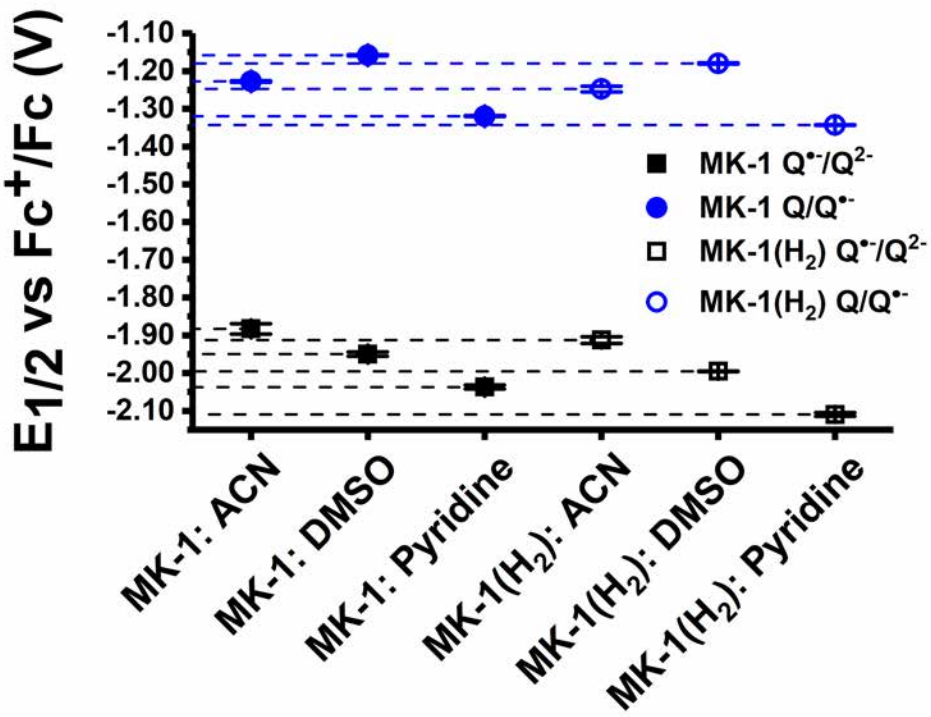

Figure 4.3.6. Measured $E_{1/2}$ (vs Fc^{+}/Fc in V) of MK-1 and MK-1(H_2) $Q/Q^{\bullet-}$ and $Q^{\bullet-}/Q^{2-}$ redox process versus solvent. Each solvent was run in triplicate, with error bars shown as standard deviations. Added horizontal lines show the distinction between each solvent for each redox process. All solvent comparisons (ACN vs DMSO, etc.) for each redox process half-wave potential for MK-1 or MK-1(H_2) are statistically different with Student's *t* test confidence intervals of 99.9% ($p < 0.0001$) except the ACN vs DMSO $Q/Q^{\bullet-}$ of MK-1, which was 99.5% ($p < 0.0016$), (at four degrees of freedom). Comparisons between MK-1 vs MK-1(H_2) half-wave potentials of $Q/Q^{\bullet-}$ and $Q^{\bullet-}/Q^{2-}$ for each solvent were at the 99.9% ($p < 0.0001$) confidence level except for ACN, which were 98% ($p < 0.0089$) and 95% ($p < 0.0355$), respectively, (at four degrees of freedom). See Supporting Information for data.

We also observed a trend in the data of the potential difference for the $Q/Q^{\bullet-}$ process as compared by solvent versus degree of saturation (see Supporting Information). For both MK-1 and MK-1(H_2), the potential difference of the $Q/Q^{\bullet-}$ process between ACN and DMSO is 69.250 (± 0.003) mV and 67.950 (± 0.008) mV, respectively. The other solvent comparisons also have values that agree with each other. For MK-1 and MK-1(H_2), the potential difference of the $Q/Q^{\bullet-}$ process between DMSO and pyridine is 161.050 (± 0.002) mV and 163.633 (± 0.002) mV, respectively. Similarly, MK-1 and MK-1(H_2) have a potential difference of the $Q/Q^{\bullet-}$ process

between ACN and pyridine is 91.800 (± 0.003) mV and 95.683 (± 0.008) mV, respectively. This conserved difference of the $Q/Q^{\bullet-}$ half-wave potentials between MK-1 vs MK-1(H_2) in each solvent may signify that how the isoprenyl side chain folds is truly solvent dependent and/or it may also suggest that the conformation of the short isoprenyl side chain (5 carbons) of MK-1 has little effect on the observed quinone redox potential in the one isoprene unit system.

In summary, both MK-1 and MK-1(H_2) during the first electrochemical process producing the semiquinone has the most positive potential in DMSO and the most negative potential in pyridine, demonstrating MK-1 or MK-1(H_2) is slightly more reducible in DMSO than ACN or pyridine. Remarkably, the observation of a ~20 mV change in quinone $Q/Q^{\bullet-}$ $E_{1/2}$ between MK-1 and MK-1(H_2) supports our second hypothesis that saturation of the isoprenyl side chain of MK-1 affects the observed quinone redox potential. This is the first time this has been demonstrated in a quinone/MK system and the difference is presumably most in part due to a through bond indirect effect, where there is an electronic perturbation of the quinone system upon saturation of the isoprenyl side chain. There was not a large difference between the MK-1 analog conformations and therefore changes in the observed redox potentials are not likely due to conformational differences. However, a potential correlation should be investigated using the appropriate fully unsaturated and partially saturated MK-2 analogs in combination with computational methods to determine if conformational folding of the second isoprene unit can alter the quinone redox potential in MK analogs with an unsaturated vs partially saturated isoprenyl side chain.

4.3.5 Interaction of Langmuir Phospholipid Monolayers with Menaquinone-1 and Menaquinone-1(H_2)

To understand the interaction and conformation of fundamental MK analogs within a membrane environment, we focused on characterizing the interaction of the most simple, truncated MK analogs, MK-1 and MK-1(H_2), with model membrane interfaces. Model membrane systems, such as Langmuir phospholipid monolayers, liposomes, micelles, and RM microemulsions, have been used to characterize the interaction and location of probe molecules with membrane-like interfaces (Figure 4.3.7).[43, 51-59] Langmuir phospholipid monolayers and RMs are two complementary model membrane systems that together can characterize the interaction, location, placement, and conformation of MKs within a model membrane interface. Using these two model membrane systems together allowed us to determine whether MK-1 analogs interact with model membrane interfaces and if a folded conformation is adopted within the RM model membrane interface.

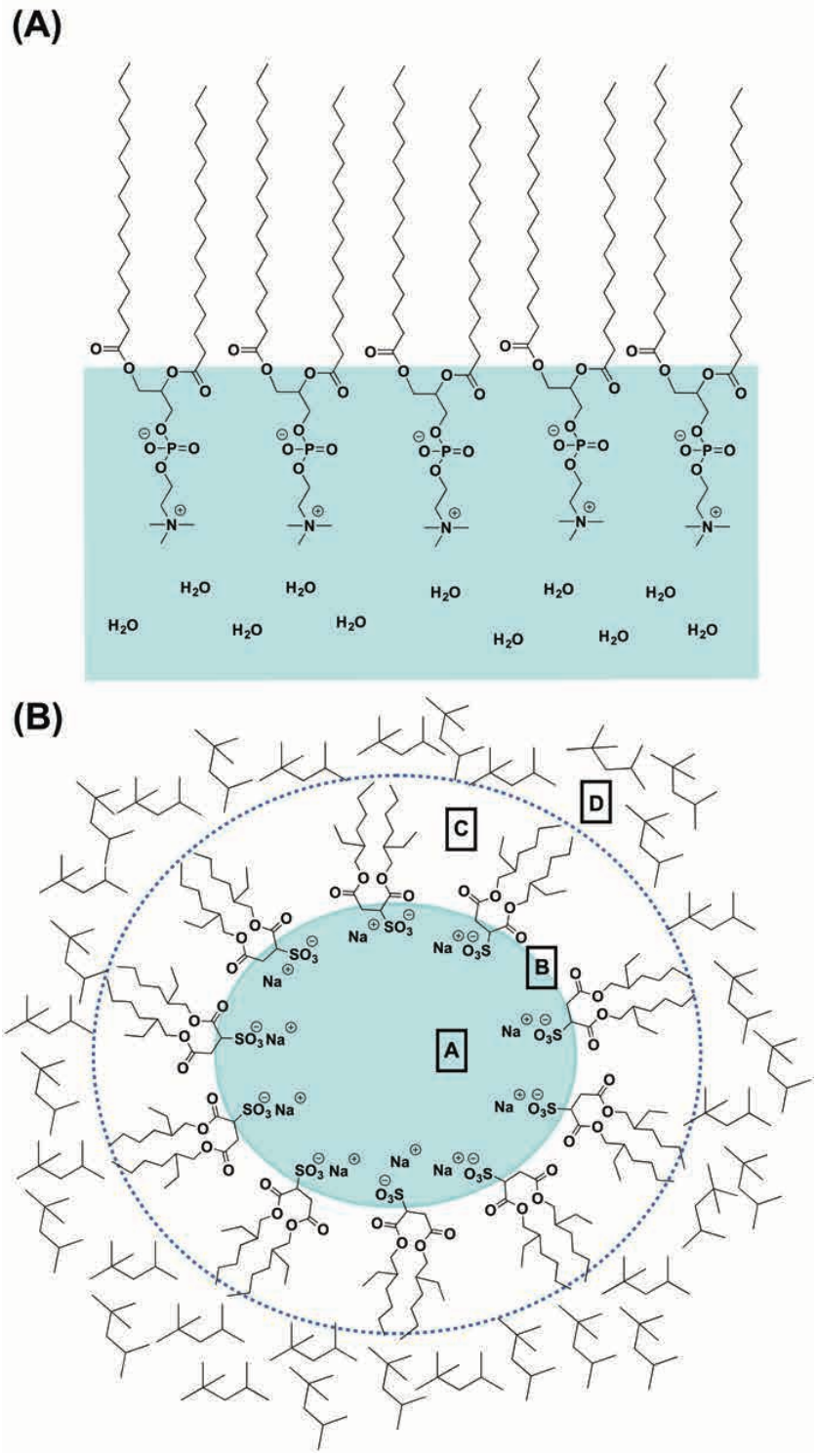

Figure 4.3.7. Schematic diagram of (A) a Langmuir phospholipid monolayer (top) and (B) a RM (bottom) present in a microemulsion with labeling as follows: the water pool (A), the Stern layer (B), the hydrophobic surfactant tails (C), and the organic solvent, isooctane (D). Adapted with permission from *J. Org. Chem.*, 2018, *83* (1), pp 275–288. Copyright 2018 American Chemical Society.

Surface pressure compression isotherm experiments using Langmuir monolayers (Figure 4.3.7A) have been useful in characterizing interactions between lipids and other lipids, lipids and fatty acids[38, 60-63], and lipids and hydrophilic molecules.[41, 51, 60] During a surface pressure compression isotherm experiment, condensing and expanding effects caused by the presence of another lipid (such as MK) can be observed and changes in phase transitions of the phospholipids can indicate an interaction between the two lipids. To establish that the two MK analogs interact with membrane interfaces, compression isotherms of Langmuir monolayers were used to characterize the interactions of MK-1 and MK-1(H_2) with phospholipid interfaces of common phospholipids found in biological systems such as dipalmitoylphosphatidylcholine (DPPC) or dipalmitoylphosphatidylethanolamine (DPPE).[64-66] Therefore, surface pressure compression isotherms of Langmuir monolayers consisting of DPPC, DPPE, MK-1, MK-1(H_2), or a mixture of phospholipid and MK analog were performed to determine if the MK analogs had any effect on the packing and compressibility of the phospholipids. The resulting compression isotherms are shown in Figure 4.3.8. The control monolayers of DPPC and DPPE are comparable to what has been found in literature.[61, 67] The DPPC monolayers both show a characteristic gas-liquid phase transition at 5 mN/m and collapse at 55 mN/m. The DPPE monolayers also collapsed at 55 mN/m, which aligns well with literature.[61, 67]

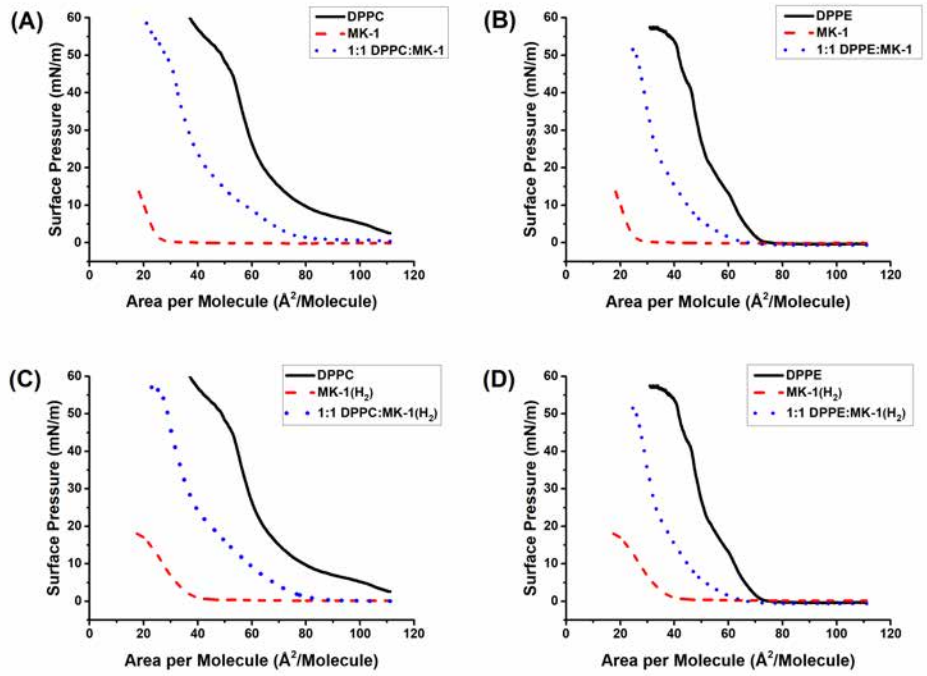

Figure 4.3.8. Compression isotherms of MK-1 and MK-1(H_2) films (dashed red lines), DPPC or DPPE phospholipid monolayers (solid black lines), or a 50:50 mixture of MK-1 or MK-1(H_2) and phospholipid (dotted blue lines). On the top left (A) are the resulting compression isotherms of MK-1 and DPPC, on the top right (B) are the resulting compression isotherms of MK-1 and DPPE, on the bottom left (C) are the resulting compression isotherms of MK-1(H_2) and DPPC, and on the bottom right (D) are the resulting compression isotherms of MK-1(H_2) and DPPE.

The MK-1 and MK-1(H_2) pure films were compressed in the same manner as the phospholipid films. Both MK-1 and MK-1(H_2) monolayers did not reach a pressure above 20 mN/m similar to findings reported for ubiquinone-10 (UQ-10) and plastoquinone.[61-62, 68] The films were not able to reach a high pressure similar to other lipoquinones, suggesting that the MK films were either slightly soluble in the sub phase (similar to UQ-2[61]) as the pressure was increased or aggregation was occurring, which has been shown for lipoquinones with longer isoprenyl side chains.[61-62] Most likely, the MK-1 analogs are aggregating as neither analog was soluble in D_2O (see solution 1D NMR studies section).

When the MK's are mixed with DPPC or DPPE phospholipids, differences in phase transitions and compression moduli indicate that an interaction with the MK analogs and phospholipids occurred. First of which, the gas to liquid phase transition for DPPC is non-existent when either MK-1 or MK-1(H_2) is present. This suggests a condensing effect at low pressures. Within all the compression isotherms of the mixed monolayers, a change in slope occurs at about 20 mN/m [similar to collapse pressure of MK-1 and MK-1(H_2)], which follows the pattern in literature with the MK analogs being compressed out of the monolayer to the top of the monolayer similar to UQ.[61-62] To determine if the MK-1 analogs still affected the phospholipid monolayers even at higher surface pressures, the compression moduli of each curve were compared in the Supporting Information (see Supporting Information for compression moduli data and interpretation). In each case, the mixed monolayer exhibited a decrease in compression modulus (easier to compress) than the pure phospholipid monolayers, indicating that the MK analogs affect the phospholipid monolayer throughout compression even at physiologically relevant surface pressures (~30-35 mN/m).[69]

Overall, the MK analogs do not form stable monolayers at high pressures (above 20 mM/m), have a compressing effect on the phospholipid monolayers, and at higher pressures, the MK analogs most likely are compressed out of the monolayer onto the phospholipid tails similar to previously reported lipoquinones with longer isoprenyl side chains.[38, 61-62, 68] It is important to note that the Langmuir phospholipid monolayer studies do not provide evidence for a folded MK conformation due to the nature of the experiment; however, they do demonstrate that MK-1 and MK-1(H_2) interact with the phospholipid model membrane interface even at physiological

surface pressures similarly to other quinones and there was not a large difference observed between the unsaturated and saturated MK-1 analog.[38, 61-62, 68]

4.3.6 1D ^{1}H NMR Spectroscopic Studies of Menaquinone-1 and Menaquinone-1(H_2) in Reverse Micelles

The studies carried out using Langmuir phospholipid monolayers established that the two MKs interacted with the phospholipid interface. However, the placement, orientation, and conformation of the MK-1 analogs within an interface was still uncertain. Therefore, to fully characterize the location, orientation, and conformation of the MKs within a model membrane interface, we used RMs (Figure 4.3.7B), which are a ternary microemulsion system in which surfactant is dissolved in an organic solvent and the addition of water creates nano-sized water droplets encased in surfactant.[43, 54-56, 70-71] MK-1 or MK-1(H_2) were placed in RMs of various sizes (w_0 4, 8, 12, 16, 20; where $w_0 = [H_2O]/[AOT]$) and then 1D ^{1}H NMR spectra were obtained for each RM size as well as a spectrum in isooctane (2,2,4-trimethylpentane), Figure 4.3.9.

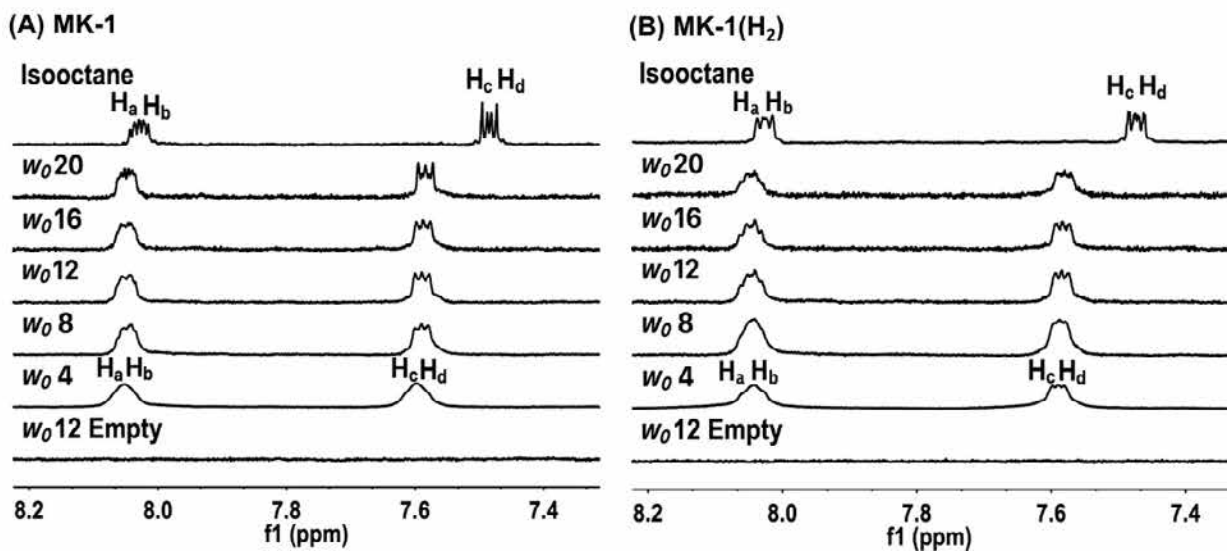

Figure 4.3.9. 1D ^{1}H NMR (400 MHz) spectra of (A) MK-1 and (B) MK-1(H_2) aromatic hydrogens H_a, H_b, H_c, and H_d in different sized RMs (w_0 4, 8, 12, 16, and 20). MK-1 or MK-1(H_2) in isooctane is used as a comparison reference spectrum and w_0 12 Empty is a control spectrum where MK-1 or MK-1(H_2) is absent. Peaks are labeled with corresponding hydrogens for MK-1 and MK-1(H_2) (refer to Figure 4.3.2 and Figure 4.3.3 for hydrogen labelling scheme key). Hydrogens, H_a, H_b, H_c, and H_d, undergo a shift upon insertion into the RMs for both MKs.

The chemical shift difference between MK-1 aromatic hydrogens, H_a/H_b and H_c/H_d, is greater with a value of 0.55 ppm in isooctane versus that of MK-1 in w_0 20 = 0.47 ppm or w_0 4 = 0.45 ppm RMs, which is diagnostic of a change in the environment surrounding MK-1 (Figure 4.3.9). Similarly, the chemical shift difference between MK-1(H_2) aromatic hydrogens, H_a/H_b and H_c/H_d, is greater with a value of 0.56 ppm in isooctane versus that of MK-1(H_2) in w_0 20 = 0.47 ppm or w_0 4 = 0.45 ppm RMs (Figure 4.3.9). The loss of splitting (peak broadening) observed for the aromatic hydrogens as the RM size decreases is attributed to the reduced ability of MK-1 or MK-1(H_2) to tumble freely within the RM interface. We were unable to obtain a spectrum in D_2O as neither MK was soluble even after extended sonication due to the hydrophobicity of the two MK analogs and it is not likely that either of the MKs are in the water pool due to the very poor water solubility of these compounds. Together, the results demonstrated that there was a significant chemical shift difference between the aromatic hydrogens in isooctane vs. the RMs for both MK-

1 analogs. Therefore, it can be concluded that neither of the MK-1 analogs are interacting with the isooctane and are either residing at the RM interface or within the AOT hydrophobic alkyl tail region. Furthermore, dynamic Light Scattering (DLS) experiments were carried out and demonstrated that inserting MK-1 or MK-1(H_2) into the RM does not alter the size of the RM nor destroy the RMs once inside and are stable over the time course of NMR experiments (see Supporting Information). Overall, we concluded that MK-1 and MK-1(H_2) interacted with RMs and resided within the RM model membrane interface.

4.3.7 ^{1}H-^{1}H 2D NOESY and ^{1}H-^{1}H 2D ROESY NMR Spectroscopic Studies of Menaquinone-1 and Menaquinone-1(H_2) in a Reverse Micelle Model Membrane System

The 1D ^{1}H NMR spectra of MK-1 and MK-1(H_2) demonstrated that MK-1 analogs reside within the interface of RMs. However, more information was needed to determine the orientation, position, and conformation while residing inside the RM interface. MK-1 was placed inside a w_0 12 RM and ^{1}H-^{1}H 2D NOESY and ^{1}H-^{1}H 2D ROESY NMR spectra were obtained (Figure 4.3.10, Figure 4.3.11, and Figures A4.10-11). NOE/ROE cross peaks between MK-1 and AOT provide evidence for the location, orientation, and conformation within the RM interface.

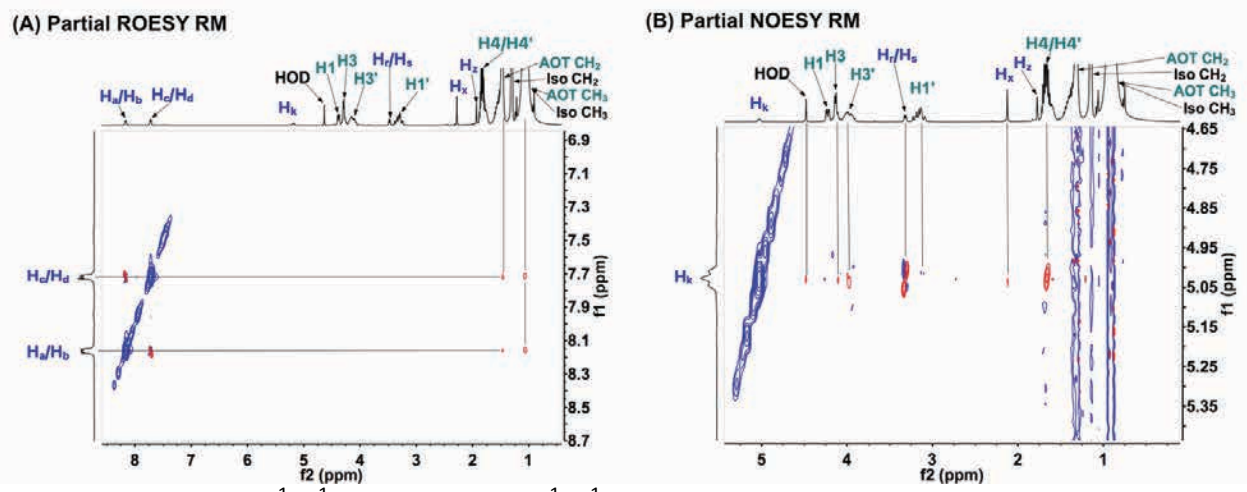

Figure 4.3.10: Partial ^{1}H-^{1}H 2D ROESY and ^{1}H-^{1}H 2D NOESY NMR (400 MHz) spectra of MK-1 in a w_0 12 RM. (A) Partial ROESY spectrum illustrating MK-1 aromatic hydrogens interactions with AOT. (B) Partial NOESY spectrum illustrating MK-1 H_k hydrogen interactions with AOT. Blue to blue hydrogen text labelling shows MK-1 to MK-1 interactions, and blue to teal hydrogen text labelling shows MK-1 to AOT interactions. Blue intensity contours represent negative NOE's or ROE's and red intensity contours represent positive NOE's or ROE's. See Figure 4.3.2 for MK-1 hydrogen labelling scheme key and Figure 4.3.12 for AOT hydrogen labelling scheme key. A standard NOESY pulse sequence was used consisting of 256 transients with 16 scans in the f1 domain using a 200 ms mixing time and a 1.5 sec relaxation delay. A standard ROESYAD pulse sequence was used consisting of 256 transients with 16 scans in the f1 domain using a 200 ms mixing time and a 2.0 sec relaxation delay.

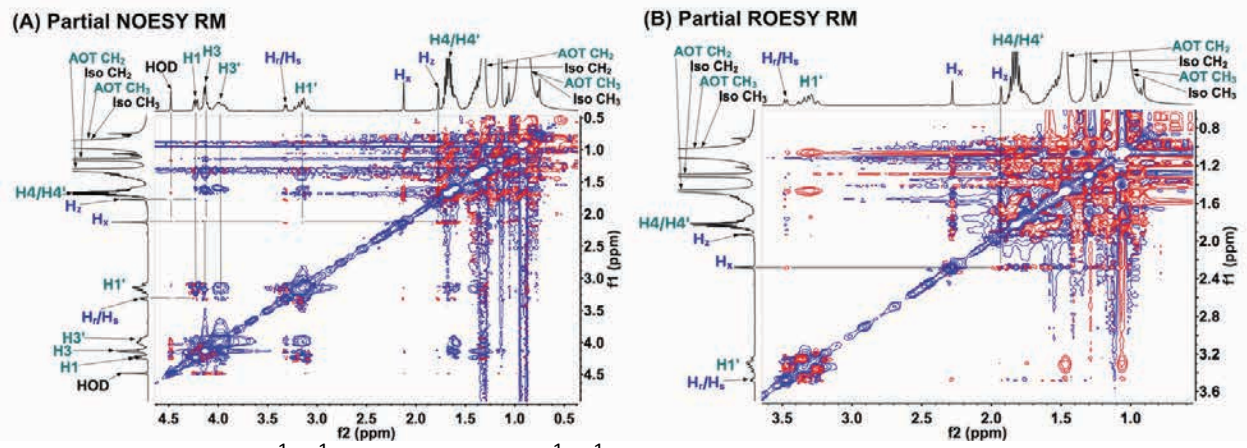

Figure 4.3.11: Partial ^{1}H-^{1}H 2D NOESY and ^{1}H-^{1}H 2D ROESY NMR (400 MHz) spectra of MK-1 in a w_0 12 RM.(A) Partial ^{1}H-^{1}H 2D NOESY NMR spectrum in a w_0 12 RM. (B) Partial ^{1}H-^{1}H 2D ROESY NMR spectrum in a w_0 12 RM. Blue to blue hydrogen text labelling shows MK-1 to MK-1 interactions, and blue to teal hydrogen text labelling shows MK-1 to AOT interactions. Blue intensity contours represent negative NOE's or ROE's and red intensity contours represent positive NOE's or ROE's. See Figure 4.3.2 for MK-1 hydrogen labelling scheme key and Figure 4.3.12 for AOT hydrogen labelling scheme key. A standard NOESY pulse sequence was used consisting of 256 transients with 16 scans in the f1 domain using a 200 ms mixing time and a 1.5 sec relaxation delay. A standard ROESYAD pulse sequence was used consisting of 256 transients with 16 scans in the f1 domain using a 200 ms mixing time and a 2.0 sec relaxation delay.

Figure 4.3.10A shows ROE cross peaks between all four aromatic hydrogens of MK-1 and the CH_2/CH_3 groups of the AOT alkyl tails. Figure 4.3.10B shows cross peaks between MK-1's alkene hydrogen H_k with HOD, H1, H3/H3', and H4/H4'. Figure 4.3.11A also shows cross peaks between hydrogens H_r/H_s with H1, H3, H3', which together indicates that MK-1 is located within the RM interface. Figure 4.3.11A-B shows NOE/ROE cross peaks between H_r/H_s and H_z, between H_x and H_z, between H_z and H1, H3, and a lack of a cross peak between H_x and H_k, which supports a folded conformation for MK-1 while residing in the interface (see Figure A4.22 for ROE/NOE correlation traces). Based on these observations, MK-1 is orientated in a manner where the naphthoquinone is positioned toward the AOT alkyl tails and the folded isoprenyl side chain is positioned between hydrogens H1/H1' and H3/H3' as illustrated in Figure 4.3.12). A proposed folded MK-1 conformation that is consistent with the 2D NOESY and ROESY spectral data is illustrated in Figure

4.3.13. The phase of the MK-1 to MK-1 cross peaks observed in the NOESY spectrum (Figures 4.3.10-11) within the RM interface are opposite phase of the diagonal, indicating MK-1 is behaving as a small molecule within the RM interface and likely tumbling freely but maintaining interactions with the AOT regions shown in Figure 4.3.12.

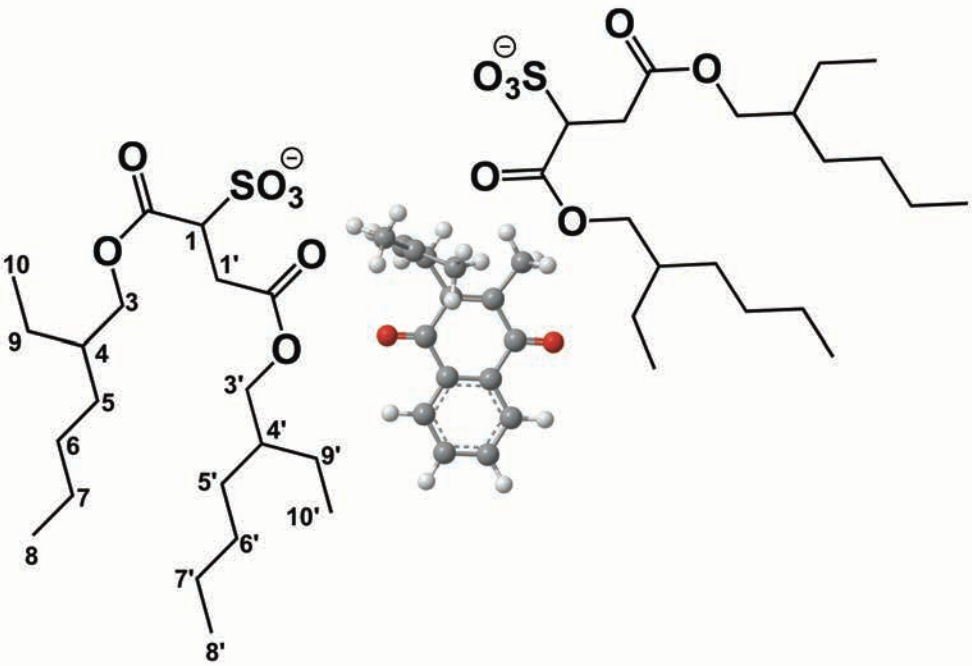

Figure 4.3.12: Illustration of the placement and proposed conformation of MK-1 inside the RM interface. This arrangement is consistent with the ^{1}H-^{1}H 2D NOESY and ^{1}H-^{1}H 2D ROESY NMR spectral data obtained in a w_0 12 RM. However, MK-1 likely tumbles freely within the interface but maintains interactions with the region of AOT shown in the illustration. AOT hydrogen labelling scheme key is shown.

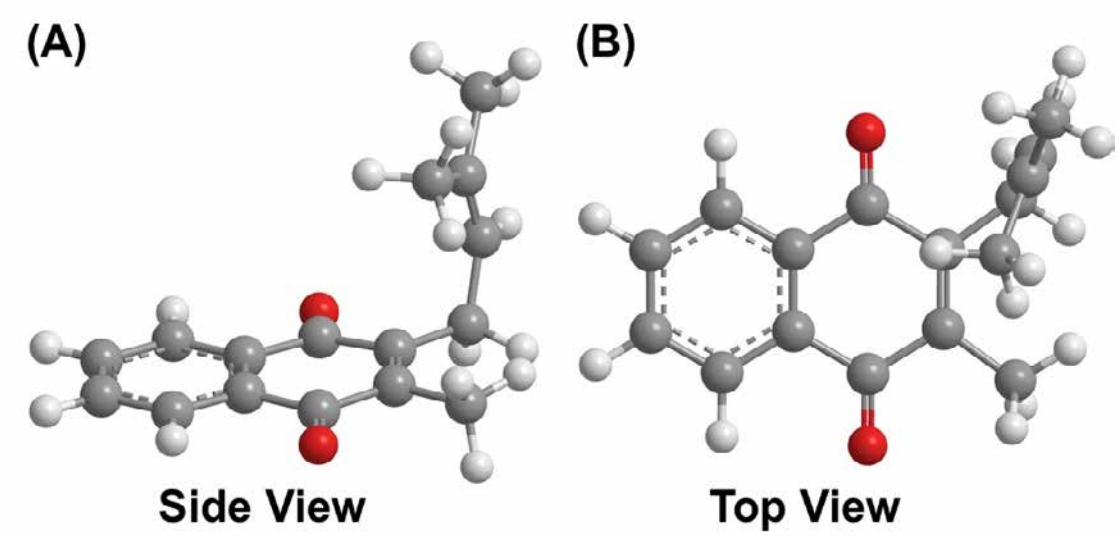

Figure 4.3.13: Proposed conformation of MK-1 at an RM interface illustrated using Merck Molecular Force Field 94 (MMFF94) calculations that is consistent with ^{1}H-^{1}H 2D NOESY and ^{1}H-^{1}H 2D ROESY NMR spectral data. (A) Side view of energy minimized folded MK-1 conformation (50.3 kcal/mol, and internuclear distance H_x-H_z: 2.8 Å). (B) Top view of the energy minimized proposed MK-1 conformation showing the isoprene methyl groups positioned folded upwards.

To determine if saturation of the isoprenyl side chain affects location and orientation within the RM interface, the same experiment was carried out with MK-1(H_2) (Figure A4.21). NOE cross peaks are observed between MK-1(H_2) aromatic hydrogens, H_a, H_b, H_c, and H_d, and AOT's CH_2 and CH_3 alkyl tail groups (Figure A4.21). NOE cross peaks are observed between methylene hydrogens, H_r/H_s, and HOD, H1/H1', H3/H3', and H4/H4'. NOE cross peaks are observed between the naphthoquinone methyl, H_x, and HOD, H1/H1', H3/H3', and H4/H4' (Figure A4.21). The AOT and isooctane hydrogens overlapped with MK-1(H_2)'s terminal methyl hydrogens, H_z and H_y, and the methine hydrogen, H_I, signals in the spectrum for MK-1(H_2) within the RM interface; therefore, we were unable to determine the conformation of MK-1(H_2) within the interface with confidence. Despite this, we would anticipate that MK-1(H_2) adopts a similar folded conformation as MK-1 within the RM interface based on similar interactions observed in the 1D and 2D NMR experiments carried out for MK-1. Together, these observations demonstrate that MK-1(H_2)

interacted with the interface and has a similar position and orientation as MK-1, indicating that saturation of the isoprenyl side chain does induce an observable change in the position and orientation within the RM interface.

Overall, the ^{1}H-^{1}H 2D NOESY and ROESY NMR spectral data of MK-1 inside a RM interface is consistent with MK-1 adopting a folded conformation within a RM model membrane interface. Interestingly, the conformation of MK-1 inside the RM interface remains folded but differs slightly from the folded conformations observed in organic solution. The observation that MK-1 adopts a folded conformation within the RM model membrane interface is important as understanding the conformational preferences of the first isoprene unit of MK will be crucial in determining and understanding conformations of the naturally occurring longer MK analogs within cellular membranes.

4.4 Summary and Conclusions

Lipoquinones such as MK, are special types of lipid-quinones and are essential components of the ETS. Partial saturation of MK in these biological systems is necessary for some organisms to survive such as pathogenic *M. tuberculosis*.[8-9, 12] The rationale for the observation of partially saturated MK derivatives in various organisms remains unclear and may be responsible for proper recognition by respiratory enzymes within the ETS or may affect electron transfer efficiency within the ETS. It is intriguing as the double bonds present in the isoprenyl side chain of MK are not conjugated with each other nor to the redox active quinone system and therefore would not be expected to affect the redox potential. Interestingly, we showed in chapter three that MK-2 adopts a folded conformation where the double bond in the second isoprene unit lies

in close proximity to the quinone carbonyl groups on the naphthoquinone and may potentially have an influence on the reactivity of the quinone.[38] The studies described in this chapter help to further understand the chemical, conformational, and biochemical properties on an important class of quinone containing compounds involved in electron transfer processes. The partially saturated MKs represent an unrecognized group of biologically significant molecules essential for pathogenic taxonomic classification.

In this chapter, we first demonstrated using a semi-quantitative 2D NMR spectroscopy approach that the two simplest most fundamental MK analogs, unsaturated MK-1 and saturated MK-1(H_2), adopt similar folded-extended conformations in each organic solvent but differ slightly between each organic solvent environment. We also observed that the degree of saturation in the isoprenyl side chain of MK-1 only slightly alters the conformation. Importantly, the conformations observed for MK-1 closely resembled the conformation of the first isoprene unit in MK-2, which we previously showed adopted folded conformations in solution and within a model membrane interface.[38] Together, these results support the first hypothesis that MK-1 analogs adopt folded conformations regardless of the degree of saturation in their isoprenyl side chain

The quinone redox potentials of MK-1 and MK-1(H_2) were measured in various anhydrous organic solvent environments. The organic solvent environments studied more closely resemble the environment of the cellular membrane where native MKs are located and serve as better comparisons for biological reactivity than those carried out in aqueous solutions. We demonstrated that the measured quinone redox potentials of MK-1 and MK-1(H_2) varied with the solvent environment (presumably due to differences in dielectric constants) where the ease

of quinone reduction for the $Q/Q^{\bullet-}$ process follows the trend: DMSO > ACN > pyridine. Remarkably, we report for the first time that the degree of saturation in the isoprenyl side chain of MK-1 influences the observed quinone redox potential, where unsaturation in the isoprenyl side chain of MK-1 makes the quinone easier to reduce by ~20 mV and the difference is conserved across several organic solvents (pyridine, ACN, DMSO). The observed ~20 mV redox potential difference is presumably due mostly in part by a perturbation of the electronics of the quinone system upon saturation of the double bond by an indirect through bond effect. The observation of a 20 mV difference in the redox potential between the two MK-1 derivatives with a saturated and unsaturated isoprenyl side chain observed in three different solvents is unexpected and may reflect some important general reactivity pattern of this system. We speculate that if such a difference is also observed for the MKs with longer isoprenyl side chains that it may reflect the biological function of these molecules and provide evidence for the possibility that such a small difference in redox potential may be biologically significant. However, in the simple MK-1 system containing one isoprene unit, the side chain may not have the spatial reach needed present in the MK-9 system and therefore, more data is needed to properly evaluate the longer MK derivatives. The consistent redox potential difference observed is small in magnitude but may be relevant in a biological context. The electrochemical results confirm our second hypothesis that saturation of the isoprenyl side chain of MK-1 affects the observed quinone redox potential.

Finally, combining results, MK-1 and MK-1(H_2) both interacted with Langmuir phospholipid monolayers and RM model membrane interfaces, where MK-1 and MK-1(H_2) had very similar interactions with the Langmuir phospholipid monolayers (DPPC and DPPE phospholipids) and similar placement and location within the RM interface. Importantly, MK-1 also adopted a folded

conformation within the RM model membrane interface further supporting our first hypothesis. The results combined from all the conformational analysis studies presented in this chapter for MK-1 and MK-1(H_2) indicated a folded-extended conformation to be a favorable and stable conformation for MK-1 analogs. All together, these results are significant as the conformation and reactivity of these MKs in organic solution and model membrane interfaces provides a first prediction/consideration of the form that exists within the native hydrophobic cellular membrane interface.

Overall, the findings of the studies presented herein help to further understand how the conformation and the degree of saturation in the isoprenyl side chain affects the reactivity and function of biologically relevant molecules. The elucidation of MK-1 and MK-1(H_2) conformation in solution and at a model membrane interface is essential and necessary as understanding the conformational preferences of the first isoprene unit of MK is useful for predicting conformations of the naturally occurring longer MK analogs within solution and cellular membranes. We observed that partial saturation in the isoprenyl side chain only minimally alters the conformation of MK-1 but may potentially affect the recognition, reactivity, and function within biologically relevant environments because a difference in the redox potential is observed. MK analogs with longer isoprenyl side chains (e.g., MK-9) may also adopt folded conformations although much more complex. Saturation of the double bond in the first isoprene unit of the isoprenyl side chain serves to only minimally alter the preferred conformation although distinctly affecting the redox function. The results of the studies in this chapter provide a working model involving the role of structure and redox potential that explains why partial saturation of MK is

observed in pathogenic *M. tuberculosis*, which is responsible for the deaths of ~1.3 million people annually.[8-9, 72]

References

1. Koehn, J. T.; Beuning, C. N.; Peters, B. J.; Dellinger, S. K.; Van Cleave, C.; Crick, D. C.; Crans, D. C., Investigating Substrate Analogues for Mycobacterial MenJ: Truncated and Partially Saturated Menaquinones. *Biochemistry* **2019,** *58* (12), 1596-1615.
2. Aguilar-Martínez, M.; Macías-Ruvalcaba, N. A.; Bautista-Martínez, J. A.; Gómez, M.; González, F. J.; González, I., Review: Hydrogen Bond and Protonation as Modifying Factors of the Quinone Reactivity. *Curr. Org. Chem.* **2004,** *8*, 1721-1738.
3. Astudillo-Sánchez, P. D.; Morales-Martínez, D.; Sánchez, A.; Rocha-Ortiz, G.; Salas-Reyes, M., Electrochemical Study of the Interactions Between Anionic Species of Menadione and Alkylated Nucleobases in Dimethylsulfoxide. *J. Electroanal. Chem.* **2017,** *801*, 104-113.
4. Gunner, M. R.; Madeo, J.; Zhu, Z., Modification of Quinone Electrochemistry by the Proteins in the Biological Electron Transfer Chains: Examples from Photosynthetic Reaction Centers. *J. Bioenerg. Biomembr.* **2008,** *40* (5), 509-519.
5. Monks, T. J.; Hanzlik, R. P.; Cohen, G. M.; Ross, D.; Graham, D. G., Quinone Chemistry and Toxicity. *Toxicol. Appl. Pharmacol* **1992,** *112* (1), 2-16.
6. Abraham, I.; Joshi, R.; Pardasani, P.; Pardasani, R. T., Recent Advances in 1,4-Benzoquinone Chemistry. *J. Braz. Chem. Soc.* **2011,** *22* (3), 385-421.
7. Nowicka, B.; Kruk, J., Occurrence, Biosynthesis and Function of Isoprenoid Quinones. *Biochim. Biophys. Acta* **2010,** *1797*, 1587-1605.
8. Upadhyay, A.; Fontes, F. L.; Gonzalez-Juarrero, M.; McNeil, M. R.; Crans, D. C.; Jackson, M.; Crick, D. C., Partial Saturation of Menaquinone in *Mycobacterium tuberculosis*: Function and Essentiality of a Novel Reductase, MenJ. *ACS Cent. Sci.* **2015,** *1* (6), 292-302.
9. Upadhyay, A.; Kumar, S.; Rooker, S. A.; Koehn, J. T.; Crans, D. C.; McNeil, M. R.; Lott, J. S.; Crick, D. C., Mycobacterial MenJ: An Oxidoreductase Involved in Menaquinone Biosynthesis. *ACS Chem. Biol.* **2018,** *13*, 2498-2507.
10. da Costa, M. S.; Albuquerque, L.; Nobre, M. F.; Wait, R., The Extraction and Identification of Respiratory Lipoquinones of Prokaryotes and Their Use in Taxonomy. In *Methods in Microbiology, Vol 38: Taxonomy of Prokaryotes*, Rainey, F.; Oren, A., Eds. Elsevier Academic Press Inc: San Diego, 2011; Vol. 38, pp 197-206.
11. Kroppenstedt, R. M.; Mannheim, W., Lipoquinones in Members of the Family Pasteurellaceae. *Int. J. Syst. Evol. Bacteriol.* **1989,** *39* (3), 304-308.
12. Collins, M. D.; Jones, D., Distribution of Isoprenoid Quinone Structural Types in Bacteria and Their Taxonomic Implications. *Microbiol. Rev.* **1981,** *45* (2), 316-354.
13. Meganathan, R., Biosynthesis of Menaquinone (Vitamin K_2) and Ubiquinone (Coenzyme Q): A Perspective on Enzymatic Mechanisms. In *Vitam. Horm.*, 2001; Vol. 61, pp 173-218.
14. Jarchow-Choy, S. K.; Koppisch, A. T.; Fox, D. T., Synthetic Routes to Methylerythritol Phosphate Pathway Intermediates and Downstream Isoprenoids. *Curr. Org. Chem.* **2014,** *18*, 1050-1072.
15. Collins, M. D.; Shah, H. N.; Minnikin, D. E., A Note on the Separation of Natural Mixtures of Bacterial Menaquinones Using Reverse-phase Thin-layer Chromatography. *J. Appl. Bacteriol.* **1980,** *48* (2), 277-282.
16. Thomson, R. H., *Naturally Occurring Quinones.* Academic Press Inc: 1971.
17. Kurosu, M.; Begari, E., Vitamin K_2 in Electron Transport System: Are Enzymes Involved in Vitamin K_2 Biosynthesis Promising Drug Targets? *Molecules* **2010,** *15* (3), 1531-1553.

18. Nakagawa, K.; Hirota, Y.; Sawada, N.; Yuge, N.; Watanabe, M.; Uchino, Y.; Okuda, N.; Shimomura, Y.; Suhara, Y.; Okano, T., Identification of UBIAD1 as a Novel Human Menaquinone-4 Biosynthetic Enzyme. *Nature* **2010,** *468*, 117-121.
19. Vos, M.; Esposito, G.; Edirisinghe, J. N.; Vilain, S.; Haddad, D. M.; Slabbaert, J. R.; Van Meensel, S.; Schaap, O.; De Strooper, B.; Meganathan, R.; Morais, V. A.; Verstreken, P., Vitamin K_2 Is a Mitochondrial Electron Carrier That Rescues Pink1 Deficiency. *Science* **2012,** *336*, 1306-1310.
20. Josey, B. J.; Inks, E. S.; Wen, X.; Chou, C. J., Structure−Activity Relationship Study of Vitamin K Derivatives Yields Highly Potent Neuroprotective Agents. *J. Med. Chem.* **2013,** *56*, 1007-1022.
21. Rahn, J. J.; Bestman, J. E.; Josey, B. J.; Inks, E. S.; Stackley, K. D.; Rogers, C. E.; Chou, C. J.; Chan, S. S. L., Novel Vitamin K Analogs Suppress Seizures in Zebrafish and Mouse Models of Epilepsy. *Neuroscience* **2014,** *259*, 142-154.
22. Chadar, D.; Camilles, M.; Patil, R.; Khan, A.; Weyhermuller, T.; Salunke-Gawali, S., Synthesis and Characterization of *n*-alkylamino Derivatives of Vitamin K3: Molecular Structure of 2-propylamino-3-methyl-1,4-naphthoquinone and Antibacterial Activities. *J. Mol. Struct.* **2015,** *1086*, 179-189.
23. Kathawate, L.; Joshi, P. V.; Dash, T. K.; Pal, S.; Nikalje, M.; Weyhermuller, T.; Puranik, V. G.; Konkimalla, V. B.; Salunke-Gawali, S., Reaction Between Lawsone and Aminophenol Derivatives: Synthesis, Characterization, Molecular Structures and Antiproliferative Activity. *J. Mol. Struct.* **2014,** *1075*, 397-405.
24. Klauda, J. B.; Brooks, B. R., An Ab Initio Study on the Torsional Surface of Alkanes and Its Effect on Molecular Simulations of Alkanes and a DPPC Bilayer. *J. Phys. Chem. B* **2005,** *109*, 5300-5311.
25. Woodward, R. B.; Bloch, K., The Cyclization of Squalene in Cholesterol Synthesis. *J. Am. Chem. Soc.* **1953,** *75*, 2023-2024.
26. Chum, S. P.; Knight, G. W.; Ruiz, J. M., Computer Modeling of {110} Adjacent Reentry of Polyethylene Molecules. *Macromolecules* **1994,** *27*, 656-659.
27. Robertson, M. B.; Klein, P. G.; Ward, I. M.; Packer, K. J., NMR Study of the Energy Difference and Population of the *gauche* and *trans* Conformations in Solid Polyethylene. *Polymer* **2001,** *42*, 1261-1264.
28. Nikki, K.; Inakura, H.; Wu-Le; Suzuki, N.; Endo, T., Remarkable Changes in Conformations of *n*-alkanes with thier Carbon Numbers and Aromatic Solvents. *J. Chem. Soc., Perkin Trans. 2* **2001,** (2370-2373).
29. Nikki, K.; Nakagawa, N., Elucidation of the Structure of Alkane Chains in Solution by Means of 1H NMR. *Org. Magn. Reson.* **1983,** *21* (9), 552-554.
30. Nikki, K., 1H and 13C NMR Aromatic Solvent-induced Shifts of *n*-alkanes. *Magn. Reson. Chem.* **1990,** *28* (5), 385-388.
31. Schramm, M. P.; Rebek Jr., J., Moving Targets: Recognition of Alkyl Groups. *Chem. Eur. J.* **2006,** *12*, 5924-5933.
32. Choudhury, R.; Barman, A.; Prabhakar, R.; Ramamurthy, V., Hydrocarbons Depending on the Chain Length and Head Group Adopt Different Conformations within a Water-Soluble Nanocapsule: 1H NMR and Molecular Dynamics Studies. *J. Phys. Chem. B* **2013,** *117*, 398-407.
33. Ho Ko, Y.; Kim, Y.; Kim, H.; Kim, K., U-Shaped Conformation of Alkyl Chains Bound to a Synthetic Receptor Cucurbit[8]uril. *Chem. Asian J.* **2011,** *6*, 652-657.
34. Ho Ko, Y.; Kim, H.; Kim, Y.; Kim, K., U-Shaped Conformation of Alkyl Chain Bound to a Synthetic Host. *Angew. Chem. Int. Ed.* **2008,** *47*, 4106-4109.
35. Zakharov, A. V.; Vogt, N., Conformational Analysis of Vitamin K_1 Model Molecule: A Theoretical Study. *Struct. Chem.* **2011,** *22* (2), 305-311.
36. Tynkkynen, T.; Hassinen, T.; Tiainen, M.; Soininen, P.; Laatikainen, R., 1H NMR Spectral Analysis and Conformational Behavior of *n*-alkanes in Different Chemical Environments. *Magn. Reson. Chem.* **2012,** *50*, 598-607.
37. Ishihara, M.; Sakagami, H., QSAR of Molecular Structure and Cytotoxic Activity of Vitamin K_2 Derivatives with Concept of Absolute Hardness. *Anticancer Res.* **2007,** *27*, 4059-4063.

38. Koehn, J. T.; Magallanes, E. S.; Peters, B. J.; Beuning, C. N.; Haase, A. A.; Zhu, M. J.; Rithner, C. D.; Crick, D. C.; Crans, D. C., A Synthetic Isoprenoid Lipoquinone, Menaquinone-2, Adopts a Folded Conformation in Solution and at a Model Membrane Interface. *J. Org. Chem.* **2018,** *83*, 275-288.
39. Stahla, M. L.; Baruah, B.; James, D. M.; Johnson, M. D.; Levinger, N. E.; Crans, D. C., 1H NMR Studies of Aerosol-OT Reverse Micelles with Alkali and Magnesium Counterions: Preparation and Analysis of MAOTs. *Langmuir* **2008,** *24* (12), 6027-6035.
40. Samart, N.; Beuning, C. N.; Haller, K. J.; Rithner, C. D.; Crans, D. C., Interaction of a Biguanide Compound with Membrane Model Interface Systems: Probing the Properties of Antimalaria and Antidiabetic Compounds. *Langmuir* **2014,** *30* (29), 8697-8706.
41. Peters, B. J.; Groninger, A. S.; Fontes, F. L.; Crick, D. C.; Crans, D. C., Differences in Interactions of Benzoic Acid and Benzoate with Interfaces. *Langmuir* **2016,** *32* (37), 9451-9459.
42. Peters, B. J.; Van Cleave, C.; Haase, A. A.; Hough, J. P. B.; Giffen-Kent, K. A.; Cardiff, G. M.; Sostarecz, A. G.; Crick, D. C.; Crans, D. C., Structure Dependence of Pyridine and Benzene Derivatives on Interactions with Model Membranes. *Langmuir* **2018,** *34*, 8939-8951.
43. Maitra, A., Determination of Size Parameters of Water-aerosol-OT Oil Reverse Micelles From Their Nuclear Magnetic-resonance Data. *J. Phys. Chem.* **1984,** *88* (21), 5122-5125.
44. Jones, C. R.; Butts, C. P.; Harvey, J. N., Accuracy in Determining Interproton Distances using Nuclear Overhauser Effect Data from a Flexible Molecule. *Beilstein J. Org. Chem.* **2011,** *7*, 145-150.
45. Cooper, G. M.; Hausman, R. E., *The Cell A Molecular Approach.* 5th ed.; Sinauer Associates, INC.: Sunderland, Massachusetts, USA, 2009; p 820.
46. Nelson, D. L.; Cox, M. M., *Lehninger Principles of Biochemistry.* 5th ed.; W.H. Freeman and Company: New York, USA, 2008; p 1158.
47. Dryhurst, G., Kadish, K. M., Scheller, F., Renneberg, R. , *Biological Eletrochemistry.* Academic Press: New York, 1982.
48. Wawzonek, S.; Berkey, R.; Blaha, E. W.; Runner, M. E., Polarographic Studies in Acetonitrile and Dimethylformamide: III. Behavior of Quinones and Hydroquinones. *J. Electroanal. Chem. Soc.* **1956,** *103* (8), 456-459.
49. Jaworski, J. S.; Leniewska, E.; Kalinowski, M. K., Solvent Effect on the Redox Potential of Quinone-semiquinone Systems. *J. Electroanal. Chem.* **1979,** *105* (2), 329-334.
50. Prince, R. C.; Leslie Dutton, P.; Malcolm Bruce, J., Electrochemistry of Ubiquinones. *FEBS Lett.* **1983,** *160* (1), 273-276.
51. Sostarecz, A. G.; Gaidamauskas, E.; Distin, S.; Bonetti, S. J.; Levinger, N. E.; Crans, D. C., Correlation of Insulin-Enhancing Properties of Vanadium-Dipicolinate Complexes in Model Membrane Systems: Phospholipid Langmuir Monolayers and AOT Reverse Micelles. *Chem. Eur. J.* **2014,** *20* (17), 5149-5159.
52. Riter, R. E.; Kimmel, J. R.; Undiks, E. P.; Levinger, N. E., Novel Reverse Micelles Partitioning Nonaqueous Polar Solvents in a Hydrocarbon Continuous Phase. *J. Phys. Chem. B* **1997,** *101* (41), 8292-8297.
53. Durantini, A. M.; Falcone, R. D.; Silber, J. J.; Correa, N. M., Effect of Confinement on the Properties of Sequestered Mixed Polar Solvents: Enzymatic Catalysis in Nonaqueous 1,4-Bis-2-ethylhexylsulfosuccinate Reverse Micelles. *ChemPhysChem* **2016,** *17* (11), 1678-1685.
54. Lepori, C. M. O.; Correa, N. M.; Silber, J. J.; Falcone, R. D., How the Cation 1-butyl-3-methylimidazolium Impacts the Interaction Between the Entrapped Water and the Reverse Micelle Interface Created with an Ionic Liquid-like Surfactant. *Soft Matter* **2016,** *12* (3), 830-844.
55. Baruah, B.; Roden, J. M.; Sedgwick, M.; Correa, N. M.; Crans, D. C.; Levinger, N. E., When Is Water Not Water? Exploring Water Confined in Large Reverse Micelles Using a Highly Charged Inorganic Molecular Probe. *J. Am. Chem. Soc.* **2006,** *128*, 12758-12765.

56. Odella, E.; Falcone, R. D.; Silber, J. J.; Correa, N. M., Nanoscale Control Over Interfacial Properties in Mixed Reverse Micelles Formulated by Using Sodium 1,4-bis-2-ethylhexylsulfosuccinate and Tri-n-octyl Phosphine Oxide Surfactants. *ChemPhysChem* **2016,** *17* (15), 2407-2414.
57. Diaz-Fernandez, Y.; Foti, F.; Mangano, C.; Pallavicini, P.; Patroni, S.; Perez-Gramatges, A.; Rodriguez-Calvo, S., Micelles for the Self-Assembly of "Off–On–Off" Fluorescent Sensors for pH Windows. *Chem. Eur. J.* **2006,** *12*, 921-930.
58. Pallavicini, P.; Diaz-Fernandez, Y.; Pasotti, L., Micelles as Nanosized Containers for the Self-assembly of Multicomponent Fluorescent Sensors. *Coord. Chem. Rev.* **2009,** *253*, 2226-2240.
59. Stefaniu, C.; Brezesinski, G.; Mohwald, H., Langmuir Monolayers as Models to Study Processes at Membrane Surfaces. *Adv. Colloid Interface Sci.* **2014,** *208*, 197-213.
60. Choi, Y.; Attwood, S. J.; Hoopes, M. I.; Drolle, E.; Karttunen, M.; Leonenko, Z., Melatonin Directly Interacts with Cholesterol and Alleviates Cholesterol Effects in Dipalmitoylphosphatidylcholine Monolayers. *Soft Matter* **2014,** *10*, 206-213.
61. Quinn, P. J.; Esfahani, M. A., Ubiquinones have Surface-Active Properties Suited to Transport Electrons and Protons Across Membranes. *Biochem. J.* **1980,** *185*, 715-722.
62. Hoyo, J.; Torrent-Burgues, J.; Guas, E., Biomimetic Monolayer Films of Monogalactosyldiacylglycerol Incorporating Ubiquinone. *J. of Colloid and Interface Sci.* **2012,** *384*, 189-197.
63. Panda, A. K.; Nag, K.; Harbottle, R. R.; Possmayer, F.; Petersen, N. O., Thermodynamic Studies on Mixed Molecular Langmuir Films: Part 2. Mutual Mixing of DPPC and Bovine Lung Surfactant Extract with Long-chain Fatty Acids. *Colloids Surf., A* **2004,** *247* (1), 9-17.
64. Veldhuizen, E. J. A.; Batenburg, J. J.; van Golde, L. M. G.; Haagsman, H. P., The Role of Surfactant Proteins in DPPC Enrichment of Surface Films. *Biophys. J.* **2000,** *79*, 3164-3171.
65. Wustneck, R.; Perez-Gil, J.; Wustneck, N.; Cruz, A.; Fainerman, V. B.; Pison, U., Interfacial Properties of Pulmonary Surfactant Layers. *Adv. Colloid Interface Sci.* **2005,** *117* (1), 33-58.
66. Sohlenkamp, C.; Geiger, O., Bacterial Membrane Lipids: Diversity in Structures and Pathways. *FEMS Microbiol. Rev.* **2016,** *40* (1), 133-159.
67. Toimil, P.; Prieto, G.; Minones Jr, J.; Sarmiento, F., A Comparative Study of F-DPPC/DPPC Mixed Monolayers. Influence of Subphase Temperature on F-DPPC and DPPC Monolayers. *Phys. Chem. Chem. Phys.* **2010,** *12*, 13323-13332.
68. Hoyo, J.; Guas, E.; Torrent-Burgues, J.; Sanz, F., Biomimetic Monolayer Films of Digalactosyldiacylglycerol Incorporating Plastoquinone. *Biochim. Biophys. Acta, Biomembr.* **2015,** *1848* (6), 1341-1351.
69. Jones, M. N.; Chapman, D., *Micelles, Monolayers, and Biomembranes.* Wiley-Liss: New York, 1995.
70. Sedgwick, M. A.; Trujillo, A. M.; Hendricks, N.; Levinger, N. E.; Crans, D. C., Coexisting Aggregates in Mixed Aerosol OT and Cholesterol Microemulsions. *Langmuir* **2011,** *27* (3), 948-954.
71. Zan, G. T.; Wu, Q. S., Biomimetic and Bioinspired Synthesis of Nanomaterials/Nanostructures. *Adv. Mater.* **2016,** *28* (11), 2099-2147.
72. Glaziou, P.; Sismanidis, C.; Floyd, K.; Raviglione, M., Global Epidemiology of tuberculosis. *Cold Spring Harbor Perspect. Med.* **2015,** *5*, a017798.

Chapter 5: Hydrophobicity May Enhance Membrane Affinity and Anti-Cancer Effects of Schiff Base Vanadium(V) Catecholate Complexes[1]

5.1 Hydrophobic and Redox-Active Vanadium(V) Catecholate Complexes

Medicinal applications of metal complexes in the past has been dominated by the anti-cancer platinum drugs, as well as a range of complexes used for imaging diagnostics and nuclear medicinal applications.[1-8] However, several additional metal-based classes of complexes have been of interest for decades and are increasing in importance. Vitamins and nutritional additives often include metal-ion containing supplements.[9-13] The large number of different formulations for iron and vanadium are testament to the existence of a range of methodologies that can be applied to increase the efficacy of absorption.[14] Furthermore, Lipinski's rules[15] based on an empirical and statistical evaluation of efficacy suggest that statistically successful drugs are of certain size, hydrophobicity, polarity, or reactivity, which thus limits the chemical space to search for available drugs. However, some of the more successful drugs do not follow these empirical rules, such as cisplatin; therefore, drug and supplement design continues to include the entire chemical space. For example, recent investigations have introduced promising hydrophobic titanium and vanadium drugs.[16-20] The water solubility of these compounds and other hydrophobic drugs is very limited, and as a result, the methods for *in vivo* studies with these compounds involve dissolving the compounds in methanol, ethanol, or DMSO or dissolution in assays containing surfactants and/or DMSO. In this chapter, we examine the solubility, stability,

[1]This chapter was reproduced by permission of The Royal Society of Chemistry and is published in *Dalton Transactions*.[1]

and interactions of representative hydrophobic metal complexes (Figure 5.1.1) and free ligand H_2shed with a model membrane interface and their anti-cancer effects.

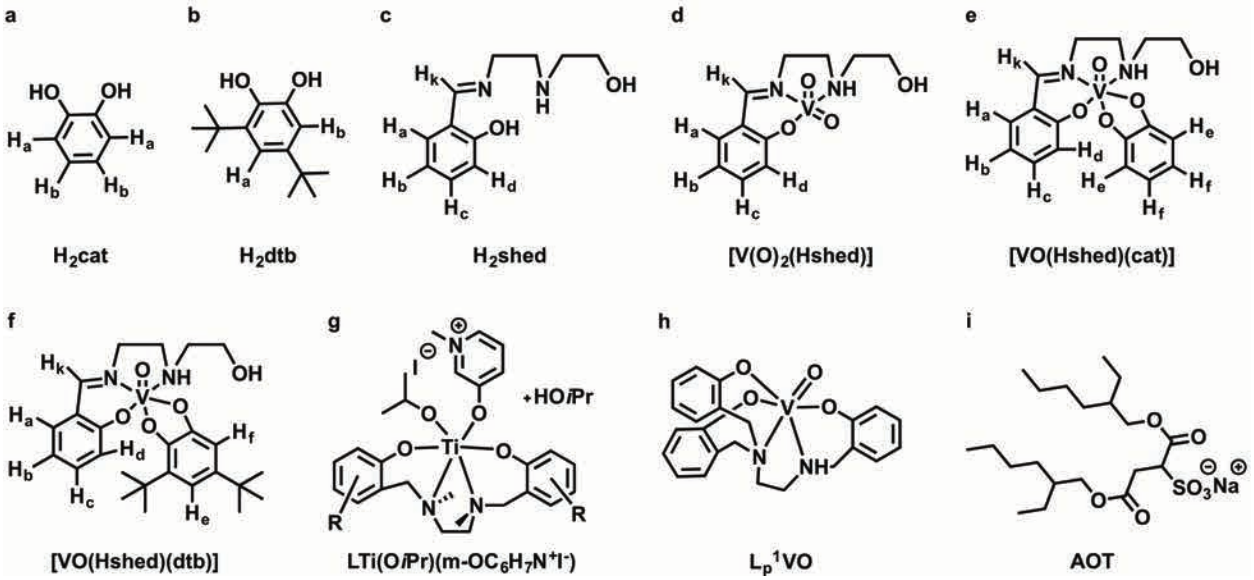

Figure 5.1.1. The structures are labelled as follows: (a) H_2cat; (b) H_2dtb; (c) H_2shed, (d) [$V(O)_2$(Hshed)], (e) [VO(Hshed)(cat)], (f) [VO(Hshed)dtb], (g) Example of a hydrolytically stable titanium complex,[21] (h) Example of a hydrolytically stable vanadium complex,[22] and (i) AOT.

Identification of inhibitors for signal transduction remains an important target in drug discovery. Phosphatase inhibitors that are particularly potent, or effective in animal studies, include a series of titanium, vanadium, and zinc coordination complexes.[18, 23-27] In several studies,[21-22, 28-29] series of compounds were tested, and a correlation with hydrophobicity and stability with potency was highlighted, for example, see a representative compound in Figure 5.1.1g.[21] The Tshuva group used this approach with vanadium compounds and prepared a hydrophobic vanadium complex (Figure 5.1.1h), which was found to have anti-cancer properties as well.[22] The high hydrophobicity of these compounds tend to protect the complexes against initial hydrolysis making them more likely to penetrate membranes and extend their lifetime and get into cells intact. An example of such a compound is shown in Figure 5.1.1h; a vanadium complex that was more effective in growth inhibition than cisplatin of human colon HT-29 and

ovarian OVCAR-3 cells.[22] Studies using data mining of vanadium-containing phosphatase complexes[27] and synchrotron studies indicate most vanadium complexes lose their ligands when binding to phosphatases[27] or transferrin, [30] in blood, and in cell medium.[31-38] In contrast, these same complexes interact with human serum albumin and in some cases can form a protein adduct that maintains the ligands.[37, 39-40] It is possible that complexes containing hydrophobic ligands with steric hindrance preventing substitution reactions may enable uptake of the intact complex and delivery to the cellular target and thus be a particularly potent cytotoxin to breast and pancreatic cancer cells.[41]

To explore how these hydrophobic complexes will interact with membrane interfaces, we have investigated the behavior of V(V) complexes with an ideal representation of a simple microemulsion ternary model membrane system shown in Figure 5.1.2.[42-43] The reverse micelle (RM) is a ternary system, H_2O/AOT/organic solvent, where AOT = sodium bis[2-ethylhexyl]sulfosuccinate, is used as a simple but effective model system to explore the ability of these hydrophobic coordination complexes to penetrate the interface, Figure 5.1.2. These self-assembled structures form in a region of the phase diagram where there is little H_2O, but significant amounts of surfactant and organic solvent.[44-48] The interface system is dynamic, but the overall stability of the system is governed by thermodynamic considerations rather than kinetic ones and, thus, the most thermodynamically stable arrangements are preserved. In the past, we have used mainly *iso*-octane or cyclohexane (or d_{16}-cyclohexane) as the organic solvent[49], but others have used pentane, benzene, chloroform, and carbon tetrachloride.[50] The microemulsion forms RMs, but the interfacial chemistry enables studies of how such metal complexes will transverse interfaces[51-52] and NMR spectroscopy provides evidence on whether

the complexes decompose and where they interact with the interfaces in this simple model system.

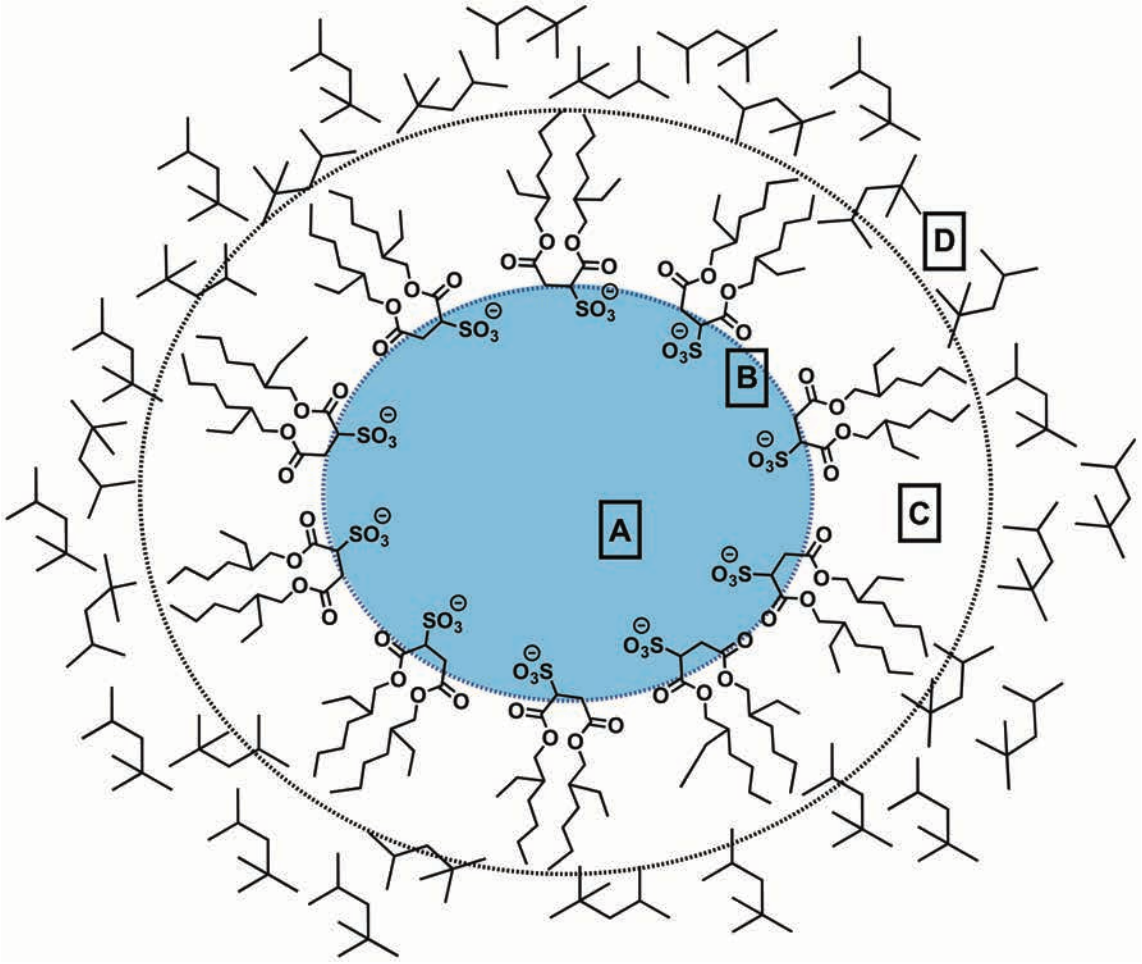

Figure 5.1.2. Schematic diagram of an RM present in a microemulsion. The four distinct locations for potential solutes are labelled as follows: (a) the water pool, (b) the Stern layer, (c) the surfactant hydrophobic layer, and (d) the organic solvent layer, *iso*-octane.

Studies with the BMOV/$[VO_2(ma)_2]^-$ system[53] and the V-dipic systems have demonstrated remarkable differences in how even simple compounds interact with model membrane systems. The BMOV/$[VO_2(ma)_2]^-$ compounds hydrolyze as they approach the interface,[53] whereas the V-dipic complexes react differently depending on the oxidation state.[54] The V(V) complex $[VO_2dipic]^-$ is able to penetrate the interface, whereas the V(III) complex $[V(dipic)_2]^-$ is found in the water pool associating with the interface.[54] The V(IV)-dipic system can form two complexes,

a neutral 1:2 complex $[VO(dipic)_2]^-$ that is generally prepared upon synthesis, as well as a 1:1 complex $[VO(H_2O)_2(dipic)]^-$. The former readily associates with the interface partially penetrating the surface, whereas the 1:1 complex is interacting further up in the hydrophobic part of the interface similarly to the V(V)-dipic complex. These studies demonstrate the versatile modes of actions of these complexes, [55-56] and considering that V-complexes are known to cycle between redox states in the biological systems, this factor undoubtedly is involved in the mode of action of the vanadium complexes.[11, 13, 20, 55-59] Indeed, the redox chemistry of vanadium compounds is likely to be associated with the generation of reactive oxygen species (ROS), which have been implicated in the mode of action of vanadium compounds. This topic is beyond the scope of this chapter and we refer the reader elsewhere on more information on this important topic.[55-56]

Using this simple model membrane system, the chemistry of the ternary V(V) complex $[V(O)_2(Hshed)]$ and two more hydrophobic analogs prepared from its complexation with catecholate (cat) or di-*tert*-butylcatecholate (dtb) (Figure 5.1.1). These compounds belong to the family of complexes formed from non-innocent ligands, and as a result, exhibit a broad spectrum of redox chemistry.[60] It is well known that V-compounds redox cycle upon administration, and a number of studies have been done exploring the details of these processes. For the V-catecholate complexes described in this chapter, the redox chemistry is mainly metal centred.[60] There have only been a few studies with vanadium-catechol complexes exploring their biological activities.[61-64] A recent study demonstrated that these compounds affected cell growth in MDA-MB-231 and PANC-1 cells with varying amounts of effectiveness.[41] Furthermore, a number of vanadium compounds have been reported with naturally occurring non-polar flavonoids including mechanistic studies probing the redox chemistry involved in these processes.[65] It is, therefore,

important to investigate how these hydrophobic complexes interact in interface model systems to explore how this may impact their anti-cancer activities.

5.2 Materials and Methods

5.2.1 Chemicals, Biochemicals, and General Methods

Most reagents were used without further purification including 2,2,4-trimethyl-pentane (*iso*-octane, Sigma-Aldrich, ≥99.0%), deuterium oxide (D_2O, Cambridge Isotope Laboratories, 99.9%), Acetone HPLC grade, *n*-pentane, and argon. Sodium bis(2-ethylhexyl)sulfosuccinate (AOT, Sigma-Aldrich, 99.8%) was purified using activated charcoal and methanol to remove acidic impurities using a modified procedure of that previously reported (see below).[11, 66-67] Salicylaldehyde (SalA) was purified *via* vacuum distillation to remove impurities prior to synthesis. $[V(O)_2(Hshed)]$, H_2shed, [VO(Hshed)(cat)], and [VO(Hshed)(dtb)] were prepared according to literature procedures.[68-70] All pH measurements were conducted using a Thermo Orion 2 Star pH meter with a VWR semi-micro pH probe.[71] When samples were prepared for RM or D_2O NMR experiments, deuterium oxide was used instead of H_2O and the pH was adjusted to consider the presence of deuterium (pD = pH + 0.4) and therefore, we report values for both pD and pH for clarity.[67, 72] Pre-sterilized media and sterile plastic ware used in cell culture were purchased from Life Technologies Australia. Human chondrosarcoma SW1353 cells were purchased from the American Type Culture Collection (ATCC, Cat. No. HTB-94) and cultured using standard techniques[73-74] in Advanced DMEM (where DMEM = Dulbecco's modified Eagle's medium; Thermo Fischer Scientific, Cat. No. 12491-015). Abbreviations are as follows: aot, bis(2-ethylhexyl) sulfosuccinate sodium salt; cat, catecholate; dtb, di-*tert*-butylcatecholate; DLS,

dynamic light scattering; HEPES, (4-(2-hydroxyethyl)-1-piperazine-ethanesulfonic acid; H_2shed, condensation product of salicylaldehyde and *N*-(2-hydroxyethyl)-1,2-ethanediamine; pdi, polydispersity index; SalA, salicylaldehyde; HyDA, *N*-(2-hydroxyethyl)-1,2-ethanediamine; CCR2, CC chemokine receptor 2; CCL2, CC chemokine ligand 2; CCR5, CC chemokine receptor 5.

5.2.2 Purification of NaAOT

NaAOT was purified by a slightly modified procedure from that reported previously.[44, 75] AOT (60.0 g) was dissolved in methanol (150 mL) and the solution was shaken for a period of two weeks in the presence of mesh activated charcoal (15.0 g).[44, 75] The suspension was then vacuum filtered through a bed of celite and then the methanol was removed, first *via* rotary evaporation under reduced pressure at room temperature and then *via* high vacuum (~150 milliTorr) until desired dryness was achieved. The residual water content ranged from 0.019 to 0.300 waters per AOT and was measured as previously reported by NMR analysis.

5.2.3 Preparation of AOT/iso-octane Stock Solution and Reverse Micelle Samples

The 750 mM AOT/*iso*-octane stock solution was prepared by dissolving AOT (8.333 g, 18.80 mmol) in *iso*-octane in a volumetric flask (25.00 mL), diluting to the mark, and vortexing until clear. For all six probe molecules studied, a 52.75 mM stock solution was used to prepare RM containing suspensions. The stock solution was prepared by dissolving the probe molecule (0.5275 mmol) in 750 mM AOT/*iso*-octane stock in a volumetric flask (10.00 mL), mixing until solubilized, and then diluting to the mark. The probe AOT/*iso*-octane stock solutions containing either vanadium or the H_2shed ligand were mixed by hand and not vortexed to have as little outside impact on hydrolysis as possible. Before the preparation of the 1 mL RM samples, 2 mL solutions of varying concentrations of probe stock were created by diluting various aliquots of

the 52.75 mM probe stock with the 750 mM AOT/*iso*-octane stock. Then, the 1 mL RM samples (w_0 = 6, 8, 12, 16, and 20) were made by diluting specific aliquots of the 2 mL solutions with various amounts of D_2O (pH = 6.6, pD = 7.0, see General Methods for pH measurements). The addition of the D_2O resulted in the formation of a white flocculent at the bottom of the samples and, when shaken, a homogenous solution resulted. For the free H_2cat and H_2dtb ligand RM samples, NMR studies were done immediately after preparation while the free H_2SHED ligand, [$V(O)_2$(Hshed)], [VO(Hshed)dtb], and [VO(Hshed)cat] RM samples were allowed to equilibrate before the NMR spectroscopic studies were performed. The total V-concentration for the 1.0 mL [$V(O)_2$(Hshed)] RM samples are as follows: w_0 20, 2.41 mM; w_0 16, 5.17 mM; w_0 12, 11.05 mM; w_0 8, 23.53 mM; and w_0 6, 36.72 mM. The overall concentrations for the 1.0 mL H_2shed RM samples are as follows: w_0 20, 2.71 mM; w_0 16, 5.65 mM; w_0 12, 11.77 mM; w_0 8, 24.48 mM; and w_0 6, 37.87 mM. The total V-concentration for the 1.0 mL [VO(Hshed)(dtb)] RM samples are as follows: w_0 20, 2.46 mM; w_0 16, 5.23 mM; w_0 12, 11.09 mM; w_0 8, 23.55 mM; w_0 6, 36.78 mM. The total V-concentration for the 1.0 mL [VO(Hshed)(cat)] RM samples are as follows: w_0 20, 2.41 mM; w_0 16, 5.17 mM; w_0 12, 11.05 mM; w_0 8, 23.53 mM; w_0 6, 36.72 mM.

5.2.4 Stability of Probe in Aqueous Solution and Reverse Micelles

The stability of the precursor complex [$V(O)_2$(Hshed)], vanadium(V) catecholates [VO(Hshed)dtb] and [VO(Hshed)cat], and the free ligand H_2shed in aqueous solution was determined by solution NMR spectroscopy. NMR measurements of the hydrolysis of each probe molecule in D_2O (pH = 6.6, pD = 7.0, see General Methods for pH measurements) were done until the probe molecule had reached equilibrium as evidenced by the NMR peak integrations changing over time. Similar equilibrium stability measurements were taken for each V-compound

in a w_0 = 12 RM. Once the equilibrium had been determined for each probe molecule in a RM system, complete RM studies were performed at the determined equilibrium time point.

5.2.5 ^{1}H and ^{51}V NMR Spectroscopic Studies on Reverse Micelles

All ^{51}V solution NMR spectra were taken on a Varian 400MR NMR spectrometer with a spectral window of -700 ppm to 700 ppm, 4096 scans, RD = 0.001 sec, and 90° pulse angle at 26 °C. The ^{1}H NMR spectroscopic experiments on the RMs were performed using a 400 MHz Varian iNova NMR spectrometer or a 400 MHz MR400 spectrometer, using standard parameters at 22 or 26 °C, respectively. The 1D ^{1}H spectra in $CDCl_3$ or d_6-DMSO were referenced to the internal solvent peak at 7.26 ppm and 2.50 ppm, respectively. The 1D ^{1}H spectra in RMs were referenced to the *iso*-octane methyl peak (0.904 ppm) as previously reported.[67] ^{51}V solution chemical shifts in DMSO are determined relative to external neat liquid $VOCl_3$ reference (0.00 ppm).[76] ^{51}V solution chemical shifts in D_2O or RMs are measured relative to an external 1 M sodium metavanadate reference (pH = 12) which, in aqueous solution, produces two signals at -535.7 ppm (used as auxiliary reference) and -560.4 ppm, relative to $VOCl_3$.[77] Spectral data was processed using MestReNova NMR processing software version 10.0.1.

5.2.6 Reverse Micelle Sample Preparation for Dynamic Light Scattering (DLS) Studies

RMs for DLS studies were prepared in a similar manner to those used for the NMR spectroscopic experiments except that Distilled Deionized (DDI) H_2O (pH = 6.6) was used as the water pool instead of D_2O, and the 0.750 M AOT/RM solution was diluted to a 0.1 M AOT/RM solution with *iso*-octane after the RMs were formed.

5.2.7 Dynamic Light Scattering (DLS) Measurements

The hydrodynamic radius of w_0 = 12 and w_0 = 20 RMs was determined by DLS measurements performed on a Malvern Zetasizer Nano ZS instrument (Malvern Instruments, Malvern, UK). The DLS cuvette (1 cm X 1 cm, glass) was washed three times with *iso*-octane followed by three washes with the RM sample (prepared at pH 6.6). Then, the cuvette was filled with 1 mL of the RM sample and closed with a Teflon cap. Each experiment was conducted at 25 °C and consisted of a 700 sec. sample equilibration period followed by 10 measurements each made of 15 scans.[78] Each sample was measured in triplicate, and the diameter and pdi were recorded and compared to those values in the literature.[79] The data were analyzed using Malvern DLS Software. See Supplementary Information.

5.2.8 Stability Studies by Electronic Absorption Spectroscopy

Freshly prepared stock solutions of [VO(Hshed)(cat)] or [VO(Hshed)(dtbc)] (10 mM V-complex in DMSO) were diluted 100-fold either with DMSO or with cell culture medium (Advanced DMEM, containing 2.0% vol. of fetal calf serum and 10 mM HEPES buffer, pH 7.4)[31]. The spectra in the 350-1200 nm range (resolution, 1 nm; acquisition rate, 600 nm min^{-1}) were acquired on an Agilent Cary 5000 spectrometer at 295 K. The corresponding solvents were used in background scans.

5.2.9 Cytotoxicity Experiments

Advanced DMEM medium (Thermo Fisher Scientific Cat. No. 12491-015, where DMEM = Dulbecco's modified Eagle's medium) was supplemented with L-glutamine (2.0 mM), antibiotic-antimycotic mixture (100 U mL^{-1} penicillin, 100 mg mL^{-1} streptomycin and 0.25 mg mL^{-1} amphotericin B) and fetal calf serum (FCS; heat-inactivated; 2% vol.). For proliferation experiments, cells were seeded in 96-well plates at an initial density of 1.0×10^3 viable cells per

well (counted using Invitrogen Countess device with trypan blue staining)[73-74] in 100 µL medium and left to attach overnight. Freshly prepared 10 mM stock solutions in DMSO ([VO(Hshed)(dtb)] or [VO(Hshed)(cat)]) or in Milli-Q H_2O (Na_3VO_4, 99.98%, Aldrich Cat. No. 450243) were used for cell assays. All the cell treatments, including controls, contained 0.50% (vol.) of DMSO.[80] Stock solutions of the treatment compounds were diluted with fully supplemented cell culture media to the required final concentrations, and the resultant media were either added to the cells within one minute (fresh solutions) or left in cell culture incubator (310 K, 5% CO_2) for 24 prior to the cell treatments (aged solutions). For end-point viability assays, cells were incubated with fresh or aged treatment compounds for 72 h, after which WST-8 reagent (Cell counting kit-8, Dojindo Molecular Technologies) or Alamar Blue reagent (Thermo Fisher Scientific Cat. No. DAL1025) was added at 10 µL/well. The cells were then incubated for further six hours, and the absorbance at 450 nm (WST-8) or fluorescence at 570/585 nm (Alamar Blue) were measured using Victor V^3 multi-well plate reader. For each treatment, six replicate cell-containing wells and two background wells (containing all the components except cells) were used, and statistical analysis of the data was performed using Origin software.[81] Preliminary calibration experiments with WST-8 assay have shown that the A_{450} values in the entire working range (0.25-1.5) were linearly dependent on the number of viable SW1353 cells (~10^2-10^4 cells per well).

5.3 Results and Discussion

5.3.1 Synthesis

[$V(O)_2$(Hshed)], [VO(Hshed)(cat)], and [VO(Hshed)(dtb)] and free ligand H_2shed were synthesized as previously described and the spectroscopic data was found to be consistent with

that in literature.[68-70] The free ligand, H_2shed, is the condensation product of salicylaldehyde (SalA) and *N*-(2-hydroxyethyl)-1,2-ethanediamine ($NH_2CH_2CH_2NHCH_2CH_2OH$, abbreviated HyDA).

5.3.2 Solubility of Free Ligands and V(V) Complexes and Stability of Free Ligand H_2shed and $[V(O)_2$(Hshed)] in Reverse Micelle Samples

The three free ligands (Hshed and cat and dtb catechols) were all dissolved in aqueous solution and *iso*-octane. The three complexes, $[V(O)_2$(Hshed)], [VO(Hshed)(cat)], and [VO(Hshed)(dtb)] are all soluble in dimethylsulfoxide (DMSO), but have less solubility in aqueous solution and no measurable solubility in *iso*-octane (2,2,4-trimethylpentane) as confirmed by NMR spectroscopy. All three complexes had to be forced into aqueous solvents such as D_2O *via* vortexing and at that point, the Schiff base ligand is subject to hydrolysis as shown in eq. (1) and the $[V(O)_2$(Hshed)] complex as shown in eq. (2).

The stability of the precursor V(V) complex, $[V(O)_2$(Hshed)], was measured in aqueous solution prior to the addition to the model membrane RM microemulsion system. We observed that the vanadium complexes hydrolyzed as shown in eq. (2) at a faster rate in aqueous solution than in the RM mixture. Due to the presence of the Schiff base in the ligand, once the complex hydrolyzed, the ligand could continue to fragment into salicylaldehyde (SalA) and *N*-(2-hydroxyethyl)-1,2-ethanediamine (HyDA) as shown in eq. (1) below. The equilibrium mixture of both the ligand and $[V(O)_2$(Hshed)] complex in aqueous solution was reached as evident by the NMR spectra recorded.

$$Hshed^- + H_3O^+ \rightarrow SalA + HyDA \quad (1)$$

$$2[V(O)_2(Hshed)] + 4HO^- \rightarrow 2\ H_2VO_4^- + 2\ Hshed^- \quad (2)$$

Once the equilibrium mixture of H_2shed ligand had been reached in aqueous solution, the solution was added to form RMs from two concentrations of AOT/*iso*-octane stock solution (0.200 and 0.750 M). Since the highest resolution ^{1}H NMR spectra were obtained using 0.750 M AOT stock solution, the rest of the studies were carried out using this stock solution concentration (see below). ^{51}V NMR spectra recorded for the precursor complex [$V(O)_2$(Hshed)] in D_2O confirmed that it hydrolyzed in aqueous solution, and that equilibrium was reached by 20 min after sample preparation (see below). Compared to the aqueous solution, the equilibrium reaction was reached slower in RMs and the equilibrium concentration was achieved after 40 min. These studies provided the time-scale of the experiments of the precursor [$V(O)_2$(Hshed)] complex sample and provided guidelines for the timeframe of the studies with this complex as well as the vanadium complexes with the catechol ligands studied, where the lower solubility is problematic and causes issues with detecting the V-complex.

5.3.3 ^{51}V NMR Spectra of the [$V(O)_2$(Hshed)] Complex

In aqueous solutions, the equilibrium concentration of [$V(O)_2$(Hshed)] is about 60% of the total vanadium. ^{51}V NMR spectra of [$V(O)_2$(Hshed)] in DMSO, D_2O, and in a series of RMs (w_0 = 6, 8, 12, 16 and 20 prepared from 0.750 M AOT/*iso*-octane stock solution) are given in Figure 5.3.1. Upon placement into the RM, the stability ratio was changed significantly and the amount of [$V(O)_2$(Hshed)] complex in the RM environment is much smaller than in D_2O (H_2O), Figure 5.3.1. These studies convincingly show that [$V(O)_2$(Hshed)] is destabilized by the RM environment more so than in aqueous solution. Slightly more [$V(O)_2$(Hshed)] complex was observed in larger RMs over smaller RMs.

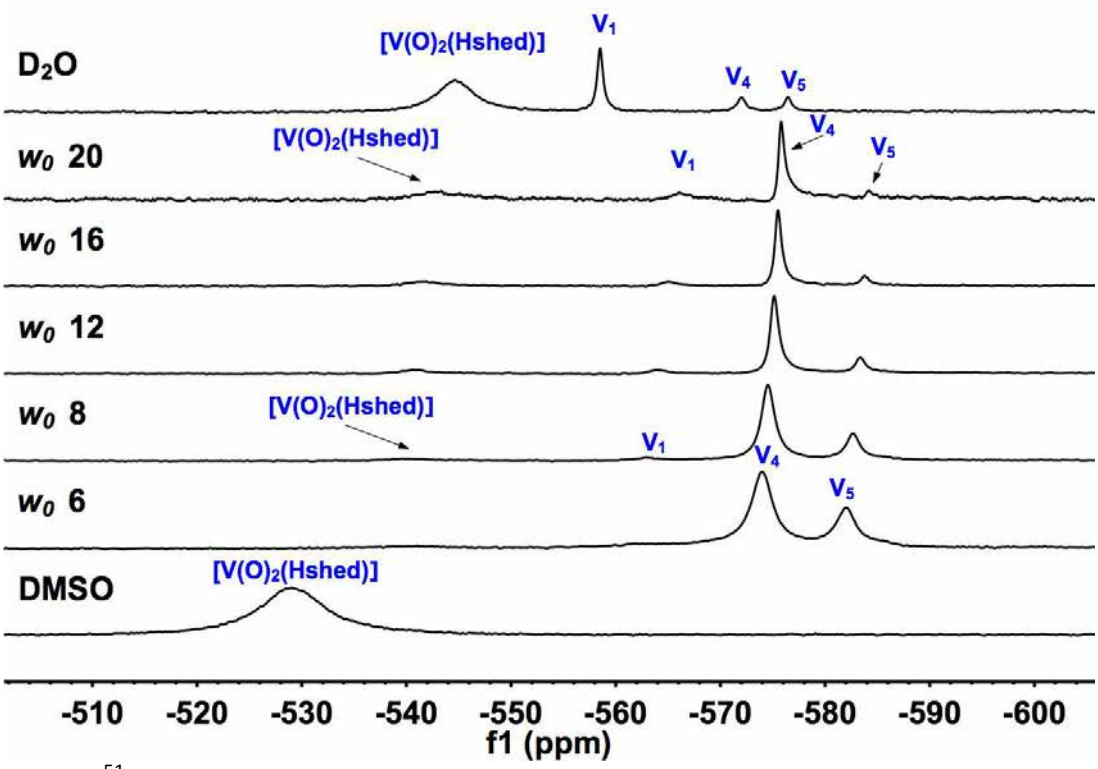

Figure 5.3.1. ^{51}V NMR spectra of $[V(O)_2(Hshed)]$ in D_2O and in a series of RMs (w_0 = 6, 8, 12, 16 and 20 prepared form a in 0.750 M AOT/*iso*-octane stock solution). The spectra were recorded after equilibration was reached after 20 min for D_2O samples and after 40 min in RM samples. The pH for D_2O and RMs was 6.6 and the pD was 7.0. The total V-concentration for the 1.0 mL $[V(O)_2(Hshed)]$ RM samples are as follows: w_0 20, 2.41 mM; w_0 16, 5.17 mM; w_0 12, 11.05 mM; w_0 8, 23.53 mM; and w_0 6, 36.72 mM.

5.3.4 ^{1}H NMR Spectra of $[V(O)_2(Hshed)]$ and H_2shed

A series of ^{1}H NMR spectroscopic studies in RMs were carried out using $[V(O)_2(Hshed)]$ and the corresponding free ligand, H_2shed. The RM studies with the $[V(O)_2(Hshed)]$ complex confirmed that the free H_2shed ligand was formed from hydrolysis of complex, which was then followed by subsequent hydrolysis of the H_2shed ligand to SalA and HyDA. The hydrolysis was confirmed in the D_2O spectra by the imine hydrogen signal (HC=N) at 8.81 ppm converting into an aldehyde hydrogen (HC=O) at 9.98 pm (Figure 5.3.2). These peaks are not present in the d_6-DMSO spectrum for $[V(O)_2(Hshed)]$ (Figure 5.3.2). The spectra are shown for RM sizes w_0 8 through w_0 20 and although the ligand hydrolysis is complete, increased reactions are taking

place because increasing SalA: [$V(O)_2$(Hshed)] (the latter measured by H_k) ratio is observed in the spectra as the RM size continues to increase (see spectrum at w_0 20).

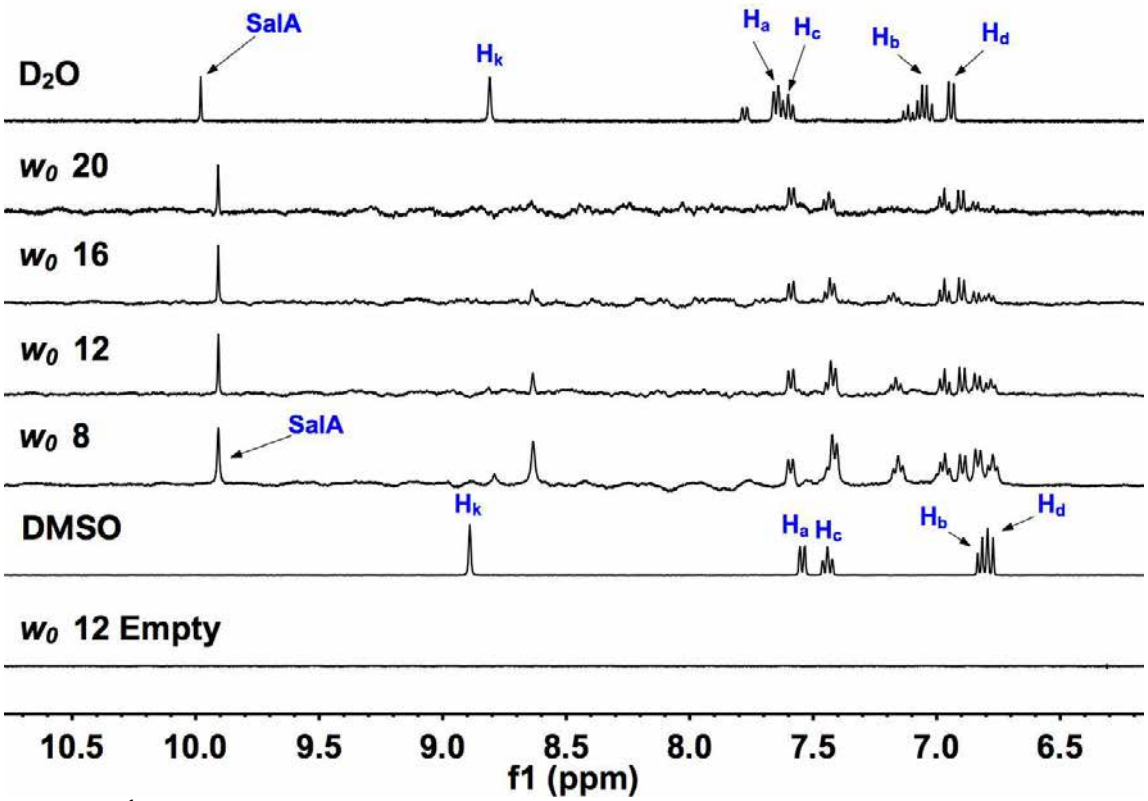

Figure 5.3.2. ^{1}H NMR spectra of [$V(O)_2$(Hshed)] in D_2O and in a series of RMs (w_0 = 8, 12, 16, and 20 prepared from 0.750 M AOT/iso-octane stock solution. The spectrum in D_2O was recorded after 20 min and the RM spectra were recorded after 40 min once equilibrium had been established. SalA = salicylaldehyde. The pH for D_2O and RMs was 6.6 and the pD was 7.0. The total V-concentration for the 1.0 mL [$V(O)_2$(Hshed)] RM samples are as follows: w_0 20, 2.41 mM; w_0 16, 5.17 mM; w_0 12, 11.05 mM; w_0 8, 23.53 mM; and w_0 6, 36.72 mM.

To further confirm the formation of the ligand hydrolysis product, SalA, a study of the non-complexed free ligand, H_2shed, in a series of RMs was carried out (Figure 5.3.3). By monitoring the ^{1}H NMR chemical shifts, it is apparent that the free ligand is hydrolyzing upon contact with the water pool (Figure 5.3.3). Formation of an aldehyde group signal (HC=O) at 9.90 ppm and a decrease in the imine signal (HC=N) near 8.5 ppm readily shows the formation of one of the starting materials of the Schiff base, SalA and almost complete conversion is seen after an

equilibrium time of 45 min in D_2O. The ^1H NMR spectra demonstrated that the equilibrium mixture was different in the RMs compared to the H_2shed ligand in aqueous solution, and that the Schiff base is more stable in the environment of the smaller RMs in contrast to the $[V(O)_2$(Hshed)] complex. Combined, these results show that the SalA and the H_2shed begin to form both in solutions with uncomplexed free ligand H_2shed (Figure 5.3.3) and with the precursor $[V(O)_2$(Hshed)] complex (Figure 5.3.2).

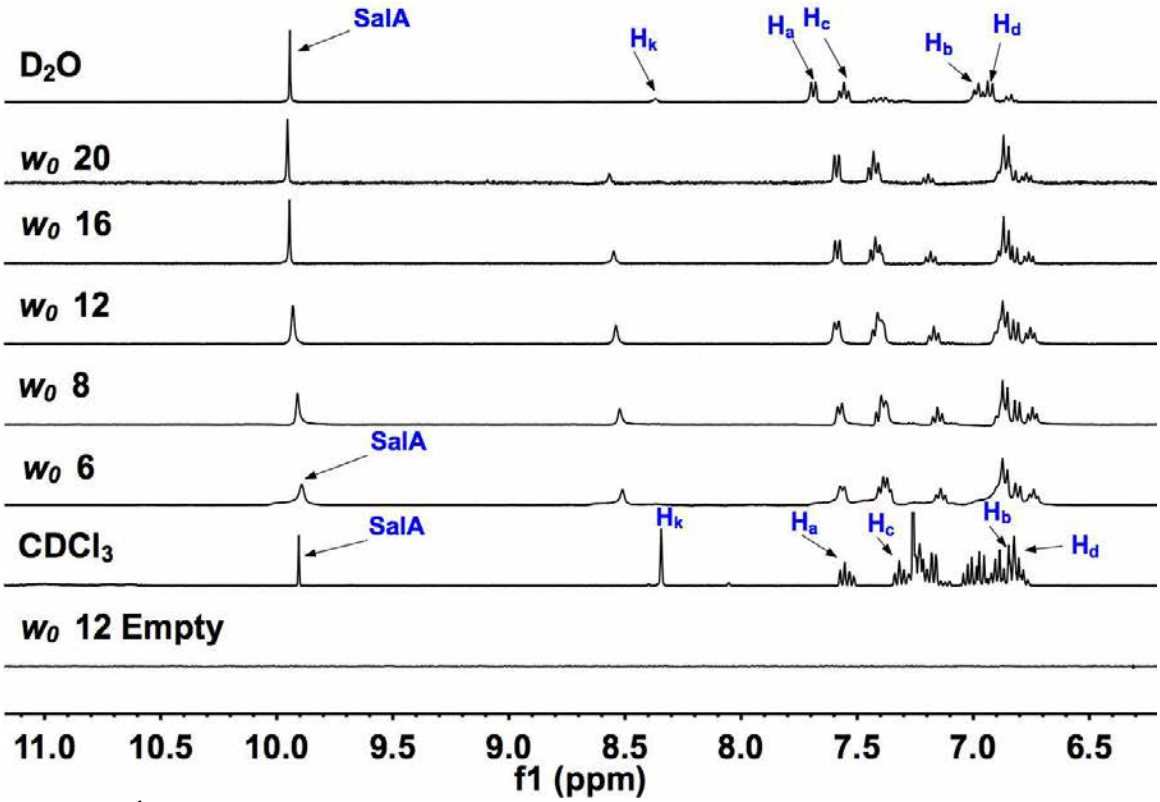

Figure 5.3.3. ^1H NMR spectra of H_2shed in D_2O and in a series of RMs (w_0 = 6, 8, 12, 16, and 20 prepared from 0.750 M AOT/*iso*-octane stock solution. The spectrum in D_2O was recorded after 35 min and the spectra in RMs were recorded after 45 min once equilibrium had been established. Hydrogen labelling scheme is found in Figure 5.1.1. SalA = salicylaldehyde. The pH for D_2O and RMs was 6.6 and the pD was 7.0. The overall concentrations for the 1.0 mL H_2shed RM samples are as follows: w_0 20, 2.71 mM; w_0 16, 5.65 mM; w_0 12, 11.77 mM; w_0 8, 24.48 mM; and w_0 6, 37.87 mM.

There is a chemical shift change observed for $[V(O)_2$(Hshed)] hydrogens H_a, H_b, H_c, H_d, and H_k upon addition to the RM, which showed a change in chemical environment and supported the

interpretation that the [$V(O)_2$(Hshed)] complex penetrated at least partially into the RM interfacial layer (Figure 5.3.2). The free ligand H_2shed hydrolyzed as evidenced by a peak at 9.94 ppm in D_2O and at 9.89 ppm in w_0 8 RM (Figure 5.3.2). There is a chemical shift change observed for H_2shed hydrogens H_a, H_b, H_c, H_d, and H_k, which also showed a change in chemical environment and supported significant interaction of the H_2shed ligand with the RM interface (Figure 5.3.3).

5.3.5 NMR Spectra of [VO(Hshed)(dtb)] in Aqueous Solution and in Reverse Micelle Samples

^{51}V NMR spectra were recorded to determine if the [VO(Hshed)(dtb)] complex hydrolyzed in aqueous solution and within RMs. This was non-trivial considering the low solubility of the V-complex in aqueous solution; therefore, these samples were prepared by dissolving the compound into the AOT/*iso*-octane stock solution rather than in the D_2O stock solution. The equilibrium for the hydrolysis products was observed in a saturated [VO(Hshed)(dtb)]/D_2O sample that was sonicated for 5 min, then vortexed for ~1 min, and then allowed to sit for 60 min (Figure 5.3.4). [VO(Hshed)(dtb)] hydrolyzed to form [$V(O)_2$(Hshed)] first and further hydrolysis formed vanadate and the H_2shed ligand according to eq. (3) and (4). The sample in d_6-DMSO (Figure 5.3.4) contained three signals for [VO(Hshed)(dtb)], the major peak signal is consistent with literature[68] and in addition, we also observed two minor peaks, which we attribute to association and concentration phenomena. When placed in RMs, the equilibration was established slightly faster in this system (~50 min) after which time point the spectra no longer changed.

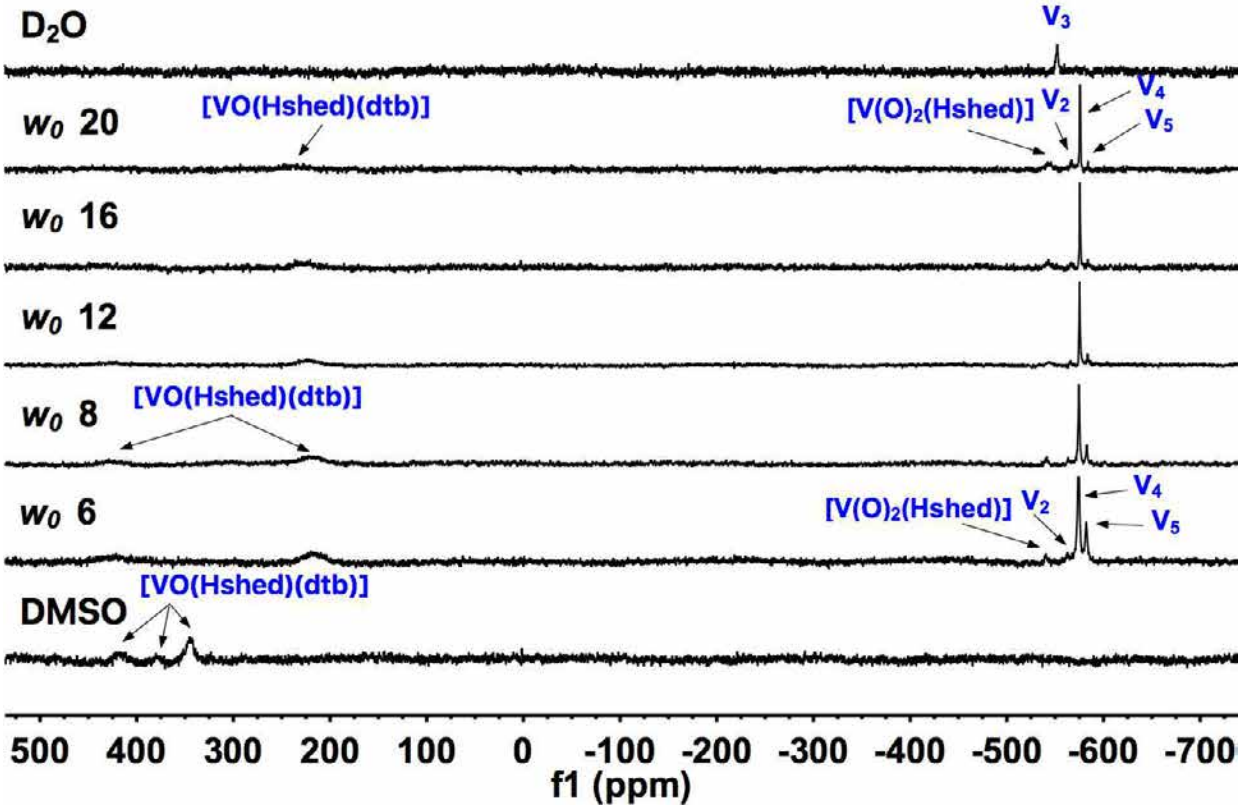

Figure 5.3.4. ^{51}V NMR spectra of [VO(Hshed)(dtb)] in d_6-DMSO, *iso*-octane, and in a series of RMs (w_0 = 6, 8, 12, 16, 20 prepared from 0.750 M AOT/*iso*-octane stock solution). The spectrum in D_2O was recorded after 60 min and the spectra in RMs was recorded after 50 min once equilibrium had been established. The pH for D_2O and RMs was 6.6 and the pD was 7.0. The total V-concentration for the 1.0 mL [VO(Hshed)(dtb)] RM samples are as follows: w_0 20, 2.46 mM; w_0 16, 5.23 mM; w_0 12, 11.09 mM; w_0 8, 23.55 mM; w_0 6, 36.78 mM.

$$[VO(Hshed)(dtb)] + H_2O \rightarrow [V(O)_2(Hshed)] + H_2dtb \qquad (3)$$

$$[V(O)_2(Hshed)] + 3H_2O \rightarrow SalA + HyDAH^+ + H_2VO_4^- \qquad (4)$$

The ^{51}V NMR spectra recorded for [VO(Hshed)(dtb)] in d_6-DMSO, D_2O, and in RMs (RMs (w_0 = 6, 8, 12, 16, and 20) are shown in Figure 5.3.4. The spectrum in d_6-DMSO shows three signals (see above). No complex is observed in the D_2O spectrum documenting that this compound is not soluble but does form vanadate oligomers when attempting to dissolve the material. In the RM samples, more vanadate oligomers, possibly a little $[V(O)_2(Hshed)]$, and two signals, which are

attributed to the [VO(Hshed)(dtb)] complex are observed (Figure 5.3.4). Both ^{51}V and ^{1}H NMR spectra confirm that in RMs at higher concentration of the complex, more [VO(Hshed)(dtb)] is observed than in pure D_2O. When placing [VO(Hshed)(dtb)] in RMs, some of the complex hydrolyzed, and there was a large change in chemical shifts from the d_6-DMSO sample and the distribution of signals varied depending on the size of the RM. This suggests that the [VO(Hshed)(dtb)] complex is in an environment different from aqueous solution. As the size of the RM changed, the chemical shifts did not significantly change consistent with the possibility that the compound is in similar environments in the different sized RMs. These results are consistent with an interpretation that the [VO(Hshed)(dtb)] complex increases stability through association or interactions with the interface and although still separated from the water pool, the water reaches the complex, initiating hydrolysis of [VO(Hshed)(dtb)] and resulting in the formation of vanadate oligomers and [$V(O)_2$(Hshed)] (Figure 5.3.4). As the RM size increases, the amount of hydrolysis increases because the [VO(Hshed)(dtb)] complex signal decreases and the increase in vanadate oligomers formed is observed (as evidenced by the changes in the metal speciation).[82]

The ^{1}H NMR spectra of [VO(Hshed)(dtb)] in D_2O, d_6-DMSO, and various sized RMs were collected (see Supporting Information Figure A5.1). The spectrum in D_2O does not show all the hydrogen peaks present in the [VO(Hshed)(dtb)] complex due to limited solubility of the complex; however, the ligand of the complex was also hydrolyzed as evidenced by an aldehyde peak at 10.04 ppm in D_2O and at 9.91 ppm in RMs. These peaks are not present in the d_6-DMSO spectrum. There is a chemical shift change for [VO(Hshed)(dtb)] aromatic hydrogens H_b, H_d, H_e, and H_f, which showed a change in environment of the complex and supports the interpretation based

on the ^{51}V NMR spectra of an association and possible penetration of the complex into the RM interface. Combined, these studies show that the aqueous insoluble [VO(Hshed)(dtb)] complex can solubilize and partition in a heterogeneous environment, but such an environment also facilitates increased hydrolysis of the complex and its Schiff base ligand.

5.3.6 NMR Spectra of [VO(Hshed)(cat)] in Aqueous Solution and in Reverse Micelle Samples

^{51}V NMR spectra were recorded as a function of time to determine if the [VO(Hshed)(cat)] complex hydrolyzed after it was dissolved in aqueous solution, as well as in AOT/*iso*-octane RMs (Figure 5.3.5). The solubility of [VO(Hshed)(cat)] was limited in aqueous solution; therefore, ~1 min of vortexing was needed to prepare a saturated sample of [VO(Hshed)(cat)] in D_2O. This system also had the potential of forming [$V(O)_2$(Hshed)] and the H_2shed ligand according to equations (5) and (6).

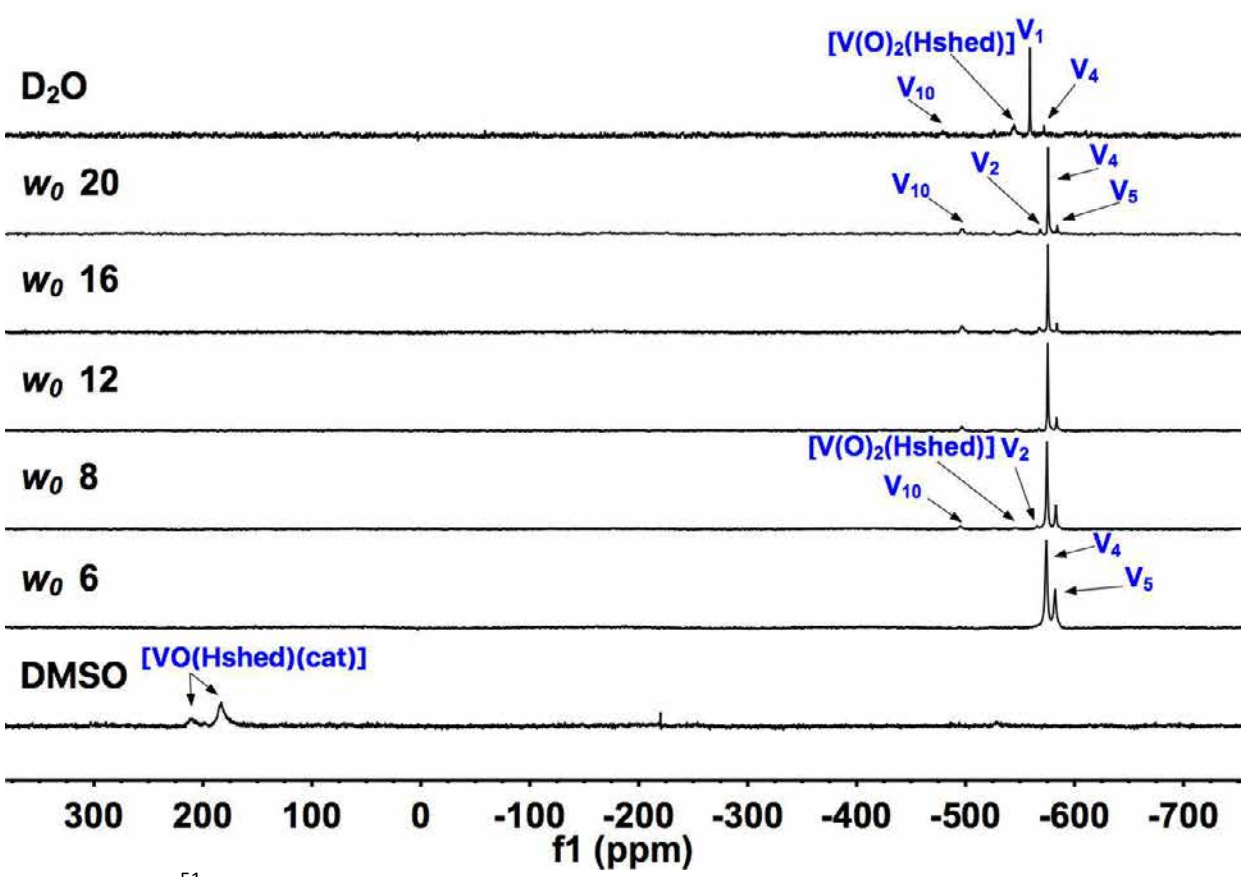

Figure 5.3.5. ^{51}V NMR spectra of [VO(Hshed)(cat)] in D_2O and in a series of RMs (w_0 = 6, 8, 12, 16, and 20 prepared from 0.750 M AOT/isooctane stock solution). The spectra were recorded after equilibration was reached after 50 min for D_2O samples and after 40 min for RM samples. The pH for D_2O and RMs was 6.6 and the pD was 7.0. The total V-concentration for the 1.0 mL [VO(Hshed)(cat)] RM samples are as follows: w_0 20, 2.41 mM; w_0 16, 5.17 mM; w_0 12, 11.05 mM; w_0 8, 23.53 mM; and w_0 6, 36.72 mM.

$$[VO(Hshed)(cat)]+H_2O \rightarrow [V(O)_2(Hshed)]+H_2cat \qquad (5)$$

$$[V(O)_2(Hshed)]+3H_2O \rightarrow SalA+HyDAH^+ +H_2VO_4^- \qquad (6)$$

[VO(Hshed)(cat)] was dissolved in d_6-DMSO and in aqueous solution as well as in AOT/*iso*-octane RMs. By ^{51}V NMR, no [VO(Hshed)(cat)] remained after being added to the D_2O solution or the RM mixture and intact [VO(Hshed)(cat)] was only observed in d_6-DMSO (Figure 5.3.5). These results suggest that the equilibrium favors complex hydrolysis upon dissolution in D_2O and that the energetics are not sufficiently favorable for the complex to reform in RM samples. ^{1}H NMR

spectra shows that the H_2shed ligand from the complex does hydrolyze more slowly, because some C=NH signal remains in w_0 8-12 samples (see Figure A5.2). These studies do confirm that the [VO(Hshed)(cat)] complex has significantly different properties than the [VO(Hshed)(dtb)] complex.

5.3.7 Examining the AOT/*iso*-octane Reverse Micelles Containing H_2shed, [$V(O)_2$(Hshed)], [VO(Hshed)(cat)], [VO(Hshed)(dtb)], using Dynamic Light Scattering

To determine if RMs formed in the AOT/RM samples, w_0 = 12 and w_0 = 20 RM samples were investigated using Dynamic Light Scattering (DLS). In Table A5.1 the RM samples are listed with the no cargo, with H_2shed, with [$V(O)_2$(Hshed)], with [VO(Hshed)(cat)] or with [VO(Hshed)(dtb)]. The results show that AOT/*iso*-octane RM structures form in all cases and that the sizes are comparative with literature values.[79] Furthermore, there were no significant differences observed between the hydrodynamic radii of the empty RM samples and those containing cargo. This suggests that no significant changes in the structures of the RMs are induced upon placement of any of the probe molecules inside the RMs.

5.3.8 The Anti-Cancer Effects of V(V) Catecholate Complexes on Bone Cancer Cells (SW1353 cells).

The hydrophobicity of the [VO(Hshed)(dtb)] complex may enhance complex stability to hydrolysis and thus increase the ability of the compound to enter cells intact. The question whether increased uptake due to hydrophobicity will be reflected in increased cytotoxicity was investigated in human chondrosarcoma cells, SW1353. However, before these studies were carried out we determined the stability of the compounds in cell culture media (Advanced

DMEM, supplemented with 2.0% vol. of fetal calf serum and 10 mM of HEPES buffer to maintain pH = 7.4 under ambient atmosphere)[31] using electronic absorption spectroscopy, because both [VO(Hshed)(cat)] and [VO(Hshed)(dtb)] showed strong absorbance bands in the visible and near-IR range in accord with literature.[68]

As shown in Figure 5.3.6, the absorption spectra of the [VO(Hshed)(dtb)] complex show intact complex in DMSO and fresh media (DMSO shown with black lines in Figure 5.3.6; fresh media are red). Although the complex is intact in DMSO, the [VO(Hshed)(dtb)] complex is only partially stable over time in cell media where it ultimately undergoes hydrolysis. However, after 24 h the [VO(Hshed)(dtb)] complex had degraded (shown with green lines in Figure 5.3.6). In contrast, addition of [VO(Hshed)(cat)] (0.10 mM V-complex) to cell culture medium instantly caused disappearance of the characteristic absorbance bands of the complex at ~530 nm and ~870 nm (red line in Figure 5.3.6a). The [VO(Hshed)(cat)] complex is therefore much less stable than the [VO(Hshed)(dtb)] complex. These results are consistent with the results by NMR spectroscopic studies described above (Figures 5.3.4-5). Both complexes decomposed after 24 h incubation with the cell culture medium at 310 K. The following cell culture studies were therefore done with both fresh (1-2 min.) and aged solutions (24 h). This allowed us to compare the effects over time for the two different V(V) Schiff base/catecholate compounds and vanadate in bone cancer cells (human chondrosarcoma, SW1353 cells). This also permitted us to explore when [VO(Hshed)(dtb)] was still intact and when both complexes were hydrolysed.

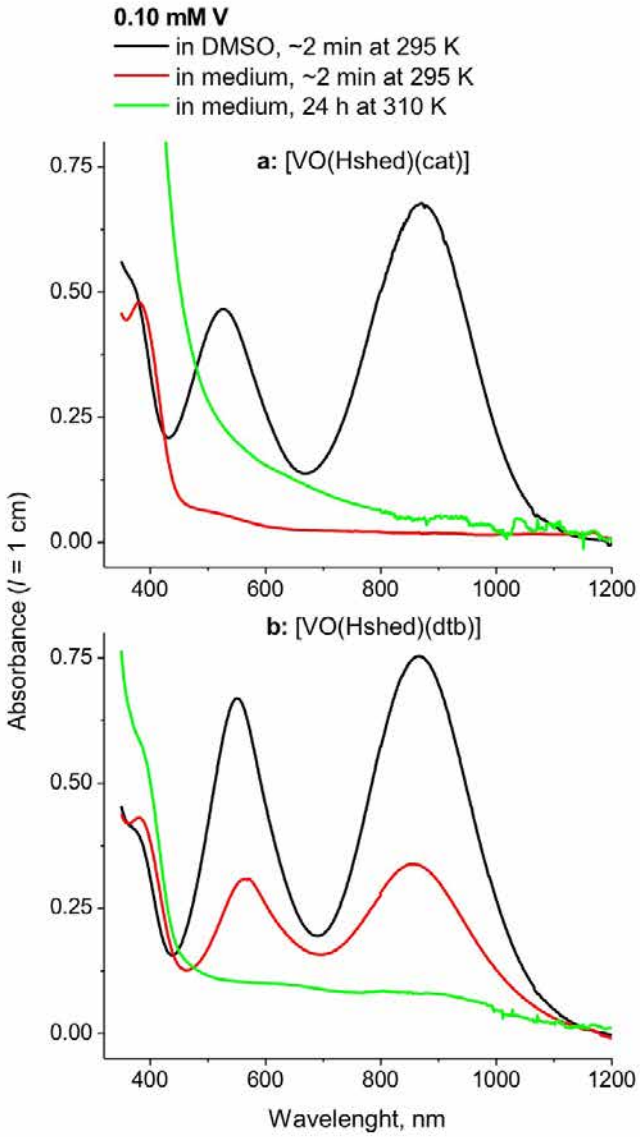

Figure 5.3.6. Representative electronic absorption spectra of fresh (2 min after dissolution) and aged (24 h after dissolution) of (A) [VO(Hshed)(cat)] and (B) [VO(Hshed)(dtb)] (0.10 mM V-compound) in DMSO solutions or in cell culture medium (Advanced DMEM, containing 2.0% vol. of fetal calf serum and 10 mM HEPES buffer, pH 7.4).

Initial experiments on the anti-proliferative activities of the [VO(Hshed)(cat)] and [VO(Hshed)(dtb)] complexes in SW1353 cells (Figure 5.3.7a) were carried out with the consideration of their different hydrolysis rates in aqueous solutions, in cell culture media and in artificial membrane systems (Figures 5.3.4-7). Stock solutions of both complexes in DMSO, which

were stable for at least 24 h under ambient conditions (verified by electronic absorption spectroscopy, Figure 5.3.6) were added to cell culture medium to the required final concentrations (typically, 5.0 μM V). The resultant medium was either immediately added to the cells (within 1 min. fresh medium), or allowed to age for 24 h (310 K, 5% CO_2) prior to addition to the cells.[38, 83] Vanadate (Na_3VO_4, either fresh or aged in the medium) was used as a reference compound.[33] Previous studies by XANES spectroscopy[35] and EPR spectroscopy[84] have shown that vanadate converts to a mixture of V(V) (predominantly) and V(IV) complexes with medium components upon aging. As shown in Figure 5.3.7a, [VO(Hshed)(cat)] was moderately active at 5.0 μM V-complex (cell viability after 72 h treatment was 40-50% of control), while Na_3VO_4 added to the media resulted in 70-75% of the control. For [VO(Hshed)(cat)] and vanadate, no significant difference in anti-proliferative activity was observed between fresh and aged solutions in cell culture medium.

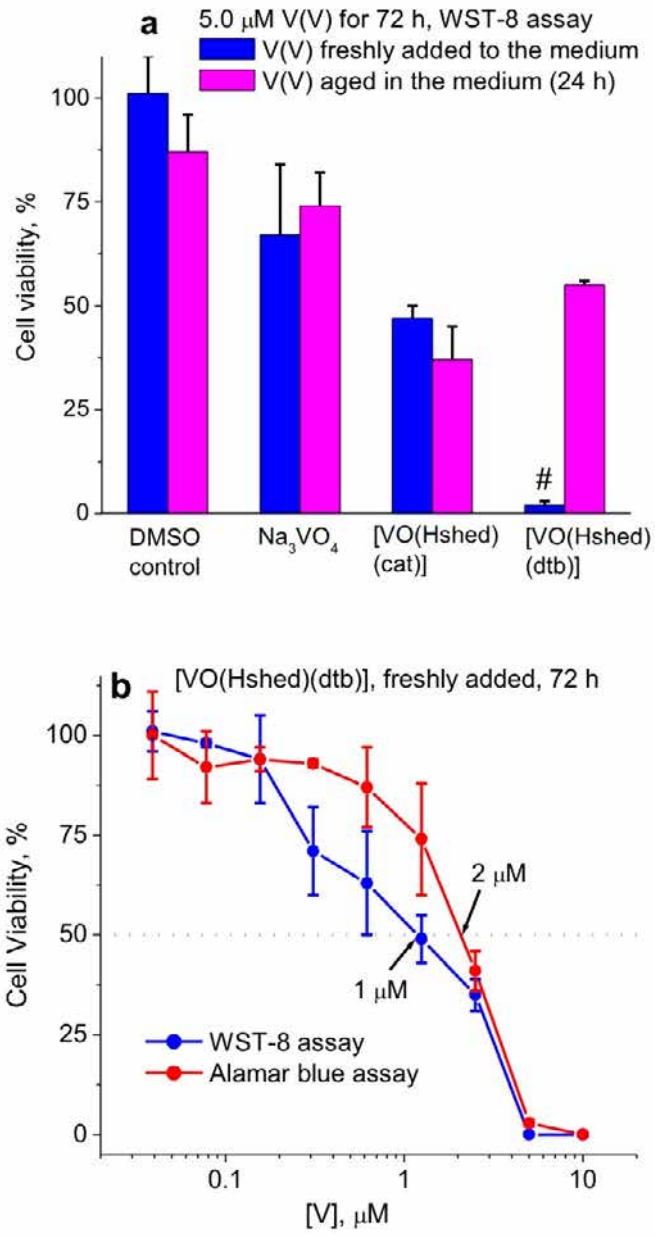

Figure 5.3.7. Anti-proliferative activity of [VO(Hshed)(cat)], [VO(Hshed)(dtb)] and Na_3VO_4 in human chondrosarcoma (SW1353) cells: (A) comparative effects of V(V) complexes at 5.0 μM V; and (B) concentration-dependent effects for fresh solutions of [VO(Hshed)(dtb)]. Treatment media were added to cells either within 1 min. after the addition of V(V) complexes (fresh media), or pre-incubated with the V(V) complexes for 24 h at 310 K and 5% CO_2 before the addition to cells (aged media). In both cases, cells were treated for 72 h (310 K, 5% CO_2) before the determination of cell viability by endpoint colorimetric assays (WST-8 or Alamar Blue). All the treatments, including controls, contained 0.50% vol. DMSO. Error bars represent the mean values and standard deviations of six replicate wells. The # sign shows highly significant difference ($P < 0.001$) in activity between fresh and decomposed solutions of [VO(Hshed)(dtb)].

The [VO(Hshed)(dtb)] complex showed much stronger anti-proliferative activity when freshly added to the medium (only ~2% of control), compared with the aged solution (50-60% of control) (Figure 5.3.7a). Furthermore, compared to the less hydrophobic [VO(Hshed)(cat)] complex or the ionic vanadate, the fresh solution of the more hydrophobic and intact [VO(Hshed)(dtb)] complex was significantly more potent. As a result, we were interested in exploring the anti-proliferative activity of [VO(Hshed)(dtb)] further. Concentration-dependent studies of fresh [VO(Hshed)(dtb)] solutions using two different assays for cell viability, WST-8[85] and Alamar Blue,[86] gave consistent results with IC_{50} = 1.3 ± 0.3 μM V and a plateau is seen at high V-concentrations (5-10 μM) (Figure 5.3.7b). This level of activity is similar or higher compared to that of well-established Pt(II) anti-cancer drugs in typical human cancer cell lines (IC_{50} ~1-5 μM Pt)[87]. Taken together, data from Figures 5.3.4-6 shows that higher stability of [VO(Hshed)(dtb)] compared with [VO(Hshed)(cat)] in cell culture medium and in the hydrophobic environment of cell membranes is likely to lead to its significant cellular uptake before hydrolysis in aqueous medium is complete.[88] The observed higher cytotoxicity of fresh solutions in cell culture medium compared to aged ones correlates with the greater stability of the [VO(Hshed)(dtb)] complex. High hydrolysis rates of [VO(Hshed)(cat)] in cell culture medium (Figure 5.3.6) are likely to prevent cellular uptake of the intact complex, which means that the anti-proliferative activity is due to decomposition products as have been recognized previously in multiple biological systems.[5, 11, 33, 89-96] Similar relation between aqueous stability, cellular uptake, and anti-proliferative activity was observed previously for Ru complexes.[97-98] We conclude that the increased hydrophobicity of the dtb catechol ligand is preventing early hydrolysis leading to the enhanced cellular uptake of intact [VO(Hshed)(dtb)] complex.

5.3.9 Discussion

Numerous studies were carried out with different V compounds exploring the mode of action and the identity of the active species when V-compounds were considered for treatment of diabetes.[5, 57, 71, 93, 99] It is well-known that V-compounds are protein tyrosine phosphatase inhibitors,[57, 100-101] however, much work has been done on the transport of V-compounds from the administration site to the site of action.[40, 102-104] Specifically, studies have been done exploring the transport of V-compounds in blood,[37, 39, 103, 105-106] and the speciation of these compounds[14, 57, 107] have been investigated in detail both in model systems,[39, 106] in blood,[37, 103, 105] in animal model studies[108] and in human studies.[12] Interaction of V-compounds with transferrin, human serum albumin, or other blood components have demonstrated that V-compounds can lose one or more of their ligands and remain active.[37, 103, 105, 109] How the vanadium compounds enter and what properties dictate entrance into the cells remains an important question.

These studies have shown that the interface dramatically impacted the stability of the vanadium precursor complex, $[V(O)_2(Hshed)]$, as well as two hydrophobic vanadium complexes, [VO(Hshed)(cat)] and [VO(Hshed)(dtb)]. Both ternary mixed-ligand complexes are soluble in the polar organic solvents such as DMSO and less so in nonpolar organic solvents (e.g., 2,2,4-trimethylpentane). However, the inhomogeneous environment of a microemulsion supports these V-complexes even if they have been hydrolyzed in the presence of interfacial water. Based on the NMR spectroscopic studies presented in this work, the interaction with the RM interface protects the V-compound against rapid initial hydrolysis. The slowed hydrolysis effect was more pronounced for the more sterically-hindered hydrophobic dtb ligand. This effect could be due to sterics or hydrophobicity of the ligand or a combination of both and studies with additional

compounds will shed light as to the origin of this observation. Alternatively, it may be possible that pKa values of the catechols can affect the inherent thermodynamic stability of the coordination complexes. The pKa value of the parent catechol is higher than that of the t-butyl substituted catechol and thus, the coordinated complex of the latter would be more stable. Initial V-complex stability may be important for the anti-cancer activity of the compounds as shown by the study in human bone cancer cells (chondrosarcoma). The anti-cancer effects reduce with decreased hydrophobicity and decreased hydrolytic stability of the V-compounds. Future studies with additional related V-compounds will shed further light on the exact origin of the anti-cancer effects.

The kinetic stability of [VO(Hshed)(dtb)] in water and aqueous media is unusual for a V-complex but in this case, provides sufficient stability to enable this complex to enter cancer cells intact. The hydrophobic environment of the cell membrane is likely to further stabilize this compound.[41] This unusual short-term stability of this highly cytotoxic V-complex may show considerable promise in cancer treatment, particularly against aggressive cancers such as prostate cancer. Since such hydrophobic complexes are likely to undergo cellular uptake *via* passive diffusion through the cell membrane, it is important to investigate if hydrophobicity or hydrolytic stability of these compounds correlates with uptake in membrane model systems.

The results presented here with two different hydrophobic catecholate complexes based on studies in AOT-*iso*-octane microemulsion system shows that although the [VO(Hshed)(dtb)] complex may be stabilized, the membrane system is not able to completely prevent hydrolysis from the water penetrating the interface. If a complex remains intact for some limited time, this will allow the drug to reach the cellular target intact. Importantly, the current results show that

the intact complexes indeed interact with the interface and hence, the results are consistent with the observation of increased cytotoxicity of fresh versus aged drug preparation. That is, the freshly prepared solution contains more intact complex and the hydrolyzed aged solution contains less intact complex. Accordingly, the solution with more intact [VO(Hshed)(dtb)] complex is much more cytotoxic compared to the aged solution with degraded V-complex towards the bone cancer cells investigated. Importantly, the results with the aged solutions shows dramatically decreased cytotoxic effect for both V-complexes against SW1353 bone cancer cells, consistent with the free ligands having no significant cytotoxicity (free ligands alone are significantly less cytotoxic (unpublished data)).

Given the fact that humans are largely composed of water and cell assay studies generally are done using water-based approaches, administration of hydrophobic drugs remains a challenge. However, there are ways of delivering a drug into the body that does not require water solubility but in the case of these very hydrophobic drugs, cell assays in aqueous solution remains problematic. The studies described herein may imply that hydrophobic metallo-compounds with increased hydrolytic stability will continue to be of interest and suggests that alternative approaches for effective drug delivery that will circumvent significant decomposition should be developed.

5.4 Summary and Conclusions

The [VO(Hshed)(cat)] complex is found to have lower thermodynamic stabilities in both water and cell culture medium compared to the [VO(Hshed)(dtb)] complex. Although the complexes show limited stability in the presence of model membrane systems, this may be a consequence of the pre-equilibrium that resulted in partial hydrolyzed complex(es). The greater activities

observed in fresh solutions of V-catecholate complexes containing higher amounts of intact compound in *in vitro* cytotoxicity assays in bone cancer cells and are in line with additional studies in MDA-MB-231 and PANC-1 cells.[41] Importantly, the membrane model results shown here demonstrate that the intact V(V) catacholate complexes will penetrate the membrane, which supports the cell cytotoxicity assays that indicate the intact complexes are taken up before they are decomposed in the cell medium.

In summary, the hydrophobic V(V) catecholate compounds presented here are found to interact with model membrane systems and the V-complex with the highest stability is found to have the most potent anti-cancer properties. It is possible that complexes containing hydrophobic ligands with sterically hindered V-atom preventing substitution reactions may enable uptake of the intact complex and delivery to the cellular target. Alternatively, similar behavior could arise from different thermodynamic stabilities. Regardless of the origin, the hydrophobic V(V) catecholate complexes were found to be a particularly potent cytotoxin to bone cancer cells. These results warrant future studies of these and similarly stable hydrophobic vanadium compounds as potential anti-cancer agents.

References

1. Crans, D. C.; Koehn, J. T.; Petry, S. M.; Glover, C. M.; Wijetunga, A.; Kaur, R.; Levina, A.; Lay, P. A., Hydrophobicity May Enhance Membrane Affinity and Anti-Cancer Effects of Schiff Base Vanadium(V) Catecholate Complexes. *Dalton Trans.* **2019,** *48*, 6383-6395.
2. Sherman, S. E.; Lippard, S. J., Structural Aspects of Platinum Anticancer Drug-Interactions with DNA. *Chem. Rev.* **1987,** *87* (5), 1153-1181.
3. Evangelou, A. M., Vanadium in Cancer Treatment. *Crit. Rev. Oncol. Hematol.* **2002,** *42* (3), 249-265.
4. Farrell, N., Current Status of Structure-activity Relationships of Platinum Anticancer Drugs: Activation of the *trans*-geometry. *Met. Ions Biol. Syst.* **1996,** *32*, 603-639.
5. Pessoa, J. C.; Etcheverry, S.; Gambino, D., Vanadium Compounds in Medicine. *Coord. Chem. Rev.* **2015,** *301*, 24-48.
6. Yang, X.; Wang, K., Perspectives in Medicinal Chemistry - Focusing on the Link Between Diabetes, Alzheimer's Disease and Cancer for the Discovery of New Medicines. *Curr. Top. Med. Chem.* **2016,** *16* (7), 675-676.
7. Petanidis, S.; Kioseoglou, E.; Domvri, K.; Zarogoulidis, P.; Carthy, J. M.; Anestakis, D.; Moustakas, A.; Salifoglou, A., In vitro and ex vivo Vanadium Antitumor Activity in (TGF-β)-induced EMT. Synergistic Activity with Carboplatin and Correlation with Tumor Metastasis in Cancer Patients. *Int. J. Biochem. Cell Biol.* **2016,** *74*, 121-134.
8. Vieira, A. P.; Wegermann, C. A.; Da Costa Ferreira, A. M., Comparative Studies of Schiff base-copper(II) and Zinc(II) Complexes Regarding their DNA Binding Ability and Cytotoxicity against Sarcoma Cells. *New J. Chem.* **2018,** *42*, 13169-13179.
9. Gruzewska, K.; Michno, A.; Pawelczyk, T.; Bielarczyk, H., Essentiality and Toxicity of Vanadium Supplements in Health and Pathology. *J. Physiol. Pharmacol.* **2014,** *65* (5), 603-11.
10. Rehder, D.; Pessoa, J. C.; Geraldes, C.; Castro, M.; Kabanos, T.; Kiss, T.; Meier, B.; Micera, G.; Pettersson, L.; Rangel, M.; Salifoglou, A.; Turel, I.; Wang, D. R., In vitro Study of the Insulin-mimetic Behaviour of Vanadium(IV, V) Coordination Compounds. *J. Biol. Inorg. Chem.* **2002,** *7* (4-5), 384-396.
11. Thompson, K. H.; Lichter, J.; LeBel, C.; Scaife, M. C.; McNeill, J. H.; Orvig, C., Vanadium Treatment of Type 2 Diabetes: A View to the Future. *J. Inorg. Biochem.* **2009,** *103*, 554–558.
12. Willsky, G. R.; Halvorsen, K.; Godzala, M. E., III; Chi, L.-H.; Most, M. J.; Kaszynski, P.; Crans, D. C.; Goldfine, A. B.; Kostyniak, P. J., Coordination Chemistry May Explain Pharmacokinetics and Clinical Response of Vanadyl Sulfate in Type 2 Diabetic Patients. *Metallomics : integrated biometal science* **2013,** *5* (11), 1491-1502.
13. Crans, D. C.; Yang, L.; Haase, A. A.; Yang, X., Health Benefits of Vanadium and Its Potential as an Anticancer Agent. *Met. Ions Life Sci.* **2017,** *18* (1), 251-280.
14. Crans, D. C.; Woll, K. A.; Prusinskas, K.; Johnson, M. D.; Norkus, E., Metal Speciation in Health and Medicine Represented by Iron and Vanadium. *Inorg. Chem.* **2013,** *52* (21), 12262-12275.
15. Lipinski, C. A.; Lombardo, F.; Dominy, B. W.; Freeney, P. J., Experimental and Computational Approaches to Estimate Solubility and Permeability in Drug Discovery and Development Settings. *Adv. Drug Delivery Rev.* **2001,** *46*, 3-26.
16. Köpf-Maier, P., Antitumor Bis(cyclopentadienyl) Metal Complexes. *Met. Complexes Cancer Chemother.* **1993**, 259-296.

17. Ghosh, P.; D'Cruz, O. J.; Narla, R. K.; Uckun, F. M., Apoptosis-inducing Vanadocene Compounds Against Human Testicular Cancer. *Clin. Cancer Res.* **2000,** *6* (4), 1536-1545.
18. Kostova, I., Titanium and Vanadium Complexes as Anticancer Agents. *Anti-Cancer Agents Med. Chem.* **2009,** *9* (8), 827-842.
19. León, I.; Butenko, N.; Di Virgilio, A.; Muglia, C.; Baran, E.; Cavaco, I.; Etcheverry, S., Vanadium and Cancer Treatment: Antitumoral Mechanisms of Three Oxidovanadium (IV) Complexes on a Human Osteosarcoma Cell Line. *J. Inorg. Biochem.* **2014,** *134*, 106-117.
20. León, I.; Cadavid-Vargas, J.; Di Virgilio, A.; Etcheverry, S., Vanadium, Ruthenium and Copper Compounds: A New Class of Non-platinum Metallodrugs with Anticancer Activity. *Curr. Med. Chem.* **2017,** *24*, 112-148.
21. Glasner, H.; Meker, S.; Tshuva, E. Y., Cationic Phenolato Titanium(IV) Complexes of Enhanced Solubility as Active and Biologically Accessible Anti-tumor Compounds. *J. Organomet. Chem.* **2015,** *788*, 33-35.
22. Reytman, L.; Braitbard, O.; Hochman, J.; Tshuva, E. Y., Highly Effective and Hydrolytically Stable Vanadium(V) Amino Phenolato Antitumor Agents. *Inorg. Chem.* **2016,** *55*, 610-618.
23. Posner, B. I.; Shaver, A.; Fantus, I. G., Insulin Mimetic Agents: Vanadium and Peroxovanadium Compounds. In *New Antidiabetic Drugs*, Bailey, C. J.; Flatt, P. R., Eds. Smith-Gordon: London, 1990; Vol. Chapter 8, pp 107-118.
24. Li, M.; Ding, W.; Baruah, B.; Crans, D. C.; Wang, R., Inhibition of Protein Tyrosine Phosphatase 1B and Alkaline Phosphatase by Bis(maltolato)oxovanadium (IV). *J. Inorg. Biochem.* **2008,** *102* (10), 1846-1853.
25. Lu, L. P.; Zhu, M. L., Metal-Based Inhibitors of Protein Tyrosine Phosphatases. *Anti-Cancer Agents Med. Chem.* **2011,** *11* (1), 164-171.
26. Crans, D. C.; Tarlton, M. L.; McLauchlan, C. C., Trigonal Bipyramidal or Square Pyramidal Coordination Geometry? Investigating the Most Potent Geometry for Vanadium Phosphatase Inhibitors. *Eur. J. Inorg. Chem.* **2014,** (27), 4450-4468.
27. McLauchlan, C. C.; Peters, B. J.; Willsky, G. R.; Crans, D. C., Vanadium–phosphatase Complexes: Phosphatase Inhibitors Favor the Trigonal Bipyramidal Transition State Geometries. *Coord. Chem. Rev.* **2015,** *301-302*, 163-199.
28. Clede, S.; Lambert, F.; Saint-Fort, R.; Plamont, M.-A.; Bertrand, H.; Vessieres, A.; Policar, C., Influence of the Side-Chain Length on the Cellular Uptake and the Cytotoxicity of Rhenium Triscarbonyl Derivatives: A Bimodal Infrared and Luminescence Quantitative Study. *Chem. Eur. J.* **2014,** *20* (28), 8714-8722.
29. Khosravi-Shahi, P.; Cabezón-Gutiérrez, L.; Custodio-Cabello, S., Metastatic Triple Negative Breast Cancer: Optimizing Treatment Options, New and Emerging Targeted Therapies. *Asia-Pac. J. Clin. Oncol.* **2018,** *14*, 32-39.
30. Correia, I.; Chorna, L.; Cavaco, I.; Roy, S.; Kuznetsov, M. L.; Ribeiro, N.; Justino, G.; Marques, F.; Santos-Silva, T.; Santos, M. F. A.; Santos, H. M.; Capelo, J. L.; Doutch, J.; Pessoa, J. C., Interaction of [VIVO(acac)$_2$] with Human Serum Transferrin and Albumin. *Chem. Asian J.* **2017,** *12*, 2062.
31. Levina, A.; Crans, D. C.; Lay, P. A., Speciation of Metal Drugs, Supplements and Toxins in Media and Bodily Fluids Controls in vitro Activities. *Coord. Chem. Rev.* **2017,** *325*, 473-498.
32. Levina, A.; Lay, P. A., Metal-based Anti-diabetic Drugs: Advances and Challenges. *Dalton Trans.* **2011,** *40*, 11675-11686.
33. Levina, A.; Lay, P. A., Stabilities and Biological Activities of Vanadium Drugs: What is the Nature of the Active Species? *Chem. Asian J.* **2017,** *12*, 1692-1699.
34. Levina, A.; McLoud, A. I.; Gasparini, S. J.; Nguyen, A.; De Silva, W. G. M.; Aitken, J. B.; Harris, H. H.; Glover, C.; Johannessen, B.; Lay, P. A., Reactivity and Speciation of Anti-Diabetic Vanadium Complexes in

Whole Blood and Its Components: The Important Role of Red Blood Cells. *Inorg. Chem.* **2015,** *54*, 7753-7766.
35. Levina, A.; McLoud, A. I.; Pulte, A.; Aitken, J. B.; Lay, P. A., Biotransformations of Antidiabetic Vanadium Prodrugs in Mammalian Cells and Cell Culture Media: A XANES Spectroscopic Study. *Inorg. Chem.* **2015,** *54*, 6707-6718.
36. Sanna, D.; Ugone, V.; Serra, M.; Garribba, E., Speciation of Potential Anti-diabetic Vanadium Complexes in Real Serum Samples. *J. Inorg. Biochem.* **2017,** *173*, 52-65.
37. Sanna, D.; Ugone, V.; Micera, G.; Buglyo, P.; Biro, L.; Garribba, E., Speciation in Human Blood of Metvan, a Vanadium Based Potential Anti-tumor Drug. *Dalton Trans.* **2017,** *46*, 8950-8967.
38. Le, M.; Rathje, O.; Levina, A.; Lay, P. A., High Cytotoxicity of Vanadium(IV) Complexes with 1,10-phenanthroline and Related Ligands is Due to Decomposition in Cell Culture Medium. *J. Biol. Inorg. Chem.* **2017,** *22* (5), 663-672.
39. Sanna, D.; Micera, G.; Garribba, E., Interaction of Insulin-Enhancing Vanadium Compounds with Human Serum holo-Transferrin. *Inorg. Chem.* **2013,** *52* (20), 11975-11985.
40. Sanna, D.; Ugone, V.; Sciortino, G.; Buglyo, P.; Bihari, Z.; Parajdi-Losonczi, P. L.; Garribba, E., (VO)-O-IV Complexes with Antibacterial Quinolone Ligands and their Interaction with Serum Proteins. *Dalton Trans.* **2018,** *47* (7), 2164-2182.
41. Levina, A.; Wijetunga, A.; Kaur, R.; Koehn, J. T.; Crans, D. C.; Lay, P. A., A Short-Lived but Highly Cytotoxic Vanadium(V) Complex: A Potential New Approach to Pancreatic Cancer Treatment. *To Be Submitted*.
42. Stahla, M. L.; Baruah, B.; James, D. M.; Johnson, M. D.; Levinger, N. E.; Crans, D. C., ^{1}H NMR Studies of Aerosol-OT Reverse Micelles with Alkali and
Magnesium Counterions: Preparation and Analysis of MAOTs. *Langmuir* **2008,** *24*, 6027-6035.
43. Crans, D. C.; Rithner, C. D.; Baruah, B.; Gourley, B. L.; Levinger, N. E., Molecular Probe Location in Reverse Micelles Determined by NMR Dipolar Interactions. *J. Am. Chem. Soc.* **2006,** *128*, 4437-4445.
44. Eastoe, J.; Robinson, B. H.; Heenan, R. K., Water-in-Oil Microemulsions Formed by Ammonium and Tetrapropylammonium Salts of Aerosol OT. *Langmuir* **1993,** *9* (11), 2820-2824.
45. Giddings, L. D.; Olesik, S. V., A Study of AOT Reverse Micelles in Liquids at Ambient
and High Pressure. *Langmuir* **1994,** *10*, 2877-2883.
46. Fernando Silva, O.; Fernandez, M. A.; Silber, J. J.; de Rossi, R. H.; Mariano Correa, N., Inhibited Phenol Ionization in Reverse Micelles: Confinement Effect at the Nanometer Scale. *ChemPhysChem* **2012,** *13* (1), 124-130.
47. Silva, O. F.; de Rossi, R. H.; Correa, N. M., The Hydrolysis of Phenyl Trifluoroacetate in AOT/n-heptane RMs as a Sensor of the Encapsulated Water Structure. *RSC Adv.* **2015,** *5* (44), 34878-34884.
48. Falcone, R. D.; Correa, N. M.; Biasutti, M. A.; Silber, J. J., Properties of AOT Aqueous and Nonaqueous Microemulsions Sensed by Optical Molecular Probes. *Langmuir* **2000,** *16* (7), 3070-3076.
49. Baruah, B.; Roden, J. M.; Sedgwick, M. A.; Correa, N. M.; Crans, D. C.; Levinger, N. E., When is Water Not Water? Exploring Water Confined in Large Reverse Micelles Using a Highly Charged Inorganic Molecular Probe. *J. Am. Chem. Soc.* **2006,** *128*, 12758-12765.
50. Correa, N. M.; Silber, J. J.; Riter, R. E.; Levinger, N. E., Nonaqueous Polar Solvents in Reverse Micelle Systems. *Chem. Rev.* **2012,** *112*, 4569-4602.
51. Vodolazkaya, N. A.; Mchedlov-Petrossyan, N. O.; Salamanova, N. V.; Surov, Y. N.; Doroshenko, A. O., Molecular Spectroscopy Studies of Solvent Properties of Dispersed 'water pools': Fluorescein and 2,7-dichlorofluorescein in Reversed AOT-based Microemulsions. *J. Mol. Liq. 157*, 105-112.
52. Vodolazkaya, N. A.; Kleshchevnikova, Y. A.; Mchedlov-Petrossyan, N. O., Differentiating Impact of the AOT-stabilized Droplets of Water-in-octane Microemulsions as Examined using Halogenated Fluoresceins as Molecular Probes. *J. Mol. Liq. 187*, 381-388.

53. Crans, D. C.; Schoeberl, S.; Gaidamauskas, E.; Baruah, B.; Roess, D. A., Antidiabetic Vanadium Compound and Membrane Interfaces: Interface-Facilitated Metal Complex Hydrolysis. *J. Biol. Inorg. Chem.* **2011,** *16* (6), 961-972.
54. Sostarecz, A. G.; Gaidamauskas, E.; Distin, S.; Bonetti, S. J.; Levinger, N. E.; Crans, D. C., Correlation of Insulin-Enhancing Properties of Vanadium- Dipicolinate Complexes in Model Membrane Systems: Phospholipid Langmuir Monolayers and AOT Reverse Micelles. *Chem. Eur. J.* **2014,** *20*, 5149-5159.
55. Willsky, G. R.; Chi, L.-H.; Godzala, M., III; Kostyniak, P. J.; Smee, J. J.; Trujillo, A. M.; Alfano, J. A.; Ding, W.; Hu, Z.; Crans, D. C., Anti-diabetic Effects of a Series of Vanadium Dipicolinate Complexes in Rats with Streptozotocin-induced Diabetes. *Coord. Chem. Rev.* **2011,** *255* (19-20), 2258-2269.
56. Li, M.; Ding, W.; Smee, J. J.; Baruah, B.; Willsky, G. R.; Crans, D. C., Anti-diabetic Effects of Vanadium (III, IV, V) – Chlorodipicolinate Complexes in Streptozotocin-Induced Diabetic Rats. *BioMetals* **2009,** *103*, 585-905.
57. Crans, D. C., Antidiabetic, Chemical, and Physical Properties of Organic Vanadates as Presumed Transition-State Inhibitors for Phosphatases. *J. Org. Chem.* **2015,** *80*, 11899-11915.
58. Scior, T.; Guevara-Garcia, J. A.; Do, Q.-T.; Bernard, P.; Laufer, S., Why Antidiabetic Vanadium Complexes are Not in the Pipeline of "Big Pharma" Drug Research? A Critical Review. *Curr. Med. Chem.* **2016,** *23*, 2874-2891.
59. Sanna, D.; Palomba, J.; Lubinu, G.; Buglyo, P.; Nagy, S.; Perdih, F.; Garribba, E., Role of Ligands in the Uptake and Reduction of V(V) Complexes in Red Blood Cells. *J. Med. Chem.* **2019,** *62*, 654-664.
60. Milsmann, C.; Levina, A.; Harris, H. H.; Foran, G. J.; Turner, P.; Lay, P. A., Charge Distribution in Chromium and Vanadium Catecholato Complexes: X-ray Absorption Spectroscopic and Computational Studies. *Inorg. Chem.* **2006,** *45*, 4743-4754.
61. Sanna, D.; Ugone, V.; Fadda, A.; Micera, G.; Garribba, E., Behavior of the Potential Antitumor (VO)-O-IV Complexes Formed by Flavonoid Ligands. Antioxidant Properties and Radical Production Capability. *J. Inorg. Biochem.* **2016,** *161*, 18-26.
62. Jakusch, T.; Enyedy, E. A.; Kozma, K.; Paar, Z.; Benyei, A.; Kiss, T., Vanadate Complexes of 3-hydroxy-1,2-dimethyl-pyridinone: Speciation, Structure and Redox Properties. *Inorg. Chim. Acta* **2014,** *420*, 92-102.
63. Chi, Z.; Zhu, L.; Lu, X.; Yu, H.; Liu, B., Comparative Study of three Mononuclear Vanadium-Aromatic 1, 2-Diol Complexes: Structure, Characterization and Anti-Proliferating Effects Against Cancer Cells. *Z. Anorg. Allg. Chem.* **2012,** *638* (10), 1523-1530.
64. Chi, Z.; Zhu, L.; Lu, X., Comparison of Two Binuclear Vanadium-catecholate Complexes: Synthesis, X-ray Structure and Effects in Cancer Cells. *J. Mol. Struct.* **2011,** *1001*, 111-117.
65. Leon, I. E.; Cadavid-Vargas, J. F.; Tiscornia, I.; Porro, V.; Castelli, S.; Katkar, P.; Desideri, A.; Bollati-Fogolin, M.; Etcheverry, S. B., Oxidovanadium(IV) Complexes with Chrysin and Silibinin: Anticancer Activity and Mechanisms of Action in a Human Colon Adenocarcinoma Model. *J. Biol. Inorg. Chem.* **2015,** *20*, 1175-1191.
66. Yoshikawa, Y.; Sakurai, H.; Crans, D. C.; Micera, G.; Garribba, E., Structural and Redox Requirements for the Action of Anti-diabetic Vanadium Compounds. *Dalton Trans.* **2014,** *43*, 6965–6972
67. Samart, N.; Beuning, C. N.; Haller, K. J.; Rithner, C. D.; Crans, D. C., Interaction of a Biguanide Compound with Membrane Model Interface Systems: Probing the Properties of Antimalaria and Antidiabetic Compounds. *Langmuir* **2014,** *30*, 8697-8706.
68. Cornman, C. R.; Colpas, G. J.; Hoeschele, J. D.; Kampf, J.; Pecoraro, V. L., Implications for the Spectroscopic Assignment of Vanadium Biomolecules: Structural and Spectroscopic Characterization of Monooxovanadium(V) Complexes Containing Catecholate and Hydroximate Based Noninnocent Ligands. *J. Am. Chem. Soc.* **1992,** *114*, 9925-9933.

69. Li, X.; Lah, M. S.; Pecoraro, V. L., Vanadium Complexes of the Tridentate Schiff Base Ligand N-Salicylidene-N'-(2-hydroxyethy1)ethylenediamine: Acid-Base and Redox Conversion between Vanadium(1V) and Vanadium(V) Imino Phenolates. *Inorg. Chem.* **1988,** *27* (25), 4657-4664.
70. Rajendiran, V.; Karthik, R.; Palaniandavar, M.; Stoeckli-Evans, H.; Periasamy, V. S.; Akbarsha, M. A.; Srinag, B. S.; Krishnamurthy, H., Mixed-Ligand Copper(II)-phenolate Complexes: Effect of Coligand on Enhanced DNA and Protein Binding, DNA Cleavage, and Anticancer Activity. *Inorg. Chem.* **2007,** *46*, 8208-8221.
71. Willsky, G. R.; Chi, L.-H.; Godzala, M., III; Kostyniak, P. J.; Smee, J. J.; Trujillo, A. M.; Alfano, J. A.; Ding, W.; Hu, Z.; Crans, D. C., Anti-diabetic Effects of a Series of Vanadium Dipicolinate Complexes in Rats with Streptozotocin-induced Diabetes. *Coord. Chem. Rev.* **2011,** *255*, 2258–2269.
72. Glasoe, P. K.; Long, F. A., Use of Glass Electrodes to Measure Acidities in Deuterium Oxide. *J. Phys. Chem.* **1960,** *64* (1), 188-190.
73. Levina, A.; Harris, H. H.; Lay, P. A., X-ray Absorption and EPR Spectroscopic Studies of the Biotransformations of Chromium(VI) in Mammalian Cells. Is Chromodulin an Artifact of Isolation Methods? *J. Am. Chem. Soc.* **2007,** *129* (5), 1065-1075.
74. Freshney, R. I., *Culture of Animal Cells: A Manual of Basic Technique and Specialized Applications*. 7th ed.; Wiley-Blackwell: Hoboken, NJ, 2016.
75. Schweigert, N.; Zehnder, A. J. B.; Eggen, R. I. L., Chemical Properties of Catechols and their Molecular Modes of Toxic Action in Cells, from Microorganisms to Mammals. *Environ. Microbiol.* **2001,** *3* (2), 81-91.
76. Pooransingh-Margolis, N.; Renirie, R.; Hasan, Z.; Wever, R.; Vega, A. J.; Polenova, T., 51V Solid-State Magic Angle Spinning NMR Spectroscopy of Vanadium Chloroperoxidase. *J. Am. Chem. Soc.* **2006,** *128*, 5190-5208.
77. Zizic, M.; Miladinovic, Z.; Stanic, M.; Hadzibrahimovic, M.; Zivic, M.; Zakrzekska, J., ^{51}V NMR Investigation of Cell-associated Vanadate Species in *Phycomyces blakesleeanus* Mycelium. *Res. Microbiol.* **2016,** *167*, 521-528.
78. Peters, B. J.; Groninger, A. S.; Fontes, F. L.; Crick, D. C.; Crans, D. C., Differences in Interactions of Benzoic Acid and Benzoate with Interfaces. *Langmuir* **2016,** *32* (37), 9451-9459.
79. Maitra, A., Determination of Size Parameters of Water-Aerosol OT-Oil Reverse Micelles from Their Nuclear Magnetic Resonance Data. *J. Phys. Chem.* **1984,** *88*, 5122-5125.
80. Timm, M.; Saaby, L.; Moesby, L.; Hansen, E. W., Considerations regarding use of solvents in in vitro cell based assays. *Cytotechnology* **2013,** *65* (5), 887-894.
81. Microcal Ltd. Microcal Origin Version 6.1. Northampton MA USA.
82. Crans, D. C., Aqueous Chemistry of Labile Oxovanadates: Relevance to Biological Studies. *Comments Inorg. Chem.* **1994,** *16*, 1-33.
83. Samart, N.; Arhouma, Z.; Kumar, S.; Murakami, H. A.; Crick, D. C.; Crans, D. C., Decavanadate Inhibits Mycobacterial Growth More Potently Than Other Oxovanadates. *Front. Chem.* **2018,** *6*, article 519.
84. Willsky, G. R.; White, D. A.; McCabe, B. C., Metabolism of Added Orthovanadate to Vanadyl and High-molecular-weight Vanadates by Saccharomyces cerevisiae. *J. Biol. Chem.* **1984,** *259* (21), 13273-13281.
85. Tominaga, H.; Ishiyama, M.; Ohseto, F.; Sasamoto, K.; Hamamoto, T.; Suzuki, K.; Watanabe, M., A Water-soluble Tetrazolium Salt Useful for Colorimetric Cell Viability Assay. *Anal. Commun.* **1999,** *36* (2), 47-50.
86. Hamid, R.; Rotshteyn, Y.; Rabadi, L.; Parikh, R.; Bullock, P., Comparison of Alamar Blue and MTT Assays for High Through-put Screening. *Toxicol. in Vitro* **2004,** *18* (5), 703-710.
87. Hall, M. D.; Telma, K. A.; Chang, K.-E.; Lee, T. D.; Madigan, J. P.; Lloyd, J. R.; Goldlust, I. S.; Hoeschele, J. D.; Gottesman, M. M., Say No to DMSO: Dimethylsulfoxide Inactivates Cisplatin, Carboplatin, and Other Platinum Complexes. *Cancer Res.* **2014,** *74* (14), 3913-3922.

88. Levina, A.; Mitra, A.; Lay, P. A., Recent Developments in Ruthenium Anticancer Drugs. *Metallomics : integrated biometal science* **2009,** *1* (6), 458-470.
89. Yang, X. G.; Wang, K.; Lu, J. F.; Crans, D. C., Membrane Transport of Vanadium Compounds and the Interaction with the Erythrocyte Membrane. *Coord. Chem. Rev.* **2003,** *237*, 103-111.
90. Crans, D. C.; Yang, L. Q.; Alfano, J. A.; Chi, L. H.; Jin, W. Z.; Mahroof-Tahir, M.; Robbins, K.; Toloue, M. M.; Chan, L. K.; Plante, A. J.; Grayson, R. Z.; Willsky, G. R., (4-hydroxypyridine-2,6-dicarboxylato)oxovanadate(V) - A New Insulin-like Compound: Chemistry, Effects on Myoblast and Yeast Cell Growth and Effects on Hyperglycemia in Rats with STZ-induced Diabetes. *Coord. Chem. Rev.* **2003,** *237*, 13-22.
91. Crans, D. C., Chemistry and Insulin-like Properties of Vanadium(IV) and Vanadium(V) Compounds *J. Inorg. Biochem.* **2000,** *80*, 123–131.
92. Yang, X. G.; Yang, X. D.; Yuan, L.; Wang, K.; Crans, D. C., The Permeability and Cytotoxicity of Insulin-mimetic Vanadium Compounds. *Pharm. Res.* **2004,** *21* (6), 1026-1033.
93. Thompson, K.; Orvig, C., Vanadium in diabetes: 100 years from Phase 0 to Phase I. *J. Inorg. Biochem.* **2006,** *100* (12), 1925-1935.
94. Rehder, D., The Potentiality of Vanadium in Medicinal Applications. *Future Med. Chem.* **2012,** *4* (14), 1823-1837.
95. Chasteen, N. D., *Copper, Molybdenum, and Vanadium in Biological Systems*. Springer: 1983.
96. Alessio, E.; Messori, L., The Deceptively Similar Ruthenium(III) Drug Candidates KP1019 and NAMI-A Have Different Actions. What Did We Learn in the Past 30 Years? In *Metallo-Drugs: Development and Action of Anticancer Agents*, Sigel, A.; Sigel, H.; Freisinger, E.; Sigel, R., Eds. 2018; pp 141-170.
97. Levina, A.; Aitken, J. B.; Gwee, Y. Y.; Lim, Z. J.; Liu, M.; Singharay, A. M.; Wong, P. F.; Lay, P. A., Biotransformations of Anticancer Ruthenium(III) Complexes: An X-Ray Absorption Spectroscopic Study. *Chem. Eur. J.* **2013,** *19* (11), 3609-3619.
98. Thota, S.; Rodrigues, D. A.; Crans, D. C.; Barreiro, E. J., Ru(II) Compounds: Next-Generation Anticancer Metallotherapeutics? *J. Med. Chem.* **2018,** *61* (14), 5805-5821.
99. Niu, X.; Xiao, R.; Wang, N.; Wang, Z.; Zhang, Y.; Xia, Q.; Yang, X., The Molecular Mechanisms and Rational Design of Anti-Diabetic Vanadium Compounds. *Curr. Top. Med. Chem.* **2016,** *16* (8), 811-822.
100. McLauchlan, C. C.; Peters, B. J.; Willsky, G. R.; Crans, D. C., Vanadium–phosphatase Complexes: Phosphatase Inhibitors Favor the Trigonal Bipyramidal Transition State Geometries. *Coord. Chem. Rev.* **2015,** *301*, 163-199.
101. Posner, B. I.; Faure, R.; Burgess, J. W.; Bevan, A. P.; Lachance, D.; Zhang-Sun, G.; Fantus, I. G.; Ng, J. B.; Hall, D. A.; Soo Lum, B.; Shaver, A., Peroxovanadium Compounds: a New Class of Potent Phosphotyrosine Phosphatase Inhibitors which are Insulin Mimetics. *J. Biol. Chem.* **1994,** *269* (6), 4596-4604.
102. Sciortino, G.; Sanna, D.; Ugone, V.; Micera, G.; Lledos, A.; Marechal, J.-D.; Garribba, E., Elucidation of Binding Site and Chiral Specificity of Oxidovanadium Drugs with Lysozyme through Theoretical Calculations. *Inorg. Chem.* **2017,** *56* (21), 12938-12951.
103. Kiss, T.; Jakusch, T.; Hollender, D.; Dörnyei, Á.; Enyedya, É. A.; Pessoa, J. C.; Sakurai, H.; Sanz-Medel, A., Biospeciation of Antidiabetic VO(IV) Complexes. *Coord. Chem. Rev.* **2008,** *252*, 1153–1162.
104. Dornyei, A.; Marcao, S.; Pessoa, J. C.; Jakusch, T.; Kiss, T., Interactions of Insulin-mimetic Vanadium Complexes with the Cell Constituents ATP and glutathione. *Eur. J. Inorg. Chem.* **2006,** *18*, 3614-3621.
105. Sanna, D.; Ugone, V.; Buglyo, P.; Nagy, S.; Kacsir, I.; Garribba, E., Speciation in Aqueous Solution and Interaction with Low and High Molecular Mass Blood Bioligands of [(VO)-O-IV(oda)(H_2O)($_2$)], a V Compound with in vitro Anticancer Activity. *Inorg. Chim. Acta* **2018,** *472*, 127-138.
106. Sanna, D.; Serra, M.; Micera, G.; Garribba, E., Interaction of Antidiabetic Vanadium Compounds with Hemoglobin and Red Blood Cells and Their Distribution between Plasma and Erythrocytes. *Inorg. Chem.* **2014,** *53* (3), 1449-1464.

107. Doucette, K. A.; Hassell, K. N.; Crans, D. C., Selective Speciation Improves Efficacy and Lowers Toxicity of Platinum Anticancer and Vanadium Antidiabetic Drugs. *J. Inorg. Biochem.* **2016,** *165*, 56-70.
108. Dikanov, S. A.; Liboiron, B. D.; Orvig, C., Two-dimensional (2D) Pulsed Electron Paramagnetic Resonance Study of VO2+-triphosphate Interactions: Evidence for Tridentate Triphosphate Coordination, and Relevance to Bone Uptake and Insulin Enhancement by Vanadium Pharmaceuticals. *J. Am. Chem. Soc.* **2002,** *124* (12), 2969-2978.
109. Pessoa, J. C.; Tomaz, I., Transport of Therapeutic Vanadium and Ruthenium Complexes by Blood Plasma Components. *Curr. Med. Chem.* **2010,** *17* (31), 3701-3738.

Chapter 6: Summary, Concluding Remarks, and Future Directions

6.1 Summary and Concluding Remarks

The research presented in this dissertation builds a foundation for further research into understanding biologically important, hydrophobic, redox-active molecules.

Chapter two described the synthesis and characterization of eight truncated MK analogs, as well as the separation and characterization of geometric isomers formed in the reactions. The fully unsaturated MK derivatives, MK-1, MK-2, and MK-3 were successfully synthesized from menadione in two steps using a Lewis acid catalyst and the respective corresponding allylic alcohol isoprenoid side chain. MK-1(H_2) was successfully synthesized in single step from 1-iodo-3-methylbutane utilizing a key radical alkylation reaction. The partially saturated MK-2(II-H_2) was successfully synthesized in a single step from menadiol and isophytol, and the *trans* isomer was separated from the *cis* isomer byproduct by preparative TLC followed by characterization. The novel fully saturated MK-2(I,II-H_4) was successfully synthesized in three steps from 3,7-dimethyloctan-1-ol. The partially saturated MK-3(II-H_2) was successfully synthesized in seven steps from β-citronellol and the *trans* isomer was readily separated from the *cis* isomer byproduct by preparative TLC followed by characterization. Finally, the novel fully saturated MK-3(I,II,III-H_6) was successfully synthesized in four steps from farnesol. The use of benzene-d_6 as a diagnostic NMR solvent for the rapid evaluation of *cis*/*trans* mixtures for MK/vitamin K analogs was essential as *cis*/*trans* peaks often coalesce in chloroform-d. Access to these MK derivatives containing varying isoprenyl side chain length and degrees of saturation is crucial for determining

why partial saturation of MK is observed in pathogenic *M. tuberculosis* and why mycobacterial electron transport efficiency was decreased 3-fold when MenJ expression was disrupted.

Chapter three characterized the conformational and chemical properties of the hydrophobic MK-2 molecule. Using 2D NMR spectroscopy, we established for the first time that MK-2 has a folded conformation defined by the isoprenyl side chain folding back over the naphthoquinone in a U-shape, which depends on the specific environmental conditions found in different solvents. We used molecular mechanics to illustrate the conformations found by the NMR experiments. The measured redox potentials of MK-2 differed in three organic solvents, where MK-2 was most easily reduced in DMSO, which may suggest a combination of solvent effect (presumably in part because of differences in dielectric constants) and/or conformational differences of MK-2 in different organic solvents. Furthermore, MK-2 was found to associate with the interface of model membranes represented by Langmuir phospholipid monolayers and RMs. MK-2 adopts a slightly different U-shaped conformation within RMs compared to within solution, which is in sharp contrast to the extended conformations illustrated in literature for MKs. These findings are important because they show that even a truncated MK analog adopts a folded conformation within hydrophobic environments, which may be important for recognition by respiratory enzymes within the ETS or may affect electron transfer efficiency.

In chapter four, the conformations of the simplest MK analogs, MK-1 and MK-1(H_2), within organic solvents were elucidated by 1D and 2D ^{1}H NMR spectroscopy. MK-1 and MK-1(H_2) adopted similar folded-extended conformations in each solvent but the preferred folded-extended conformations differed slightly between solvent environments. The quinone redox potentials of MK and MK-1(H_2) were measured in three organic solvents, where a solvent effect

(presumably due to a change in dielectric constant) was observed and most interestingly, a ~20 mV difference in semiquinone redox potential was observed between MK-1 and MK-1(H_2). The interaction of MK-1 and MK-1(H_2) with phospholipid monolayers was characterized using Langmuir phospholipid monolayers and the two MK-1 analogs were found to interact with the phospholipid interface. Finally, using a complementary study, the location, orientation, and conformation of MK-1 and MK-1(H_2) within a RM model membrane interface was determined using 1D and 2D NMR spectroscopy. The two MK-1 analogs interacted similarly with the RM model membrane interface and MK-1 adopted a slightly different folded conformation within the RM interface compared to that observed in organic solution. The elucidation of MK-1 and MK-1(H_2) conformation in solution and at a model membrane interface is essential and necessary as understanding the conformational preferences of the first isoprene unit of MK is useful for predicting conformations of the naturally occurring longer MK analogs within solution and cellular membranes. We observed that partial saturation in the isoprenyl side chain only minimally alters the conformation of MK-1 but may potentially affect the reactivity and function within biologically relevant environments because a difference in the redox potential is observed. MK analogs with longer isoprenyl side chains (e.g., MK-9) may also adopt folded conformations although much more complex. Saturation of the double bond in the first isoprene unit of the isoprenyl side chain serves to only minimally alter the preferred conformation although distinctly affecting the redox function. The results of the studies herein provide a working model involving the role of structure and redox potential that explains why partial saturation of MK is observed in pathogenic *M. tuberculosis*, which is responsible for the deaths of ~1.3 million people annually.

Chapter five demonstrates that certain hydrophobic vanadium(V) Schiff base/catecholate compounds, shown herein, have increased stability in aqueous media and affinity for membrane interfaces. Depending on their hydrophobicity, they may be able to enter cells intact. Two hydrophobic V(V) catecholate substituted analogues, [VO(Hshed)(cat)] and [VO(Hshed)(dtb)], (Hshed = N-(salicylideneami- nato)-N'-(2-hydroxyethyl)-1,2-ethanediamine, cat = pyrocatechol, and dtb = 3,5-di(tert-butyl)catechol and the vanadium(V) precursor [$V(O)_2$(Hshed)]) were synthesized for their ability to interact with membranes and their anti-cancer effects. Using ^{51}V and ^{1}H NMR spectroscopy, the presence and location of the free ligand, H_2shed, and the three V(V) complexes were examined in a model membrane microemulsion system. The stability of the three complexes was measured in aqueous solution, cell media, and an inhomogeneous microemulsion system. Our results demonstrated that free ligand H_2shed and the intact V(V) complexes associated with the interface but that the V-complexes hydrolyzed to some extent because oxovanadates were observed by ^{51}V NMR spectroscopy and decreasing complex by electronic absorption spectroscopy in cell media. When determining the effects of V(V) catecholate complexes on bone cancer cells, the strongest effects were observed with the more stable hydrophobic complex [VO(Hshed)(dtb)] that was able to best associate and penetrate the model membrane system intact. These studies are consistent with the membrane permeability studies being a good predictor for *in vitro* cytotoxicity assays because [VO(Hshed)(dtb)] can pass through the cellular membrane intact, which may enhance its anti-cancer activities. Importantly, the model membrane results shown herein demonstrate that the intact V(V) catacholate complexes will penetrate the membrane, which supports the cell cytotoxicity assays that indicate the intact complexes are taken up before they are decomposed in the cell medium. In summary,

the hydrophobic V(V) catecholate compounds presented herein are found to interact with membrane model systems and the V-complex with the highest stability is found to have the most potent anti-cancer properties. It is possible that complexes containing hydrophobic ligands with sterically hindered V-atom preventing substitution reactions may enable uptake of the intact complex and delivery to the cellular target. Alternatively, similar complex stability behavior could arise from different thermodynamic stabilities. Regardless of the origin, the hydrophobic Schiff base V(V) catecholate complexes were found to be a particularly potent cytotoxin to bone cancer cells. These results warrant future studies of these and similarly stable hydrophobic vanadium compounds as potential anti-cancer agents, where one could envision cytotoxic V-complex solutions being directly injected into the tumor *via* endoscopy to exhibit potent cytotoxic activity.

Overall, the findings of the studies presented in this dissertation help to further understand how the conformation and the degree of saturation in the isoprenyl side chain of MK affects the recognition, reactivity, and function of MK within the ETS of bacterial pathogens. These studies are important because they begin to elucidate and provide a working model to explain the chemical rationale as to why partially saturated MK-9 is observed in pathogenic *M. tuberculosis*, which is responsible for the infection of ~2 billion people worldwide and the deaths of ~1.3 million annually. Furthermore, the studies with the hydrophobic vanadium(V) catecholate metallo-complexes underpin a drug design concept exploiting hydrolytic stability imparted by hydrophobicity and steric bulk of a non-innocent ligand. Metal complexes designed on these principles may be successful anti-cancer drug candidates utilizing non-conventional drug delivery strategies that circumvent solubility and stability issues such as direct injection of cytotoxic solution into the tumor *via* endoscopy.

6.2 Future Directions

The following discusses an amalgam of future studies that would provide more fundamental information on the MK and MenJ system. These studies should shed further light on the role and function of partial saturation of MK that is observed in pathogenic *M. tuberculosis*. Partial saturation of the isoprenyl side chain of MK may be necessary for proper substrate recognition by respiratory enzymes within the ETS, or may be able to affect electron transport efficiency of the MK within the ETS, or may be a combination of both. The following also discusses future studies that would explore hydrophobic vanadium(V) catecholate complexes as potential anti-cancer drugs.

We have carried out a lot of electrochemical studies on truncated MK analogs. We have demonstrated that saturation of the isoprene unit on MK-1 affects the redox potential by ~20 mV, which was discussed in chapter four. We have carried out further preliminary studies on the eight synthesized MK derivatives as well as MK-7 and MK-9 and have observed an effect on redox potential based on isoprenyl side chain length and degree of saturation for the longer MK derivatives. These studies are the topic of a manuscript in preparation. An extract of mycobacterial MK-9(II-H_2) would be of great interest to characterize by electrochemistry to determine how much the redox potential differs from that of MK-9. This experiment would shed light on the 3-fold decrease observed in mycobacterial electron transport efficiency when MenJ expression is disrupted.

Preliminary structure-activity relationship studies with MenJ have been carried out by the Crick group using our synthesized MK derivatives and some interesting *in vitro* results were observed. These studies are the topic of a manuscript in preparation. Further structure activity

relationship studies are warranted. It would be interesting if MenJ took a fully saturated ring system on the naphthoquinone of a MK analog as a substrate because such a substrate would have no redox functioning capacity and may be a potential inhibitor of the electron transport system or attenuate electron transport efficiency enough to compromise the bacteria. Another MK analog that would be of interest to study would be to replace the branched methyl group on the second isoprene unit of MK-2 or MK-3 with a C-F group to determine if this affected the catalytic activity of MenJ. Truncated MK analogs should be evaluated to determine their capacity as electron transfer reagents *in vivo* within the mycobacterial ETS.

The studies presented within this dissertation concern the oxidized forms of MK derivatives. This is mostly in part because the reduced form or quinol form of MK is highly susceptible to spontaneous oxidation by atmospheric oxygen, which makes isolation or synthetic access to these MK derivatives challenging. We speculate that the quinol form has different physical and chemical properties, may adopt different conformations, and have different placement within the cellular membrane. Interestingly, the quinol form of UQ is much more stable and may be a good alternative to study than the air sensitive MK-quinol form. Efforts should be carried out to synthesize the quinol analogs of UQ and then their conformations and interactions within model membrane systems should be explored.

The synthetic procedures to carry out the C-C bond formation between the isoprenyl side chain and the naphthoquinone head group could be optimized to improve the yield. The current routes provide adequate material and in pure form; therefore, extensive time and effort was not spent optimizing the procedures beyond the yields shown herein. Efforts should be put forth to

optimize synthetic coupling procedures to access MK analogs where current yields are less than 30%.

Efforts should be put forth to further purify synthetic MK analogs to a crystalline state or recrystallization efforts should be carried out to obtain suitable crystals for single crystal x-ray diffraction analysis. MK-1(H_2), MK-2, MK-4, MK-7 and MK-9 are crystalline powders and efforts should be carried out to determine their solid state crystalline structure. These studies would provide valuable information as to the solid-state conformation of MKs derivatives, which would be useful for understanding solution conformations or the conformation adopted within cellular membranes for MKs.

The synthesis of partially saturated MK derivatives leads to the formation of the undesirable *cis* isomer. We could effectively purify the *trans* MK isomer from the *cis*/*trans* MK isomer mixture. However, efforts to obtain the *cis* isomer from the *cis*/*trans* isomer were unsuccessful. Efforts should be carried out to isolate the *cis* isomer from the *trans*/*cis* isomer mixture. It may be worthwhile to try reverse phase preparative tlc, silver impregnated silica column, or gravitron centrifugation tlc. The *cis* MK isomer would be desirable to have because *cis* and *trans* isomers may have very different conformational, chemical, and biological properties. It would be interesting to know if activity is observed with MenJ for the *cis* isomer of any fully unsaturated truncated MK analog.

Inhibitor development should be explored for MenJ if the catalytic function of MenJ is determined to be what is necessary for *M. tuberculosis* survival in macrophages. If the survival of *M. tuberculosis* is dependent upon the presence of the protein and not related to the enzymatic function, then development of an inhibitor may be very challenging. High-throughput screening

efforts should be carried out such as fragment based screening for inhibitor development. The synthesis of a tethered MK analog where the methyl is tethered in a ring system back to the isoprenyl side chain may lock the molecule in a conformation where it is no longer able to fit into the active site and redox cycle and may inhibit the ETS or provide us more information on what conformation of MK MenJ recognizes.

MenJ knockout rescue experiments should be pursued where mutant variants of *M. tuberculosis* that lack expression of MenJ are infected inside a macrophage and then partially saturated MK is introduced to see if it rescues the bacteria and restores survival. These experiments are challenging from the standpoint that the hydrophobic MK derivative must traverse two membranes to observe an effect, where one is the almost wax like membrane of *M. tuberculosis* made up of very hydrophobic structural lipids such as the mycolic acids. This may be circumvented by pre-soaking the bacteria with cell media containing partially saturated MK derivative and then carrying out the macrophage infection experiments to see if rescue occurs. However, experiments are currently being pursued where mutants of MenJ that fold correctly but have no catalytic activity will be expressed in *M. tuberculosis* while infecting a macrophage to determine exactly if the virulence factor is the enzyme MenJ or partially saturated MK-9. It would be interesting to synthesize an MK analog that is substituted on the MK ring system that has a small redox change magnitude (~20 mV) and see it rescues *M. tuberculosis* MenJ knockouts infecting macrophage like cells or increases electron transfer efficiency within the ETS.

MK analogs of interest not already synthesized or commercially available should be synthesized. Efforts were carried out and we were able to successfully synthesize MK-2(I-H_2) that is saturated at the first isoprene. However, the yield was less than 1% and we have since

developed a better proposed synthetic method that should be carried out in the future. This molecule is thought to not function properly in electron transport and it would be interesting to explore the chemical rationale behind this observation further. Other MK analogs that have substituents on the naphthoquinone ring that would perturb the redox potential would be interesting to study. Benzophenone has been showed to mimic the structure of an isoprene unit within the isoprenyl side chan. Therefore, MK-benzophenone analogs could be synthesized and investigated for their chemical and biochemical properties. It would be very informative to synthesize a MK analog that could covalently link to the active site of MenJ once bound, which may provide information on the interactions of MK with MenJ and the active site since a crystal structure of MenJ still has not been obtained.

Preliminary conformational analysis of partially saturated MK analogs such as MK-2(II-H_2) and MK-3(II-H_2) should be extended to other organic solvents and further into model membrane systems. Preliminary studies show these partially saturated MK analogs can also adopt folded conformations in organic solution. These compounds are crucial to study as they are truncated mimics of the partially saturated MK product of the MenJ catalyzed reaction.

Computational studies should be carried out on these MK derivatives. Rigorous calculation and comparison of the energies of conformations should be carried out. NMR chemical shift calculations should be carried out to determine how closely the experimental chemical shifts match predicted chemical shifts based on a proposed conformation. Computational studies characterizing the HOMO-LUMO band gap energy should be carried out on the MK derivatives described herein.

Studies in model membrane systems should extended to more physiologically relevant environments. Conformational analysis of truncated MKs in deuterated liposomes would be a logical next step.

Rigorous studies on the chromatographic separation of MK homologs (varying side chain length) would be very beneficial from both a synthetic standpoint and a fundamental chemical information standpoint. HPLC work with truncated MK analogs for separation analysis (retention times on a reverse phase column) based on isoprenyl side chain length and degree of saturation would be very valuable.

We have begun characterizing the MK derivatives by spectroelectrochemistry looking at the absorbance spectra under reduced and oxidized conditions and determining diffusion coefficients of the MK analogs, which is the topic of a manuscript in preparation. However, UV-Vis experiments should be carried out on truncated MK analogs for absorbance characterization and at varying concentrations to study aggregation and possible stacking interactions. These experiments would provide valuable information on the solution and association chemistry of these compounds.

Studies should be extended to other essential to life lipoquinones such as ubiquinones. We have already carried out a lot of studies in this area but due to length consideration of this dissertation, this chapter was omitted. We carried out a 6-step synthesis to yield gram quantities of ubiquinone-2 (UQ-2) and conformational analysis in two organic solvents and a reverse micelle environment was carried out. Preliminary findings suggest a folded conformation for UQ-2 in organic solutions and at the interface of RMs similar to lipoquinone analog, MK-2. These studies are the topic of a manuscript that is in preparation.

The chapter describing vanadium(V) catecholates set forth a concept exploiting hydrophobicity and steric bulk of a ligand to slow initial hydrolysis of a metal complex, which imparted increased stability in a model membrane system and exhibited potent cytotoxic effects against bone cancer cell lines. These studies should be extended to other vanadium(V) catecholate complexes with different substituents with varying amount of steric bulk and hydrophobicity to determine the best structure for cytotoxic activity. Studies should also be extended to exploring different tertiary stabilizing ligands other than H_2shed. Many of these studies are currently underway and will be the topic of future manuscripts. These vanadium(V) catecholate complexes exhibit very interesting redox chemistry and a wide range of NMR chemical shifts, which we have studied extensively and is the topic of a manuscript in preparation.

In summary, chapters two through four lay a solid foundation for a working model to describe why partial saturation is observed in pathogenic *M. tuberculosis*, which has infected around one third of the global population of humans with TB and is responsible for the deaths of ~1.3 million worldwide. While these chapters have made significant discoveries such as truncated MK derivatives adopting folded conformations and that saturation of the isoprenyl side chain on MK-1 can affect the redox potential, there are still many key experiments to determine the chemical rationale for why partial saturation is observed in MK within *M. tuberculosis*. This is an exciting field and we hope that the studies presented herein and published elsewhere will spark an interest in answering these perplexing biological questions. Chapter five explored a concept exploiting hydrophobicity and steric bulk of a ligand to slow initial hydrolysis of a metal complex and enhance membrane affinity and anti-cancer effects of vanadium(V) catecholate complexes.

These concepts will be extended to other vanadium and metal complexes for potential novel metallo-drugs to target hard to treat cancers such as pancreatic cancer.

Appendix I: Contributions to Work

The material in chapter one is primarily from literature, background knowledge, or insights gained from experience. Figures were prepared from original material or adapted for this dissertation.

Some of the material in chapter two is published[1] in *ACS Omega* with Jordan T. Koehn as the primary author. Coauthors include Dean C. Crick and Debbie C. Crans. For this work, Jordan T. Koehn carried out all the synthetic and experimental work, wrote the manuscript, prepared the figures, and prepared the supporting information. Dean C. Crick gave input and advice on what menaquinone derivatives would be of interest to make and helped with editing the manuscript. Debbie C. Crans gave input and advice on what menaquinone derivatives to make and helped with editing of the manuscript.

The material in chapter three is published[2] in *the Journal of Organic Chemistry* with Jordan T. Koehn as the primary author. Coauthors include Estella S. Magallanes, Benjamin J. Peters, Cheryle N. Beuning, Allison A. Haase, Michelle J. Zhu, Christopher D. Rithner, Dean C. Crick, and Debbie C. Crans. For this work, Jordan T. Koehn helped write the manuscript, created most of the figures, prepared the supporting information, synthesized menaquinone-2, carried out and analyzed the organic solution 2D NMR experiments and data, and carried out and analyzed the 2D reverse micelle NMR experiments and data. Estella S. Magallanes helped originally obtain 1D NMR data in reverse micelles and outlined a rough draft of the manuscript. Benjamin J. Peters designed the reverse micelle experiments and prepared and analyzed the Langmuir monolayer section.

Cheryle N. Beuning acquired the electrochemical data and contributed to the electrochemistry section. Allison A. Haase also helped acquire the Langmuir monolayer data. Michelle J. Zhu helped acquire preliminary data of menaquinone-2 within reverse micelles. Christopher D. Rithner gave valuable help for NMR interpretation and acquisition. Debbie C Crans helped write the manuscript and gave valuable input on experiments and writing. Dean C. Crick and Debbie C. Crans gave valuable advice and help preparing and editing the manuscript.

The material in chapter four is published[3] in *Biochemistry* with Jordan T. Koehn as the primary author. Coauthors include Cheryle N. Beuning, Benjamin J. Peters, Sara K. Dellinger, Cameron Van Cleave, Dean C. Crick, and Debbie C. Crans. For this work, Jordan T. Koehn wrote the manuscript, created most of the figures, synthesized MK-1 and MK-1(H_2), carried out and analyzed the organic solution 2D NMR experiments and data, carried out and analyzed the 1D and 2D NMR data in reverse micelles, and prepared the supporting information. Cheryle N Beuning acquired the electrochemical data and contributed to the electrochemistry section. Benjamin J. Peters prepared, analyzed, and helped write the Langmuir monolayer section. Sara K. Dellinger helped acquire some of the original 1D ^{1}H NMR spectra of MK-1 in different solvents. Cameron Van Cleave also helped acquire the Langmuir monolayer data. Dean C. Crick gave valuable input on the project. Debbie C. Crans gave valuable input and helped edit the manuscript.

The material in chapter five is published[4] in *Dalton Transactions* with Debbie C. Crans as the primary author. Coauthors include Jordan T. Koehn, Stephanie M. Petry, Caleb M. Glover, Asanka Wijetunga, Ravinder Kaur, Aviva Levina, and Peter A. Lay. For this work, Jordan T. Koehn synthesized the vanadium complexes, trained and supervised undergraduate students (Stephanie and Caleb) in synthesis and how to make and run reverse micelle experiments,

prepared the figures, prepared the supporting information, analyzed data, and helped write and edit the manuscript. Stephanie M. Petry carried out the NMR experiments in solution and within reverse micelles and carried out the dynamic light scattering experiments. Caleb M. Glover carried out the initial experiments in reverse micelles and helped getting the project running. UV-Vis and cytotoxicity experiments were carried out by Asanka Wijetunga, Ravinder Kaur and Aviva Levina. Peter A. Lay and Aviva Levina wrote the UV-Vis and cytotoxicity sections, gave valuable advice, and helped edit the manuscript. Debbie C. Crans wrote the original outline and draft of the manuscript, helped edit the manuscript, and provided valuable advice and input.

The material in chapter six provides a summary and concluding remarks of the work in the preceding chapters. In addition, a future direction sections details where the author believes the project should go and what experiments should be carried out in the future.

The following appendices state contributions to the published works that are not discussed within the chapters of this dissertation or are supporting figures useful for further interpretations of the data.

References

1. Koehn, J. T.; Crick, D. C.; Crans, D. C., Synthesis and Characterization of Partially and Fully Saturated Menaquinone Derivatives. *ACS Omega* **2018,** *3*, 14889-14901.
2. Koehn, J. T.; Magallanes, E. S.; Peters, B. J.; Beuning, C. N.; Haase, A. A.; Zhu, M. J.; Rithner, C. D.; Crick, D. C.; Crans, D. C., A Synthetic Isoprenoid Lipoquinone, Menaquinone-2, Adopts a Folded Conformation in Solution and at a Model Membrane Interface. *J. Org. Chem.* **2018,** *83*, 275-288.
3. Koehn, J. T.; Beuning, C. N.; Peters, B. J.; Dellinger, S. K.; Van Cleave, C.; Crick, D. C.; Crans, D. C., Investigating Substrate Analogues for Mycobacterial MenJ: Truncated and Partially Saturated Menaquinones. *Biochemistry* **2019,** *58* (12), 1596-1615.
4. Crans, D. C.; Koehn, J. T.; Petry, S. M.; Glover, C. M.; Wijetunga, A.; Kaur, R.; Levina, A.; Lay, P. A., Hydrophobicity May Enhance Membrane Affinity and Anti-Cancer Effects of Schiff Base Vanadium(V) Catecholate Complexes. *Dalton Trans.* **2019,** *48*, 6383-6395.

Appendix II: Supporting Information for Chapter 2

General Methods & Information. All non-aqueous reactions were carried out under an atmosphere of argon in flame-dried glassware and were stirred on a magnetic stir plate using anhydrous solvent unless otherwise noted. All solvents were purchased from commercial sources and either used directly or after drying. Solvents were dried either by passing through an alumina drying column (Solv-Tek Inc.) under argon pressure (i.e. benzene, methanol, and trimethylamine), or by passing through a column packed with activated neutral alumina under argon pressure (i.e. *n*-pentane), or dried over activated 3 Å molecular sieves for 48-72 h under argon atmosphere (i.e. tertbutanol, 10 g sieves / 100 mL solvent). Reactions were monitored by thin layer chromatography (TLC) on Whatman Partisil® K6F TLC plates (silica gel 60 Å, 0.250 mm thickness) or Merck TLC Silica gel 60 F_{254} plates and visualized using a UV lamp (366 or 254 nm), Seebachs stain (and heated to visualize), or $KMnO_4$ stain (and heated to visualize) and preparative TLC was carried out using full size 20 X 20 cm Merck TLC Silica gel 60 F_{254} plates and visualized using a UV lamp. Products were purified by flash chromatography (SiliCycle®SiliaFlash® F60, 43-60 μm 60 Å). Yields refer to dried, chromatographically and spectroscopically (^{1}H NMR) homogenous materials unless otherwise noted. All chemicals were used without purification unless otherwise noted. ^{1}H and ^{13}C spectra were recorded on a 400 MHz Varian Model MR400 or a Bruker Model Avance Neo400 equipped with BBFO smart probe operating at 400 MHz or 101 MHz, respectively. Chemical shift values (δ) are reported in ppm and referenced against the internal solvent peaks in ^{1}H NMR ($CDCl_3$, δ at 7.26 ppm; benzene-d_6, δ at 7.16 ppm) and in ^{13}C NMR ($CDCl_3$, δ at 77.16 ppm; benzene-d_6, δ at 128.06 ppm). All NMR spectra were acquired either at 25 or 26 °C. Integral values were determined using standard, uncalibrated NMR experiments and should be viewed accordingly. ^{1}H NMR spectra are reported as follows: chemical shift (multiplicity, coupling constant, integration). The following abbreviations are used to indicate multiplicities: s, singlet; d, doublet; t, triplet; q, quartet; m, multiplet; br, broad. NMR spectra were processed using MestReNova version 10.0.1. or 12.0.2 Details of NMR experiments are provided in representative experimental sections and captions of figures.

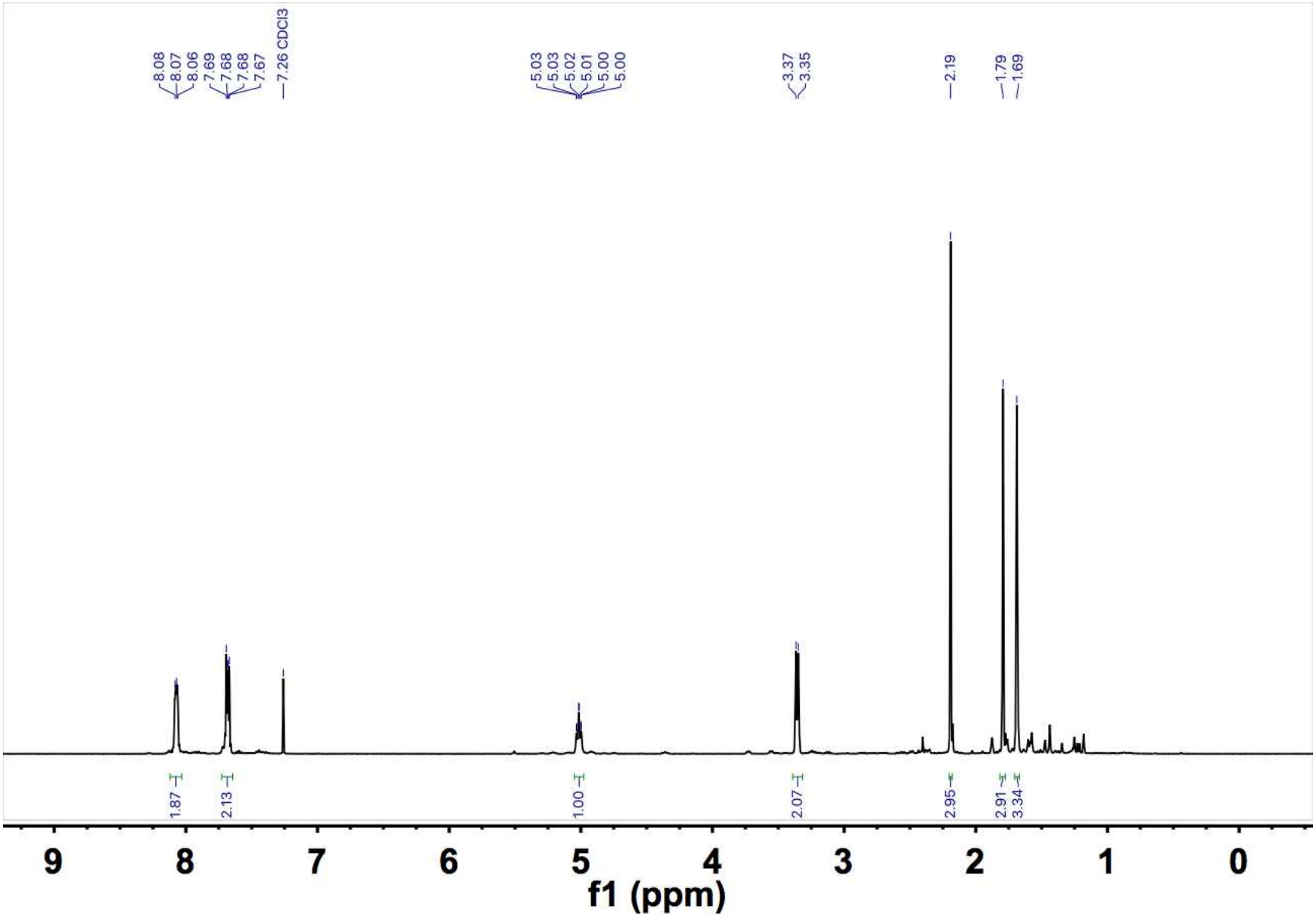

Figure A2.1: 1D ^{1}H NMR (400 MHz) spectrum of MK-1 (2.4) at 26 °C in $CDCl_3$.

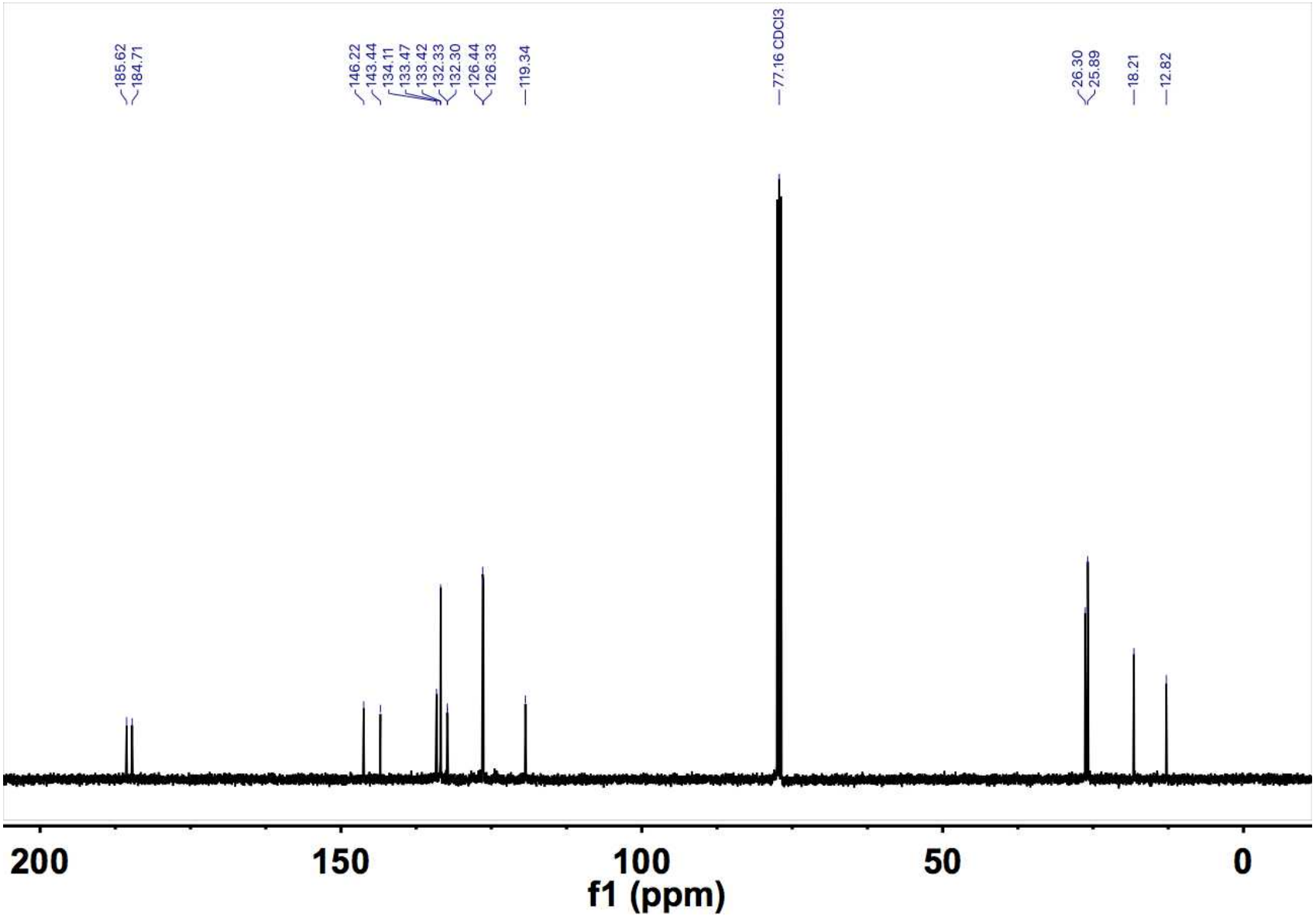

Figure A2.2: 1D ^{13}C NMR (101 MHz) spectrum of MK-1 (2.4) at 26 °C in $CDCl_3$.

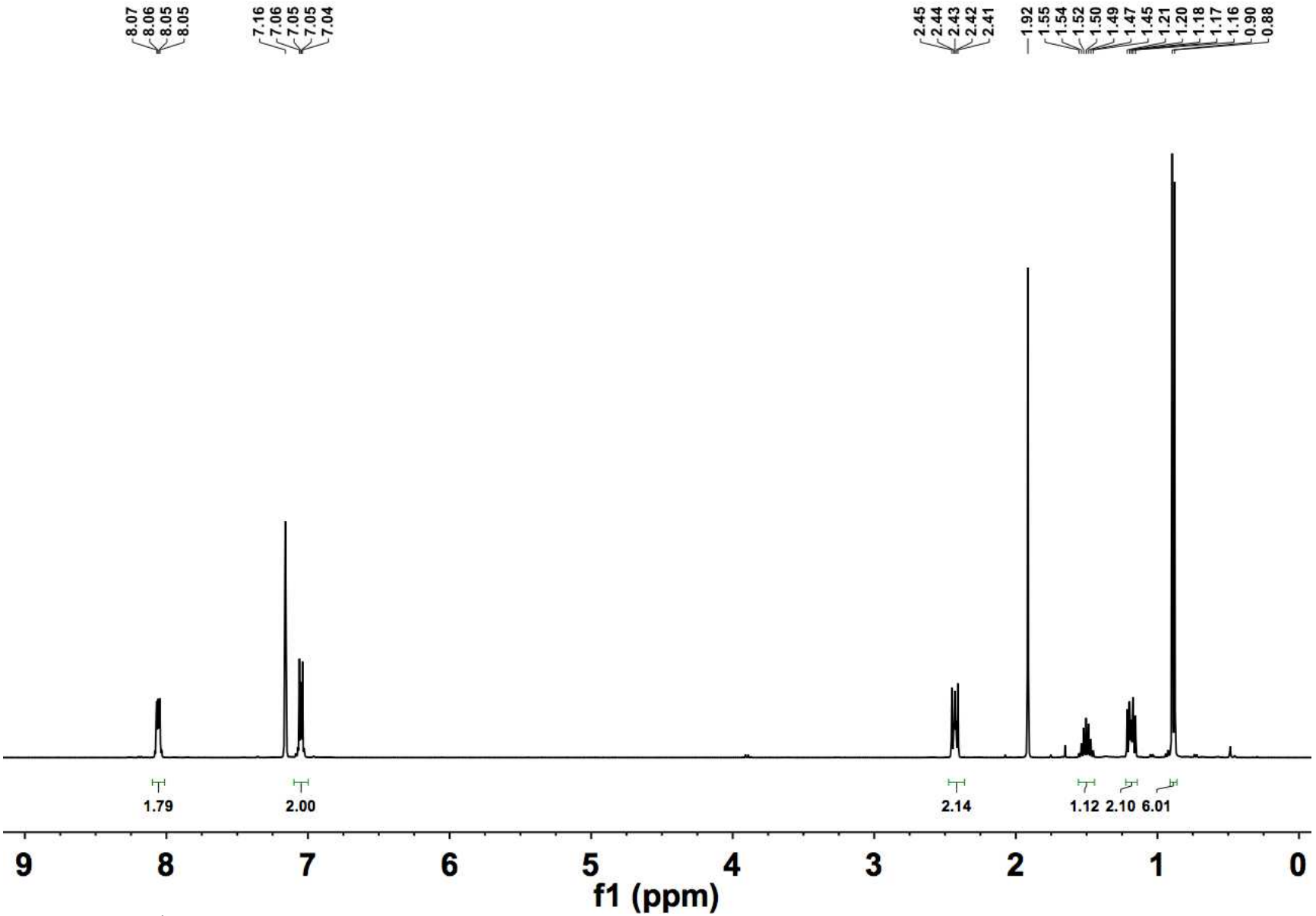

Figure A2.3: 1D ^{1}H NMR (400 MHz) spectrum of MK-1(H_2) (2.6) at 26 °C in d_6-benzene.

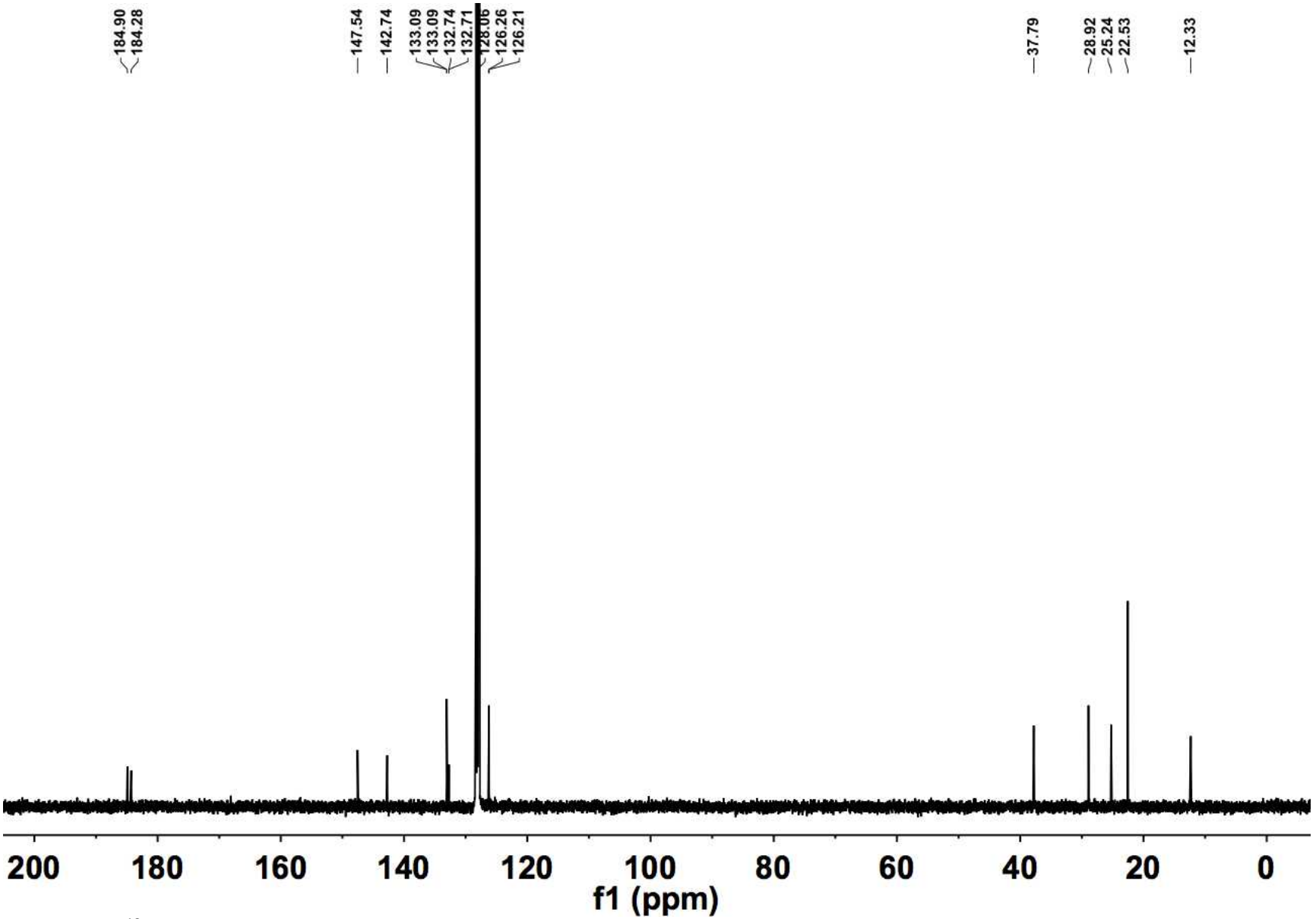

Figure A2.4: ^{13}C NMR (101 MHz) spectrum of MK-1(H_2) (2.6) at 26 °C in d_6-benzene.

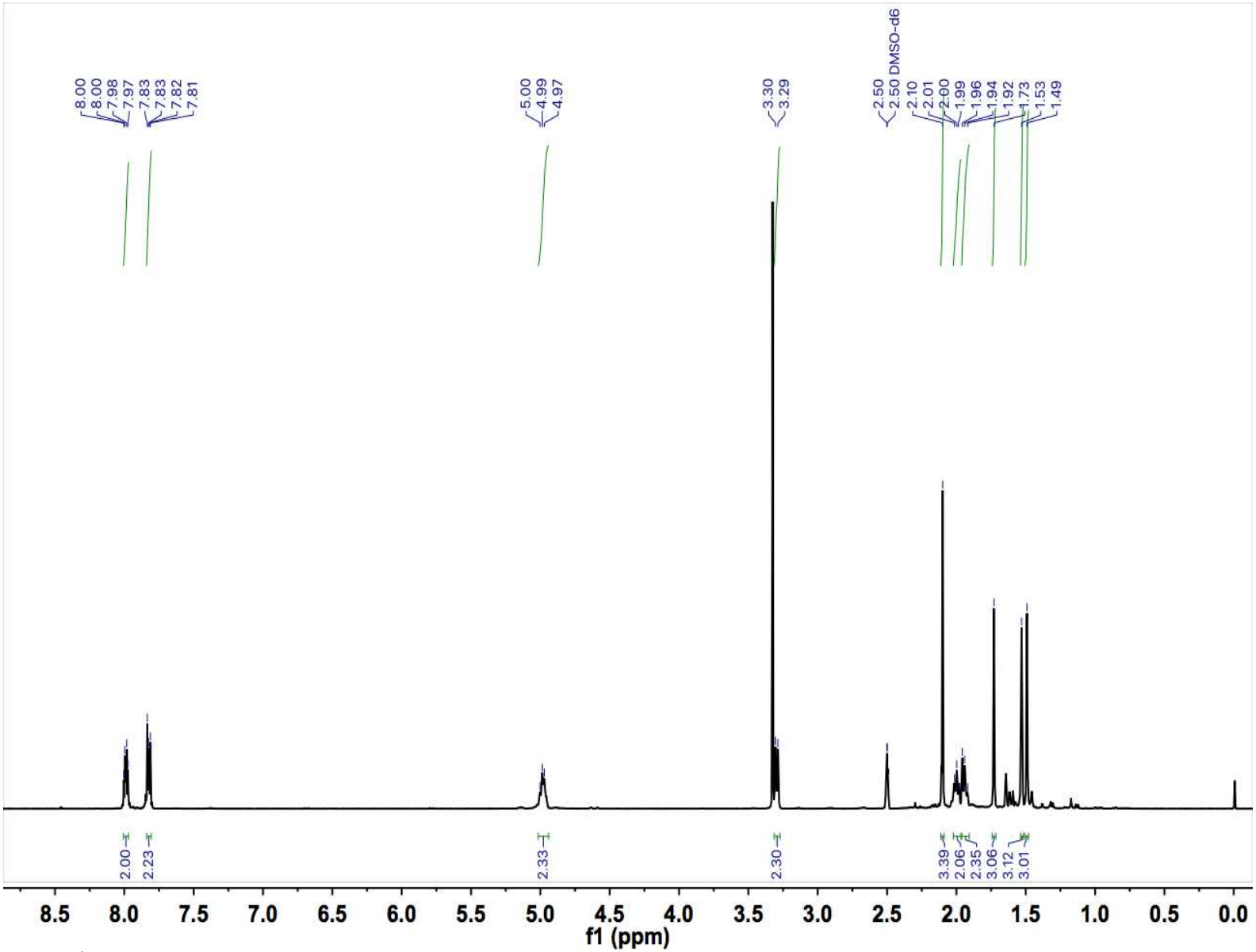

Figure A2.5. ^{1}H NMR (400 MHz) spectrum of MK-2 (2.8) at 26 °C in d_6-DMSO.

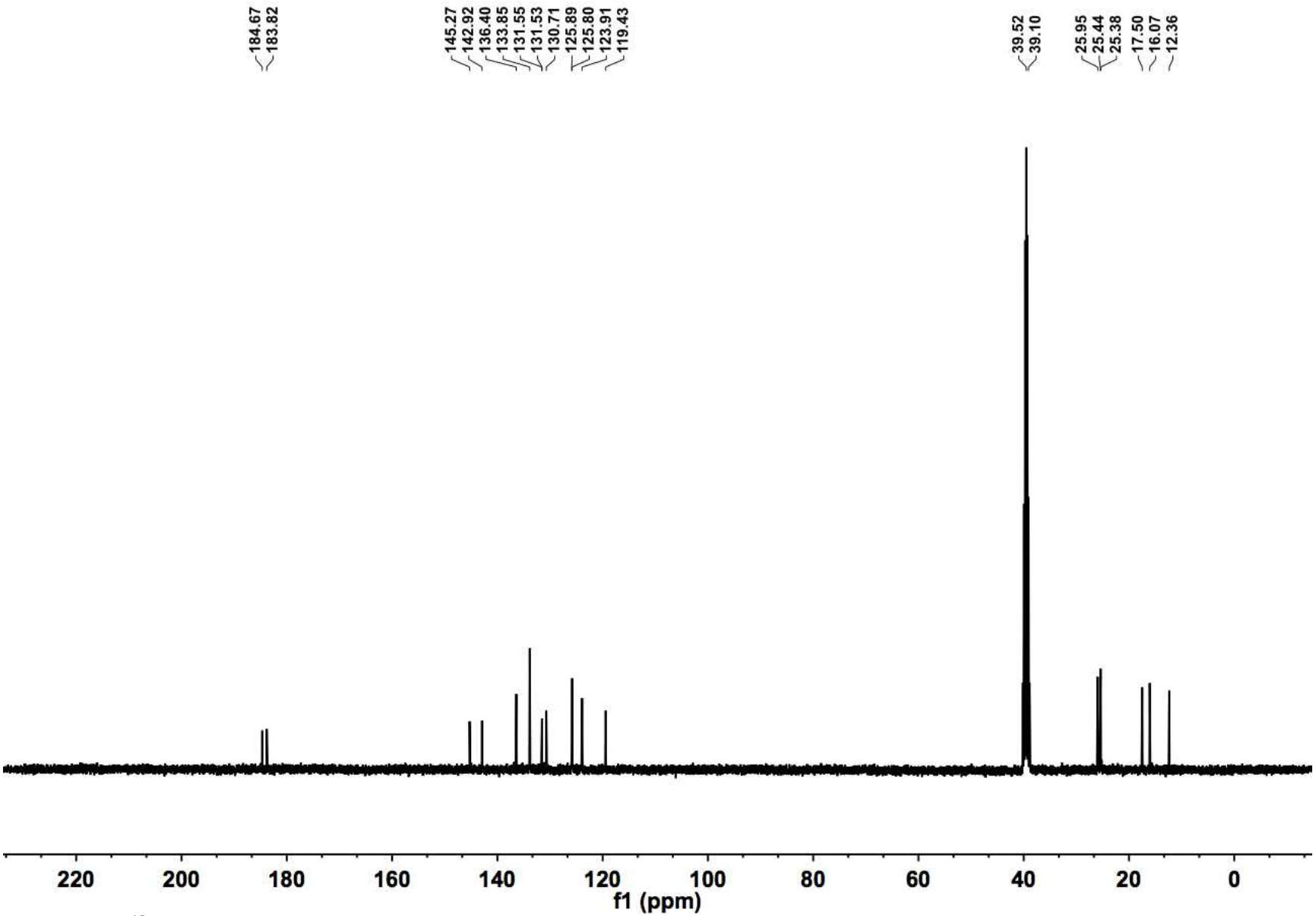

Figure A2.6. ^{13}C NMR (400 MHz) spectrum of MK-2 (2.8) at 26 °C in d_6-DMSO.

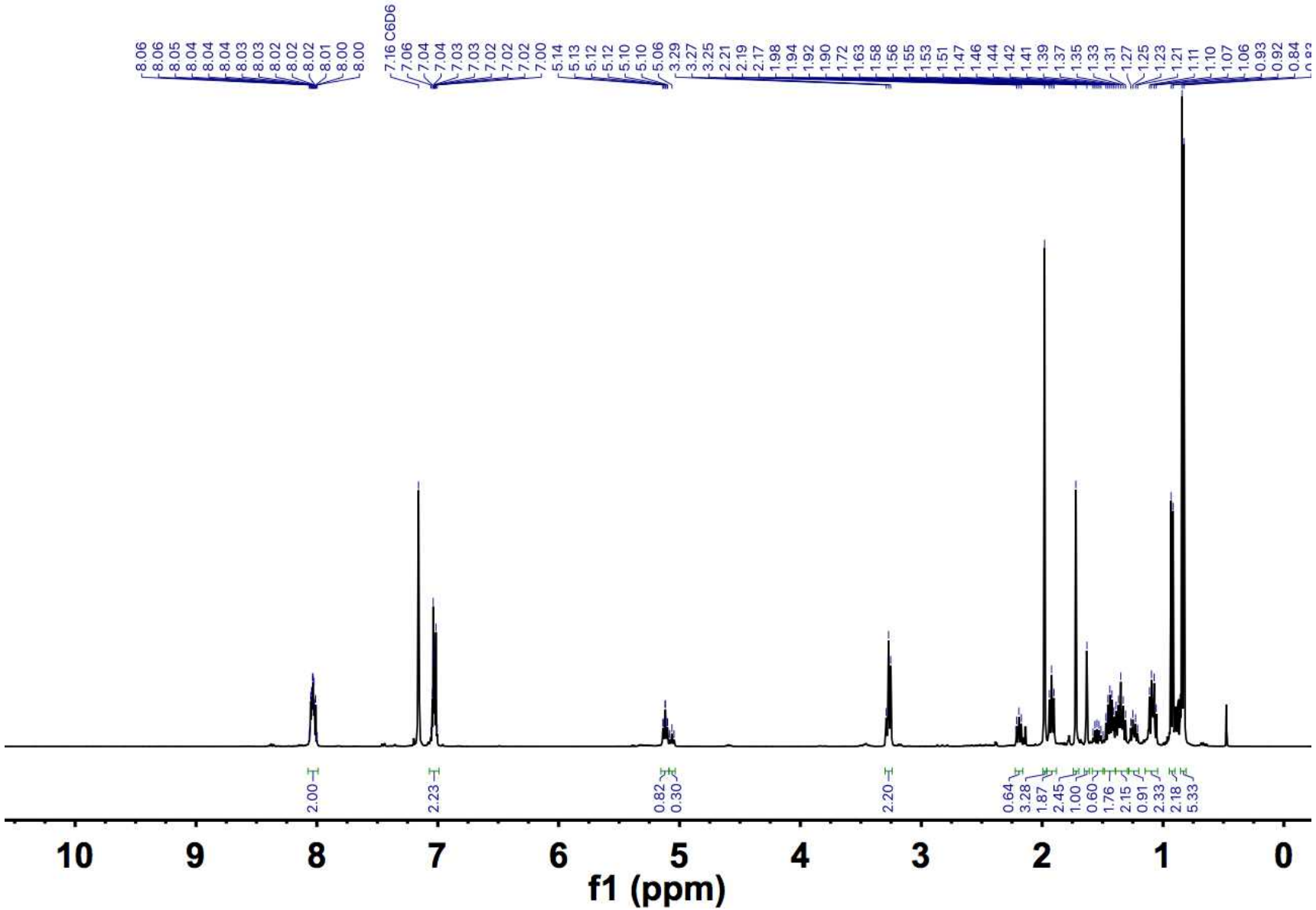

Figure A2.7: 1D ^{1}H NMR (400 MHz) spectrum of 30 mM cis/trans MK-2(II-H_2) (2.10) at 25 °C in C_6D_6.

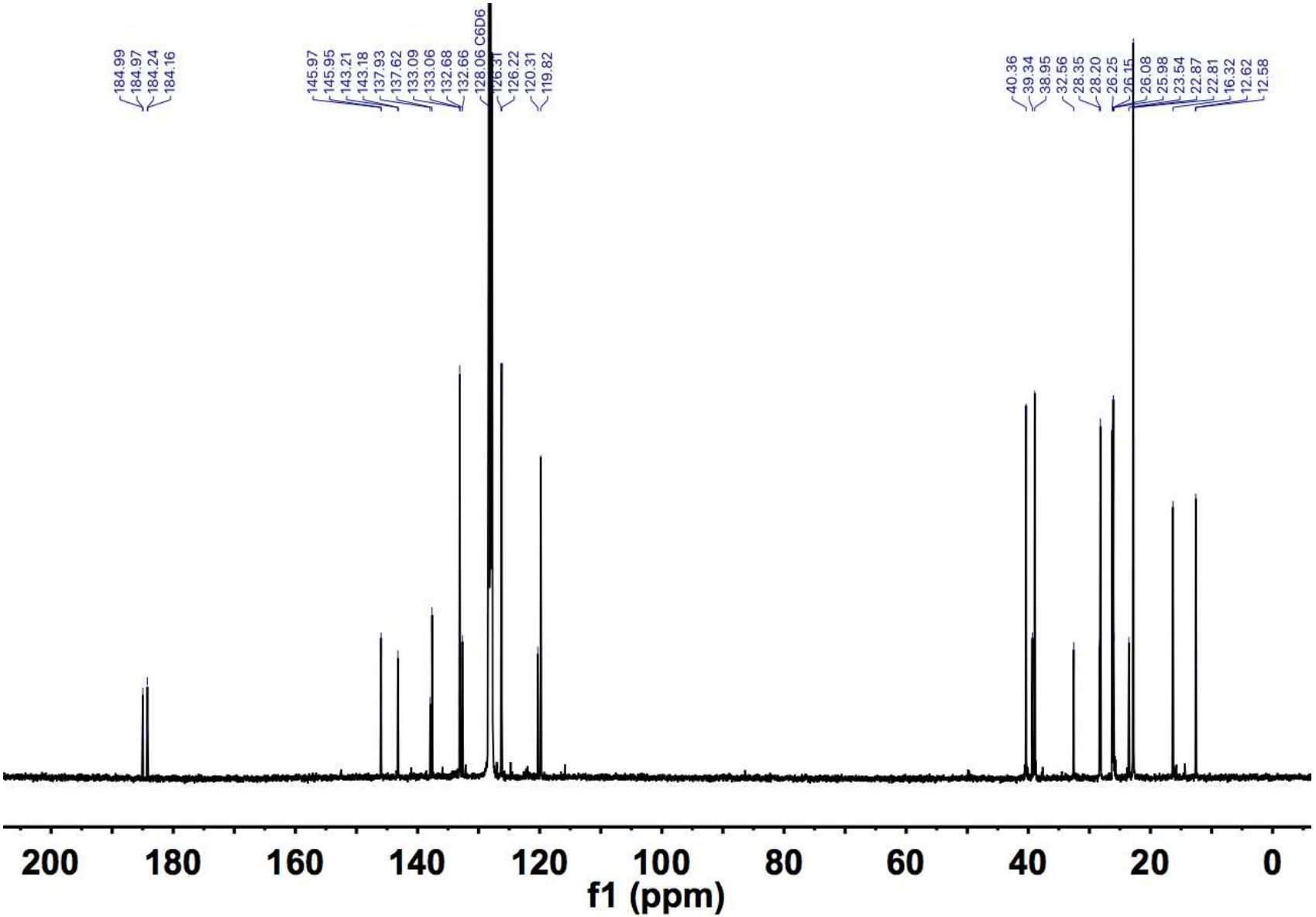

Figure A2.8: 1D ^{13}C NMR (101 MHz) spectrum of 64 mM cis/trans MK-2(II-H_2) (2.10) at 25 °C in C_6D_6 using 2000 scans.

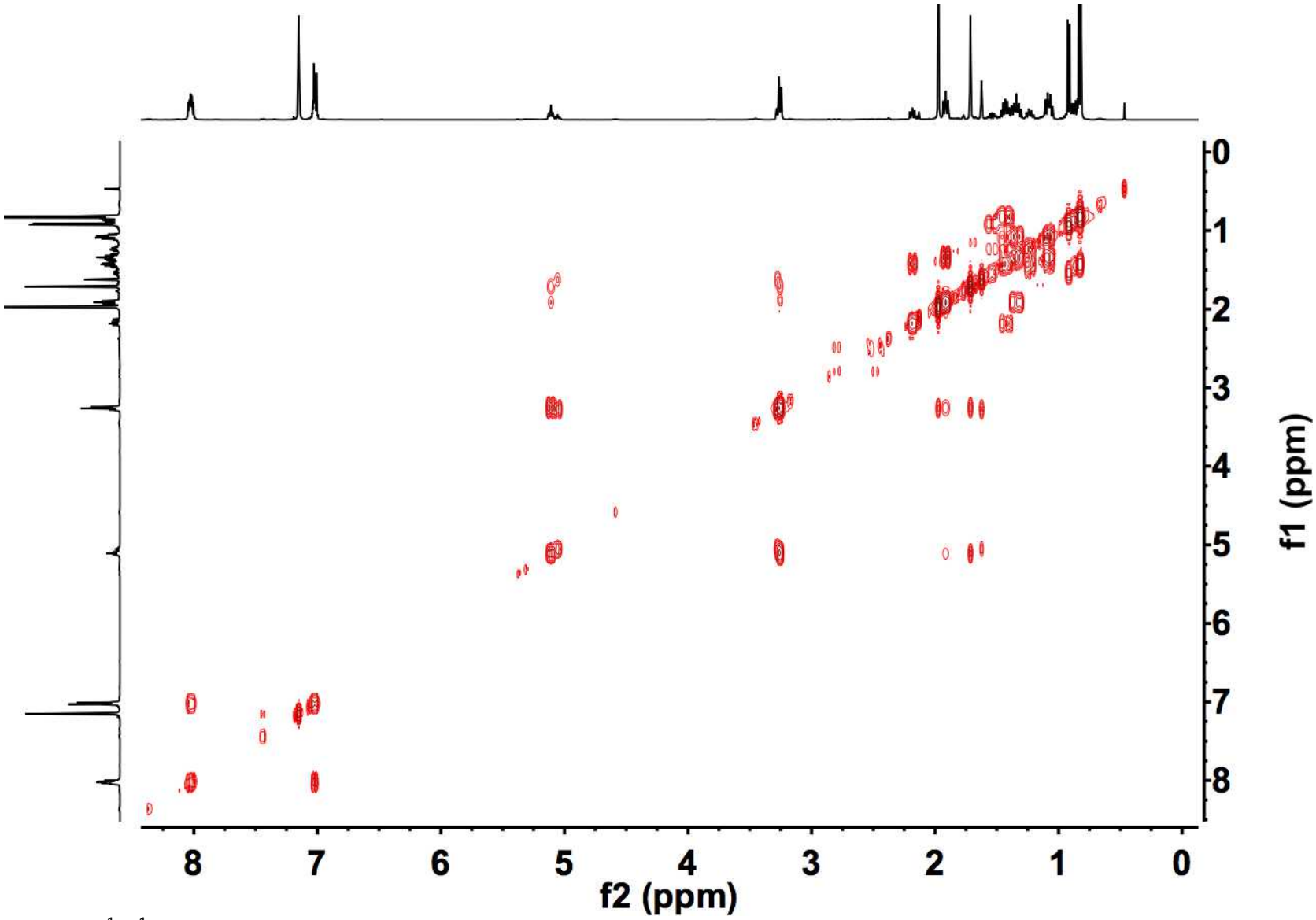

Figure A2.9: ^{1}H-^{1}H 2D gCOSY NMR (400 MHz) spectrum of 64 mM *cis*/*trans* MK-2(II-H_2) (2.10) in C_6D_6 at 25 °C. A standard gCOSY pulse sequence was used consisting of 128 t1 increments with 8 scans per t1 increment.

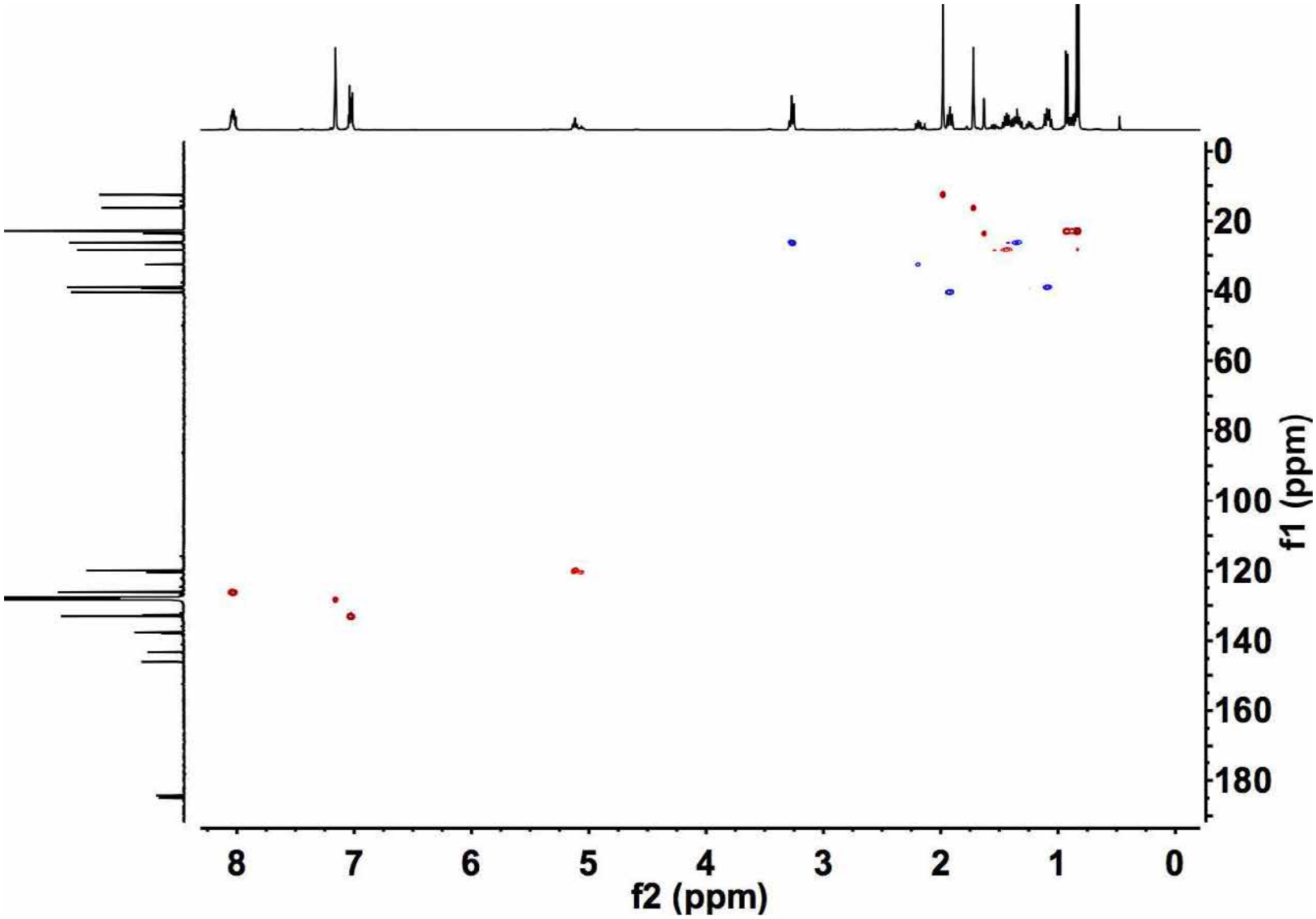

Figure A2.10: ^{1}H-^{13}C 2D HSQC NMR (400 MHz) spectrum of 64 mM cis/trans MK-2(II-H_2) (2.10) in C_6D_6 at 25 °C. A standard gHSQC pulse sequence was used consisting of 128 t1 increments with 8 scans per t1 increment. Red contour peaks correspond to methyl (-CH_3) and methine (>CH-) groups and blue contour peaks correspond to methylene (-CH_2 -) groups.

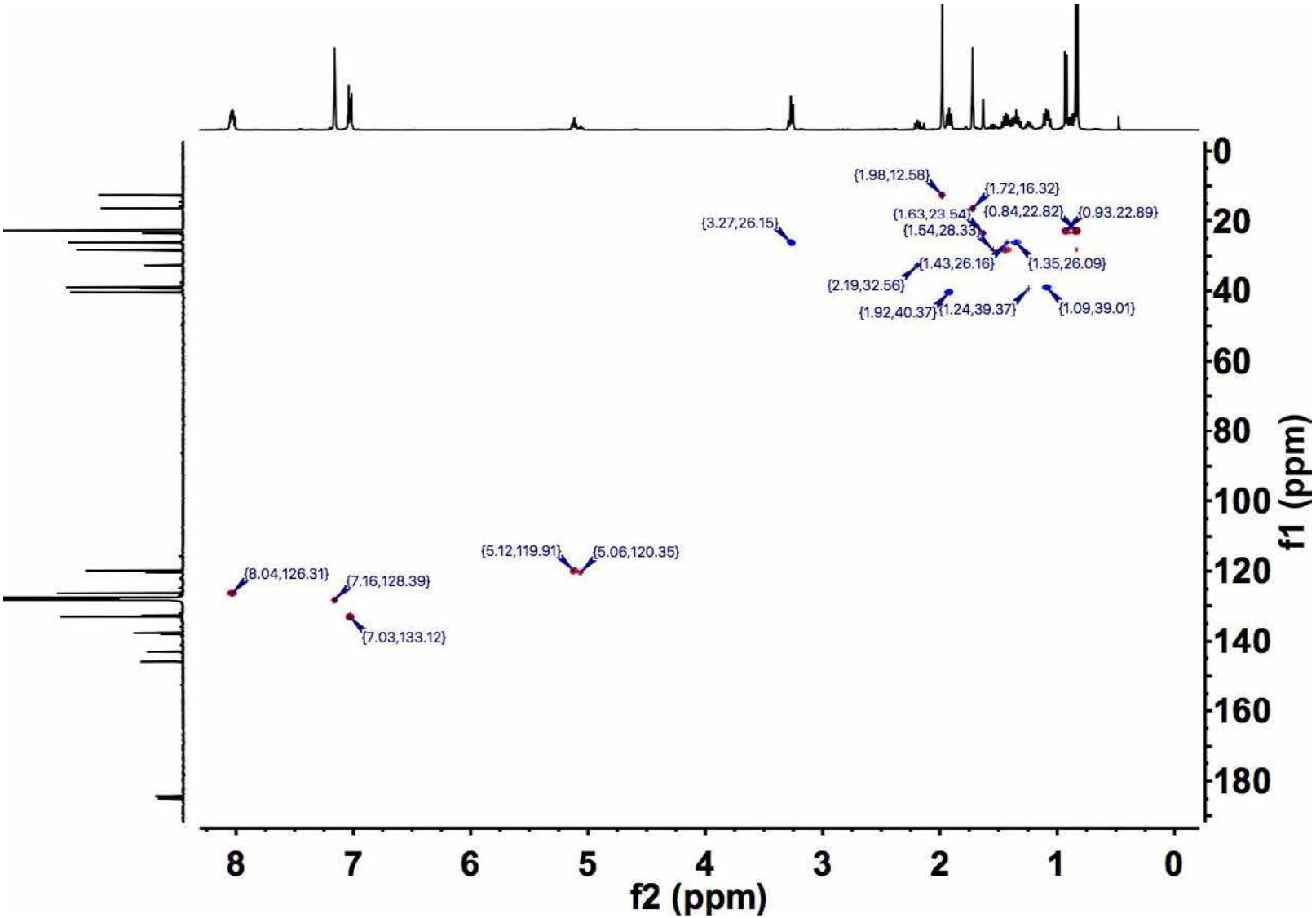

Figure A2.10.1: ^{1}H-^{13}C 2D HSQC NMR (400 MHz) spectrum of 64 mM cis/trans MK-2(II-H_2) (2.10) in C_6D_6 at 25 °C. A standard gHSQC pulse sequence was used consisting of 128 t1 increments with 8 scans per t1 increment. Red contour peaks correspond to methyl (-CH_3) and methine (>CH-) groups and blue contour peaks correspond to methylene (-CH_2 -) groups.

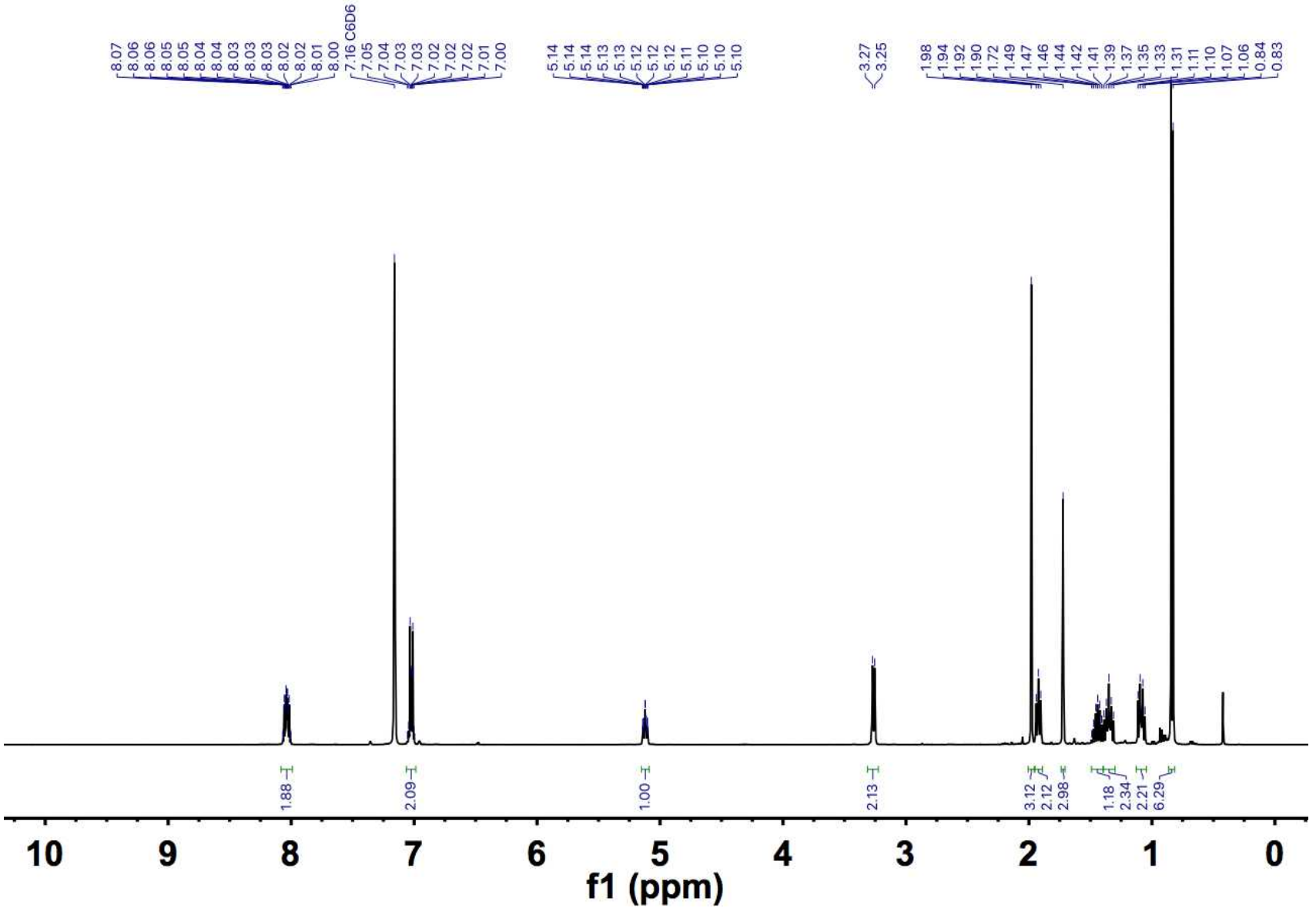

Figure A2.11: 1D ^{1}H NMR (400 MHz) spectrum of 30 mM *trans*-MK-2(II-H_2) (2.10) at 25 °C in C_6D_6.

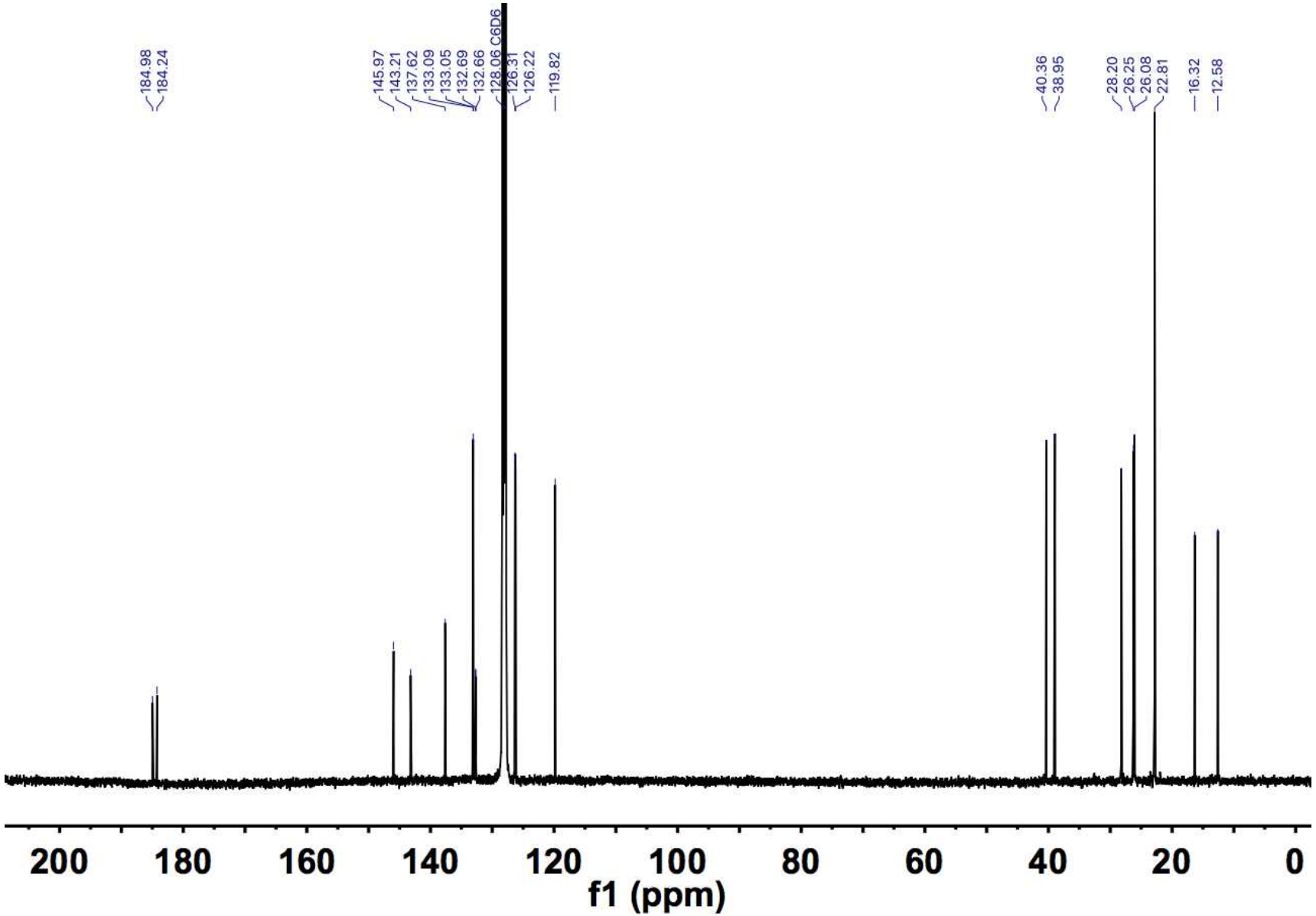

Figure A2.12: 1D ^{13}C NMR (101 MHz) spectrum of 30 mM trans-MK-2(II-H_2) (2.10) at 25 °C in C_6D_6.

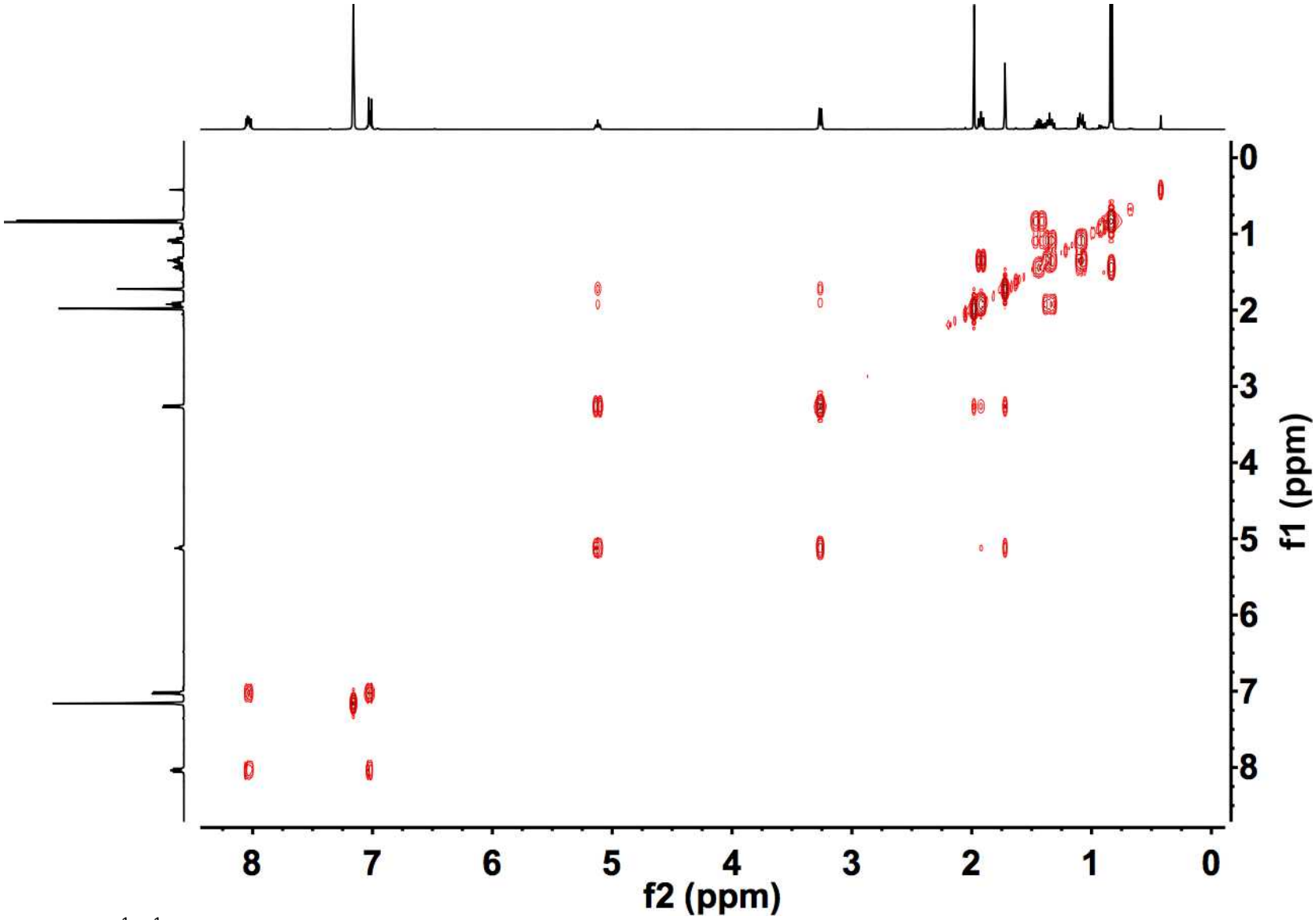

Figure A2.13: ^{1}H-^{1}H 2D gCOSY NMR (400 MHz) spectrum of 30 mM trans-MK-2(II-H_2) (2.10) in C_6D_6 at 25 °C. A standard gCOSY pulse sequence was used consisting of 128 t1 increments with 8 scans per t1 increment.

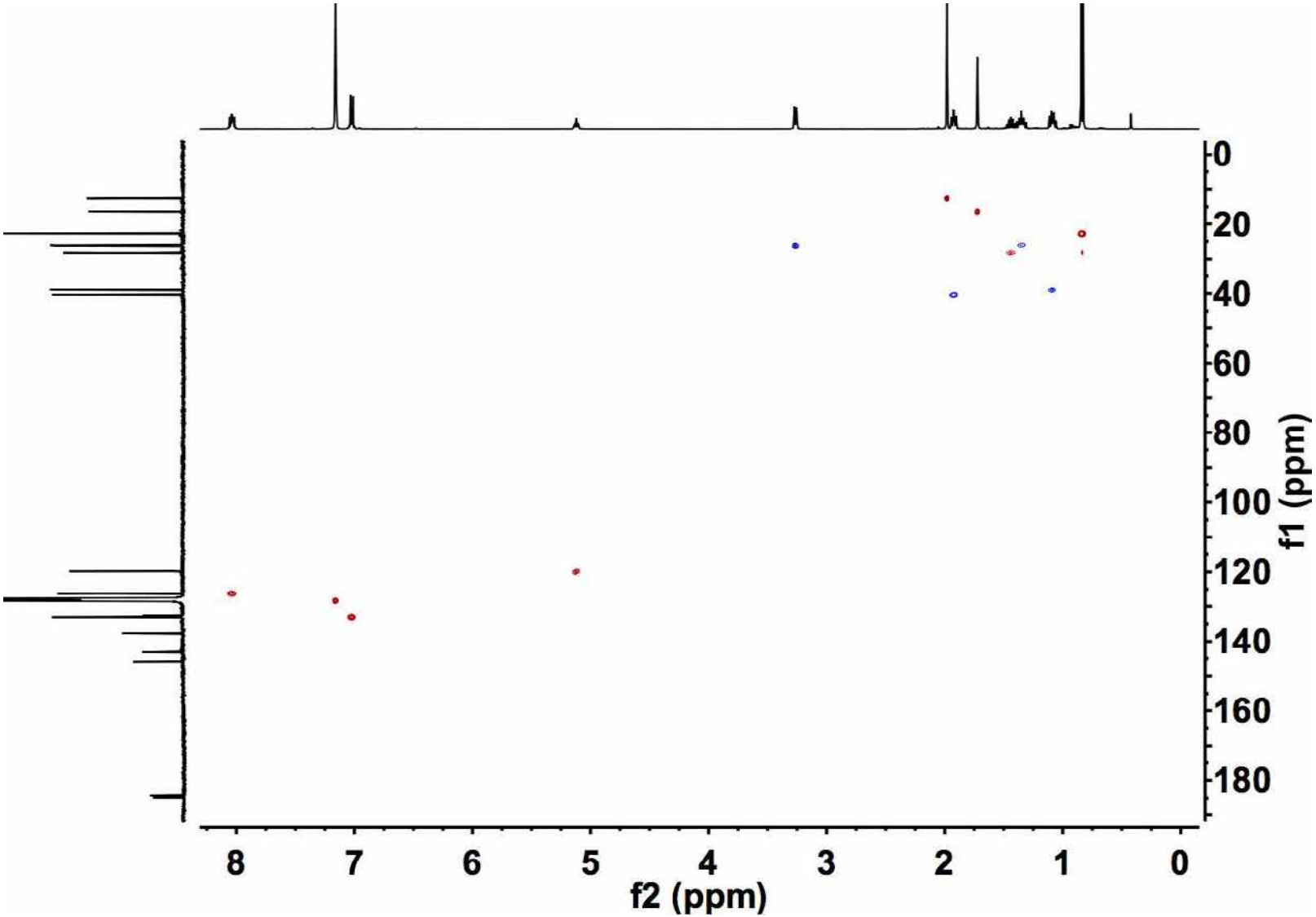

Figure A2.14: ^{1}H-^{13}C 2D HSQC NMR (400 MHz) spectrum of 30 mM trans-MK-2(II-H_2) (2.10) in C_6D_6 at 25 °C. A standard gHSQC pulse sequence was used consisting of 128 t1 increments with 8 scans per t1 increment. Red contour peaks correspond to methyl (-CH_3) and methine (>CH-) groups and blue contour peaks correspond to methylene (-CH_2 -) groups.

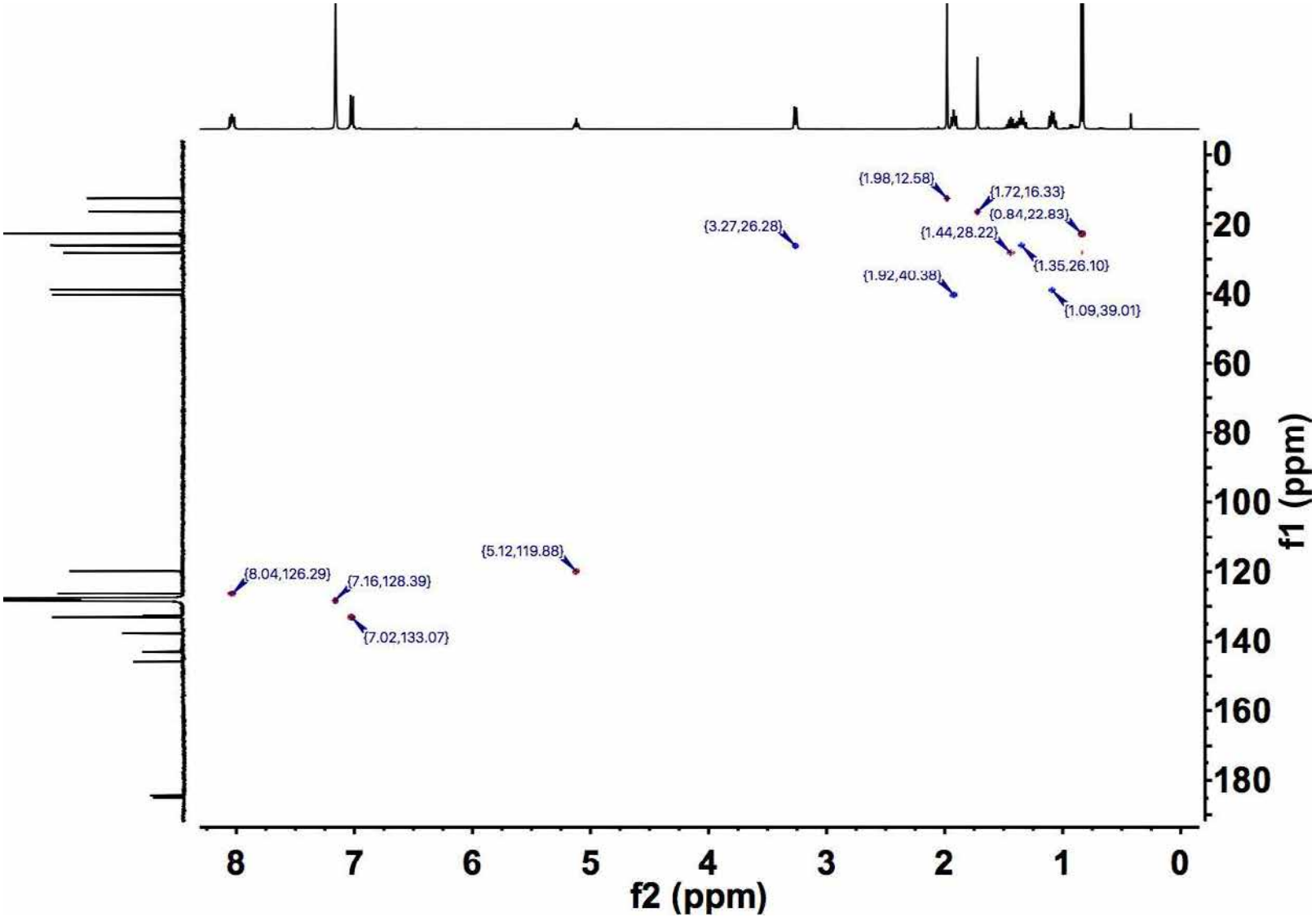

Figure A2.14.1: ^{1}H-^{13}C 2D HSQC NMR (400 MHz) spectrum of 30 mM trans-MK-2(II-H_2) (2.10) in C_6D_6 at 25 °C. A standard gHSQC pulse sequence was used consisting of 128 t1 increments with 8 scans per t1 increment. Red contour peaks correspond to methyl (-CH_3) and methine (>CH-) groups and blue contour peaks correspond to methylene (-CH_2 -) groups.

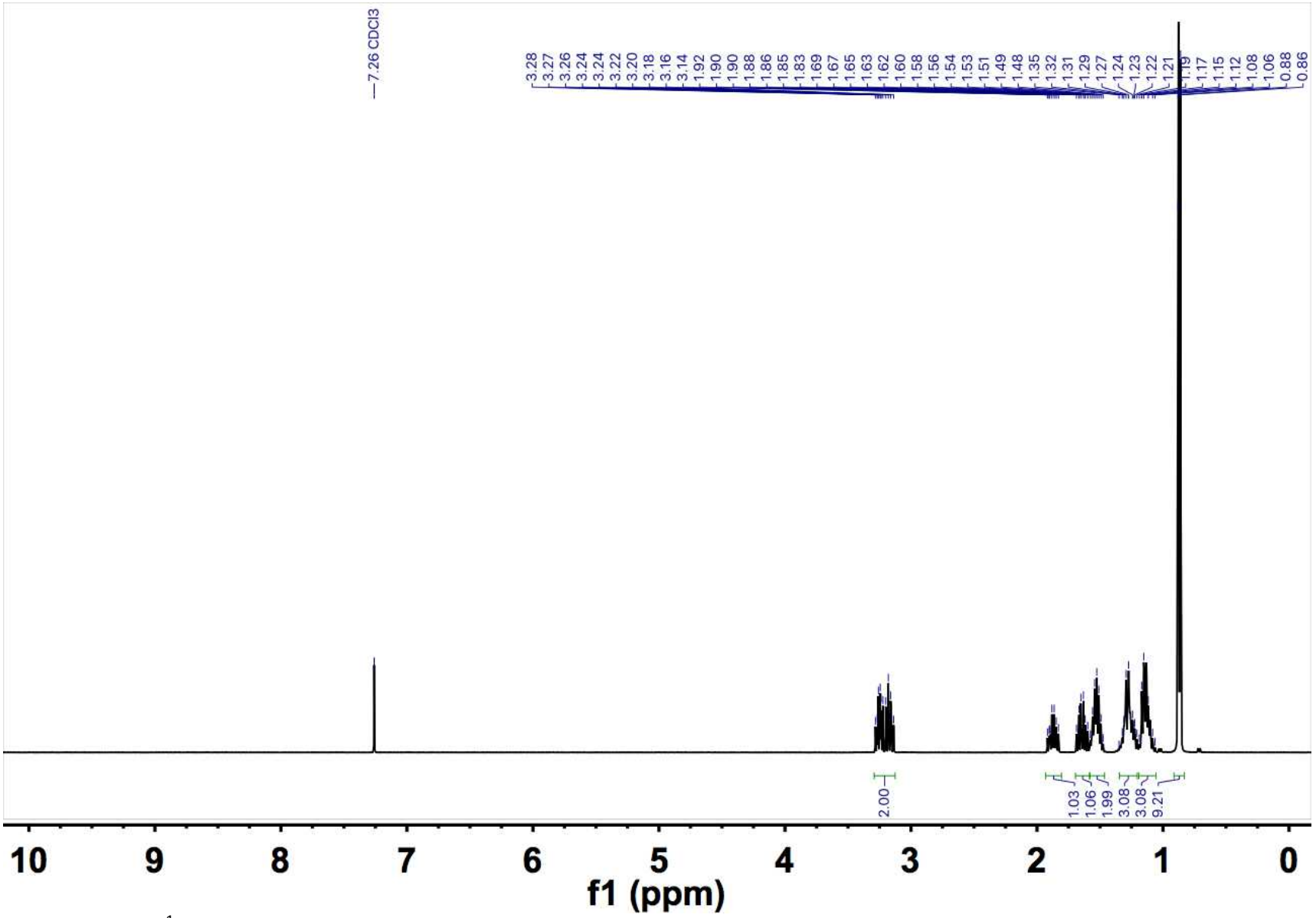

Figure A2.15: 1D ^{1}H NMR (400 MHz) spectrum of 1-Iodo-3,7-dimethyloctane (2.12) at 26 °C in $CDCl_3$.

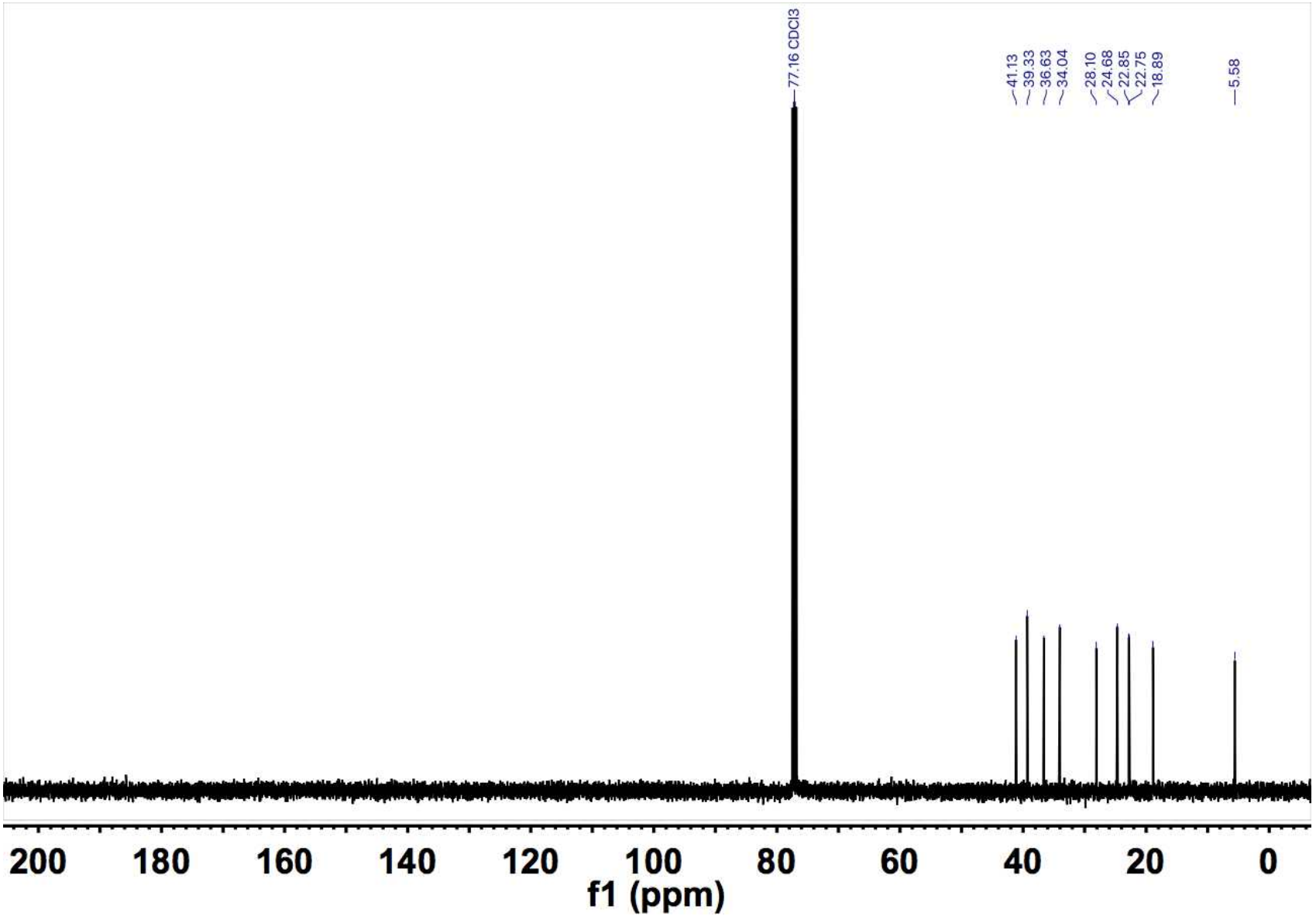

Figure A2.16: 1D ^{13}C NMR (101 MHz) spectrum of 1-Iodo-3,7-dimethyloctane (2.12) at 26 °C in $CDCl_3$.

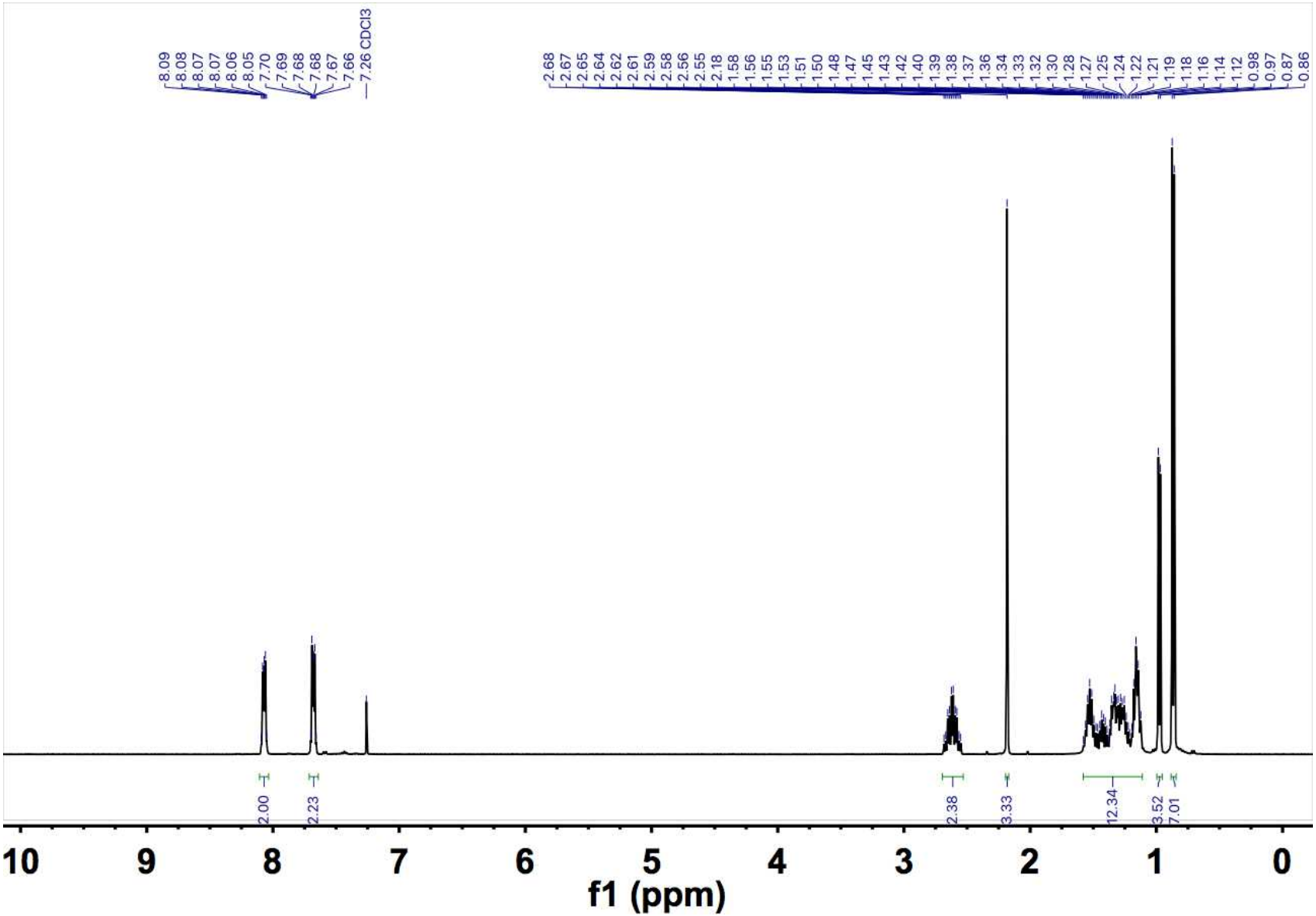

Figure A2.17: 1D ^{1}H NMR (400 MHz) spectrum of 100 mM MK-2(I,II-H_4) (2.13) at 26 °C in $CDCl_3$.

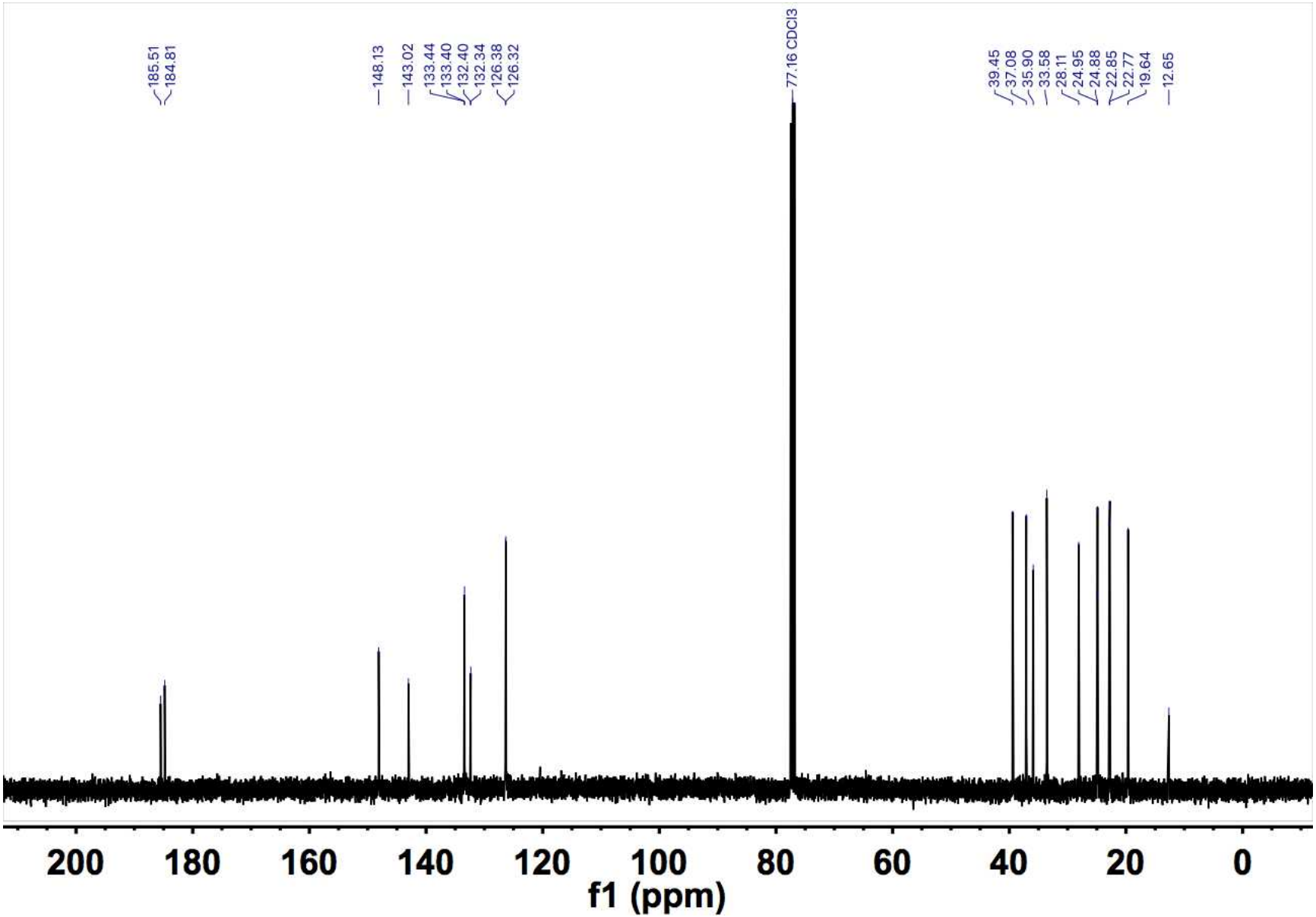

Figure A2.18: 1D ^{13}C NMR (101 MHz) spectrum of 100 mM MK-2(I,II-H_4) (2.13) at 26 °C in $CDCl_3$.

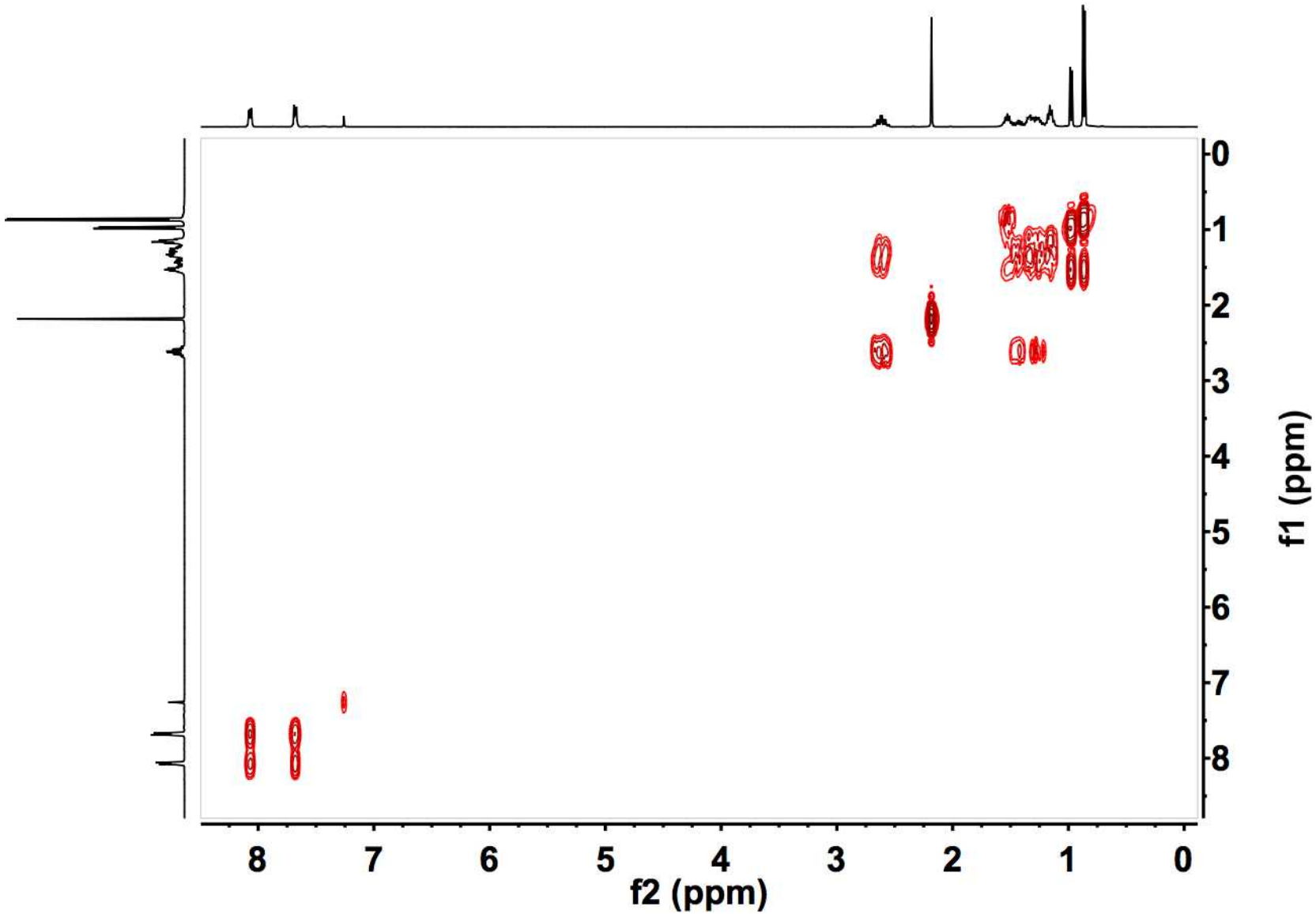

Figure A2.19: ^{1}H-^{1}H 2D gCOSY NMR (400 MHz) spectrum of 100 mM MK-2(I,II-H_4) (2.13) in $CDCl_3$ at 26 °C. A standard gCOSY pulse sequence was used consisting of 128 t1 increments with 8 scans per t1 increment.

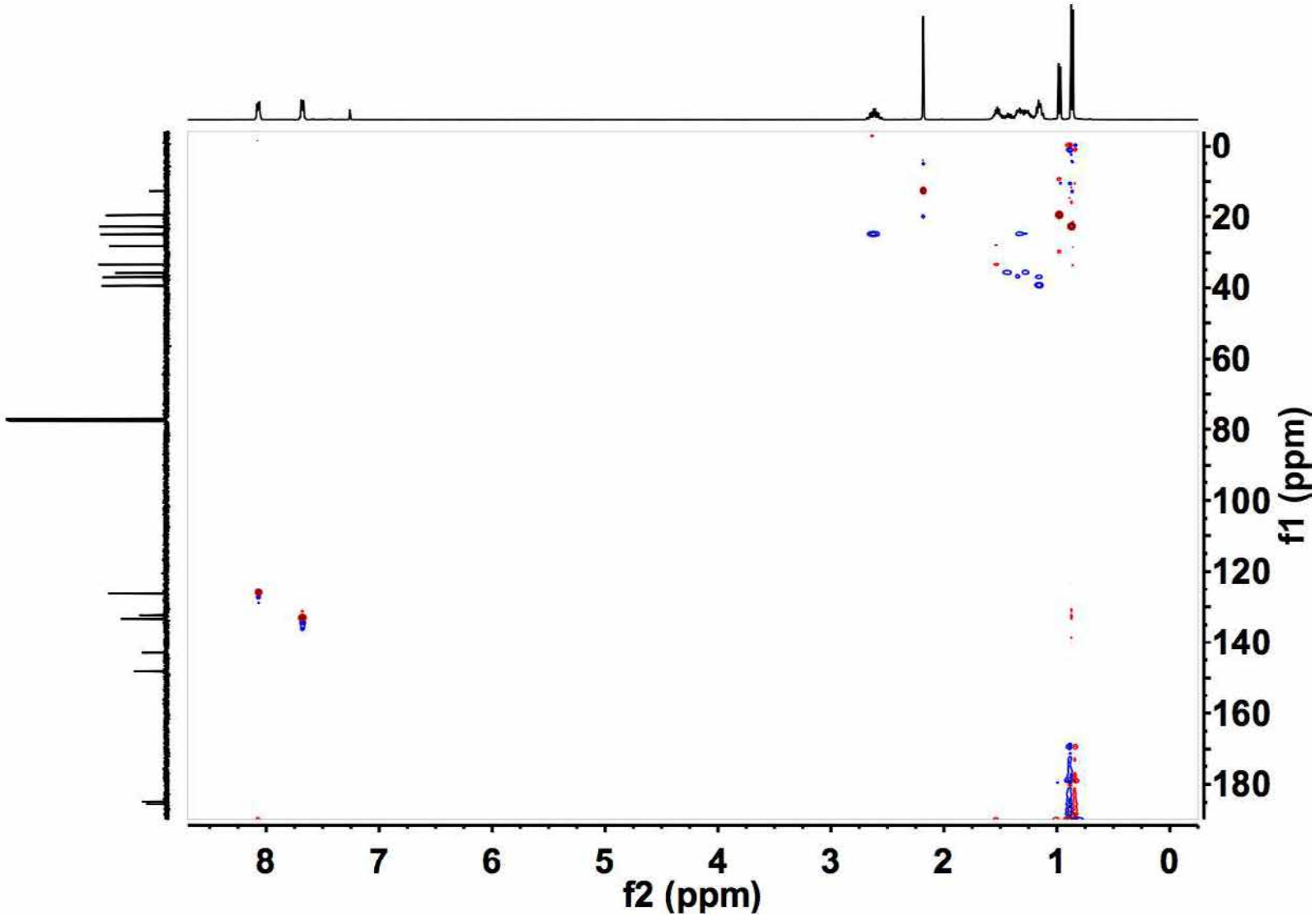

Figure A2.20: ^{1}H-^{13}C 2D HSQC NMR (400 MHz) spectrum of 100 mM MK-2(I,II-H_4) (2.13) in $CDCl_3$ at 26 °C. A standard HSQCAD pulse sequence was used consisting of 128 t1 increments with 4 scans per t1 increment. Red contour peaks correspond to methyl (-CH_3) and methine (>CH-) groups and blue contour peaks correspond to methylene (-CH_2 -) groups.

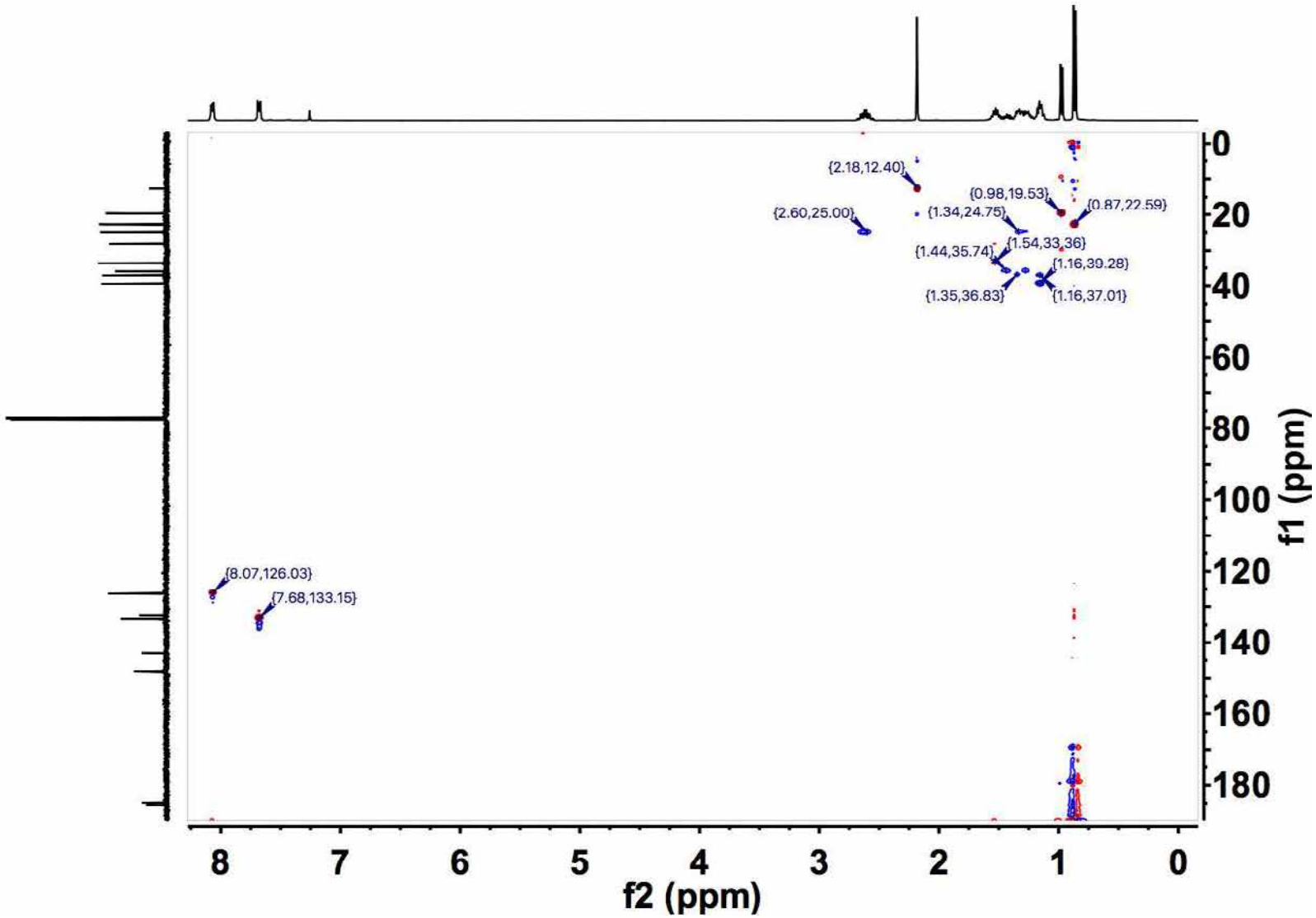

Figure A2.20.1: ^{1}H-^{13}C 2D HSQC NMR (400 MHz) spectrum of 100 mM MK-2(I,II-H_4) (2.13) in $CDCl_3$ at 26 °C. A standard HSQCAD pulse sequence was used consisting of 128 t1 increments with 4 scans per t1 increment. Red contour peaks correspond to methyl (-CH_3) and methine (>CH-) groups and blue contour peaks correspond to methylene (-CH_2 -) groups.

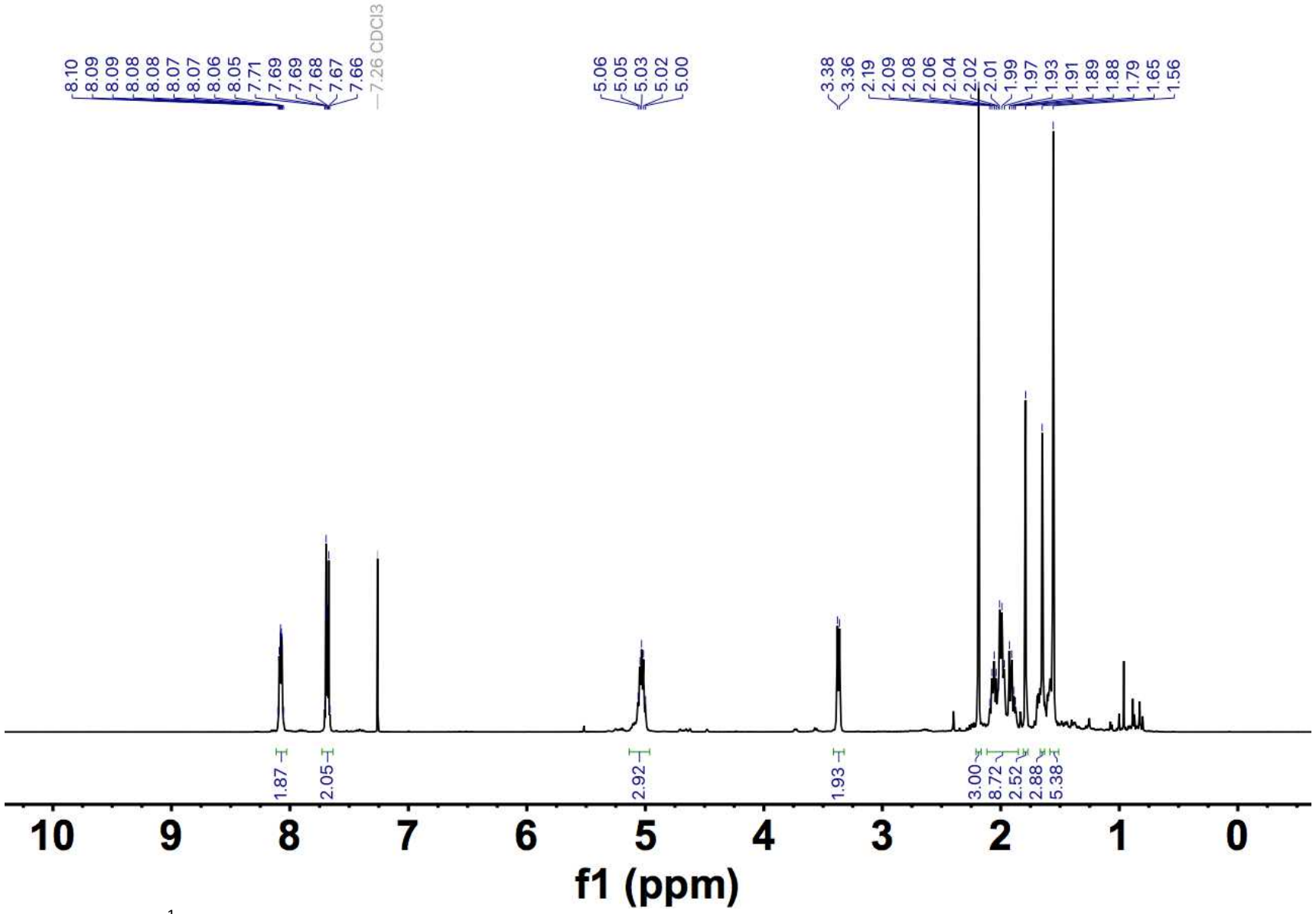

Figure A2.21: 1D ^{1}H NMR (400 MHz) spectrum of 55 mM MK-3 (2.15) at 25 °C in $CDCl_3$.

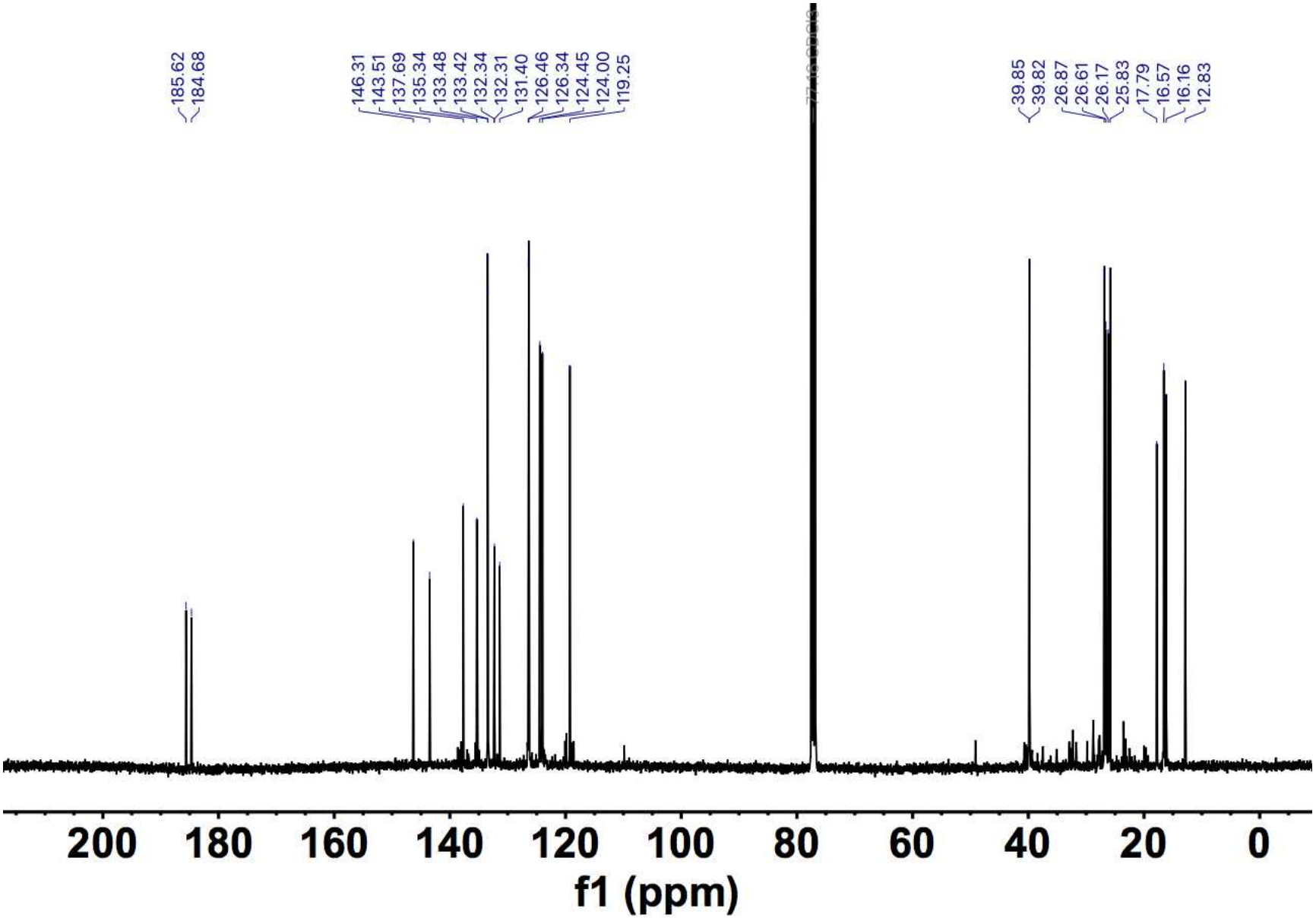

Figure A2.22: 1D ^{13}C NMR (101 MHz) spectrum of 55 mM MK-3 (2.15) at 25 °C in $CDCl_3$.

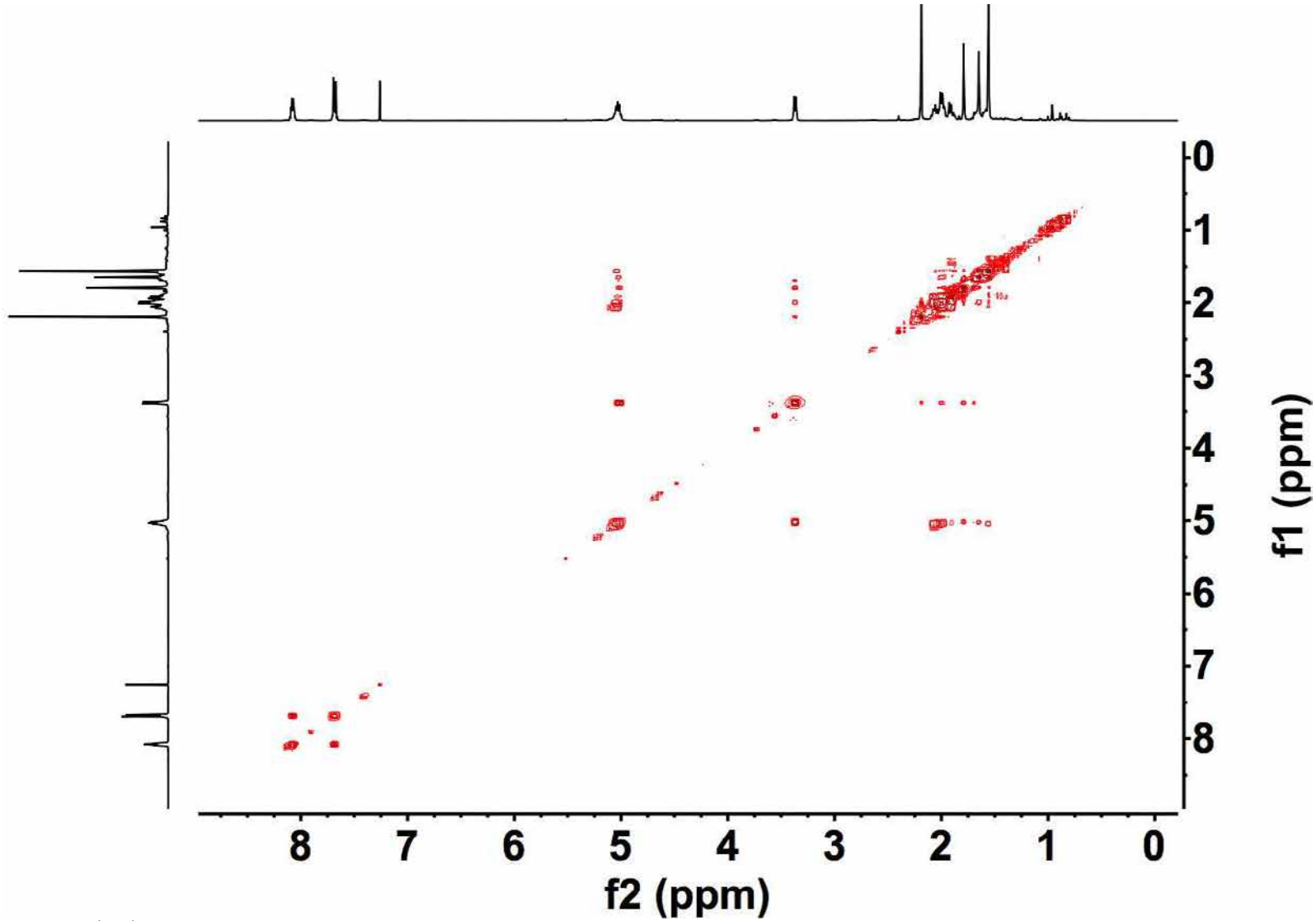

Figure A2.23: ^{1}H-^{1}H 2D gCOSY NMR (400 MHz) spectrum of 55 mM MK-3 (2.15) in $CDCl_3$ at 25 °C. A standard gCOSY pulse sequence was used consisting of 128 t1 increments with 8 scans per t1 increment.

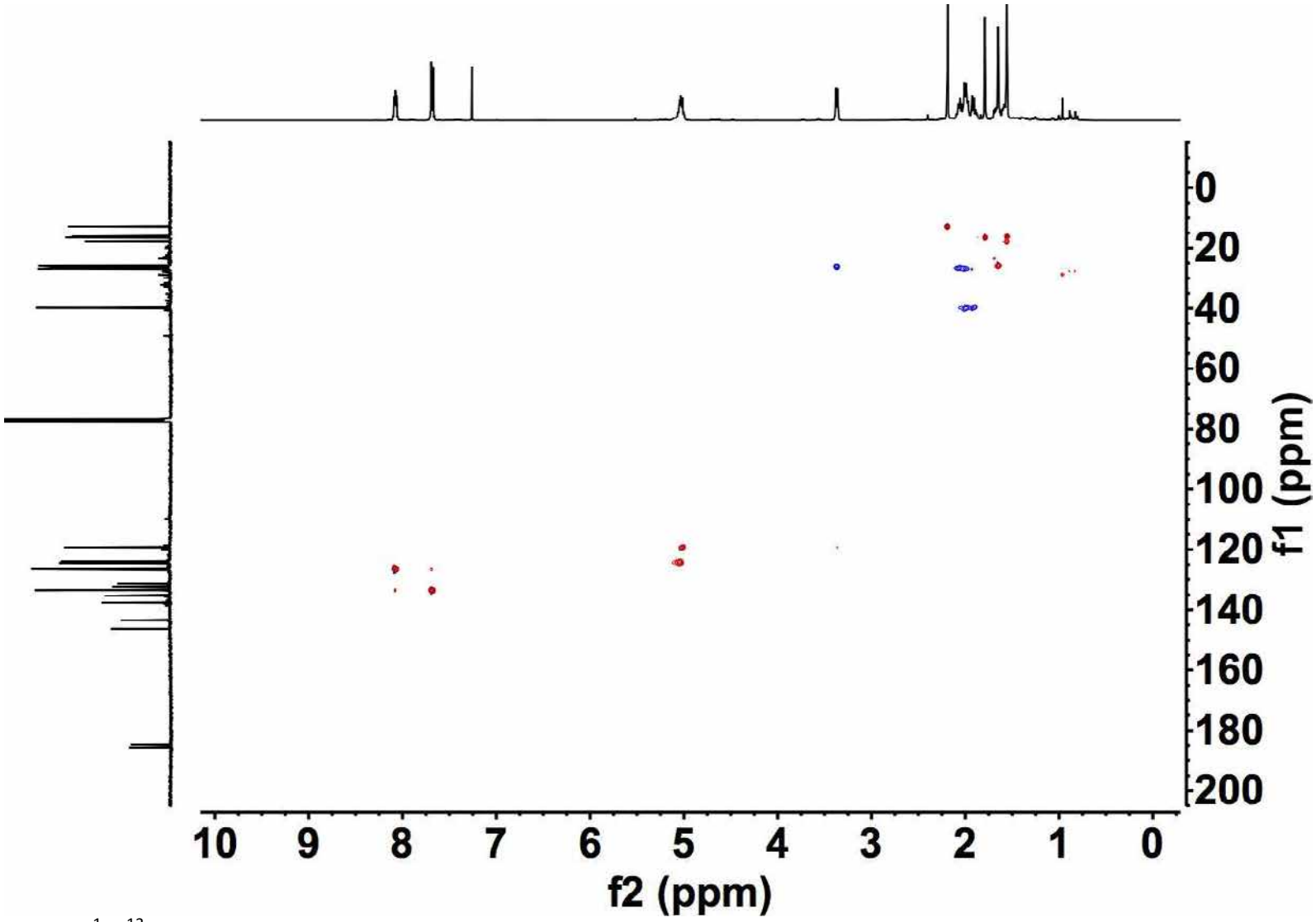

Figure A2.24: ^{1}H-^{13}C 2D HSQC NMR (400 MHz) spectrum of 55 mM MK-3 (2.15) in $CDCl_3$ at 25 °C. A standard HSQCAD pulse sequence was used consisting of 128 t1 increments with 8 scans per t1 increment. Red contour peaks correspond to methyl (-CH_3) and methine (>CH-) groups and blue contour peaks correspond to methylene (-CH_2 -) groups.

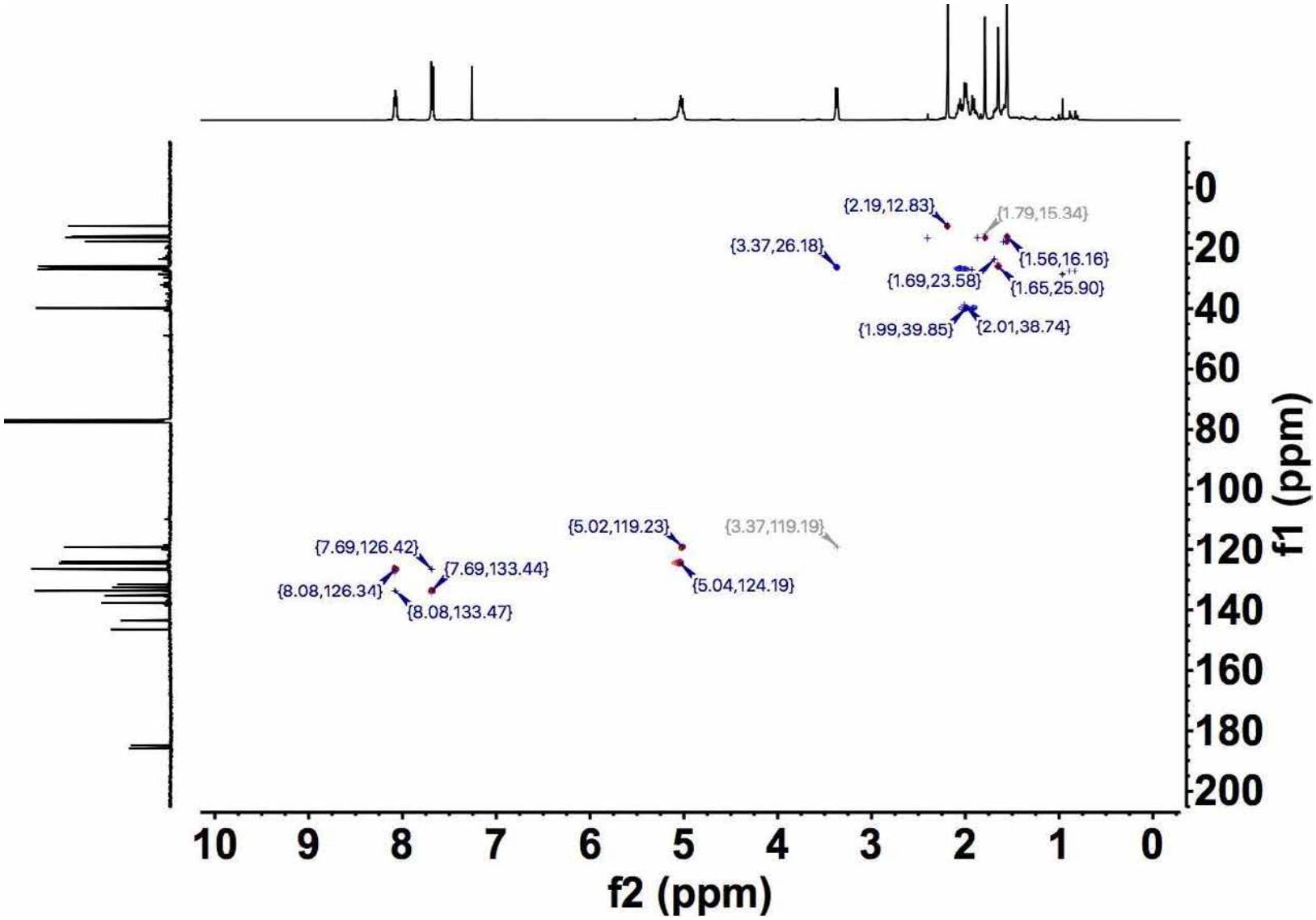

Figure A2.24.1: ^{1}H-^{13}C 2D HSQC NMR (400 MHz) spectrum of 55 mM MK-3 (2.15) in $CDCl_3$ at 25 °C. A standard HSQCAD pulse sequence was used consisting of 128 t1 increments with 8 scans per t1 increment. Red contour peaks correspond to methyl ($-CH_3$) and methine (>CH-) groups and blue contour peaks correspond to methylene ($-CH_2-$) groups.

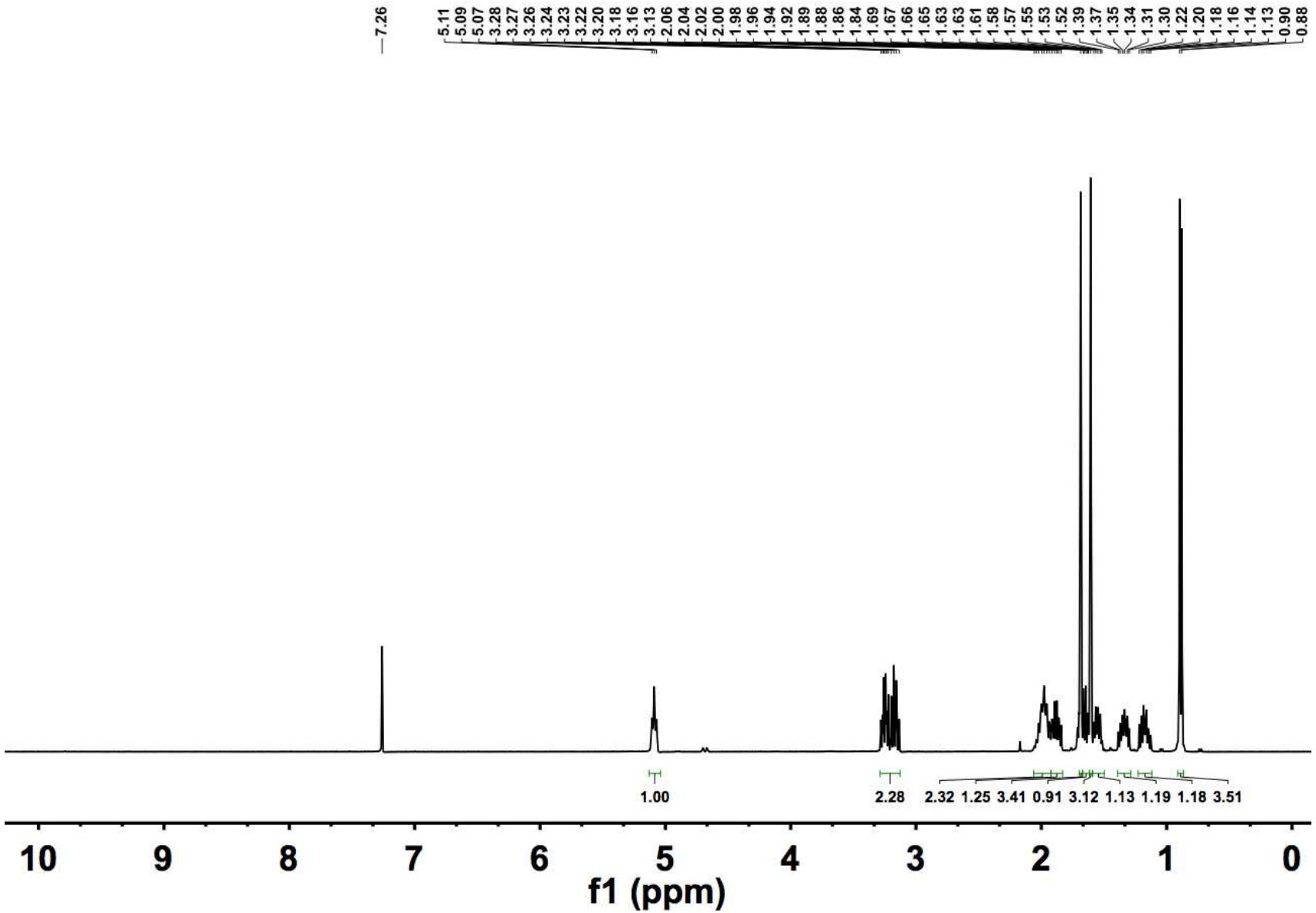

Figure A2.25: 1D ^{1}H NMR (400 MHz) spectrum of 8-iodo-2,6-dimethyloct-2-ene (2.17) at 26 °C in $CDCl_3$.

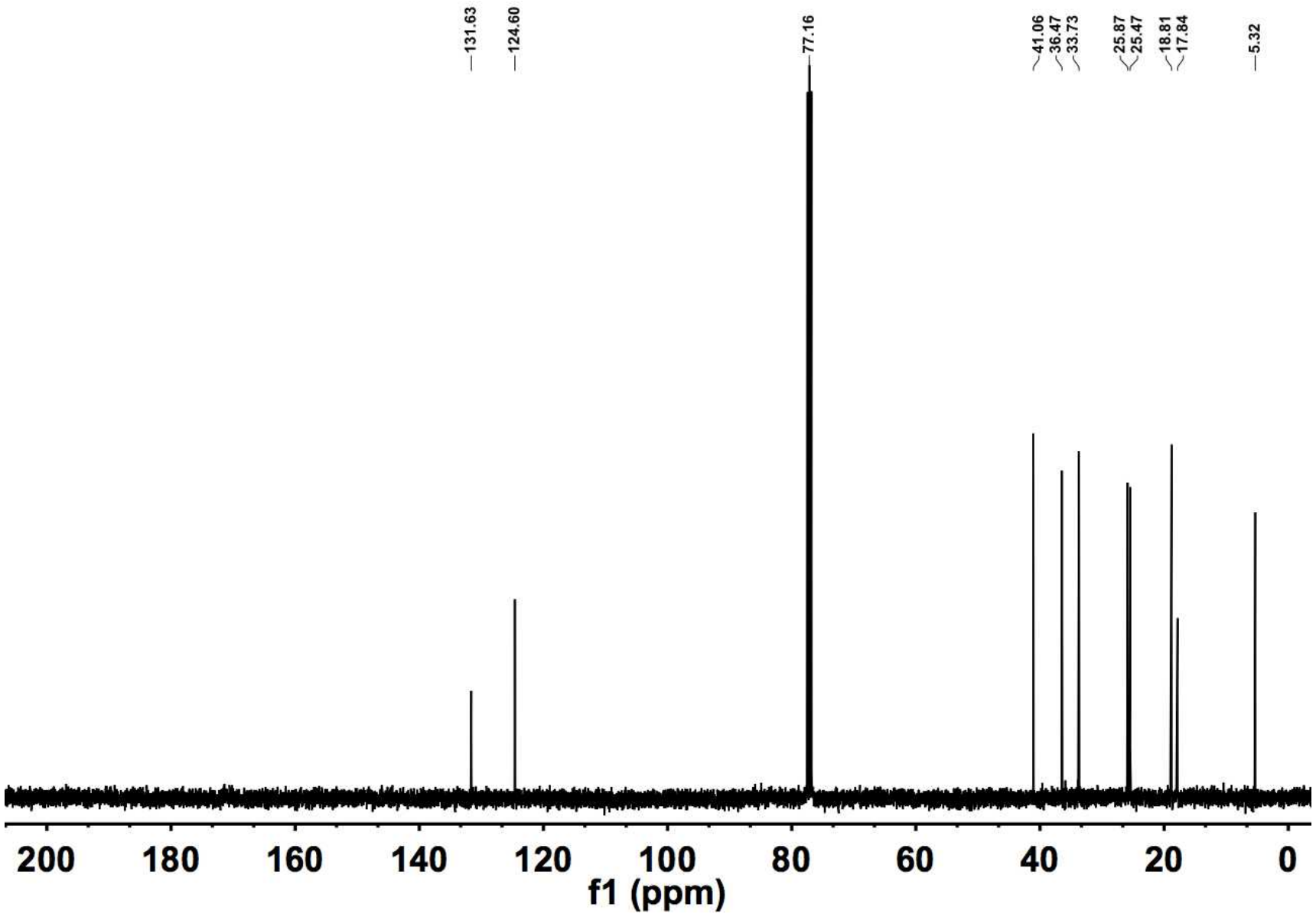

Figure A2.26: 1D ^{13}C NMR (101 MHz) spectrum of 8-iodo-2,6-dimethyloct-2-ene (2.17) at 26 °C in $CDCl_3$.

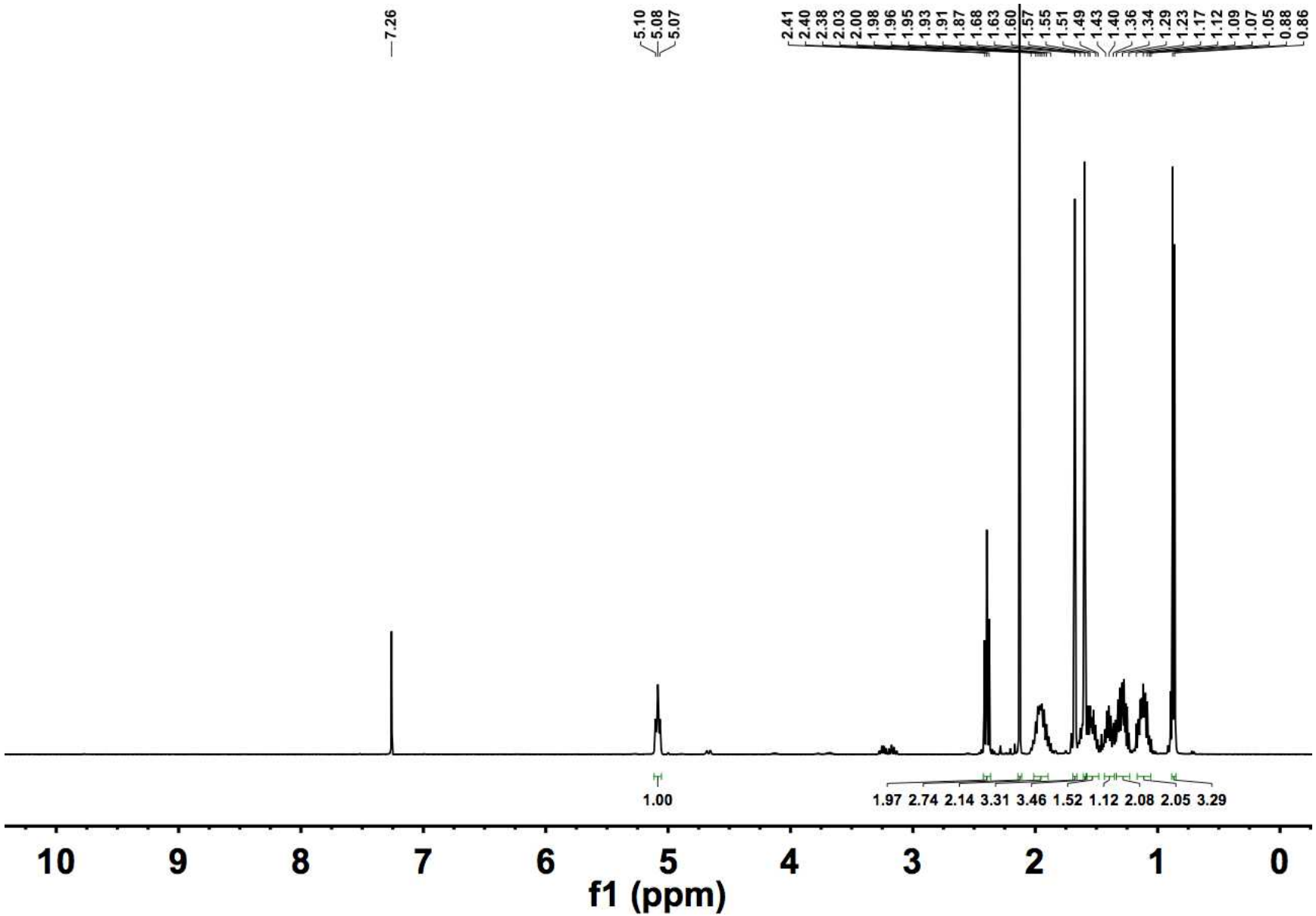

Figure A2.27: 1D ^{1}H NMR (400 MHz) spectrum of 6,10-dimethylundec-9-en-2-one (2.18) at 26 °C in $CDCl_3$.

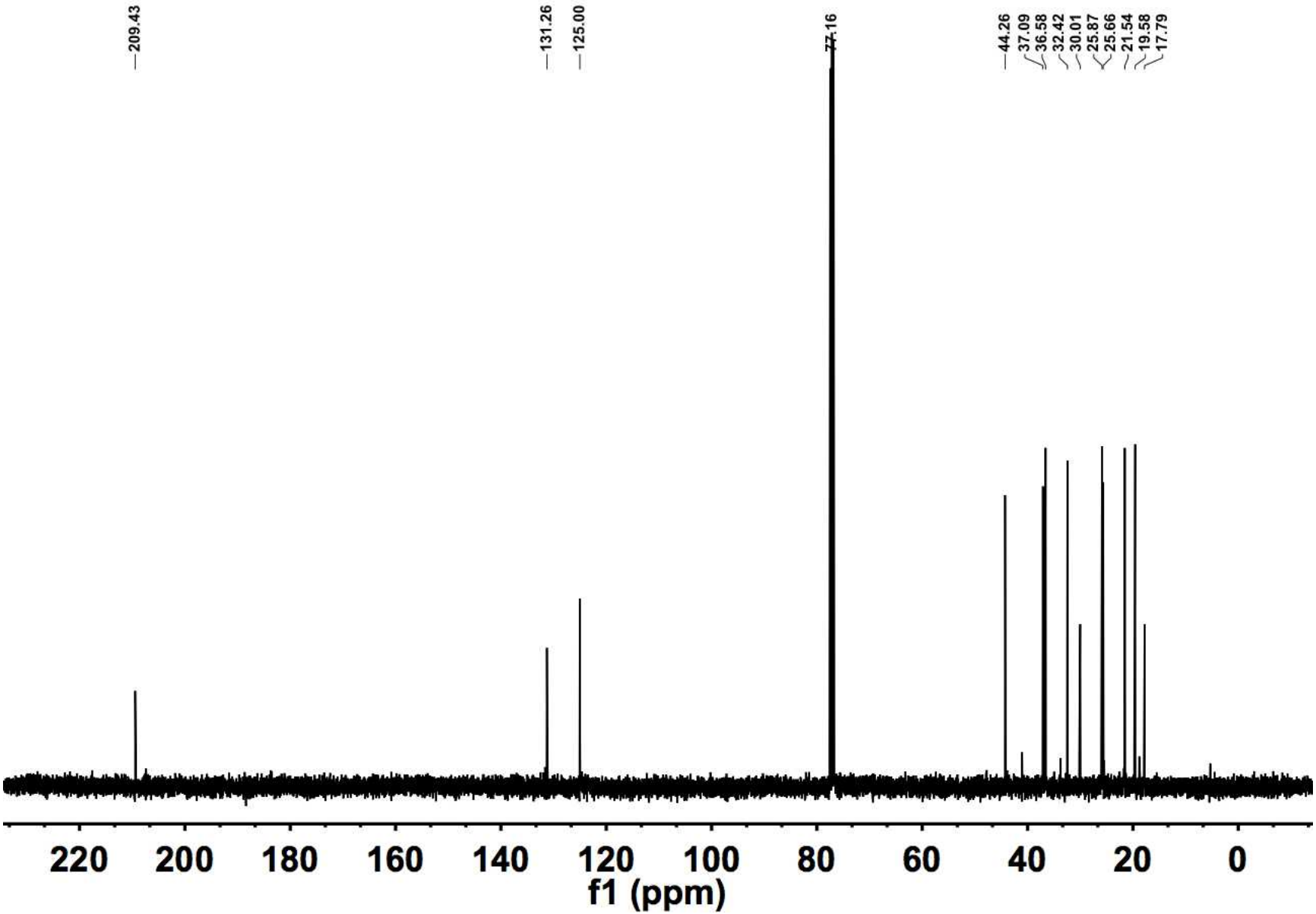

Figure A2.28: 1D ^{13}C NMR (101 MHz) spectrum of 6,10-dimethylundec-9-en-2-one (2.18) at 26 °C in $CDCl_3$.

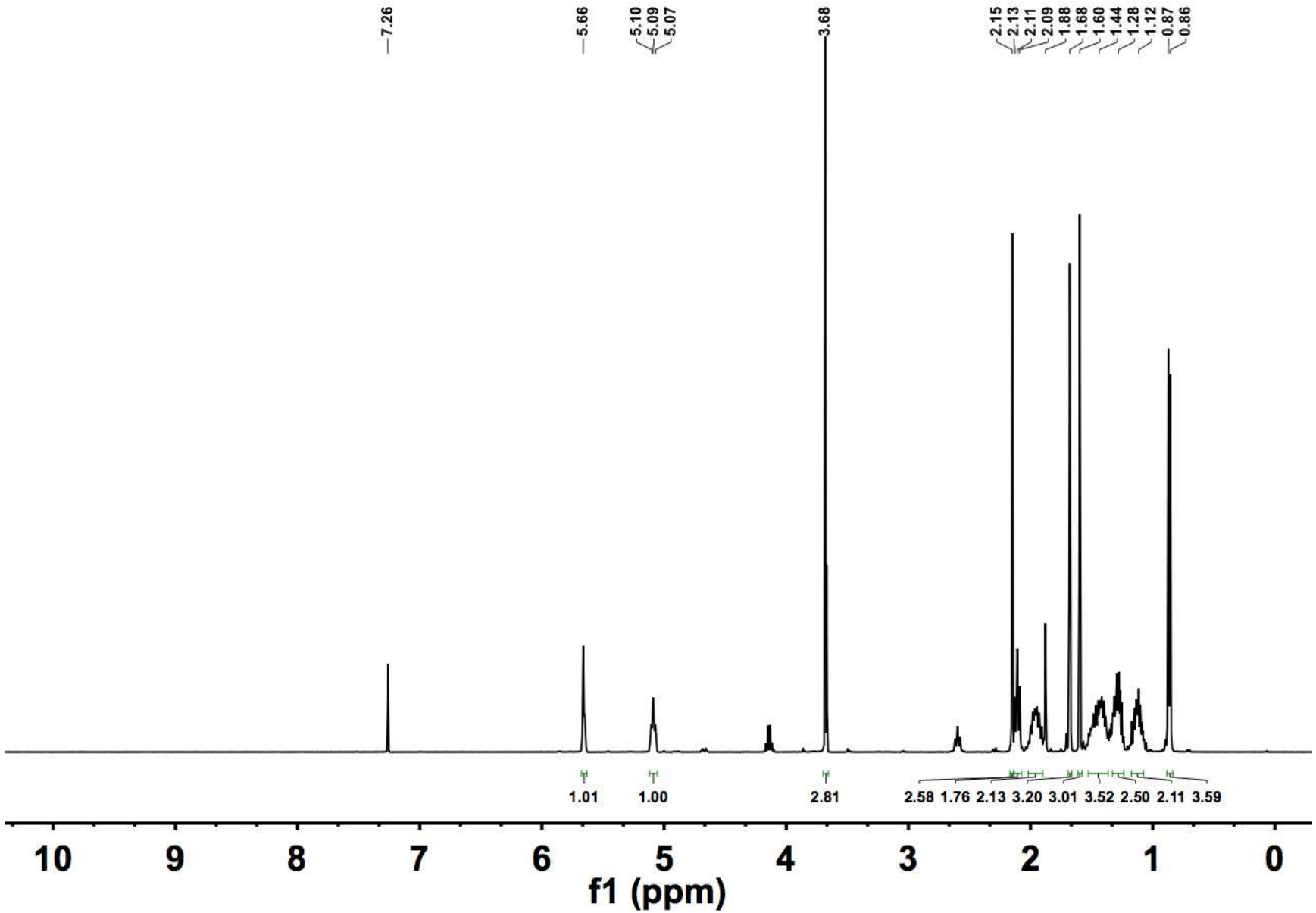

Figure A2.29: 1D ^{1}H NMR (400 MHz) spectrum of Methyl 3,7,11-trimethyldodeca-2,10-dienoate (2.19) at 26 °C in $CDCl_3$.

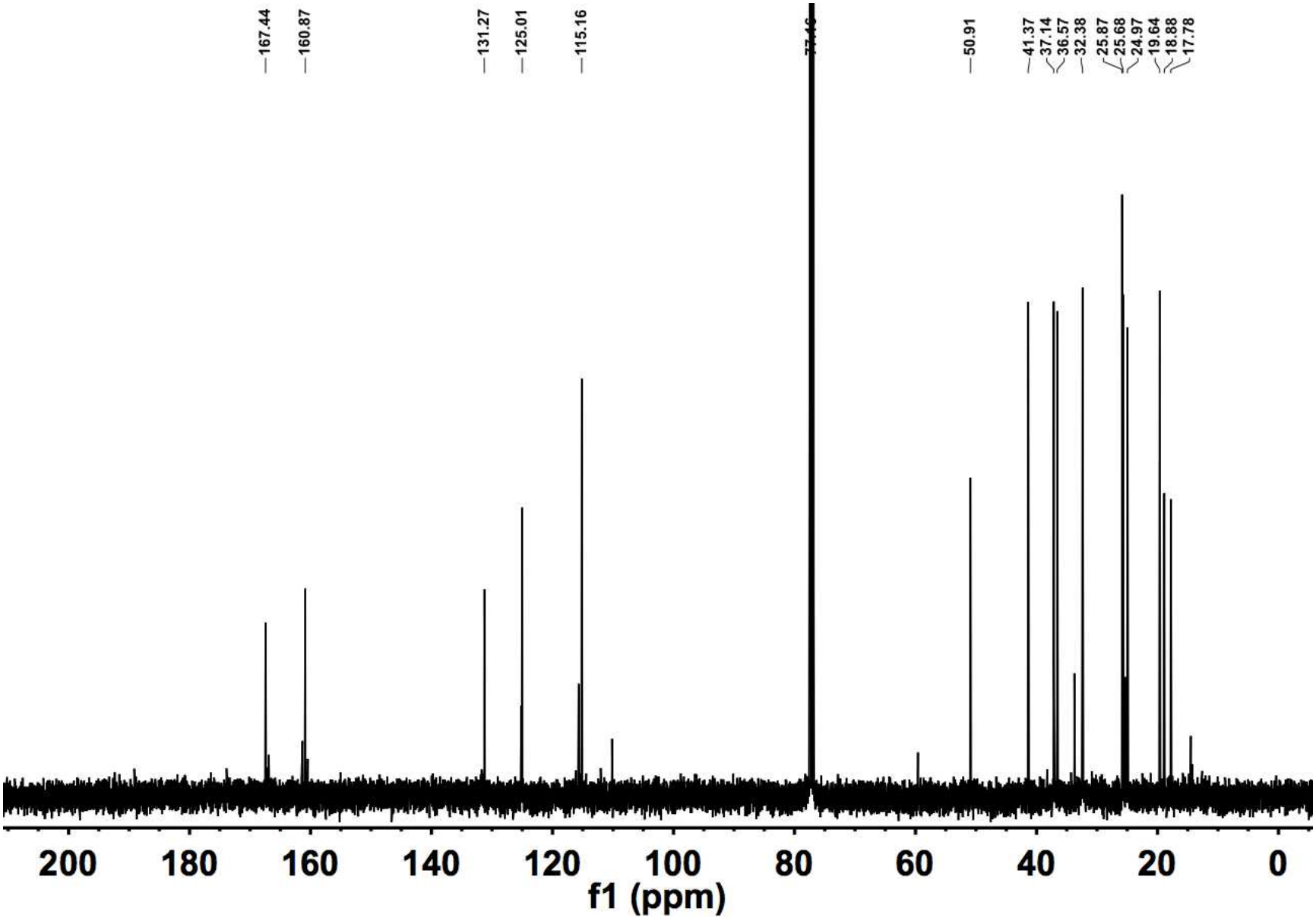

Figure A2.30: 1D ^{13}C NMR (101 MHz) spectrum of Methyl 3,7,11-trimethyldodeca-2,10-dienoate (2.19) at 26 °C in $CDCl_3$.

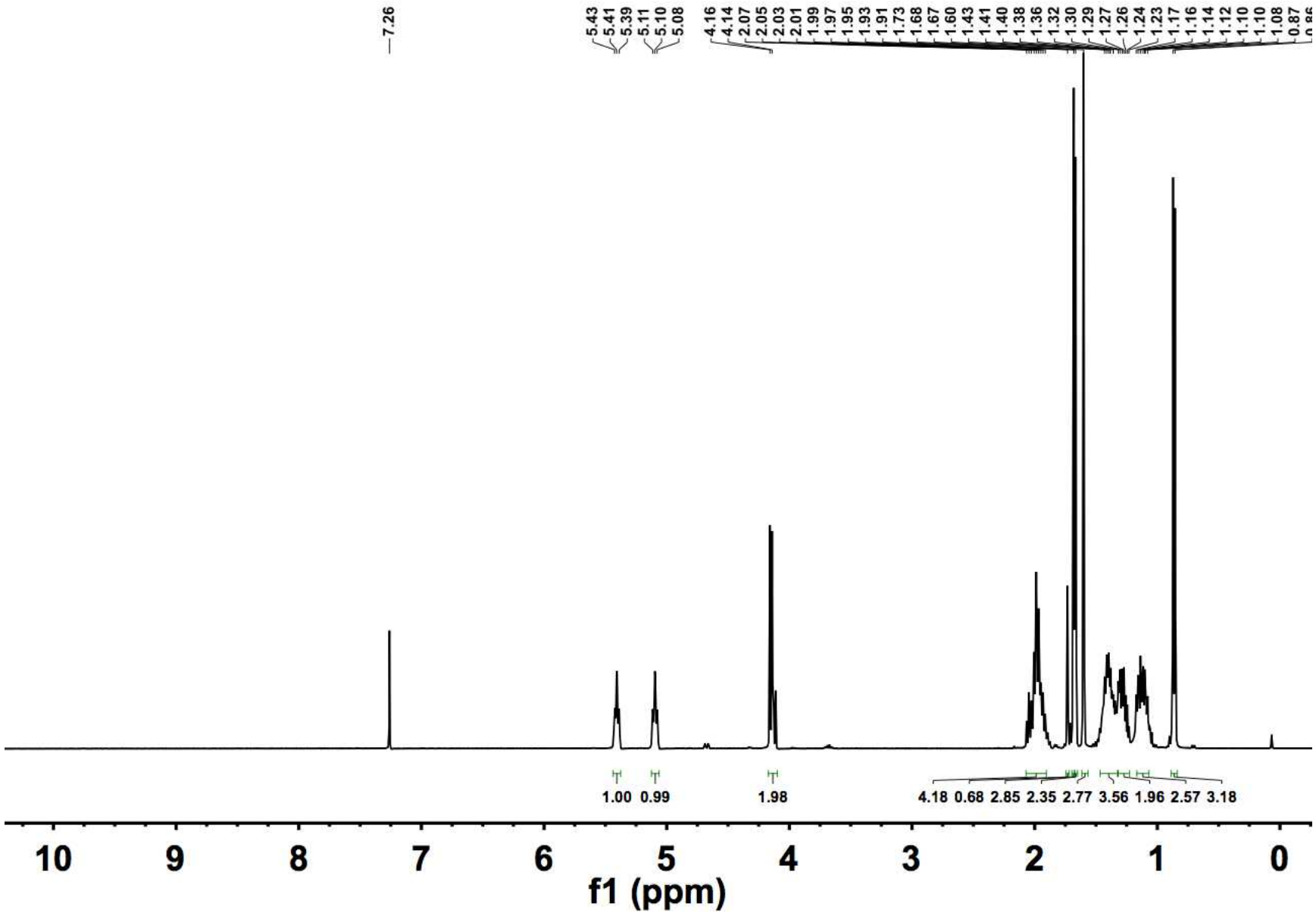

Figure A2.31: 1D ^{1}H NMR (400 MHz) spectrum of 3,7,11-trimethyldodeca-2,10-dien-1-ol (2.20) at 26 °C in $CDCl_3$.

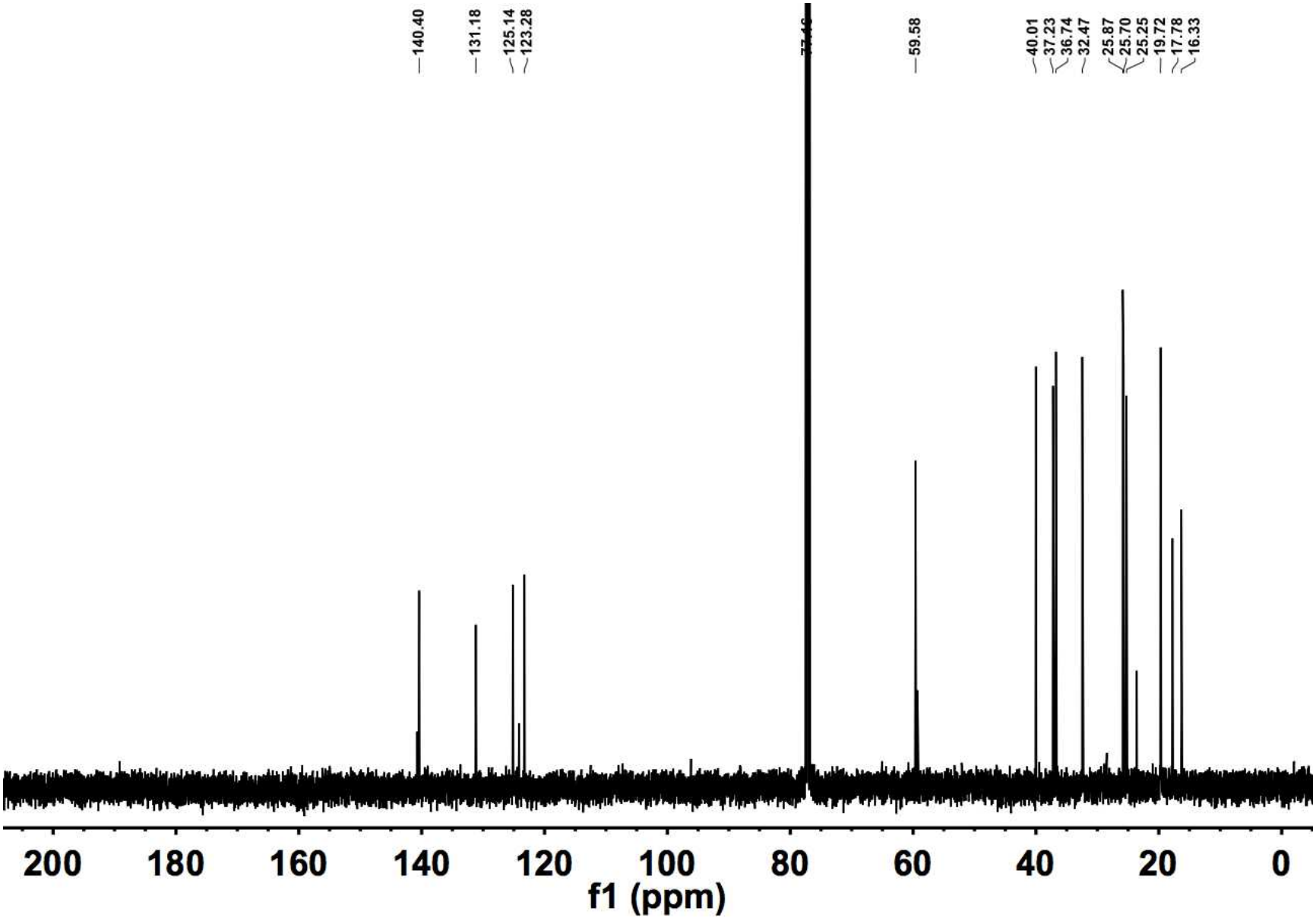

Figure A2.32: 1D ^{13}C NMR (101 MHz) spectrum of 3,7,11-trimethyldodeca-2,10-dien-1-ol (2.20) at 26 °C in $CDCl_3$.

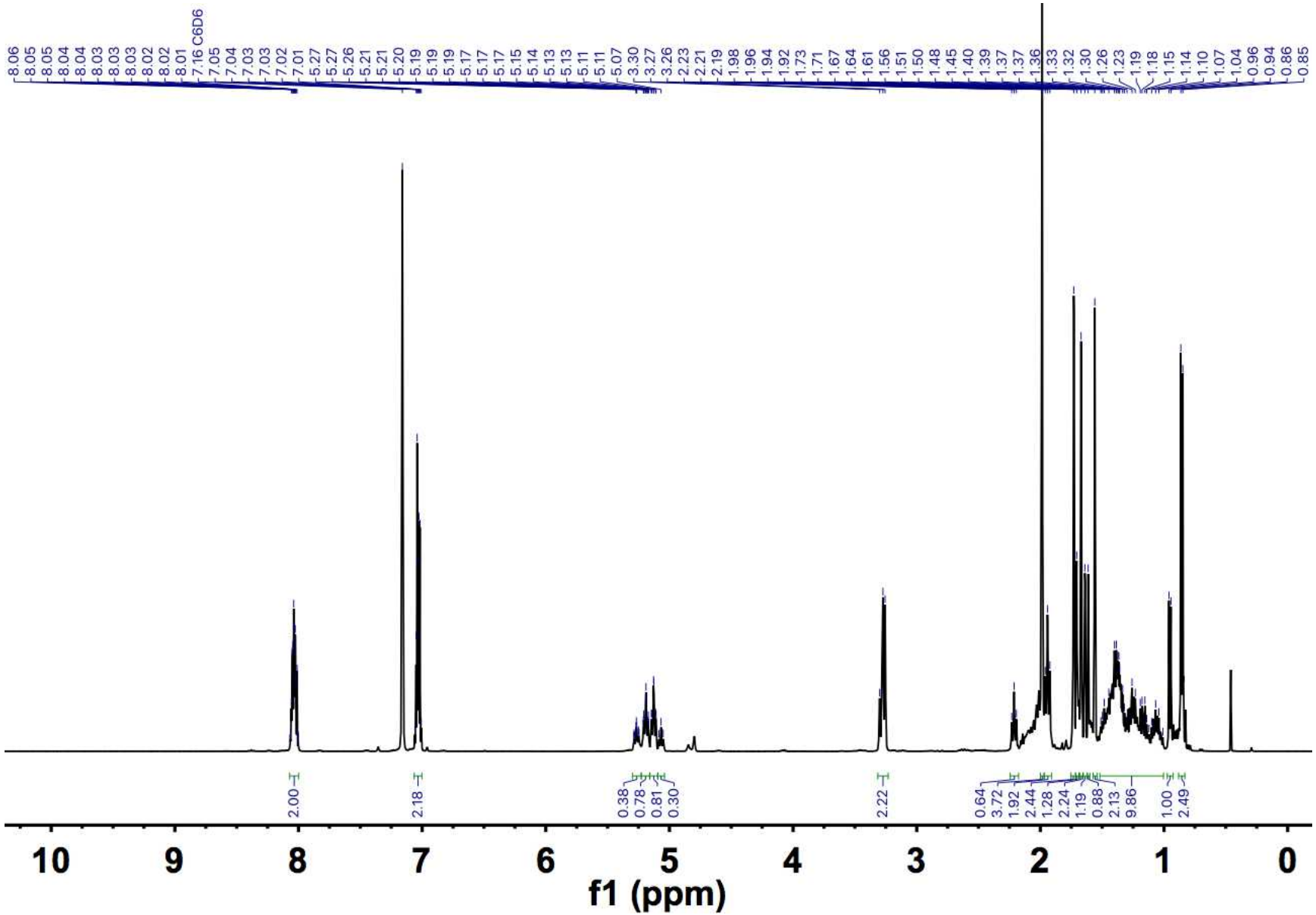

Figure A2.33: 1D ^{1}H NMR (400 MHz) spectrum of 53 mM cis/trans MK-3(II-H_2) (2.21) at 25 °C in C_6D_6.

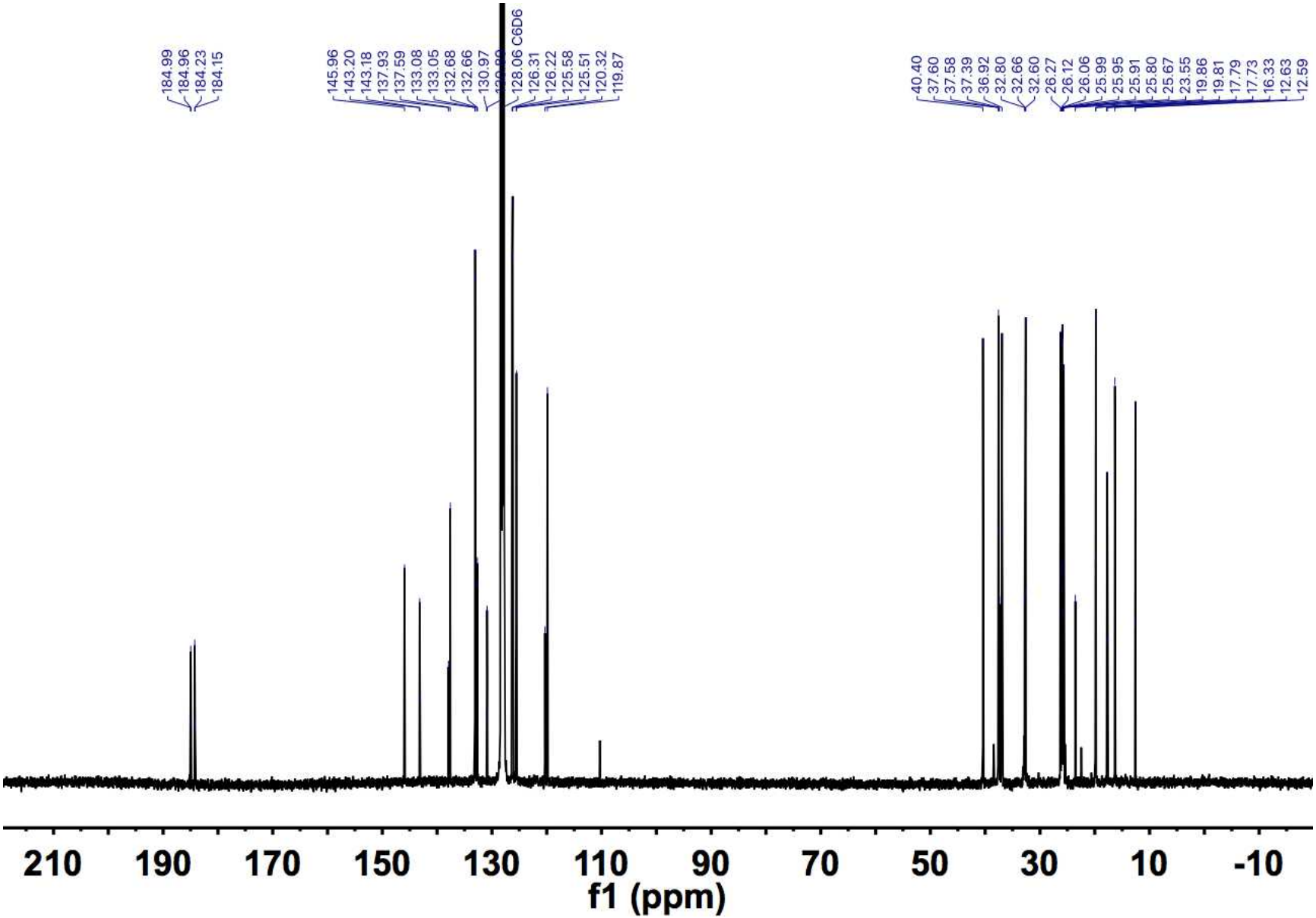

Figure A2.34: 1D ^{13}C NMR (101 MHz) spectrum of 53 mM cis/trans MK-3(II-H_2) (2.21) at 25 °C in C_6D_6 using 2000 scans.

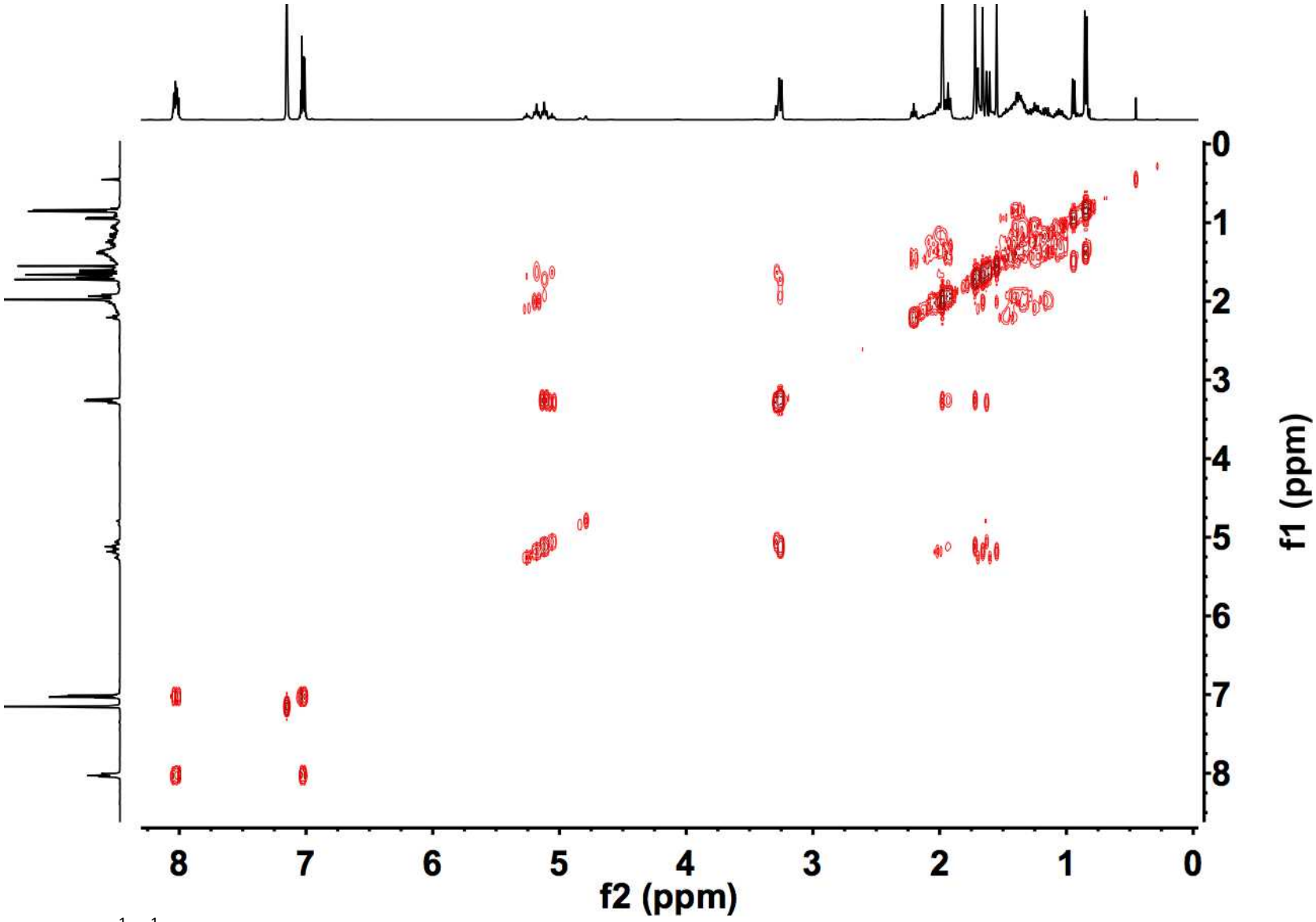

Figure A2.35: ^{1}H-^{1}H 2D gCOSY NMR (400 MHz) spectrum of 53 mM cis/trans MK-3(II-H_2) (2.21) in C_6D_6 at 25 °C. A standard gCOSY pulse sequence was used consisting of 128 t1 increments with 8 scans per t1 increment.

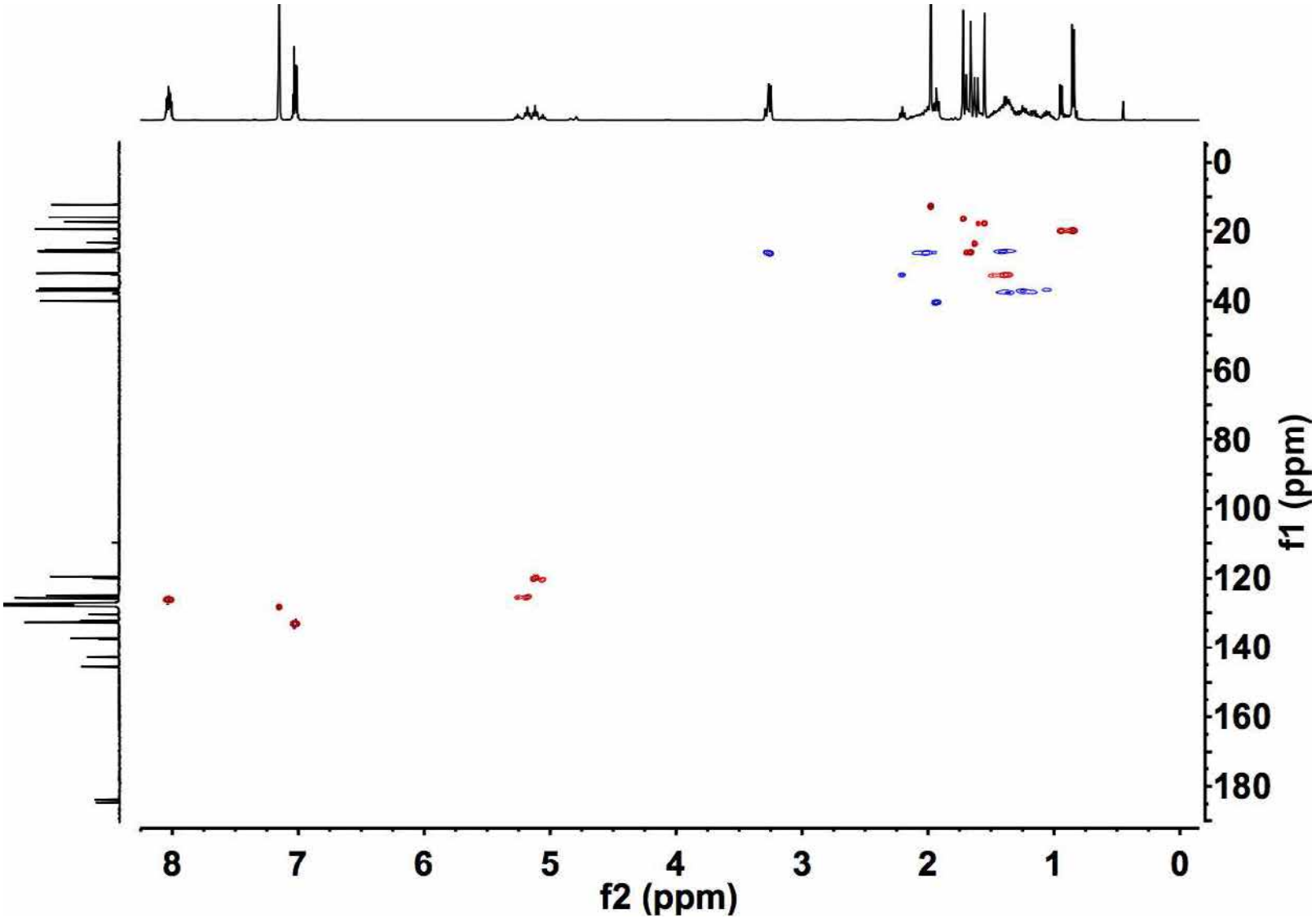

Figure A2.36: ^{1}H-^{13}C 2D HSQC NMR (400 MHz) spectrum of 53 mM cis/trans MK-3(II-H_2) (2.21) in C_6D_6 at 25 °C. A standard gHSQC pulse sequence was used consisting of 128 t1 increments with 8 scans per t1 increment. Red contour peaks correspond to methyl (-CH_3) and methine (>CH-) groups and blue contour peaks correspond to methylene (-CH_2 -) groups.

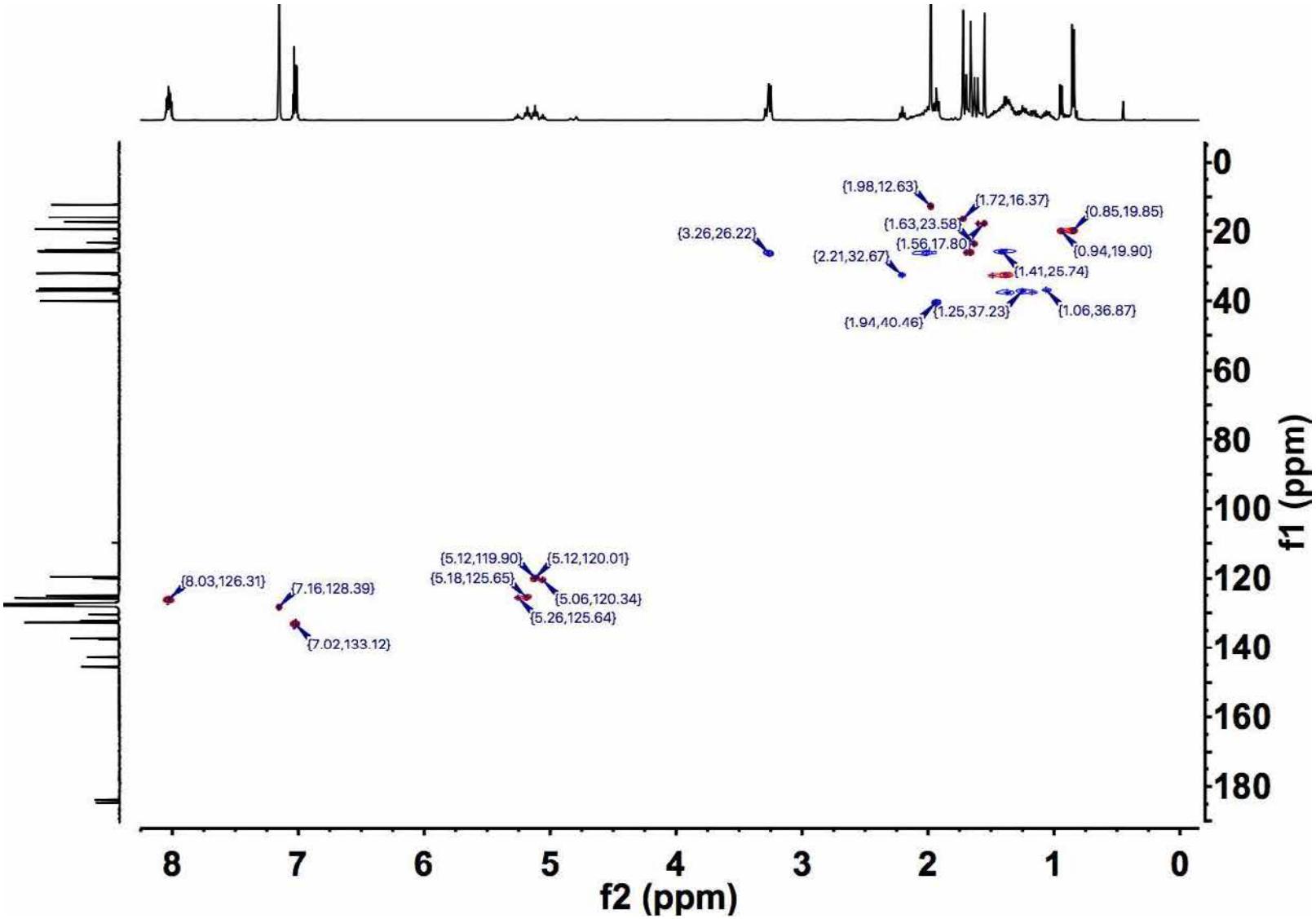

Figure A2.36.1: ^{1}H-^{13}C 2D HSQC NMR (400 MHz) spectrum of 53 mM cis/trans MK-3(II-H_2) (2.21) in C_6D_6 at 25 °C. A standard gHSQC pulse sequence was used consisting of 128 t1 increments with 8 scans per t1 increment. Red contour peaks correspond to methyl (-CH_3) and methine (>CH-) groups and blue contour peaks correspond to methylene (-CH_2 -) groups.

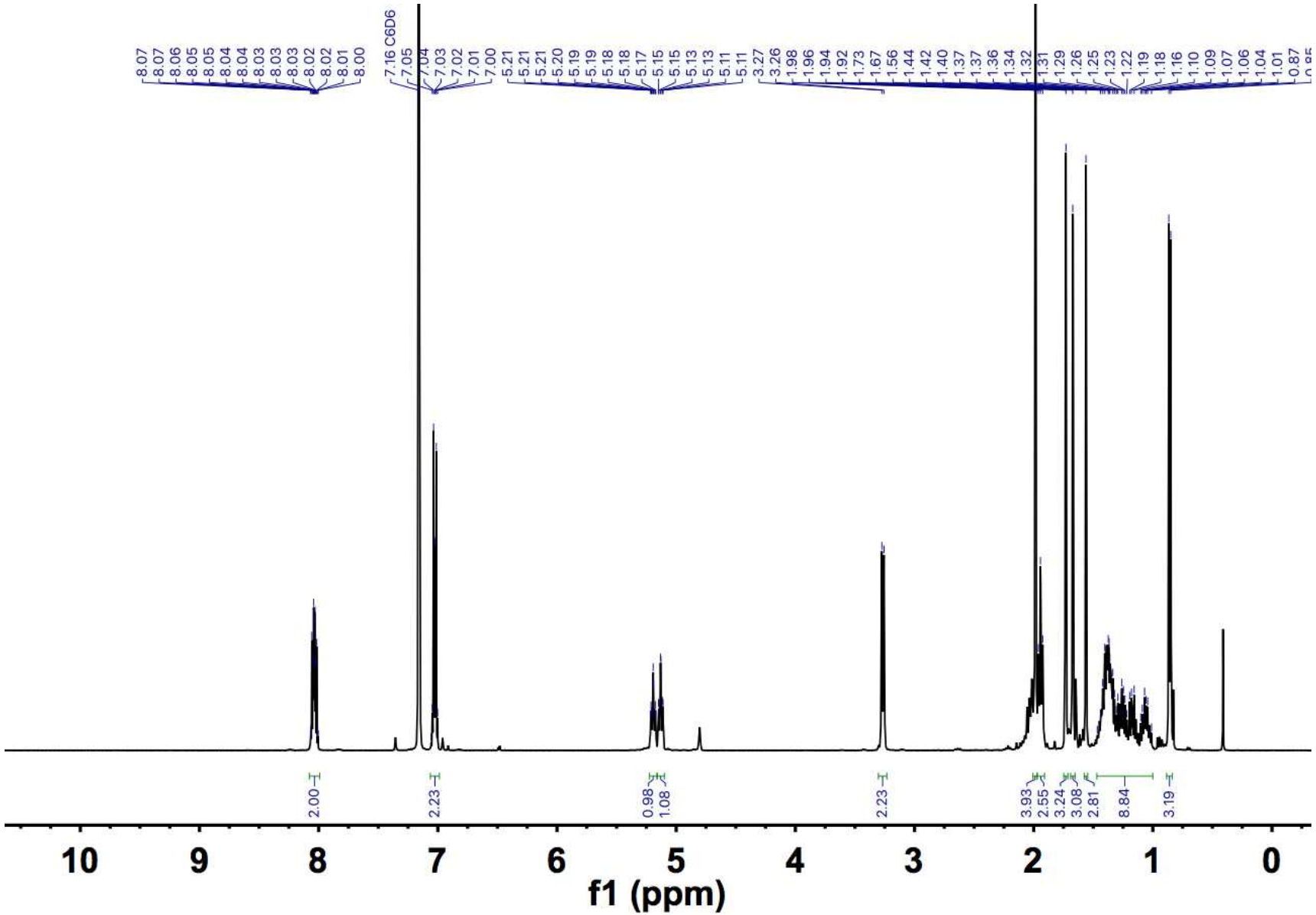

Figure A2.37: 1D ^{1}H NMR (400 MHz) spectrum of 20 mM trans-MK-3(II-H_2) (2.21) at 25 °C in C_6D_6.

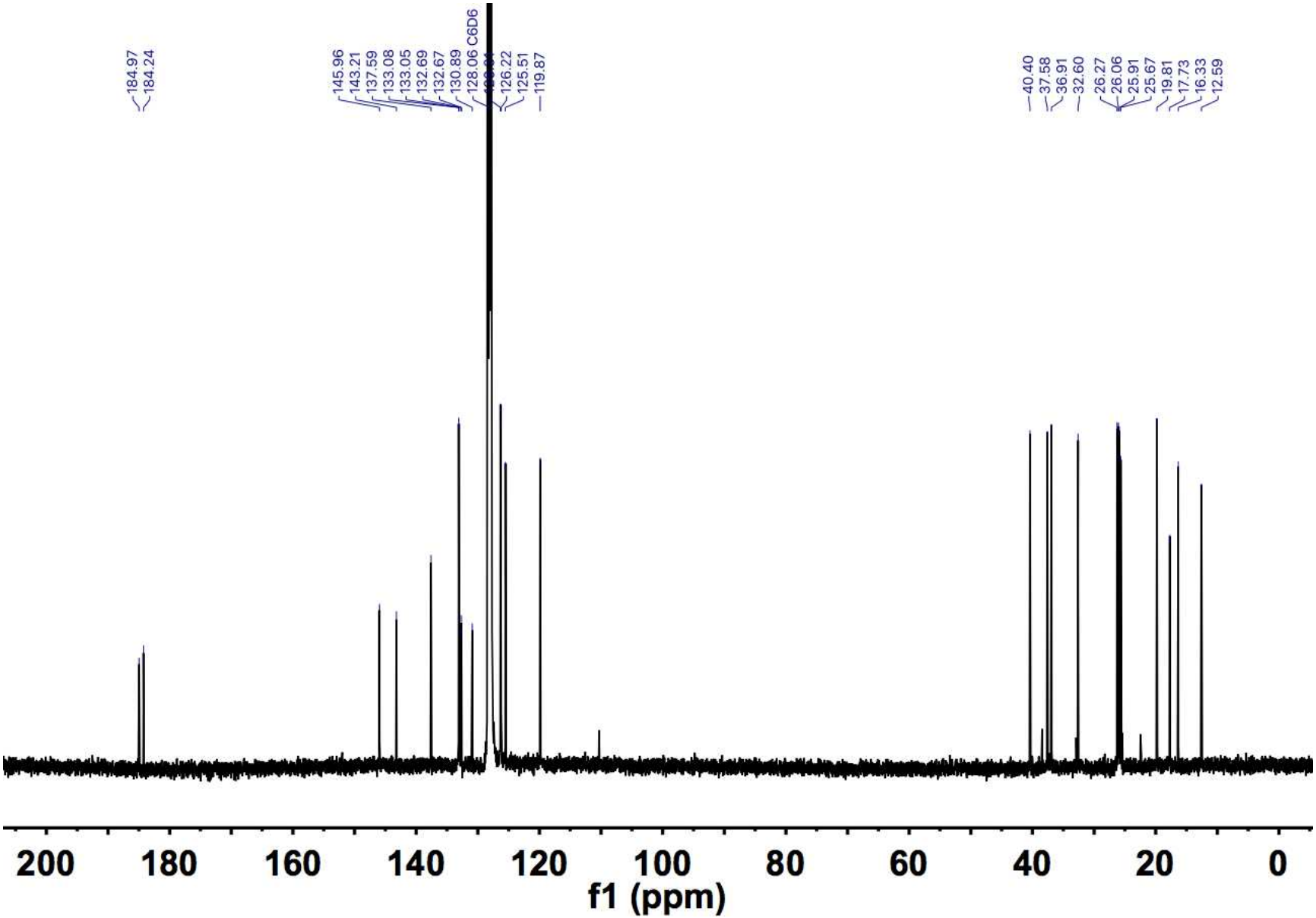

Figure A2.38: 1D ^{13}C NMR (101 MHz) spectrum of 20 mM trans-MK-3(II-H_2) (2.21) at 25 °C in C_6D_6 using 2000 scans.

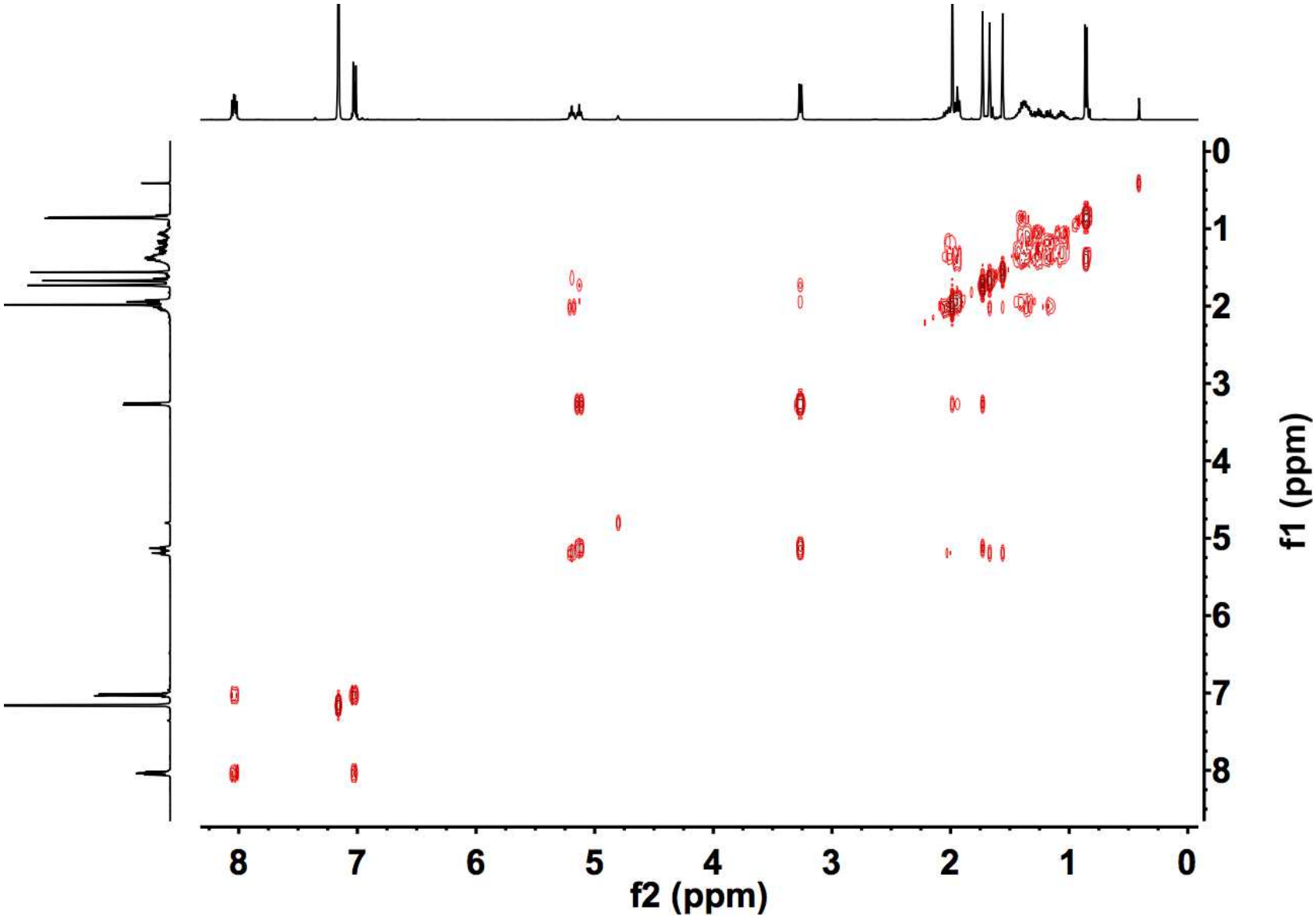

Figure A2.39: ^{1}H-^{1}H 2D gCOSY NMR (400 MHz) spectrum of 20 mM trans-MK-3(II-H_2) (2.21) in C_6D_6 at 25 °C. A standard gCOSY pulse sequence was used consisting of 128 t1 increments with 8 scans per t1 increment.

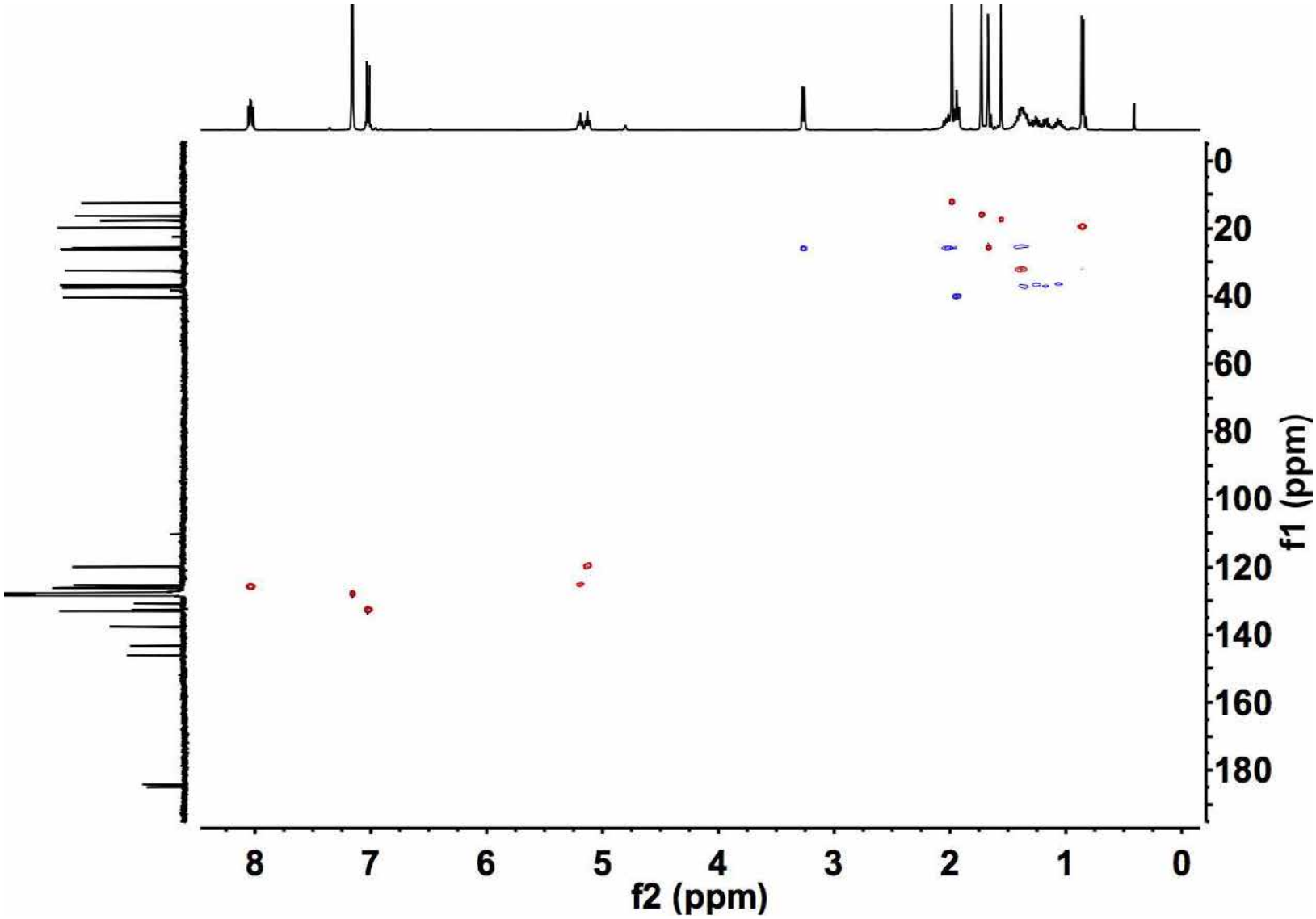

Figure A2.40: ^{1}H-^{13}C 2D HSQC NMR (400 MHz) spectrum of 20 mM trans-MK-3(II-H_2) (2.21) in C_6D_6 at 25 °C. A standard gHSQC pulse sequence was used consisting of 128 t1 increments with 8 scans per t1 increment. Red contour peaks correspond to methyl (-CH_3) and methine (>CH-) groups and blue contour peaks correspond to methylene (-CH_2 -) groups.

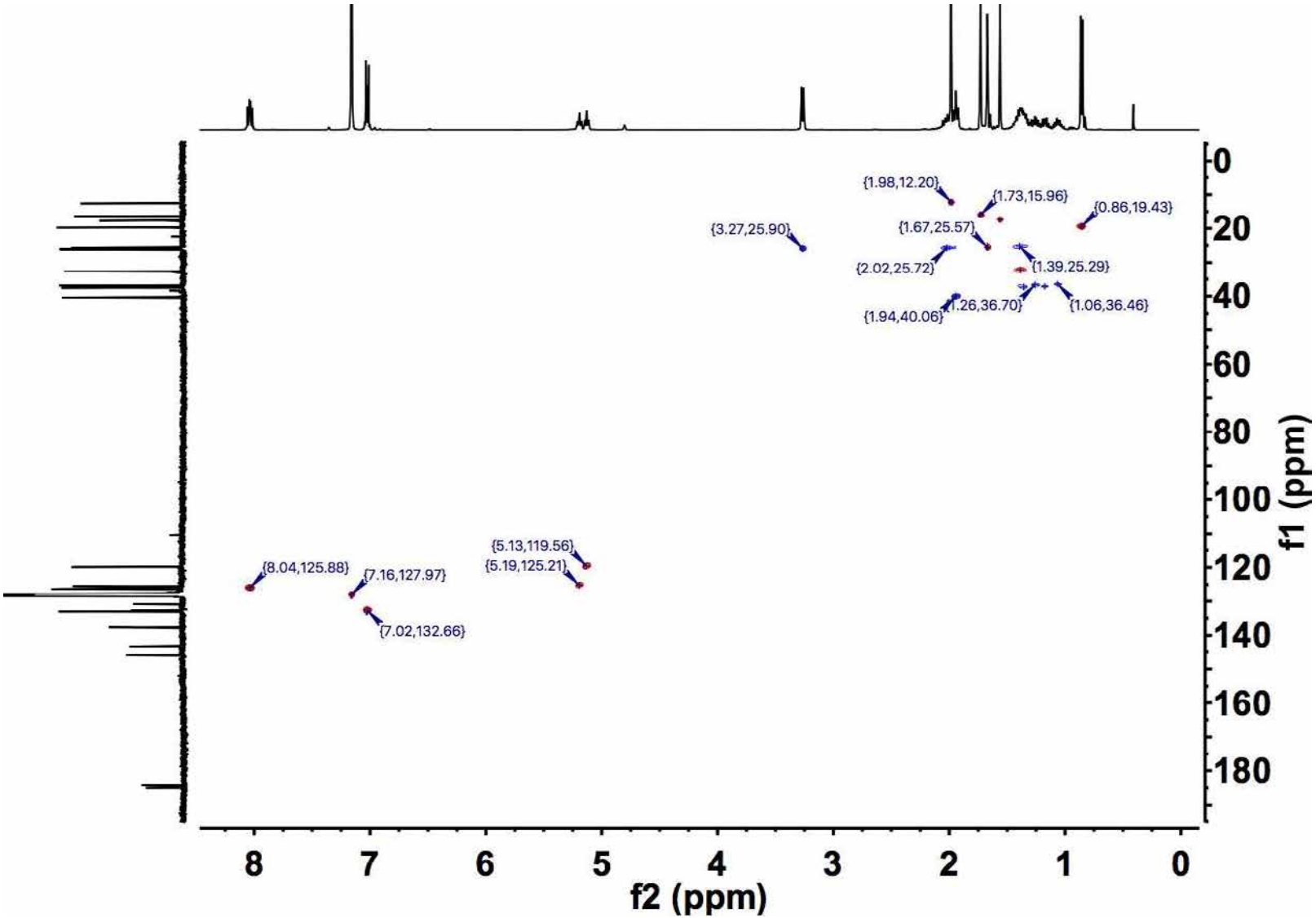

Figure A2.40.1: ^{1}H-^{13}C 2D HSQC NMR (400 MHz) spectrum of 20 mM trans-MK-3(II-H_2) (2.21) in C_6D_6 at 25 °C. A standard gHSQC pulse sequence was used consisting of 128 t1 increments with 8 scans per t1 increment. Red contour peaks correspond to methyl (-CH_3) and methine (>CH-) groups and blue contour peaks correspond to methylene (-CH_2 -) groups.

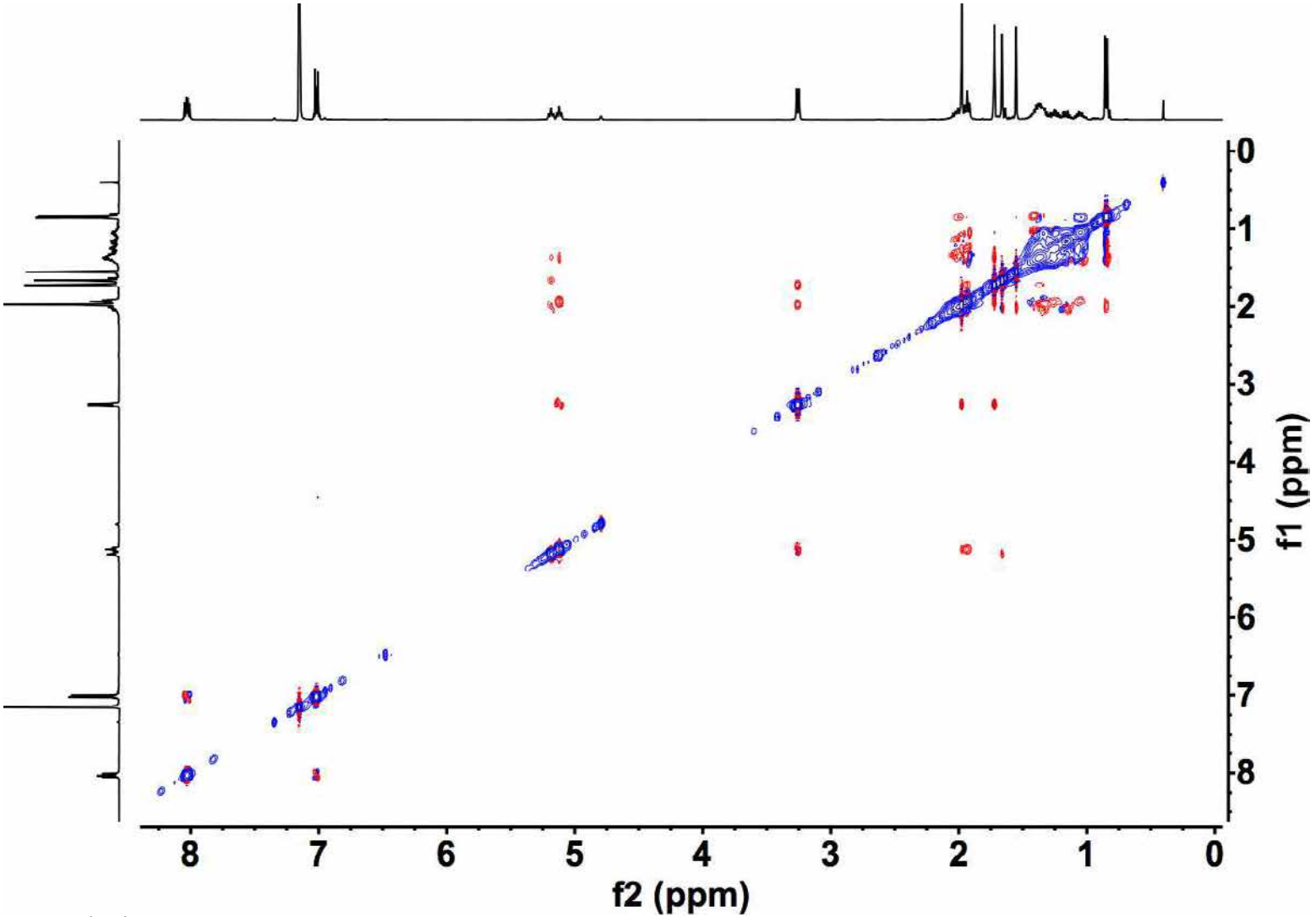

Figure A2.41. ^{1}H-^{1}H 2D ROESY NMR (400 MHz) spectrum of 20 mM trans-MK-3(II-H_2) (2.21) at 25 °C in C_6D_6. A standard ROESY pulse sequence was used consisting of 256 transients with 16 scans in the f1 domain using a 400 ms mixing time and 2.0 sec. relaxation delay. Blue intensity contours represent negative ROE's and red intensity contours represent positive ROE's. A sine square 90° weighting function was used in the F1 and F2 dimensions.

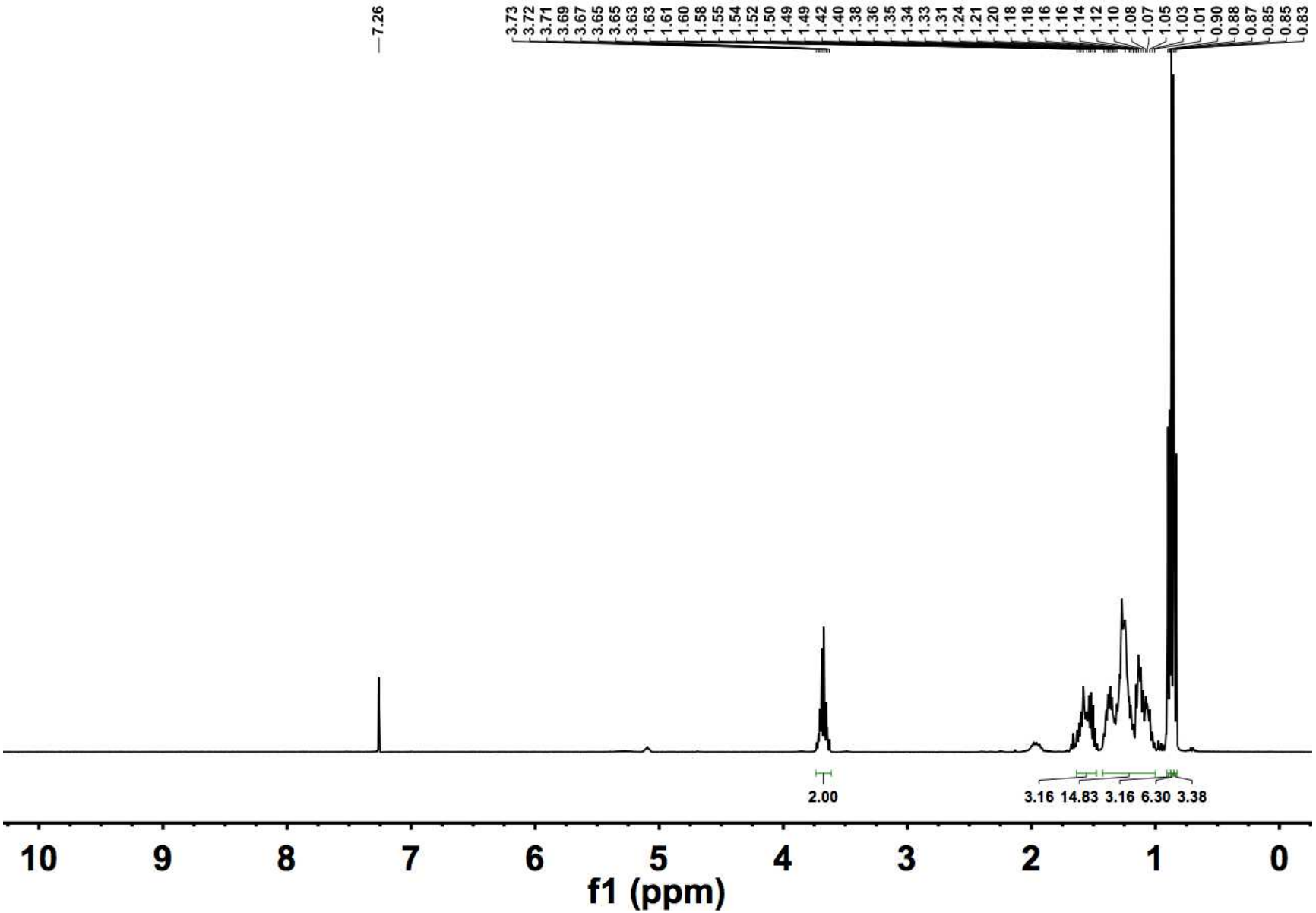

Figure A2.42: 1D ^{1}H NMR (400 MHz) spectrum of 3,7,11-trimethyldodecan-1-ol (2.23) at 26 °C in $CDCl_3$.

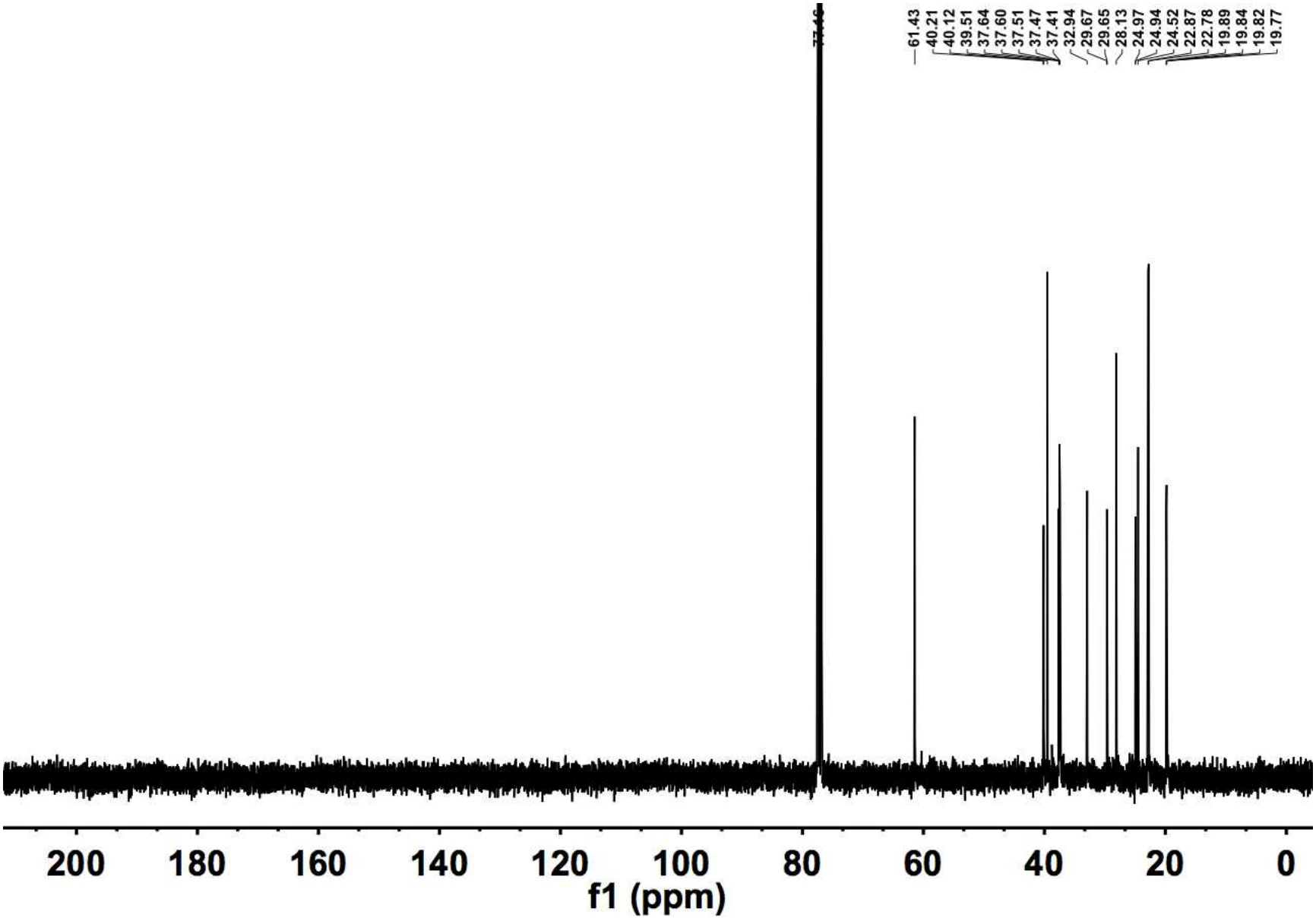

Figure A2.43: 1D ^{13}C NMR (101 MHz) spectrum of 3,7,11-trimethyldodecan-1-ol (2.23) at 26 °C in $CDCl_3$.

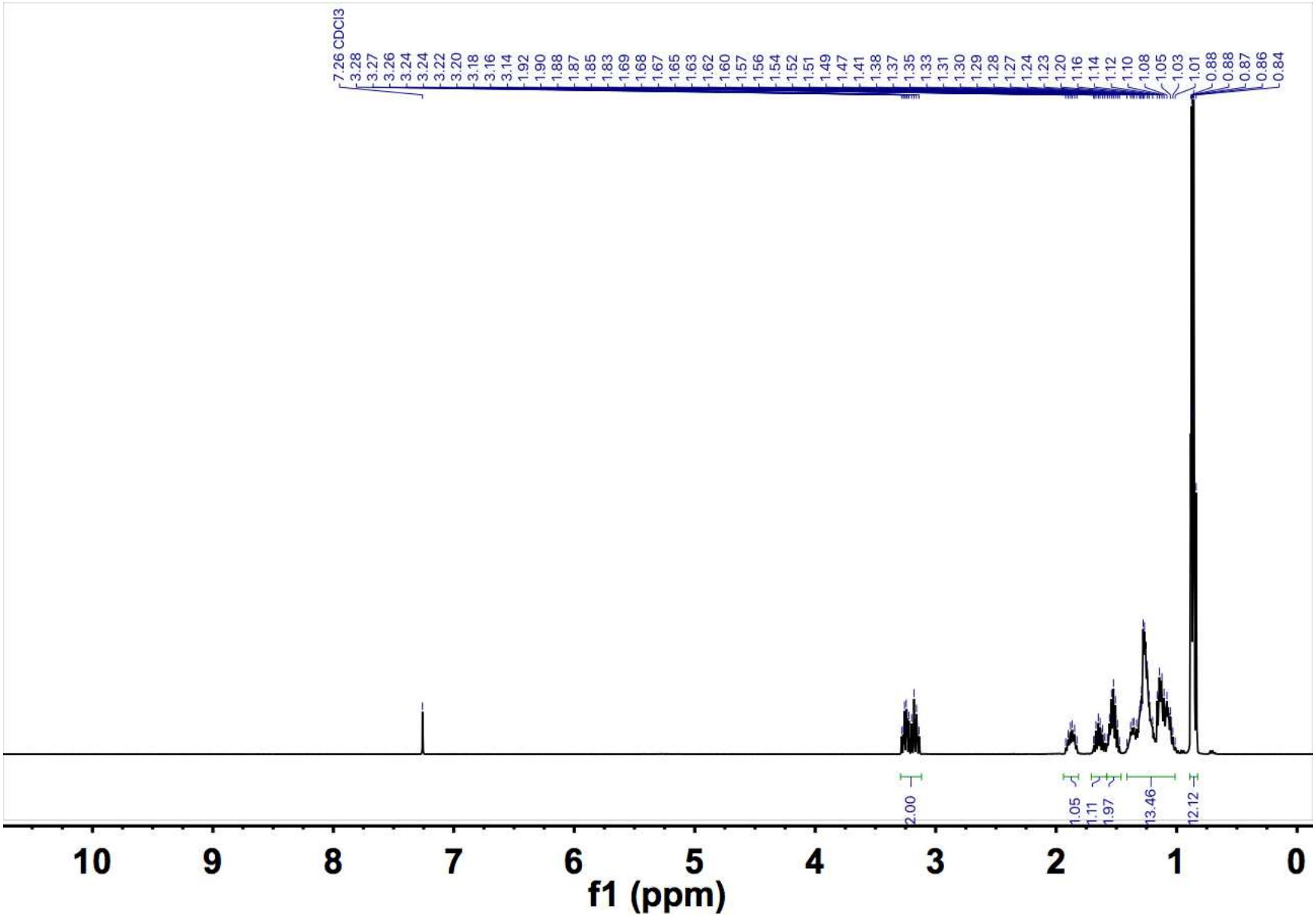

Figure A2.44: 1D ^{1}H NMR (400 MHz) spectrum of 80 mM 1-iodo-3,7,11-trimethyldodecane (2.24) at 26 °C in $CDCl_3$.

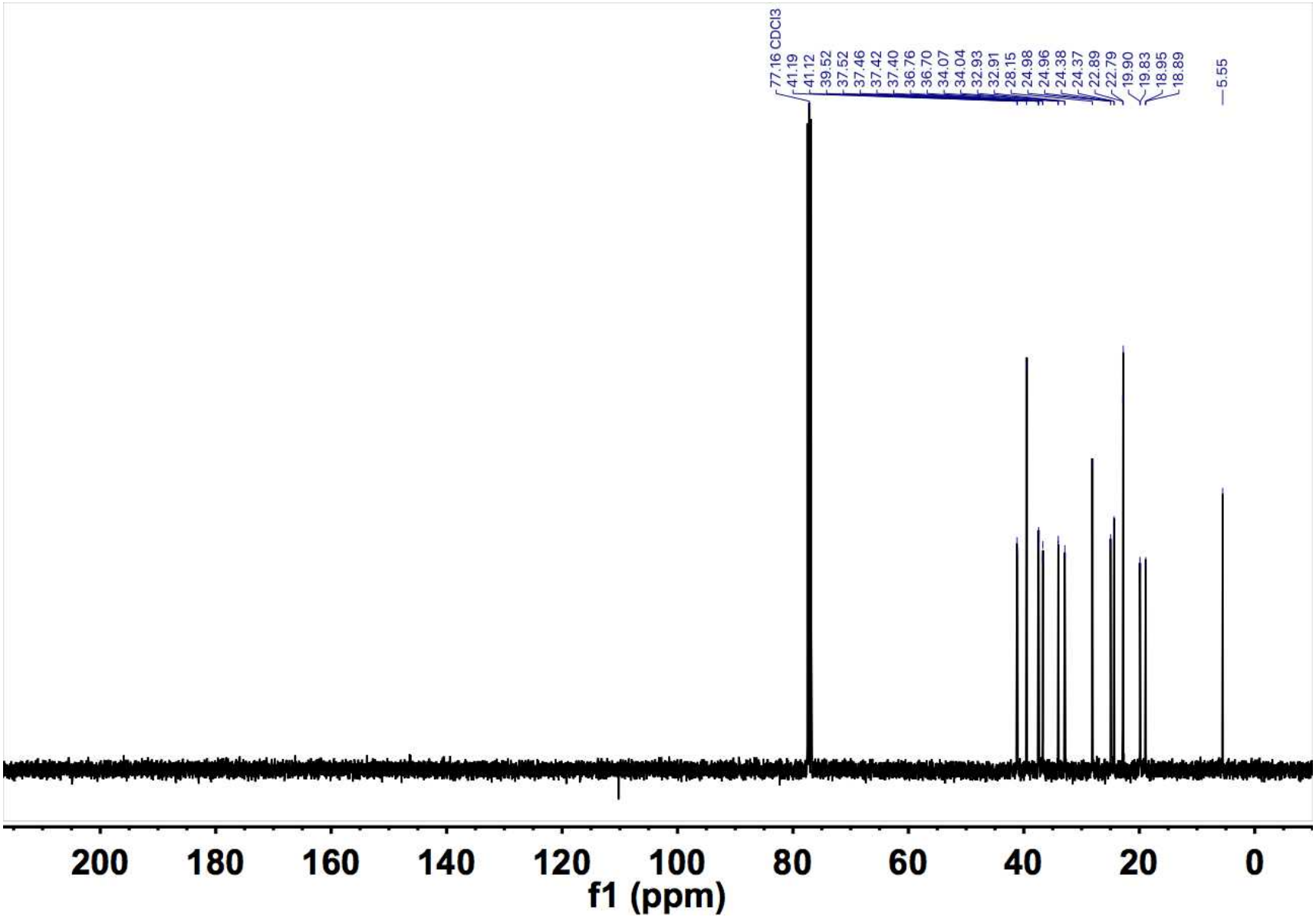

Figure A2.45: 1D ^{13}C NMR (101 MHz) spectrum of 80 mM 1-iodo-3,7,11-trimethyldodecane (2.24) at 26 °C in $CDCl_3$.

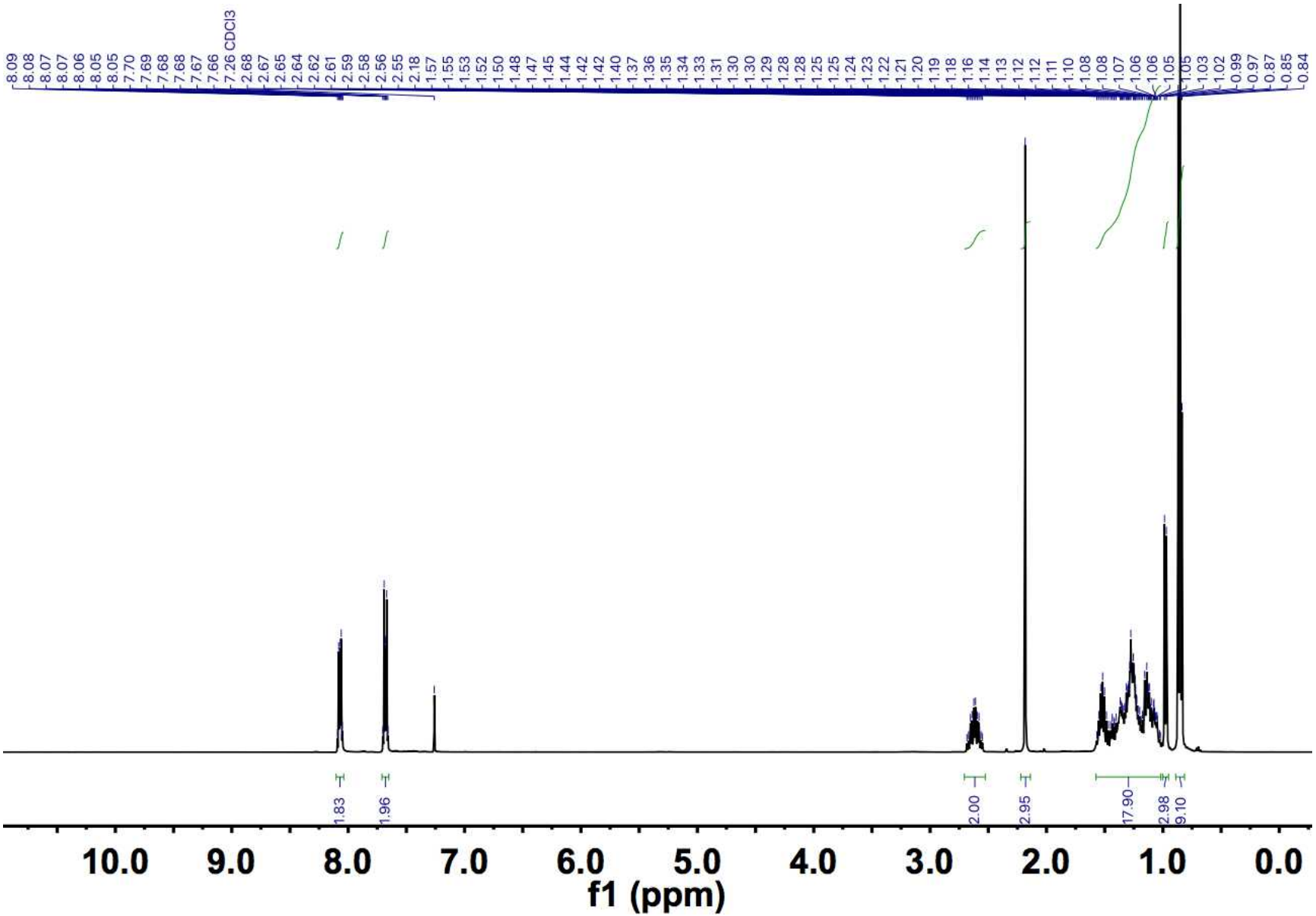

Figure A2.46: 1D ^{1}H NMR (400 MHz) spectrum of 80 mM MK-3(I,II,III-H_6) (2.25) at 25 °C in $CDCl_3$.

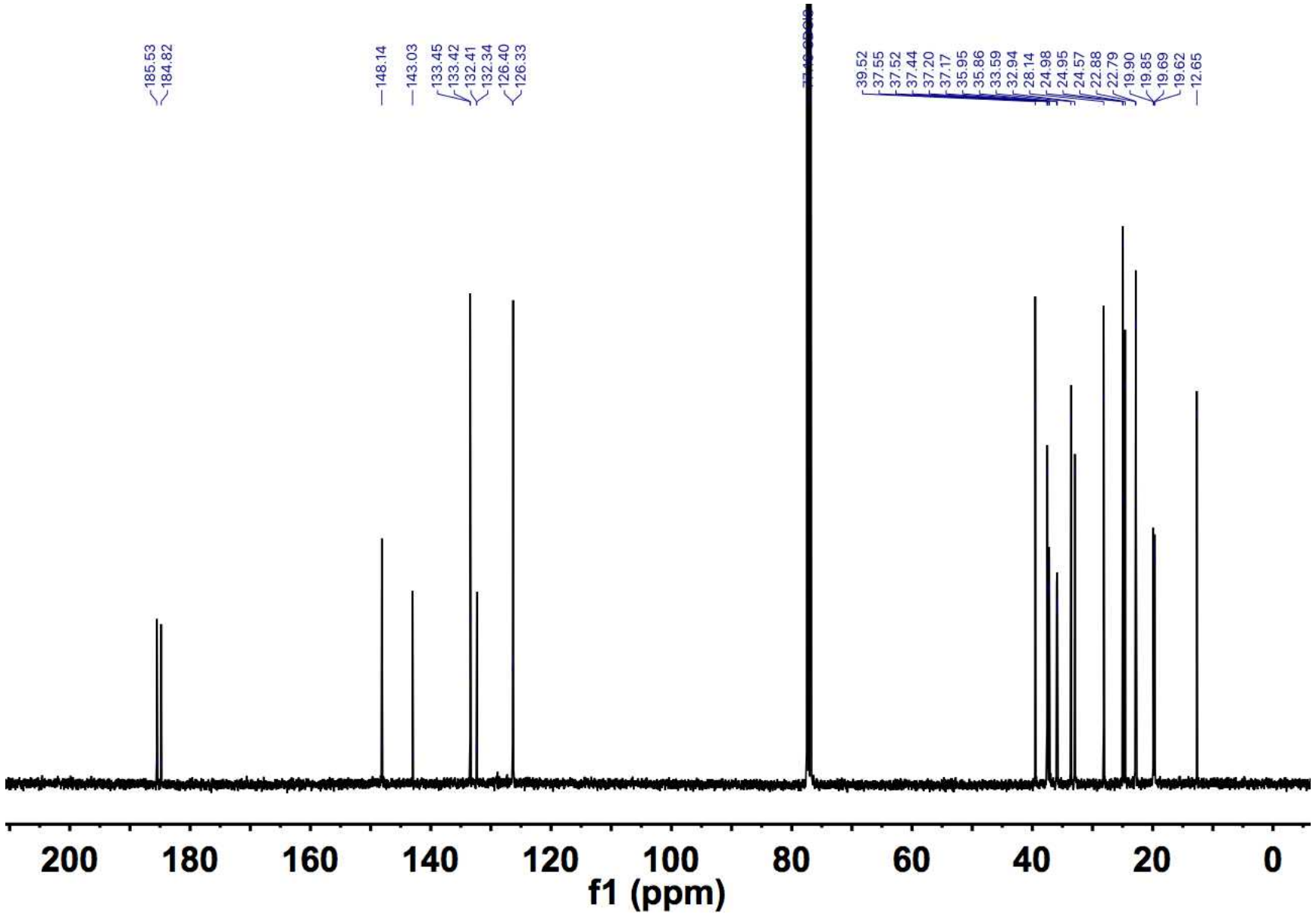

Figure A2.47: 1D ^{13}C NMR (101 MHz) spectrum of 80 mM MK-3(I,II,III-H_6) (2.25) at 25 °C in $CDCl_3$.

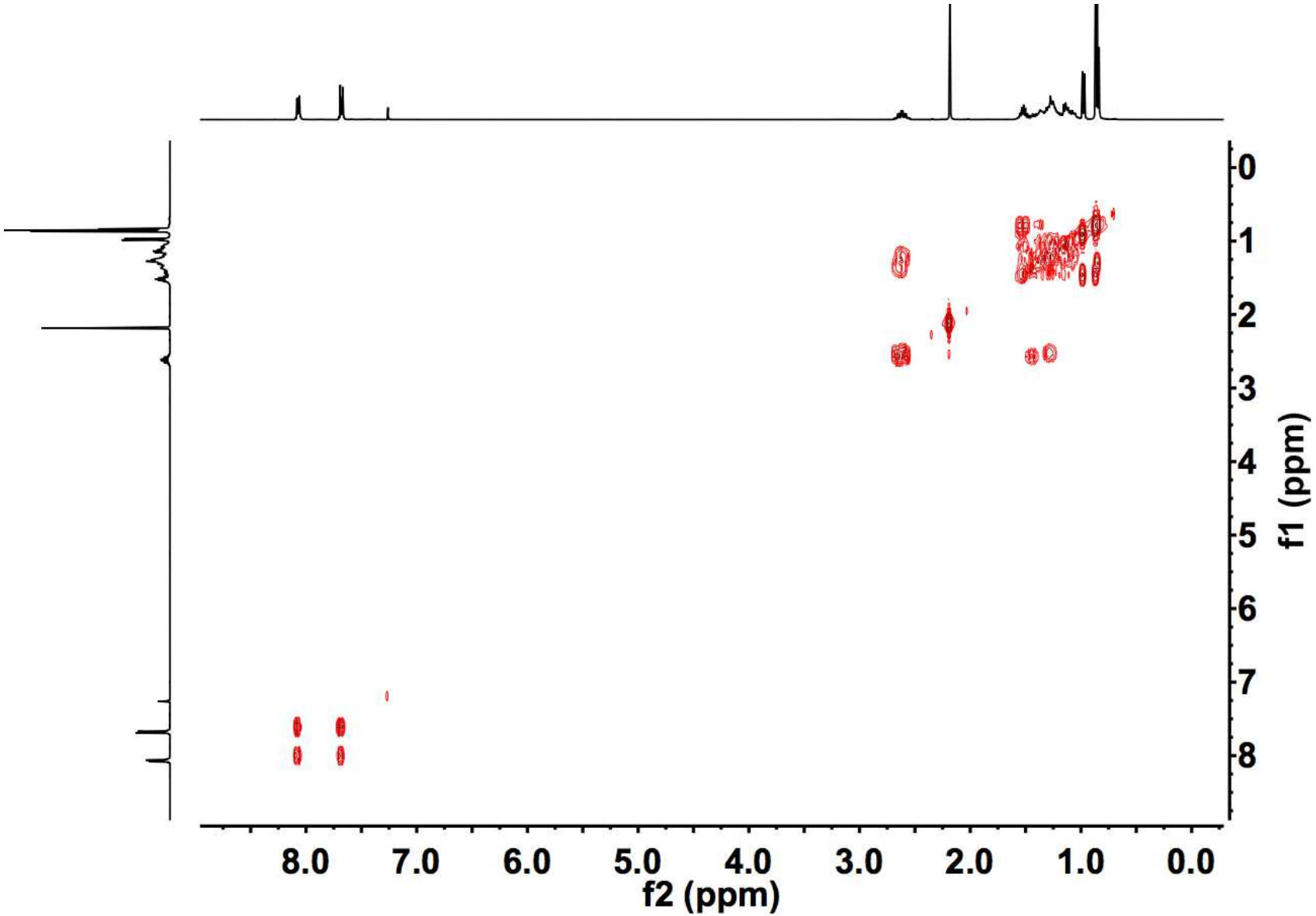

Figure A2.48: ^{1}H-^{1}H 2D gCOSY NMR (400 MHz) spectrum of MK-3(I,II,III-H_6) (2.25) in $CDCl_3$ at 25 °C. A standard gCOSY pulse sequence was used consisting of 128 t1 increments with 8 scans per t1 increment.

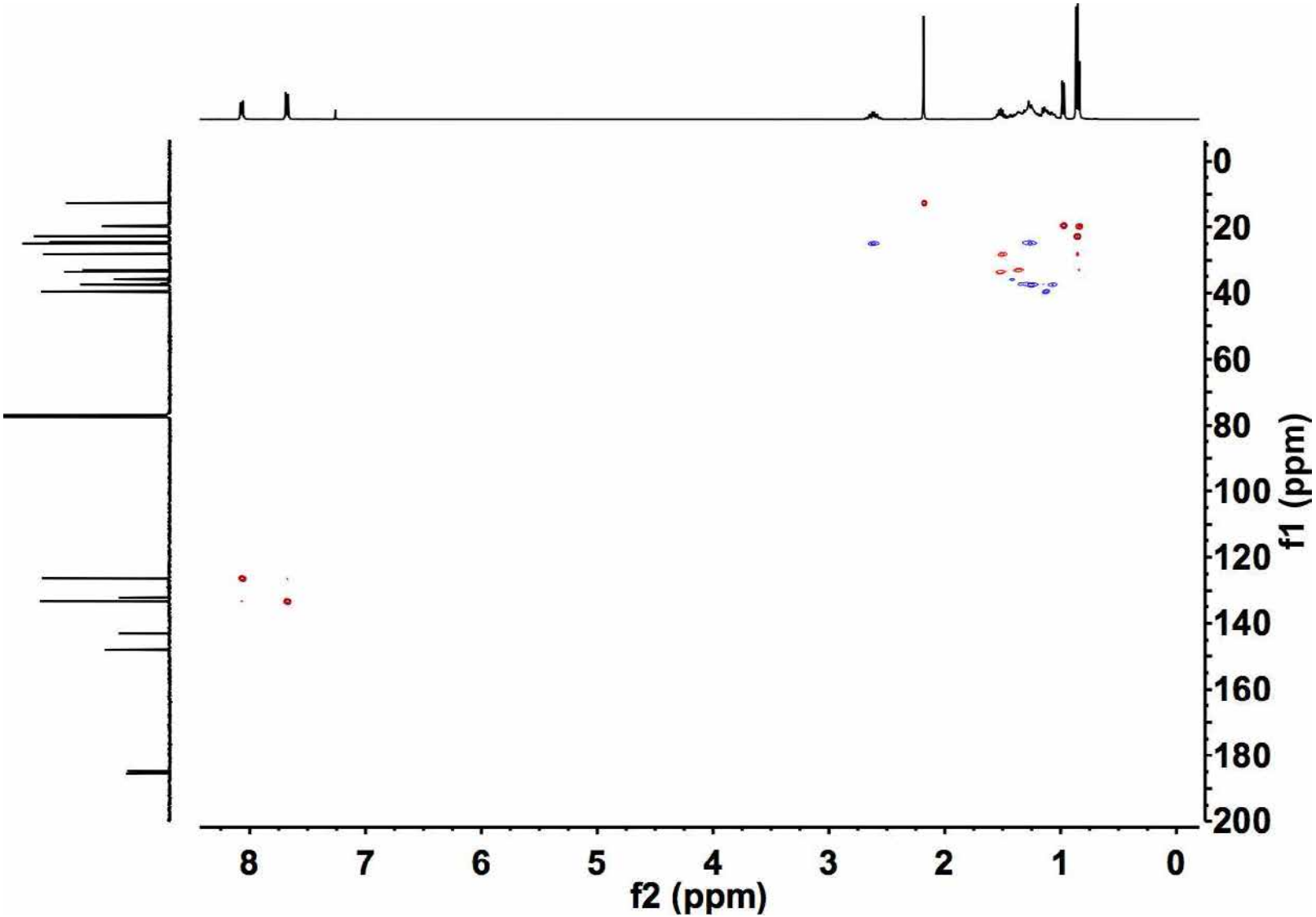

Figure A2.49: ^{1}H-^{13}C 2D HSQC NMR (400 MHz) spectrum of 80 mM MK-3(I,II,III-H_6) (2.25) in $CDCl_3$ at 25 °C. A standard gHSQC pulse sequence was used consisting of 128 t1 increments with 8 scans per t1 increment. Red contour peaks correspond to methyl (-CH_3) and methine (>CH-) groups and blue contour peaks correspond to methylene (-CH_2 -) groups.

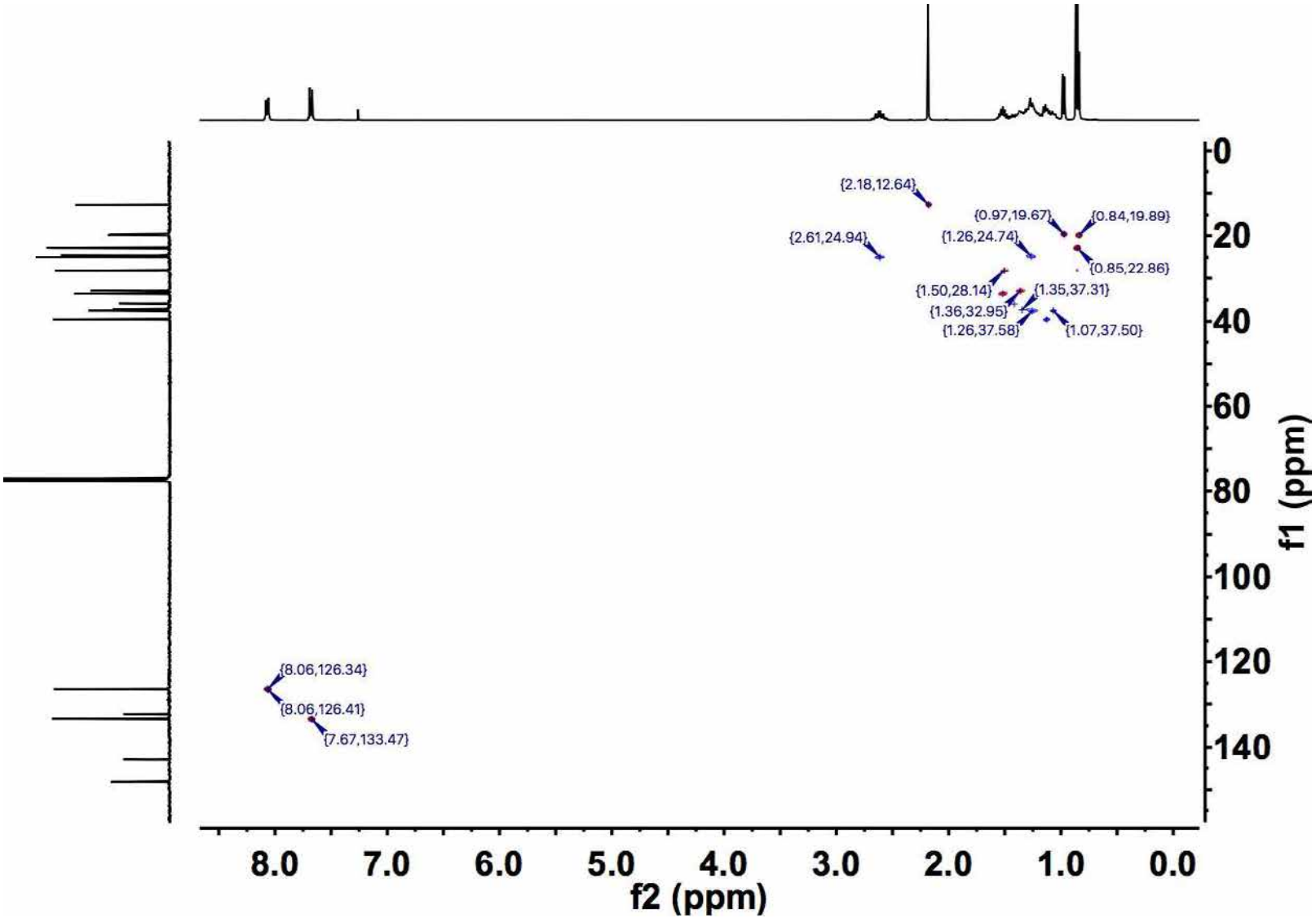

Figure A2.49.1: ^{1}H-^{13}C 2D HSQC NMR (400 MHz) spectrum of 80 mM MK-3(I,II,III-H_6) (2.25) in $CDCl_3$ at 25 °C. A standard gHSQC pulse sequence was used consisting of 128 t1 increments with 8 scans per t1 increment. Red contour peaks correspond to methyl (-CH_3) and methine (>CH-) groups and blue contour peaks correspond to methylene (-CH_2 -) groups.

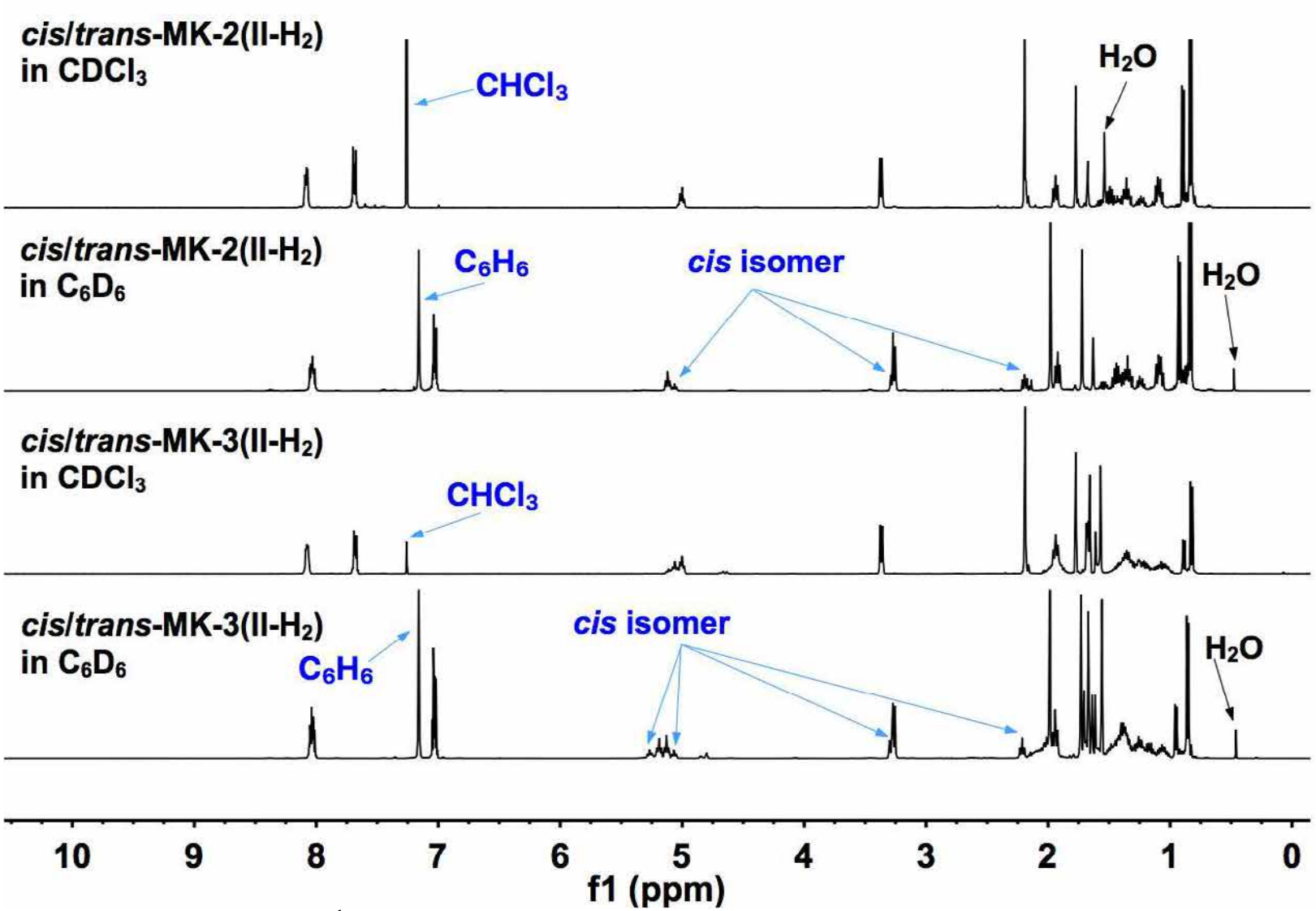

Figure A2.50: Comparison between ^{1}H NMR (400 MHz) spectrum of cis/trans-MK-2(II-H_2) in $CDCl_3$ vs C_6D_6 and comparison between ^{1}H NMR (400 MHz) spectrum of cis/trans-MK-3(II-H_2) in $CDCl_3$ vs. C_6D_6. The NMR spectra were recorded typically using 32 scans, at 25 or 26 °C and referenced to the internal solvent peak (see experimental for details). Not all the cis isomer peaks are labelled.

Appendix III: Supporting Information for Chapter 3

General 2D NMR Methods. Spectra were processed using MestReNova version 10.0.1. Details of experiments are provided in representative experimental sections and captions of figures. Spectra were collected both at 500 MHz and 400 MHz giving consistent results; however, all the data presented herein was at 400 MHz due to less noise in the spectrum. The interpretations of distances from NOE and ROE data were based off semi-quantitative examination of cross peak intensity and then a distance extrapolated by using a modeled 3D energy minimized molecular mechanics MK-2 conformation. Conformations were matched based off our interpretations; however, more sophisticated methods need to be executed in the future to further confirm our suggested conformations.

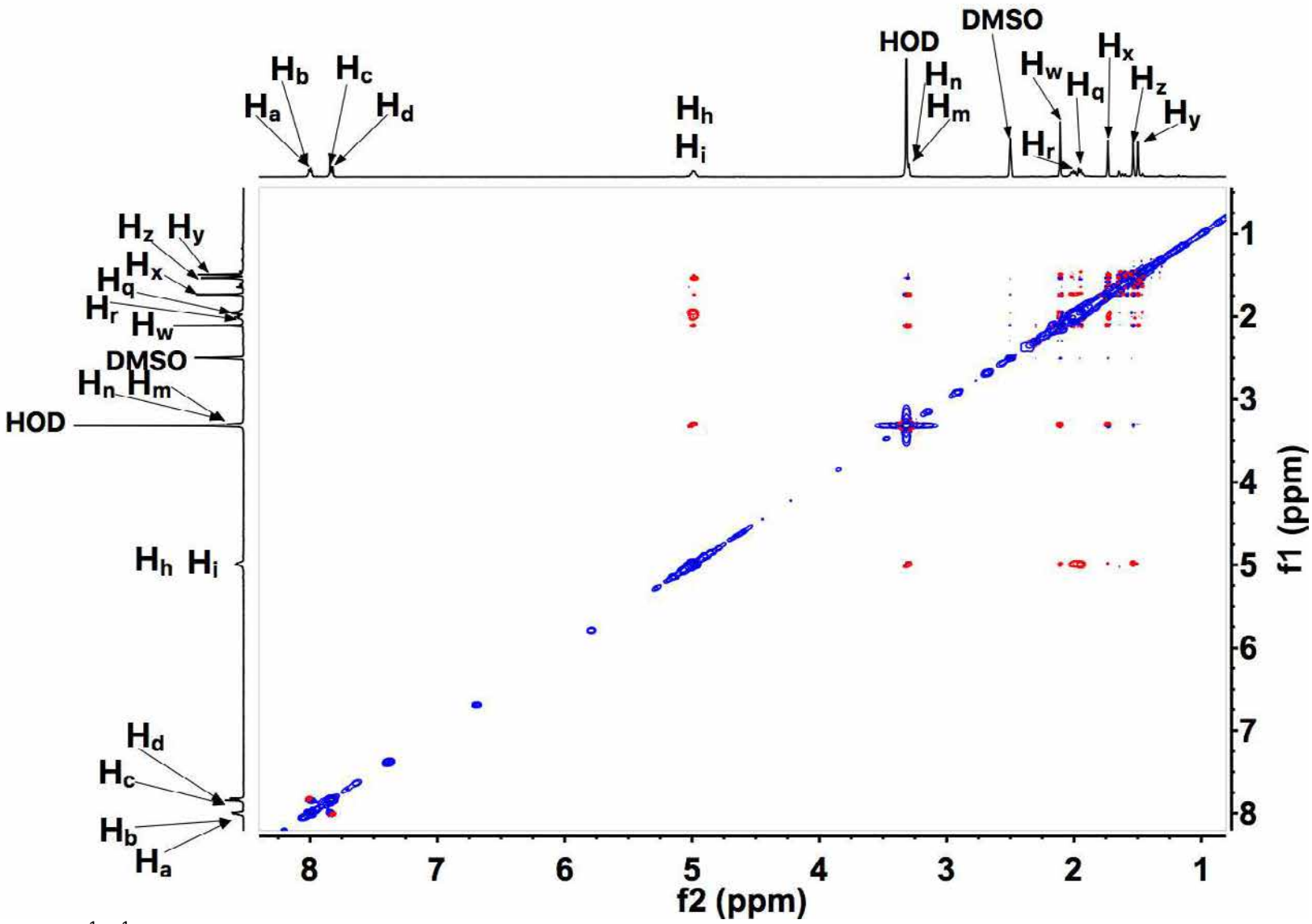

Figure A3.1. ^{1}H-^{1}H 2D NOESY NMR (400 MHz) spectrum of 20 mM MK-2 at 26 °C in d_6-DMSO. A standard NOESY pulse sequence was used consisting of 256 transients with 16 scans in the f1 domain using a 500 ms mixing time and 1.5 sec relaxation delay.

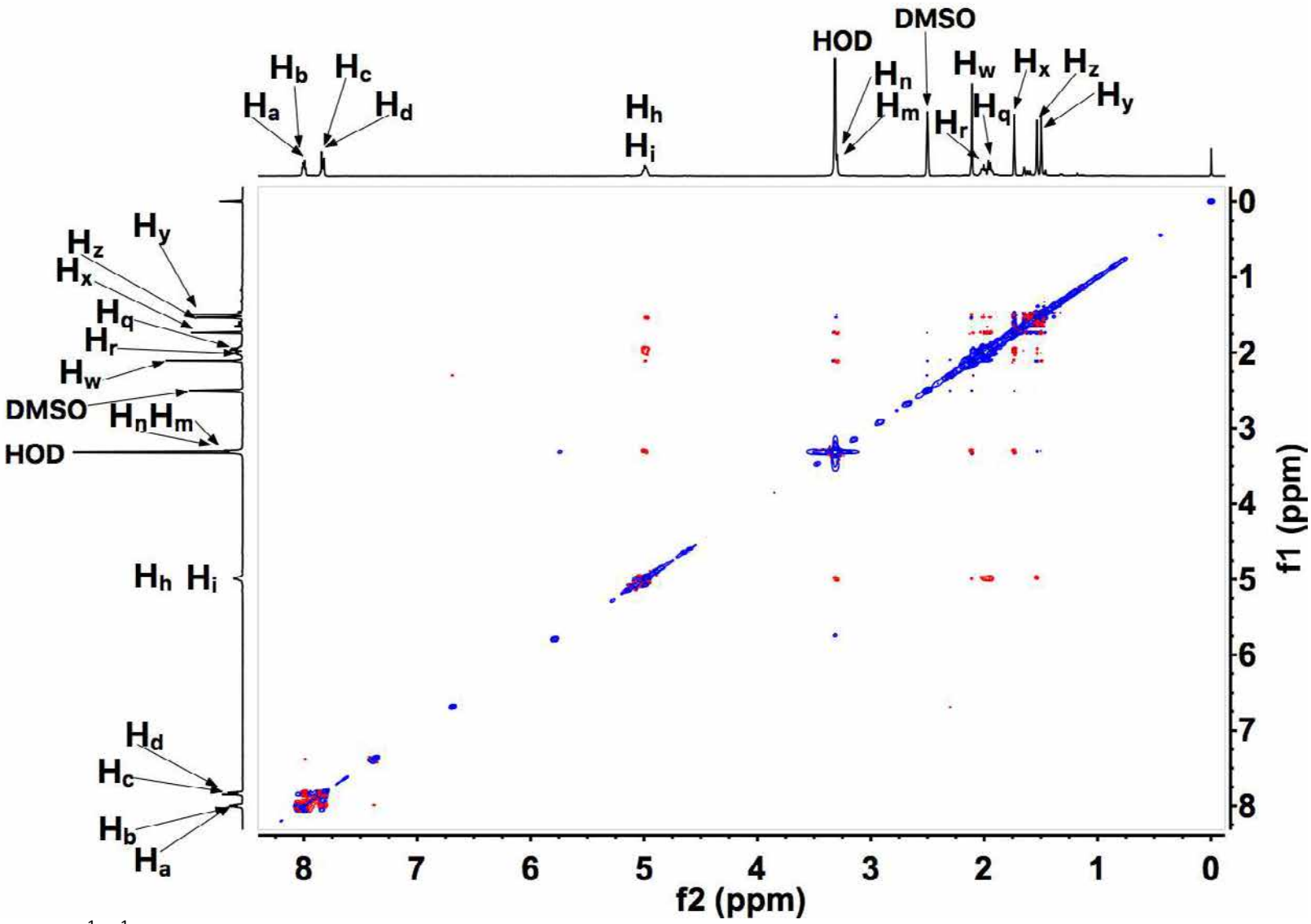

Figure A3.2. ^{1}H-^{1}H 2D ROESY NMR (400 MHz) spectrum of 20 mM MK-2 at 26 °C in d_6-DMSO. A standard ROESYAD pulse sequence was used consisting of 256 transients with 16 scans in the f1 domain using a 400 ms mixing time and 2.0 sec. relaxation delay.

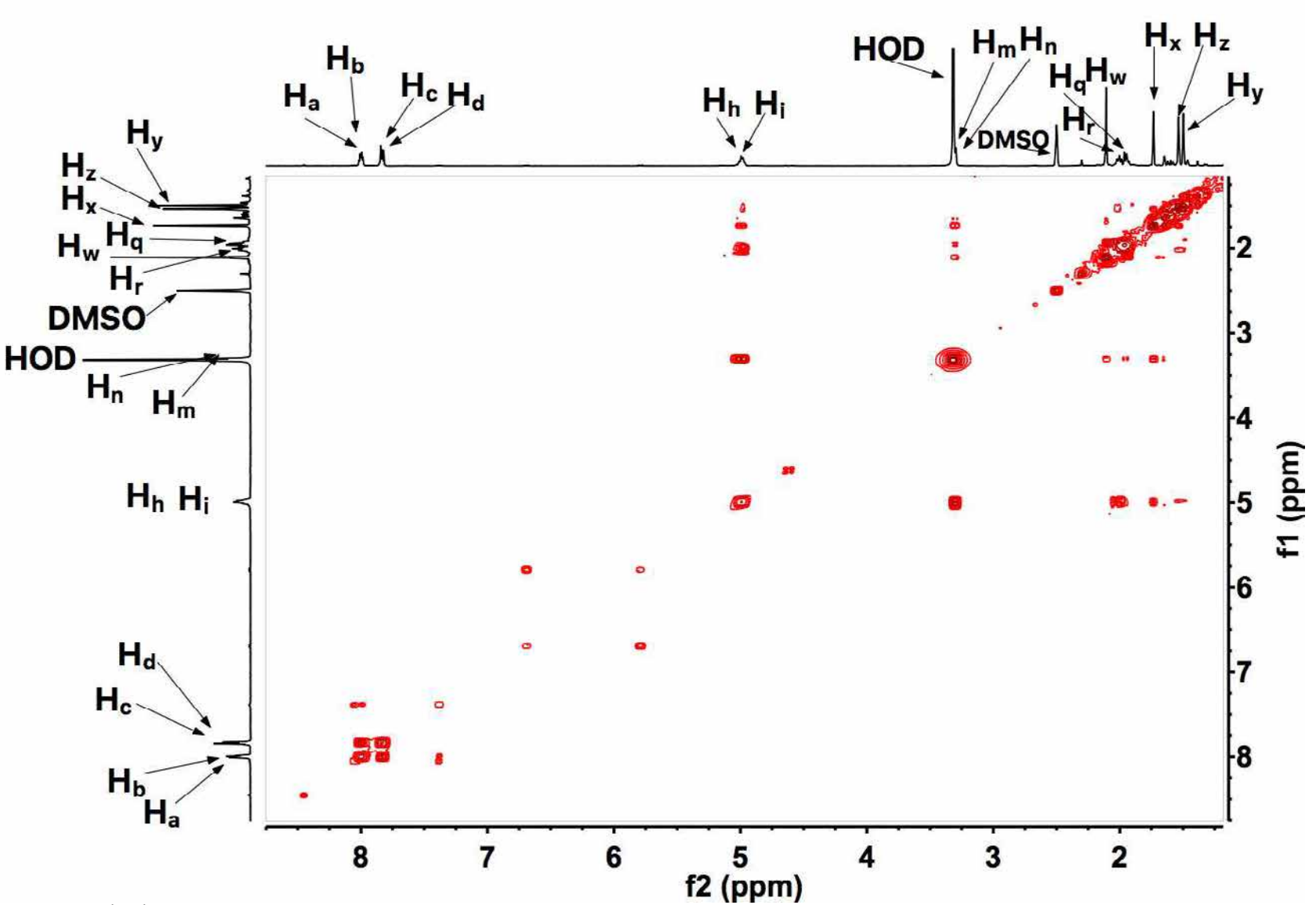

Figure A3.3. ^{1}H-^{1}H 2D gCOSY NMR (400 MHz) spectrum of MK-2 in d_6-DMSO at 26 °C. A standard gCOSY pulse sequence was used consisting of 200 t1 increments with 8 scans per t1 increment.

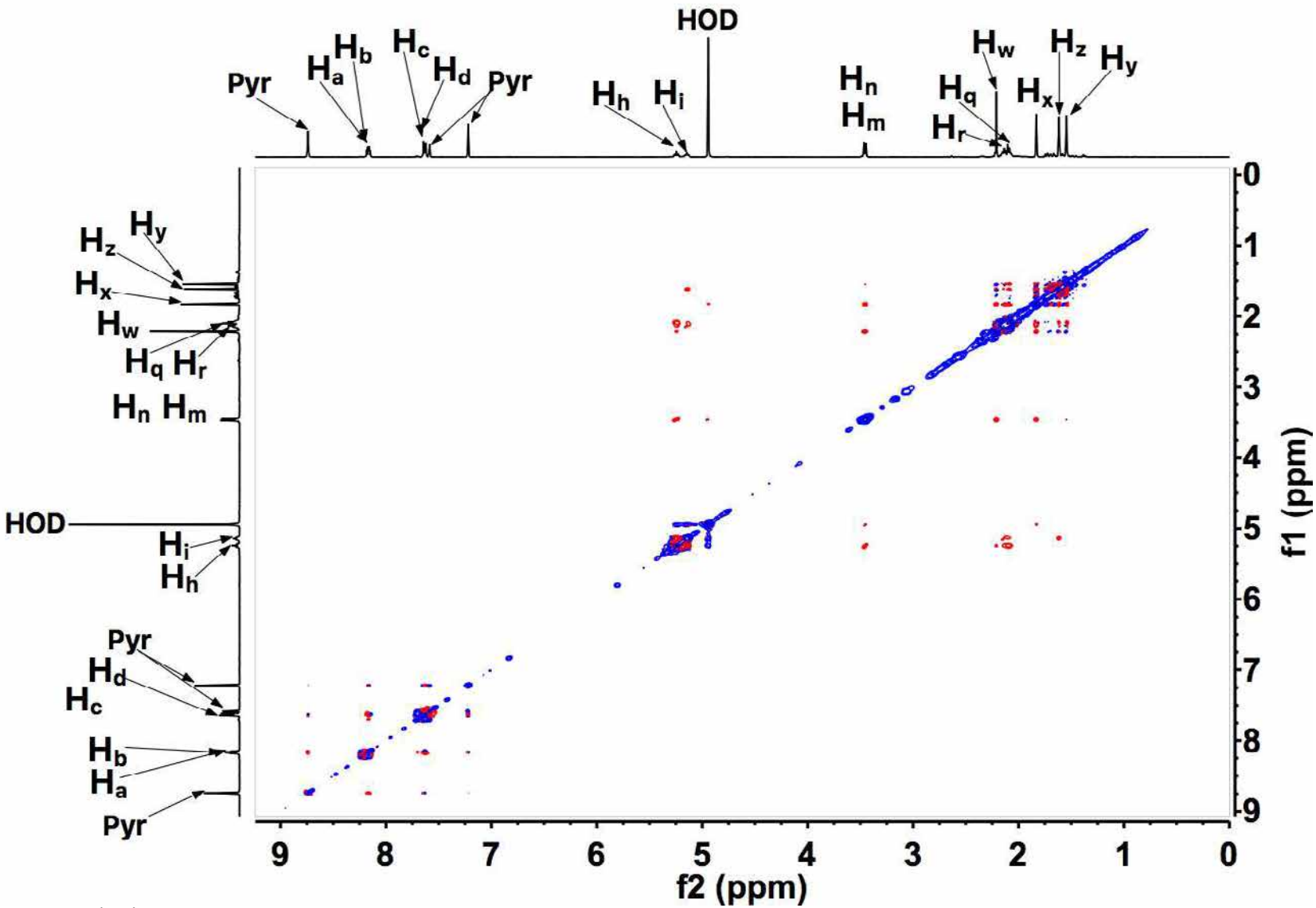

Figure A3.4. ^{1}H-^{1}H 2D NOESY NMR (400 MHz) spectrum of 20 mM MK-2 at 26 °C in d_5-pyridine. A standard NOESY pulse sequence was used consisting of 200 transients with 16 scans in the f1 domain using a 500 ms mixing time and 1.5 sec relaxation delay.

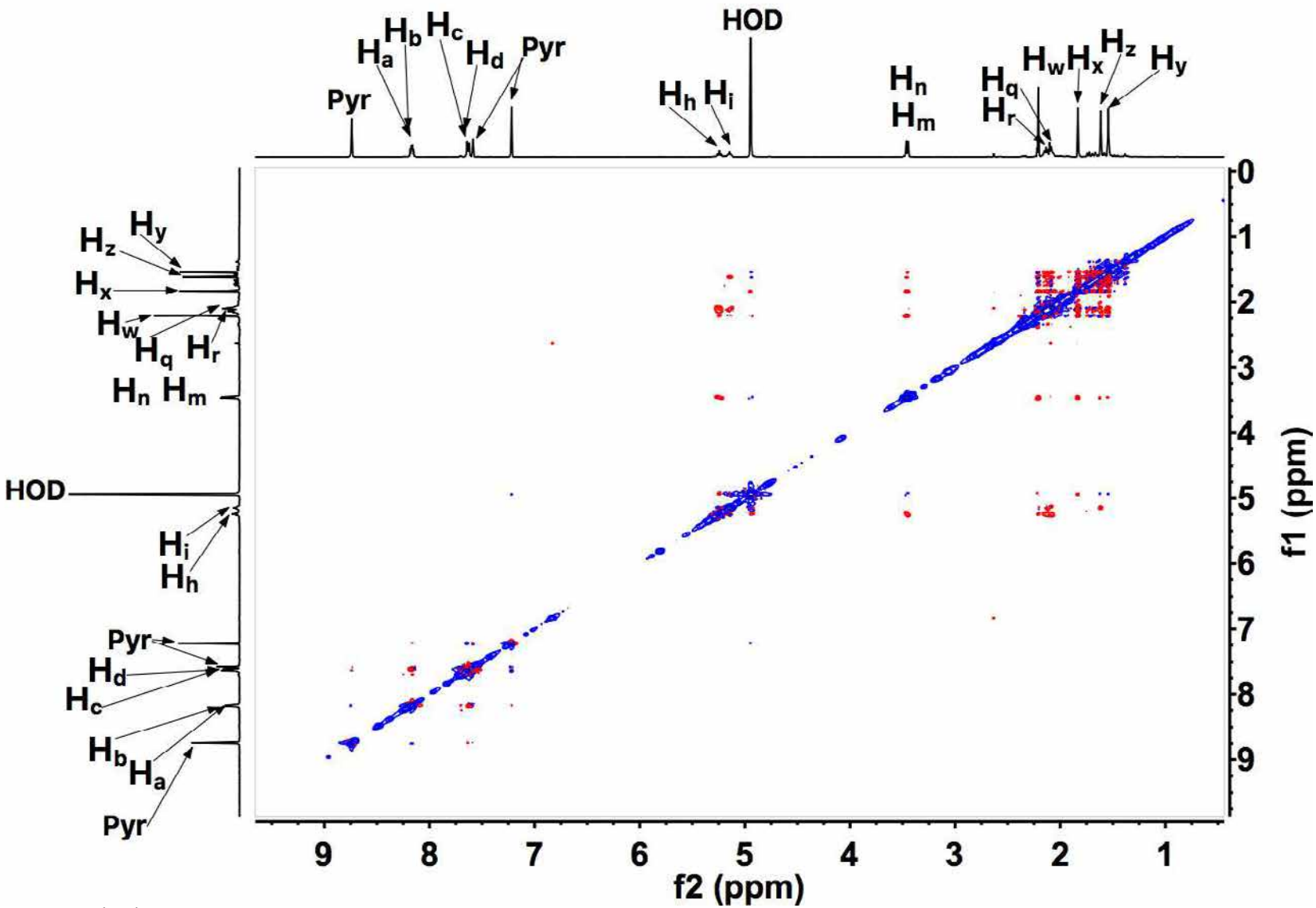

Figure A3.5. ^{1}H-^{1}H 2D ROESY NMR (400 MHz) spectrum of 20 mM MK-2 at 26 °C in d_5-pyridine. A standard ROESYAD pulse sequence was used consisting of 200 transients with 16 scans in the f1 domain using a 400 ms mixing time and 2.0 sec. relaxation delay.

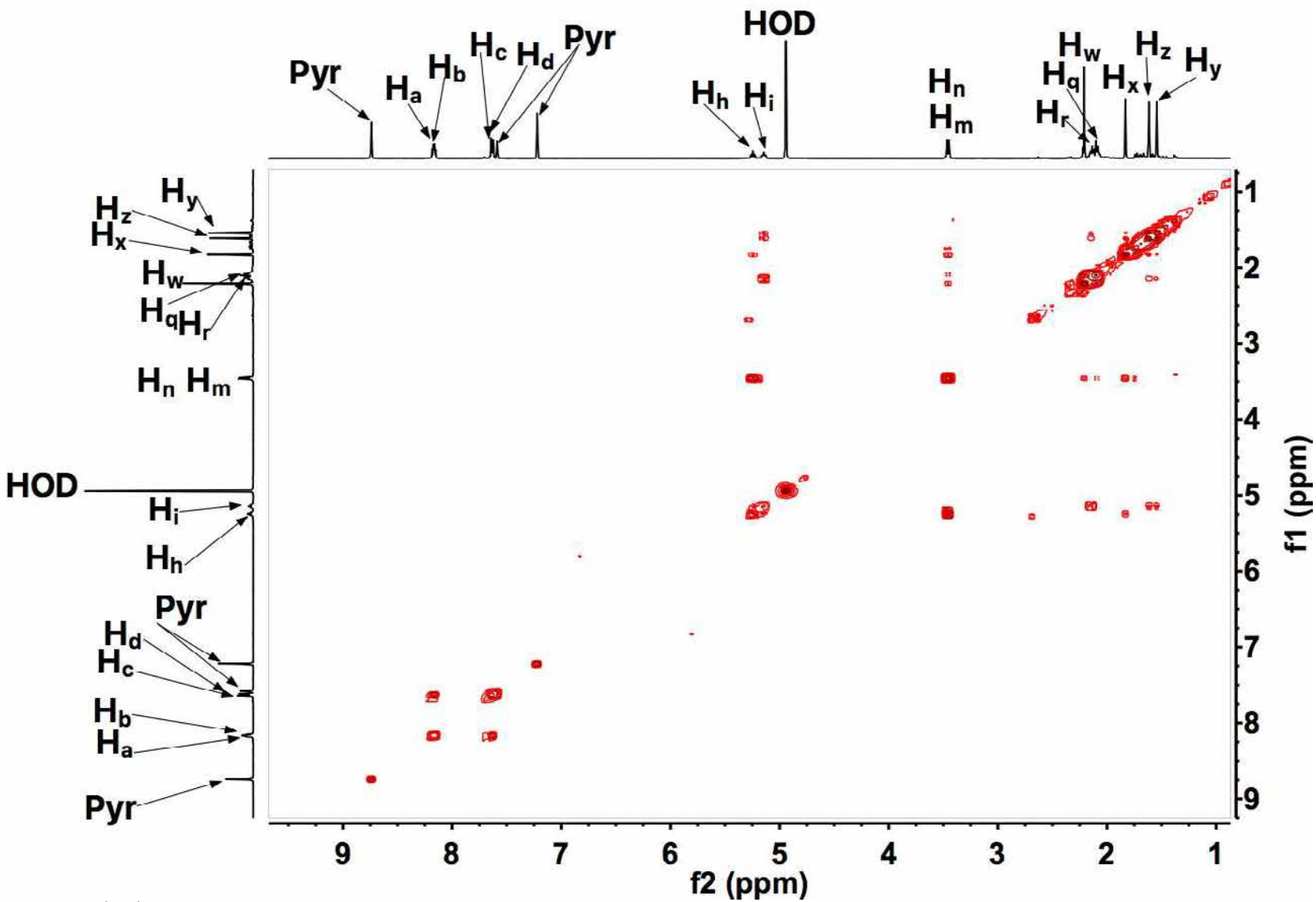

Figure A3.6. ^{1}H-^{1}H 2D gCOSY NMR (400 MHz) spectrum of 20 mM MK-2 in d_5-pyridine at 26 °C. A standard gCOSY pulse sequence was used consisting of 200 t1 increments with 8 scans per t1 increment.

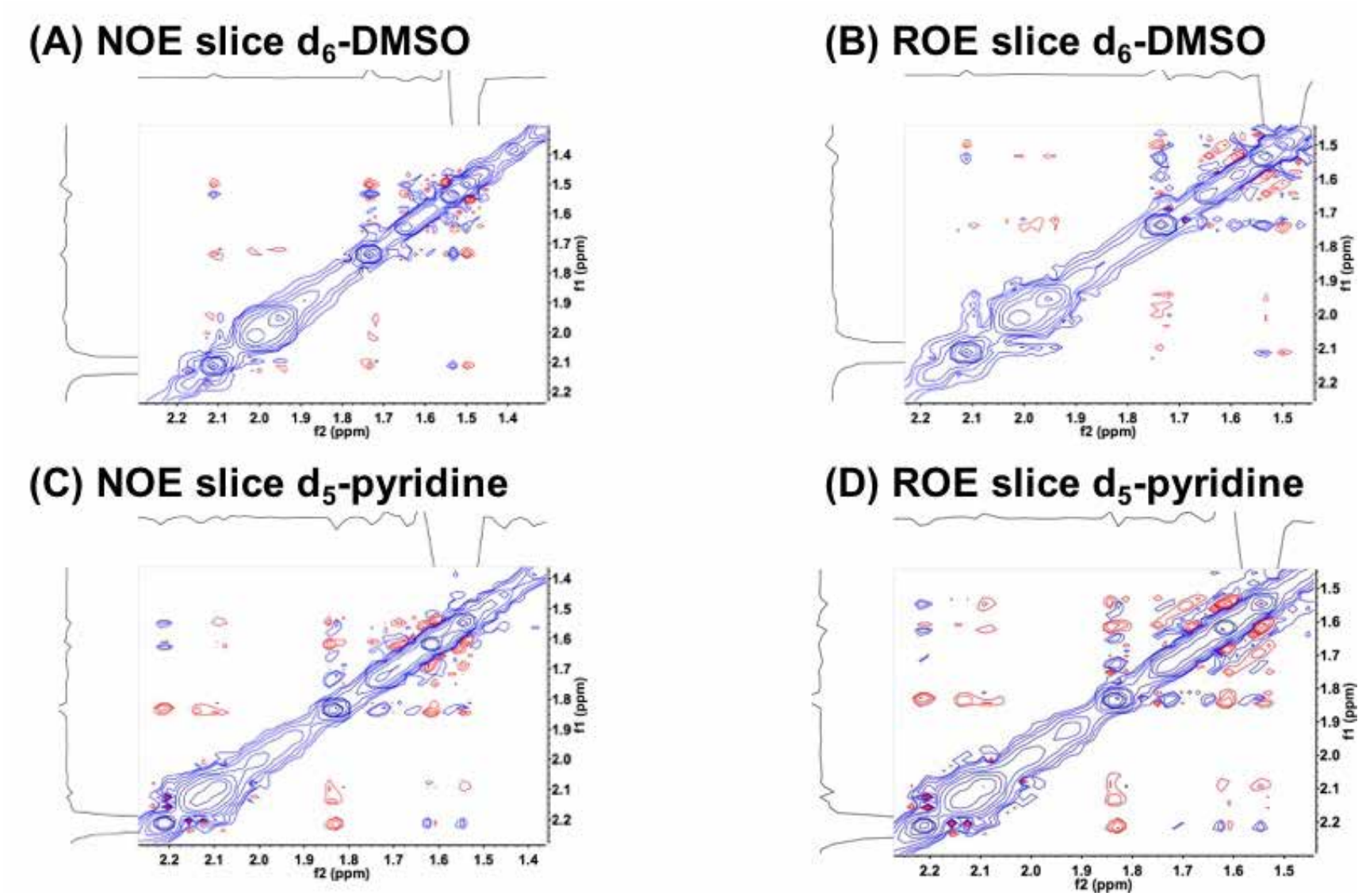

Figure A3.7. NOE/ROE slices for MK-2 correlation H_w to H_y. (A) NOE slice for MK-2 correlation H_w to H_y in d_6-DMSO, (B) ROE slice for MK-2 correlation H_w to H_y in d_6-DMSO, (C) NOE slice for MK-2 correlation H_w to H_y in d_5-pyridine, (D) ROE slice for MK-2 correlation H_w to H_y in d_5-pyridine.

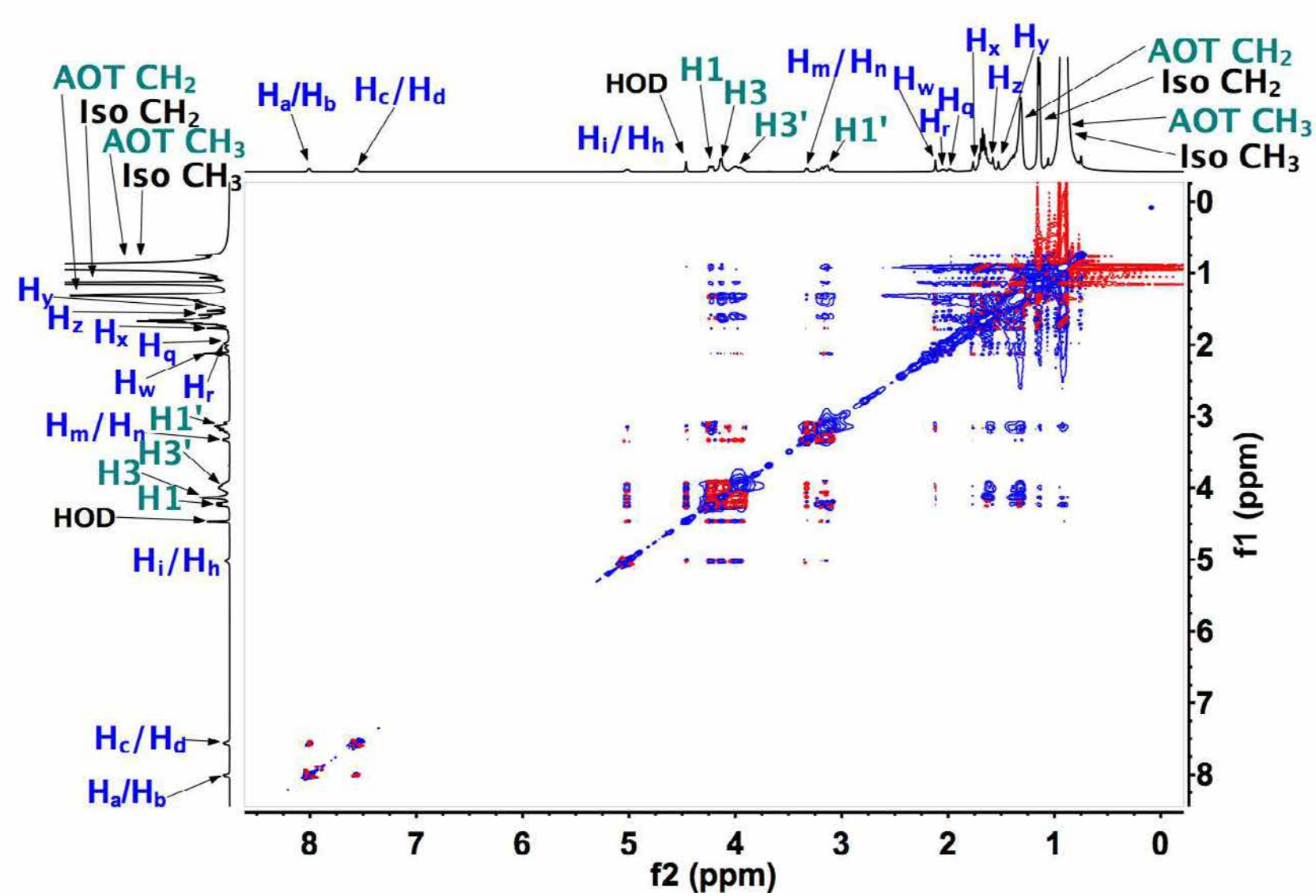

Figure A3.8. ^{1}H-^{1}H 2D NOESY NMR (400 MHz) spectrum of 100 mM MK-2 in w_0 12 reverse micelle at 26 °C. A standard NOESY pulse sequence was used consisting of 256 transients with 16 scans in the f1 domain using a 200 ms mixing time and 1.5 sec. relaxation delay.

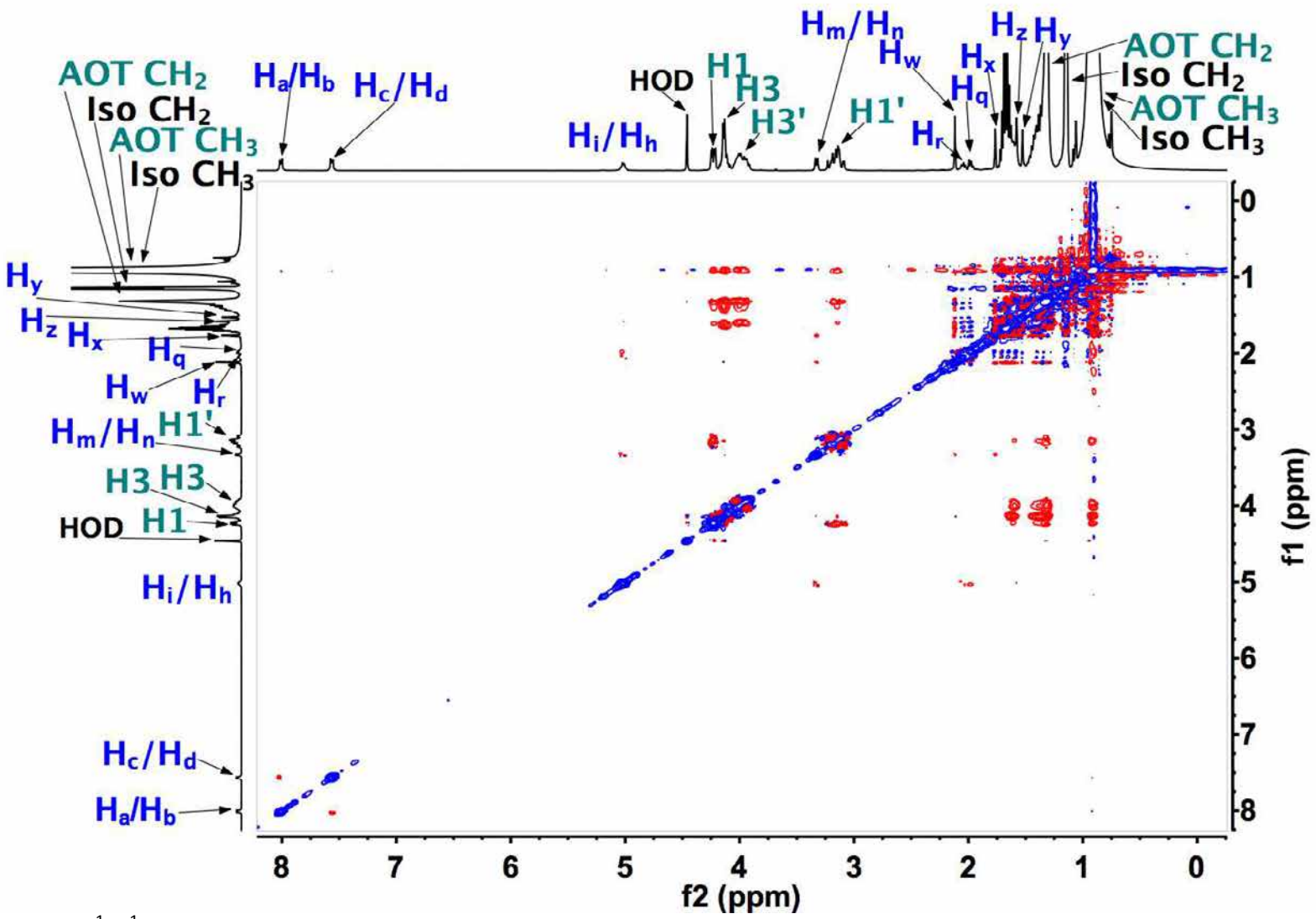

Figure A3.9. ^{1}H-^{1}H 2D ROESYAD NMR (400 MHz) spectrum of 100 mM MK-2 in w_0 12 reverse micelle at 26 °C. A standard ROESY pulse sequence was used consisting of 256 transients with 16 scans in the f1 domain using a 200 ms mixing time and 2.0 sec. relaxation delay.

Molecular Mechanics: MK-2 Conformational Analysis, Energies, and Hydrogen Distances.

Conformational analysis methods. These calculations were done to provide visual aids to help interpret the NMR results. Specifically, calculations were done to characterize the local minima with parameters similar to that obtained by the solution NMR studies. All the conformations (Figure A3.10) were constructed by drawing the molecule and rotating bonds until a desired conformation was obtained (except for conformation C). An energy minimization was then carried out to obtain a conformation with realistic bond lengths and angles. Finally, a molecular mechanics energy calculation was done to determine if the resulting conformation had similar stability as the local minima obtained. Conformation C was obtained by drawing an extended conformation and then 10,000 iterations were run leading to a sampling of different parts of the energy surface for MK-2. These calculations were followed by an energy minimization and finally a Molecular Mechanics energy calculation. It is important to note that conformations A and B (in d_6-DMSO and d_5-pyridine, respectively) were generated and then the internuclear distances between 6-8 hydrogens (i.e. H_w-H_y, H_w-H_z, H_w-H_x, etc., see Table A3.1) were matched (i.e. bonds rotated to move selected hydrogen of interest closer or farther away until internuclear distance agreed with observed NOE or ROE intensity) to the interpreted NOE and ROE cross peak intensity observed from experiment. As seen in Table A3.1, the conformations in d_6-DMSO and d_5-pyridine differed in energy by less than 0.5 kcal/mol.

Table A3.1. Conformation energies of MK-2 and selected internuclear distances between hydrogens.

MK-2 Conformation	Energy (kcal/mol)	H_w-H_m [a] (Å)	H_w-H_n [a] (Å)	H_w-H_q [a] (Å)	H_w-H_r [a] (Å)	H_w-H_y [a] (Å)	H_w-H_z [a] (Å)	H_w-H_x [a] (Å)	H_w-H_h [a] (Å)	H_w-H_i [a] (Å)
(A) DMSO	66.8	3.7	2.2	4.7	5.9	2.6	4.8	2.5	4.1	6.5
(B) Pyridine	66.7	3.5	2.0	5.4	6.6	6.1	7.0	2.7	4.7	7.1
(C) Representative low energy folded	60.2	3.7	2.1	5.5	4.9	2.6	4.5	2.3		
(D) Extended chain conformation	83.5	3.6	4.0	3.5	5.8	8.3	7.9	5.4	2.0	5.5
(E) Extended chain rotated up	83.1	2.2	2.5	6.6	7.5	10.0	11.4	4.0		
(F) Extended chain out of quinone plane out of the board	78.0	2.6	4.0	4.8	6.5	9.0	9.5	5.5		
(G) Extended chain out of quinone plane into the board	77.7	2.3	3.8	5.0	6.7	9.2	9.5	4.1		
(H) Bent extended chain	80.3	4.0	3.6	5.4	6.4	8.3	9.5	3.5		
MK-2 conformation inside RM interface	63.5	3.7	2.2	4.6	5.6	4.2	4.0	2.7		

[a]All internuclear distances were determined using the closest hydrogens. For example, the closest H_w hydrogen was used to determine the distance to the closest H_q hydrogen.

Supplemental Conformational Analysis. The following discussion relating to the details of the U-shape was omitted from the main paper due to space constraints. It is included here for the readers interested in more details. When starting from an energy minimized extended planar conformation of MK-2, kinks in the isoprenyl chain were observed in as little as 200 iterations and folding of the isoprenyl chain was observed in as few as 500 iterations in most simulations. The folded, U-shaped segment in the isoprenyl chain of MK-2 contains at least one g^+g^- conformation. MK-2's alkyl chain carbons, C2-C6, distance was 3.5 Å in d_6-DMSO. Conformational analysis of pentane is a logical comparison as it takes five carbons in the isoprenyl chain of MK-2 to create the U-shaped fold observed in experiment and computation. Pentane's C1-C5 g^+g^- conformation distance was reported to be 3.42 Å, whereas the g^+g^+ conformation was 3.72 Å (and for comparison the tg conformation distance was 4.57 Å).[1] The g^+g^- conformation in pentane is energetically unfavorable due to the destabilizing "pentane effect."[1] This destabilizing effect describes the steric hindrance present in a conformation with *gauche* interactions, where one of

the hydrogens distance between the ends of the chain is 2.24 Å in pentane. This distance is minimized in MK-2 due to the presence of the two double bonds in the isoprenyl chain. These double bonds decrease the amount of hydrogen atoms present in the chain and increases the end to end distance between the two alkene hydrogens. Furthermore, favorable π-π stacking within the alkenes in the isoprenyl chain may also stabilize the g^+g^- conformation more with a larger favorable enthalpy contribution over entropic considerations. It was demonstrated using microwave spectroscopy and computational calculations for the conformational isomers of 1,6-heptadiyne that the presence of π bonds favors the molecule acquiring the *gauche* conformations that are disfavored by steric repulsion in alkanes; this observation was attributed to a stabilizing CH/π interaction (mostly dispersive in nature rather than electrostatic).[2] In MK-2, two possibilities for this type of stabilization occur in a folded isoprenyl chain conformation because of the presence of the two alkene units.

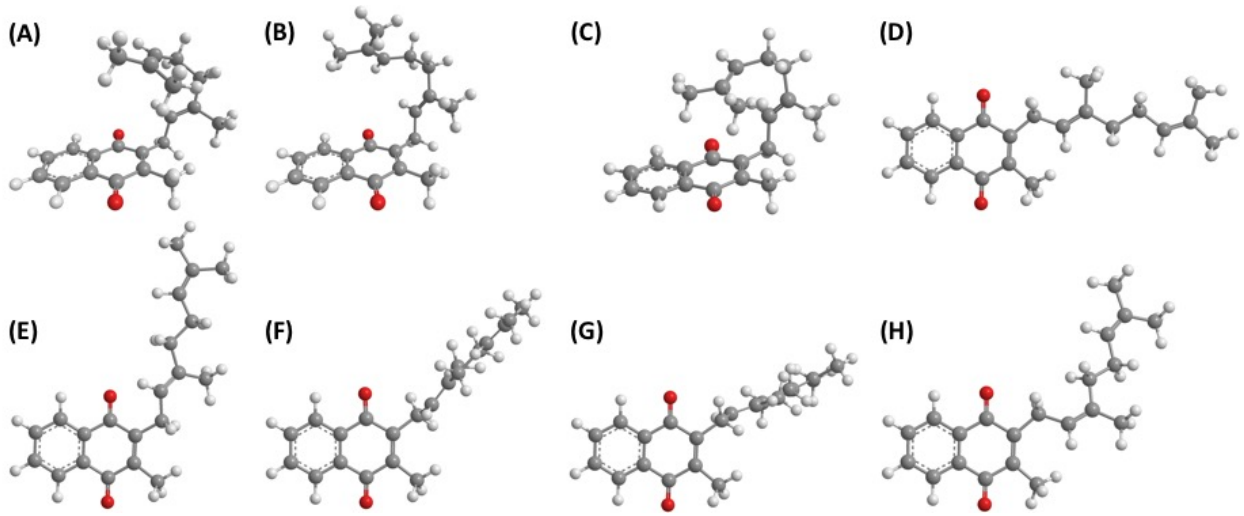

Figure A3.10. MK-2 conformations generated using MMFF94 calculations in the gas phase at 300° K. (A) MK-2 conformation in d_6-DMSO determined from NOESY and ROESY spectrum (66.8 kcal/mol, and internuclear distance H_w-H_y: 2.6 Å), (B) Potential MK-2 conformation in d_5-pyridine consistent with NOESY and ROESY spectrum (66.7 kcal/mol, and internuclear distance H_w-H_y: 6.1 Å), (C) Low energy structure of MK-2 found using 10,000 iterations and energy minimization (60.2 kcal/mol, and internuclear distance H_w-H_y: 2.6 Å), (D) Commonly drawn MK conformation in literature with MK-2 planar and chain extended (83.5 kcal/mol, and internuclear distance H_w-H_y: 7.9 Å), (E) Planar MK-2 conformation with extended chain extended up (83.1 kcal/mol, and internuclear distance H_w-H_y: 11.4 Å), (F) MK-2 conformation with extended chain out of quinone plane out of the plane of paper (78.0 kcal/mol, and internuclear distance H_w-H_y: 10.0 Å), (G) MK-2 conformation with extended chain out of quinone plane into the plane of paper (77.7 kcal/mol, and internuclear distance H_w-H_y: 9.9 Å), (H) MK-2 conformation with bent extended chain (80.3 kcal/mol, and internuclear distance H_w-H_y: 8.3 Å).

Refer to the published manuscript[3] and corresponding supporting information for Electrochemistry Experimental, Methods, and Data.

Refer to the published manuscript[3] and corresponding supporting information for Langmuir Monolayer Studies Experimental, Methods, and Data.

References

1. Klauda, J. B.; Brooks, B. R., An Ab Initio Study on the Torsional Surface of Alkanes and Its Effect on Molecular Simulations of Alkanes and a DPPC Bilayer. *J. Phys. Chem. B* **2005,** *109*, 5300-5311.
2. Restrepo, A. A.; Bohn, R. K., Alkyl Chians with CN and CCH Substituents Prefer *gauche* Conformations. *J. Mol. Struct.* **2007,** *833*, 189-196.
3. Koehn, J. T.; Magallanes, E. S.; Peters, B. J.; Beuning, C. N.; Haase, A. A.; Zhu, M. J.; Rithner, C. D.; Crick, D. C.; Crans, D. C., A Synthetic Isoprenoid Lipoquinone, Menaquinone-2, Adopts a Folded Conformation in Solution and at a Model Membrane Interface. *J. Org. Chem.* **2018,** *83*, 275-288.

Appendix IV: Supporting Information for Chapter 4

Further Information for Processing of 2D NMR Spectra. Spectra were processed using MestReNova version 10.0.1. Details of experiments are provided in representative experimental sections and captions of figures. Spectra were collected both at 500 MHz and 400 MHz giving consistent results; however, all the data presented herein was at 400 MHz (unless otherwise noted) due to less noise in the spectrum. The interpretations of distances from NOE and ROE data were based off qualitative examination of observed cross peak intensity and then a distance extrapolated by using a modeled 3D energy minimized molecular mechanics MK-1 or MK-1(H_2) conformation. Conformations were created based on our interpretations; however, more sophisticated methods need to be executed in the future to further confirm our suggested conformations.

^{1}H-^{1}H 2D NOESY and ^{1}H-^{1}H 2D ROESY NMR spectra collected in organic solutions were processed using MestReNova version 10.0.1. A Sine Square 90° weighting function was applied in the f2 (t2) dimension and a Sine Bell 90° weighting function was applied in the f1 (t1) dimension. The spectra were then phased and a Bernstein Polynomial Fit was applied with a polynomial order of 3 in both dimensions separately. Symmeterize->Cosy-like command was then applied to clean up the small amount of t1 noise in the spectra. We were cautious and the use of this command did not introduce artifacts and did not seem to distort the cross peaks in the spectra as the background noise was not strong but was necessary as t1 noise overlapped cross peaks in most spectra. Spectra worked up using simple processing were compared to spectra worked up using simple processing plus the symmeterize command and the cross peaks appeared identical except the t1 noise was removed thus making the spectra much more interpretable. The symmeterize command or function replaces the larger of two symmetrical points with a point that has the same magnitude as the smaller one (as stated in the MestReNova 2015 MESTRELAB Research manual on pgs. 207-208). Unsymmetrically positioned noise and artifacts are removed by this command but symmetrical noise or artifacts will be preserved. Most importantly, the complementary experiments of ^{1}H-^{1}H 2D NOESY and ^{1}H-^{1}H 2D ROESY NMR spectra in organic solution produce the same results and agree with each other, demonstrating the spectra were processed reliably.

^{1}H-^{1}H 2D NOESY and ^{1}H-^{1}H 2D ROESY NMR spectra collected in reverse micelle solutions were processed using MestReNova version 10.0.1. These spectra are more complex and much more challenging to process compared to spectra in simple organic solutions. A Sine Square 90° and Gaussian weighting function was applied in the f2 (t2) dimension and a Gaussian weighting function was applied in the f1 (t1) dimension. We used these weighting functions as they appeared to produce the best signal/noise in the spectra. The spectra were then phased and a Bernstein Polynomial Fit was applied with a polynomial order of 3 in both dimensions separately. Symmeterize->Cosy-like was then applied to the spectra as the background noise in the 1-4.5 ppm range made the cross peaks undiscernible without applying this command. There are several internal controls that demonstrate the reverse micelle spectra were processed reliably. For

instance, lack of a cross peak between H_k and H_z, which agrees with expected results and the results from the organic solution spectra. Also, there is a cross peak observed between $H_{r/s}$ and H_z and not between $H_{r/s}$ and H_y (H_y is overshadowed by H4/H4' but a cross peak is not observed where one would expect one), which agrees with expected results and that observed in the organic solution spectra. Most importantly, the ^{1}H-^{1}H 2D NOESY and ^{1}H-^{1}H 2D ROESY NMR spectra in reverse micelles produce the same results and agree with each other, demonstrating the spectra were processed reliably.

Further Information on the Assignment of the MK-1 Terminal Methyl Hydrogens (H_y & H_z). The ambiguity in the hydrogen peak assignment for the terminal methyls on the isoprenyl side chain of MK-1 was clarified using ^{1}H-^{1}H 2D NOESY and ^{1}H-^{1}H 2D ROESY NMR. In all three solvents, a strong NOE/ROE cross peak (expected for a cis relationship) was observed between the alkene hydrogen, H_k, and the methyl singlet further up field, while a very weak or no cross peak (expected for a trans relationship) was observed between H_k and the methyl singlet further downfield. In addition, $H_{r/s}$ only interacts with the methyl singlet that is further downfield and not the methyl singlet that is further up field. This led to the determination that H_z is the methyl further downfield and H_y is the methyl further up field.

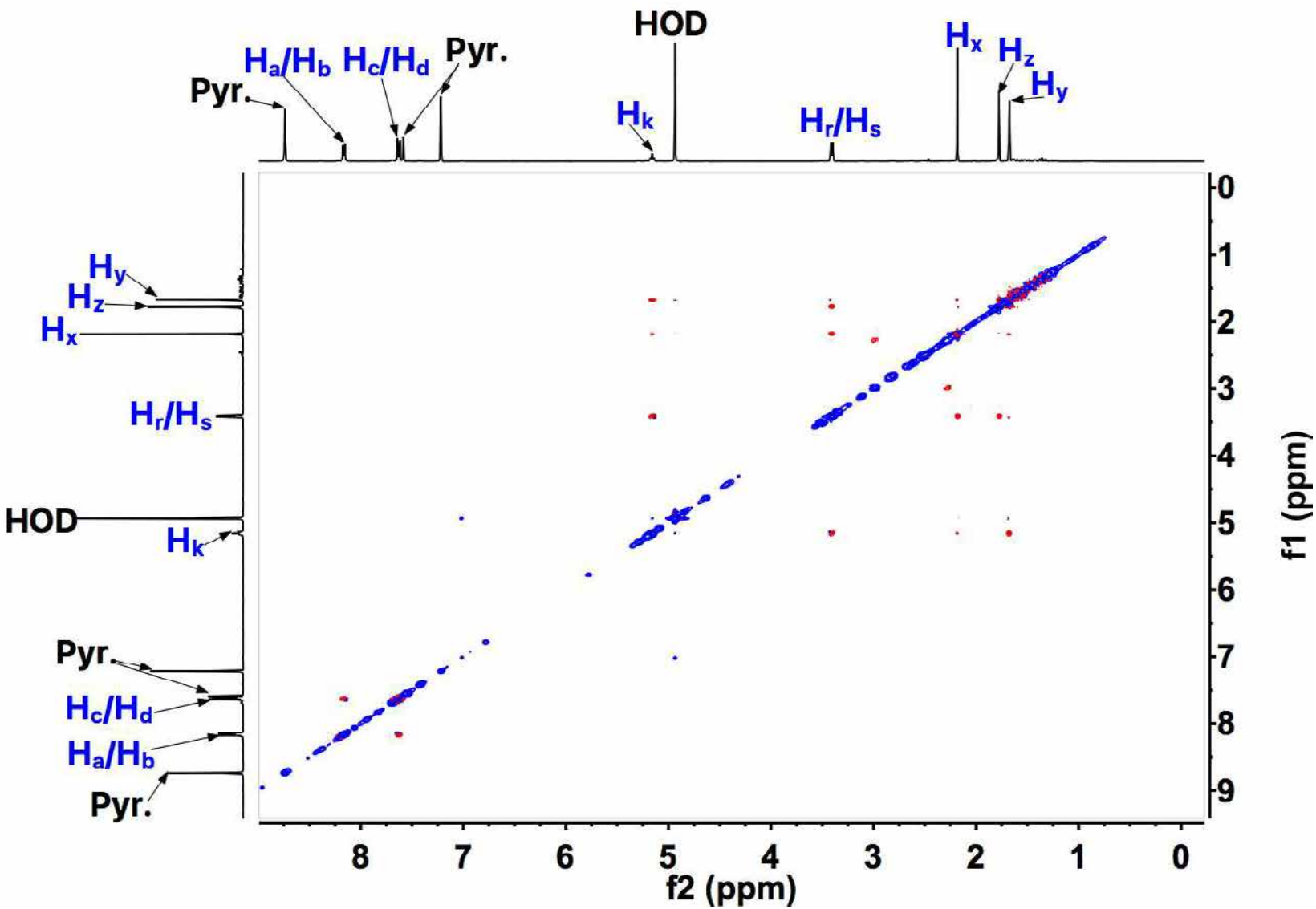

Figure A4.1: ^{1}H-^{1}H 2D NOESY NMR (400 MHz) spectrum of MK-1 in d_5-pyridine at 26 °C. A standard NOESY pulse sequence was used consisting of 256 transients with 16 scans in the f1 domain using a 500 ms mixing time and 1.5 sec. relaxation delay.

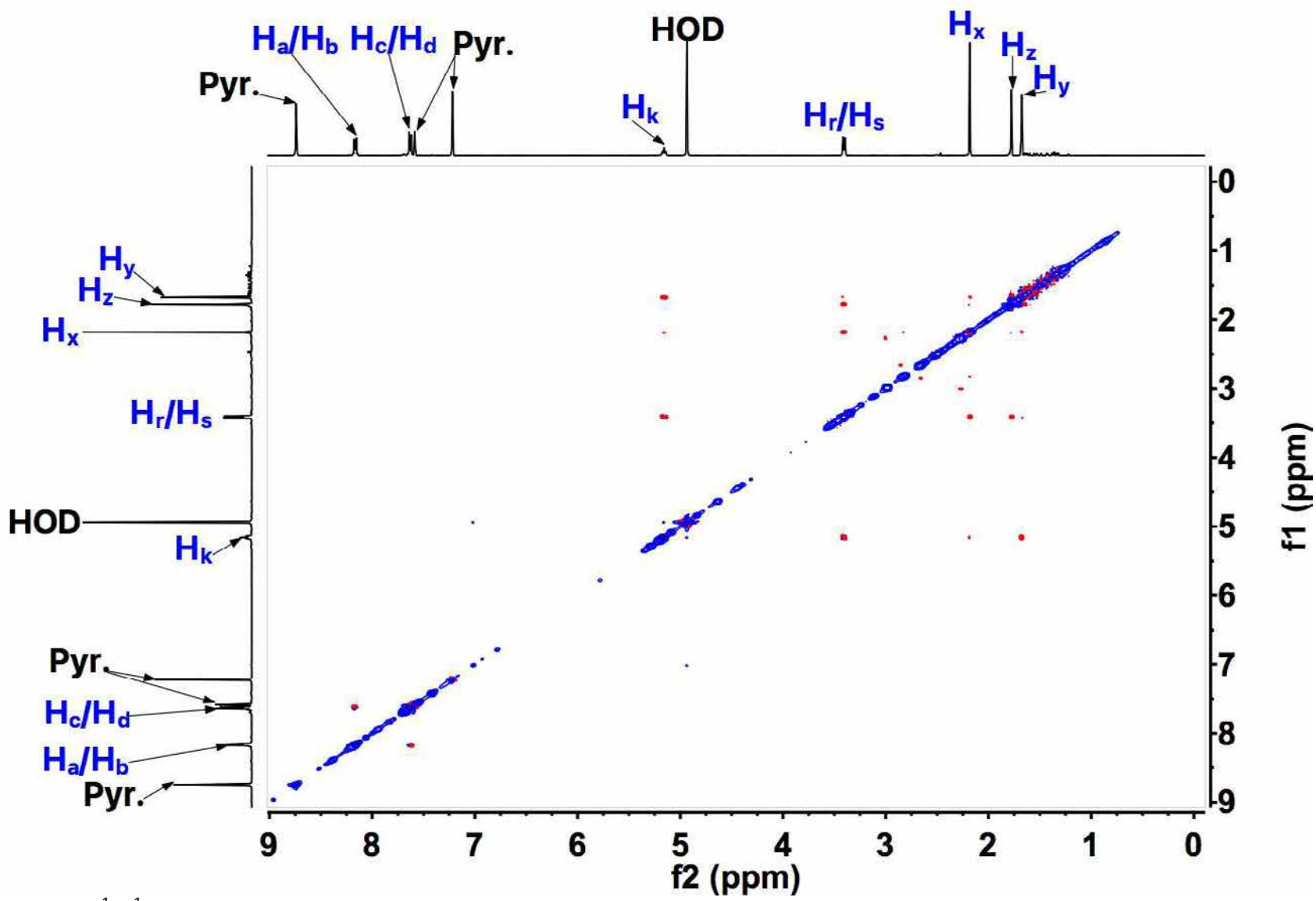

Figure A4.2: ^{1}H-^{1}H 2D ROESY NMR (400 MHz) spectrum of MK-1 in d_5-pyridine at 26 °C. A standard ROESYAD pulse sequence was used consisting of 256 transients with 16 scans in the f1 domain using a 400 ms mixing time and 2 sec. relaxation delay.

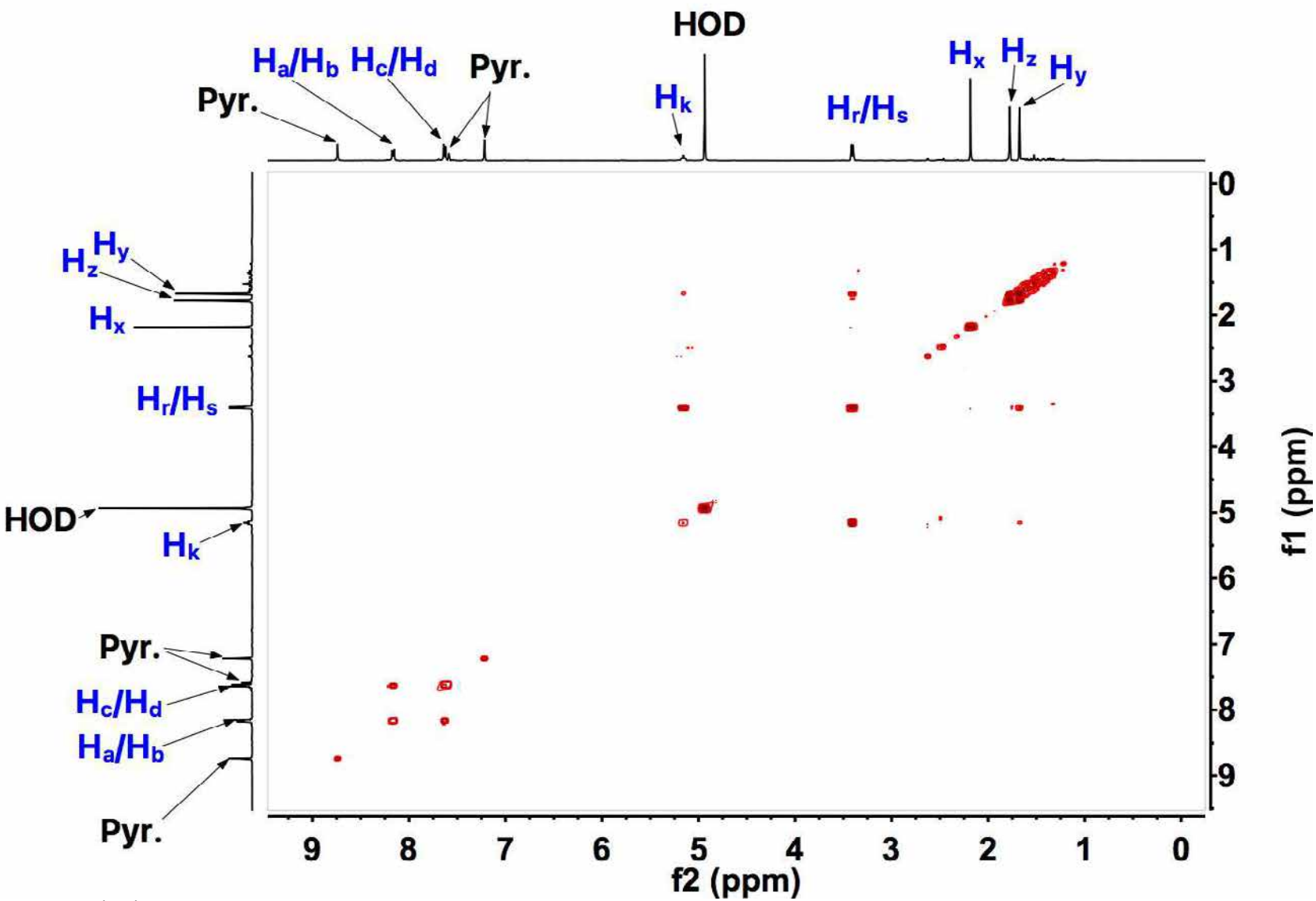

Figure A4.3: ^{1}H-^{1}H 2D gCOSY NMR (400 MHz) spectrum of MK-1 in d_5-pyridine at 26 °C. A standard gCOSY pulse sequence was used consisting of 200 t1 increments with 8 scans per t1 increment

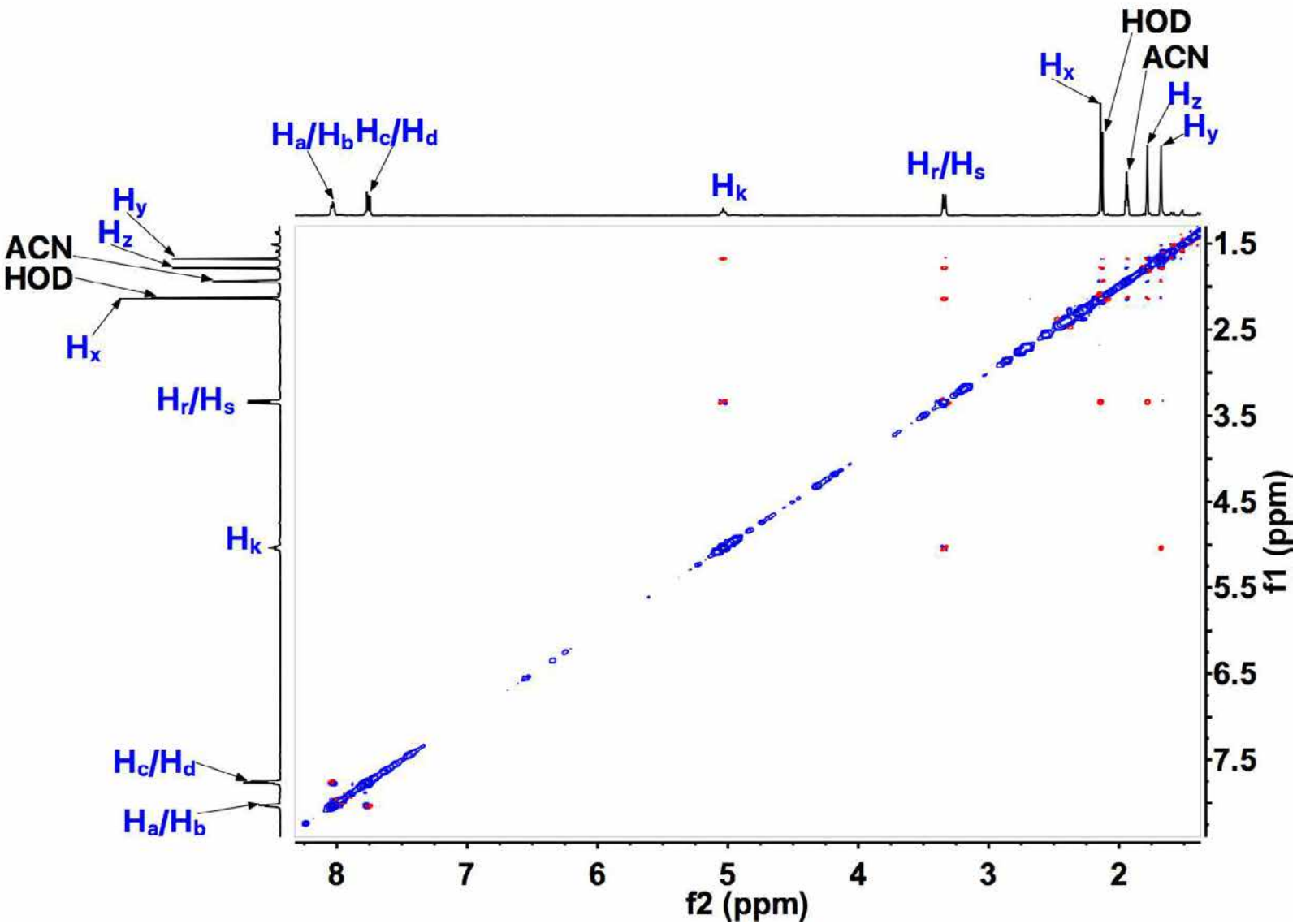

Figure A4.4: ^{1}H-^{1}H 2D NOESY NMR (400 MHz) spectrum of MK-1 in d_3-acetonitrile at 26 °C. A standard NOESY pulse sequence was used consisting of 256 transients with 16 scans in the f1 domain using a 500 ms mixing time and 1.5 sec. relaxation delay.

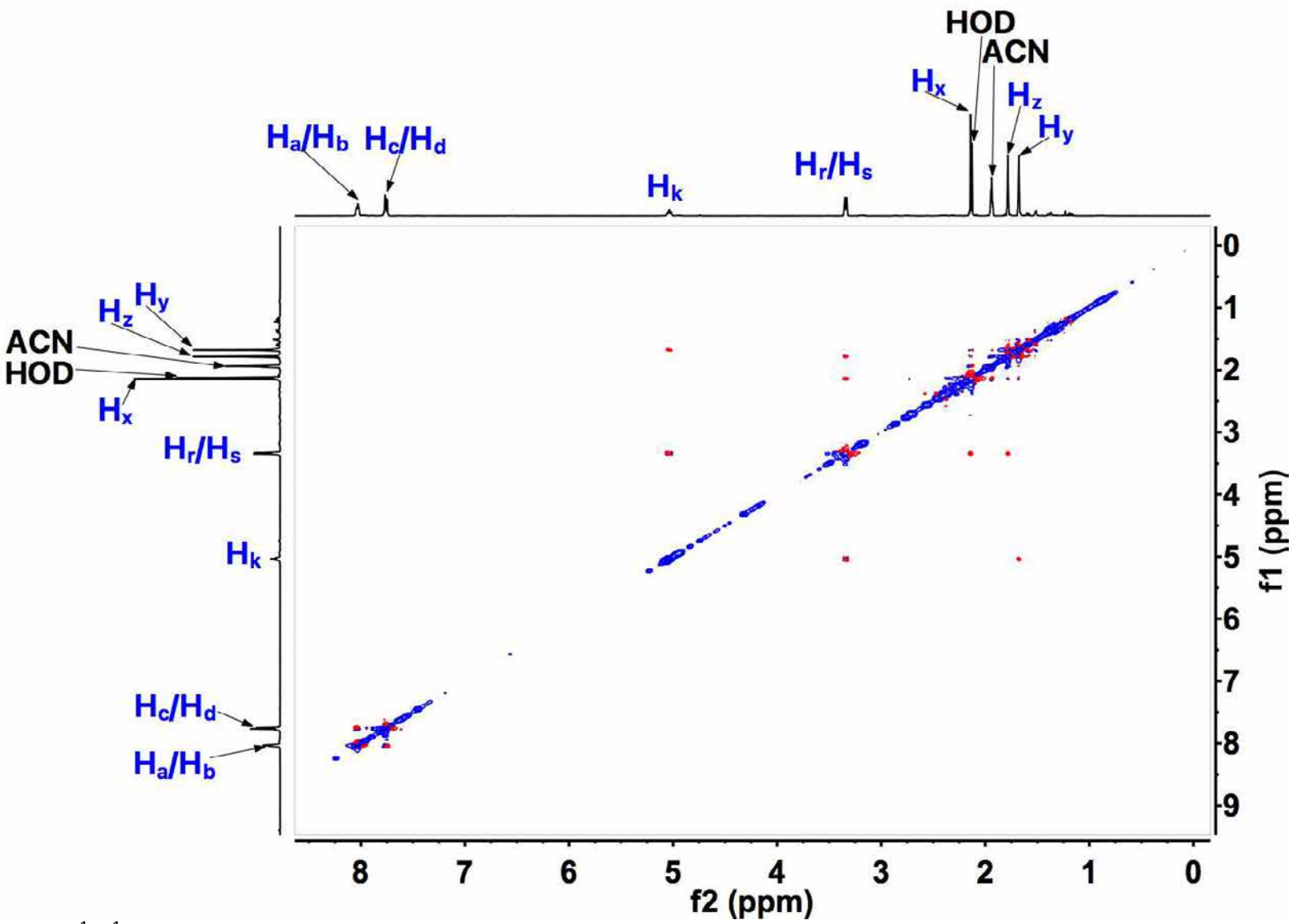

Figure A4.5: ^{1}H-^{1}H 2D ROESY NMR (400 MHz) spectrum of MK-1 in d_3-acetonitrile at 26 °C. A standard ROESYAD pulse sequence was used consisting of 256 transients with 16 scans in the f1 domain using a 400 ms mixing time and 2.0 sec. relaxation delay.

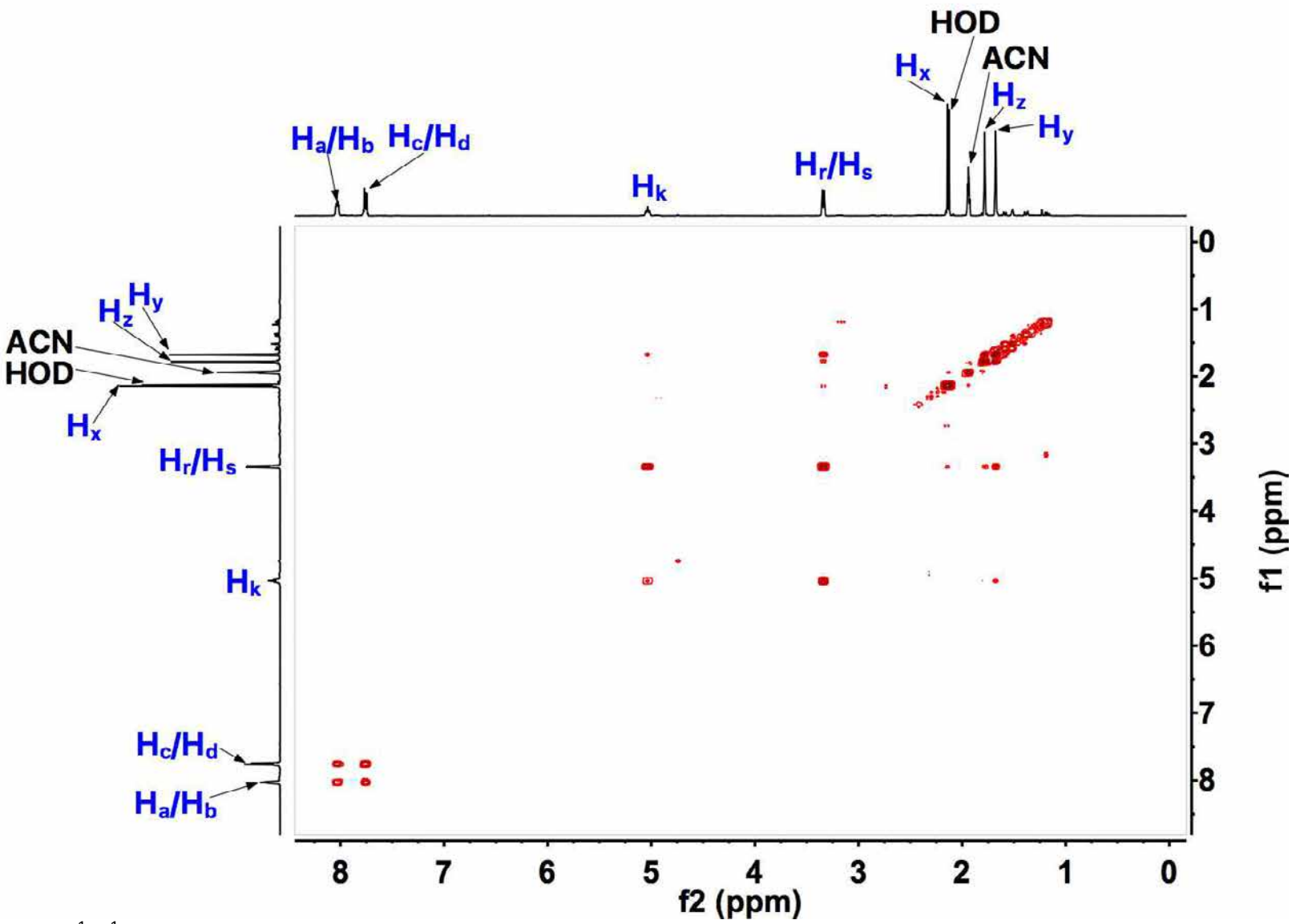

Figure A4.6: ^{1}H-^{1}H 2D gCOSY NMR (400 MHz) spectrum of MK-1 in d_3-acetonitrile at 26 °C. A standard gCOSY pulse sequence was used consisting of 200 t1 increments with 8 scans per t1 increment.

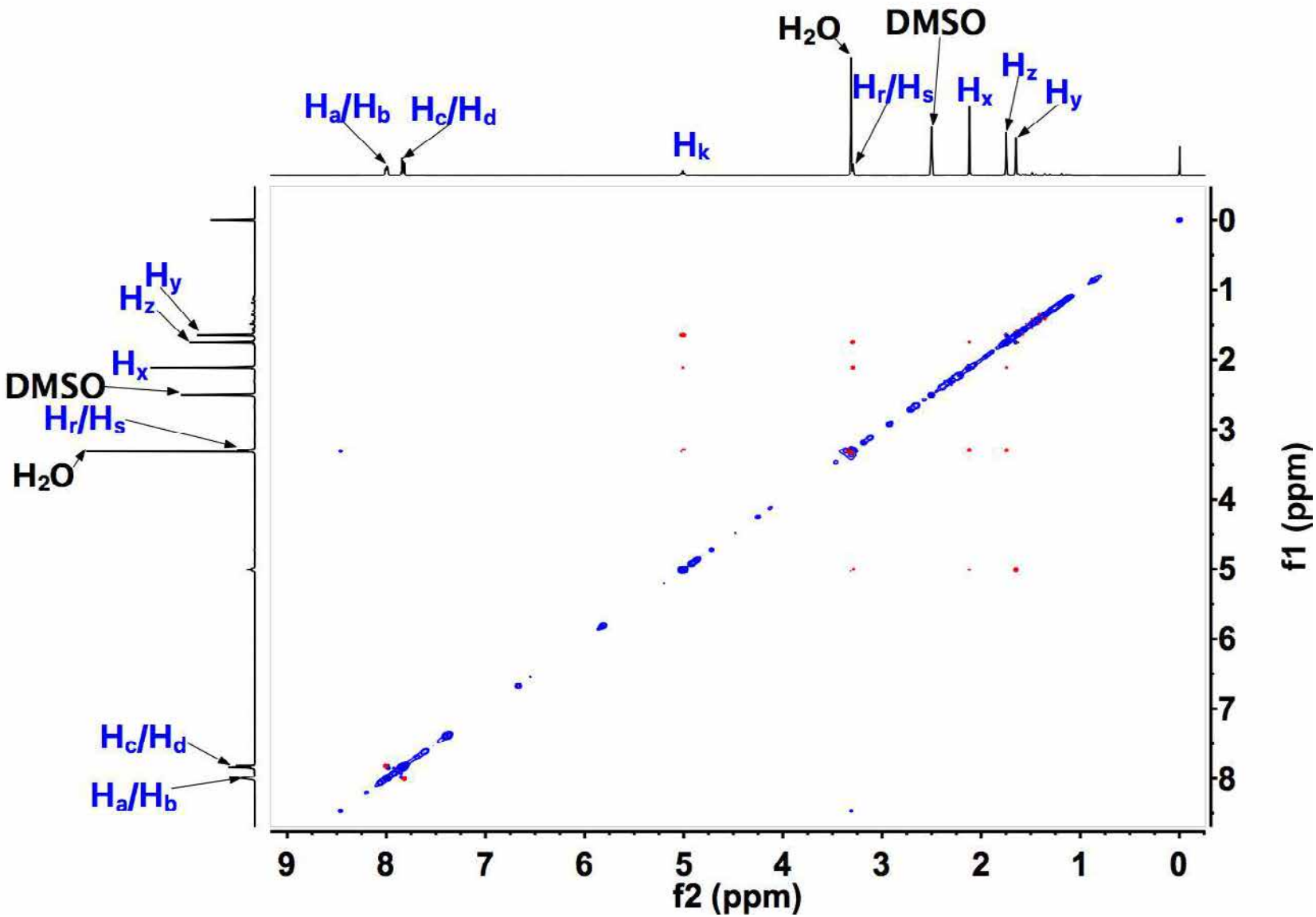

Figure A4.7: ^{1}H-^{1}H 2D NOESY NMR (400 MHz) spectrum of MK-1 in d_6-DMSO at 26 °C. A standard NOESY pulse sequence was used consisting of 256 transients with 16 scans in the f1 domain using a 500 ms mixing time and 1.5 sec. relaxation delay.

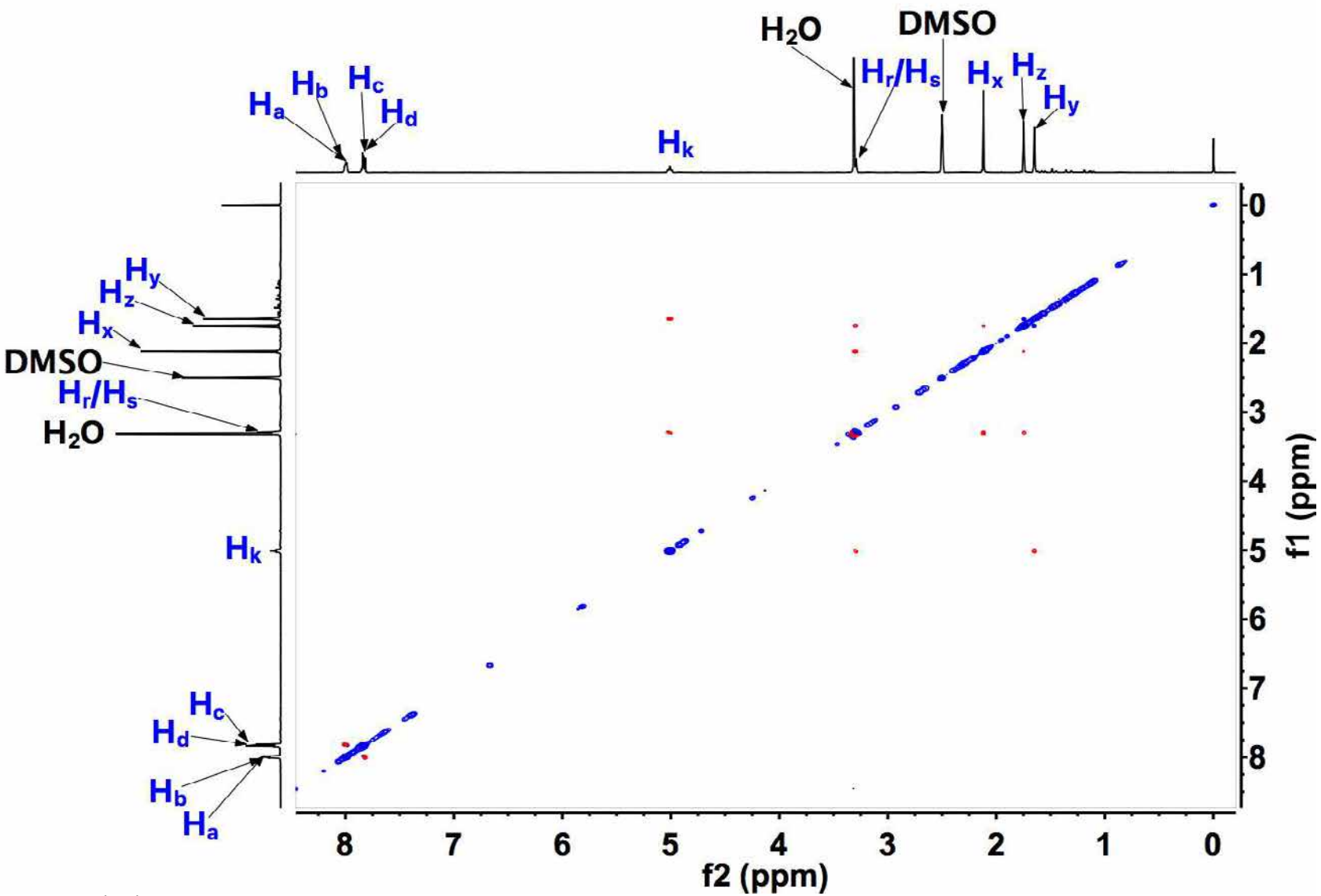

Figure A4.8: ^{1}H-^{1}H 2D ROESY NMR (400 MHz) spectrum of MK-1 at in d_6-DMSO at 26 °C. A standard ROESYAD pulse sequence was used consisting of 256 transients with 16 scans in the f1 domain using a 400 ms mixing time and 2 sec. relaxation delay.

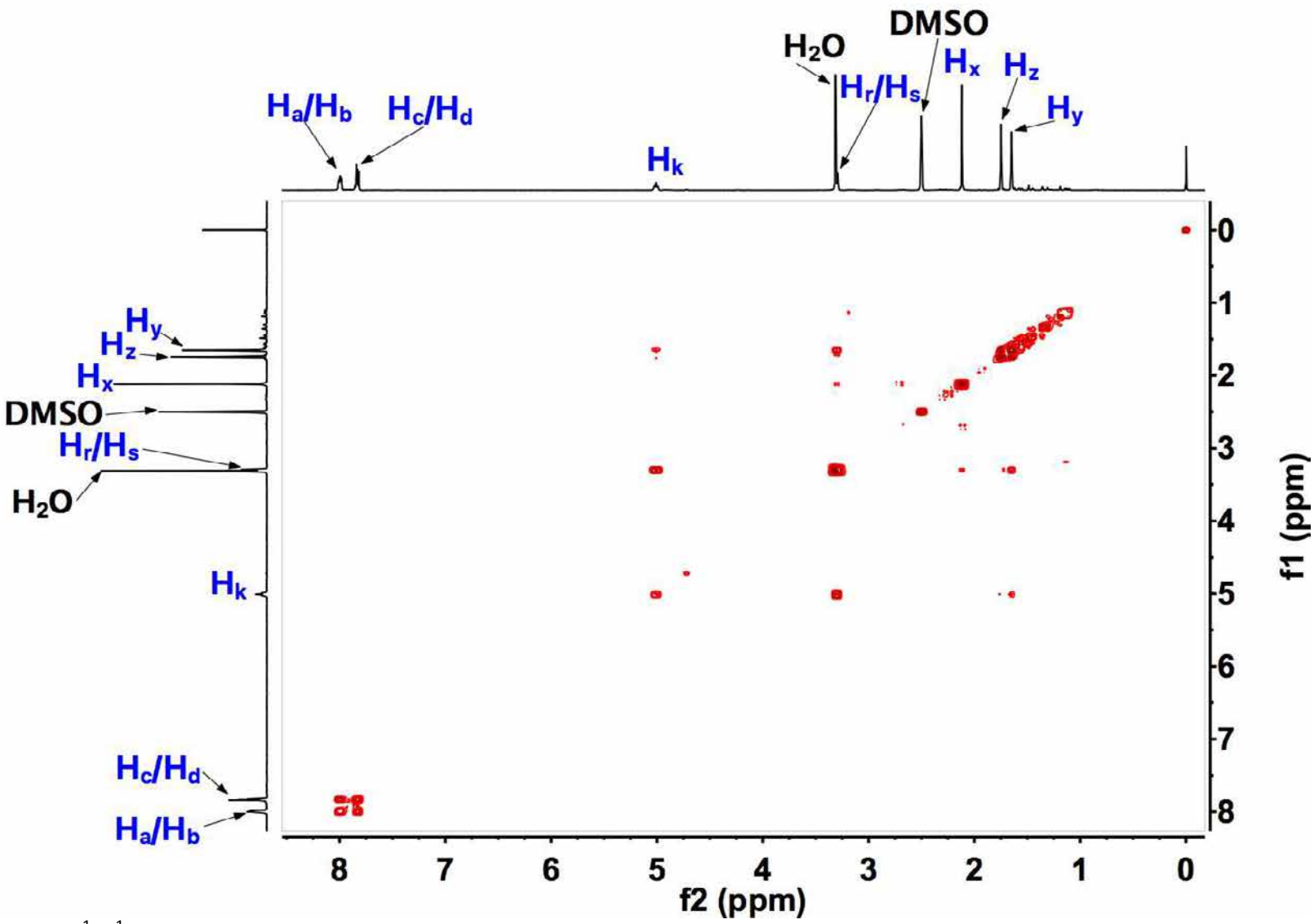

Figure A4.9: ^{1}H-^{1}H 2D gCOSY NMR (400 MHz) spectrum of MK-1 in d_6-DMSO at 26 °C. A standard gCOSY pulse sequence was used consisting of 200 t1 increments with 8 scans per t1 increment.

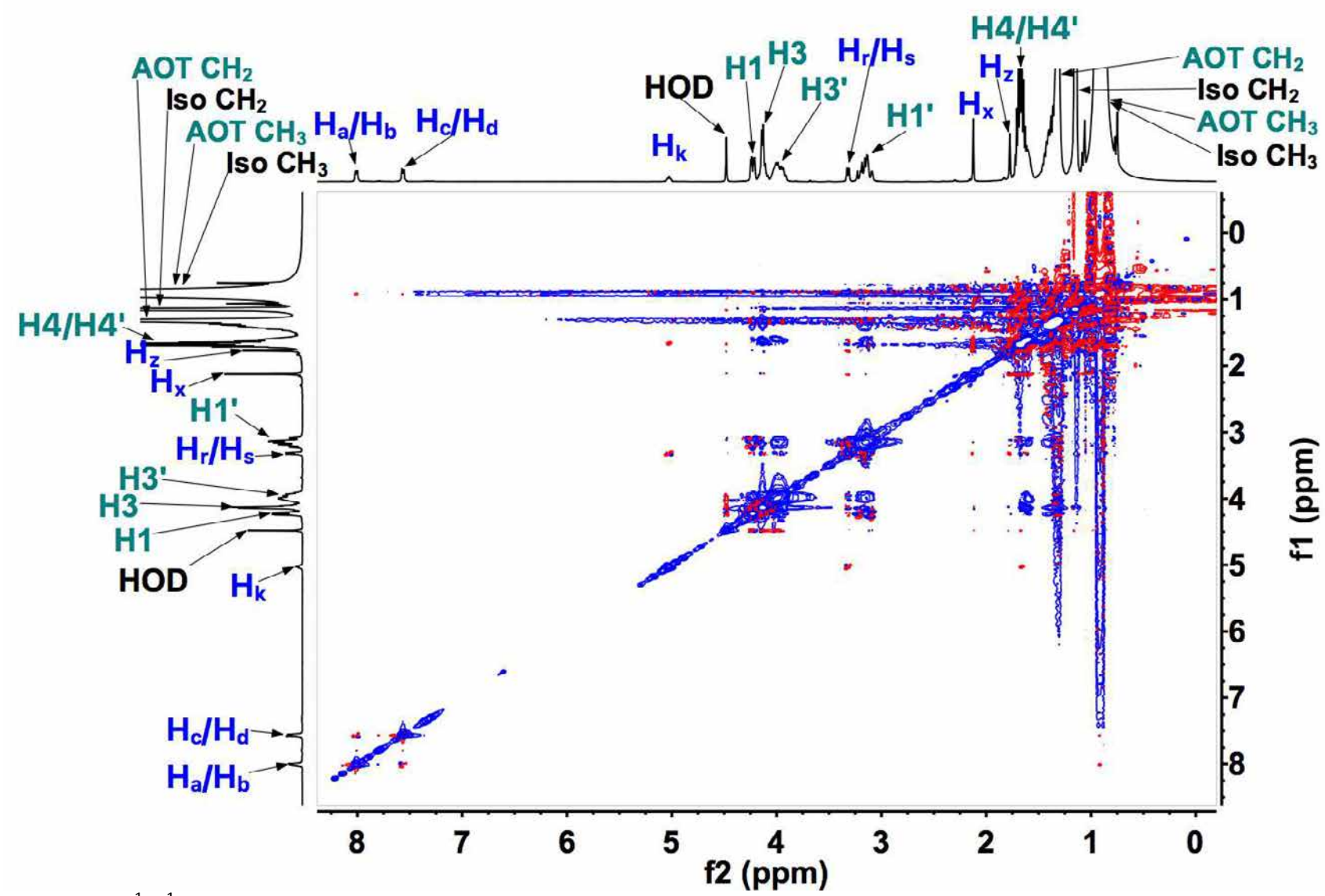

Figure A4.10: ^{1}H-^{1}H 2D NOESY NMR (400 MHz) spectrum of MK-1 in a w_0 12 reverse micelle at 26 °C. A standard NOESY pulse sequence was used consisting of 256 transients with 16 scans in the f1 domain using a 200 ms mixing time and 1.5 sec. relaxation delay.

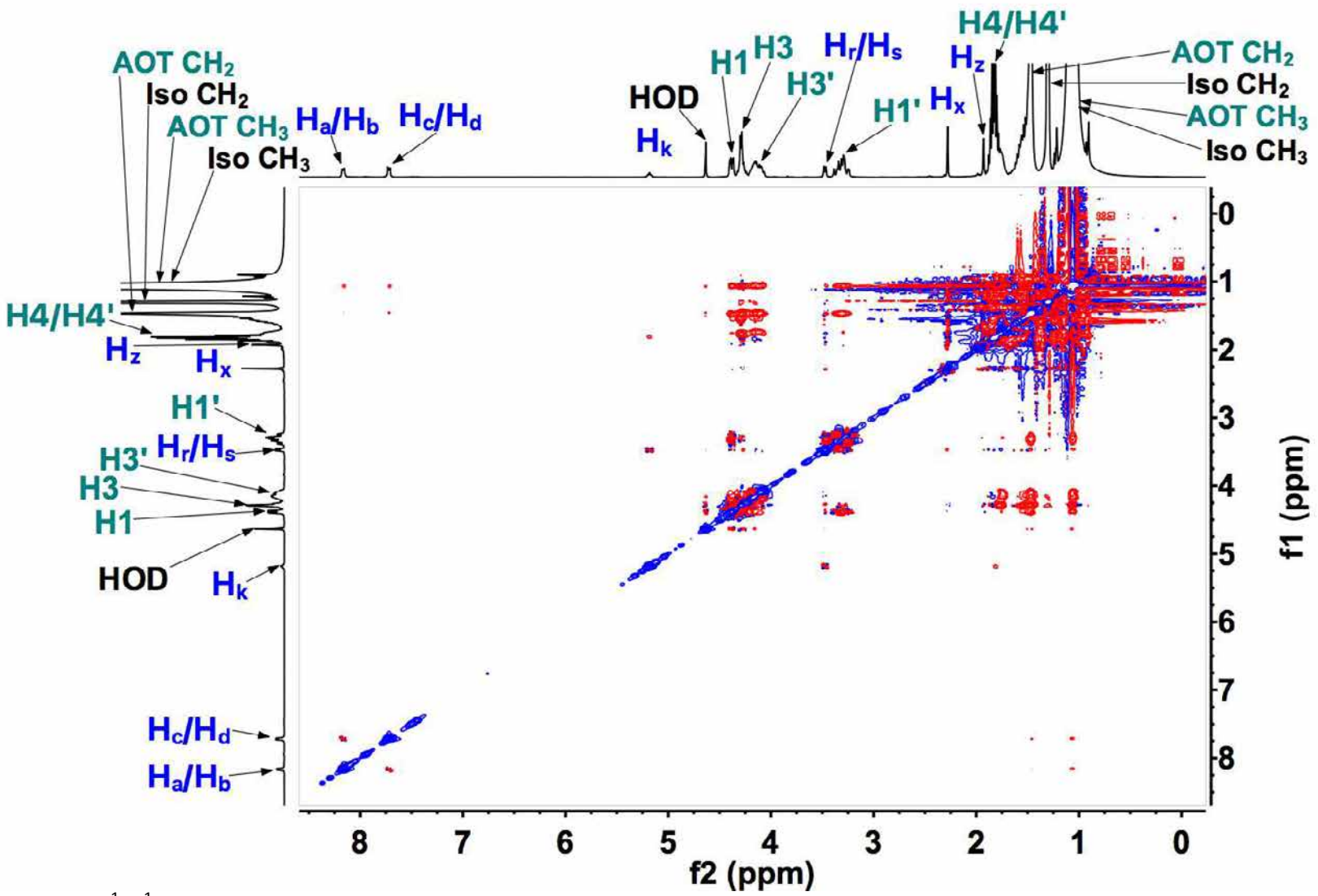

Figure A4.11: ^{1}H-^{1}H 2D ROESY NMR (400 MHz) spectrum of MK-1 in a w_0 12 reverse micelle at 26 °C. A standard ROESYAD pulse sequence was used consisting of 256 transients with 16 scans in the f1 domain using a 200 ms mixing time and 1.5 sec. relaxation delay.

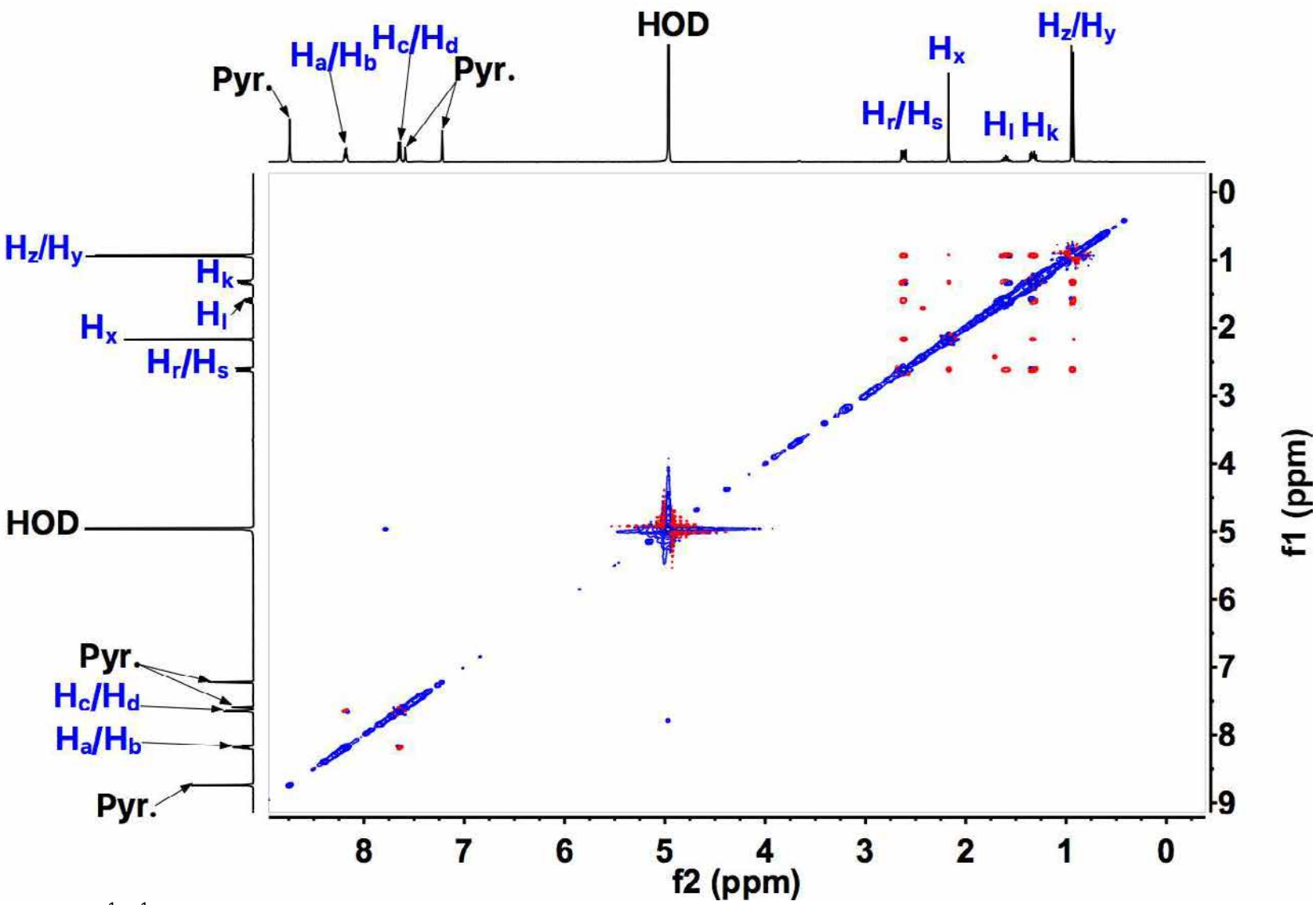

Figure A4.12: ^{1}H-^{1}H 2D NOESY NMR (400 MHz) spectrum of MK-1(H_2) in d_5-pyridine at 26 °C. A standard NOESY pulse sequence was used consisting of 256 transients with 16 scans in the f1 domain using a 500 ms mixing time and 1.5 sec. relaxation delay.

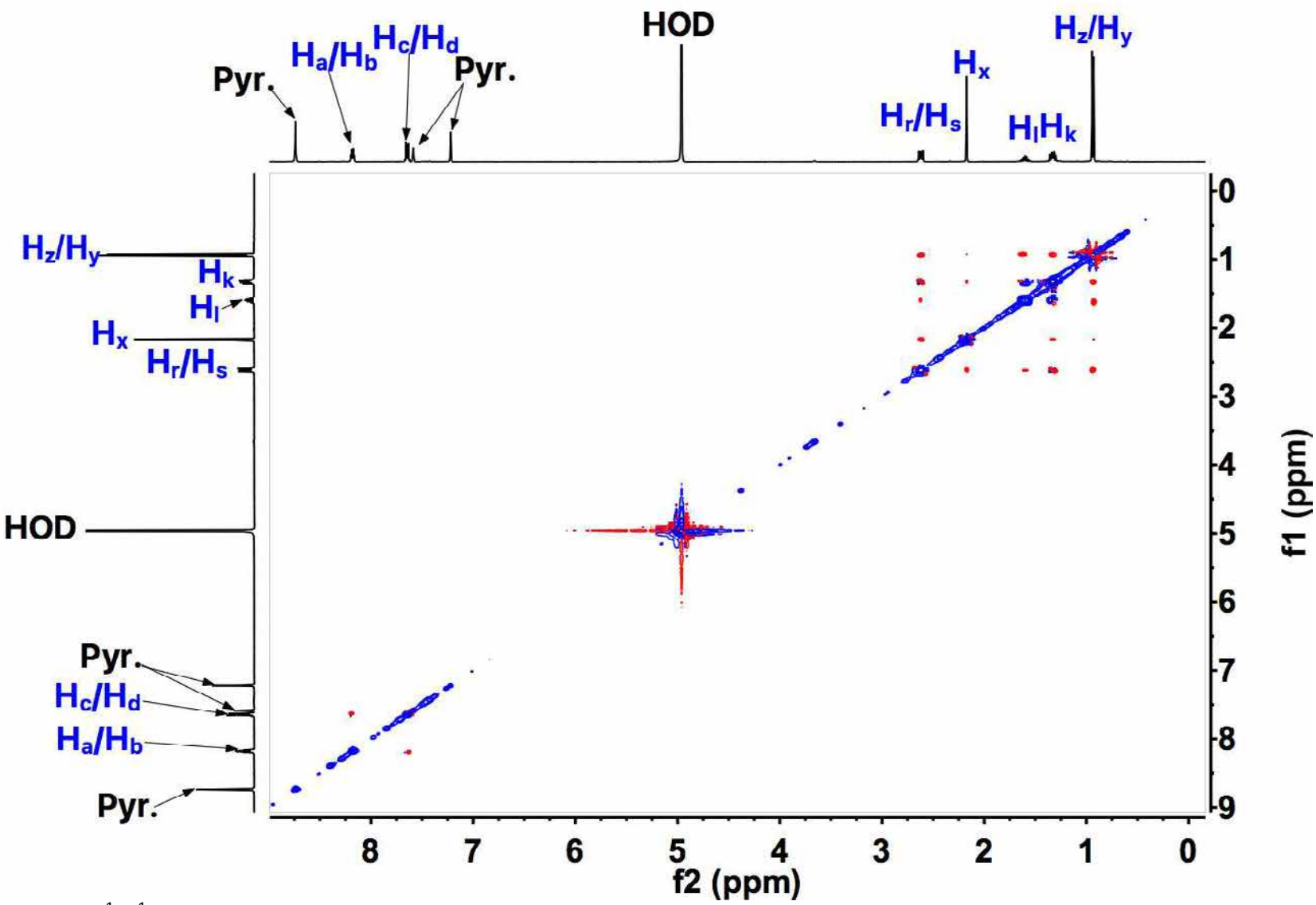

Figure A4.13: ^{1}H-^{1}H 2D ROESY NMR (400 MHz) spectrum of MK-1(H_2) in d_5-pyridine at 26 °C. A standard ROESYAD pulse sequence was used consisting of 256 transients with 16 scans in the f1 domain using a 400 ms mixing time and 2 sec. relaxation delay.

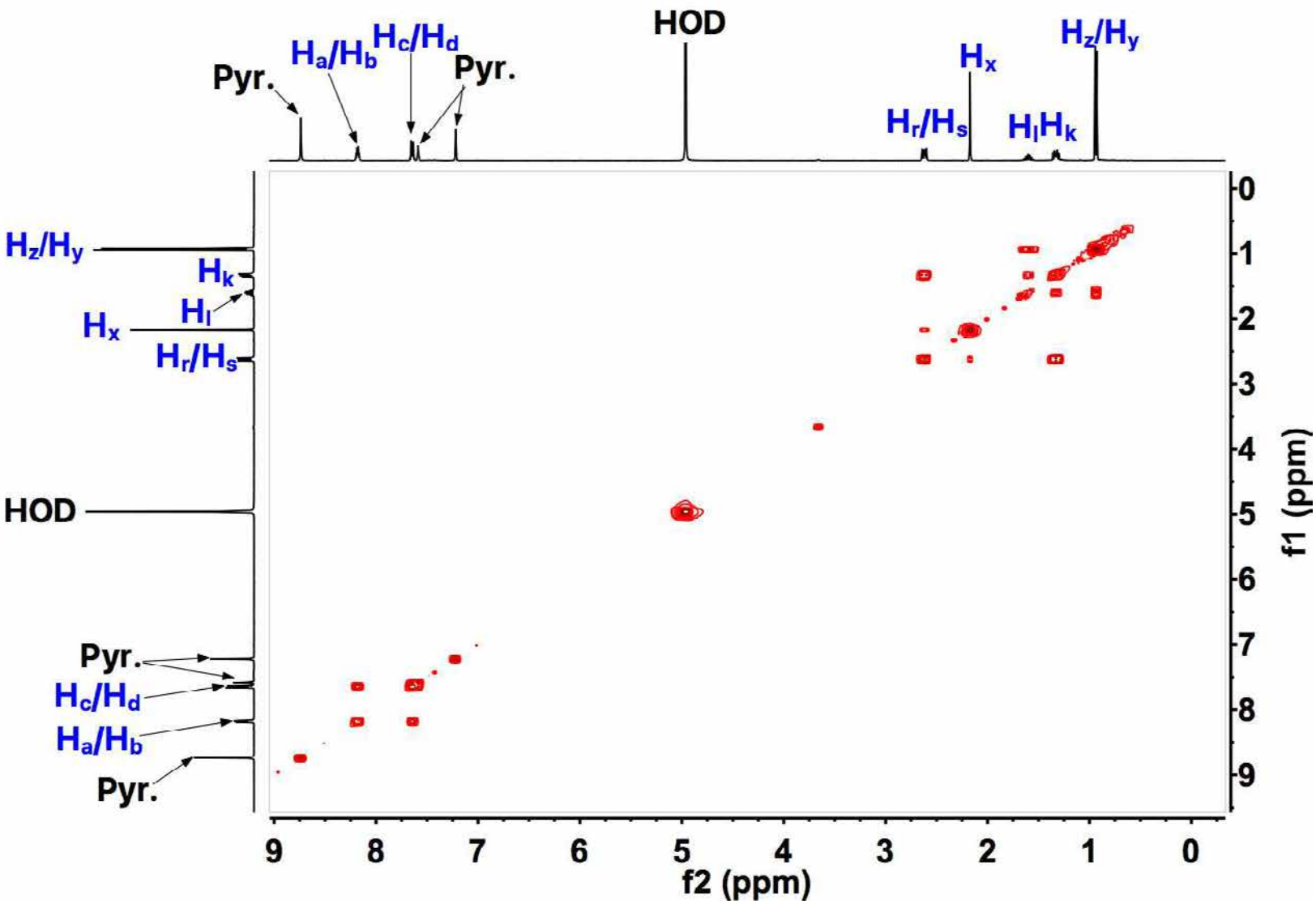

Figure A4.14: ^{1}H-^{1}H 2D gCOSY NMR (400 MHz) spectrum of MK-1(H_2) in d_5-pyridine at 26 °C. A standard gCOSY pulse sequence was used consisting of 200 t1 increments with 8 scans per t1 increment.

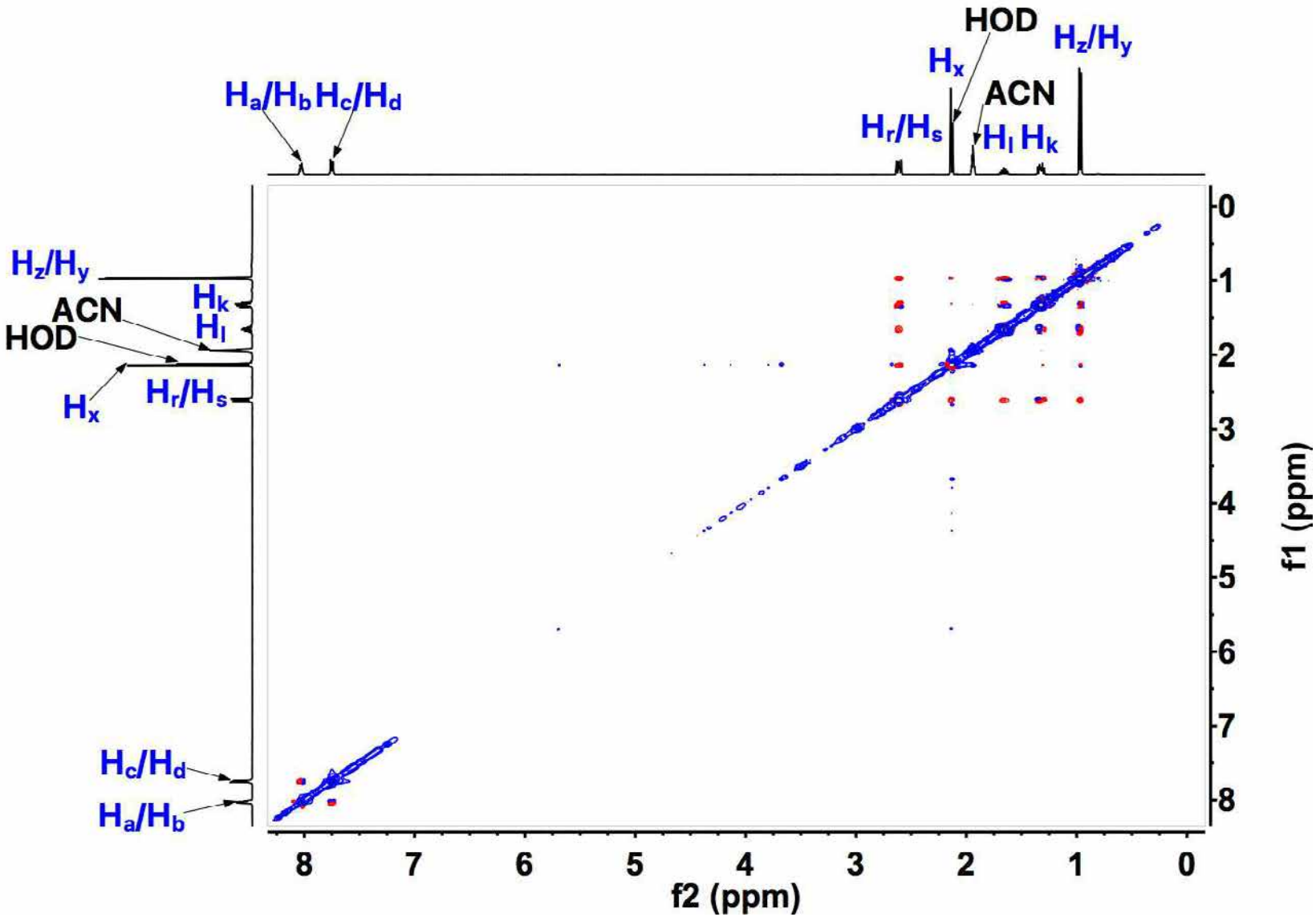

Figure A4.15: ^{1}H-^{1}H 2D NOESY NMR (400 MHz) spectrum of MK-1(H_2) in d_3-acetonitrile at 26 °C. A standard NOESY pulse sequence was used consisting of 256 transients with 16 scans in the f1 domain using a 500 ms mixing time and 1.5 sec. relaxation delay.

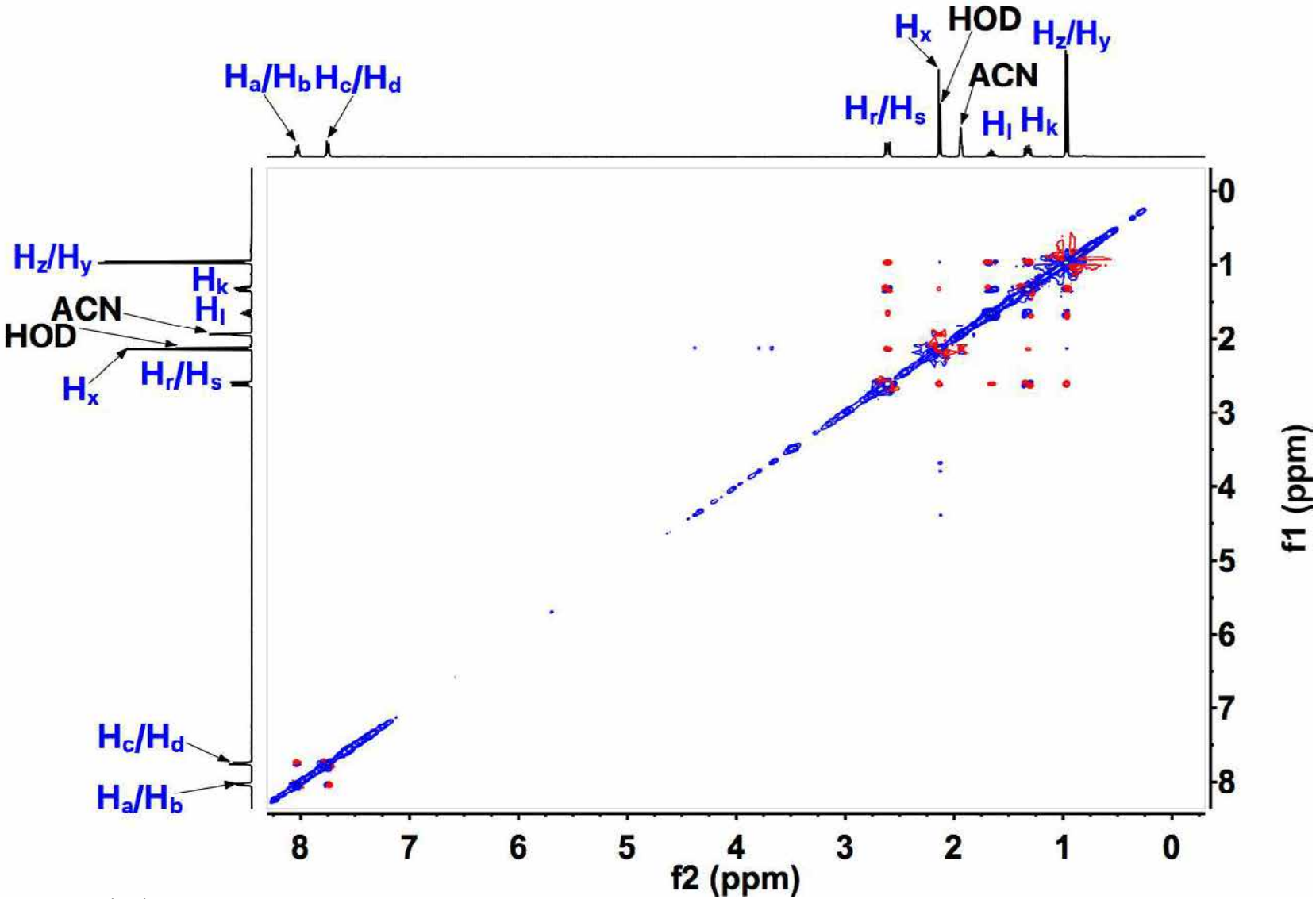

Figure A4.16: ^{1}H-^{1}H 2D ROESY NMR (400 MHz) spectrum of MK-1(H_2) in d_3-acetonitrile at 26 °C. A standard ROESYAD pulse sequence was used consisting of 256 transients with 16 scans in the f1 domain using a 400 ms mixing time and 2.0 sec. relaxation delay.

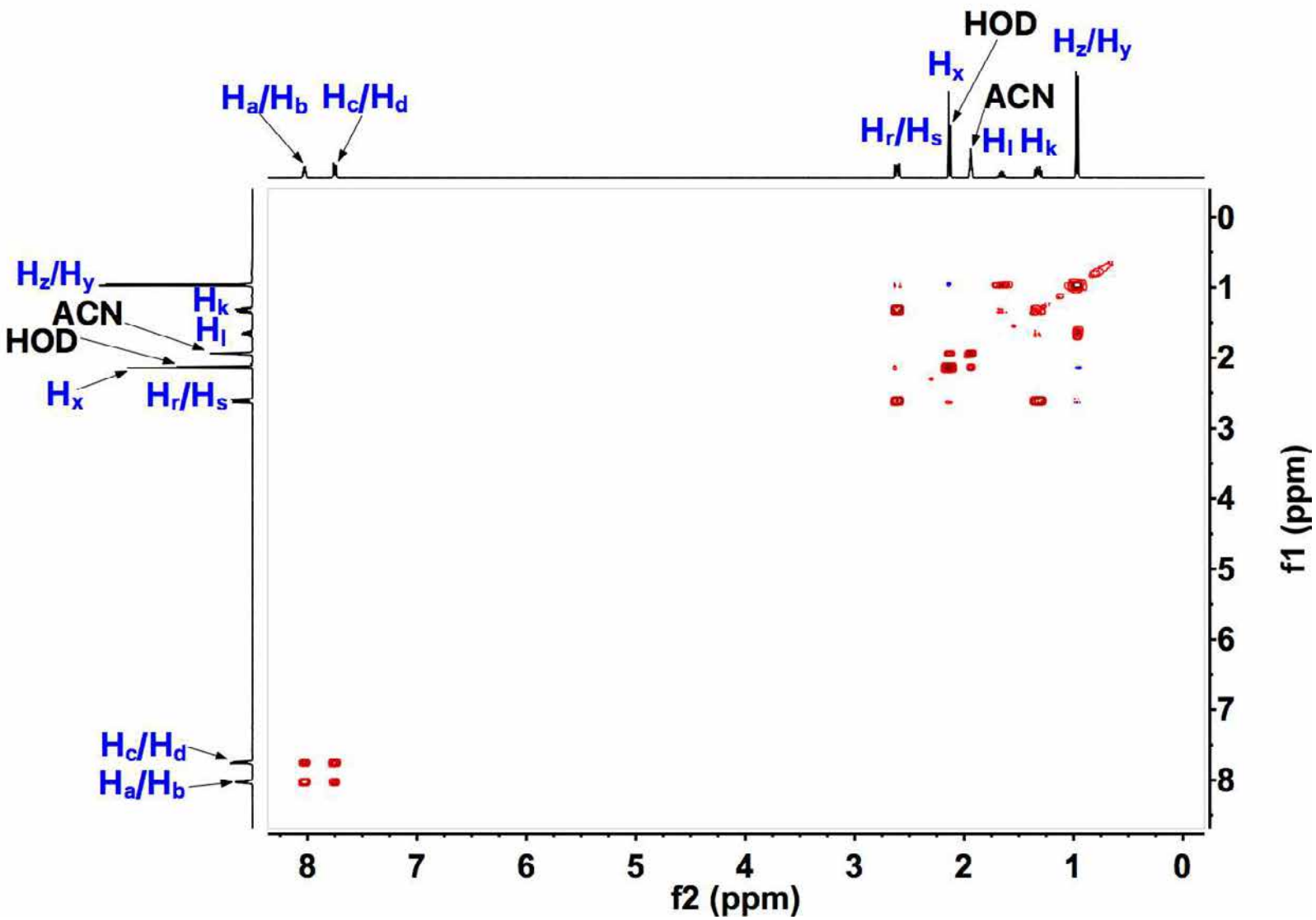

Figure A4.17: ^{1}H-^{1}H 2D gCOSY NMR (400 MHz) spectrum of MK-1(H_2) in d_3-acetonitrile at 26 °C. A standard gCOSY pulse sequence was used consisting of 200 t1 increments with 8 scans per t1 increment.

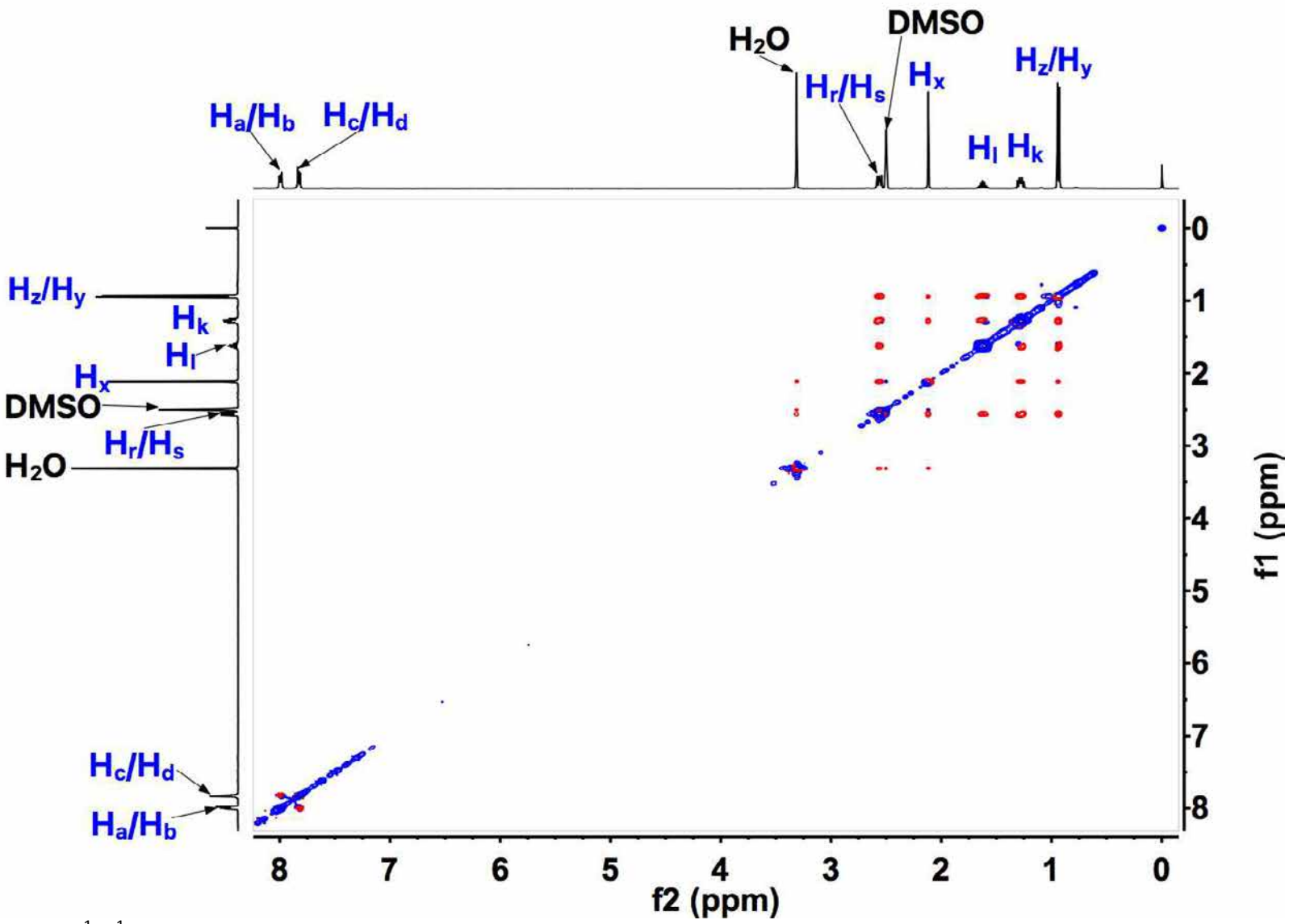

Figure A4.18: ^{1}H-^{1}H 2D NOESY NMR (400 MHz) spectrum of MK-1(H_2) in d_6-DMSO at 26 °C. A standard NOESY pulse sequence was used consisting of 256 transients with 16 scans in the f1 domain using a 500 ms mixing time and 1.5 sec. relaxation delay.

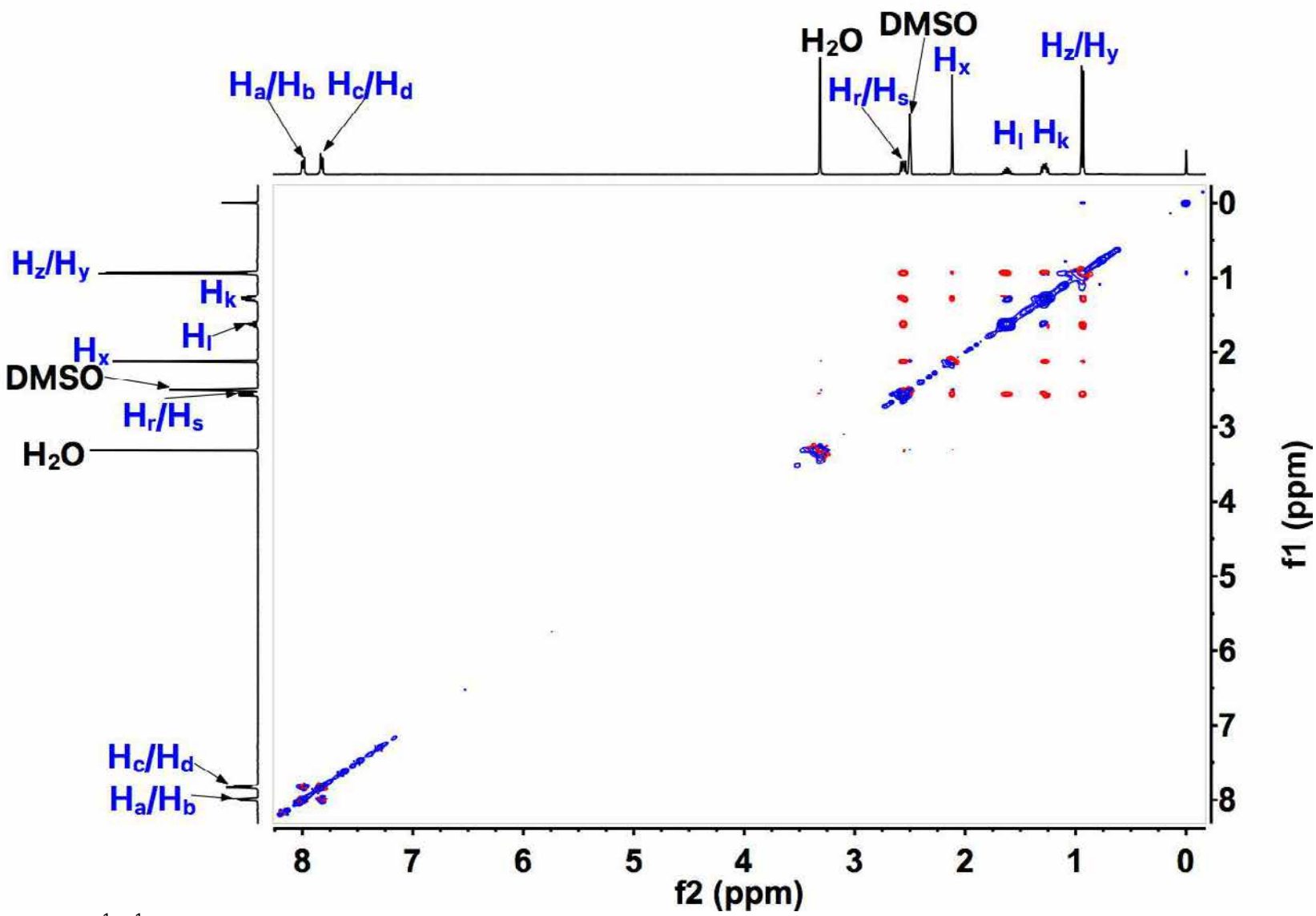

Figure A4.19: ^{1}H-^{1}H 2D ROESY NMR (400 MHz) spectrum of MK-1(H_2) at in d_6-DMSO at 26 °C. A standard ROESYAD pulse sequence was used consisting of 256 transients with 16 scans in the f1 domain using a 400 ms mixing time and 2 sec. relaxation delay.

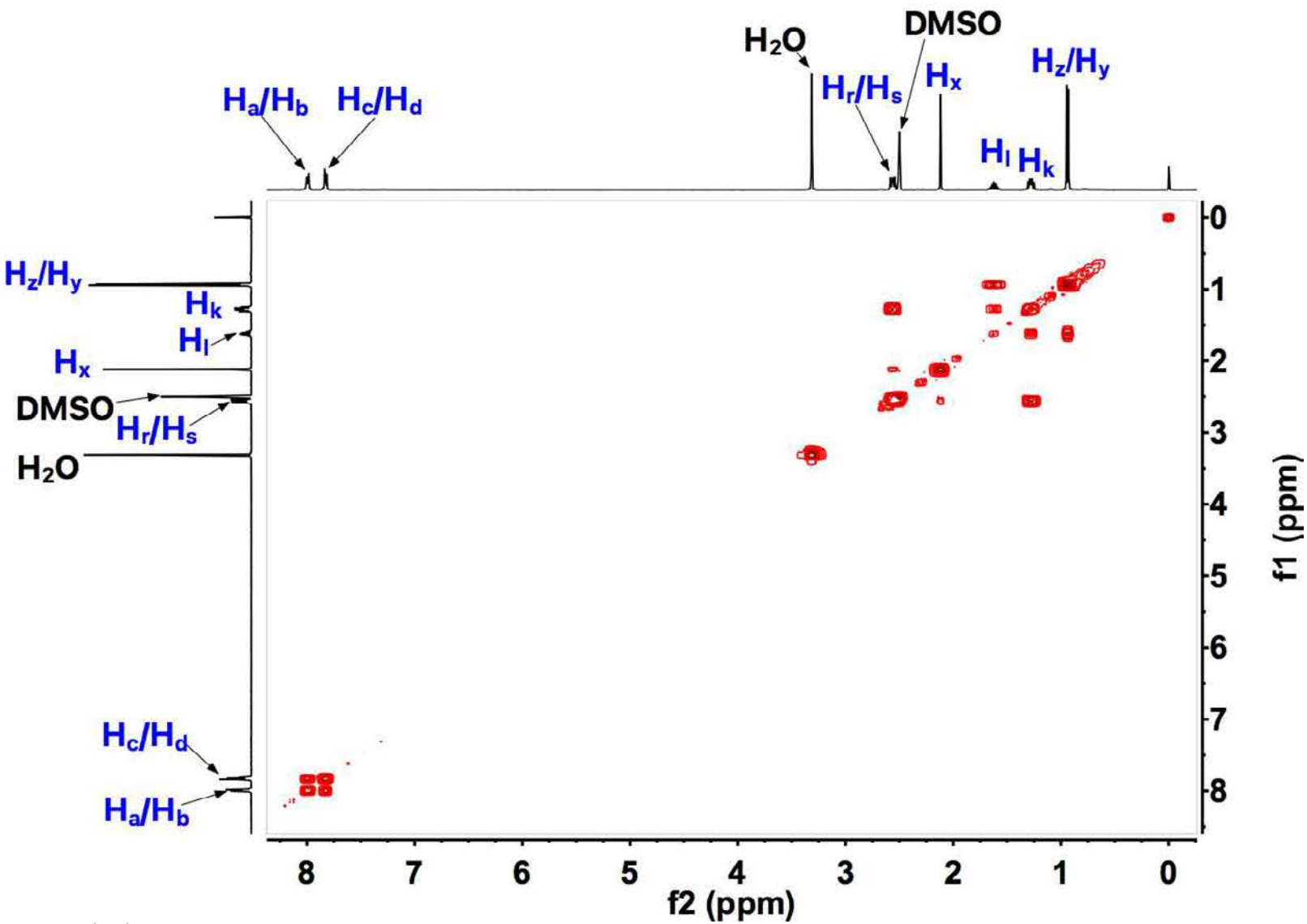

Figure A4.20: ^{1}H-^{1}H 2D gCOSY NMR (400 MHz) spectrum of MK-1(H_2) in d_6-DMSO at 26 °C. A standard gCOSY pulse sequence was used consisting of 200 t1 increments with 8 scans per t1 increment.

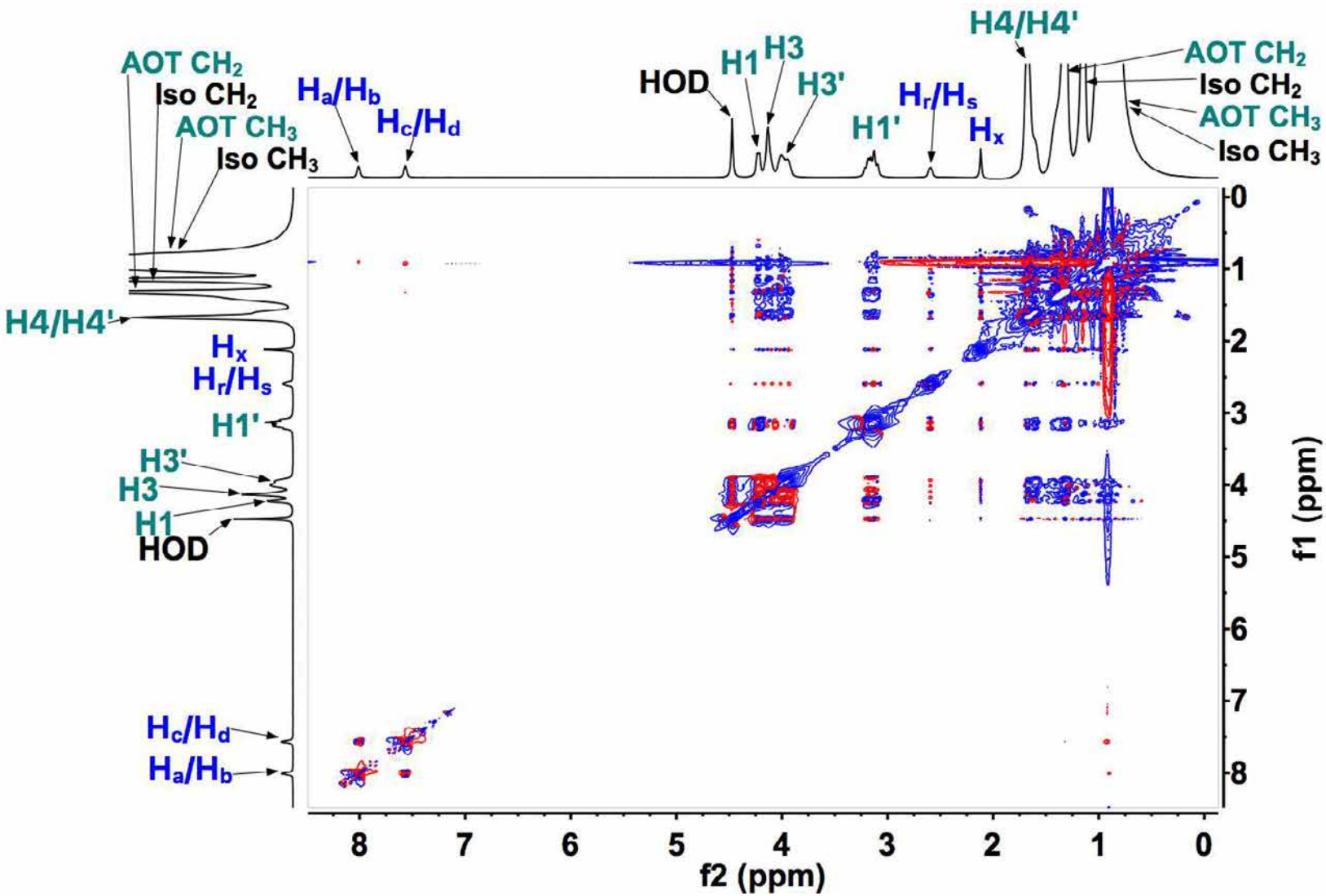

Figure A4.21: ^{1}H-^{1}H 2D NOESY NMR (500 MHz) spectrum of MK-1(H_2) in a w_0 12 reverse micelle at 25 °C. A standard NOESY pulse sequence was used consisting of 200 transients with 32 scans in the f1 domain using a 200 ms mixing time and a 1.5 sec. relaxation delay.

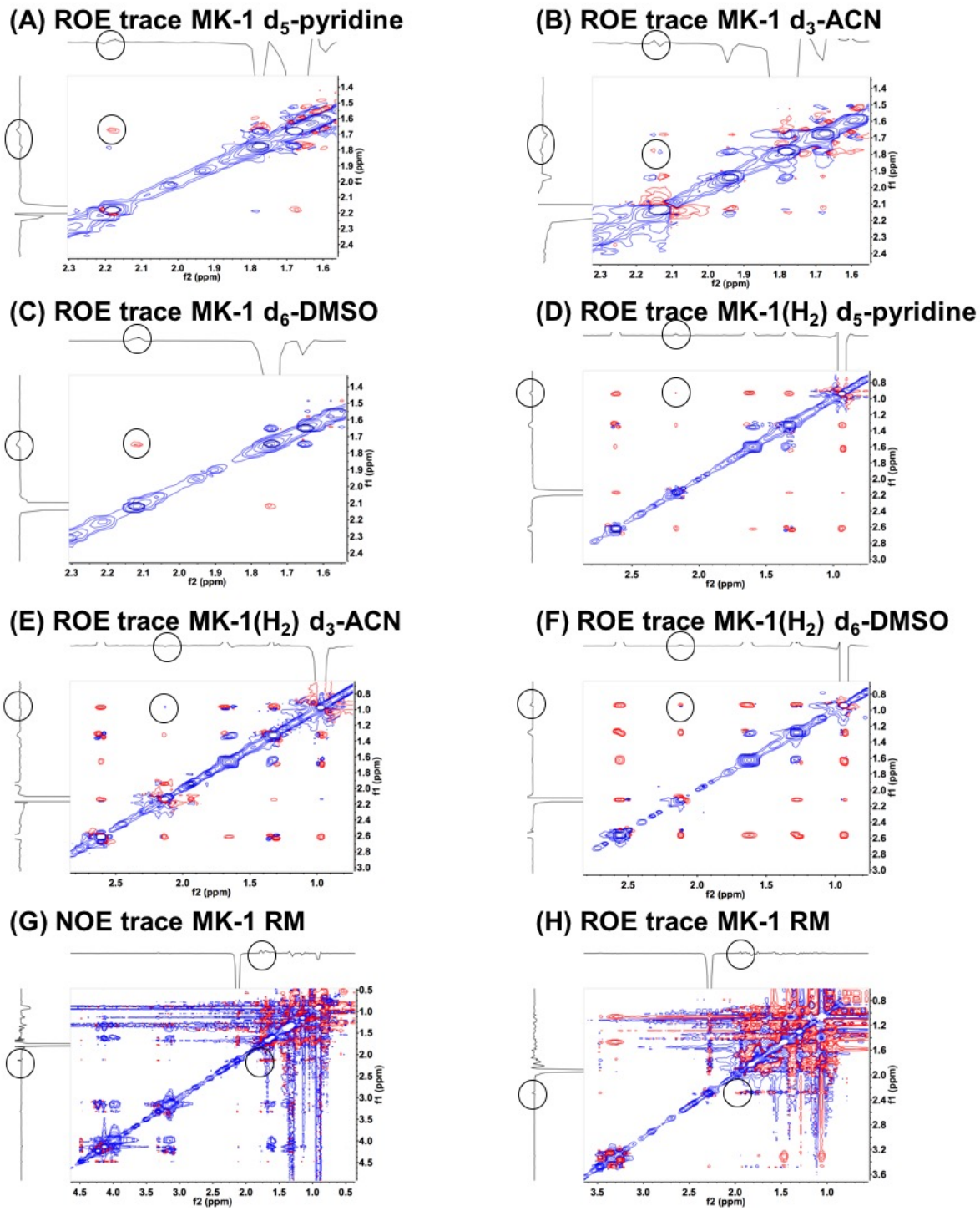

Figure A4.22: ROE/NOE traces for MK-1 and MK-1(H_2) correlations. (A) ROE trace for MK-1 correlation H_x to H_y in d_5-pyridine, (B) ROE trace for MK-1 correlation H_x to H_z in d_3-ACN, (C) ROE trace for MK-1 correlation H_x to H_z in d_6-DMSO, (D) ROE trace for MK-1(H_2) correlation H_x to $H_{y/z}$ in d_5-pyridine, (E) ROE trace for MK-1(H_2) correlation H_x to $H_{y/z}$ in d_3-ACN, (F) ROE trace for MK-1(H_2) correlation H_x to $H_{y/z}$ in d_6-DMSO, (G) NOE trace for MK-1 correlation H_x to H_z in a w_0 12 RM, (H) ROE trace for MK-1 correlation H_x to H_z in a w_0 12 RM.

Molecular Mechanics: MK-1 and MK-1(H_2) Conformational Analysis, Energies, Hydrogen Distances, & Cartesian Coordinates.

Conformational Analysis. Molecular mechanics (MM) calculations were carried out to provide visual aids to understand the 2D NMR spectral results. Specifically, calculations were carried out to characterize the local minima with parameters similar to that obtained by the solution 2D NMR spectroscopic studies. All the conformations (Figure A4.23) were constructed by building the molecule and then rotating bonds until a desired conformation was obtained (except for conformation D and D1). An energy minimization was then performed to obtain a conformation with realistic bond lengths and angles as well as provide an energy value to determine if the resulting conformation had similar stability to other conformations obtained. Conformations D and D1 were obtained by building an extended-flat conformation and then subjecting it to 10,000 iterations (leading to a sampling of different parts of the energy surface for MK-1 or MK-1(H_2) conformations) and then an energy minimization was carried out to produce realistic bond lengths and angles and to provide an energy value for the conformation. As seen in Table S1, the conformations of MK-1 in d_5-pyridine, d_3-acetonitrile, and d_6-DMSO differed by less than 5 kcal/mol and for MK-1(H_2) by ~1 kcal/mol.

Table A4.1. Conformation energies of MK-1 and MK-1(H_2) and selected distances between hydrogens.

	MK-1 Conformation	Energy (kcal/mol)	H_x-H_z[a] (Å)	H_x-H_y[a] (Å)	H_x-H_x[a] (Å)	H_x-H_i[a] (Å)	H_x-H_z[a] (Å)	H_x-H_y[a] (Å)	H_x-$H_{r/s}$[a] (Å)	H_{rs}-H_y[a] (Å)	H_{rs}-H_z[a] (Å)
(A)	Pyridine	51.8	4.6	4.3	3.0	2.6	3.8	2.6	2.9	4.5	2.5
(B)	Acetonitrile	48.6	3.9	5.2	4.0	2.1	3.8	2.3	2.8	4.7	2.3
(C)	DMSO	47.3	3.2	4.7	4.0	2.1	3.8	2.3	2.6	4.8	2.1
(D)	Low Energy MM Conformation	46.0	2.5	4.7	4.1	2.2	3.8	2.3	2.5	4.6	2.1
(E)	Extended Planar Side Chain	65.8	5.1	2.6	2.0	3.6	3.8	2.3	2.7	4.9	2.9
(F)	Extended Planar Side Chain Rotated Upwards	63.4	4.1	6.9	4.8	2.2	3.8	2.1	2.9	4.6	2.7
	Reverse Micelle Proposed Conformation	50.3	2.8	5.5	4.4	2.3	3.8	2.3	2.3	4.5	3.1

	MK-1 (H_2) Conformation	Energy (kcal/mol)	H_x-H_z[a] (Å)	H_x-H_y[a] (Å)	H_x-H_x[a] (Å)	H_x-H_{rs}[a] (Å)	H_x-H_z[a] (Å)	H_x-H_y[a] (Å)	H_x-$H_{r/s}$[a] (Å)	H_{rs}-H_y[a] (Å)	H_{rs}-H_z[a] (Å)	H_i-H_x (Å)
(A1)	Pyridine	42.1	3.6	5.2	2.8	2.1	2.6	2.6	2.5	4.3	2.3	4.9
(B1)	Acetonitrile	43.0	4.0	5.3	3.0	2.1	2.7	2.5	2.4	4.4	2.8	5.3
(C1)	DMSO	41.9	3.4	4.8	2.6	2.2	2.6	2.6	2.5	4.5	2.3	4.9
(D1)	Low Energy MM Conformation	41.9	5.0	4.6	2.7	2.1	2.6	2.4	2.5	4.3	2.3	3.6
(E1)	Extended Planar Side Chain	56.1	4.7	3.2	2.0	3.8	2.8	2.3	2.4	4.1	2.5	4.0
(F1)	Extended Planar Side Chain Rotated Upwards	53.2	3.3	6.6	4.6	2.3	2.9	2.3	2.4	4.0	2.3	4.8

[a]All distances were determined using the closest hydrogens. For example, the closest H_x hydrogen was used to determine the distance to the closest H_z hydrogen.

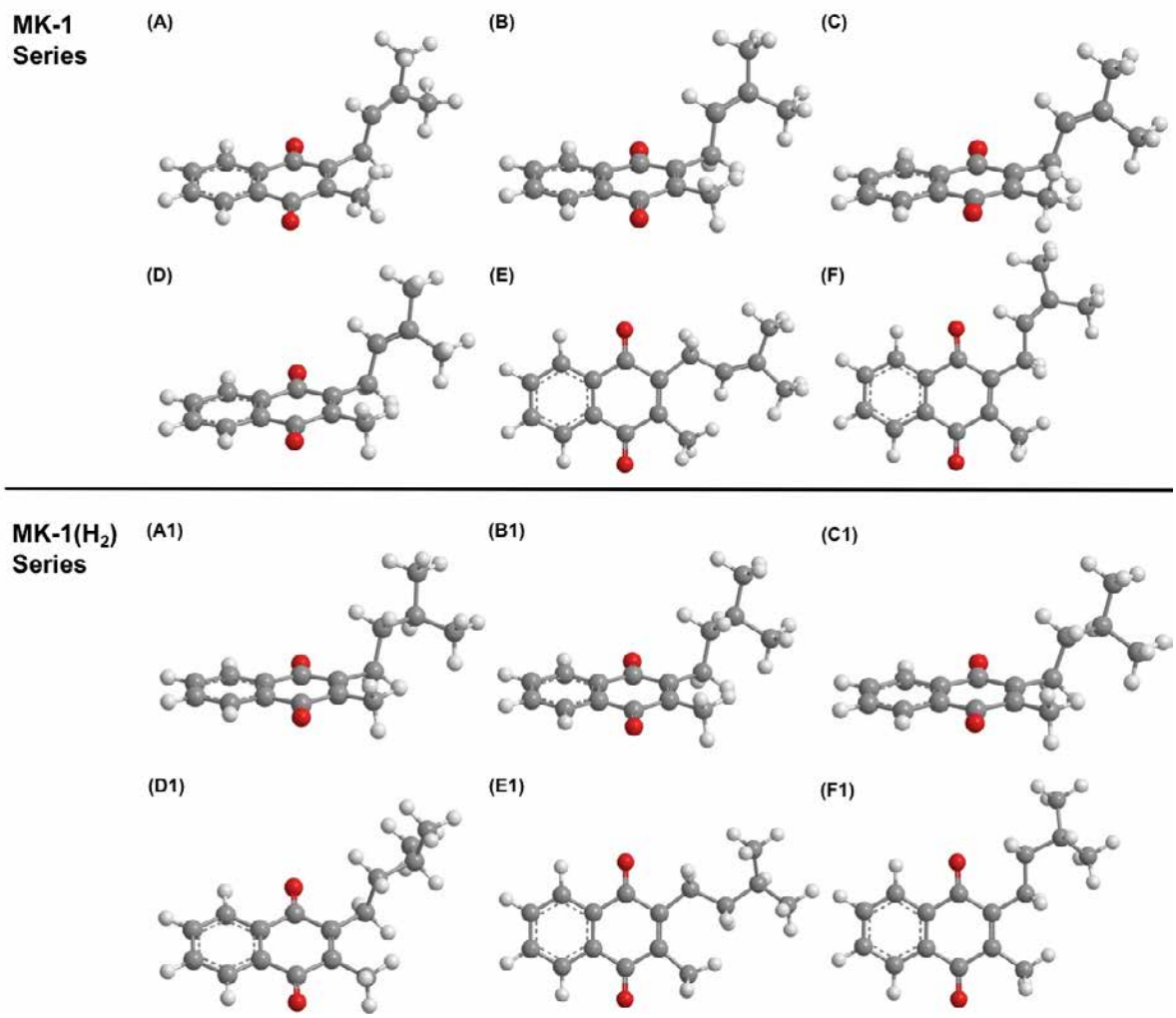

Figure A4.23. MK-1 and MK-1(H_2) conformations illustrated using MMFF94 calculations. MK-1 Series: (A) Illustrates proposed MK-1 conformation in d_5-pyridine determined from 2D NOESY and ROESY NMR spectra (51.8 kcal/mol, H_x-H_y: 4.3 Å), (B) Illustrates proposed MK-1 conformation in d_3-acetonitrile determined from 2D NOESY and ROESY NMR spectra (48.6 kcal/mol, H_x-H_z: 3.9 Å), (C) Illustrates proposed MK-1 conformation in d_6-DMSO determined from 2D NOESY and ROESY NMR spectra (47.3 kcal/mol, H_x-H_z: 3.2 Å), (D) Low energy MM conformation of MK-1 found using 10,000 iterations and energy minimization (46.0 kcal/mol, H_x-H_z: 2.5 Å), (E) Commonly illustrated MK conformation in literature with MK-1 extended-flat side chain (65.8 kcal/mol, H_x-H_z: 5.1 Å), (F) MK-1 conformation with extended planar side chain rotated up (63.4 kcal/mol, H_x-H_z: 4.1 Å). MK-1(H_2) Series: (A1) Illustrates proposed MK-1(H_2) conformation in d_5-pyridine determined from 2D NOESY and ROESY NMR spectra (42.1 kcal/mol, H_x-H_z: 3.6 Å), (B1) Illustrates proposed MK-1(H_2) conformation in d_3-acetonitrile determined from 2D NOESY and ROESY NMR spectra (43.0 kcal/mol, H_x-H_z: 4.0 Å), (C1) Illustrates proposed MK-1(H_2) conformation in d_6-DMSO determined from 2D NOESY and ROESY NMR spectra (41.9 kcal/mol, H_x-H_z: 3.4 Å), (D1) Low energy MM conformation of MK-1(H_2) found using 10,000 iterations and energy minimization (41.9 kcal/mol, H_x-H_z: 5.0 Å), (E1) Commonly illustrated MK conformation in literature with MK-1(H_2) extended-flat side chain (56.1 kcal/mol, H_x-H_z: 4.7 Å), (F1) MK-1(H_2) conformation with extended planar side chain rotated up (53.2 kcal/mol, H_x-H_z: 3.3 Å).

Table A4.2. Cartesian coordinates for the proposed conformation of MK-1 in d_5-pyridine obtained from the xyz file.

34									
1	C	-4.3552	0.918053	0.212182	2	2	6	19	
2	C	-4.34055	0.717934	1.59071	2	1	3	20	
3	C	-3.27499	0.038296	2.18288	2	2	4	21	
4	C	-2.21579	-0.438753	1.39499	2	3	5	7	
5	C	-2.23094	-0.242801	0.020261	2	4	6	10	
6	C	-3.30577	0.435837	-0.574051	2	1	5	22	
7	C	-1.09416	-1.1471	2.03385	3	4	8	11	
8	C	0.071214	-1.54273	1.18714	2	7	9	12	
9	C	0.071774	-1.32885	-0.145605	2	8	10	14	
10	C	-1.12855	-0.748128	-0.818388	3	5	9	13	
11	O	-1.12656	-1.38165	3.23617	7	7			
12	C	1.23297	-2.15957	1.91728	1	8	23	24	25
13	O	-1.21215	-0.685136	-2.04009	7	10			
14	C	1.2307	-1.68009	-1.06158	1	9	15	26	27
15	C	2.23936	-0.560442	-1.16218	2	14	16	28	
16	C	3.35406	-0.544522	-1.92157	2	15	17	18	
17	C	4.24905	0.668451	-1.90662	1	16	29	30	31
18	C	3.79741	-1.66232	-2.82286	1	16	32	33	34
19	H	-5.18512	1.447	-0.252148	5	1			
20	H	-5.15825	1.08822	2.20484	5	2			
21	H	-3.27271	-0.117018	3.26085	5	3			
22	H	-3.32937	0.592054	-1.65176	5	6			
23	H	2.16399	-1.63506	1.6791	5	12			
24	H	1.12618	-2.12094	3.00531	5	12			
25	H	1.33685	-3.21414	1.63924	5	12			
26	H	1.73522	-2.5819	-0.691911	5	14			
27	H	0.865508	-1.93771	-2.06214	5	14			
28	H	2.03015	0.326999	-0.565543	5	15			
29	H	4.54559	0.91791	-0.882394	5	17			
30	H	5.16698	0.498979	-2.47922	5	17			
31	H	3.73531	1.52809	-2.34892	5	17			
32	H	3.16531	-2.55095	-2.74445	5	18			
33	H	3.78283	-1.33173	-3.86662	5	18			
34	H	4.82015	-1.9671	-2.57614	5	18			

Table A4.3. Cartesian coordinates for the proposed conformation of MK-1 in d_3-acetonitrile obtained from the xyz file.

34									
1	C	-3.4403	-3.41969	2.11734	2	2	6	19	
2	C	-2.59961	-4.20659	2.9009	2	1	3	20	
3	C	-1.21833	-3.99674	2.87514	2	2	4	21	
4	C	-0.674514	-2.99209	2.06013	2	3	5	7	
5	C	-1.51404	-2.21567	1.27246	2	4	6	10	
6	C	-2.89942	-2.43027	1.29868	2	1	5	22	
7	C	0.782562	-2.76735	2.03511	3	4	8	11	
8	C	1.31463	-1.5957	1.27569	2	7	9	12	
9	C	0.495306	-0.838201	0.510346	2	8	10	14	
10	C	-0.958661	-1.17281	0.397034	3	5	9	13	
11	O	1.53403	-3.51871	2.64993	7	7			
12	C	2.78683	-1.36019	1.46982	1	8	23	24	25
13	O	-1.69811	-0.582697	-0.378647	7	10			
14	C	0.915901	0.352225	-0.332668	1	9	15	26	27
15	C	0.540238	1.66791	0.304672	2	14	16	28	
16	C	1.11591	2.86566	0.087631	2	15	17	18	
17	C	0.628495	4.10159	0.796317	1	16	29	30	31
18	C	2.24608	3.11179	-0.876349	1	16	32	33	34
19	H	-4.5159	-3.5798	2.13348	5	1			
20	H	-3.01911	-4.98236	3.53611	5	2			
21	H	-0.56853	-4.61354	3.4965	5	3			
22	H	-3.55854	-1.81718	0.687786	5	6			
23	H	3.12164	-0.38486	1.10638	5	12			
24	H	3.04593	-1.39128	2.53504	5	12			
25	H	3.36983	-2.13122	0.952265	5	12			
26	H	1.99291	0.323787	-0.521304	5	14			
27	H	0.446869	0.274188	-1.32414	5	14			
28	H	-0.297896	1.63113	0.995094	5	15			
29	H	-0.154584	3.88134	1.52363	5	17			
30	H	1.45033	4.58639	1.32828	5	17			
31	H	0.220274	4.81078	0.072728	5	17			
32	H	2.36964	2.30544	-1.6073	5	18			
33	H	2.06669	4.03026	-1.44799	5	18			
34	H	3.18667	3.23383	-0.328655	5	18			

Table A4.4. Cartesian coordinates for the proposed conformation of MK-1 in d_6-DMSO obtained from the xyz file.

34									
1	C	-4.84183	-0.361719	-0.146168	2	2	6	19	
2	C	-4.84756	-1.2823	0.899869	2	1	3	20	
3	C	-3.64043	-1.73964	1.43002	2	2	4	21	
4	C	-2.42161	-1.27881	0.911377	2	3	5	7	
5	C	-2.41542	-0.365379	-0.134451	2	4	6	10	
6	C	-3.62938	0.097346	-0.664636	2	1	5	22	
7	C	-1.15759	-1.77215	1.47817	3	4	8	11	
8	C	0.12676	-1.29374	0.886669	2	7	9	12	
9	C	0.137797	-0.413758	-0.135745	2	8	10	14	
10	C	-1.14311	0.124567	-0.689368	3	5	9	13	
11	O	-1.17271	-2.55691	2.42207	7	7			
12	C	1.35837	-1.87032	1.53265	1	8	23	24	25
13	O	-1.15383	0.955617	-1.59199	7	10			
14	C	1.38824	0.116984	-0.811331	1	9	15	26	27
15	C	1.95798	1.31204	-0.093449	2	14	16	28	
16	C	3.25426	1.58378	0.167538	2	15	17	18	
17	C	3.63623	2.8362	0.912728	1	16	29	30	31
18	C	4.42395	0.739677	-0.255718	1	16	32	33	34
19	H	-5.78084	-0.002147	-0.56043	5	1			
20	H	-5.79025	-1.64347	1.30556	5	2			
21	H	-3.65215	-2.45866	2.24706	5	3			
22	H	-3.63442	0.817616	-1.48146	5	6			
23	H	2.22075	-1.88008	0.862556	5	12			
24	H	1.62355	-1.28488	2.41731	5	12			
25	H	1.20388	-2.91141	1.8453	5	12			
26	H	2.11784	-0.69028	-0.906738	5	14			
27	H	1.17224	0.407247	-1.8455	5	14			
28	H	1.2119	2.04224	0.220831	5	15			
29	H	2.76267	3.41554	1.22924	5	17			
30	H	4.20821	2.58201	1.81141	5	17			
31	H	4.25246	3.48151	0.278066	5	17			
32	H	4.1466	-0.103295	-0.892086	5	18			
33	H	5.13431	1.34708	-0.828206	5	18			
34	H	4.94202	0.341834	0.622958	5	18			

Table A4.5. Cartesian coordinates for the proposed conformation of MK-1(H_2) in d_5-pyridine obtained from the xyz file.

36									
1	C	-4.30468	0.017264	2.33954	2	2	6	19	
2	C	-4.17819	-1.22687	2.95394	2	1	3	20	
3	C	-3.02635	-1.98876	2.75268	2	2	4	21	
4	C	-1.99333	-1.50387	1.93762	2	3	5	7	
5	C	-2.11759	-0.263155	1.32675	2	4	6	10	
6	C	-3.27783	0.499812	1.52595	2	1	5	22	
7	C	-0.781125	-2.31429	1.74039	3	4	8	12	
8	C	0.335252	-1.74599	0.927757	2	7	9	11	
9	C	0.217519	-0.542668	0.333189	2	8	10	14	
10	C	-1.0362	0.260223	0.476729	3	5	9	13	
11	C	1.55536	-2.62423	0.876184	1	8	23	24	25
12	O	-0.697268	-3.43061	2.24052	7	7			
13	O	-1.16939	1.34185	-0.086822	7	10			
14	C	1.2805	0.099722	-0.534478	1	9	15	26	27
15	C	2.10936	1.12012	0.256986	1	14	16	28	29
16	C	3.08152	1.9269	-0.623747	1	15	17	18	30
17	C	3.67001	3.08889	0.180769	1	16	31	32	33
18	C	4.21401	1.06507	-1.18446	1	16	34	35	36
19	H	-5.20165	0.612896	2.49484	5	1			
20	H	-4.97501	-1.60469	3.59065	5	2			
21	H	-2.93465	-2.95983	3.23649	5	3			
22	H	-3.3846	1.47354	1.05068	5	6			
23	H	2.43126	-2.12678	0.452803	5	11			
24	H	1.84254	-2.9413	1.8847	5	11			
25	H	1.35354	-3.51764	0.276762	5	11			
26	H	1.93563	-0.659912	-0.972088	5	14			
27	H	0.809133	0.58373	-1.39903	5	14			
28	H	1.43235	1.8191	0.765917	5	15			
29	H	2.66933	0.602486	1.04608	5	15			
30	H	2.52198	2.35252	-1.46583	5	16			
31	H	4.33947	3.69307	-0.441052	5	17			
32	H	2.87566	3.74619	0.549882	5	17			
33	H	4.23968	2.72849	1.04406	5	17			
34	H	4.89834	1.67239	-1.7872	5	18			
35	H	3.83208	0.270798	-1.8323	5	18			
36	H	4.7958	0.599938	-0.381446	5	18			

Table A4.6. Cartesian coordinates for the proposed conformation of MK-1(H_2) in d_3-acetonitrile obtained from the xyz file.

36									
1	C	-3.01031	1.07664	-4.77074	2	2	6	19	
2	C	-2.15895	0.291051	-5.54714	2	1	3	20	
3	C	-1.06146	-0.345036	-4.95815	2	2	4	21	
4	C	-0.816146	-0.192095	-3.5859	2	3	5	7	
5	C	-1.66198	0.59468	-2.81629	2	4	6	10	
6	C	-2.76308	1.23119	-3.40801	2	1	5	22	
7	C	0.33791	-0.866483	-2.97037	3	4	8	12	
8	C	0.54316	-0.730932	-1.49353	2	7	9	13	
9	C	-0.276821	0.036174	-0.749097	2	8	10	14	
10	C	-1.41093	0.778991	-1.38362	3	5	9	11	
11	O	-2.13096	1.52878	-0.73159	7	10			
12	O	1.10595	-1.52672	-3.66316	7	7			
13	C	1.71146	-1.52895	-0.977383	1	8	23	24	25
14	C	-0.152102	0.291948	0.738978	1	9	15	26	27
15	C	-1.16652	-0.5224	1.55508	1	14	16	28	29
16	C	-1.41941	0.041176	2.96831	1	15	17	18	30
17	C	-2.36921	-0.886115	3.73176	1	16	31	32	33
18	C	-0.133196	0.253736	3.76304	1	16	34	35	36
19	H	-3.86618	1.57099	-5.22603	5	1			
20	H	-2.34666	0.173802	-6.61192	5	2			
21	H	-0.401737	-0.954311	-5.57149	5	3			
22	H	-3.43112	1.84672	-2.80533	5	6			
23	H	1.7362	-1.60543	0.111704	5	13			
24	H	1.6762	-2.55783	-1.3554	5	13			
25	H	2.65079	-1.0725	-1.30939	5	13			
26	H	0.862373	0.079252	1.09409	5	14			
27	H	-0.292727	1.36728	0.922874	5	14			
28	H	-2.13315	-0.558887	1.03522	5	15			
29	H	-0.818805	-1.56253	1.62003	5	15			
30	H	-1.91781	1.01312	2.86672	5	16			
31	H	-2.61102	-0.472699	4.7169	5	17			
32	H	-3.31002	-1.0179	3.18609	5	17			
33	H	-1.92012	-1.87535	3.87935	5	17			
34	H	-0.356666	0.538264	4.79851	5	18			
35	H	0.466854	1.05953	3.33072	5	18			
36	H	0.476008	-0.656151	3.78214	5	18			

Table A4.7. Cartesian coordinates for the proposed conformation of MK-1(H_2) in d_6-DMSO obtained from the xyz file.

34									
1	C	-4.84183	-0.361719	-0.146168	2	2	6	19	
2	C	-4.84756	-1.2823	0.899869	2	1	3	20	
3	C	-3.64043	-1.73964	1.43002	2	2	4	21	
4	C	-2.42161	-1.27881	0.911377	2	3	5	7	
5	C	-2.41542	-0.365379	-0.134451	2	4	6	10	
6	C	-3.62938	0.097346	-0.664636	2	1	5	22	
7	C	-1.15759	-1.77215	1.47817	3	4	8	11	
8	C	0.12676	-1.29374	0.886669	2	7	9	12	
9	C	0.137797	-0.413758	-0.135745	2	8	10	14	
10	C	-1.14311	0.124567	-0.689368	3	5	9	13	
11	O	-1.17271	-2.55691	2.42207	7	7			
12	C	1.35837	-1.87032	1.53265	1	8	23	24	25
13	O	-1.15383	0.955617	-1.59199	7	10			
14	C	1.38824	0.116984	-0.811331	1	9	15	26	27
15	C	1.95798	1.31204	-0.093449	2	14	16	28	
16	C	3.25426	1.58378	0.167538	2	15	17	18	
17	C	3.63623	2.8362	0.912728	1	16	29	30	31
18	C	4.42395	0.739677	-0.255718	1	16	32	33	34
19	H	-5.78084	-0.002147	-0.56043	5	1			
20	H	-5.79025	-1.64347	1.30556	5	2			
21	H	-3.65215	-2.45866	2.24706	5	3			
22	H	-3.63442	0.817616	-1.48146	5	6			
23	H	2.22075	-1.88008	0.862556	5	12			
24	H	1.62355	-1.28488	2.41731	5	12			
25	H	1.20388	-2.91141	1.8453	5	12			
26	H	2.11784	-0.69028	-0.906738	5	14			
27	H	1.17224	0.407247	-1.8455	5	14			
28	H	1.2119	2.04224	0.220831	5	15			
29	H	2.76267	3.41554	1.22924	5	17			
30	H	4.20821	2.58201	1.81141	5	17			
31	H	4.25246	3.48151	0.278066	5	17			
32	H	4.1466	-0.103295	-0.892086	5	18			
33	H	5.13431	1.34708	-0.828206	5	18			
34	H	4.94202	0.341834	0.622958	5	18			

Table A4.8. Cartesian coordinates for the proposed conformation of MK-1 in a w_0 12 reverse micelle obtained from the xyz file.

34									
1	C	-4.66912	-0.236265	-0.011421	2	2	6	19	
2	C	-4.82158	-1.44273	0.669263	2	1	3	20	
3	C	-3.69561	-2.14427	1.10217	2	2	4	21	
4	C	-2.41153	-1.63905	0.851532	2	3	5	7	
5	C	-2.25802	-0.438292	0.171887	2	4	6	10	
6	C	-3.39066	0.266751	-0.26084	2	1	5	22	
7	C	-1.23409	-2.39432	1.30263	3	4	8	12	
8	C	0.120197	-1.80498	1.08452	2	7	9	11	
9	C	0.273519	-0.627298	0.44402	2	8	10	14	
10	C	-0.914497	0.090921	-0.115053	3	5	9	13	
11	C	1.23305	-2.63911	1.65989	1	8	23	24	25
12	O	-1.37351	-3.4827	1.85033	7	7			
13	O	-0.793124	1.09025	-0.815598	7	10			
14	C	1.59894	0.032426	0.138442	1	9	15	26	27
15	C	1.89564	1.32549	0.859584	2	14	16	28	
16	C	1.60811	1.74793	2.10761	2	15	17	18	
17	C	1.98713	3.14307	2.53859	1	16	29	30	31
18	C	0.928088	0.942251	3.17547	1	16	32	33	34
19	H	-5.54507	0.311799	-0.351426	5	1			
20	H	-5.81599	-1.83952	0.862264	5	2			
21	H	-3.82164	-3.08718	1.6323	5	3			
22	H	-3.28031	1.2087	-0.795894	5	6			
23	H	2.19322	-2.12057	1.6956	5	11			
24	H	1.00668	-2.92439	2.69324	5	11			
25	H	1.36337	-3.55216	1.06987	5	11			
26	H	2.4496	-0.639835	0.283202	5	14			
27	H	1.61784	0.244753	-0.940246	5	14			
28	H	2.42762	2.02709	0.213762	5	15			
29	H	2.4652	3.71385	1.7354	5	17			
30	H	1.09553	3.69548	2.85299	5	17			
31	H	2.68837	3.10328	3.3789	5	17			
32	H	1.11425	-0.12676	3.06865	5	18			
33	H	1.3079	1.21476	4.16671	5	18			
34	H	-0.150331	1.12807	3.16314	5	18			

Refer to the published manuscript[1] and corresponding supporting information for Electrochemistry Experimental, Methods, and Data.

Refer to the published manuscript[1] and corresponding supporting information for Langmuir Monolayer Studies Experimental, Methods, and Data.

Dynamic Light Scattering Data for MK-1 and MK-1(H_2).

Table A4.9. Dynamic Light Scattering measurements on MK-1 and MK-1(H_2) in 0.1 M AOT/isooctane RMs.

w_0	N (probes)	N (Micelles)	N (probes) / N (Micelles)	MK-1 r_h[a] (nm)	MK-1 PDI	MK-1(H_2) rh[a] (nm)	MK-1(H_2) PDI	Blank r_h[a] (nm)	r_h[b] Literature (nm)	Blank PDI
20	8.43 X 10^{17}	8.18 X 10^{17}	1.03	4.5 (± 0.4)	0.37 (± 0.04)	4.2 (± 0.2)	0.36 (± 0.04)	4.5 (± 0.3)	4.4	0.38 (± 0.28)
12	2.11 X 10^{18}	2.08 X 10^{18}	1.01	3.4 (± 0.1)	0.27 (± 0.03)	3.4 (± 0.1)	0.27 (± 0.06)	3.72 (± 0.02)	3.7	0.19 (± 0.01)
4	8.31X 10^{19}	8.30 X 10^{19}	1.00	2.1 (± 0.1)	0.51 (± 0.17)	2.2 (± 0.1)	0.42 (± 0.02)	2.0 (± 0.1)	2.5	0.31 (± 0.05)

[a]Radius measurements were taken from the volume distribution
[b] Ref. 2.

Interpretation of DLS measurements on MK-1 or MK-1(H_2) Containing AOT/isooctane RMs. DLS established the formation of RMs. Samples of MK-1 or MK-1(H_2) RMs were prepared using 0.10 M AOT/isooctane and the results are shown in Table A4.9. The average radius obtained from w_0 sizes 4, 12, and 20 compared favorably with those reported previously in the literature.[2, 3, 4] These results were observed with RMs prepared with and without MK-1 or MK-1(H_2). These results showed that RMs formed, and that the presence of MK-1 or MK-1(H_2) did not significantly affect the size or stability of the RM.

References

1. Koehn, J. T.; Beuning, C. N.; Peters, B. J.; Dellinger, S. K.; Van Cleave, C.; Crick, D. C.; Crans, D. C., Investigating Substrate Analogues for Mycobacterial MenJ: Truncated and Partially Saturated Menaquinones. *Biochemistry* **2019,** *58* (12), 1596-1615.
2. Maitra, A., Determination of Size Parameters of Water-aerosol-OT Oil Reverse Micelles From Their Nuclear Magnetic-resonance Data. *J. Phys. Chem.* **1984,** *88* (21), 5122-5125.
3. Eicke, H. F.; Rehak, J., Formation of Water-oil-microemulsions. *Helv. Chim. Acta* **1976,** *59* (8), 2883-2891.
4. Zulauf, M.; Eicke, H. F., Inverted Micelles and Microemulsions in the Ternary-system H_2O-areosol-OT-isooctane as Studied by Proton Correlation Spectroscopy. *J. Phys. Chem.* **1979,** *83* (4), 480-486.

Appendix V: Supporting Information for Chapter 5

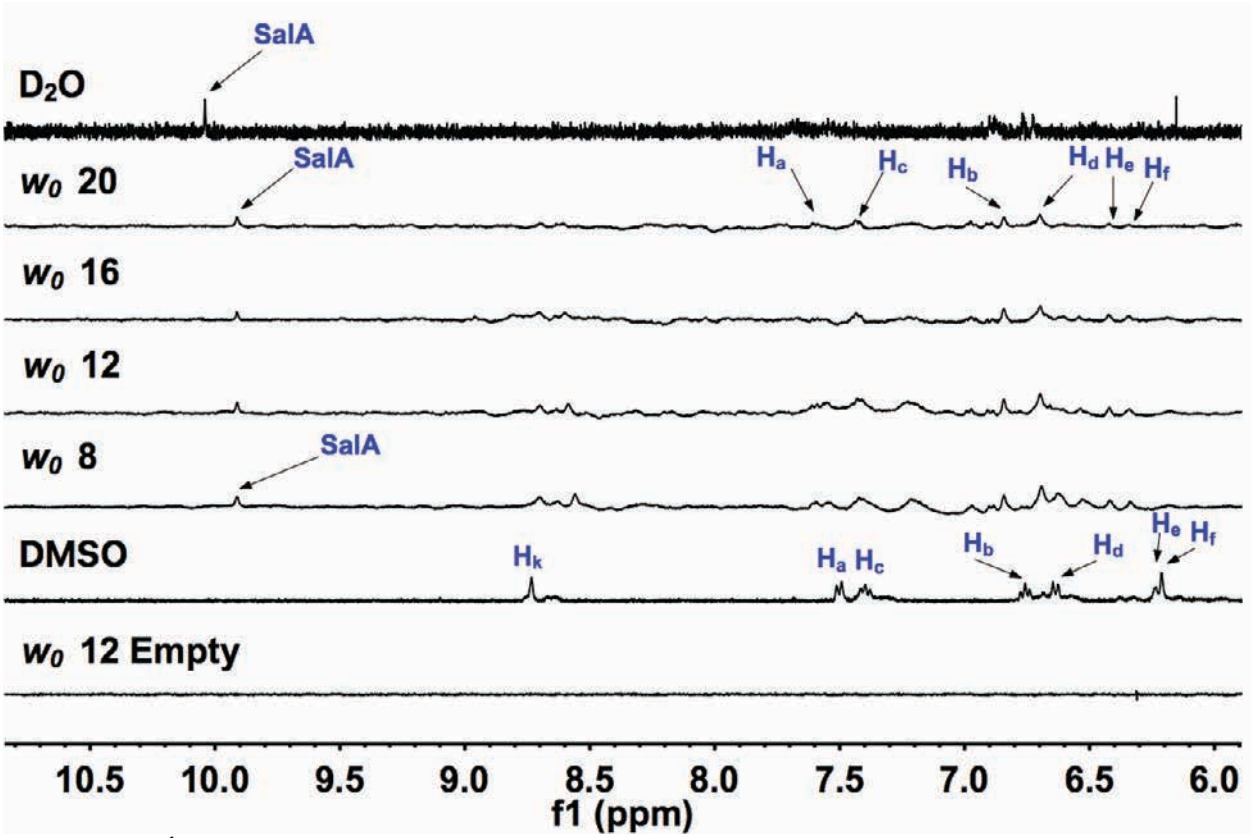

Figure A5.1: ^{1}H NMR spectra of [VO(Hshed)(dtb)] in d_6-DMSO, iso-octane, and in a series of RMs (w_0 = 8, 12, 16, and 20 prepared from 0.750 M AOT/iso-octane stock solution). The spectrum in D_2O was recorded after 60 min. and the spectra in RMs was recorded after 50 min. once equilibrium had been established. Hydrogen labeling scheme is found in Figure 5.1.1. SalA = Salicylaldehyde.

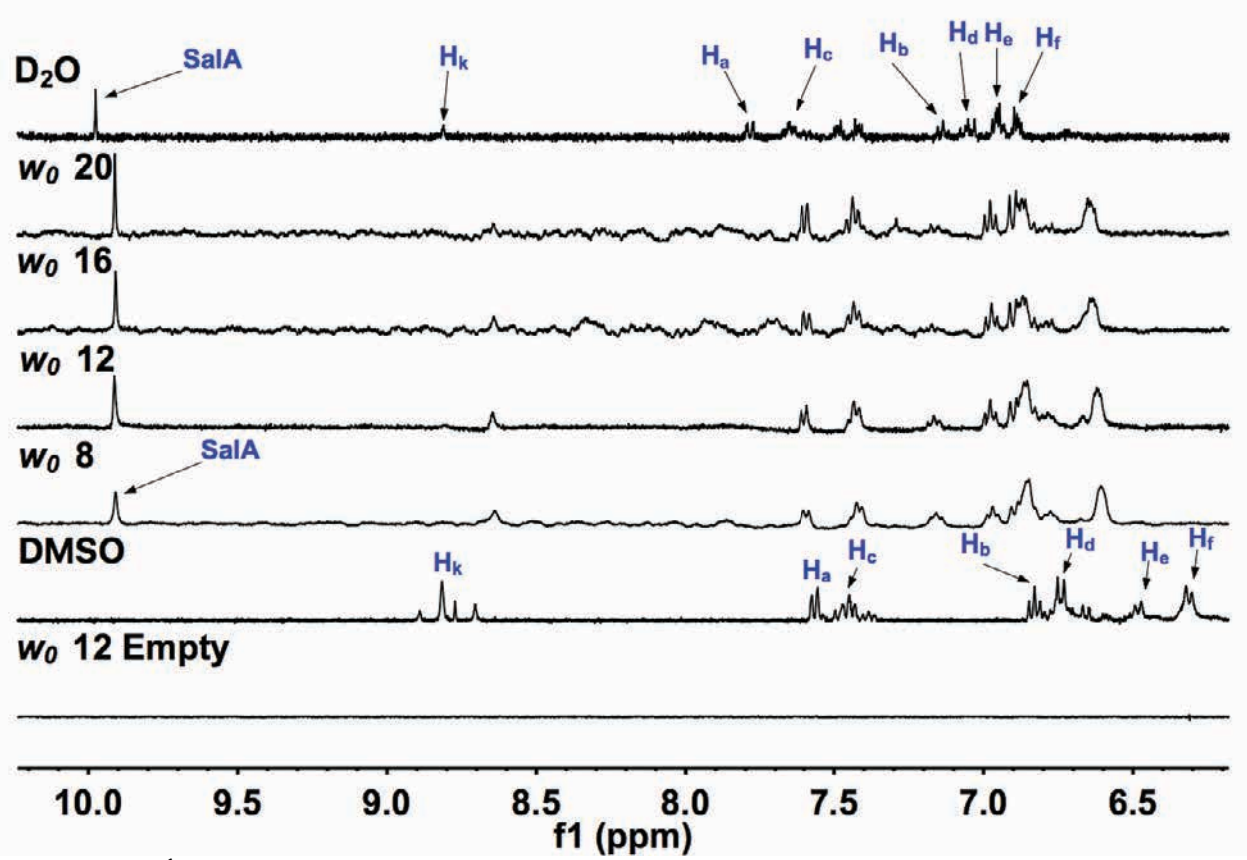

Figure A5.2: ^{1}H NMR spectra of [VO(Hshed)(cat)] in d_6-DMSO, D_2O, and in a series of RMs (w_0 = 8, 12, 16, and 20 prepared from 0.750 M AOT/iso-octane stock solution). The spectrum in D_2O was recorded after 50 min. and the spectra in RMs was recorded after 40 min. once equilibrium had been reached. Hydrogen labeling scheme is found in Figure 5.1.1. SalA = Salicylaldehyde.

Table A5.1. Dynamic Light Scattering measurements on $[V(O)_2(Hshed)]$, H_2shed, $[VO(Hshed)(cat)]$, H_2cat, $[VO(Hshed)(dtb)]$, and H_2dtb in 0.1 M AOT/isooctane RMs.

	$w_0 = 12$	$w_0 = 20$
N(probe)/N(micelle)	2.3	1.4
$[V(O)_2(Hshed)]$ r_h[a] (nm)	3.9 (± 0.3)	4.5 (± 0.3)
PDI $[V(O)_2(Hshed)]$	0.33 (±0.16)	0.52 (±0.17)
H_2shed r_h[a] (nm)	4.0 (± 0.3)	4.3 (± 0.3)
PDI H_2shed	0.20 (±0.08)	0.60 (±0.20)
$[VO(Hshed)(cat)]$ r_h[a] (nm)	3.5 (±0.3)	4.3 (± 0.4)
PDI $[VO(Hshed)(cat)]$	0.27 (±0.12)	0.46 (±0.18)
H_2cat r_h[a] (nm)	3.8 (±0.2)	4.4 (± 0.3)
PDI H_2cat	0.43 (±0.16)	0.23 (±0.09)
$[VO(Hshed)(dtb)]$ r_h[a] (nm)	3.6 (±0.5)	4.1 (±0.3)
PDI $[VO(Hshed)(dtb)]$	0.45 (±0.08)	0.16 (±0.05)
H_2dtb r_h[a] (nm)	3.8 (±0.2)	4.3 (±0.3)
PDI H_2dtb	0.22 (±0.08)	0.48 (±0.11)
Blank r_h[a] (nm)	3.6 (± 0.3)	4.6 (± 0.3)
PDI Blank	0.42 (±0.17)	0.50 (±0.19)
Lit. r_h[b] (nm)	3.7	4.4

[a]Radius measurements were taken from the volume distribution
[b] Ref. 1.

Interpretation of DLS measurements on $[V(O)_2(Hshed)]$, H_2shed, $[VO(Hshed)(cat)]$, H_2cat, $[VO(Hshed)(dtb)]$, and H_2dtb Containing AOT/isooctane RMs.

DLS established the formation of RMs. Samples of $[V(O)_2(Hshed)]$, H_2shed, $[VO(Hshed)(cat)]$, H_2cat, $[VO(Hshed)(dtb)]$, or H_2dtb RMs were prepared using 0.10 M AOT/isooctane and the results are shown in Table A5.1. The average radius obtained from w_0 sizes 12, and 20 compared favorably with those reported previously in the literature.[1, 2, 3] These results were observed with RMs prepared with and without $[V(O)_2(Hshed)]$, H_2shed, $[VO(Hshed)(cat)]$, H_2cat, $[VO(Hshed)(dtb)]$, or H_2dtb. These results showed that RMs formed, and that the presence of $[V(O)_2(Hshed)]$, H_2shed, $[VO(Hshed)(cat)]$, H_2cat, $[VO(Hshed)(dtb)]$, or H_2dtb did not significantly affect the size or stability of the RM.

References

1. Maitra, A., Determination of Size Parameters of Water-aerosol-OT Oil Reverse Micelles From Their Nuclear Magnetic-resonance Data. *J. Phys. Chem.* **1984,** *88* (21), 5122-5125.
2. Eicke, H. F.; Rehak, J., Formation of Water-oil-microemulsions. *Helv. Chim. Acta* **1976,** *59* (8), 2883-2891.
3. Zulauf, M.; Eicke, H. F., Inverted Micelles and Microemulsions in the Ternary-system H_2O-areosol-OT-isooctane as Studied by Proton Correlation Spectroscopy. *J. Phys. Chem.* **1979,** *83* (4), 480-486.

Appendix VI: Synthesis and Characterization of Partially and Fully Saturated Menaquinone Derivatives

This is the manuscript that corresponds to chapter two and is published in *ACS Omega*.[1]

References

1. Koehn, J. T.; Crick, D. C.; Crans, D. C., Synthesis and Characterization of Partially and Fully Saturated Menaquinone Derivatives. *ACS Omega* **2018,** *3*, 14889-14901.

This is an open access article published under a Creative Commons Attribution (CC-BY) License, which permits unrestricted use, distribution and reproduction in any medium, provided the author and source are cited.

ACS OMEGA

Article

Cite This: ACS Omega 2018, 3, 14889−14901

http://pubs.acs.org/journal/acsodf

Synthesis and Characterization of Partially and Fully Saturated Menaquinone Derivatives

Jordan T. Koehn,[†] Dean C. Crick,[‡,§] and Debbie C. Crans*[,†,‡]

[†]Chemistry Department, [‡]Cell and Molecular Biology Program, and [§]Microbiology, Immunology, and Pathology Department, Colorado State University, Fort Collins, Colorado 80523, United States

Supporting Information

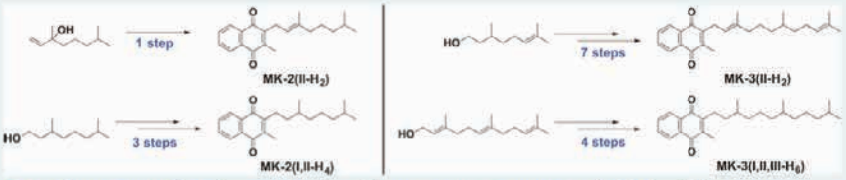

ABSTRACT: Menaquinones (MKs) contain both a redox active quinone moiety and a hydrophobic repeating isoprenyl side chain of varying lengths and degrees of saturation. This characteristic structure allows MKs to play a key role in the respiratory electron transport system of some prokaryotes by shuttling electrons and protons between membrane-bound protein complexes, which act as electron acceptors and donors. Hydrophobic MK molecules with partially and fully saturated isoprenyl side chains are found in a wide range of eubacteria and archaea, and the structural variations of the MK analogues are evolutionarily conserved but poorly understood. For example, *Mycobacterium tuberculosis*, the causative agent of tuberculosis, uses predominantly MK-9(II-H_2) (saturated at the second isoprene unit) as its electron carrier and depends on the synthesis of MK-9(II-H_2) for survival in host macrophages. Thus, MKs with partially saturated isoprenyl side chains may represent a novel virulence factor. Naturally occurring longer MKs are very hydrophobic, whereas MK analogues that have a truncated (i.e., one to three isoprenes) isoprenyl side chain are less hydrophobic. This improves their solubility in aqueous solutions, allowing rigorous study of their structure and biological activity. We present the synthesis and characterization of two partially saturated MK analogues, MK-2(II-H_2) and MK-3(II-H_2), and two novel fully saturated MK derivatives, MK-2(I,II-H_4) and MK-3(I,II,III-H_6).

INTRODUCTION

Menaquinones (or naphthoquinones, MKs) belong to the class of lipoquinones, which are a type of lipid-quinone containing isoprenoids that have a variety of biological roles. These molecules contain both a redox active quinone moiety and a hydrophobic repeating isoprenyl side chain of varying lengths and degrees of saturation (Figure 1) depending on the organism. Although the naturally occurring lipoquinones generally have longer isoprenyl side chains, these MK analogues have very low water solubility, which causes problems for biological assays; therefore, the use of truncated MK derivatives can circumvent solubility issues in aqueous assays. The 1943 Nobel prize in physiology or medicine was awarded to Henrik Dam and Edward Doisy for the discovery and characterization of vitamin K (a MK), a key cofactor in blood coagulation.[1] The interest in and the importance of MK/vitamin K, its derivatives, and vitamers (e.g., vitamins K_1, K_2, and K_3) have remained strong. Vitamin K_1, also known as phylloquinone, is found in green plants and contains four isoprene units with the terminal three saturated and functions as an electron acceptor during photosynthesis within photosystem I.[2] Vitamin K_2, also known as menaquinone-4 (MK-4), has been the subject of interesting reports, demonstrating its biological roles and applications over the last 10 years.[3−6] Vitamin K_3 (or menadione), the simplest 1,4-naphthoquinone derivative, which lacks the isoprenyl side chain and non-naturally occurring N-alkylated MK derivatives has also shown interesting biological properties.[7−11] In 2017, the potent cyclic peptide antibiotic, Lotilibcin, was demonstrated to be effective against Gram-positive bacteria including methicillin-resistant *Staphylococcus aureus*.[12] The activity of Lotilibcin was attributed to lysis of the bacterial membrane, where its membrane-disrupting effects depended on the presence of MK, which leaves the question if other MK derivatives have the same effect.[12] This report underlines the importance of understanding the relationship between the MK structure, its biological role, and its biological function.

MK analogues that contain partially and fully saturated isoprenyl side chains of various lengths are found in eubacteria and archaea. These characteristics are evolutionarily conserved and have long been used in taxonomic classification efforts and phenotypic organization of bacteria.[13−15] MK analogues with

Received: October 1, 2018
Accepted: October 10, 2018
Published: November 5, 2018

ACS Publications © 2018 American Chemical Society

DOI: 10.1021/acsomega.8b02620
ACS Omega 2018, 3, 14889−14901

Downloaded via COLORADO STATE UNIV on November 5, 2018 at 19:35:04 (UTC).
See https://pubs.acs.org/sharingguidelines for options on how to legitimately share published articles.

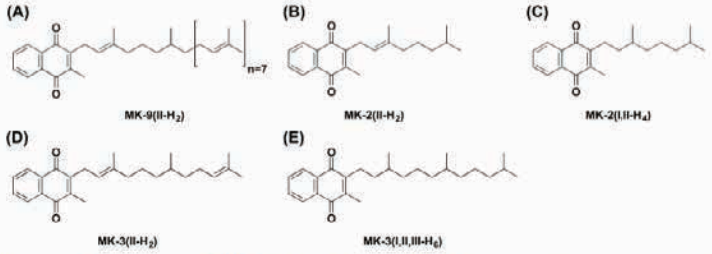

Figure 1. (A) Partially saturated menaquinone-9(II-H_2) [abbreviated as MK-9(II-H_2)] present within *M. tuberculosis*, (B) partially saturated menaquinone-2(II-H_2) [abbreviated as MK-2(II-H_2)], (C) fully saturated menaquinone-2(I,II-H_4) [abbreviated as MK-2(I,II-H_4)], (D) partially saturated menaquinone-3(II-H_2) [abbreviated as MK-3(II-H_2)], and (E) fully saturated menaquinone-3(I,II,III-H_6) [abbreviated as MK-3(I,II,III-H_6)].

one or more saturated isoprene units are found in some members of Gram-positive and Gram-negative bacteria, and the systematic preparation and characterization of a few selected truncated partially and fully saturated MK derivatives are described in this manuscript.[14−17] In contrast to partial saturation, the fully saturated MK-7(14H) has been observed in archaea, which are single-celled microbes comprising part of the human microbiota.[18,19] It is thought that the full saturation of the isoprenyl side chain observed in archaea makes the cellular membrane more tolerant to extreme environments (e.g., high temperature, high salinity, and low/high pH).[18] Thus, many MK homologues that contain various degrees of saturation in their isoprenyl side chains have been isolated, but there is a limited understanding of the function of partially saturated derivatives.[16,20] Menaquinone-9(II-H_2) [abbreviated as MK-9(II-H_2), Figure 1A], which is saturated at the second isoprene, has been observed in a number of bacteria including *Mycobacterium phlei* and pathogenic *Mycobacterium tuberculosis*.[14,16,17,21,22] The biological significance of the partial saturation of MK-9 has remained unclear even 50 years after its first description.[20] Remarkably, the synthesis of MK-9(II-H_2) was recently shown to be essential for *M. tuberculosis* survival in host macrophages (white blood cells of the immune system); thus, MK-9(II-H_2) represents a potential novel virulence factor involved in tuberculosis (TB) disease progression.[23]

Part of our ongoing studies includes why partial saturation of MK-9 increases the virulence of pathogens such as *M. tuberculosis*.[23] Therefore, we need access to MK analogues containing partially and fully saturated isoprenyl side chains. However, in general, they are neither commercially available nor sold as a pure geometric isomer as in the case of vitamin K_1. The potential for the formation of cis and trans MK isomers and the separation and characterization of these geometric isomers are sometimes overlooked in the literature, but it is critical for their applications in biological systems. The use of cis/trans MK mixtures in biological systems would lead to inaccurate biological activities. Recently, the separation and nuclear magnetic resonance (NMR) analysis of cis/trans mixtures of the dietary supplement menaquinone-7 (MK-7) was reported, demonstrating the importance in understanding the different chemical, biochemical, conformational, and physical properties exhibited between cis and trans MK isomers.[24,25] Truncated MK analogues (i.e., one to three isoprene units) have the advantage of being less hydrophobic, which can improve their biological activity compared to longer isoprenyl MK analogues (e.g., MK-7 and MK-9) and can be prepared using a similar methodology described in this manuscript and reports elsewhere.[26,27]

In this manuscript, we have synthesized and characterized four partially and fully saturated truncated isoprenyl MK derivatives (Figure 1B−E) as well as separated and characterized the geometric isomers formed in the reactions. We have adopted the simple naming system where MK-2 with a saturated double bond at the second isoprene unit is denoted as menaquinone-2(II-H_2) and abbreviated as MK-2(II-H_2), where II denotes the second isoprene unit and H_2 denotes the saturation of one double bond (Figure 1B).[23,28] This naming system follows for higher degrees of saturation such as MK-2(I,II-H_4), that is, saturated at isoprenes I and II and MK-3(I,II,III-H_6), that is, saturated at isoprenes I, II, and III (Figure 1C,E). Although MK-2(II-H_2) and menaquinone-3(II-H_2) [abbreviated as MK-3(II-H_2)] were known in literature reports mostly in the 1950s[29−34] and MK-2(II-H_2) was considered in a computational model study,[35] there are no modern syntheses reported, and these analogues have not been extensively characterized nor have their geometric isomers been resolved and characterized in the literature. Evidence supports the trans MK isomer as the only biologically active isomer.[27] Therefore, the separation and isolation of geometric isomers of MK derivatives is critical when testing these compounds in biological assays.

The synthesis and characterization of partially and fully saturated isoprenyl MK analogues, such as the two novel fully saturated MK derivatives described in this work, are important for understanding their requirement in biological systems, as little is known about their physical properties, reactivity, or 3D-conformation within solution or cell membranes. Access to these partially and fully saturated truncated MK analogues in the pure geometric form is critical, considering the recent discovery and timeliness for understanding why partially saturated MKs [e.g., MK-9(II-H_2), Figure 1A] may be a potential virulence factor against pathogenic *M. tuberculosis*, when currently around one-third of the world's population is infected with latent TB and over 1.3 million people worldwide die annually from TB.[36]

RESULTS AND DISCUSSION

In the following, we describe the synthesis and characterization of two partially saturated MK analogues, MK-2(II-H_2) and MK-3(II-H_2), using modified and adapted procedures. We also describe the synthesis and characterization of two novel fully saturated MK analogues, MK-2(I,II-H_4) and MK-3(I,II,III-

DOI: 10.1021/acsomega.8b02620
ACS Omega 2018, 3, 14889−14901

Scheme 1. Synthetic Scheme for the Coupling Reaction Using a MgF_2-48 Catalyst To Obtain MK-2(II-H_2) 3 from Menadiol 1 and Isophytol 2[40]

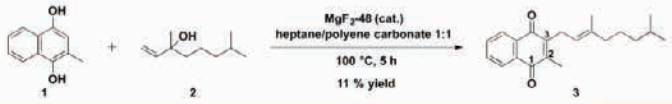

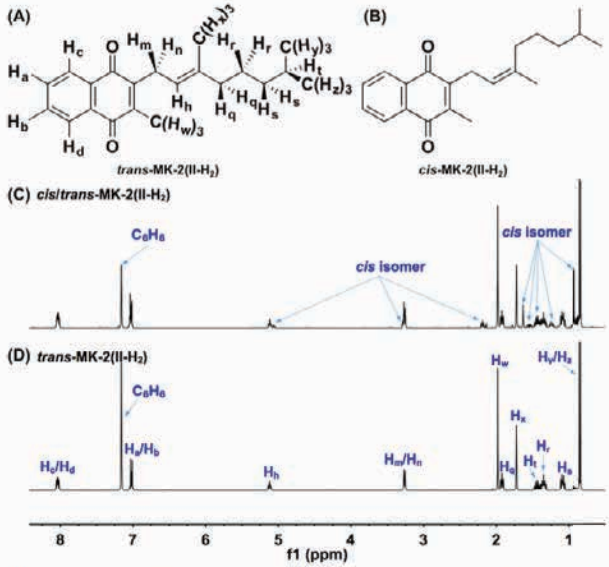

Figure 2. Comparison of the 1D ^{1}H NMR (400 MHz) spectra for the mixture of *cis*/*trans*-MK-2(II-H_2) and *trans*-MK-2(II-H_2) in C_6D_6 at 25 °C. (A) Structure of *trans*-MK-2(II-H_2) with the proton labeling scheme key, (B) structure of *cis*-MK-2(II-H_2), (C) 1D ^{1}H NMR spectrum of the cis/trans mixture of MK-2(II-H_2) in C_6D_6, and (D) 1D ^{1}H NMR spectrum of *trans*-MK-2(II-H_2) in C_6D_6.

H_6), utilizing a key radical alkylation reaction. This is the first report on a preparatory scale utilizing a primary alkyl radical coupling reaction to access fully saturated MK derivatives, although in situ analysis of menaquinone-1(H_2) was reported previously.[37] Importantly, a convenient analysis can be carried out by rapid detection using benzene-d_6 as an NMR solvent for the evaluation of cis and trans MK mixtures (peaks coalesce in $CDCl_3$ disguising potential isomers formed). The cis/trans isomers can then be readily separated using preparative thin-layer chromatography (TLC) and analyzed.

Synthesis and Characterization of MK-2(II-H_2). The partially saturated MK analogue, MK-2(II-H_2) **3**, was synthesized in a single step using Friedel–Crafts coupling between menadiol **1** and isophytol **2** (Scheme 1). The precursor menadiol was synthesized, as previously described, from menadione.[26,38] The partly hydroxylated heterogeneous Lewis–Brønsted acid catalyst, MgF_2-48, was synthesized as previously described.[39−41] We chose MgF_2-48 over other catalysts because it was readily prepared from inexpensive methanol and Mg^0 powder as well as from commonly available 48% aqueous hydrofluoric acid.[39−41] Furthermore, the partly hydroxylated MgF_2 catalyst was recently used with a biphasic *n*-heptane/polyene carbonate solvent system to synthesize vitamin K_1 and K_1-chromanol.[40] Therefore, we thought this catalyst would be an excellent choice to synthesize the partially saturated MK-2(II-H_2), which has the analogous (but truncated) structure of vitamin K_1 [or MK-4(II,III,IV-H_6)].

The Friedel–Crafts alkylation of **1** and **2** (Scheme 1) followed by in situ oxidation of dihydro-MK-2(II-H_2) formed the desired product **3** in an 11% yield. The low yield may be attributed to the formation of the undesired C2 isomeric side product (see Scheme 1), which was readily separated using column chromatography. The inherent instability of menadiol, which is prone to auto-oxidation even when purified immediately before use may also contribute to the low yield. MK-2(II-H_2) 3 was obtained as a yellow/red oil. The reaction was carried out in the dark, and the product was exposed minimally to light as previous studies have shown that interconversion to undesirable geometric isomers can occur through photo-oxidation if exposed to light.[16,42,43]

We considered other possible catalysts to carry out the transformation shown in Scheme 1. For instance, we also explored a commercially available strong Brønsted acid catalyst (Nafion perfluorinated powdered resin and Nafion perfluorinated ion-exchange resin in 10 wt % dispersion in water); however, the yields were significantly lower with the increased formation of the C2 prenylated isomeric side product (see Scheme 1). Furthermore, we were concerned about the Nafion catalyst (containing super acidic sites) dehydrating isophytol to

DOI: 10.1021/acsomega.8b02620
ACS Omega 2018, 3, 14889−14901

Scheme 2. Synthetic Scheme for the Three-Step Synthesis To Obtain MK-2(I,II-H_4) 7[a]

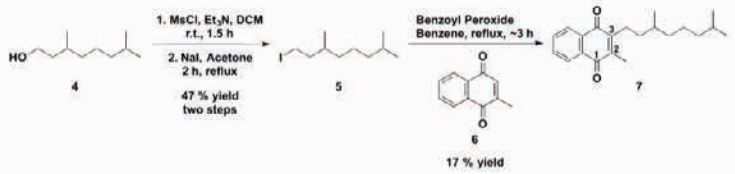

[a]The first step forms the mesylate from **4**. The second step forms aliphatic iodide **5** via a S_N2 reaction. The final step couples menadione **6** and aliphatic iodide **5** using a radical alkylation initiated by benzoyl peroxide.

Scheme 3. Synthetic Scheme for the Seven-Step Synthesis To Obtain MK-3(II-H_2) 13 from β-Citronellol 8[33,38]

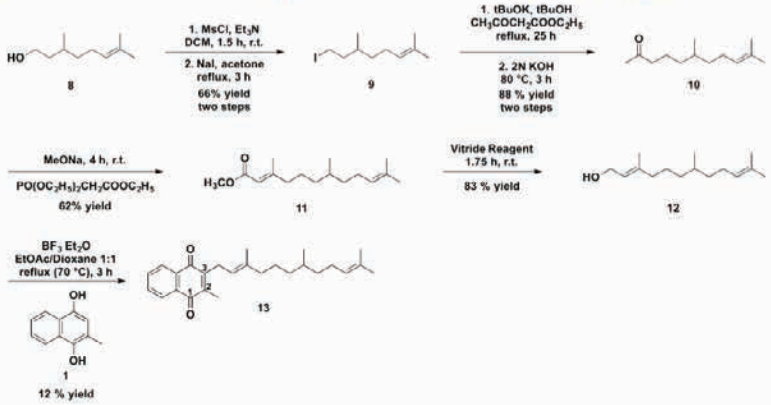

form undesirable phytadienes,[40] which presumably contribute to it being a less desirable catalyst for this purpose.

An interesting feature of MKs is the possibility of geometric isomer formation (Figure 2A,B). The biologically active trans isomer of vitamin K_1 is the natural biological form of vitamin K_1.[27] Evidence also demonstrates that biological MKs have an all-trans configuration of the double bonds within the isoprenyl side chain.[27] The geometric isomers of vitamin K_1, MK-7 and MK-9(II-H_2) (isolated from *M. phlei*, Figure 1A), have been successfully separated; therefore, efforts to isolate the trans isomer of MK-2(II-H_2) from its cis isomer byproduct (Figure 2B) were carried out.[16,24,27] MK-2(II-H_2) **3** was initially isolated as a 2.7:1 mixture of trans/cis isomers (by NMR integration of alkene peaks in benzene-d_6) after column chromatography. The trans isomer of MK-2(II-H_2) **3** can be isolated using preparative TLC, similar to reports for vitamin K_1 analogues[34] and MK analogues.[16]

The successful separation of the trans isomer of **3** by preparative TLC allowed for characterization of a single pure geometric isomer of MK-2(II-H_2), Figure 2. The structural assignment of *trans*-MK-2(II-H_2) (Figure 2) was elucidated using two-dimensional (2D) NMR spectroscopic methods [$^1H-^1H$ correlation spectroscopy (COSY) and $^1H-^{13}C$ heteronuclear single quantum correlation (HSQC) spectroscopy; see the Supporting Information for spectra, Figures S1–S4.1 and S7–S8.1]. Spectra obtained in benzene-d_6 (C_6D_6) result in less overlap of the NMR signals for the cis/trans isomer mixture (Figure 2C,D), compared to $CDCl_3$ where some of the geometric isomer peaks overlap (e.g., cis/trans alkene protons coalesce in $CDCl_3$) and the formation of isomers is not obvious. Therefore, the use of C_6D_6 as a diagnostic NMR solvent for the evaluation of cis/trans mixtures for MK analogues was critical and is in line with a recently reported NMR analysis of cis/trans isomer mixtures of MK-7[24] (see the Supporting Information for spectra in $CDCl_3$ versus C_6D_6, Figure S40).

Synthesis and Characterization of MK-2(I,II-H_4). The fully saturated isoprenyl MK analogue, MK-2(I,II-H_4) **7**, was synthesized in three steps from commercially available 3,7-dimethyloctan-1-ol **4** (Scheme 2). The first step converted aliphatic alcohol **4** to the mesylate, which was then subjected to an S_N2 reaction using NaI to yield 1-iodo-3,7-dimethyloctane **5** in 47% yield over two steps.[38] The alkyl iodide **5** was then coupled to menadione **6** via radical alkylation using benzoyl peroxide[37] as a radical initiator to yield MK-2(I,II-H_4) **7** in 17% yield. The yield for the coupling reaction is close in range with that reported in the literature for other coupling reactions for the synthesis of MK analogues.[26,27,38] The unreacted alkyl iodide **5** can be recovered during column chromatography. In an effort to ensure selectivity of prenylation at C3 versus C2 (Scheme 2), the slow addition of napthoquinone **6** during the reaction was carried out so that the naphthoquinone stationary concentration in the reaction mixture is low compared to the prenyl iodide concentration.[37] MK-2(I,II-H_4) **7** was obtained as a yellow oil. This is the first report of the synthesis and characterization of MK-2(I,II-H_4) **7** (see the Supporting Information for the 2D NMR spectra, Figures S13–S14.1), the fully saturated analogue of MK-2.

DOI: 10.1021/acsomega.8b02620
ACS Omega 2018, 3, 14889−14901

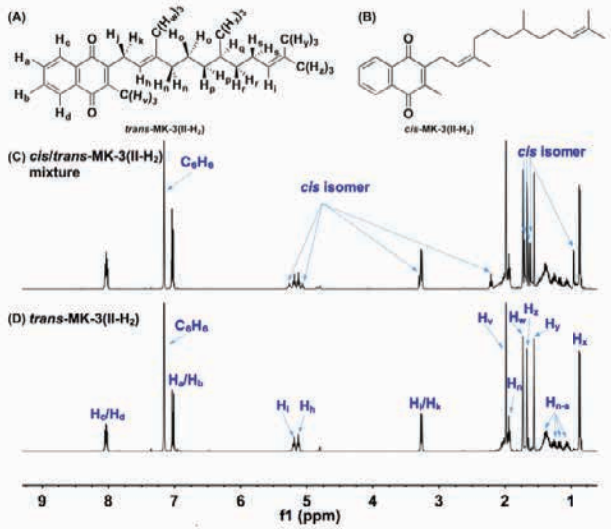

Figure 3. Comparison of the 1D ^{1}H NMR (400 MHz) spectra for the mixture of *cis*/*trans*-MK-3(II-H_2) and *trans*-MK-3(II-H_2) in C_6D_6 at 25 °C. (A) Structure of *trans*-MK-3(II-H_2) with the proton labeling scheme key, (B) structure of *cis*-MK-3(II-H_2), (C) 1D ^{1}H NMR spectrum of the cis/trans mixture of MK-3(II-H_2) in C_6D_6, and (D) 1D ^{1}H NMR spectrum of *trans*-MK-3(II-H_2) in C_6D_6. Overlapping cis/trans peaks have been left unlabeled.

Synthesis and Characterization of MK-3(II-H_2). The partially saturated isoprenyl MK analogue, MK-3(II-H_2) **13**, was synthesized in seven steps from commercially available β-citronellol **8** (Scheme 3) via a modified adaptation of a combination of a reported synthesis of MK-4(II-H_2)[38] and a less recent 1965 synthesis of MK-3(II-H_2).[33] First, the hydroxyl group of β-citronellol **8** was converted into iodide **9** through methane sulfonate in 66% yield over two steps.[38] The introduction of a carbonyl group to produce citronellylacetone **10** was accomplished under basic conditions in 88% yield over two steps.[45] This was followed by a Horner−Wadsworth−Emmons reaction to give methyl ester **11** in 62% yield.[38] Reduction of **11** with the Vitride reagent produced 6,7-dihydrofarnesol **12** in 83% yield.[38,46] Finally, MK-3(II-H_2) **13** was obtained from the BF_3-catalyzed coupling between the partially saturated allylic alcohol **12** and menadiol **1** (prepared from menadione)[26,38] in 12% yield.[26,38] The low yield may be attributed to the formation of the undesired C2 isomeric side product (see Scheme 3), which was readily separated using column chromatography. MK-3(II-H_2) **13** was obtained as a yellow oil.

Similar to MK-2(II-H_2) **3**, MK-3(II-H_2) **13** was initially isolated as a 2.7:1 mixture (by NMR integration of alkene peaks in C_6D_6) of trans/cis isomers. However, the trans isomer (Figure 3A) can be isolated from the cis isomer byproduct (Figure 3B) using preparative TLC, similar to a report on cis/trans vitamin K_1 analogues.[44] MK analogues can be very sensitive; for example, during purification, we observed degradation of *trans*-MK-3(II-H_2) (Figure 3A) within a solution of dichloromethane (DCM) that was not stabilized with amylene. This was evidenced by a decreased integration value for the alkene proton at 5.19 ppm and the appearance of two extra peaks at ~1.3 ppm and a peak at 1.12 ppm in C_6D_6. Amylene is a radical scavenger, and it is likely that the alkene is undergoing a radical reaction with chloride radicals present in the unstabilized DCM. Similar to MK-2(II-H_2) **3**, the use of benzene-d_6 as a diagnostic NMR solvent for the evaluation of cis/trans mixtures of MK-3(II-H_2) **13** (Figure 3C,D) was essential because the presence of the cis isomer was not well-observed in $CDCl_3$ (see the Supporting Information for spectra in $CDCl_3$ vs benzene-d_6, Figure S40).

The structural assignment of *trans*-MK-3(II-H_2) (Figure 3) was elucidated using 2D NMR spectroscopic methods [^{1}H−^{1}H COSY, ^{1}H−^{13}C HSQC, and ^{1}H−^{1}H rotating frame Overhauser effect spectroscopy (ROESY); see the Supporting Information for spectra, Figures S23−S26.1 and S29−S31]. The assignment of the alkene proton H_h at 5.13 ppm was determined by the following: the observation of a cross peak in the COSY spectrum at 5.13 and 1.73 ppm (assignment H_w, Figure 3), the observation of a cross peak at 5.13 and 1.94 ppm (assignment H_n, Figure 3), and the lack of an observed cross peak at 5.19 and 1.73 ppm (H_w). The assignment of alkene proton H_i at 5.19 ppm was determined by the observation of a cross peak at 5.19 and 1.67 ppm and the lack of a cross peak at 5.19 and 1.73 ppm (H_w). ^{1}H−^{1}H 2D ROESY NMR spectroscopy (see the Supporting Information) also supported the alkene assignment by the observation of a ROE cross peak at 5.19 and 1.67 ppm (H_i−H_z interaction) and the lack of a ROE cross peak at 5.19 ppm and 1.56 ppm. The assignment of the terminal methyl groups, H_y and H_x, was also determined by ^{1}H−^{1}H 2D ROESY NMR spectroscopy. It is anticipated that a ROE cross peak would be observed between the alkene proton H_i and the methyl group, that is, cis to H_i, because of the close spatial proximity, and a ROE cross peak is observed, as expected, at 5.19 and 1.67 ppm (H_i−H_z interaction) (see the Supporting Information). Although H_y and H_i are within the spatial limits of an expected ROE cross peak observation, an ROE cross peak is not observed at 5.19 ppm and 1.56 ppm. This supports

DOI: 10.1021/acsomega.8b02620
ACS Omega 2018, 3, 14889−14901

Scheme 4. Synthetic Scheme for the Four-Step Synthesis To Obtain MK-3(I,II,III-H_6) 17[a]

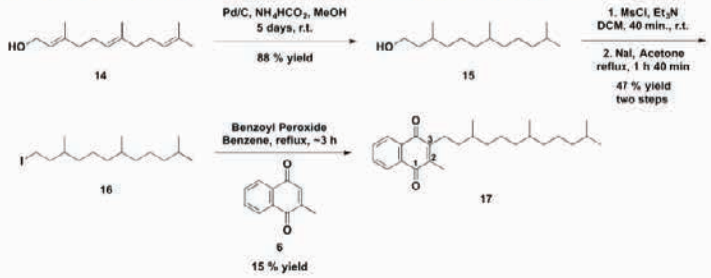

[a]The first step is a transfer hydrogenation to produce the fully saturated alcohol **15** from farnesol **14**. The second step forms the mesylate from **15**. The third step forms aliphatic iodide **16** via a S_N2 reaction. The final step couples menadione **6** and aliphatic iodide **16** using a radical alkylation initiated by benzoyl peroxide.

the structural assignment of H_y as trans to the alkene proton H_i, as H_y is further away, spatially, from H_i compared to H_z.

Synthesis and Characterization of MK-3(I,II,III-H_6). The fully saturated isoprenyl MK analogue, MK-3(I,II,III-H_6) **17**, was synthesized in four steps (Scheme 4) from the commercially available allylic alcohol, farnesol **14**. The first step was the Pd- catalyzed transfer hydrogenation of farnesol to yield the fully saturated alcohol **15** in 88% yield.[47] Subsequent mesylation of the alcohol of product **15** followed by substitution with NaI gave aliphatic iodide **16** in 47% yield over two steps.[38,48] The final step was the radical coupling of menadione **6** and aliphatic iodide **16** using benzoyl peroxide[37] as the radical initiator to yield the desired final product, MK-3(I,II,III-H_6) **17**, in 15% yield. This yield is similar to that attained for the coupling reaction to obtain MK-2(I,II-H_4) **7**. The unreacted aliphatic iodide **16** can be recovered during purification. Similar to MK-2(I,II-H_4) **7**, in an attempt to ensure good selectivity of prenylation (C3 over C2, Scheme 4), slow addition of napthoquinone **6** to the prenyl iodide solution during the course of the reaction was carried out.[37] Similar to the synthesis of MK-2(I,II-H_4) **7** above, this is the second report of this type of primary alkyl radical coupling reaction to access MK and the first report on a preparatory scale. MK-3(I,II,III-H_6) **17** was obtained as a yellow oil. This is the first report for the synthesis and characterization of MK-3(I,II,III-H_6) **17** (see the Supporting Information for 2D NMR spectra, Figures S38–S39.1), the fully saturated analogue of MK-3.

■ CONCLUSIONS

The results of these studies will allow for the synthesis of various MK analogues and give access to previously unexplored compounds with unknown biological activity. In summary, this manuscript described the synthesis and characterization of four truncated partially and fully saturated isoprenyl MK analogues as well as separated and characterized the geometric isomers formed in the reactions. The partially saturated MK-2(II-H_2) was successfully synthesized in a single step from menadiol and isophytol, and the trans isomer was separated from the cis isomer byproduct by preparative TLC, followed by characterization. The novel fully saturated MK-2(I,II-H_4) was successfully synthesized in three steps from 3,7-dimethyloctan-1-ol. The partially saturated MK-3(II-H_2) was successfully synthesized in seven steps from β-citronellol, and the trans isomer was readily separated from the cis isomer byproduct by preparative TLC, followed by characterization. Finally, the novel fully saturated MK-3(I,II,III-H_6) was successfully synthesized in four steps from farnesol. The use of benzene-d_6 as a diagnostic NMR solvent for the rapid evaluation of cis/trans mixtures for MK/vitamin K analogues was essential as cis/trans peaks often coalesce in chloroform-*d*.

The separation and characterization of an MK analogue's trans isomer is essential for use of these compounds in biological systems or for understanding biological systems that use MK because evidence shows that the cis isomer is not biologically active. The partially and fully saturated MK analogues synthesized in this manuscript are substrate analogues for enzymes involved in MK/vitamin K metabolism and are essential for understanding the structure–activity relationships of these biological systems.[49] They are also critical for understanding the function, reactivity, and conformation of partially saturated MK analogues as little is currently known. These MK analogues are also of interest from a therapeutic and medicinal standpoint. For instance, MK-4 (vitamin K_2) was recently shown to be a potential new therapeutic strategy to treat rheumatoid arthritis; it is a proposed drug for the effective treatment of osteoporosis and has anticancer properties. Nevertheless, the synthesis of partially saturated MK analogues remains a challenge as there is currently not a suitable catalyst to selectively saturate an individual isoprene unit on an MK analogue while leaving the other double bonds unaffected. Importantly, the synthesis and characterization of these partially and fully saturated MK substrate analogues is essential for understanding why they are necessary for various organisms to survive, and most importantly, understanding the reason MK-9(II-H_2) (i.e., saturated at the second isoprene unit) is a potential virulence factor for pathogenic *M. tuberculosis*, which is responsible for the deaths of ~1.3 million people annually.

■ EXPERIMENTAL SECTION

General Information. Menadiol **1** was synthesized as previously described[26,38] from menadione, and the MgF_2-48 sol–gel catalyst was synthesized, as previously described.[39–41] For clarity, any mention of MK-2(II-H_2) or MK-3(II-H_2) is assumed to be the cis/trans mixture, whereas the trans isomer is specifically written as *trans*-MK-2(II-H_2) or *trans*-MK-3(II-H_2). We used the standard abbreviations adopted by the American Chemical Society, for example, ethyl acetate

DOI: 10.1021/acsomega.8b02620
ACS Omega 2018, 3, 14889–14901

(EtOAc), methanol (MeOH), distilled-deionized water (DDI-H_2O), chloroform-*d* ($CDCl_3$), benzene-d_6 (C_6D_6), equivalent (equiv), room temperature (r.t.), R_f (retention factor), high-resolution mass spectrometry (HRMS), calculated (calcd), megahertz (MHz), Hz (hertz), and so forth. See the Supporting Information for general methods and information, materials, and one-dimensional (1D) and 2D NMR spectra of synthesized compounds.

NMR Spectroscopic Studies. The synthesized compounds were dried under vacuum for ~2−4 days (~150−200 mTorr), unless otherwise noted, to ensure as much residual solvent from purification was removed as possible. Samples for NMR studies were prepared immediately prior to running the samples using deuterated solvents sealed under an inert atmosphere in glass ampules. The NMR sample solutions were placed under an argon atmosphere immediately and capped, and then the spectra were acquired, unless otherwise noted. NMR samples of MKs were protected from light by wrapping the samples in an aluminum foil while not in the NMR instrument because of potential degradation. ^1H and ^{13}C spectra were recorded using a Varian model MR400 or a Bruker model AVANCE Neo400 spectrometer equipped with a BBFO smart probe and an automated tuning module operating at 400 or 101 MHz, respectively. Chemical shift values (δ) are reported in ppm and referenced against the internal solvent peaks in ^1H NMR ($CDCl_3$, δ at 7.26 ppm; benzene-d_6, δ at 7.16 ppm) and in ^{13}C NMR ($CDCl_3$, δ at 77.16 ppm; benzene-d_6, δ at 128.06 ppm). All NMR spectra were recorded at either 25 or 26 °C. NMR spectra were processed using MestReNova version 10.0.1. or 12.0.2. See the Supporting Information for 1D & 2D NMR spectra and NMR experimental details.

Mass Spectrometry and Elemental Analysis. HRMS experiments were conducted either on an Agilent 6224 TOF LC/MS [O-time-of-flight (TOF)] interfaced with the Direct Analysis in Real Time (DART) source (IonSense DART-100) or on a Bruker MaXis TOF MS (Q-TOF) interfaced with the DART source (IonSense DART-SVP). A standard of Jeffamine was used as an internal standard calibration for HRMS DART experiments carried out in the positive mode. Combustion elemental analysis was carried out by ALS Environmental located in Tucson, AZ.

Preparation of MK-2(II-H_2) (3). Compound **3** was accessed from **1** and **2**.

Preparation of 2-(3,7-Dimethyloct-2-en-1-yl)-3-methylnaphthalene-1,4-dione MK-2(II-H_2) (3). To a dry 150 mL round-bottom thick-walled pressure flask was added a dry stir bar, dry heptane (21 mL), and polyene carbonate (21 mL). The solution was bubbled with argon for several min. Then, menadiol **1** (1.22 g, 7.00 mmol) was added and stirred until dissolution occurred under argon bubbling. Then, isophytol **2** (1.09 g, 7.00 mmol) was added, followed by MgF_2-48 (350 mg). The biphasic reaction mixture was bubbled with argon for ~1 min and then sealed tightly with a Teflon screw cap. The sealed reaction mixture was covered in an aluminum foil to minimize light exposure and was stirred for 5 h at 100 °C under an argon atmosphere. The yellow biphasic suspension was then cooled to an ambient temperature. The ^1H NMR spectrum of the crude product confirmed product formation by the presence of a doublet at 3.37 ppm ($CDCl_3$). The layers were separated, and the polyene carbonate layer (bottom layer) was extracted with *n*-pentane (3 × 100 mL). The combined yellow organic extracts were washed with DDI H_2O (100 mL), washed with sat. $NaHCO_3$ (100 mL), washed with brine (100 mL), dried over anhydrous Na_2SO_4, and concentrated under reduced pressure at an ambient temperature. The crude oil was dried overnight under reduced pressure to yield 1.31 g of crude red oil. The crude red oil was purified by flash column chromatography (300 mL of 230−400 mesh SiO_2, 20:1 *n*-pentane/EtOAc, 40 mm column) to yield 0.235 g (0.757 mmol, 10.8% yield) as a yellow/red oil after drying under vacuum (200 mTorr). The C2 isomeric side product was readily separated by flash column chromatography eluting after the C3 desired product. The product was obtained as a mixture of trans/cis isomers (ratio of trans/cis = 2.7:1 by NMR integration of alkene peaks), as has similarly been reported for vitamin K_1 analogues[44] and various MK analogues.[27] ^1H NMR (400 MHz, C_6D_6): δ 8.00−8.06 (m, 2H), 7.0−7.06 (m, 2H), 5.12 (t, J = 7.0 Hz, 1H, trans isomer), 5.06 (t, J = 7.0 Hz, 1H, cis isomer), 3.28 (d, J = 7.7 Hz, 2H, cis isomer), 3.26 (d, J = 7.1 Hz, 2H, trans isomer), 2.19 (t, J = 7.8 Hz, 2H, cis isomer), 1.98 (s, 3H), 1.92 (t, J = 7.5 Hz, 2H, trans isomer), 1.72 (s, 3H, trans isomer), 1.63 (s, 3H, cis isomer), 1.50−1.58 (m, 1H, cis isomer),1.40−1.49 (m, 1H, trans isomer), 1.40−1.48 (m, 2H, cis isomer), 1.31−1.39 (m, 2H, trans isomer), 1.21−1.27 (q, 2H, cis isomer), 1.06−1.11 (q, 2H, trans isomer), 0.93 (d, J = 6.6 Hz, 6H, cis isomer), 0.83 (d, J = 6.6 Hz, 6H, trans isomer). ^{13}C NMR (101 MHz, C_6D_6): δ 184.99, 184.97, 184.24, 184.16, 145.97, 145.95, 143.21, 143.18, 137.93, 137.62, 133.09, 133.06, 132.68, 132.66, 126.31, 126.22, 120.31, 119.82, 40.36, 39.34, 38.95, 32.56, 28.35, 28.20, 26.25, 26.15, 26.08, 25.98, 23.54, 22.87, 22.81, 16.32, 12.62, 12.58. HRMS (DART, Q-TOF): calcd for $C_{21}H_{27}O_2$ [$(M + H)^+$], 311.2006; found, 311.2018.

A sample for analytical characterization of *trans*-MK-2(II-H_2) was purified by normal phase preparative TLC (see experimental below) on silica gel using (30:1) *n*-pentane/EtOAc as the eluting solvent; R_f cis: 0.37, R_f trans: 0.32; ratio of trans/cis before separation was 2.7:1 (the ratio was measured from the NMR integration of alkene peaks). Although we isolated the pure trans isomer, the cis isomer coeluted with the trans isomer, and efforts to obtain a sample of the pure cis isomer were not successful. The cis and the trans isomers have different NMR spectra in C_6D_6 for the protons and carbons within the isoprenyl side chain. Data for *trans*-MK-2(II-H_2): ^1H NMR (400 MHz, C_6D_6): δ 8.00−8.07 (m, 2H), 7.00−7.05 (m, 2H), 5.12 (t, J = 7.0 Hz, 1H), 3.26 (d, J = 7.0 Hz, 2H), 1.98 (s, 3H), 1.92 (t, J = 7.5 Hz, 2H), 1.72 (s, 3H), 1.40−1.49 (m, 1H), 1.31−1.39 (m, 2H), 1.06−1.11 (q, 2H), 0.83 (d, J = 6.6 Hz, 6H). ^{13}C NMR (101 MHz, C_6D_6): δ 184.98, 184.24, 145.97, 143.21, 137.62, 133.09, 133.05, 132.69, 132.66, 126.31, 126.22, 119.82, 40.36, 38.95, 28.20, 26.25, 26.08, 22.81, 16.32, 12.58. HRMS (DART, Q-TOF): calcd for $C_{21}H_{27}O_2$ [$(M + H)^+$], 311.2006; found, 311.1991. NMR data for the cis isomer (obtained from spectra with both cis and trans isomers present): ^1H NMR (400 MHz, C_6D_6): δ 8.00−8.06 (m, 2H), 7.00−7.06 (m, 2H), 5.06 (t, J = 7.0 Hz, 1H), 3.28 (d, J = 7.7 Hz, 2H), 2.19 (t, J = 7.8 Hz, 2H), 1.98 (s, 3H), 1.63 (s, 3H), 1.50−1.58 (m, 1H), 1.40−1.48 (m, 2H), 1.21−1.27 (q, 2H), 0.93 (d, J = 6.6 Hz, 6H).

A sample for analytical characterization of *trans*-MK-2(II-H_2) was prepared by using normal phase preparative TLC. First, 8.0 mg of *cis*/*trans*-MK-2(II-H_2) (dissolved in a minimal amount of DCM) was loaded onto a preparative TLC plate via a capillary tube and then eluted once using 30:1 *n*-pentane/EtOAc and an elution time of 45 min. The TLC plate was

DOI: 10.1021/acsomega.8b02620
ACS Omega 2018, 3, 14889−14901

briefly air-dried and then eluted a second time under the same conditions. The yellow band was illuminated under ultraviolet light, and while illuminated, the band was divided into a top two-third and a bottom one-third. The bottom one-third was carefully removed with a razor blade, extracted with DCM, filtered through a disposable Pasteur pipette filled with glass wool (prerinsed with DCM), concentrated under reduced pressure at an ambient temperature, and dried for 4 days at reduced pressure (200 mTorr) to provide 2.5 mg of *trans*-MK-2(II-H_2) as a yellow oil (31.3% recovery).

Preparation of MK-2(I,II-H_4) (7). Compound **7** was accessed through compound **5** from commercially available compound **4**.

1-Iodo-3,7-dimethyloctane (5). To a dry 250 mL round-bottom Schlenk flask was added a dry stir bar, 3,7-dimethyl-1-octanol **4** (8.61 g, 54.4 mmol), and dry DCM (100 mL), which was then purged/evacuated with argon repeatedly. The solution was cooled to 0 °C in an ice−H_2O bath. Then, methanesulfonyl chloride (2.16 mL, 3.20 g, 27.9 mmol, 1.2 equiv) was added under an argon atmosphere followed by dropwise addition of dry triethylamine (11.39 mL, 8.26 g, 81.6 mmol, 1.5 equiv) over 5 min at 0 °C. The resulting solution was stirred at an ambient temperature for 1.5 h under argon. The reaction was quenched with sat. $NaHCO_3$ (100 mL), and then the phases were separated. The aqueous layer was extracted with diethyl ether (3 × 100 mL). The combined organic extracts were washed with sat. $NaHCO_3$ (100 mL), washed with brine (100 mL), dried over anhydrous Na_2SO_4, and then concentrated under reduced pressure at an ambient temperature (residual triethylamine can be removed by vacuum pumping for ∼1 h) to yield 9.65 g of crude yellow oil. The crude mesylate was dissolved in dry and degassed acetone (100 mL, dried over anhydrous K_2CO_3 immediately prior for ∼10 min) in a dry 250 mL round-bottom Schlenk flask. Then, NaI (16.50 g, 110.0 mmol, 2.0 equiv) was added, and the solution was refluxed for 2 h under argon. The white reaction mixture was diluted with ice−DDI H_2O (100 mL) and diethyl ether (100 mL), and then the phases were separated. The aqueous layer was extracted with diethyl ether (3 × 100 mL). The combined organic extracts were washed with sat. $NaHCO_3$ (100 mL), washed with brine (100 mL), dried over anhydrous Na_2SO_4, and then concentrated under reduced pressure at an ambient temperature to yield 9.83 g of crude clear and yellow oil. The crude product was purified by flash column chromatography (800 mL of 230−400 mesh SiO_2, 10:1 *n*-pentane/EtOAc, 70 mm column) to yield 6.91 g (25.8 mmol, 47.4% yield) as a clear and colorless oil after drying under vacuum (150 mTorr). ^{1}H NMR (400 MHz, $CDCl_3$): δ 3.14−3.28 (m, 2H), 1.83−1.92 (m, 1H), 1.60−1.69 (m, 1H), 1.48−1.58 (m, 2H), 1.21−1.35 (m, 3H), 1.06−1.21 (m, 3H), 0.87 (d, J = 6.6 Hz, 9H). ^{13}C NMR (101 MHz, $CDCl_3$): δ 41.13, 39.33, 34.04, 28.10, 24.68, 22.85, 22.75, 18.89, 5.58. Anal. Calcd for $C_{10}H_{21}I$: C, 44.79; H, 7.89. Found: C, 44.81; H, 7.72.

2-(3,7-Dimethyloctyl)-3-methylnaphthalene-1,4-dione MK-2(I,II-H_4) (7). To a dry 100 mL round-bottom Schlenk flask was added a dry stir bar and dry and degassed benzene (30 mL) followed by 1-iodo-3,7-dimethyloctane **5** (2.68 g, 10.0 mmol, 1 equiv). To a dry 20 mL vial was added dry and degassed benzene (15 mL) followed by menadione **6** (1.72 g, 10.0 mmol) and benzoyl peroxide (2.42 g, 10.0 mmol, 1 equiv) and then sonicated until dissolution occurred under argon. The naphthoquinone−benzoyl peroxide solution was added dropwise for over 2 h 15 min to the refluxing prenyl iodide solution, which was under an argon atmosphere during the reaction. After the addition was complete, the solution was refluxed for an additional 1 h. The solution was diluted with sat. $NaHCO_3$ (100 mL) and diethyl ether (100 mL), and then the phases were separated. The aqueous layer was extracted with diethyl ether (3 × 100 mL). The combined organic extracts were washed with sat. $NaHCO_3$ (100 mL), washed with brine (100 mL), dried over anhydrous Na_2SO_4, and then concentrated under reduced pressure at an ambient temperature to yield a crude yellow powder. The crude powder was purified by flash column chromatography (10:1.5 *n*-pentane/EtOAc) to yield 0.539 g (1.73 mmol, 17.3% yield) after drying under vacuum (150 mTorr) as a yellow oil. ^{1}H NMR (400 MHz, $CDCl_3$): δ 8.05−8.09 (m, 2H), 7.66−7.70 (m, 2H), 2.55−2.68 (m, 2H), 2.18 (s, 3H), 1.12−1.58 (m, 10H), 0.98 (d, J = 6.6 Hz, 3H), 0.87 (d, J = 6.6 Hz, 6H). ^{13}C NMR (101 MHz, $CDCl_3$): δ 185.51, 184.81, 148.13, 143.02, 133.44, 133.40, 132.40, 132.34, 126.38, 126.32, 39.45, 37.08, 35.90, 33.58, 28.11. HRMS (DART, O-TOF): calcd for $C_{21}H_{29}O_2$ [$(M + H)^+$], 313.2162; found, 313.2158.

Preparation of MK-3(II-H_2) (13). Compound **13** was accessed through compounds **9**, **10**, **11**, and **12** starting from commercially available compound **8**.

8-Iodo-2,6-dimethyloct-2-ene (9). To a dry 500 mL round-bottom Schlenk flask was added a dry stir bar, (±)β-citronellol **8** (17.00 g, 108.8 mmol), dry DCM (200 mL), and dry trimethylamine (22.8 mL, 16.52 g, 163.2 mmol, 1.5 equiv), which was then purged/evacuated with argon repeatedly. Then, methanesulfonyl chloride (10.4 mL, 15.33 g, 133.8 mmol, 1.23 equiv) was added dropwise for over 5 min at 0 °C under argon. The resulting solution was stirred at an ambient temperature for 1.5 h under argon. The reaction was quenched with sat. $NaHCO_3$ (200 mL), and then the phases were separated. The aqueous layer was extracted with diethyl ether (3 × 100 mL). The combined organic extracts were washed with sat. $NaHCO_3$ (100 mL), washed with brine (100 mL), dried over anhydrous Na_2SO_4, and concentrated under reduced pressure at an ambient temperature (residual triethylamine can be removed by vacuum pumping for ∼1 h) to yield a crude orange oil. The crude mesylate was dissolved in dry acetone (200 mL) in a dry 500 mL round-bottom Schlenk flask. Then, NaI (33.00 g, 220.2 mmol, 2.02 equiv) was added, and the solution was refluxed for 3 h under argon. The resulting white reaction mixture was diluted with ice−DDI H_2O (200 mL) and diethyl ether (100 mL), and then the phases were separated. The aqueous layer was extracted with diethyl ether (3 × 100 mL). The combined organic extracts were washed with sat. $NaHCO_3$ (100 mL), washed with brine (100 mL), dried over anhydrous Na_2SO_4, and concentrated under reduced pressure at an ambient temperature to yield 22.56 g of crude yellow oil. The crude yellow oil was purified by flash column chromatography (800 mL of 230−400 mesh SiO_2, 10:1 *n*-pentane/EtOAc, 70 mm column) to yield 19.10 g (71.8 mmol, 66.0% yield) after vacuum pumping (150 mTorr) overnight as a clear and colorless oil. ^{1}H NMR (400 MHz, $CDCl_3$): δ 5.09 (t, J = 7.0 Hz, 1H), 3.13−3.28 (m, 2H), 1.92−2.02 (m, 2H), 1.84−1.92 (m, 1H), 1.69 (s, 3H), 1.62−1.67 (m, 1H), 1.61 (s, 3H), 1.51−1.59 (m, 1H), 1.29−1.39 (m, 1H), 1.13−1.22 (m, 1H), 0.89 (d, J = 6.6 Hz, 3H). ^{13}C NMR (101 MHz, $CDCl_3$): δ 131.63, 124.60, 41.06, 36.47, 33.73, 25.87, 25.47, 18.81, 17.84, 5.32. HRMS

DOI: 10.1021/acsomega.8b02620
ACS Omega 2018, 3, 14889−14901

(DART, Q-TOF): calcd for $C_{10}H_{20}I$ [$(M + H)^+$], 267.0604; found: 267.0613.

6,10-Dimethylundec-9-en-2-one (10). To a dry 250 mL round-bottom Schlenk flask was added a dry stir bar and dry *tert*-butanol (60 mL, dried over activated 3 Å molecular sieves 10 g sieves/100 mL solvent) followed by *t*-BuOK (4.92 g, 40.3 mmol, 1.2 equiv), and the solution was refluxed for 30 min under argon to dissolve *t*-BuOK and then cooled to 60 °C. Then, ethyl acetoacetate (4.81 g, 36.9 mmol, 1.1 equiv) was added dropwise, and the reaction mixture was stirred for 30 min at 60 °C under argon. Then, 8-iodo-2,6-dimethyloct-2-ene **9** (8.94 g, 33.6 mmol) was added dropwise. The reaction mixture was refluxed for 25 h under argon. The reaction mixture was then vacuum-filtered and washed with diethyl ether (50 mL). The filtrate solvent was removed under reduced pressure at an ambient temperature. To the crude residue was added 2 N KOH (128 mL), and the reaction mixture was stirred for 3 h at 80 °C under argon. The reaction mixture was cooled to ambient temperature, and then the alkaline solution was acidified with acetic acid (20 mL). The acidified solution was extracted with diethyl ether (3 × 100 mL). The combined organic extracts were washed with sat. $NaHCO_3$ (100 mL), washed with brine (100 mL), dried over anhydrous Na_2SO_4, and then concentrated under reduced pressure at an ambient temperature to yield 6.37 g of crude clear and colorless oil. The crude oil was purified by vacuum distillation (bp: 108−111 °C/4 mmHg)[45] to yield 5.82 g (29.6 mmol, 88.1% yield) as a clear and colorless oil after drying under vacuum (150 mTorr). ^{1}H NMR (400 MHz, $CDCl_3$): δ 5.09 (t, J = 7.2 Hz, 1H), 2.40 (t, J = 7.5 Hz, 2H), 2.13 (s, 3H), 1.87−2.03 (m, 2H), 1.68 (s, 3H), 1.60 (s, 3H), 1.49−1.63 (m, 2H), 1.34−1.43 (m, 1H), 1.23−1.34 (m, 2H), 1.05−1.17 (m, 2H), 0.87 (d, J = 6.5 Hz, 3H). ^{13}C NMR (101 MHz, $CDCl_3$): δ 209.43, 131.26, 125.00, 44.26, 37.09, 36.58, 32.42, 30.01, 25.87, 25.66, 21.54, 19.58, 17.79. HRMS (DART, O-TOF): calcd for $C_{13}H_{25}O$ [$(M + H)^+$], 197.1905; found, 197.1894.

Methyl 3,7,11-Trimethyldodeca-2,10-dienoate (11). To a 50 mL dry round-bottom Schlenk flask that was purged/evacuated with argon was added NaOMe (4.87 g, 90.2 mmol, 1.36 equiv to triethyl phosphonoacetate) followed by MeOH (12.51 g), and this solution was stirred for 5 min under argon. To this solution was added triethyl phosphonoacetate (14.86 g, 66.3 mmol, 1.54 equiv) dropwise and allowed to stir at an ambient temperature for 30 min under argon. To a dry 250 mL round-bottom Schlenk flask was added dry pentane (80 mL, dried by passing through an activated neutral alumina column under argon immediately prior) followed by 6,10-dimethylundec-9-en-2-one **10** (8.45 g, 43.0 mmol). Then, the phosphonium ylide solution was added dropwise over 10 min under argon. The reaction mixture was stirred for 4 h at an ambient temperature under argon. Then, DDI H_2O (100 mL) was added to terminate the reaction. The reaction mixture was extracted with pentane (3 × 100 mL). The combined organic extracts were washed with sat. $NaHCO_3$ (100 mL), washed with DDI H_2O (100 mL), washed with brine (100 mL), dried over anhydrous Na_2SO_4, and then concentrated under reduced pressure at an ambient temperature to yield 9.60 g of crude oil after vacuum pumping overnight. The crude oil was purified by flash column chromatography (95:5 *n*-pentane/EtOAc) to yield 6.71 g (26.6 mmol, 61.9% yield) as a clear and colorless oil after drying under vacuum (150 mTorr). ^{1}H NMR (400 MHz, $CDCl_3$): δ 5.66 (s, 1H), 5.09 (t, J = 7.1 Hz, 1H), 3.68 (s, 3H), 2.15 (s, 3H), 2.11 (t, J = 7.6 Hz, 2H), 1.90−2.00 (m, 2H), 1.68 (s, 3H), 1.60 (s, 3H), 1.37−1.57 (m, 3H), 1.24−1.33 (m, 2H), 1.08−1.17 (m, 2H), 0.87 (d, J = 6.6 Hz, 3H). ^{13}C NMR (101 MHz, $CDCl_3$): δ 167.44, 160.87, 131.27, 125.01, 115.16, 50.91, 41.37, 37.14, 36.57, 32.38, 25.87, 25.68, 24.97, 19.64, 18.88, 17.78. HRMS (DART, O-TOF): calcd for $C_{15}H_{32}NO$ [$(M + NH_4)^+$], 242.2478; found, 242.2484.

3,7,11-Trimethyldodeca-2,10-dien-1-ol (12). To a dry 250 mL round-bottom Schlenk flask was added a dry stir bar, dry pentane (85 mL, dried over an activated alumina column under argon immediately prior), and methyl 3,7,11-trimethyldodeca-2,10-dienoate **11** (8.31 g, 32.9 mmol). The flask was purged/evacuated with argon repeatedly. Then, Vitride reagent (Red-Al sodium bis(2-methoxyethoxy)aluminum hydride solution, 32.1 mL of ≥60 wt % solution in toluene, 98.7 mmol, 3.0 equiv) was added dropwise via a dry glass syringe. The reaction mixture turned milky white upon addition of the Vitride reagent. The reaction mixture was stirred for 1.75 h at an ambient temperature under argon and was completed by TLC analysis (10:1 *n*-pentane/EtOAc, stain with $KMnO_4$ to visualize) and by ^{1}H NMR analysis. A Fieser method quench was used as follows.[46] The reaction solution was cooled to −78 °C (dry ice/acetone), and then DDI H_2O (20 mL) was slowly added (dropwise) under argon purge to quench the reaction. The reaction solution was removed from the −78 °C (dry ice/acetone) bath, and then 15% aq NaOH (20 mL) was added slowly followed by DDI H_2O (60 mL) and *n*-pentane (100 mL). The solution was stirred at an ambient temperature for 30 min. The solution was filtered through a pad of Celite and washed with *n*-pentane (200 mL), and then the phases were separated. The aqueous layer was extracted with *n*-pentane (3 × 100 mL). The combined organic extracts were washed with sat. $NaHCO_3$ (100 mL), washed with DDI H_2O (100 mL), washed with brine (100 mL), dried over anhydrous Na_2SO_4, and then concentrated under reduced pressure at an ambient temperature. The crude oil was vacuum-pumped over night to yield 6.34 g as a crude opaque colorless oil. The crude oil was purified via flash column chromatography (1000 mL of 230−400 mesh SiO_2, 5:1 *n*-pentane/EtOAc, 70 mm column) to yield 6.09 g (27.2 mmol, 82.7% yield) as an opaque colorless oil after drying under vacuum (150 mTorr). ^{1}H NMR (400 MHz, $CDCl_3$): δ 5.41 (t, J = 7.5 Hz, 1H), 5.10 (t, J = 7.1 Hz, 1H), 4.15 (d, J = 7.0 Hz, 2H), 1.90−2.07 (m, 4H), 1.73 (s, 3H, cis isomer*), 1.68 (s, 3H), 1.67 (s, 3H, trans isomer*), 1.60 (s, 3H), 1.33−1.47 (m, 3H), 1.23−1.32 (m, 2H), 1.06−1.17 (m, 2H), 0.87 (d, J = 6.6 Hz, 3H). ^{13}C NMR (101 MHz, $CDCl_3$): δ 140.40, 131.18, 125.14, 123.28, 59.58, 40.01, 37.23, 36.74, 32.47, 25.87, 25.70, 25.25, 19.72, 17.78, 16.33. HRMS (DART, Q-TOF): calcd for $C_{15}H_{32}NO$ [$(M + NH_4)^+$], 242.2478; found, 242.2473. *Determined from the ^{1}H−^{13}C 2D HSQC and ^{1}H−^{1}H 2D COSY NMR spectra (data not shown).

2-Methyl-3-(3,7,11-trimethyldodeca-2,10-dien-1-yl)-naphthalene-1,4-dione MK-3(II-H$_2$) (13). To a 100 mL round-bottom Schlenk flask was added a stir bar, EtOAc (16 mL), and 1,4 dioxane (16 mL), and then the flask was purged/evacuated with argon repeatedly. Then, menadiol **1** (2.50 g, 11.5 mmol, 4:1 menadiol/menadione by NMR integration in $CDCl_3$, menadiol is unstable in $CDCl_3$) and 3,7,11-trimethyldodeca-2,10-dien-1-ol **12** (2.81 g, 12.5 mmol, 1.09 equiv) were added followed by dropwise addition of distilled BF_3 etherate (0.8 mL, fresh bottle) under argon. The reaction mixture refluxed at 70 °C for 3 h under argon. The reaction mixture turned dark orange and was quenched with ice−DDI H_2O (100 mL) and then extracted with diethyl ether (3 × 100

DOI: 10.1021/acsomega.8b02620
ACS Omega 2018, 3, 14889−14901

mL). The combined yellow organic extracts were washed with sat. $NaHCO_3$ (100 mL), washed with DDI H_2O (100 mL), washed with brine (100 mL), dried with anhydrous Na_2SO_4, and then concentrated under reduced pressure at an ambient temperature to yield 5.06 g of the crude red solid. The crude solid was purified by flash column chromatography (1000 mL of 230−400 mesh SiO_2, 20:1 *n*-pentane/EtOAc) to yield 1.28 g (yield at this stage = 29.4%, 3.38 mmol) as a red oil, but further purification was needed as evidenced by ^{1}H NMR analysis. The C2 isomeric side product was readily separated by flash column chromatography eluting after the C3 desired product. The red oil was subjected to a second column chromatography purification using the same conditions as the first purification, and then the material was dried under reduced pressure (150 mTorr) overnight to yield 0.501 g (1.32 mmol, 11.5% yield) as a yellow oil. Similar to vitamin K_1 analogues,[44] various MK analogues[27] and MK-2(II-H_2) **3**, the product was obtained as a mixture of trans/cis isomers (ratio of trans/cis = 2.7:1 by NMR integration of alkene peaks). ^{1}H NMR (400 MHz, C_6D_6): δ 8.00−8.07 (m, 2H), 7.01−7.06 (m, 2H), 5.27 (t, J = 7.1 Hz, 1H, cis isomer), 5.19 (t, J = 7.1 Hz, 1H, trans isomer), 5.13 (t, J = 7.0 Hz, 1H, trans isomer), 5.07 (t, J = 7.0 Hz, 1H, cis isomer), 3.29 (d, J = 7.2 Hz, 2H, cis isomer), 3.26 (d, J = 7.1 Hz, 2H, trans isomer), 2.21 (t, J = 7.5 Hz, 2H, cis isomer), 1.98 (s, 3H), 1.94 (t, J = 7.5 Hz, 2H, trans isomer), 1.73 (s, 3H, trans isomer), 1.71 (s, 3H, cis isomer), 1.67 (s, 3H, trans isomer), 1.64 (s, 3H, cis isomer), 1.61 (s, 3H, cis isomer), 1.56 (s, 3H, trans isomer), 1.01−1.51 (m, 9H), 0.95 (d, J = 6.6 Hz, 3H, cis isomer), 0.86 (d, J = 6.5 Hz, 3H, trans isomer). ^{13}C NMR (101 MHz, C_6D_6): δ 184.99, 184.96, 184.23, 184.15, 145.96, 143.20, 143.18, 137.93, 137.59, 133.08, 133.05, 132.68, 132.66, 130.97, 130.89, 126.31, 126.22, 125.58, 125.51, 120.32, 119.87, 40.40, 37.60, 37.58, 37.39, 36.92, 32.80, 32.66, 32.60, 26.27, 26.12, 26.06, 25.99, 25.95, 25.91, 25.80, 25.67, 23.55, 19.86, 19.81, 17.79, 17.73, 16.33, 12.63, 12.59. HRMS (DART, Q-TOF): calcd for $C_{26}H_{35}O_2$ $[(M + H)^+]$, 379.2632; found, 379.2643.

A sample for analytical characterization of *trans*-MK-3(II-H_2) was prepared similarly as described (see experimental below) for *trans*-MK-2(II-H_2) above by normal phase preparative TLC on silica gel using (30:1) *n*-pentane/EtOAc as the eluting solvent; R_f cis: 0.35, R_f trans: 0.30; ratio of trans/cis before separation was 2.7:1 (ratio by NMR integration of alkene peaks). Importantly, the bottom one-half of the band was isolated, instead of the bottom one-third of the band as was done to obtain *trans*-MK-2(II-H_2). This purification provided 3.7 mg of *trans*-MK-3(II-H_2) as a yellow oil (43.5% recovery) from the initial 8.5 mg cis/trans mixture loaded onto the TLC plate after drying under vacuum (200 mTorr) for 4 days. Similar to MK-2(II-H_2) **3**, we isolated the pure trans isomer; however, the cis isomer coeluted with the trans isomer, and efforts to obtain a sample of the pure cis isomer were not successful. Similar to MK-2(II-H_2) **3**, the cis and trans isomers of MK-3(II-H_2) have different NMR spectra in C_6D_6 for the protons and carbons that belong to the isoprenyl side chain. Data for *trans*-MK-3(II-H_2): ^{1}H NMR (400 MHz, C_6D_6): δ 8.00−8.07 (m, 2H), 7.00−7.06 (m, 2H), 5.19 (t, J = 7.1 Hz, 1H), 5.13 (t, J = 7.0 Hz, 1H), 3.27 (d, J = 7.1 Hz, 2H), 1.98 (s, 3H), 1.94 (t, J = 7.5 Hz, 2H), 1.73 (s, 3H), 1.67 (s, 3H), 1.56 (s, 3H), 1.01−1.47 (m, 9H), 0.86 (d, J = 6.5 Hz, 3H). ^{13}C NMR (101 MHz, C_6D_6): δ 184.97, 184.24, 145.96, 143.21, 137.59, 133.08, 133.05, 132.69, 132.67, 130.89, 126.31, 126.22, 125.51, 119.87, 40.40, 37.58, 36.91, 32.60, 26.27, 26.06, 25.91, 25.67, 19.81, 17.73, 16.33, 12.59. HRMS (DART, Q-TOF): calcd for $C_{26}H_{35}O_2$ $[(M + H)^+]$, 379.2632; found, 379.2639. NMR data for the cis isomer (obtained from spectra with both cis and trans isomers present): ^{1}H NMR (400 MHz, C_6D_6): δ 8.00−8.06 (m, 2H), 7.01−7.06 (m, 2H), 5.27 (t, J = 7.1 Hz, 1H), 5.07 (t, J = 7.0 Hz, 1H), 3.29 (d, J = 7.2 Hz, 2H), 2.21 (t, J = 7.5 Hz, 2H), 1.98 (s, 3H), 1.71 (s, 3H), 1.64 (s, 3H), 1.61 (s, 3H), 1.01−1.51 (m, 9H), 0.95 (d, J = 6.6 Hz, 3H).

Preparation of MK-3(I,II,III-H_6) (17). Compound **17** was accessed through compounds **15** and **16** starting from commercially available compound **14**.

3,7,11-Trimethyldodecan-1-ol (15). To a dry 500 mL round-bottom Schlenk flask was added a dry stir bar, dry methanol (200 mL), ammonium formate (29.15 g, 462.3 mmol, 9.28 equiv), and farnesol **14** (11.08 g, 49.83 mmol), followed by careful addition of the palladium catalyst by a funnel (2.14 g, 20.1 mmol, 0.4 equiv). The reaction mixture was stirred at an ambient temperature for 5 days under positive pressure from an argon balloon, and ^{1}H NMR analysis showed only residual alkene present. The reaction mixture was filtered through a pad of Celite and washed with MeOH (600 mL). MeOH was removed under reduced pressure at an ambient temperature. The crude product was then filtered through a silica plug (4:1 *n*-pentane/EtOAc, 500 mL eluent) and washed with EtOAc (300 mL). The organic filtrate was concentrated under reduced pressure at an ambient temperature to yield a crude clear and colorless oil. The crude oil was suspended in diethyl ether (200 mL), washed with sat. $NaHCO_3$ (200 mL), washed with brine (100 mL), dried over anhydrous Na_2SO_4, and then concentrated under reduced pressure at an ambient temperature to yield a crude clear and colorless oil. The crude oil was purified by flash column chromatography (1000 mL of 230−400 mesh SiO_2, 4:1 *n*-pentane/EtOAc, 70 mm column) to yield 9.99 g (43.7 mmol, 87.8% yield) as a clear and colorless oil after drying under vacuum (150 mTorr). ^{1}H NMR (400 MHz, $CDCl_3$): δ 3.63−3.73 (m, 2H), 1.49−1.63 (m, 3H), 1.01−1.42 (m, 14H), 0.89 (d, J = 6.5 Hz, 3H), 0.86 (d, J = 6.6 Hz, 6H), 0.84 (d, J = 6.8 Hz, 3H). ^{13}C NMR (101 MHz, $CDCl_3$): δ 61.43, 40.21, 40.12, 39.51, 37.64, 37.60, 37.51, 37.47, 37.41, 32.94, 29.67, 29.65, 28.13, 24.97, 24.94, 24.52, 22.87, 22.78, 19.89, 19.84, 19.32, 19.77. HRMS (DART, Q-TOF): calcd for $C_{15}H_{36}NO$ $[(M + NH_4)^+]$, 246.2791; found, 246.2796.

1-Iodo-3,7,11-trimethyldodecane (16). To a dry 250 mL round-bottom Schlenk flask was added a dry stir bar, 3,7,11-trimethyldodecan-1-ol **15** (9.41 g, 41.2 mmol), and dry DCM (125 mL). The flask was purged/evacuated with argon repeatedly. The solution was cooled to 0 °C in an ice−H_2O bath. Then, dry triethylamine (8.61 mL, 6.25 g, 61.8 mmol, 1.5 equiv) was added to the flask followed by dropwise addition of methanesulfonyl chloride (3.82 mL, 5.66 g, 49.4 mmol, 1.2 equiv) at 0 °C for over 5 min while stirring under argon. The reaction mixture was stirred at an ambient temperature for 40 min under argon. The off-white reaction mixture was quenched with sat. $NaHCO_3$ (100 mL), and then the phases were separated. The aqueous layer was extracted with diethyl ether (3 × 100 mL). The combined organic extracts were washed with sat. $NaHCO_3$ (100 mL), washed with brine (100 mL), dried over anhydrous $MgSO_4$, vacuum-filtered, and then concentrated under reduced pressure at an ambient temperature (residual triethylamine can be removed by vacuum pumping for ∼1 h) to yield 12.98 g of crude clear and light-yellow oil. To another dry 250 mL round-bottom Schlenk flask

DOI: 10.1021/acsomega.8b02620
ACS Omega 2018, 3, 14889−14901

was added dry and degassed acetone (100 mL, dried over anhydrous K_2CO_3 for ~10 min immediately prior) and crude mesylate followed by NaI (15.44 g, 103.0 mmol, 2.5 equiv). The reaction mixture turned bright yellow upon addition of NaI and was refluxed for 1 h and 40 min under argon. The yellow reaction mixture was diluted with diethyl ether (100 mL) and DDI H_2O (100 mL), and then the phases were separated. The aqueous layer was extracted with diethyl ether (3 × 100 mL). The combined organic extracts were washed with sat. $NaHCO_3$ (100 mL), washed with brine (100 mL), dried over anhydrous $MgSO_4$, vacuum-filtered, and then concentrated under reduced pressure at an ambient temperature to yield a crude yellow murky oil. To remove the salt impurities, the crude oil was suspended in *n*-pentane (100 mL) and washed with DDI H_2O (100 mL), and then the phases were separated. The aqueous layer was extracted with *n*-pentane (3 × 100 mL). The combined organic extracts were washed with sat. $NaHCO_3$ (100 mL), washed with brine (100 mL), dried over anhydrous $MgSO_4$, vacuum-filtered, and then concentrated under reduced pressure at an ambient temperature to yield 13.19 g of crude clear and light-yellow oil. The crude oil was purified by flash column chromatography (1000 mL of 230−400 mesh SiO_2, 100% *n*-pentane, R_f = 0.71, 70 mm column) to yield 6.52 g (19.3 mmol, 46.8% yield) after drying under vacuum (200 mTorr) as a clear and colorless oil. ^{1}H NMR (400 MHz, $CDCl_3$): δ 3.14−3.28 (m, 2H), 1.83−1.92 (m, 1H), 1.60−1.69 (m, 1H), 1.47−1.57 (m, 2H), 1.01−1.41 (m, 13H), 0.84−0.88 (m, 12H). ^{13}C NMR (101 MHz, $CDCl_3$): δ 41.19, 41.12, 39.52, 37.52, 37.46, 37.42, 37.40, 36.76, 36.70, 34.07, 34.04, 32.93, 32.91, 28.15, 24.98, 24.96, 24.38, 24.37, 22.89, 22.79, 19.90, 19.83, 18.95, 18.89, 5.55. Anal. Calcd for $C_{15}H_{31}I$: C, 53.25; H, 9.24. Found: C, 53.78; H, 9.38.

*2-Methyl-3-(3,7,11-trimethyldodecyl)naphthalene-1,4-dione MK-3(I,II,III,H$_6$) (**17**).* To a dry 100 mL round-bottom Schlenk flask was added under argon, a dry stir bar, dry and degassed benzene (30 mL), and 1-iodo-3,7,11-trimethyldodecane **16** (3.38 g, 10.0 mmol, 1.00 equiv). To a dry 20 mL vial was added benzene (15 mL), which was degassed via argon needle purge, followed by menadione **6** (1.72 g, 10.0 mmol, 1.00 equiv) and benzoyl peroxide (2.42 g, 10.0 mmol, 1.00 equiv) and then sonicated until dissolution occurred under argon. The naphthoquinone−benzoyl peroxide solution was added dropwise to the refluxing prenyl iodide solution for over 2 h and 15 min while the reaction mixture was refluxing under argon. The solution was then refluxed for an additional 1 h. The reaction mixture was diluted with sat. $NaHCO_3$ (100 mL) and DDI H_2O (100 mL), and then the phases were separated. The aqueous layer was extracted with diethyl ether (3 × 100 mL). The combined yellow organic extracts were washed with sat. $NaHCO_3$ (100 mL), washed with brine (100 mL), dried over anhydrous $MgSO_4$, and concentrated under reduced pressure at an ambient temperature to yield 6.63 g of crude yellow powder. The crude product was purified by flash column chromatography (1000 mL of 230−400 mesh SiO_2, 10:1 *n*-pentane/EtOAc, 70 mm column) to yield 0.555 g (1.45 mmol, 14.5% yield) after drying under vacuum (200 mTorr) as a yellow oil. ^{1}H NMR (400 MHz, $CDCl_3$): δ 8.05−8.09 (m, 2H), 7.66−7.70 (m, 2H), 2.55−2.68 (m, 2H), 2.18 (s, 3H), 1.02−1.57 (m, 17H), 0.98 (d, J = 6.6 Hz, 3H), 0.84−0.87 (m, 9H). ^{13}C NMR (101 MHz, $CDCl_3$): δ 185.53, 184.82, 148.14, 143.03, 133.45, 133.42, 132.41, 132.34, 126.40, 126.33, 39.52, 37.55, 37.52, 37.44, 37.20, 37.17, 35.95, 35.86, 33.59, 32.94, 28.14, 24.98, 24.95, 24.57, 22.88, 22.79, 19.90, 19.85, 19.69, 19.62, 12.65. HRMS (DART, Q-TOF): calcd for $C_{26}H_{39}O_2$ [$(M + H)^+$], 383.2945; found, 383.2935.

■ ASSOCIATED CONTENT

Supporting Information

The Supporting Information is available free of charge on the ACS Publications website at DOI: 10.1021/acsomega.8b02620.

General experimental information, materials, and 1D (^{1}H & ^{13}C) and 2D NMR (^{1}H−^{1}H gCOSY, ^{1}H−^{13}C HSQC, and ^{1}H−^{1}H ROESY) spectroscopic and structural data for synthesized compounds (PDF)

■ AUTHOR INFORMATION

Corresponding Author

*E-mail: Debbie.Crans@colostate.edu.

ORCID

Jordan T. Koehn: 0000-0003-3008-6303
Dean C. Crick: 0000-0001-9281-7058
Debbie C. Crans: 0000-0001-7792-3450

Notes

The authors declare no competing financial interest.

■ ACKNOWLEDGMENTS

Drs. Crans and Crick thank NIH for funding (grant #AI119567) and NSF for funding (grant #CHE-1709564). Dr. Crans also thanks the Arthur Cope Foundation administered by the American Chemical Society for the partial support. We also thank Colorado State University Libraries Open Access Research and Scholarship Fund for partial funding of open access option. We also thank Thomas J. Olson for early contributions to the MK-3(I,II,III-H_6) synthesis.

■ REFERENCES

(1) Kurosu, M.; Begari, E. Vitamin K_2 in Electron Transport System: Are Enzymes Involved in Vitamin K_2 Biosynthesis Promising Drug Targets? *Molecules* **2010**, *15*, 1531−1553.

(2) van der Est, A. Electron Transfer Involving Phylloquinone in Photosystem I. In *Photosystem I*; Golbeck, J. H., Ed.; Advances in Photosynthesis and Respiration; Springer: Dordrecht, 2006; Vol. 24.

(3) Nakagawa, K.; Hirota, Y.; Sawada, N.; Yuge, N.; Watanabe, M.; Uchino, Y.; Okuda, N.; Shimomura, Y.; Suhara, Y.; Okano, T. Identification of UBIAD1 as a Novel Human Menaquinone-4 Biosynthetic Enzyme. *Nature* **2010**, *468*, 117−121.

(4) Vos, M.; Esposito, G.; Edirisinghe, J. N.; Vilain, S.; Haddad, D. M.; Slabbaert, J. R.; Van Meensel, S.; Schaap, O.; De Strooper, B.; Meganathan, R.; Morais, V. A.; Verstreken, P. Vitamin K_2 Is a Mitochondrial Electron Carrier That Rescues Pink1 Deficiency. *Science* **2012**, *336*, 1306−1310.

(5) Dragh, M. A.; Xu, Z.; Al-Allak, Z. S.; Hong, L. Vitamin K_2 Prevents Lymphoma in Drosophila. *Sci. Rep.* **2017**, *7*, 17047.

(6) Okamoto, H.; Shidara, K.; Hoshi, D.; Kamatani, N. Anti-arthritis Effects of Vitamin K_2 (Menaquinone-4) - a New Potential Therapeutic Strategy for Rheumatoid Arthritis. *FEBS J.* **2007**, *274*, 4588−4594.

(7) Astudillo-Sánchez, P. D.; Morales-Martínez, D.; Sánchez, A.; Rocha-Ortiz, G.; Salas-Reyes, M. Electrochemical Study of the Interactions Between Anionic Species of Menadione and Alkylated Nucleobases in Dimethylsulfoxide. *J. Electroanal. Chem.* **2017**, *801*, 104−113.

(8) Josey, B. J.; Inks, E. S.; Wen, X.; Chou, C. J. Structure-Activity Relationship Study of Vitamin K Derivatives Yields Highly Potent Neuroprotective Agents. *J. Med. Chem.* **2013**, *56*, 1007−1022.

DOI: 10.1021/acsomega.8b02620
ACS Omega 2018, 3, 14889−14901

(9) Rahn, J. J.; Bestman, J. E.; Josey, B. J.; Inks, E. S.; Stackley, K. D.; Rogers, C. E.; Chou, C. J.; Chan, S. S. L. Novel Vitamin K Analogs Suppress Seizures in Zebrafish and Mouse Models of Epilepsy. *Neuroscience* **2014**, *259*, 142−154.
(10) Chadar, D.; Camilles, M.; Patil, R.; Khan, A.; Weyhermüller, T.; Salunke-Gawali, S. Synthesis and Characterization of *n*-alkylamino Derivatives of Vitamin K3: Molecular Structure of 2-propylamino-3-methyl-1,4-naphthoquinone and Antibacterial Activities. *J. Mol. Struct.* **2015**, *1086*, 179−189.
(11) Kathawate, L.; Joshi, P. V.; Dash, T. K.; Pal, S.; Nikalje, M.; Weyhermüller, T.; Puranik, V. G.; Konkimalla, V. B.; Salunke-Gawali, S. Reaction Between Lawsone and Aminophenol Derivatives: Synthesis, Characterization, Molecular Structures and Antiproliferative Activity. *J. Mol. Struct.* **2014**, *1075*, 397−405.
(12) Itoh, H.; Tokumoto, K.; Kaji, T.; Paudel, A.; Panthee, S.; Hamamoto, H.; Sekimizu, K.; Inoue, M. Total Synthesis and Biological Mode of Action of WAP-8294A2: A Menaquinone-Targeting Antibiotic. *J. Org. Chem.* **2018**, *83*, 6924−6935.
(13) Thomson, R. H. *Naturally Occurring Quinones*; Academic Press Inc., 1971.
(14) Collins, M. D.; Jones, D. Distribution of Isoprenoid Quinone Structural Types in Bacteria and Their Taxonomic Implications. *Microbiol. Rev.* **1981**, *45*, 316−354.
(15) Collins, M. D.; Shah, H. N.; Minnikin, D. E. A Note on the Separation of Natural Mixtures of Bacterial Menaquinones using Reverse Phase Thin-layer Chromatography. *J. Appl. Bacteriol.* **1980**, *48*, 277−282.
(16) Dunphy, P. J.; Brodie, A. F. The Structure and Function of Quinones in Respiratory Metabolism. *Methods in Enzymology*; Academic Press, 1971; Vol. *18*, pp 407−461.
(17) Dunphy, P. J.; Gutnick, D. L.; Phillips, P. G.; Brodie, A. F. A New Natural Naphthoquinone in *Mycobacterium phlei*. Cis-dihydromenaquinone-9, Structure and Function. *J. Biol. Chem.* **1968**, *243*, 398−407.
(18) Ogawa, T.; Isobe, K.; Mori, T.; Asakawa, S.; Yoshimura, T.; Hemmi, H. A novel geranylgeranyl reductase from the methanogenic archaeon Methanosarcina acetivorans displays unique regiospecificity. *FEBS J.* **2014**, *281*, 3165−3176.
(19) Bang, C.; Schmitz, R. A. Archaea Associated with Human Surfaces: Not To Be Underestimated. *FEMS Microbiol. Rev.* **2015**, *39*, 631−648.
(20) Gale, P. H.; Arison, B. H.; Trenner, N. R.; Page, A. C.; Folkers, K.; Brodie, A. F. Characterization of Vitamin K9(H) from *Mycobacterium phlei*. *Biochemistry* **1963**, *2*, 200−203.
(21) Azerad, R.; Cyrot, M.-O.; Lederer, E. Structure of the Dihydromenaquinone-9 of *Mycobacterium phlei*. *Biochem. Biophys. Res. Commun.* **1967**, *27*, 249−252.
(22) Azerad, R.; Cyrot-Pelletier, M.-O. Structure and Configuration of the Polyprenoid Side Chain of Dihydromenaquinones from *Myco-* and *Corynebacteria*. *Biochimie* **1973**, *55*, 591−603.
(23) Upadhyay, A.; Fontes, F. L.; Gonzalez-Juarrero, M.; McNeil, M. R.; Crans, D. C.; Jackson, M.; Crick, D. C. Partial Saturation of Menaquinone in Mycobacterium tuberculosis: Function and Essentiality of a Novel Reductase, MenJ. *ACS Cent. Sci.* **2015**, *1*, 292−302.
(24) Sitkowski, J.; Bocian, W.; Szterk, A. The application of multidimensional NMR analysis to cis/trans isomers study of menaquinone-7 (vitamine K2MK-7), identification of the (E,Z3,E2,ω)-menaquinone-7 isomer in dietary supplements. *J. Mol. Struct.* **2018**, *1171*, 449−457.
(25) Szterk, A.; Zmysłowski, A.; Bus, K. Identification of cis/trans isomers of menaquinone-7 in food as exemplified by dietary supplements. *Food Chem.* **2018**, *243*, 403−409.
(26) Koehn, J. T.; Magallanes, E. S.; Peters, B. J.; Beuning, C. N.; Haase, A. A.; Zhu, M. J.; Rithner, C. D.; Crick, D. C.; Crans, D. C. A Synthetic Isoprenoid Lipoquinone, Menaquinone-2, Adopts a Folded Conformation in Solution and at a Model Membrane Interface. *J. Org. Chem.* **2018**, *83*, 275−288.
(27) Daines, A. M.; Payne, R. J.; Humphries, M. E.; Abell, A. D. The Synthesis of Naturally Occurring Vitamin K and Vitamin K Analogues. *Curr. Org. Chem.* **2003**, *7*, 1625−1634.
(28) IUPAC-IUB. Nomenclature of Quinones with Isoprenoid Side-Chains. *Pure Appl. Chem.* **1974**, *38*, 439−447.
(29) Phoenix, J.; Edwards, R. H. T.; Jackson, M. J. The effect of vitamin E analogues and long hydrocarbon chain compounds on calcium-induced muscle damage. A novel role for α-tocopherol? *Biochim. Biophys. Acta, Mol. Basis Dis.* **1991**, *1097*, 212−218.
(30) Wiss, O.; Weber, F.; Rüegg, R.; Isler, O. The Biological Activity of Vitamins K_1 and K_2 and their Isoprenologs. *Hoppe-Seyler's Z. Physiol. Chem.* **1959**, *314*, 245−249.
(31) Noll, H. Physicochemical Characterization of Vitamin K Homologs. I. Identification by a Novel Method of Quantitative Infrared Spectrophotometry. *J. Biol. Chem.* **1960**, *235*, 2207−2216.
(32) Isler, O.; Rüegg, R.; Studer, A.; Jürgens, R. Specificity of the Vitamin K_1 Constitution and its Analogs Toward Coumarin Linkages. *Hoppe-Seyler's Z. Physiol. Chem.* **1953**, *295*, 290−309.
(33) Azerad, R.; Cyrot, M. O. Synthesis of Two Dihydrofarnesylnaphthoquinones Related to Vitamin K2(45)H from *Mycobacterium phlei*. *Bull. Soc. Chim. Fr.* **1965**, *12*, 3740−3745.
(34) Karrer, P.; Yap, K. S. Über ein weiteres niederes Homologe des α-Tocopherols. *Helv. Chim. Acta* **1940**, *23*, 581−584.
(35) Zakharov, A. V.; Vogt, N. Conformational Analysis of Vitamin K_1 Model Molecule: A Theoretical Study. *Struct. Chem.* **2011**, *22*, 305−311.
(36) Glaziou, P.; Sismanidis, C.; Floyd, K.; Raviglione, M. Global Epidemiology of tuberculosis. *Cold Spring Harbor Perspect. Med.* **2015**, *5*, a017798.
(37) Coppa, F.; Fontana, F.; Minisci, F.; Barbosa, M. C. N.; Vismara, E. Homolytic alkylation of naphthoquinone and methyl-naphtoquinone. Enthalpic steric and polar effects. *Tetrahedron* **1991**, *47*, 7343−7352.
(38) Suhara, Y.; Wada, A.; Tachibana, Y.; Watanabe, M.; Nakamura, K.; Nakagawa, K.; Okano, T. Structure-activity Relationships in the Conversion of Vitamin K Analogues into Menaquinone-4. Substrates Essential to the Synthesis of Menaquinone-4 in Cultured Human Cell Lines. *Bioorg. Med. Chem.* **2010**, *18*, 3116−3124.
(39) Wuttke, S.; Coman, S. M.; Scholz, G.; Kirmse, H.; Vimont, A.; Daturi, M.; Schroeder, S. L. M.; Kemnitz, E. Novel Sol−Gel Synthesis of Acidic $MgF_{2-x}(OH)_x$ Materials. *Chem.—Eur. J.* **2008**, *14*, 11488−11499.
(40) Coman, S. M.; Parvulescu, V. I.; Wuttke, S.; Kemnitz, E. Synthesis of Vitamin K_1 and E-Chromanol by Friedel−Crafts Alkylation in Heterogeneous Catalysis. *ChemCatChem* **2010**, *2*, 92−97.
(41) Coman, S. M.; Patil, P.; Wuttke, S.; Kemnitz, E. Cyclisation of citronellal over heterogeneous inorganic fluorides-highly chemo- and diastereoselective catalysts for (±)-isopulegol. *Chem. Commun.* **2009**, 460−462.
(42) DiMari, S. J.; Rapoport, H. The Reconstitution of Oxidative Phosphorylation in *Mycobacterium phlei* with *cis*- and *trans*-Phylloquinone. Evidence against Isomerization. *Biochemistry* **1968**, *7*, 2650−2652.
(43) Creed, D.; Werbin, H.; Daniel, T. The Mechanism of Photooxidation of the Menaquinones. *Tetrahedron Lett.* **1981**, *22*, 2039−2042.
(44) Lowenthal, J.; Chowdhury, M. N. R. Synthesis of Vitamin K_1 analogs. A New Class of Vitamin K Antagonists. *Can. J. Chem.* **1970**, *48*, 3957−3958.
(45) Kim, J.; Matsuyama, S.; Suzuki, T. Deuterated Analogues of 4,8-dimethyldecanal, the Aggregation Pheromone of Tribolium castaneum: Synthesis and Pheromonal Activity. *J. Labelled Compd. Radiopharm.* **2004**, *47*, 921−934.
(46) Fieser, L. F.; Fieser, M. *Reagents for Organic Synthesis*; Wiley: New York, 1967; Vol. *1*, pp 581−595.
(47) Lerman, L.; Weinstock-Rosin, M.; Nudelman, A. An Improved Synthesis of Hydroxyindoles. *Synthesis* **2004**, *18*, 3043−3046.

DOI: 10.1021/acsomega.8b02620
ACS Omega 2018, 3, 14889−14901

(48) Bennett, C. J.; Caldwell, S. T.; McPhail, D. B.; Morrice, P. C.; Duthie, G. G.; Hartley, R. C. Potential Therapeutic Antioxidants that Combine the Radical Scavenging Ability of Myricetin and the Lipophilic Chain of Vitamin E to Effectively Inhibit Microsomal Lipid Peroxidation. *Bioorg. Med. Chem.* **2004**, *12*, 2079−2098.
(49) Upadhyay, A.; Kumar, S.; Rooker, S. A.; Koehn, J. T.; Crans, D. C.; McNeil, M. R.; Lott, J. S.; Crick, D. C. Mycobacterial MenJ: An Oxidoreductase Involved in Menaquinone Biosynthesis. *ACS Chem. Biol.* **2018**, *13* (9), 2498−2507.

DOI: 10.1021/acsomega.8b02620
ACS Omega 2018, 3, 14889−14901

Appendix VII: A Synthetic Isoprenoid Lipoquinone, Menaquinone-2, Adopts a Folded Conformation in Solution and at a Model Membrane Interface

This is the manuscript that corresponds to chapter three and is published in *the Journal of Organic Chemistry*.[1]

References

1. Koehn, J. T.; Magallanes, E. S.; Peters, B. J.; Beuning, C. N.; Haase, A. A.; Zhu, M. J.; Rithner, C. D.; Crick, D. C.; Crans, D. C., A Synthetic Isoprenoid Lipoquinone, Menaquinone-2, Adopts a Folded Conformation in Solution and at a Model Membrane Interface. *J. Org. Chem.* **2018,** *83*, 275-288.

JOC The Journal of Organic Chemistry
Article
Cite This: J. Org. Chem. 2018, 83, 275−288
pubs.acs.org/joc

A Synthetic Isoprenoid Lipoquinone, Menaquinone-2, Adopts a Folded Conformation in Solution and at a Model Membrane Interface

Jordan T. Koehn,[†] Estela S. Magallanes,[†] Benjamin J. Peters,[†] Cheryle N. Beuning,[†] Allison A. Haase,[†] Michelle J. Zhu,[†] Christopher D. Rithner,[†] Dean C. Crick,[‡,§] and Debbie C. Crans*[,†,‡]

[†]Chemistry Department, [‡]Cell and Molecular Biology Program, and [§]Microbiology, Immunology, and Pathology Department, Colorado State University, Fort Collins, Colorado 80523, United States

Supporting Information

ABSTRACT: Menaquinones (naphthoquinones, MK) are isoprenoids that play key roles in the respiratory electron transport system of some prokaryotes by shuttling electrons between membrane-bound protein complexes acting as electron acceptors and donors. Menaquinone-2 (MK-2), a truncated MK, was synthesized, and the studies presented herein characterize the conformational and chemical properties of the hydrophobic MK-2 molecule. Using 2D NMR spectroscopy, we established for the first time that MK-2 has a folded conformation defined by the isoprenyl side-chain folding back over the napthoquinone in a U-shape, which depends on the specific environmental conditions found in different solvents. We used molecular mechanics to illustrate conformations found by the NMR experiments. The measured redox potentials of MK-2 differed in three organic solvents, where MK-2 was most easily reduced in DMSO, which may suggest a combination of solvent effect (presumably in part because of differences in dielectric constants) and/or conformational differences of MK-2 in different organic solvents. Furthermore, MK-2 was found to associate with the interface of model membranes represented by Langmuir phospholipid monolayers and Aerosol-OT (AOT) reverse micelles. MK-2 adopts a slightly different U-shaped conformation within reverse micelles compared to within solution, which is in sharp contrast to the extended conformations illustrated in literature for MKs.

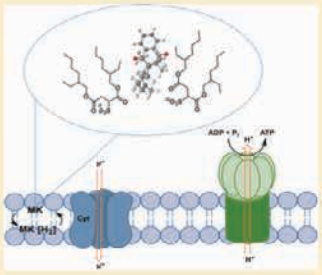

INTRODUCTION

Isoprenoids are among the most numerous and diverse compounds found in nature.[1−3] It was reported that 55,000 of these naturally occurring compounds had been identified by 2007;[3] an estimate that increased to 70,000 in 2015.[1] Classes of isoprenoids include lipoquinones, sterols, carotenoids, prenylated proteins, dolichols, monoterpenes, and sesquiterpenes. These compounds are involved in diverse functions such as electron transport, hormone function, membrane structure and fluidity, vision, photoprotection, insect reproduction, fragrance, and defense. The solution structures of many of these compounds, such as the sterols, are well studied. However, the conformations of long linear polymers of isoprene units such as those found in the side-chains of lipoquinones involved in bacterial and eukaryotic electron transport systems (ETS) have not been characterized.[4−7] Lipoquinones are small hydrophobic molecules that shuttle electrons between the membrane-bound protein complexes acting as electron acceptors and donors in the respiratory ETS. Two major structural groups of lipoquinones are recognized: ubiquinones (or benzoquinones, UBQ) typically found in eukaryotes and Gram-negative prokaryotes and menaquinones (or naphthoquinones, MK) typically found in Gram-positive prokaryotes, including many pathogens such as *Mycobacterium tuberculosis*. The roles and applications of lipoquinone derivatives are currently being explored where a range of different approaches are used for combatting human diseases.[8−20] This manuscript aims to characterize the conformation of a synthetic truncated MK analog within organic solutions and within a model membrane interface as well as document the redox potential of these systems accompanying the conformational studies.

Here, we use an abbreviation system where MK with two isoprene units is MK-2 and with nine isoprene units is MK-9, Figure 1. Naturally occurring lipoquinones are characterized by the presence of an isoprenyl side-chain of varying length from 1 to 14 isoprene units[21,22] depending on the species of origin; a characteristic long used to assist taxonomic efforts. Textbooks often represent UBQ and MK as "Q" or "MQ" in illustrations of the ETS, and in primary literature they are generally shown in an extended conformation, Figure 1.[7,23,24] The extended conformation of these molecules seems highly unlikely in light of the one-step cyclization of squalene epoxide, an isoprenoid compound containing six isoprene units, to form the protosterol cation, which contains the basic steroidal ring system with eight chiral centers.[25,26] Woodward reported the cyclization of this

Received: October 18, 2017
Published: November 23, 2017

ACS Publications © 2017 American Chemical Society

DOI: 10.1021/acs.joc.7b02649
J. Org. Chem. 2018, 83, 275−288

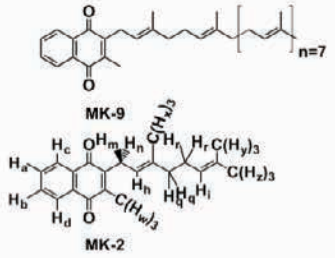

Figure 1. Structure of menaquinone-9 (MK-9), a representative MK found in *Mycobacterium tuberculosis* (top) and MK-2, a simplified MK analog (bottom), is also shown. Protons are labeled on MK-2 for spectral interpretation.

polyisoprenoid squalene epoxide forming only one stereoisomer out of the possible 256 (2^8) in 1953.[25,26] The stereospecificity of this reaction requires preorganization of the epoxide before protonation, and such a conformer is not the extended conformation commonly depicted in the literature.

Small angle X-ray diffraction experiments with the isoprenoid dolichol, an alcohol with 18−20 isoprene units, indicated that the molecule adopted a helical structure in organic solvent.[27] The conformation of the isoprenoid moiety in MK derivatives is likely important to its function as an electron-transfer agent and other biological roles. Although nothing is known about the conformation of MK derivatives, limited conformational analysis is available on different classes of compounds including alkanes, alkenes, and fatty acids with much simpler structures.[28−42] The all-*trans* conformations of alkanes are generally considered the most stable, and therefore, it is expected that the most prevalent conformation of an alkane is the fully extended alkyl chain.[28] A few studies have been reported with simple alkanes and a range of other, more complex compounds with large alkane-components such as in polyenes and fatty acids.[29,30] The U-shape in fatty acids was described when bound to a fatty acid binding protein (FABP), where the alkyl chain region of two fatty acids, palmitic and oleic acids, folds over in the shape of a U.[39,40] In 2008, X-ray crystal structure analysis, as well as NMR spectroscopy, also supported the U-shaped conformation of amphiphilic alkyl chains bound to a synthetic receptor where the folded C_8, C_{10}, and C_{12} conformations have anticlinal as well as *gauche* arrangements.[39,40] Based on these few examples, we hypothesized that MKs will adopt folded conformations depending on specific environmental conditions.

In this manuscript, we describe the synthesis and characterization of a truncated MK derivative with two isoprene units. MK-2 (Figure 1) can be characterized in detail and serves as a representative MK reference compound as it is the simplest MK containing a napthoquinone and repeating isoprenyl side-chain allowing comparison to more complex MK-derivatives found in various microorganisms.[6,43,44] First, the conformation of MK-2 was investigated in organic solvents (polar and hydrophobic). Next, because we are ultimately interested in the function of these derivatives, we measured the electrochemical potential of MK-2 in the organic solvents where the conformations were determined. Finally, the location and conformation of MK-2 in simple membrane model systems was examined. Combined, our results show that MK-2 folds into a U-shaped conformation in solution contrary to common perception and that a folded, slightly different U-shaped conformation also exists in the presence of a simple model lipid membrane interface.

RESULTS AND DISCUSSION

Synthesis of MK-2. MK-2 was synthesized using a procedure in literature (Scheme 1).[45,46] First, menadione **1** was reduced to the corresponding menadiol **2** using aqueous sodium dithionite. Geraniol **3** was coupled to menadiol **2** using the Lewis acid catalyst, boron trifluoride. This preparation produced a yield of 20% overall, which is lower than the reported MK-2 preparation with the deuterated analog in literature.[45] The lower yield appears to be due to extensive alkylation at the C2 position instead of the desired C3 position; however, this side product is readily separated using column chromatography. Highly pure material yields a yellow solid upon crystallization at −20 °C and retains this state when warmed to room temperature, while material with impurities does not crystallize and remains a red oil.

1D ^{1}H NMR Spectroscopic Studies of MK-2 in Different Solvents. MK-2 was first characterized using 1D ^{1}H NMR spectroscopy. Figure 2 shows ^{1}H NMR spectra of MK-2 in isooctane (2,2,4-trimethylpentane), d_5-pyridine, d_6-benzene, d_3-acetonitrile, d_6-DMSO, and D_2O. The observed chemical shifts of MK-2 vary dramatically in the different solvents shown. Hydrophobic solvent environments including aliphatic (isooctane) and aromatic (d_5-pyridine and d_6-benzene) as well as hydrophilic (d_3-acetonitrile, d_6-DMSO, and H_2O/D_2O) solvent environments generate very different spectroscopic signatures. For example, the pairs of aromatic protons, H_a/H_b and H_c/H_d, are significantly different in the two different classes of solvents. This observed variation in chemical shift could be attributed to conformational changes of MK-2 in the various solvent environments investigated, alterations of the electronic state due to interaction with the solvent, or most likely, a combination of both. Focusing on the ^{1}H NMR spectra of MK-2 in the three hydrophilic solvents, d_3-acetonitrile, d_6-DMSO, and D_2O, some differences and similarities are observed (Figure 2). The MK-2 spectrum in D_2O required significantly more scans to produce a reasonable spectrum because of the poor solubility in D_2O. The

Scheme 1. Synthetic Route To Prepare MK-2 4 from Menadiol 2 and Geraniol 3 using Lewis Acid Catalyst Conditions[45,46]

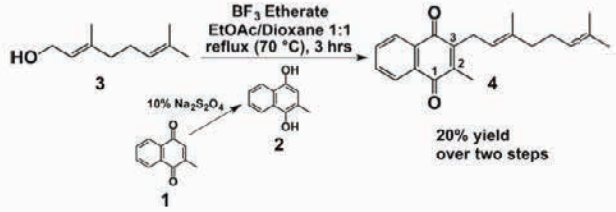

DOI: 10.1021/acs.joc.7b02649
J. Org. Chem. 2018, 83, 275−288

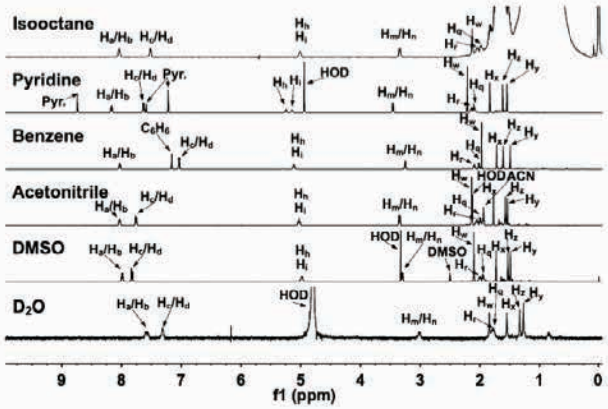

Figure 2. 1D ^{1}H NMR (400 MHz) spectra of MK-2 in hydrophilic (d_6-DMSO, d_3-acetonitrile, and D_2O) and hydrophobic [isooctane (2,2,4-trimethtylpentane), d_5-pyridine, and d_6-benzene] solvents. Proton peak text labeling corresponds to MK-2 structure in Figure 1.

proton chemical shifts generally are observed further upfield in D_2O, presumably indicative of more aggregation in this solvent. The alkene H_h and H_i proton signals are not observed in the D_2O spectrum because of overlap with the HOD peak. However, the HOD signal in the d_6-DMSO spectrum is observed at 3.3 ppm, which allows for observation of the alkene protons, H_h and H_i, at 4.9 ppm. The spectrum of MK-2 in d_6-DMSO is very similar to that in d_3-acetonitrile, and both also have some similarities to the MK-2 spectrum in D_2O. The aromatic protons, H_a/H_b, shifted about 0.2 ppm from the H_c/H_d signals in both solvents. This suggests that these protons remain in similar chemical environments in these two solvent environments. Combined, these three spectra provide a representation of the properties of the MK-2 in a hydrophilic solvent environment.

Next, the aromatic and alkene protons were examined in the hydrophobic solvents, isooctane, d_5-pyridine, and d_6-benzene (Figure 2). Here, protons H_a, H_b, H_c, H_d, H_h, and H_i are observed and readily identified. The signals from alkene protons, H_h and H_i, are both further downfield compared to the signals in hydrophilic solvents, and most interestingly, the two alkene protons become nonchemical shift equivalent in d_5-pyridine. This contrasts with the aliphatic protons in the spectrum in d_6-benzene, which are like those in d_6-DMSO except for H_q, H_r, H_w, and H_z. The changes in the chemical shifts are most distinctive in the aromatic and alkene protons, suggesting that there are some major differences in their respective environments. Together, these differences strongly indicate that MK-2 is sensitive to the solvent environment. However, information from 2D NMR experiments is needed to elucidate if this change in chemical shift is due to conformational variations and/or solvent effect.

^{1}H−^{1}H 2D NOESY and ^{1}H−^{1}H 2D ROESY NMR Spectroscopic Studies of MK-2 in d_6-DMSO and d_5-Pyridine. Differences between the conformations observed in d_6-DMSO vs d_5-pyridine are likely manifested by the conformation minimizing the unfavorable interactions with the solvent environment and maximizing favorable intramolecular interactions with the isoprenyl side-chain. To investigate the conformation of MK-2 in organic solvents, we utilized two different but complementary 2D NMR methods, ^{1}H−^{1}H 2D NOESY and ^{1}H−^{1}H 2D ROESY. Figure 3 shows the ^{1}H−^{1}H 2D NOESY and ROESY NMR spectra of MK-2 in d_6-DMSO and portions of the spectrum in d_5-pyridine. Figure 3A shows the complete ^{1}H−^{1}H 2D NOESY spectrum of MK-2 in d_6-DMSO and Figure 3B−C shows zoomed in regions of interest in the NOESY and ROESY spectra collected in d_6-DMSO, respectively (see Figures S3−S4 for full spectra). Figure 3D−F shows zoomed in regions of interest in the NOESY and ROESY spectra collected in d_5-pyridine, respectively (see Figures S6−S7 for full spectra). Figure 3B,D illustrates that MK-2 alkene protons, H_h and H_i, are in similar environments in d_5-pyridine and d_6-DMSO due to the observance of similar NOE cross peaks. In both solvents, Figure 3B,D shows NOE cross peaks illustrating that H_h and H_i interact with H_n/H_m, H_q, H_r, and H_z. Figure 3B,D shows NOE cross peaks demonstrating proton H_w interacts with protons H_h/H_i and H_m/H_n in both d_6-DMSO and d_5-pyridine. Figure 3C,E shows partial ^{1}H−^{1}H 2D ROESY NMR spectra where the focus is on proton H_w in d_6-DMSO and d_5-pyridine (see Figures S4 and S7 for full spectra and Figure S9 for NOE/ROE correlation traces (slices)). Figure 3B−C shows partial spectra for MK-2 in d_6-DMSO, where NOE and ROE cross peaks indicate the H_w proton interacts with H_q, H_r, H_z, and H_y. However, the lack of ROE cross peaks in Figure 3E shows H_w does not interact with H_y or H_z in d_5-pyridine (observed cross peaks between H_w and H_y or H_z in d_5-pyridine are likely due to TOCSY exchange). The observation of cross peaks shows that there are similar interactions between the aromatic and alkene protons in the two solvents; however, there is a twist around the C−C bond leading to closer proximity of the H_w with the H_q, H_r, H_z, and H_y protons in d_6-DMSO. The NOE and ROE cross peaks in the d_6-DMSO spectrum in Figure 3 clearly support a folded, U-shaped conformation for MK-2 in d_6-DMSO. However, evidence of a folded conformation for MK-2 is not as definitive in d_5-pyridine due to the lack of NOE and ROE cross peaks between H_w and H_y or H_z. If MK-2 did adopt a U-shaped conformation in d_5-pyridine, it would have a conformation as shown in Figure 4B, where the distance between H_w and H_y/H_z is beyond observation in the ^{1}H−^{1}H 2D NOESY and ROESY NMR experiment. This conformation for MK-2 in d_5-pyridine is based on other NOE/ROE cross peaks observed (i.e., H_w to H_h, H_w to H_q or H_r, H_w to H_a). Figure 3F illustrates $\pi-\pi$ stacking between pyridine and part of the napthoquinone ring, which could possibly explain the lack of interaction between H_w and H_y or H_z.

DOI: 10.1021/acs.joc.7b02649
J. Org. Chem. 2018, 83, 275−288

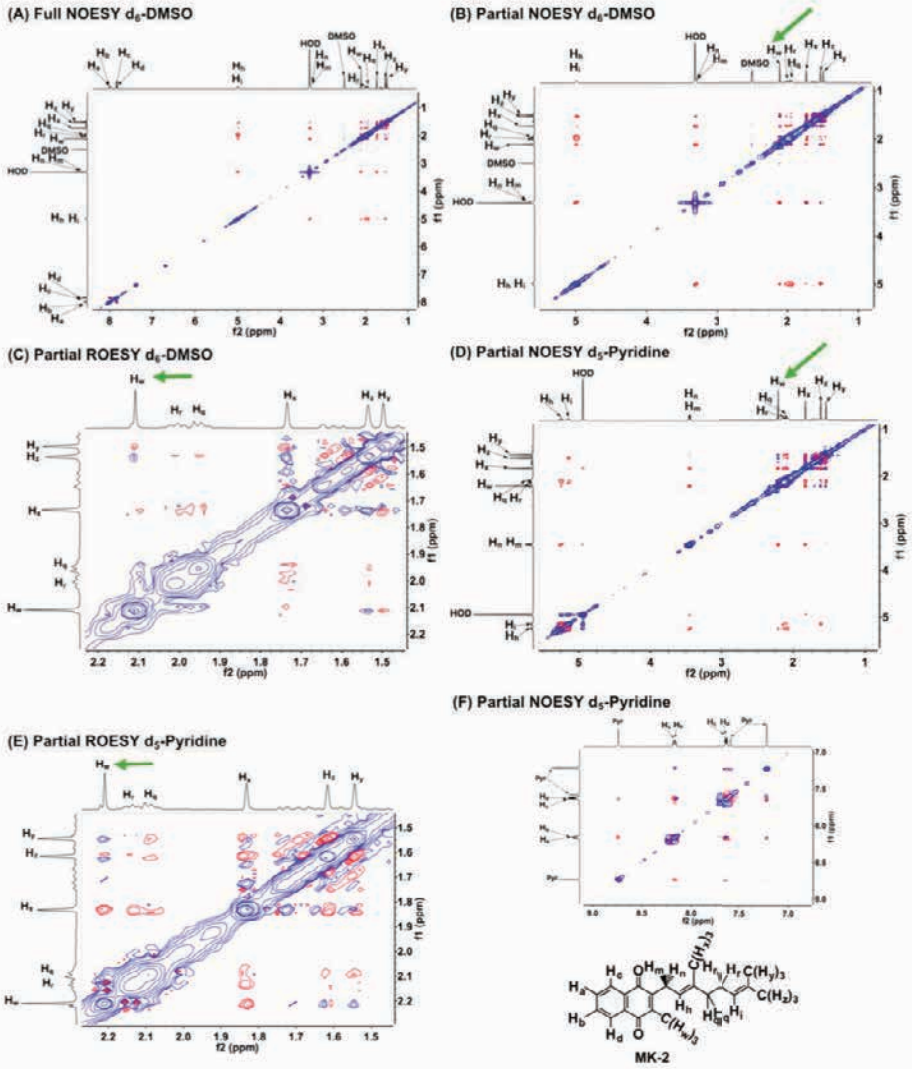

Figure 3. $^1H-^1H$ 2D NOESY and $^1H-^1H$ 2D ROESY NMR (400 MHz) spectra of 20 mM MK-2 in d_6-DMSO and d_5-pyridine at 26 °C. (A) Full $^1H-^1H$ 2D NOESY NMR spectrum of MK-2 in d_6-DMSO. (B) Partial $^1H-^1H$ 2D NOESY NMR spectrum of MK-2 in d_6-DMSO. (C) Partial $^1H-^1H$ 2D ROESY NMR spectrum of MK-2 in d_6-DMSO. (D) Partial $^1H-^1H$ 2D NOESY NMR spectrum of MK-2 in d_5-pyridine. (E) Partial $^1H-^1H$ 2D ROESY NMR spectrum of MK-2 in d_5-pyridine. (F) Partial $^1H-^1H$ 2D ROESY NMR spectrum of MK-2 in d_5-pyridine illustrating stacking interactions. Blue intensity contours represent negative NOE's or ROE's, and red intensity contours represent positive NOE's or ROE's. A standard NOESY pulse sequence was used consisting of 200−256 transients with 16 scans in the f1 domain using a 500 ms mixing time and a 1.5 s relaxation delay. A standard ROESYAD pulse sequence was used consisting of 200 or 256 transients with 16 scans in the f1 domain using a 400 ms mixing time and a 2.0 s relaxation delay. The structure of MK-2 is shown with a proton labeling scheme key. Green arrows indicate proton H_w, where the observed cross peaks differed the most between the two solvents studied.

Illustrating MK-2 Conformations using Molecular Mechanics. MK-2 has a short repeating isoprenyl chain (C_{10}) but contains enough carbons to produce numerous degrees of rotational freedom; therefore, even the truncated version of MK, MK-2, can assume many different conformations. Using molecular mechanics calculations, we explored the energy surface and visualized specific conformations defined by the $^1H-^1H$ 2D NOESY and ROESY NMR experiments of MK-2 in

DOI: 10.1021/acs.joc.7b02649
J. Org. Chem. 2018, 83, 275−288

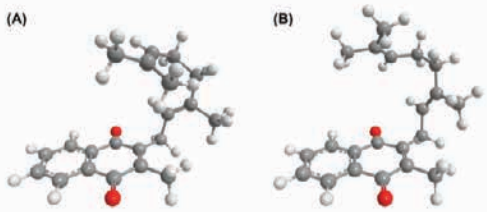

Figure 4. MK-2 conformations generated using MMFF94 calculations to illustrate the conformations elucidated by the 2D NMR studies. (A) Illustrates the MK-2 conformation in d_6-DMSO determined from ^{1}H−^{1}H 2D NOESY and ROESY NMR spectral data cross peak interactions (66.8 kcal/mol, and internuclear distance H_w−H_y: 2.6 Å). (B) Illustrates a potential U-shaped MK-2 conformation in d_5-pyridine consistent with the ^{1}H−^{1}H 2D NOESY and ROESY NMR spectral data cross peak interactions (66.7 kcal/mol, and internuclear distance H_w−H_y: 6.1 Å). See Supporting Information for a table of selected proton to proton distances for conformations A and B.

d_6-DMSO and d_5-pyridine. Specific conformations were generated based on distances imposed by the NMR data and then energy optimized to produce realistic bond lengths and angles for these conformations. Finally, an energy was calculated to ensure that the conformation was at a reasonable energy. Longer calculations generally lead to rotations around bonds and conformations not exactly as those suggested from the NMR data (see below and Supporting Information). The intent with the molecular mechanics calculations was to illustrate conformations corresponding to the ^{1}H−^{1}H 2D NOESY and ROESY NMR spectral data in d_6-DMSO and d_5-pyridine constrained by all cross peak interactions observed as well as to provide visual aids (Figure 4). One of the low-energy conformations generated for MK-2 has a conformation (Figure 4A, 66.8 kcal/mol, H_w−H_y: 2.6 Å) consistent with the 2D NOESY and ROESY spectral parameters observed in d_6-DMSO. Figure 4B illustrates a potential conformation of MK-2 that is consistent with the 2D NOESY and ROESY spectral parameters observed in d_5-pyridine (66.7 kcal/mol, H_w−H_y: 6.1 Å). See Table S1 for selected proton to proton distances for conformations seen in Figure 4A−B consistent with the 2D NOESY and ROESY NMR spectral parameters. The MK-2 conformation determined in d_6-DMSO adopts a folded, U-shaped conformation.

Fewer NOE and ROE cross peaks were observed in d_5-pyridine that would indicate a folded conformation, and although this does not preclude a U-shaped conformation, it does suggest that the H_w−H_y internuclear distance is longer and outside the observable range using the ^{1}H−^{1}H 2D NOESY and ROESY NMR experiment. We based this folded conformation off other NOE and ROE cross peaks observed, which were suggestive of folding (see Figure 3 and related discussion). However, a U-shaped conformation has been observed by NMR analysis in another aromatic solvent, d_6-benzene, for *n*-dodecane.[34] The U-shaped conformations shown in Figure 4 are representative of many possible stable conformations MK-2 could adopt. For comparison, Figure S12C shows another favorable conformation for MK-2 that has a characteristic U-shape. The energy of the conformation C shown in Figure S12C was the lowest energy we found. This conformation was obtained by subjecting an extended MK-2 conformation to 10,000 iterations followed by an energy minimization, illustrating that nonextended conformations are readily reached and energetically favorable.

Combined, the stability of the U-shaped conformations shown by these simple calculations is in line with work reported that showed ^{1}H NMR spectra of *n*-pentane and *n*-hexane measured in polar and spherical solvents such as DMSO favor *gauche* conformations as well as the reported U-shaped conformations of alkyl chains bound to synthetic receptors.[39,40,47] The folded conformations for MK-2 demonstrated herein from experiments align with reported computationally determined conformations for MK analogs.[48] However, it is contrary to the general expectation that the all-*trans* conformations of alkanes or alkyl components are the most stable.[7,23,24,28]

In addition to the U-shaped conformations seen in conformations A and B in Figure 4, a series of alternative conformations of MK-2 (Figure S12D−F) were also generated from the structures most often depicted by representations in the literature and then were energy optimized. Conformations D−H in Figure S12 were generated to compare these conformations energetically to the two U-shaped conformations shown in Figure 4A−B. The energies of conformations D−H in Figure S12 were all higher (~11 to ~23 kcal/mol) than the conformations found in d_6-DMSO, d_5-pyridine, and conformation C (Figure S12). Additional analysis of conformations and a table of selected internuclear distances of MK-2 conformations from Figure 4 and Figure S12 are given in Table S1.

Selected simple alkanes and a few other, more complex compounds with long alkyl-segments such as in polyenes and fatty acids report that the extended and folded forms are comparable in energy to the all-*trans* form.[29,30] The "pentane effect" for longer chains destabilizes the *gauche* conformations because of unfavorable g^+g^- arrangements, which increases the energy by ~0.55 kcal/mol with each kink in the chain.[29,30] In contrast, *gauche* arrangements are often energetically favored because of entropic contributions.[31,32] This is in part due to the spatial requirements that all molecules exert and can be justified using limited sphere considerations.[33] *Gauche* arrangements tend to favor folded conformations where the degree of folding of *n*-alkanes (C_5−C_{32}) in solution depends on the strength of the dispersion force of the solvent[35] and the degree of folding increases with increasing chain length of the solute.[34,36] Other molecules that contain alkyl chains such as fatty acids and polyethylene derivatives have also been reported as either extended chains or in folded conformations depending on physical and environmental conditions.[31,32,37,38] Conformational analysis of long chain allylic polyunsaturated fatty acid chains using Hartree−Fock calculations showed that conformational differences between the all-*trans* and helical folded structures are only a few kcal/mol.[37] Ultimately, there are a few but strongly convincing examples[30,39−42] that folded and/or U-shaped conformations are likely to become much more important than have been recognized previously. The studies presented herein represent a new class of compounds that adopt a U-shaped conformation, illustrating that these folded conformations are likely to be important and may impact the biological function of these lipoquinone systems. It is very important to recognize the molecular plasticity, which allows the alkyl chain to assume shapes depending on the complementary structures or influences of the immediately surrounding environment.

Electrochemistry of MK-2 in Different Solvents. Our interest in these systems relates to the fact that the redox potential of MK is important in shuttling electrons between protein complexes. Although the focus of this manuscript has been on the conformations of these compounds, we are particularly interested in redox properties because we are aiming

DOI: 10.1021/acs.joc.7b02649
J. Org. Chem. 2018, 83, 275−288

to investigate the function of these systems as well. For MKs to carry out this process, MKs must associate with the transmembrane proteins involved in the electron-transfer processes.[49] The electron-transfer processes all take place within or near the membrane interface with two one electron reduction processes sequentially forming the radical anion (semiquinone) and then the dianion.[50−52] Even though there has been many reports in literature on the redox potentials of MK derivatives, the origin of these changes is not well understood.[50−52] These processes are particularly poorly understood when the quinones are present in a hydrophobic molecule that is entirely or partly located in the membrane of a biological system. Although, it is premature to correlate conformation with redox potential, we are seeking systematic information where redox potentials and conformations are known (i.e., within different organic solvents) and the electrochemical data on this system becomes an important frame of reference because the conformational analysis has been carried out. We hypothesized that the redox potential of MK-2 will vary based on organic solvent environment.

Although this hypothesis would be anticipated to be confirmed, it is important to measure how and if the magnitude of the redox potential changes as the solvent environment changes because the function of MK-2 is tied to the redox potentials. Initially, redox studies were planned to be carried out in DMSO, acetonitrile, and benzene; however, because of low solubility of all of the electrolytes examined in benzene, benzene was replaced with pyridine as a representative aromatic solvent.[53] The electrolyte tetrabutylammonium perchlorate (TBAP) was chosen because 1D ^{1}H NMR studies showed that the addition of TBAP to MK-2 solutions (solvents: d_6-DMSO, d_5-pyridine, d_3-acetonitrile) did not affect the observed chemical shifts of the MK-2 protons, and thus no evidence for artifacts due to ion pairing would be observed (see Supporting Information for further description of the electrochemical analysis, and see Figure S13 for MK-2/TBAP NMR studies).

MK-2's first electrochemical potential is the one electron reduction of the quinone to semiquinone ($Q/Q^{\bullet-}$), and the second is the one electron reduction of the semiquinone to the dianion ($Q^{\bullet-}/Q^{2-}$), Scheme S1.[50−52] The cyclic voltammogram's (CVs) of MK-2 and an internal standard of ferrocene (Fc^+/Fc) in three organic solvents are shown in Figure 5. The $Q/Q^{\bullet-}$ $E_{1/2}$ vs Fc^+/Fc for MK-2 in DMSO, CH_3CN, and pyridine were measured to be −1.155 (±0.001) V, −1.230 (±0.003) V, and −1.331 (±0.001) V, respectively. As shown in Figure 5, we included the Fc^+/Fc reference in the data presented. These results are consistent with $Q/Q^{\bullet-}$ $E_{1/2}$ vs Fc^+/Fc values given for 1,4-naphthoquinone.[50,54] The values determined experimentally for $Q^{\bullet-}/Q^{2-}$ $E_{1/2}$ vs Fc^+/Fc for MK-2 in DMSO, CH_3CN, and pyridine were measured to be −1.863 (±0.008) V, −1.902 (±0.012) V, and −2.075 (±0.003) V, respectively (Table S2). In Figure 6, the half-wave potentials are plotted showing the trend that both redox processes are more readily reduced in DMSO than CH_3CN or pyridine similar to the trend observed in literature for 1,4-napthoquinone potentials.[54]

In summary, during the first electrochemical process producing the semiquinone, MK-2 has the most positive potential in DMSO and the most negative potential in pyridine, showing MK-2 is slightly more reducible in DMSO than pyridine or CH_3CN. The observation of differing redox potentials between organic solvents supports the second hypothesis that the redox potential of MK-2 is influenced by the specific organic solvent, where a contributing factor to the observed changes is due to the differences between the dielectric constant of each

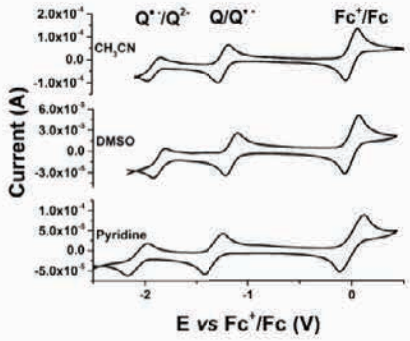

Figure 5. Three representative CVs of 2 mM MK-2 in CH_3CN, DMSO, and pyridine. The potentials are referenced to the Fc^+/Fc couple (2 mM) determined in each solvent. From left to right, redox processes are $Q^{\bullet-}/Q^{2-}$, $Q/Q^{\bullet-}$, and Fc^+/Fc. Each sample has 0.1 M TBAP and was degassed with argon gas for 10 min at ambient room temperature before spectra were recorded. Current sweeps are in the anodic direction from −2 V to 1 V and back to −2 V. A 100 mV scan rate was used.

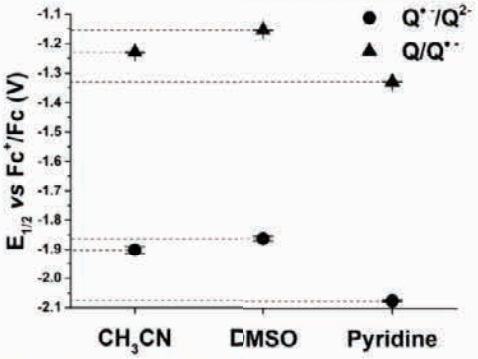

Figure 6. Measured $E_{1/2}$ (vs Fc^+/Fc in V) of MK-2 $Q/Q^{\bullet-}$ and $Q^{\bullet-}/Q^{2-}$ redox processes vs solvent. Added lines show the distinction between each solvent for each redox process. Each solvent was run in triplicate with error bars shown. Student's t test indicated the half wave potentials of each redox process are significantly different in each solvent ($p < 0.01$ for $Q^{\bullet-}/Q^{2-}$ CH_3CN-DMSO and $p < 0.0001$ for all other comparisons). See Supporting Information for details.

solvent. The different organic solvents influence the observed redox potential of MK-2, and from the 2D NMR studies on the conformation of MK-2, slight differences in conformation were observed, which may suggest that a combination of solvent effect and conformational differences of MK-2 may affect the redox potential.

Interaction of Langmuir Phospholipid Monolayers with MK-2. The physiologically relevant environment for MKs is in association with membranes; therefore, we also studied the interaction of MK-2 with a more direct model membrane interface, a phospholipid monolayer. Several membrane models exist including Langmuir phospholipid monolayers, liposomes, micelles, and reverse micelles (RM) (Figure 7).[55−61] Each model system has advantages and disadvantages, and we have chosen to investigate the

DOI: 10.1021/acs.joc.7b02649
J. Org. Chem. 2018, 83, 275−288

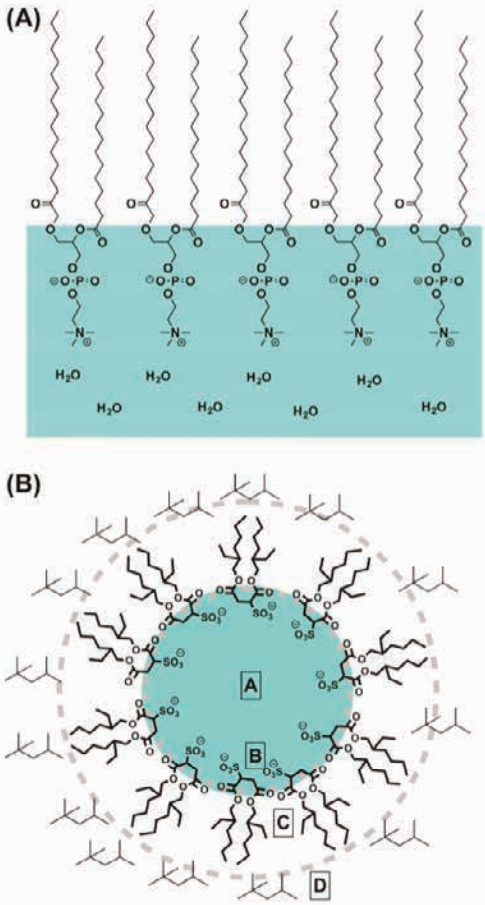

Figure 7. Schematic diagram of (A) a Langmuir phospholipid monolayer and (B) a RM present in a microemulsion. Labeling for the RM is as follows: the water pool (A), the Stern layer (B), the surfactant tails (C), and the organic solvent, isooctane (D).

phospholipid monolayer because of MKs direct association with a membrane and the RM system because RMs allow for the determination of molecular placement and conformation of MK-2 within the interface.[55−61]

First, we describe our studies with Langmuir phospholipid monolayers[60,61] consisting of phospholipids to gain insight into the interactions between two classes of phospholipids (dipalmitoylphosphatidylcholine (DPPC) or dipalmitoylphosphatidylethanolamine (DPPE)) and MK derivatives. These studies will demonstrate how the phospholipid packing is affected by the presence of MK derivatives as it interacts with the phospholipid interface (Figure 7A).[60,62−65] Due to the low solubility of MK-2 in aqueous environments, the Langmuir phospholipid monolayer studies involve experimental protocols used for other materials with low solubility in water, such as UBQ.[66,67] Figure 8 shows the change in surface pressure as a function of area per molecule of DPPC or DPPE in the presence of various amounts of MK-2. The resulting compression moduli as functions of surface pressure are shown in Figure S14.

The compression isotherm of DPPC shows a transition at ~8 mN/m and both DPPC and DPPE collapse at ~55 mN/m similar to findings reported in literature.[68] The compression isotherm of the 1:1 mixture of DPPC and MK-2 shows a disappearance of the gas to liquid phase transition at 8 mN/m, suggesting there is a condensing effect of MK-2 with DPPC at a high area per molecule/low surface pressure. Moving to DPPE, the 1:1 mixture of MK-2 with DPPE reduces the collapse pressure of the film to 50 mN/m, showing destabilization of the DPPE film. The pure MK-2 films had limited stability shown by a maximum surface pressure of ~20 mN/m. This result suggests MK-2 forms a less stable film than the phospholipids.[66−68] To understand the interactions of MK-2 with DPPE and DPPC further, the compression moduli were calculated using equation 4 (see Supporting Information), where the compression modulus is the measure of the compressibility of the film.

Our results are interpreted as MK-2 having a condensing effect on DPPC phospholipid films at high area per molecule/low pressure and destabilization of DPPE phospholipid films. The resulting mixed films (DPPC/MK-2 or DPPE/MK-2) were also consistent with reported UBQ, suggesting similar trends where UBQ was shown to be compressed out of the phospholipid interface.[66,67,69] In summary, MK-2 has a condensing effect on DPPC phospholipid films, a destabilization of DPPE phospholipid films, and is most likely compressed out of the phospholipid film similar to UBQ.[66,67,69] Unfortunately, these studies do not directly show whether a folded or extended conformation of MK-2 exists. A folded conformation occupies a larger volume than the extended conformation, which would affect packing within the phospholipid interface. Our studies do demonstrate that MK-2 interacts with the phospholipid model membrane interfaces of DPPC and DPPE even above physiologically relevant pressures. It is possible that the observation of the destabilization of the DPPE phospholipid films (not observed for DPPC) by the presence of the MK may suggest a folded MK-2 conformation that does not fit in the organization of the DPPE film (possibly related to packing of the phospholipid).

1D ^{1}H NMR Spectroscopic Studies of MK-2 in RMs. Our ultimate objective was to characterize the molecular details of MK-2's association with membrane-like interfaces. This characterization includes determining the location and conformation of MK-2; therefore, the RM model system was investigated (Figure 7B).[60,62−65,70] In the RM, a ternary microemulsion system forms when a surfactant is dissolved in an organic solvent and the addition of water creates nanosized water droplets encased in surfactant.[56,63,65,70−72] This dynamic, yet simple, model can provide molecular detail on location and conformation of MK at an interface using NMR spectroscopy, whereas the use of phospholipids such as DPPC can have overlapping proton signals with key MK proton signals making interpreting conformational information very complex.[70,73−76] RM systems provide information regarding the location, conformation, and physical interactions of MK with lipid films and potentially membranes, which allowed us to examine our third hypothesis that the membrane interface influences the conformation of the MK derivative.

To explore the location of MK-2 at a lipid/water interface further, studies were conducted using a simple microemulsion interfacial system, which allows for identification of molecular placement. Figure 9 shows a stack plot of 1D ^{1}H NMR spectra for

DOI: 10.1021/acs.joc.7b02649
J. Org. Chem. 2018, 83, 275−288

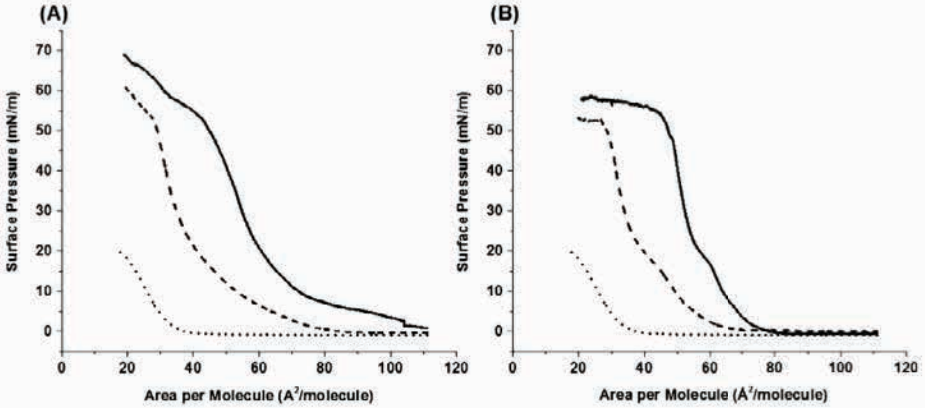

Figure 8. Compression isotherms of MK-2 films (dotted lines), DPPC or DPPE phospholipid films (solid lines), or a 50:50 mixture of MK-2 and phospholipid (dashed line). On the left (A) are the resulting compression isotherms of MK-2 and DPPC, while on the right (B) are the resulting compression isotherms of MK-2 and DPPE.

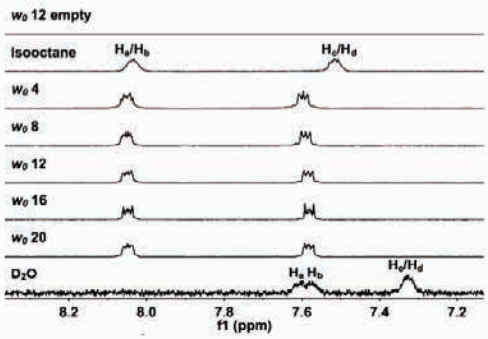

Figure 9. 1D ^{1}H NMR (400 MHz) spectra of MK-2's aromatic protons, H_a, H_b, H_c and H_d in D_2O, isooctane, and different sized RMs. Proton peak text labeling corresponds to MK-2 proton labeling scheme key found in Figure 3. H_a, H_b, H_c, and H_d protons undergo a chemical shift upon inclusion inside RMs.

the aromatic protons (H_a/H_b and H_c/H_d) of MK-2 in solutions of D_2O, isooctane, or isooctane solutions of MK-2 containing RMs (D_2O/AOT/isooctane microemulsions) of various sizes (w_0: 4, 8, 12, 16, and 20, where w_0 = [D_2O]/[AOT]) and for comparison with an empty AOT/isooctane RM. The aromatic MK-2 protons in the AOT/isooctane RMs are similar to the signals observed in isooctane but very different from the signals observed in D_2O. The distance between H_a/H_b and H_c/H_d is 0.52 ppm in isooctane, 0.47 ppm in the RM, and 0.27 ppm in D_2O. This suggests that the environment of the MK-2 protons in the AOT/isooctane RMs is more like an environment in isooctane than D_2O, where MK-2 is no longer in isooctane but associating with the AOT molecules. The signals from the H_c/H_d protons in the AOT/isooctane RMs do change slightly as the RM size increase or decreases. This observation is also consistent with MK-2 penetrating and residing in the interface.

To verify that the RMs formed in the samples used and that the properties of the samples are consistent with previous studies,[61,63,70,77,78] dynamic light scattering (DLS) experiments were carried out. These studies confirmed the formation of RMs, and that the RM did not change significantly upon the addition of MK-2. This was carried out by measuring the sizes in the presence and absence of MK-2 and confirming that the size was as those reported previously (data not shown).[63] Overall, these results are consistent with MK-2 penetrating the RM model membrane interface; however, 2D studies are described below to get more information regarding the placement and conformation of MK-2 within the RM system.

^{1}H–^{1}H 2D NOESY and ROESY NMR Spectroscopic Studies of MK-2 in a RM Model Membrane System. To provide further evidence regarding the location, orientation, and conformation of MK-2 within RMs, we obtained the ^{1}H–^{1}H 2D NOESY NMR spectrum and the ^{1}H–^{1}H 2D ROESY NMR spectrum of MK-2 in a w_0 12 RM, Figures 10 and 11. Figure 10 shows a partial ^{1}H–^{1}H 2D NOESY and ROESY NMR spectra indicating both AOT and MK-2 protons, whereas Figure 11 focused in on selected proton interactions specifically in the NOESY spectrum (see Figures S10–S11 for full spectra). Figure 11A shows cross peaks between the aromatic H_a/H_b and H_c/H_d and parts of the AOT CH_2 and CH_3 tail groups (i.e., H8′ and H10′ protons, see Figure 12 for AOT proton labeling key). Figure 11B shows cross peaks between alkene protons, H_i and H_j, with HOD and AOT's H1, H1′, H3, and H3′ protons and only evidence of a weak interaction between MK-2 and isooctane. These interactions are consistent with placement of MK-2 between the AOT tails, as shown using a depth perception drawing in Figure 12.

Regarding the conformation of MK-2 associated with the RM–water interface, the NOE and ROE cross peaks in Figure 10 show interactions between H_w and H_z/H_y and between H_w and the alkene protons, H_h/H_i, which is consistent with a folded, U-shaped conformation. In the proposed conformation, the C2–C6 atom to atom distance in MK-2's isoprenyl side-chain was found to be 3.6 Å, which is consistent with a U-shape (g^+g^- conformation, Figure 13) for MK-2 placed at the RM interface (see Supporting Information for further discussion and internuclear distances of different MK-2 conformations). An illustration of an MK-2 conformation consistent with these observations is shown in Figure 13. This U-shaped conformation

DOI: 10.1021/acs.joc.7b02649
J. Org. Chem. 2018, 83, 275–288

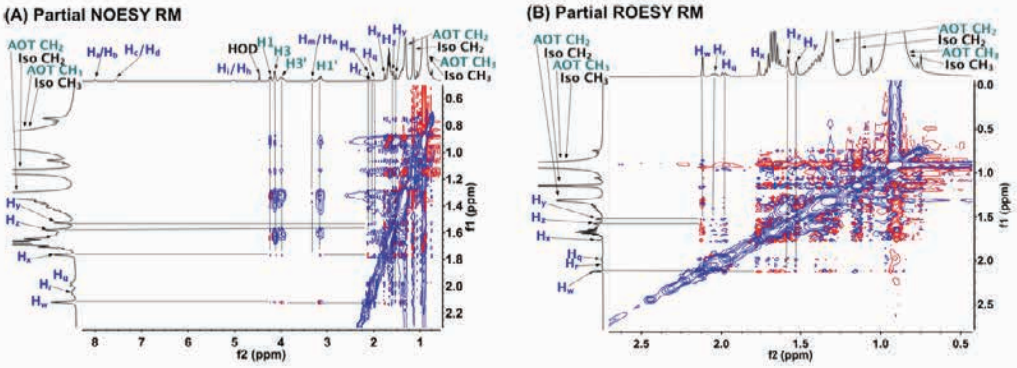

Figure 10. Partial ^{1}H−^{1}H 2D NOESY and ROESY NMR (400 MHz) spectra of MK-2 inside w_0 12 RM at 26 °C. (A) Partial ^{1}H−^{1}H 2D NOESY NMR spectrum in a w_0 12 RM. (B) Partial ^{1}H−^{1}H 2D ROESY NMR spectrum in a w_0 12 RM. Blue to blue proton text labeling shows MK-2 to MK-2 interactions, teal to teal proton text labeling shows AOT to AOT interactions, and blue to teal proton text labeling shows MK-2 to AOT interactions. Blue intensity contours represent negative NOE's or ROE's and red intensity contours represent positive NOE's or ROE's. A standard NOESY pulse sequence was used consisting of 256 transients with 16 scans in the f1 domain using a 200 ms mixing time and a 1.5 s relaxation delay. A standard ROESYAD pulse sequence was used consisting of 256 transients with 16 scans in the f1 domain using a 200 ms mixing time and a 2.0 s relaxation delay. See Figure 3 for MK-2 proton labeling scheme key and Figure 12 for AOT proton labeling scheme key.

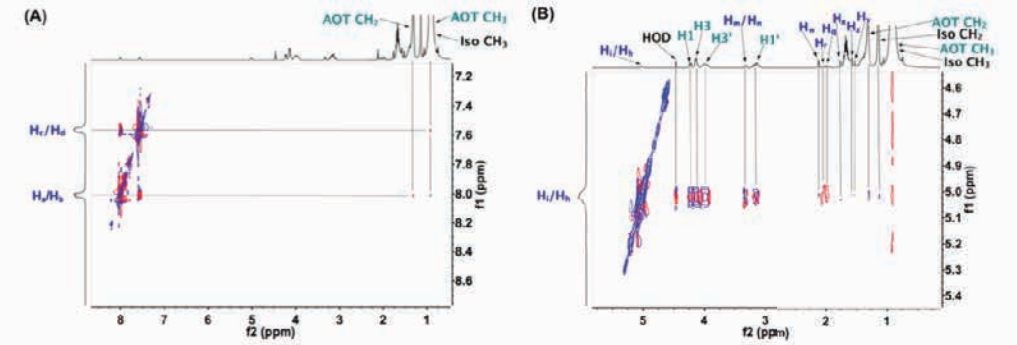

Figure 11. Partial ^{1}H−^{1}H 2D NOESY NMR (400 MHz) spectra of MK-2 inside a w_0 12 RM at 26 °C illustrating interactions of MK-2 with the AOT surfactant tails. (A) Interactions between MK-2's aromatic protons and AOT. (B) Interactions between MK-2 alkene protons and AOT. The blue to blue proton text labeling shows MK-2 to MK-2 interactions, teal to teal proton text labeling shows AOT to AOT interactions, and blue to teal proton text labeling shows MK-2 to AOT interactions. Blue intensity contours represent negative NOE's, and red intensity contours represent positive NOE's. A standard NOESY pulse sequence was used consisting of 256 transients with 16 scans in the f1 domain using a 200 ms mixing time and a 1.5 s relaxation delay. See Figure 3 for MK-2 proton labeling scheme key and Figure 12 for AOT proton labeling scheme key.

observed when MK-2 is associated within the RMs changed slightly from that observed in d_6-DMSO regarding where the double bond overlaps with the napthoquinone moiety. The overlap of the alkene and napthoquinone functionalities in the conformation associated with the interface is best illustrated by the top view in Figure 13B. Importantly, the U-shape fold remains, but slight rotation around the C−C bond facilitates the conformational changes in the U-shape.

Implications of Folded Conformations for MK Derivatives. Natural MKs contain a naphthoquinone and an isoprenyl side-chain with some variable number of repeating isoprene units, where MKs support the electron-transfer reactions in a range of systems.[6,43] MK-2 was synthesized allowing for detailed characterization of the molecule. The results presented herein for MK-2 suggests that other important MK derivatives in biology will adopt folded conformations as well and demonstrates the need to prepare and study such derivatives both experimentally and computationally.

The extended conformations of long chain biological molecules such as fatty acids and polyenes are generally shown in the literature if the structure is presented.[7,23,24] However, a few studies of isoprene conformers and 1,3 acyclic dienes show the extended *trans* alkane conformations compare in energy with folded or helical conformations.[79,80] Although the folded conformations in those studies may be slightly higher in energy than unfolded conformations, the difference is surprisingly small. The C−C single bond lengths reported for stearic acid decreases under high pressure.[42] These bond shrinkages cause conformational and shape changes in stearic acid favoring folded conformations.[42] Previous studies using high-temperature UV-absorption spectroscopy, molecular orbital calculations, and gas-phase electron diffraction found that isoprene and chloroprene

DOI: 10.1021/acs.joc.7b02649
J. Org. Chem. 2018, 83, 275−288

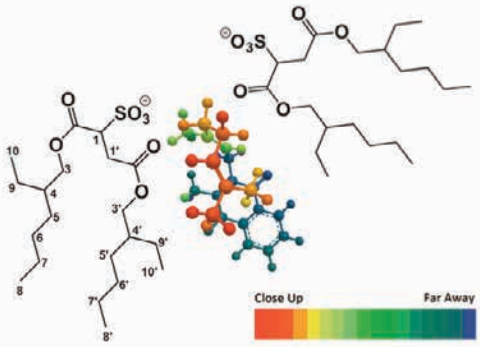

Figure 12. Illustration of MK-2's proposed folded, U-shaped conformation and placement in the RM interface. This arrangement is consistent with ^{1}H–^{1}H 2D NOESY and ROESY NMR spectral data obtained in a w_0 12 RM; however, MK-2 likely tumbles freely within the interface but maintains interactions with the region of AOT shown in the illustration. Color depth fading legend shows dark red as closer in distance and dark blue as farther in distance from the reader. AOT proton labeling scheme key is shown.

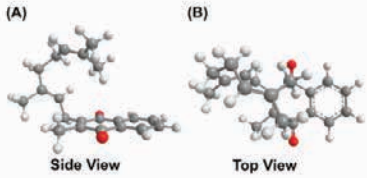

Figure 13. MK-2 conformation at an interface visualized using MMFF94 calculations. Molecular mechanics simulations generating the 3D conformation of MK-2 in a RM that is consistent with ^{1}H–^{1}H 2D NOESY and ROESY NMR spectral data. (A) Side view of energy minimized conformation (63.5 kcal/mol, and internuclear distance H_w–H_z: 4.0 Å) showing MK-2's isoprene side-chain adopting a hook-like shape also known as a folded, U-shaped conformation. (B) Top view of energy minimized conformation showing the terminal isoprene methyl groups overlapping the carbonyl groups on the napthoquinone.

conformations did, in fact, favor folded conformations.[81,82] Although these conditions are nonphysiological, they do demonstrate that changes in a physical parameter can affect the preferred conformation. Previous work has been carried out with fatty acids where the experimental studies showed that the conformations of the alkane portion of the fatty acids can and do change similar to conformations of MK-2 as shown in this work.[37] Our studies confirm the first hypothesis that MKs have different conformations depending on specific environmental conditions, which was achieved by first synthesizing MK-2 and then demonstrating that a U-shaped, folded conformation was adopted in d_6-DMSO, which was different from the conformation in d_5-pyridine.

Conformations can affect reactivity, and as in this case, the electron-transfer reactions facilitated by MK. MK forms complexes with several enzymes during the electron-transfer processes, and although kinetic characterizations of these systems have been reported,[83−85] less is known structurally. The redox potentials of MK-2 depicted in Figure 6 illustrate the trend where the most positive potential is in DMSO and the most negative potential is in pyridine, which agrees with literature reports on menadione.[50,54] These results have identified that the redox potential of MK-2 changes as a function of solvent, and the origin of this change (presumably in part due to a change in dielectric constant between solvents) and whether these observed solvent effects can be associated with changes in conformation should be investigated in the future using both suitable high-level computational methods as well as electrochemistry. Indeed, the change in redox potential is likely to be important, and since there is no conjugation between the isoprenyl side-chain and napthoquinone, these effects are very interesting and may reflect that the energy required for the reduction is determined by the energy difference of the HOMO−LUMO gap in the two different conformations.[86] Orbital analysis of the HOMO−LUMO gap could potentially be informative and describe the origin of the observed varied biological effects of a series of *N*-alkyl MK derivatives that have been reported.[87,88] For example, replacement of a CH_2 group with a N atom modifies the parent system, creating a class of compounds with a nitrogen bound directly to the "naphthoquinone group." These molecules have dramatically different biological properties than the parent MK derivatives,[87,88] and it is possible that these activities could be related to the change in fundamental physical and chemical properties that occurs with *N*-alkyl isoprenoid substitution of the naphthoquinone ring. Combined, these results confirm the second hypothesis that the redox potential of MK-2 is influenced by organic solvent environment (in part due to dielectric constant of solvent), which is likely to be important for understanding the mechanistic details in MK metabolism.

The third hypothesis involves determining if the association of MK with the membrane interface influences the conformation of the MK derivative. We investigated the interaction of MK-2 with a phospholipid Langmuir monolayer, which is a simple 2D model of a single leaflet of a cell membrane.[59,89,90] The fact that MK-2 interacts with the phospholipid monolayer is consistent with the expected MK affinity for the hydrophobic phospholipids that make up the cell membrane. Langmuir monolayer studies support interaction of MK-2 with the phospholipid monolayer interface; however, the lipoquinone is likely compressed out of the interfacial portion of the phospholipid monolayer into the more hydrophobic alkyl tail groups on the top of the monolayer as the pressure increases. Unfortunately, Langmuir phospholipid monolayer studies could not determine the conformation of MK-2; however, the RM surfactant interface complements studies with the phospholipid monolayer interface. The question of folding was further investigated by combining ^{1}H NMR spectroscopic studies of MK-2 in organic solution and in a simple model membrane system, RMs. The conformation of MK-2 was characterized in organic solvents and was found to differ slightly from the conformation when it was associated with the surfactant interface within RMs. It is to be expected that MK-2 would have an affinity for the interface because of its hydrophobicity, which agrees with results observed in the RM system. The RM interface is known to be penetrated by water molecules and thus less packed than a biological membrane and, therefore, has a lower interface pressure meaning MK-2 is unlikely to be compressed out once inside.[63,70,91] The ^{1}H NMR spectroscopic studies in RMs allowed us to observe the association of MK-2 with the interface molecules as well as with itself in its folded state. The ^{1}H–^{1}H 2D NOESY and ROESY NMR spectral data indicate that the U-shaped conformation of MK-2 (Figure 13) remained intact while

DOI: 10.1021/acs.joc.7b02649
J. Org. Chem. 2018, 83, 275−288

associating with the RM model membrane interface; however, the overlap between the alkene and the napthoquinone varies with the specific environment. The small changes in the U-shaped conformation document the environmental influence on the conformational folding of MK-2. These results are very important because they document the possibility that MK derivatives in the cell membrane environment may be folded, and if so, such folds will impact the interaction with proteins in the ETS and affect reactivity and function.

Naturally occurring lipoquinones are characterized by the presence of an isoprenyl side-chain of varying length depending on the species of origin. MK-2's isoprenyl side-chain is shorter than most lipoquinones involved in electron transport; therefore, it may not fully mimic the interactions generated by MK derivatives with longer isoprene chains with the membrane or the enzyme systems. However, these results show that the folding of MK-2 is very important and may suggest that MK derivatives with the longer isoprenyl side-chains may adopt folded conformations as well. Understanding how MK-2 and other MK derivatives fold in a hydrophobic environment is critical to gauge how these molecules will behave within a biological membrane associated with the ETS.

Investigation of the conformation of a particular MK derivative's location and conformation will also allow for a more realistic interpretation of data obtained with the novel fluorogenic probe, a vitamin K analog, reported to fluoresce after reduction to the quinol.[92] Studies with this new probe may help provide information on the role that vitamin K plays in key redox processes. Accurate information obtained from the use of this probe would provide better quality data regarding photosynthesis and cellular respiration, and future consideration of MK derivatives location and conformation will be important for proper interpretation of the results obtained from the use of this probe.[92]

■ CONCLUSIONS

Conformations exhibited by alkanes and alkenes are essential for explaining trends in reactivity and manifestation of physical properties, but little is understood regarding biological systems with hydrophobic small components containing alkyl segments. The studies presented in this manuscript describe the chemical and biochemical properties of MK, which is an essential component of the ETS in many Gram-positive bacteria, including pathogens such as *Mycobacterium tuberculosis*, *Mycobacterium leprae*, and *Staphylococcus aureus*, to name a few. We report for the first time in this class of molecules that MK-2 adopts a folded, U-shaped conformation in organic solution. The specific nature of the conformation varied within different organic solvents and thus confirmed our first hypothesis that MK-2 conformations are very sensitive to their environment. These findings contrast with the simple, extended conformation represented in textbooks and the literature that is shown for MK derivatives as well as the more common "Q", belonging to the UBQ family of lipoquinones.

The change in the observed redox potentials of MK-2 with different organic solvents confirmed our second hypothesis. This is important for future studies probing the function of the substrate and potential correlation between conformation and redox potential of MK derivatives, and although most of the studies in this manuscript are of a structural nature, it is important to recognize that the function is likely related to the conformation of the MK-derivative. The discovery that MK-2 adopts a folded conformation may suggest that other MK derivatives will have similar conformations, which ultimately will impact all the biological systems in which MKs have a role such as within the ETS in specific Gram-positive bacterial pathogens. The result of a stable U-shape conformation in solution and within an interface is important as little information is available on essential hydrophobic biological components.

Although the NMR spectral data illustrated using molecular mechanics allowed for the conclusion that MK-2's conformation is environment dependent, it was important to investigate if this U-shaped conformation remained at a membrane-like interface. We used two membrane model systems to investigate this question. The more physiologically relevant DPPC/DPPE phospholipid monolayers confirmed that MK-2 interacted with the phospholipid interface similar to UBQs; however, the conformation of MK-2 remained unspecified. Complementary studies using the AOT-RM model membrane system allowed determination of the molecular location of MK-2 as penetrating the water−surfactant interface as well as the conformation of MK-2 within the RM interface. We found that the folded, U-shaped conformations observed in organic solution remained upon association with the AOT-RM interface, but the U-shaped conformation differed slightly indicating the interface's environmental influence on conformation. Together, these results support the interpretation that the MKs conformation remains folded in a U-shape even in contact with a model membrane interface, which agrees with our third hypothesis.

More broadly, the results of this study will also enhance our understanding of folded conformations for chemically and biologically important hydrophobic small molecules in solutions and confined hydrophobic environments. The shape and, thus, the conformation of these molecules are relevant for molecular recognition motifs and the processing of these molecules within the membrane. This manuscript represents the first attempt to characterize the conformation as well as the chemical and biochemical properties manifested by the conformation of any electron transferring lipoquinone derivative. Although many studies have been carried out with these systems kinetically, the conformation and how this impacts the biological chemistry has not yet been addressed.

■ EXPERIMENTAL SECTION

Preparation of (*E*)-2-(3,7-Dimethylocta-2,6-dien-1-yl)-3-methylnaphthalene-1,4-dione (4). To a 500 mL round-bottom Schlenk flask were added a stir bar, diethyl ether (100 mL), and menadione (5.00 g, 29.0 mmol). Then, 10% aq. $Na_2S_2O_4$ (100 mL, 57.4 mmol) was added, and the solution immediately turned dark red. After 30 min of stirring at ambient temperature, the solution was clear yellow. The aqueous layer was separated and extracted with diethyl ether (3×, 100 mL). The combined organic extracts were washed with sat. $NaHCO_3$ (100 mL), followed by DDI H_2O (100 mL), and last with brine (100 mL). The combined organic extracts were dried with anhydrous Na_2SO_4 and then concentrated under reduced pressure at room temperature. The crude powder was triturated with pentane (50 mL), vacuum filtered, and washed with pentane (100 mL) to yield 4.25 g as a pale purple solid. Menadiol formation is indicative by ^{1}H NMR ($CDCl_3$) by the presence of a peak at 6.64 ppm and is consistent with literature.[93]

To a 100 mL round-bottom Schlenk flask was added ethyl acetate (16 mL) and 1,4-dioxane (16 mL), which was purged/evacuated with argon repeatedly. Then, crude menadiol (2.50 g, 4:1 menadiol:menadione by NMR integration, 11.5 mmol) was added, followed by geraniol (1.92 g, 12.5 mmol), and then dropwise addition of fresh BF_3 etherate (0.8 mL). The solution was allowed to reflux at 70−72 °C for 3 h under argon. The dark orange colored reaction mixture was quenched with ice-H_2O (100 mL) and then extracted with diethyl ether (3×, 100 mL). The yellow

DOI: 10.1021/acs.joc.7b02649
J. Org. Chem. 2018, 83, 275−288

organic extracts were washed with sat. $NaHCO_3$ (100 mL), washed with DDI H_2O (100 mL), washed with brine (100 mL), dried with anhydrous Na_2SO_4, and then concentrated under reduced pressure at room temperature to yield 3.71 g of crude red oil. The crude oil was purified by flash column chromatography (1000 mL of 230–400 mesh SiO_2, 70 mm column, 20:1 pentane/ethyl acetate). The yellow oil obtained was dried under reduced pressure (~125 mTorr) overnight to yield 0.713 g (2.31 mmol, 20.1% yield) as a yellow solid. The scale of this reaction was ~14 times larger than the previously reported synthesis.[45] ^{1}H NMR (400 MHz, d_6-DMSO) δ: 7.96–8.01 (m, 2H), 7.80–7.84 (m, 2H), 4.96–5.00 (m,2H), 3.30 (d, 2H, J = 4 Hz), 2.10 (s, 3H), 1.92–2.04 (m, 4H), 1.73 (s, 3H), 1.53 (s, 3H), 1.49 (s, 3H). ^{13}C NMR (100 MHz, d_6-DMSO) δ: 184.7, 183.6, 145.3, 142.9, 136.4, 133.9, 131.5, 130.7, 125.9, 125.8, 123.9, 119.4, 26.0, 25.4, 25.4, 17.5, 16.1, 12.4. LRMS (ESI 70 eV, EtOAc) m/z: $[(M + H)^+]$ Calcd for $C_{21}H_{25}O_2$ 309.2; found 309.2. HRMS (ESI, OTOF) m/z: $[(M + H)^+]$ Calcd for $C_{21}H_{25}O_2$ 309.1849; found 309.1851.

Mass Spectrometry. Low-resolution mass spectrometry (LRMS) experiments were conducted by electron spray ionization mass spectrometry (ESI) on an Agilent technologies 6130 Quadrupole LCMS. High-resolution mass spectrometry (HRMS) experiments were carried out using an Agilent 6220 TOF LC/MS ("OTOF") interfaced to an Agilent 1200 HPLC with electrospray (ESI) mode.

NMR Spectroscopic Studies. 1D and 2D ^{1}H studies were carried out both in organic solvents and more complex media (see below for RM studies). ^{1}H and ^{13}C spectra were recorded using a Varian Model MR400 or Model Inova400 operating at 400 and 100 MHz, respectively. Chemical shift values (δ) are reported in ppm and referenced against the internal solvent peaks in ^{1}H NMR (d_6-DMSO, δ at 2.50 ppm; $CDCl_3$, δ at 7.26 ppm; d_5-pyridine, δ at 8.74 ppm; d_3-acetonitrile, δ at 1.94 ppm; D_2O, δ at 4.79 ppm; C_6D_6, δ at 7.16 ppm) and in ^{13}C NMR (d_6-DMSO, δ at 39.52 ppm). All NMR spectra were recorded at either 22 or 26 °C.

Solution 1D ^{1}H NMR Spectroscopic Studies. Samples were prepared by dissolving ~5 mg of MK-2 in either 0.5 mL of isooctane, d_5-pyridine, C_6D_6, d_3-acetonitirle, d_6-DMSO, or D_2O. The MK-2 sample in D_2O was vortexed for ~1 h to dissolve maximum amount of MK-2. The NMR spectrum was collected by running 32 scans and was locked onto the deuterated solvent except for isooctane, which was ran unlocked using $CDCl_3$ as a spectral window reference.

Sample Preparation for Solution ^{1}H–^{1}H 2D NOESY and ROESY NMR Spectroscopic Studies. To prepare the samples in d_6-DMSO and d_5-pyridine, 0.0031 g of MK-2 was dissolved in 0.5 mL of solvent to yield a 20 mM solution of MK-2. The NMR tubes containing the MK-2 solution were purged with argon prior to data collection.

^{1}H–^{1}H 2D NOESY and ROESY NMR Spectroscopy in Organic Solution. 2D NMR spectroscopic studies in organic solution were carried out on a Varian model MR400 400 MHz magnet at 26 °C. A standard NOESY pulse sequence was used consisting of either 200 or 256 transients with 16 scans in the f1 domain using a 500 ms mixing time, 45° pulse angle, and a 1.5 s relaxation delay. A standard ROESYAD pulse sequence was used consisting of either 200 or 256 transients with 16 scans in the f1 domain using a 400 ms mixing time, 45° pulse angle, and a 2.0 s relaxation delay. The NMR was locked onto either d_6-DMSO or d_5-pyridine and referenced to the internal solvent peak. The resulting spectrum was processed using MestReNova NMR software version 10.0.1.

Molecular Mechanics Calculations. To obtain visual aids of MK-2 conformations, Merck molecular force field 94 (MMFF94) molecular mechanics gas-phase simulations were conducted using ChemBio3D Ultra 12.0 at 25 °C. Starting conformations were obtained from ChemDraw structures or by rotating desired bonds and then either had simulations run or simply an energy minimized to achieve the desired conformation. Conformations A–B in Figure 4 were generated and then energy minimized with a root-mean-square (RMS) gradient of 0.1 and up to 50 iterations to obtain conformations that agreed with our interpretation of the cross peak observations in the ^{1}H–^{1}H 2D NOESY and ROESY NMR spectral data. One simulation was run for 10,000 iterations and then energy minimized using an MMFF94 energy minimization calculation using 500 iterations with a RMS gradient of 0.001 to achieve conformation C in Figure S12C. Conformations D–H in Figure S12 were generated by rotating bonds to achieve the desired conformation followed by an energy minimization using 20–50 iterations and an RMS gradient of 0.1. A table of structural parameters such as selected distances between hydrogen atoms within the conformations and energies calculated for the 3D conformations can be found in the Supporting Information section.

Electrochemistry Methods. All electrochemistry was performed on a CHI 750D potentiostat. For the cyclic voltammetry (CV), a classical three electrode system was used with scan rate of 100 mV/s at 22 °C. The working electrode was a glassy carbon electrode (BASi MF2012, 3 mm), and the counter electrode was a platinum wire electrode (BASi MW1032). The Ag^+/Ag reference electrode (BASi MW1085) was constructed by inserting a Ag wire into a freshly prepared solution of organic solvent (CH_3CN, DMSO, or pyridine) with 0.1 M TBAP and 0.01 M $AgNO_3$. Detailed experimental, instrumentation, and analysis are available in the Supporting Information.

Langmuir Monolayer Compression Isotherms. The subphase for each experiment consisted of approximately 50 mL of a 20 mM sodium phosphate buffer (pH 7.4). The phospholipid solution was prepared by dissolving powdered phospholipid into a chloroform:methanol (9:1, v:v) solution to produce 1 mM phospholipid stock solution. The film applied to the subphase consisted of 20 μL of phospholipid stock solution or a 50:50 mole fraction mixture of MK-2 with either DPPC or DPPE. The resulting film was equilibrated for 15 min and then compressed using a Teflon ribbon at a rate of 10 mm/min (2.4 Å^2/chain). The surface pressure was measured using the Wilhemy plate method where a wire probe was used as the plate on a Kibron μTrough XS.[94] The reported compression isotherms are reported as an average of three trials (constructed by averaging the three isotherms in excel). See Supporting Information for compression modulus data and interpretation.

Sample Preparation for RM NMR Spectroscopic Studies. A 0.50 M AOT stock solution was made by dissolving AOT (5.56 g, 12.5 mmol) in isooctane (25.0 mL). RMs were prepared by mixing the 0.50 M AOT stock solution with D_2O (pH 7.0) and then vortexed until clear. MK-2 RMs were made in a similar manner except an 11.2 mM MK-2 stock solution was prepared by directly dissolving MK-2 in the 0.50 M AOT/isooctane solution. Then, the MK-2-AOT-isooctane stock solution along with D_2O (pH 7) were used to make RMs.

1D ^{1}H NMR Spectroscopic Studies of AOT/Isooctane RMs That Contain MK-2. 1D ^{1}H NMR spectroscopic experiments were carried out using a Varian Inova 400 MHz instrument using routine parameters (pulse angle: 45°, relaxation delay of 1 s) at 22 °C. The RM spectra were internally referenced using the isooctane methyl peak set to 0.904 ppm.[95] Data analysis and spectrum workup were done using the NMR software, MestReNova version 10.0.1.

Sample Preparation for ^{1}H–^{1}H 2D NOESY and ROESY NMR Spectroscopic Studies (RMs). To prepare the AOT/isooctane stock solution, 0.22 g AOT (0.50 mmol) was dissolved into isooctane (1.0 mL) for a final 0.50 M AOT stock solution. Then 0.035 g (1.10 mmol) of MK-2 was dissolved into the 0.50 M AOT stock solution for a final concentration of 110 mM MK-2. Then, 892.6 μL of MK-2 AOT/isooctane stock solution was mixed with 107.3 μL of D_2O (pH = 7) and then vortexed until clear. This final mixture results in a w_0 12 RM microemulsion with an overall concentration of MK-2 being 100 mM (~29 molecules per RM).

^{1}H–^{1}H 2D NOESY and ROESY NMR Spectroscopic Studies in AOT/Isooctane w_0 12 RM. 2D NMR samples were ran using similar conditions used previously[61] using a Varian model MR400 400 MHz magnet at 26 °C. A standard NOESY pulse sequence was used consisting of 256 transients with 16 scans in the f1 direction using a 200 ms mixing time, 45° pulse angle, and a relaxation delay of 1.5 s. A standard ROESYAD pulse sequence was used consiting of 256 transients with 16 scans in the f1 direction using a 200 ms mixing time, 45° pulse angle, and a relaxation delay of 2.0 s. The NMR was locked onto 10% D_2O, and the spectrum was referenced to the isooctane methyl peak at 0.904 ppm as previously reported.[95] The resulting spectrum was processed using MestReNova NMR software version 10.0.1. The 3D structure illustration within a RM was drawn using

DOI: 10.1021/acs.joc.7b02649
J. Org. Chem. 2018, 83, 275–288

ChemBioD Ultra 12.0 and ChemBio3D Ultra 12.0 based on spectral parameters described under results.

■ ASSOCIATED CONTENT

Supporting Information

The Supporting Information is available free of charge on the ACS Publications website at DOI: 10.1021/acs.joc.7b02649.

General experimental information; 1D and 2D NMR spectroscopic and structural data of MK-2, MK-2 conformational analysis, and relevant internuclear distances; electrochemistry experimental and data/discussion; ^{1}H NMR of MK-2 with TBAP; Langmuir monolayer compression modulus of MK-2 and interpretation (PDF)

■ AUTHOR INFORMATION

Corresponding Author

*E-mail: Debbie.Crans@colostate.edu

ORCID

Jordan T. Koehn: 0000-0003-3008-6303

Debbie C. Crans: 0000-0001-7792-3450

Notes

The authors declare no competing financial interest.

■ ACKNOWLEDGMENTS

Drs. Crans and Crick thank NIH for funding (grant no. AI119567) and the NSF for funding (grant no. CHE-1709564). Dr. Crans also thanks the Arthur Cope Foundation administered by the American Chemical Society for partial support.

■ REFERENCES

(1) Beller, H. R.; Soon Lee, T.; Katz, L. *Nat. Prod. Rep.* **2015**, *32*, 1508.
(2) Frank, A.; Groll, M. *Chem. Rev.* **2017**, *117*, 5675.
(3) Thulasiram, H. V.; Erickson, H. K.; Poulter, C. D. *Science* **2007**, *316*, 73.
(4) da Costa, M. S.; Albuquerque, L.; Nobre, M. F.; Wait, R. In *Methods in Microbiology: Taxonomy of Prokaryotes*; Rainey, F., Oren, A., Eds.; Elsevier Academic Press Inc: San Diego, CA, 2011; Vol. *38*, p 197.
(5) Kroppenstedt, R. M.; Mannheim, W. *Int. J. Syst. Bacteriol.* **1989**, *39*, 304.
(6) Collins, M. D.; Jones, D. *Microbiol. Rev.* **1981**, *45*, 316.
(7) Meganathan, R. *Vitam. Horm.* **2001**, *61*, 173.
(8) Caluwe, R.; Pyfferoen, L.; De Boeck, K.; De Vriese, A. S. *Clin. Kidney J.* **2016**, *9*, 273.
(9) Bergdoll, L.; ten Brink, F.; Nitschke, W.; Picot, D.; Baymann, F. *Biochim. Biophys. Acta, Bioenerg.* **2016**, *1857*, 1569.
(10) Epand, R. M.; Walker, C.; Epand, R. F.; Magarvey, N. A. *Biochim. Biophys. Acta, Biomembr.* **2016**, *1858*, 980.
(11) Villaume, M. T.; Sella, E.; Saul, G.; Borzilleri, R. M.; Fargnoli, J.; Johnston, K. A.; Zhang, H.; Fereshteh, M. P.; Murali Dhar, T. G.; Baren, P. S. *ACS Cent. Sci.* **2016**, *2*, 27.
(12) Choi, S. R.; Larson, M. A.; Hinrichs, S. H.; Bartling, A. M.; Frandsen, J.; Narayanasamy, P. *Future Med. Chem.* **2016**, *8*, 11.
(13) Matarlo, J. S.; Lu, Y.; Daryaee, F.; Daryaee, T.; Ruzsicska, B.; Walker, S. G.; Tonge, P. J. *ACS Infect. Dis.* **2016**, *2*, 329.
(14) Szamosvari, D.; Bottcher, T. *Angew. Chem., Int. Ed.* **2017**, *56*, 7271.
(15) Vilcheze, C.; Hartman, T.; Weinrick, B.; Jain, P.; Weisbrod, T. R.; Leung, L. W.; Freundlich, J. S.; Jacobs, W. R. *Proc. Natl. Acad. Sci. U. S. A.* **2017**, *114*, 4495.
(16) Upadhyay, A.; Fontes, F. L.; Gonzalez-Juarrero, M.; McNeil, M. R.; Crans, D. C.; Jackson, M.; Crick, D. C. *ACS Cent. Sci.* **2015**, *1*, 292.
(17) Vos, M.; Esposito, G.; Edirisinghe, J. N.; Vilain, S.; Haddad, D. M.; Slabbaert, J. R.; Van Meensel, S.; Schaap, O.; De Strooper, B.; Meganathan, R.; Morais, V. A.; Verstreken, P. *Science* **2012**, *336*, 1306.
(18) Nakagawa, K.; Hirota, Y.; Sawada, N.; Yuge, N.; Watanabe, M.; Uchino, Y.; Okuda, N.; Shimomura, Y.; Suhara, Y.; Okano, T. *Nature* **2010**, *468*, 117.
(19) Hiratsuka, T.; Furihata, K.; Ishikawa, J.; Yamashita, H.; Itoh, N.; Seto, H.; Dairi, T. *Science* **2008**, *321*, 1670.
(20) Newman, D. K.; Kolter, R. *Nature* **2000**, *405*, 94.
(21) Collins, M. D.; Shah, H. N.; Minnikin, D. E. *J. Appl. Bacteriol.* **1980**, *48*, 277.
(22) Thomson, R. H. *Naturally Occurring Quinones*; Chapman & Hall: London, 1971.
(23) Cooper, G. M.; Hausman, R. E. *The Cell: A Molecular Approach*, 5th ed.; Sinauer Associates, Inc.: Sunderland, MA, 2009.
(24) Nelson, D. L.; Cox, M. M. *Lehninger Principles of Biochemistry*, 5th ed.; W. H. Freeman and Company: New York, 2008.
(25) Woodward, R. B.; Bloch, K. *J. Am. Chem. Soc.* **1953**, *75*, 2023.
(26) Hess, B. A., Jr.; Smentek, L. *Angew. Chem., Int. Ed.* **2013**, *52*, 11029.
(27) Murgolo, N. J.; Patel, A.; Stivala, S. S.; Wong, T. K. *Biochemistry* **1989**, *28*, 253.
(28) Lowry, T. H.; Richardson, K. S. *Mechanism and Theory in Organic Chemistry*, 3rd ed.; Harper & Row Publishers: New York, 1987.
(29) Klauda, J. B.; Brooks, B. R.; et al. *J. Phys. Chem. B* **2005**, *109*, 5300.
(30) Choudhury, R.; Barman, A.; Prabhakar, R.; Ramamurthy, V. *J. Phys. Chem. B* **2013**, *117*, 398.
(31) Chum, S. P.; Knight, G. W.; Ruiz, J. M.; Phillips, P. J. *Macromolecules* **1994**, *27*, 656.
(32) Robertson, M. B.; Klein, P. G.; Ward, I. M.; Packer, K. J. *Polymer* **2001**, *42*, 1261.
(33) Cao, M.; Monson, P. A. *J. Phys. Chem. B* **2009**, *113*, 13866.
(34) Nikki, K.; Inakura, H.; Wu-Le; Suzuki, N.; Endo, T. *J. Chem. Soc., Perkin Trans. 2* **2001**, 2370.
(35) Nikki, K.; Nakagawa, N. *Org. Magn. Reson.* **1983**, *21*, 552.
(36) Nikki, K. *Magn. Reson. Chem.* **1990**, *28*, 385.
(37) Law, J. M. S.; Setiadi, D. H.; Chass, G. A.; Csizmadia, I. G.; Viskolcz, B. *J. Phys. Chem. A* **2005**, *109*, 520.
(38) Kanicky, J. R.; Shah, D. O. *J. Colloid Interface Sci.* **2002**, *256*, 201.
(39) Ko, Y. H.; Kim, Y.; Kim, H.; Kim, K. *Chem. - Asian J.* **2011**, *6*, 652.
(40) Ko, Y. H.; Kim, H.; Kim, Y.; Kim, K. *Angew. Chem., Int. Ed.* **2008**, *47*, 4106.
(41) Schramm, M. P.; Rebek, J., Jr. *Chem. - Eur. J.* **2006**, *12*, 5924.
(42) de Sousa, F. F.; Freire, P. T. C.; Saraiva, G. D.; Lima, J. A.; Alcantara, P.; Melo, F. E. A.; Mendes, J. *Vib. Spectrosc.* **2010**, *54*, 118.
(43) Collins, M. D.; Kroppenstedt, R. M. *FEMS Microbiol. Lett.* **1987**, *44*, 215.
(44) Bentley, R. *Pure Appl. Chem.* **1975**, *41*, 47.
(45) Suhara, Y.; Wada, A.; Tachibana, Y.; Watanabe, M.; Nakamura, K.; Nakagawa, K.; Okano, T. *Bioorg. Med. Chem.* **2010**, *18*, 3116.
(46) Payne, R. J.; Daines, A. M.; Clark, B. M.; Abell, A. D. *Bioorg. Med. Chem.* **2004**, *12*, 5785.
(47) Tynkkynen, T.; Hassinen, T.; Tiainen, M.; Soininen, P.; Laatikainen, R. *Magn. Reson. Chem.* **2012**, *50*, 598.
(48) Ishihara, M.; Sakagami, H. *Anticancer Res.* **2007**, *27*, 4059.
(49) Lancaster, C. R. D.; Haas, A. H.; Madej, M. G.; Mileni, M. *Biochim. Biophys. Acta, Bioenerg.* **2006**, *1757*, 988.
(50) Prince, R. C.; Leslie Dutton, P.; Malcolm Bruce, J. *FEBS Lett.* **1983**, *160*, 273.
(51) Guin, P. S.; Das, S.; Mandal, P. C. *Int. J. Electrochem.* **2011**, *2011*, 816202.
(52) Dryhurst, G., Kadish, K. M., Scheller, F., Renneberg, R. *Biological Eletrochemistry*; Academic Press: New York, 1982.
(53) Luder, W. F.; Kraus, P. B.; Kraus, C. A.; Fuoss, R. M. *J. Am. Chem. Soc.* **1936**, *58*, 255.
(54) Jaworski, J. S.; Leniewska, E.; Kalinowski, M. K. *J. Electroanal. Chem. Interfacial Electrochem.* **1979**, *105*, 329.
(55) Baruah, B.; Roden, J. M.; Sedgwick, M.; Correa, N. M.; Crans, D. C.; Levinger, N. E. *J. Am. Chem. Soc.* **2006**, *128*, 12758.
(56) Odella, E.; Falcone, R. D.; Silber, J. J.; Correa, N. M. *ChemPhysChem* **2016**, *17*, 2407.

DOI: 10.1021/acs.joc.7b02649
J. Org. Chem. 2018, 83, 275−288

(57) Diaz-Fernandez, Y.; Foti, F.; Mangano, C.; Pallavicini, P.; Patroni, S.; Perez-Gramatges, A.; Rodriguez-Calvo, S. *Chem. - Eur. J.* **2006**, *12*, 921.
(58) Pallavicini, P.; Diaz-Fernandez, Y.; Pasotti, L. *Coord. Chem. Rev.* **2009**, *253*, 2226.
(59) Stefaniu, C.; Brezesinski, G.; Mohwald, H. *Adv. Colloid Interface Sci.* **2014**, *208*, 197.
(60) Sostarecz, A. G.; Gaidamauskas, E.; Distin, S.; Bonetti, S. J.; Levinger, N. E.; Crans, D. C. *Chem. - Eur. J.* **2014**, *20*, 5149.
(61) Peters, B. J.; Groninger, A. S.; Fontes, F. L.; Crick, D. C.; Crans, D. C. *Langmuir* **2016**, *32*, 9451.
(62) Riter, R. E.; Kimmel, J. R.; Undiks, E. P.; Levinger, N. E. *J. Phys. Chem. B* **1997**, *101*, 8292.
(63) Maitra, A. *J. Phys. Chem.* **1984**, *88*, 5122.
(64) Durantini, A. M.; Falcone, R. D.; Silber, J. J.; Correa, N. M. *ChemPhysChem* **2016**, *17*, 1678.
(65) Lepori, C. M. O.; Correa, N. M.; Silber, J. J.; Falcone, R. D. *Soft Matter* **2016**, *12*, 830.
(66) Hoyo, J.; Torrent-Burgues, J.; Guas, E. *J. Colloid Interface Sci.* **2012**, *384*, 189.
(67) Quinn, P. J.; Esfahani, M. A. *Biochem. J.* **1980**, *185*, 715.
(68) Patterson, M.; Vogel, H. J.; Prenner, E. J. *Biochim. Biophys. Acta, Biomembr.* **2016**, *1858*, 403.
(69) Roche, Y.; Peretti, P.; Bernard, S. *J. Therm. Anal. Calorim.* **2007**, *89*, 867.
(70) De, T. K.; Maitra, A. *Adv. Colloid Interface Sci.* **1995**, *59*, 95.
(71) Sedgwick, M. A.; Trujillo, A. M.; Hendricks, N.; Levinger, N. E.; Crans, D. C. *Langmuir* **2011**, *27*, 948.
(72) Zan, G. T.; Wu, Q. S. *Adv. Mater.* **2016**, *28*, 2099.
(73) Kuchler, A.; Yoshimoto, M.; Luginbuhl, S.; Mavelli, F.; Walde, P. *Nat. Nanotechnol.* **2016**, *11*, 409.
(74) Dharaiya, N.; Bahadur, P. *Colloids Surf., A* **2012**, *410*, 81.
(75) Dumas, C.; Meledandri, C. J. *Langmuir* **2015**, *31*, 7193.
(76) Kaur, G.; Chiappisi, L.; Prevost, S.; Schweins, R.; Gradzielski, M.; Mehta, S. K. *Langmuir* **2012**, *28*, 10640.
(77) Sanchez-Lombardo, I.; Baruah, B.; Alvarez, S.; Werst, K. R.; Segaline, N. A.; Levinger, N. E.; Crans, D. C. *New J. Chem.* **2016**, *40*, 962.
(78) Crans, D. C.; Levinger, N. E. *Acc. Chem. Res.* **2012**, *45*, 1637.
(79) Bock, C. W.; Panchenko, Y. N.; Krasnoshchiokov, S. V.; Aroca, R. *J. Mol. Struct.* **1987**, *160*, 337.
(80) Squillacote, M. E.; Semple, T. C.; Mui, P. W. *J. Am. Chem. Soc.* **1985**, *107*, 6842.
(81) Mui, P. W.; Grunwald, E. *J. Phys. Chem.* **1984**, *88*, 6340.
(82) Gundersen, G.; Thomassen, H. G.; et al. *J. Mol. Struct.* **1991**, *243*, 385.
(83) Fujimoto, N.; Kosaka, T.; Yamada, M. *Menaquinone as Well as Ubiquinone as a Crucial Component in the Escherichia coli Respiratory Chain*; InTech: Rijeka, Croatia, 2012.
(84) Lai, C.-T.; Li, H.-J.; Yu, W.; Shah, S.; Bommineni, G. R.; Perrone, V.; Garcia-Diaz, M.; Tonge, P. J.; Simmerling, C. *Biochemistry* **2015**, *54*, 4683.
(85) Yano, T.; Rahimian, M.; Aneja, K. K.; Schechter, N. M.; Rubin, H.; Scott, C. P. *Biochemistry* **2014**, *53*, 1179.
(86) Peover, M. E. *J. Chem. Soc.* **1962**, 4540.
(87) Chadar, D.; Camilles, M.; Patil, R.; Khan, A.; Weyhermuller, T.; Salunke-Gawali, S. *J. Mol. Struct.* **2015**, *1086*, 179.
(88) Kathawate, L.; Joshi, P. V.; Dash, T. K.; Pal, S.; Nikalje, M.; Weyhermuller, T.; Puranik, V. G.; Konkimalla, V. B.; Salunke-Gawali, S. *J. Mol. Struct.* **2014**, *1075*, 397.
(89) McQuaw, C. M.; Sostarecz, A. G.; Zheng, L.; Ewing, A. G.; Winograd, N. *Langmuir* **2005**, *21*, 807.
(90) Demel, R. A.; Geurts Van Kessel, W. S. M.; Zwaal, R. F. A.; Roelofsen, B.; Van Deenen, L. M. *Biochim. Biophys. Acta, Biomembr.* **1975**, *406*, 97.
(91) Choi, Y.; Attwood, S. J.; Hoopes, M. I.; Drolle, E.; Karttunen, M.; Leonenko, Z. *Soft Matter* **2014**, *10*, 206.
(92) Belzile, M.-N.; Godin, R.; Durantini, A.; Cosa, G. *J. Am. Chem. Soc.* **2016**, *138*, 16388.
(93) Dobrinescu, C.; Iorgulescu, E. E.; Mihailciuc, C.; Macovei, D.; Wuttke, S.; Kemnitz, E.; Parvulescu, V. I.; Coman, S. M. *Adv. Synth. Catal.* **2012**, *354*, 1301.
(94) Girard-Egrot, A.; Blum, L. J. Langmuir-Blodgett Technique for Synthesis of Biomimetic Lipid Membranes. In *Nanobiotechnology of Biomimetic Membranes*; Ferrari, M., Martin, D. K., Eds.; Springer: New York, 2007; p 23.
(95) Samart, N.; Beuning, C. N.; Haller, K. J.; Rithner, C. D.; Crans, D. C. *Langmuir* **2014**, *30*, 8697.

DOI: 10.1021/acs.joc.7b02649
J. Org. Chem. 2018, 83, 275−288

Appendix VIII: Investigating Substrate Analogs for Mycobacterial MenJ: Truncated and Partially Saturated Menaquinones

This is the manuscript that corresponds to chapter four and is published in *Biochemistry*.[1]

References

1. Koehn, J. T.; Beuning, C. N.; Peters, B. J.; Dellinger, S. K.; Van Cleave, C.; Crick, D. C.; Crans, D. C., Investigating Substrate Analogues for Mycobacterial MenJ: Truncated and Partially Saturated Menaquinones. *Biochemistry* **2019,** *58* (12), 1596-1615.

Biochemistry

Article

Cite This: *Biochemistry* 2019, 58, 1596−1615

pubs.acs.org/biochemistry

Investigating Substrate Analogues for Mycobacterial MenJ: Truncated and Partially Saturated Menaquinones

Jordan T. Koehn,[†] Cheryle N. Beuning,[†] Benjamin J. Peters,[†] Sara K. Dellinger,[†] Cameron Van Cleave,[†] Dean C. Crick,[‡,§] and Debbie C. Crans*[,†,‡]

[†]Chemistry Department, [‡]Cell and Molecular Biology Program, and [§]Microbiology, Immunology, and Pathology Department, Colorado State University, Fort Collins, Colorado 80523, United States

Supporting Information

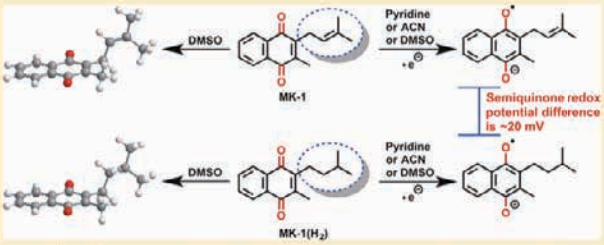

ABSTRACT: Menaquinones (MKs) are essential for electron transport in prokaryotes, and importantly, partially saturated MKs represent a novel virulence factor. However, little is known regarding how the degree of saturation in the isoprenyl side chain influences conformation or quinone redox potential. MenJ is an enzyme that selectively reduces the second isoprene unit on MK-9 and is contextually essential for the survival of *Mycobacterium tuberculosis* in J774A.1 macrophage-like cells, suggesting that MenJ may be a conditional drug target for pathogenic mycobacteria. Therefore, fundamental information about the properties of this system is important, and we synthesized the simplest MKs, unsaturated MK-1 and the saturated analogue, MK-1(H_2). Using two-dimensional nuclear magnetic resonance spectroscopy, we established that MK-1 and MK-1(H_2) adopted similar folded−extended conformations (i.e., the isoprenyl side chain folds upward) in each solvent examined but the folded−extended conformations differed slightly between organic solvents. Saturation of the isoprenyl side chain slightly altered the MK-1 analogue conformation in each solvent. We used molecular mechanics to illustrate the MK-1 analogue conformations. The measured quinone redox potentials of MK-1 and MK-1(H_2) differed between organic solvents (presumably due to differences in dielectric constants), and remarkably, an ~20 mV semiquinone redox potential difference was observed between MK-1 and MK-1(H_2) in pyridine, acetonitrile, and dimethyl sulfoxide, demonstrating that the degree of saturation in the isoprenyl side chain of MK-1 influences the quinone redox potential. Finally, MK-1 and MK-1(H_2) interacted with Langmuir phospholipid monolayers and Aerosol-OT reverse micelle (RM) model membrane interfaces, where MK-1 adopted a slightly different folded conformation within the RM model membrane interface.

Quinones are a unique type of α,β-unsaturated ketone existing as metabolites in numerous pathways where they have many functions in nature.[1−6] The importance of quinone chemistry has been recognized since the mid-1800s. Quinone-containing compounds can be antioxidants, antitumoral agents, or carcinogenic agents and are the inherent components of biological systems such as photosystem II.[1−6] Menaquinones (MKs) (or naphthoquinones) are members of the lipoquinone (lipid-quinone) class of molecules and are essential components of the respiratory electron transport system (ETS), where they shuttle electrons and protons between protein complexes by acting as electron donors and acceptors.[6] Partial saturation of the isoprenyl side chain of MK has been known for a long time, but MenJ was recently shown to selectively reduce MK-9 at the second isoprene unit, demonstrating the origin and necessity of partially saturated MKs for the survival of the bacteria.[7,8] Currently, little is known regarding the conformation of MKs in solution or within cell membranes and how partial saturation of the isoprenyl side chain affects conformation and quinone reactivity, even though the structures and biological significance of lipoquinones and isoprenoids have been known for more than 50 years.[6,9−13] It is well-known that evolutionarily conserved structural differences in the lipoquinone headgroup alter quinone redox potential,[1] but how partial saturation of the isoprenyl side chain affects quinone redox potential remains uncertain. Therefore, this work aims to characterize the conformation of the most fundamental MKs containing

Received: January 3, 2019
Revised: February 19, 2019
Published: February 21, 2019

ACS Publications © 2019 American Chemical Society

DOI: 10.1021/acs.biochem.9b00007
Biochemistry 2019, 58, 1596−1615

Downloaded via COLORADO STATE UNIV on April 9, 2019 at 18:22:29 (UTC).
See https://pubs.acs.org/sharingguidelines for options on how to legitimately share published articles.

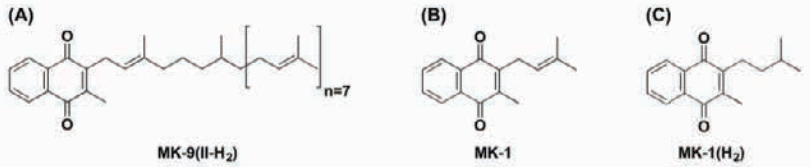

Figure 1. Structures of (A) MK-9(II-H_2), present within *Mycobacterium tuberculosis*, (B) the unsaturated MK analogue, MK-1, and (C) the saturated MK analogue, MK-1(H_2).

one isoprene unit (unsaturated vs saturated side chain) in an organic solution and a model membrane interface and to determine the quinone redox potentials of unsaturated MK-1 and saturated MK-1(H_2) in organic solutions.

MKs are structurally characterized by a naphthoquinone moiety and a repeating isoprenyl side chain of varying length (Figure 1), where the latter is a characteristic that has long been used to assist taxonomic efforts.[14,15] The most widely known MK compound is vitamin K_2 (or MK-4), which is essential for life in humans as it is a key cofactor in blood coagulation.[16] MK-4 was recently shown to be biosynthesized in humans[17] and as a part of the ETS in *Drosophila*.[18] Vitamin K_3 (or menadione), the simplest 1,4-naphthoquinone derivative lacking the isoprenyl side chain, has been reported to have significant antitumoral properties.[2] N-Alkylated MK derivatives have also been synthesized and characterized in the literature, with several exhibiting interesting biological properties.[19−22] The truncated MK analogues, menaquinone-1 (MK-1) and menaquinone-1(H_2) [MK-1(H_2)], are vital to study as they are the simplest, most fundamental MKs, where they retain the core requirements (i.e., a naphthoquinone moiety and a one-unit isoprenyl side chain). MK-1(H_2) is crucial to study as it lacks the double bond in the isoprenyl side chain, and importantly, biologically isolated MK analogues containing partial saturation (reduced double bond) in the isoprenyl side chain have been reported (Figure 1).[6−8] Truncated MK analogues are more soluble than the natural MK substrate, thus allowing rigorous characterization in aqueous assays.[8] Furthermore, MK-9 contains 80 hydrogens with significant spectral overlap, making conformational analysis nontrivial. Therefore, the conformational analysis of these two truncated MK-1 analogues is essential as the conformation of the first isoprene unit will influence the conformation of the rest of the isoprenyl side chain in naturally occurring longer MK analogues [e.g., MK-4, MK-9, or MK-9(II-H_2) (Figure 1)].

The synthesis of truncated MK analogues is necessary as it allows experimental conformational analysis to be carried out. Molecular conformations are significant for manifesting physical and chemical reactivity as well as recognition in biological systems. MKs contain alkyl side chains of varying lengths, and conformations have been reported for various alkanes, alkenes, and fatty acids, which all contain alkyl chains of varying lengths.[23−35] For example, the degree of folding of C_5−C_{32} *n*-alkanes in solution depends on the strength of the dispersion force of the solvent and increases with an increase in chain length.[27−29] Furthermore, studies of *n*-hexane and *n*-pentane in various solvents suggested that the solvent environment had only minor effects on the conformational equilibrium.[35] Interestingly, conformations observed in polar and spherical solvents such as dimethyl sulfoxide (DMSO) favored *gauche* conformations.[35] Computational studies have been carried out on MK analogues in which folded conformations were found to be favorable.[34,36] Importantly, we recently reported that menaquinone-2 (MK-2) adopts a folded, U-shaped conformation in solution and within a model membrane interface.[37] However, MK-1 contains only one isoprene unit and presents the best opportunity for a flat−extended conformation to exist, and therefore, it is important to determine if a flat−extended (i.e., trans or extended configuration of the side chain and isoprene planar), folded−extended (i.e., isoprene folded upward), or U-shaped conformation (i.e., isoprene folded up and back toward the naphthoquinone in a U shape) is preferred (see the illustration below). On the basis of these selected examples, we hypothesized that MK-1 analogues adopt folded conformations regardless of the degree of saturation in their isoprenyl side chain.

The conformation and electronic properties of a molecule can affect both the reactivity and function of a molecule in solution and within biological environments. The longer partially saturated isoprenyl side chain MK analogue, MK-9(II-H_2) (Figure 1), is an electron transporter within *Mycobacterium tuberculosis*, and the synthesis of MK-9(II-H_2) was found to be essential for the survival of pathogenic *M. tuberculosis* in host macrophages; thus, partially saturated MKs represent a novel virulence factor.[7,8] In addition, partially saturated MK analogues have been reported in other organisms such as members of the genera *Streptomyces* and *Actinomadura*.[11] It is unclear whether hydrogenation of the double bond in specific isoprene units changes the reactivity of the quinone system. The double bonds present within the isoprenyl side chain are not conjugated to the quinone system within MK. Therefore, it would not be anticipated that a significant change in the quinone redox potential would occur upon reduction of an isoprenyl unit. However, it has been reported that even when there is no direct conjugation between the quinone system and a substituent group, electrochemical reduction of the quinone system is sensitive to the electronic perturbation of the substituents.[1] Thus, it is possible that partial saturation in the isoprenyl side chain could influence the quinone redox potential, where an indirect through-bond effect could be a contributing factor and/or conformational effects of the substituent. Therefore, we hypothesized that the quinone redox potential of MK-1 may

DOI: 10.1021/acs.biochem.9b00007
Biochemistry 2019, 58, 1596−1615

be influenced by the degree of saturation in the isoprenyl side chain.

In this work, MK-1 and MK-1(H_2) (Figure 1) were first synthesized and then their conformations within organic solvents were elucidated by one-dimensional (1D) and two-dimensional (2D) ^{1}H nuclear magnetic resonance (NMR) spectroscopy. MK-1 and MK-1(H_2) adopted similar folded–extended conformations in each solvent, but the preferred folded–extended conformations differed slightly between solvent environments. The quinone redox potentials of MK and MK-1(H_2) were measured in three organic solvents, where a solvent effect (presumably due to a change in the dielectric constant) was observed, and most interestingly, an ~20 mV difference in semiquinone redox potential was observed between MK-1 and MK-1(H_2). The interaction of MK-1 and MK-1(H_2) with phospholipid monolayers was characterized using Langmuir phospholipid monolayers, and the two MK-1 analogues were found to interact with the phospholipid interface. Finally, using a complementary study, the location, orientation, and conformation of MK-1 and MK-1(H_2) within a reverse micelle (RM) model membrane interface were determined using 1D and 2D NMR spectroscopy. The two MK-1 analogues interacted similarly with the RM model membrane interface, and MK-1 adopted a slightly different folded conformation within the RM interface compared to that observed in an organic solution.

EXPERIMENTAL SECTION

Materials. Menadione (crystalline), sodium hydrosulfite (85.0%), 1,4-dioxane (99.9%), 3-methyl-2-buten-1-ol (99%), BF_3 etherate (≥46.5%), Luperox A98 benzoyl peroxide (≥98%), 1-iodo-3-methylbutane (97%), dioctyl sulfosuccinate sodium salt (AOT, 97.0%), isooctane (2,2,4-trimethylpentane, ≥99.0%), chloroform (99.8%), methanol (99.9%), tetrabutylammonium perchlorate (TBAP, ≥99.0%), ferrocene (Fc, anhydrous), silver nitrate ($AgNO_3$, ≥99.0%), and activated charcoal were purchased from Sigma-Aldrich and used as received unless otherwise noted. Absolute ethanol and ultra-high-purity argon gas (99.9%) were acquired from Pharmco-Aaper and Airgas, respectively. Deuterated solvents of acetonitrile (d_3-ACN or CD_3CN) (99.8% D), dimethyl sulfoxide (d_6-DMSO) (99.9% D, 0.05% (v/v) tetramethylsilane), and d_6-benzene (≥99.6%) were acquired from Sigma-Aldrich. Deuterium oxide (D_2O, 99.9%), d_2-dichloromethane (99.9%), and d_4-methanol (99.8%) were acquired from Cambridge Isotope Laboratories, Inc. Deuterated pyridine (99.8% D) was purchased from Arcos Organics. DPPC (1,2-dipalmitoyl-*sn*-glycero-3-phosphocholine, ≥99.0%) and DPPE (1,2-dipalmitoyl-*sn*-glycero-3-phosphoethanolamine, ≥99.0%) were purchased from Avanti Polar Lipids Inc. Monosodium phosphate (NaH_2PO_4, 96.0%) and sodium phosphate dibasic anhydrous (Na_2HPO_4) were purchased from Fisher Scientific, and distilled deionized water (DDI H_2O) was purified with a Barnstead E-pure system (~18 MΩ cm).

General Methods. All non-aqueous reactions were carried out under an argon atmosphere in flame-dried glassware, and all mixtures were stirred on a magnetic stir plate using an anhydrous solvent unless otherwise noted. Reactions were monitored by thin layer chromatography (TLC) on Whatman Partisil K6F TLC plates (silica gel 60 Å, 0.250 mm thickness) and visualized using an ultraviolet lamp (366 or 254 nm). Products were purified by flash chromatography (SiliCycle SiliaFlash F60, 43–60 μm, 60 Å). Yields refer to chromatographically and spectroscopically (^{1}H NMR) homogeneous materials unless otherwise noted. All chemicals were used without purification except AOT and the organic solvents. AOT was purified using activated charcoal and methanol to remove acidic impurities using previously reported methods.[38] Organic solvents dimethyl sulfoxide (DMSO), acetonitrile (CH_3CN or ACN), and pyridine were purified by distillation and then dried over activated 3 Å molecular sieves (40 g/200 mL of solvent) for 3 days. Benzene was dried by being passed through an alumina drying column (Solv-Tek Inc.) under argon pressure. When samples were prepared for RM NMR experiments, deuterium oxide was used instead of H_2O and the pH was adjusted to consider the presence of deuterium (pD = 0.4 + pH).[39] ^{1}H and ^{13}C NMR spectra were recorded on a 400 MHz Varian Model MR400, 400 MHz Varian iNova400, or 500 MHz Varian iNova500 spectrometer. Chemical shift values (δ) are reported in parts per million and referenced against the internal solvent peaks in ^{1}H NMR ($CDCl_3$, δ 7.26; d_3-acetonitrile, δ 1.94; d_6-DMSO, δ 2.50; d_4-methanol, δ 4.87; d_2-methylene chloride, δ 5.32; d_6-benzene, δ 7.16; d_5-pyridine, δ 8.74; D_2O, δ 4.79) and in ^{13}C NMR ($CDCl_3$, δ 77.16; d_6-benzene, δ 128.06).

Preparation of 2-Methyl-3-(3-methylbut-2-en-1-yl)-naphthalene-1,4-dione, MK-1 (3). Menadiol **2** was synthesized as previously described[37] from menadione **4**, and MK-1 **3** was synthesized previously.[8] However, in this work, the reaction to form MK-1 **3** was scaled up and characterization reported data in $CDCl_3$. To a dry 100 mL Schlenk flask were added a stir bar, EtOAc (16 mL), and 1,4-dioxane (16 mL), which was then purged/evacuated with argon repeatedly. Then, crude menadiol **2** (2.50 g, 4:1 menadiol:menadione by NMR integration; note that menadiol is prone to autoxidation in $CDCl_3$, 11.48 mmol) was added followed by 3-methyl-2-buten-1-ol **1** (1.08 g, 12.52 mmol) and then dropwise addition of distilled BF_3 etherate (0.8 mL). The reaction solution turned dark orange and was refluxed at 70 °C for 3 h under argon. The reaction was quenched with ice and H_2O (100 mL), and then the mixture extracted with diethyl ether (3 × 100 mL). The yellow organic extracts were washed with saturated $NaHCO_3$ (100 mL), washed with brine (100 mL), dried with anhydrous Na_2SO_4, and then concentrated under reduced pressure at ambient temperature to yield 3.50 g of crude red oil. The crude oil was purified by flash column chromatography (1000 mL of 230–400 mesh SiO_2, 70 mm column, 20:1 *n*-pentane:EtOAc). The red oil obtained was dried under reduced pressure (~125 mTorr) overnight to yield 0.628 g of a deep red oil (2.61 mmol, 22.7% yield): ^{1}H NMR (400 MHz, $CDCl_3$) δ 8.06–8.08 (m, 2H), 7.67–7.69 (m, 2H), 5.02 (t, J = 7.0 Hz, 1H), 3.36 (d, 2H, J = 7.0 Hz), 2.19 (s, 3H), 1.79 (s, 3H), 1.69 (s, 3H); ^{13}C NMR (101 MHz, $CDCl_3$) δ 185.6, 184.7, 146.2, 143.4, 134.1, 133.47, 133.42, 132.33, 132.30, 126.4, 126.3, 119.3, 26.3, 25.9, 18.2, 12.8; HRMS (DART) m/z [(M + H)$^+$] calcd for $C_{16}H_{17}O_2$ 241.1223, found 241.1222.

Preparation of 2-Isopentyl-3-methylnaphthalene-1,4-dione, MK-1(H_2) (6). To a dry 100 mL round-bottom Schlenk flask were added a stir bar and dry and degassed benzene (30 mL) followed by 1-iodo-3-methylbutane **5** (1.98 g, 10.0 mmol, 1 equiv), which was then purged/evacuated with argon repeatedly. To a dry 20 mL vial was added dry benzene (15 mL), which was then degassed via argon needle purge, followed by addition of menadione **4** (1.72 g, 10.0 mmol) and benzoyl peroxide (2.42 g, 10.0 mmol, 1 equiv). This solution

DOI: 10.1021/acs.biochem.9b00007
Biochemistry 2019, 58, 1596–1615

was sonicated until dissolution occurred under argon. The naphthoquinone/benzoyl peroxide solution was added dropwise over 135 min to the refluxing prenyl iodide solution, which was under an argon atmosphere during the reaction. After the addition was complete, the solution was refluxed for an additional 1 h. The solution was then diluted with saturated $NaHCO_3$ (100 mL) and diethyl ether (100 mL), and then the two phases were separated. The aqueous layer was extracted with diethyl ether (3 × 100 mL), and the combined organic extracts were washed with saturated $NaHCO_3$ (100 mL), washed with brine (100 mL), dried with anhydrous Na_2SO_4, and then concentrated under reduced pressure at ambient temperature to yield a crude yellow powder. The crude powder was purified by flash column chromatography (10:1.5 *n*-pentane:EtOAc) to yield 0.493 g of a yellow solid (2.03 mmol, 20.3% yield) after drying overnight under reduced pressure (~125 mTorr): ^{1}H NMR (400 MHz, C_6D_6) δ 8.05−8.07 (m, 2H), 7.04−7.06 (m, 2H), 2.41−2.45 (m, 2H), 1.92 (s, 3H), 1.45−1.55 (m, 1H), 1.16−1.21 (m, 2H), 0.89 (d, J = 6.6 Hz, 2H); ^{13}C NMR (101 MHz, C_6D_6) δ 184.9, 184.3, 147.5, 142.7, 133.09, 133.08, 132.74, 132.71, 126.26, 126.21, 37.8, 28.9, 25.2, 22.5, 12.3; HRMS (DART) m/z [$(M + H)^+$] calcd for $C_{16}H_{19}O_2$ 243.1380, found 243.1378.

Mass Spectrometry. High-resolution mass spectrometry (HRMS) experiments were conducted on an Agilent 6224 TOF LC/MS instrument [O-time-of-flight (TOF)] interfaced with the Direct Analysis in Real Time (DART) source (IonSense DART-100). A standard of Jeffamine was used as an internal standard calibration for HRMS DART experiments carried out in positive mode.

NMR Spectroscopic Studies. 1D and 2D ^{1}H NMR spectroscopic studies were carried out both in organic solvents and in an RM model membrane system. ^{1}H and ^{13}C NMR spectra were recorded using either a Varian model MR400, model Inova400, or model Inova500 spectrometer operating at either 400, 500, or 101 MHz, respectively. Chemical shift values (δ) are reported in parts per million and referenced against the internal solvent peaks in ^{1}H NMR ($CDCl_3$, δ 7.26; d_3-ACN, δ 1.94; d_6-DMSO, δ 2.50; d_4-methanol, δ 4.87; d_2-methylene chloride, δ 5.32; d_6-benzene, δ 7.16; d_5-pyridine, δ 8.74; D_2O, δ 4.79) and in ^{13}C NMR ($CDCl_3$, δ 77.16; d_6-benzene, δ 128.06). All NMR spectra were recorded at either 22, 25, or 26 °C. See figure captions and the Supporting Information for more details.

Solution 1D ^{1}H NMR Spectroscopic Studies. Samples were prepared by dissolving ~5.0 mg of MK-1 in 0.5 mL of either d_1-chloroform, d_2-methylene chloride, d_4-methanol, d_6-DMSO, d_5-pyridine, d_3-ACN, or d_6-benzene. The NMR instrument was locked onto the respective deuterium signal in the deuterated solvent used. NMR spectra were then collected using 32 scans for each sample. The data were processed using MestReNova NMR processing software version 10.0.1. The spectra were manually phased, and then the baseline was corrected using a Bernstein Polynomial Fit (polynomial order 3). The obtained spectra were referenced to the proper internal solvent peak.

Sample Preparation for ^{1}H−^{1}H 2D NOESY and ^{1}H−^{1}H 2D ROESY NMR Spectroscopic Studies. To prepare the solutions of MK-1 or MK-1(H_2) in d_5-pyridine, d_3-ACN, and d_6-DMSO, 0.0024 g of MK-1 or 0.0024 g of MK-1(H_2) was dissolved in 0.5 mL of a deuterated solvent to produce a 20 mM solution of MK-1 or MK-1(H_2), respectively. The NMR samples containing the MK-1 or MK-1(H_2) solution were purged with argon briefly and capped prior to data collection.

^{1}H−^{1}H 2D NOESY and ^{1}H−^{1}H 2D ROESY NMR Spectroscopic Solution Studies. ^{1}H−^{1}H 2D NOESY NMR and ^{1}H−^{1}H 2D ROESY NMR spectroscopic experiments were conducted using a 400 MHz Varian MR400 NMR spectrometer operating at 26 °C. A standard NOESY pulse sequence was used consisting of 256 transients with 16 scans in the f1 domain using a 500 ms mixing time, a 45° pulse angle, and a 1.5 s relaxation delay. The standard ROESYAD pulse sequence consisted of 256 transients with 16 scans in the f1 domain using a 400 ms mixing time, a 45° pulse angle, and a 2.0 s relaxation delay. The NMR was locked onto either d_5-pyridine, d_3-ACN, or d_6-DMSO. The resulting spectrum was processed using MestReNova NMR software version 10.0.1 (see the Supporting Information for further details). The spectra were referenced to the proper internal solvent peak.

Molecular Mechanics Calculations. To illustrate conformations for MK-1 and MK-1(H_2), Merck Molecular Force Field 94 (MMFF94) molecular mechanics gas phase simulations were conducted using ChemBio3D Ultra 12.0 at 25 °C. Starting conformations were obtained by building ChemDraw structures and rotating desired bonds, and then simulations were run followed by energy optimization or simply an energy minimization to achieve the desired conformation. Conformations A, A1, B, B1, C, and C1 in Figure 5 were constructed and then energy minimized with a root-mean-square (RMS) gradient of 0.1 and up to 50 iterations to obtain MK-1 and MK-1(H_2) conformations that agreed with our interpretation of the cross peak observations and intensities in the ^{1}H−^{1}H 2D NOESY and ROESY NMR spectral data. Two simulations were run for 10000 iterations and then energy minimized using an MMFF94 energy minimization calculation using 500 iterations with an RMS gradient of 0.001 to achieve conformations D and D1 in Figure S27. Conformations E, E1, F, and F1 in Figure S27 were generated by rotating bonds to achieve the desired conformation followed by an energy minimization using 20−50 iterations and an RMS gradient of 0.1. A table of structural parameters such as selected distances between hydrogens within the conformations in Figure 5 and Figure S27 and energies calculated for the three-dimensional (3D) conformations can be found in the Supporting Information. Tables of Cartesian coordinates for the MK-1 analogue conformations can be found in the Supporting Information.

Electrochemistry Methods. The electrochemistry was performed on a CHI 750D potentiostat. For cyclic voltammetry, a classical three-electrode system was used with a scan rate of 100 mV/s at ambient temperature. A glassy carbon working electrode (BASi MF2012, 3 mm) was lightly polished between runs with alumina powder and then rinsed with water and ethanol. A platinum wire counter electrode (BASi MW1032) was gently polished between runs with 600 grit sandpaper. A Ag^+/Ag reference electrode (BASi MW1085) was constructed by using the Ag wire gently polished with 600 grit sandpaper inserted into a freshly prepared solution of organic solvent (ACN, pyridine, or DMSO) with 0.1 M TBAP and 0.01 M $AgNO_3$. This reference electrode was equilibrated in the MK-1 or MK-1(H_2) solution (2 mM) of the same organic solvent for 10 min. The solutions were bubbled for ~5−10 min with argon gas to ensure as much dissolved O_2(g) was removed as possible before the cyclic voltammogram was recorded. All half-wave potentials recorded were referenced to

DOI: 10.1021/acs.biochem.9b00007
Biochemistry 2019, 58, 1596−1615

the internal standard Fc^+/Fc couple by subtracting the averaged potential in each solvent. The Fc^+/Fc couple against the Ag^+/Ag reference in ACN was 0.081 ± 0.002 V, in DMSO was 0.176 ± 0.004 V, and in pyridine was 0.562 ± 0.001 V. The reliability of the Fc^+/Fc couple half-wave potential in each solvent was within experimental error.

$$E_{1/2} = \frac{E_{pc} + E_{pa}}{2} \quad (1)$$

$$\frac{i_{pc}}{i_{pa}} = 1, \text{ for a reversible process} \quad (2)$$

$$\Delta E_p = E_{pc} - E_{pa}, n = x \times \frac{0.059V}{\Delta E_p} \quad (3)$$

The half-wave potentials are calculated using eq 1, where E_{pc} and E_{pa} are the cathodic and anodic peak potentials, respectively. The cathodic and anodic peak currents, i_{pc} and i_{pa}, respectively, were measured manually with a ruler on the cyclic voltammograms in centimeters to determine reversibility as a measure of the closeness to unity (eq 2). The number of electrons, n, in each process was determined using eq 3, where x is the adjustment factor in each solvent determined by setting the standard ferrocene number of electrons to 1 (n = 1). Electrochemistry performed in non-aqueous solvents may have ΔE_p values that are not indicative of the number of electrons; therefore, the ferrocene standard was used to determine the true value. See the Supporting Information for more detailed electrochemistry methods and discussion.

Langmuir Monolayer Compression Isotherms. Langmuir phospholipid monolayers were prepared using a Kibron μtroughXS. The subphase consisted of ~50 mL of a 20 mM phosphate buffer (pH 7.4). Phospholipid stock solutions of 18.4 mg (1 mM) of DPPC or 17.3 mg (1 mM) of DPPE were prepared by dissolving the phospholipid in 25 mL of a chloroform/methanol solvent [9:1 (v/v)]. Stock solutions (1 mM) of both MK-1 and MK-1(H_2) were prepared with 0.97 and 0.96 mg, respectively, in 4 mL of a chloroform/methanol solvent [9:1 (v/v)]. Then, 20 μL of a stock solution [20 nmol of DPPC, DPPE, MK-1, or MK-1(H_2)] or a mixture (10 nmol of lipid and 10 nmol of MK) was applied in dropwise fashion to the surface of the subphase. This was then allowed to equilibrate for 15 min, allowing the lipids to spread and the solvent to evaporate. The DPPC/DPPE mixed solution and MK-1 or MK-1(H_2) were prepared by mixing equimolar amounts of phospholipid and MK analogue in a separate vial before application to the subphase. The resulting monolayer was compressed at a rate of 10 mm min^{-1} (5 mm min^{-1} from two sides) with a Teflon ribbon, and the surface tension was measured using the Wilhemy plate method using a wire probe as the Wilhemy plate. The temperature of the compression isotherm experiments was kept consistent at 25 °C using a circulating water bath. The surface pressure reported is calculated from eq 4, where π is the surface pressure, γ_o is the surface tension of water without lipid (72.8 mN/m[40,41]), and γ is the surface tension of water with lipid present during compression. Each compression isotherm presented herein is an average of three measurements. The data acquired were processed using OriginPro version 9.1 graphing software. The compression modulus was calculated as described in the Supporting Information.

$$\pi = \gamma_o - \gamma \quad (4)$$

Sample Preparation for RM NMR Spectroscopic Studies. A 0.50 M AOT stock solution was prepared by dissolving AOT (5.56 g, 12.5 mmol) in isooctane (25.0 mL). Empty RMs were prepared by mixing a 0.50 M AOT stock solution with a D_2O water pool and then vortexed. MK-1 and MK-1(H_2) RMs were made in a similar manner, the only difference being a 14.3 mM stock solution for MK-1 or MK-1(H_2) was prepared by dissolving MK-1 or MK-1(H_2), respectively, in a 0.50 M AOT/isooctane solution. The RMs were then prepared using the MK-1 or MK-1(H_2) AOT/isooctane stock solution. First, 2.0 mL samples were made using specific amounts of MK-1 or MK-1(H_2) AOT/isooctane stock solution and then diluting the sample to 2.0 mL with the 0.50 M AOT/isooctane solution. From the 2.0 mL solutions, 1.0 mL RM samples were prepared using designated amounts of the 2.0 mL sample and then adding the proper amount of D_2O at pH 6.65 (see General Methods for pH measurements) for MK-1 [the D_2O pH was 6.71 for the MK-1(H_2) samples] to form RMs of the desired size. The samples were then vortexed until the solution was clear. The overall concentrations for the 1.0 mL MK-1 RM samples are as follows: w_0 4, 13.8 mM; w_0 8, 6.5 mM; w_0 12, 3.5 mM; w_0 16, 1.9 mM; and w_0 20, 1.3 mM. The overall concentrations for the 1.0 mL MK-1(H_2) RM samples are as follows: w_0 4, 13.8 mM; w_0 8, 6.4 mM; w_0 12, 3.5 mM; w_0 16, 2.0 mM; and w_0 20, 1.4 mM.

1D ^{1}H NMR Spectroscopic Studies of AOT/Isooctane RMs Containing MK-1 or MK-1(H_2). NMR spectra of MK-1 and MK-1(H_2) in various size RMs, isooctane, and D_2O were obtained using a Varian Inova 400 MHz instrument operating at 22 °C using routine parameters (45° pulse angle and 1 s relaxation delay) and 64 scans. The NMR instrument was locked onto the 10% D_2O signal for the RM samples and locked onto 100% D_2O for the sample in D_2O. The 1D ^{1}H NMR spectra of MK-1 or MK-1(H_2) in isooctane were doped with ~5% d_6-benzene for the NMR instrument to lock onto and to achieve properly shimmed spectra. The spectral data were processed using MestReNova NMR processing software version 10.0.1. The spectra were manually phased, and then the baseline was corrected using a multipoint baseline correction (cubic splines). The spectrum in D_2O was referenced to the internal D_2O peak, and the spectra in isooctane and RMs were referenced to the isooctane methyl peak (0.904 ppm) as previously reported.[39]

Sample Preparation for ^{1}H–^{1}H 2D NOESY and ^{1}H–^{1}H 2D ROESY NMR Spectroscopic Studies in AOT/Isooctane RMs. RM samples of MK-1 and MK-1(H_2) were prepared in the following manner. A 0.50 M AOT stock solution was first prepared by dissolving AOT (5.56 g, 12.5 mmol) in isooctane (25.0 mL). A 1.0 mL stock solution of 112 mM MK-1 in an AOT/isooctane solution was prepared by dissolving 27.7 mg of MK-1 in 1.0 mL of a 0.50 M AOT/isooctane stock solution. To prepare a w_0 12 RM, 894.68 μL of a 112 mM MK-1 AOT/isooctane stock solution and 105.32 μL of D_2O at pH 7.03 were mixed together and then vortexed until the solution was clear. The MK-1(H_2) w_0 12 RM sample was prepared like that of MK-1 using a 112 mM stock solution and D_2O (pH 7.01). This final mixture results in a w_0 12 RM microemulsion with an overall concentration of MK-1 or MK-1(H_2) of ~100 mM (~29 molecules per RM). The NMR samples containing the MK-1 or MK-1(H_2) RM solution were purged with argon briefly and capped prior to data collection.

^{1}H–^{1}H 2D NOESY and ^{1}H–^{1}H 2D ROESY NMR Spectroscopic Studies in a w_0 12 AOT/Isooctane RM.

DOI: 10.1021/acs.biochem.9b00007
Biochemistry 2019, 58, 1596–1615

Scheme 1. (A) Synthetic Scheme for the Allylic Alcohol Coupling Reaction To Form MK-1 3 and (B) Synthetic Scheme for the Radical Alkylation of Menadione 4 and 1-Iodo-3-methylbutane 5 To Form MK-1(H_2) 6[8,37,51–53]

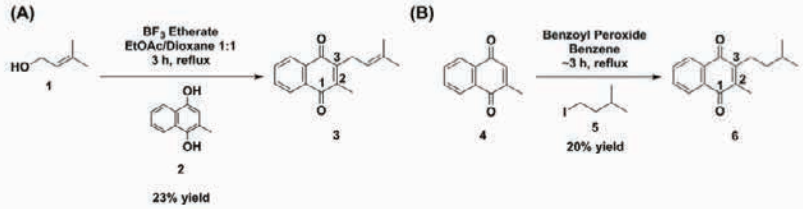

2D NMR spectra of MK-1 and MK-1(H_2) in RMs were obtained using similar conditions and methods described previously[37,42,43] using a 400 MHz Varian MR400 NMR spectrometer operating at 26 °C for MK-1 and were obtained using a 500 MHz Varian Inova 500 spectrometer operating at 25 °C for MK-1(H_2). A standard NOESY pulse sequence was used consisting of 200 or 256 transients with either 16 or 32 scans in the f1 domain using a 200 ms mixing time, a 45° pulse angle, and a 1.5 s relaxation delay. A standard ROESYAD pulse sequence was used consisting of 256 transients with 16 scans in the f1 domain using a 200 ms mixing time, a 45° pulse angle, and a 2.0 s relaxation delay. The NMR instrument was locked onto the 10% D_2O signal. The resulting spectrum was processed using MestReNova NMR software version 10.0.1 (see the Supporting Information for further details). The spectrum was referenced to the isooctane methyl peak at 0.904 ppm on both axes as previously reported.[39] The 3D conformation illustration within an RM interface was constructed using ChemDraw Professional 15.0 and Chem-Bio3D Ultra 12.0 based on spectral parameters described in Results and Discussion.

Dynamic Light Scattering (DLS) Studies. RMs for DLS studies were prepared as described for the NMR spectroscopic studies except that DDI H_2O was used as the water pool instead of D_2O and 0.50 M AOT was diluted with isooctane after the RM had formed to a final AOT concentration of 0.1 M. The hydrodynamic radius of the RMs was determined by DLS measurements performed on a Malvern Zetasizer Nano ZS instrument (Malvern Instruments, Malvern, U.K.). The DLS cuvette (1 cm × 1 cm, glass) was washed three times with isooctane followed by three washes with the RM sample. Then, the cuvette was filled with 1 mL of the RM sample and closed with a Teflon cap. Each experiment was conducted at 25 °C and consisted of a 700 s sample equilibration period followed by 10 measurements consisting of 15 scans each.[42] Each sample was measured in triplicate, and the radius and polydispersity (PDI) were recorded. The data were analyzed using Malvern Zetasizer Software version 7.11 and compared to values reported in the literature.[44] See the Supporting Information for data and interpretation.

■ RESULTS AND DISCUSSION

Synthesis and Characterization of MK-1 Analogues. We have previously synthesized MK-1,[8] and it has been synthesized by other reported routes;[45–49] however, here we present a scaled-up version and NMR spectral characterization in chloroform-*d* (Scheme 1). Menadiol **2** was synthesized as previously described from menadione **4**.[37,50,51] To introduce the isoprenyl side chain, menadiol **2** was treated with 3-methyl-2-buten-1-ol **1** in the presence of the Lewis acid catalyst, boron trifluoride.[37,51] MK-1 **3** was obtained as a red oil in a 23% yield (Scheme 1). Although the route to obtain MK-1(H_2) has been reported in the literature[52] (Scheme 1), the product was not isolated in pure form or characterized by NMR spectroscopy. We modified and optimized the reported route to increase the yield and scaled the reaction up to a preparatory scale using a similar methodology we recently reported.[53] MK-1(H_2) **6** was synthesized by a one-step radical alkylation reaction in which menadione **4** and 1-iodo-3,7-dimethylbutane **5** were coupled using benzoyl peroxide as the radical initiator.[52,53] MK-1(H_2) **6** was obtained as a yellow powder in a 20% yield (Scheme 1). The menadione/benzoyl peroxide solution was added dropwise over ~2 h to the refluxing prenyl iodide solution to keep the stationary menadione **4** concentration sufficiently low in the reaction to ensure good selectivity of alkylation, favoring alkylation at C3 over C2 (Scheme 1).[52,53]

1D ^{1}H NMR Spectroscopic Studies of MK-1 in Organic Solvents. The synthesis of MK-1 and MK-1(H_2) provided material to investigate if the solvent environment induced chemical shift changes. NMR spectra of MK-1 were collected in various organic solvents ranging from aromatic to non-aromatic and of differing polarity (Figure 2). The most drastic chemical shift change observed for MK-1 was in the aromatic solvents, d_6-benzene and d_5-pyridine, compared to the other solvents in Figure 2. This is seen by focusing on the chemical

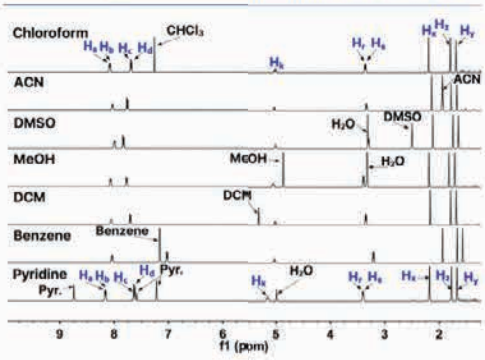

Figure 2. 1D ^{1}H NMR (400 MHz) spectra illustrating chemical shift differences of MK-1 hydrogens between various organic solvent environments. Abbreviations: ACN, d_3-acetonitrile; DMSO, d_6-dimethyl sulfoxide; MeOH, d_4-methanol; DCM, d_2-dichloromethane; Pyr, d_5-pyridine. A structure of MK-1 with a hydrogen labeling scheme key is shown in Figure 3.

DOI: 10.1021/acs.biochem.9b00007
Biochemistry 2019, 58, 1596–1615

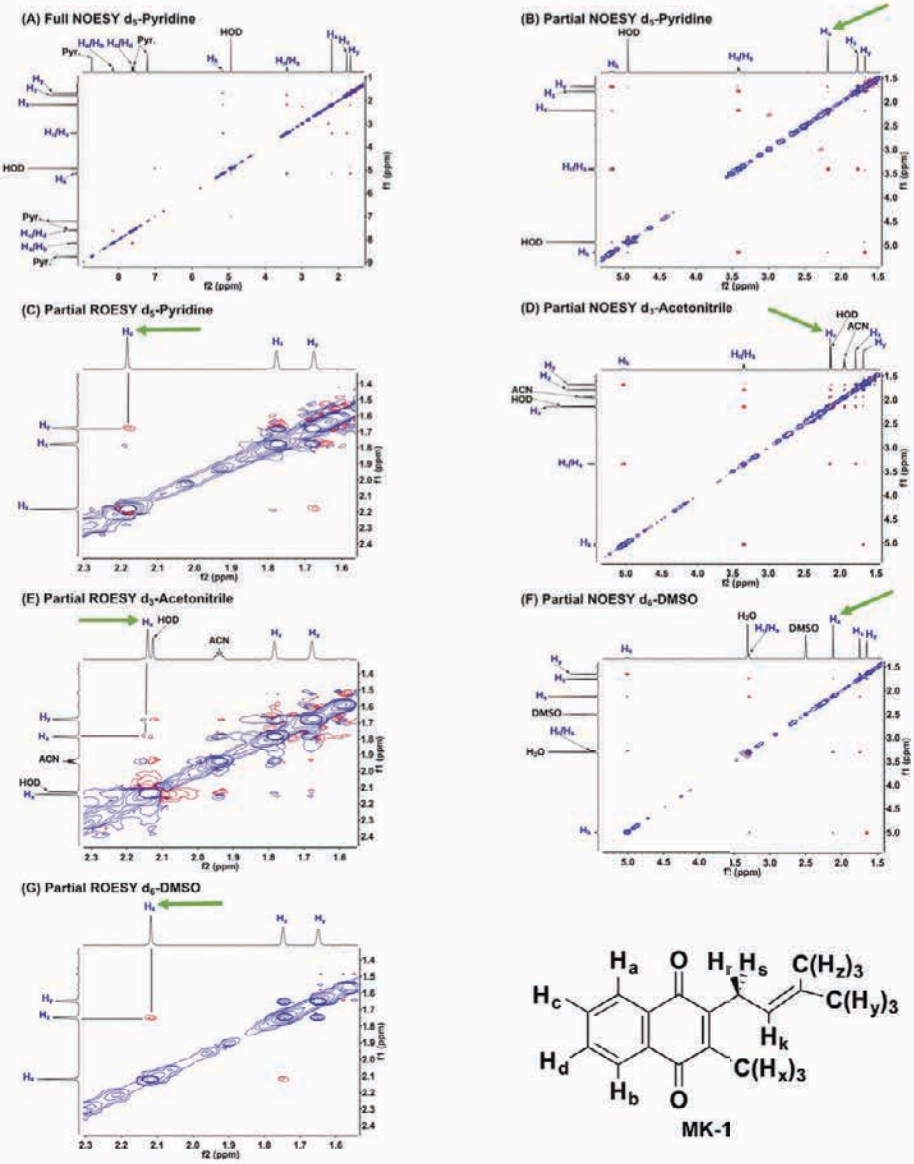

Figure 3. $^1H-^1H$ 2D NOESY and $^1H-^1H$ 2D ROESY NMR (400 MHz) spectra of 20 mM MK-1 in d_5-pyridine, d_3-acetonitrile (d_3-ACN), and d_6-DMSO at 26 °C. (A) Full $^1H-^1H$ 2D NOESY NMR spectrum of MK-1 in d_5-pyridine. (B) Partial $^1H-^1H$ 2D NOESY NMR spectrum of MK-1 in d_5-pyridine. (C) Partial $^1H-^1H$ 2D ROESY NMR spectrum of MK-1 in d_5-pyridine. (D) Partial $^1H-^1H$ 2D NOESY NMR spectrum of MK-1 in d_3-ACN. (E) Partial $^1H-^1H$ 2D ROESY NMR spectrum of MK-1 in d_3-ACN. (F) Partial $^1H-^1H$ 2D NOESY NMR spectrum of MK-1 in d_6-DMSO. (G) Partial $^1H-^1H$ 2D ROESY NMR spectrum of MK-1 in d_6-DMSO. Blue intensity contours represent negative NOEs or ROEs, and red intensity contours represent positive NOEs or ROEs. A standard NOESY pulse sequence consisting of 256 transients with 16 scans in the f1 domain using a 500 ms mixing time and a 1.5 s relaxation delay was used. A standard ROESYAD pulse sequence consisting of 256 transients with 16 scans in the f1 domain using a 400 ms mixing time and a 2.0 s relaxation delay was used. The structure of MK-1 is shown with a hydrogen labeling scheme key. Green arrows indicate hydrogen H_a, where the observed cross peaks differed the most between the three solvents studied.

DOI: 10.1021/acs.biochem.9b00007
Biochemistry 2019, 58, 1596−1615

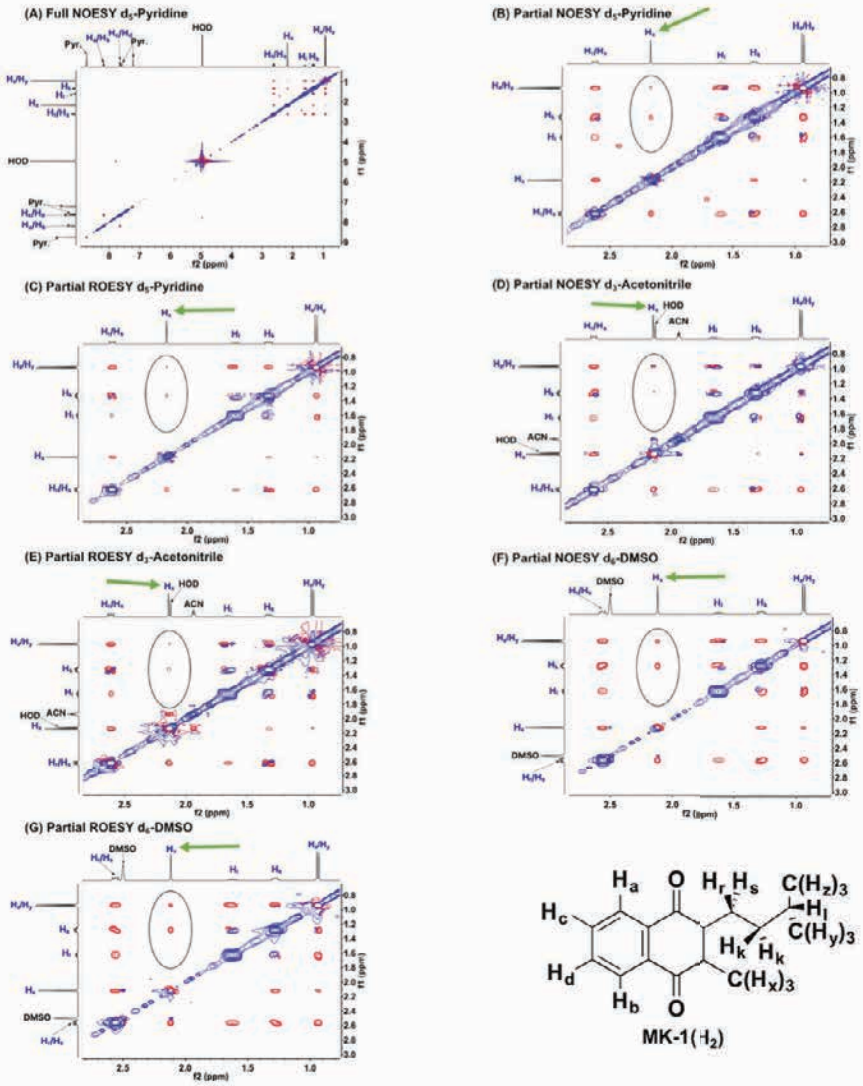

Figure 4. ^{1}H−^{1}H 2D NOESY and ^{1}H−^{1}H 2D ROESY NMR (400 MHz) spectra of 20 mM MK-1(H_2) in d_5-pyridine, d_3-acetonitrile (d_3-ACN), and d_6-DMSO at 26 °C. (A) Full ^{1}H−^{1}H 2D NOESY NMR spectrum of MK-1(H_2) in d_5-pyridine. (B) Partial ^{1}H−^{1}H 2D NOESY NMR spectrum of MK-1(H_2) in d_5-pyridine. (C) Partial ^{1}H−^{1}H 2D ROESY NMR spectrum of MK-1(H_2) in d_5-pyridine. (D) Partial ^{1}H−^{1}H 2D NOESY NMR spectrum of MK-1(H_2) in d_3-ACN. (E) Partial ^{1}H−^{1}H 2D ROESY NMR spectrum of MK-1(H_2) in d_3-ACN. (F) Partial ^{1}H−^{1}H 2D NOESY NMR spectrum of MK-1(H_2) in d_6-DMSO. (G) Partial ^{1}H−^{1}H 2D ROESY NMR spectrum of MK-1(H_2) in d_6-DMSO. Blue intensity contours represent negative NOEs or ROEs, and red intensity contours represent positive NOEs or ROEs. A standard NOESY pulse sequence consisting of 256 transients with 16 scans in the f1 domain using a 500 ms mixing time and a 1.5 s relaxation delay was used. A standard ROESYAD pulse sequence consisting of 256 transients with 16 scans in the f1 domain using a 400 ms mixing time and a 2.0 s relaxation delay was used. The structure of MK-1(H_2) is shown with a hydrogen labeling scheme key. Green arrows indicate hydrogen H_x where the observed cross peaks differed the most between the two solvents studied, and black ovals highlight the region that changes the most between spectra.

shift differences observed between the MK-1 aromatic hydrogens, H_a/H_b and H_c/H_d. The chemical shift difference is nearly 1 ppm in d_6-benzene compared to 0.2−0.4 ppm in the other solvents. The methylene hydrogens, H_r/H_s, and the

DOI: 10.1021/acs.biochem.9b00007
Biochemistry 2019, 58, 1596−1615

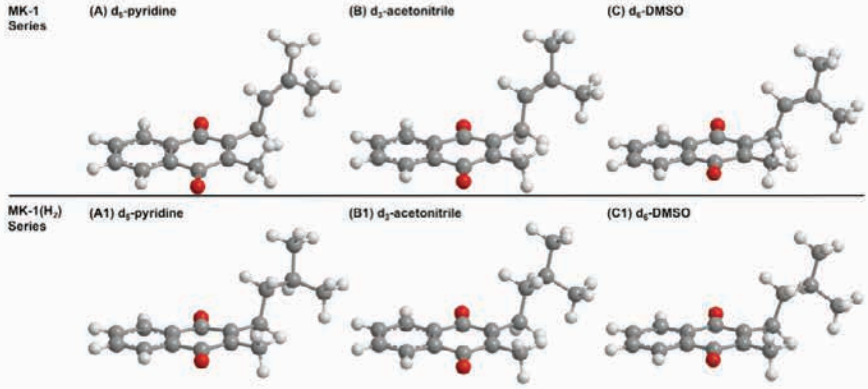

Figure 5. MK-1 and MK-1(H_2) conformations generated using MMFF94 calculations to illustrate the possible conformations consistent with the ^{1}H−^{1}H 2D NOESY and ROESY NMR spectral studies in which conformations agree with observed cross peak interactions and intensities. MK-1 series: (A) proposed MK-1 conformation in d_5-pyridine determined from ^{1}H−^{1}H 2D NOESY and ROESY NMR spectral data for cross peak interactions (51.8 kcal/mol; H_x−H_y 4.3 Å), (B) proposed MK-1 conformation in d_3-ACN determined from ^{1}H−^{1}H 2D NOESY and ROESY NMR spectral data for cross peak interactions (48.6 kcal/mol; H_x−H_y 3.9 Å), and (C) proposed MK-1 conformation in d_6-DMSO determined from ^{1}H−^{1}H 2D NOESY and ROESY NMR spectral data for cross peak interactions (47.3 kcal/mol; H_x−H_y 3.2 Å). MK-1(H_2) series: (A1) proposed MK-1(H_2) conformation in d_5-pyridine determined from ^{1}H−^{1}H 2D NOESY and ROESY NMR spectral data for cross peak interactions (42.1 kcal/mol; H_x−H_y 3.6 Å), (B1) proposed MK-1(H_2) conformation in d_3-ACN determined from ^{1}H−^{1}H 2D NOESY and ROESY NMR spectral data for cross peak interactions (43.0 kcal/mol; H_x−H_y 4.0 Å), and (C1) proposed MK-1(H_2) conformation in d_6-DMSO determined from ^{1}H−^{1}H 2D NOESY and ROESY NMR spectral data for cross peak interactions (41.9 kcal/mol; H_x−H_y 3.4 Å).

naphthoquinone methyl (H_x) also shift in d_6-benzene compared to the other solvents. Via examination of the chemical shift differences in the spectra in Figure 2, it is clear that MK-1 is influenced by solvent environment, but whether MK-1 adopts different conformations in these organic solvent environments remains unclear.

^{1}H−^{1}H 2D NOESY and ^{1}H−^{1}H 2D ROESY NMR Spectroscopic Studies of MK-1 and MK-1(H_2) in d_5-Pyridine, d_3-Acetonitrile, and d_6-DMSO. The 1D ^{1}H NMR experiments demonstrated that the solvent environment impacts the chemical environment surrounding MK-1 enough to change the observed chemical shift. However, whether the conformation of MK-1 and MK-1(H_2) changes depending on the solvent environment remained unclear. Therefore, we used two different complementary 2D NMR spectroscopic techniques (^{1}H−^{1}H 2D NOESY and ^{1}H−^{1}H 2D ROESY NMR) to elucidate the conformation of the MK analogues in organic solutions. We present the 2D NMR data for MK-1 in Figure 3, the 2D NMR data for MK-1(H_2) in Figure 4, and the 3D conformations for MK-1 and MK-1(H_2) in Figure 5. We used a semiquantitative approach for the 2D NMR conformational analysis in which NOE/ROE distance intensities are as follows: a strong cross peak intensity is an ~2−3 Å distance, a medium cross peak intensity is an ~3−4 Å distance, and a weak cross peak intensity is a >4 Å distance.[54] We standardized the signal intensities on the basis of the intensity of the H_x−H_c cross peak of MK-1 or MK-1(H_2), which was used as the internal intensity calibrant (the actual distance is 2.5 Å, which indicates a strong cross peak). Figure 3 shows ^{1}H−^{1}H 2D NOESY and ^{1}H−^{1}H 2D ROESY NMR spectra of MK-1 in d_5-pyridine, d_3-acetonitrile (d_3-ACN), and d_6-DMSO (see Figures S3−S11 and S16−S24 for full 2D NMR spectra and Figure S26 for ROE/NOE correlation traces). These organic solvents were chosen because they differed sufficiently with regard to shape, polarity, and aromatic versus non-aromatic and are well behaved in electrochemical studies.

The conformation of MK-1 in d_5-pyridine was determined by analyzing the ^{1}H−^{1}H 2D NOESY and ROESY NMR spectra (Figure 3A−C and Figures S3 and S4). Figure 3B shows a strong NOE cross peak observed between hydrogens $H_{r/s}$ and H_z and a weak NOE cross peak between $H_{r/s}$ and H_y (see the Supporting Information for hydrogen peak assignments of H_z and H_y). Weak NOE/ROE cross peaks are also observed between H_x and H_y (Figure 3B,C), which supports a folded−extended conformation in which the terminal methyl groups orient themselves in a manner to fold upward (C−C bond rotation allows the methyl groups to rotate upward) positioning H_y close enough to H_x to observe a NOE/ROE cross peak. The weak cross peak (same phase as the diagonal) observed between H_x and H_z is likely due to TOCSY exchange. The weak NOE cross peak in Figure 3B between H_x and H_k has an intensity similar to that of the NOE cross peak observed between H_x and H_y, which is not explained by an extended−flat conformation (see Figure S27E and Table S1 for structure and internuclear distances of the MK-1 flat−extended conformation). Together, these observations provide evidence that MK-1 adopts a folded-extended conformation in d_5-pyridine in which the isoprenyl side chain folds upward.

With regard to the conformation of MK-1 in d_3-ACN, panels D and E of Figure 3 (Figures S6 and S7) show a weak NOE/ROE cross peak observed between H_x and H_z and no cross peak observed between H_x and H_y. The cross peak observed is opposite in phase to the diagonal and possibly due to chemical exchange or TOCSY exchange. TOCSY exchange is more likely as are there are no readily exchangeable hydrogens in the molecule. There is a weak NOE cross peak between H_x and H_k that is visible only in the spectrum upon zooming in on lower floors, which is not consistent with an extended−flat

DOI: 10.1021/acs.biochem.9b00007
Biochemistry 2019, 58, 1596−1615

conformation and is different from that observed in d_5-pyridine, indicating slightly different conformations adopted between solvent environments. However, the cross peak intensity between $H_{r/s}$ and H_z or H_y is similar to that in d_5-pyridine. There is also a NOE/ROE cross peak observed between H_y and HOD and between H_y and the solvent, d_3-ACN, and interactions between MK and the solvent were not observed in the 2D NMR spectra of MK-1 in d_5-pyridine or d_6-DMSO. On the basis of observations described above, MK-1 likely adopts a folded−extended conformation in d_3-ACN that differs slightly from the folded−extended conformation in d_5-pyridine.

Finally, the conformation of MK-1 in d_6-DMSO was determined. Panels F and G of Figure 3 (Figures S9 and S10) show a weak NOE cross peak between H_x and H_k and a medium NOE/ROE cross peak between H_x and H_z and with no NOE/ROE cross peak observed between H_x and H_y. This is similar to the cross peaks observed in d_3-ACN, but the H_x to H_z cross peak is stronger in d_6-DMSO, indicating slightly different conformations. These observations would not be explained by a flat−extended conformation, and MK-1 likely adopts a folded−extended conformation in d_6-DMSO more similar to that in d_3-ACN than in d_5-pyridine.

To investigate whether saturation of the alkene in the isoprenyl side chain influences the conformation of MK-1(H_2), ^{1}H−^{1}H 2D NOESY and ^{1}H−^{1}H 2D ROESY NMR spectra were collected in d_5-pyridine, d_3-ACN, and d_6-DMSO (Figure 4). Similar NOE/ROE cross peaks were observed for MK-1(H_2) in d_5-pyridine and MK-1 in d_5-pyridine (Figure 4A−C and Figures S16 and S17). Specifically, a weak NOE/ROE cross peak between H_x and H_z/H_y, a medium NOE/ROE cross peak between H_x and $H_{r/s}$ and a medium NOE/ROE cross peak between $H_{r/s}$ and H_y were observed. There is also no NOE/ROE cross peak observed between H_x and H_y, which further supports a folded−extended conformation. This is suggestive of a similar conformation for MK-1(H_2) and MK-1 in d_5-pyridine, where both adopt a similar folded−extended conformation. Similar NOE/ROE cross peaks were observed for MK-1(H_2) in d_3-ACN and MK-1 in d_3-ACN (Figure 4D,E and Figures S19 and S20). Specifically, the lack of an observable cross peak between H_x and H_z/H_y (compared to a weak NOE/ROE cross peak in the case of MK-1), a medium NOE/ROE cross peak between H_x and $H_{r/s}$, a medium NOE/ROE cross peak between $H_{r/s}$ and H_y, and a very weak NOE/ROE cross peak between H_x and H_k was observed. There is also no NOE/ROE cross peak observed between H_x and H_l. This is suggestive of a similar conformation for MK-1(H_2) and MK-1 in d_3-ACN, where both adopt a similar folded−extended conformation. Comparable NOE/ROE cross peaks were observed for MK-1(H_2) in d_6-DMSO and MK-1 in d_6-DMSO (Figure 4F,G and Figures S22 and S23). For instance, a medium NOE/ROE cross peak between H_x and H_z/H_y, a medium NOE/ROE cross peak between H_x and $H_{r/s}$, a medium NOE/ROE cross peak between $H_{r/s}$ and H_y/H_z, and a medium NOE/ROE cross peak between H_x and H_k were observed. There was also no NOE/ROE cross peak observed between H_x and H_l. This is suggestive of a comparable conformation for MK-1(H_2) and MK-1 in d_6-DMSO, where both adopt a similar folded−extended conformation.

Considering the similar trends in cross peaks and intensities observed for MK-1 and MK-1(H_2) in d_5-pyridine, d_3-ACN, and d_6-DMSO, it appears that saturation does not affect the conformation significantly. The subtle differences observed for MK-1 and MK-1(H_2) in the different organic solvents suggest that slightly different folded−extended conformations are adopted between each of the organic solvents, but MK-1 and MK-1(H_2) have very similar conformations in each solvent. This suggests that there could be a correlation between a preferred conformation in each solvent environment and that a simple change such as saturation of a double bond only slightly influences this preferred conformation. Overall, these truncated MK analogues appear to adopt folded−extended conformations in organic solutions based on the 2D NMR data and the folded−extended conformations differ slightly between solvent environments. However, it is possible that an equilibrium population exists between multiple conformations (e.g., folded and/or nonfolded conformations). The observations from the 2D NMR spectroscopic studies support our first hypothesis that the most fundamental MK-1 analogues adopt folded conformations regardless of the degree of saturation in their isoprenyl side chain.

Illustrating MK-1 and MK-1(H_2) Conformations Using Molecular Mechanics. To clearly show illustrations of MK-1 and MK-1(H_2), conformations were generated on the basis of our interpretation of observed cross peak intensities in the ^{1}H−^{1}H 2D NOESY and ROESY NMR spectral data using a semiquantitative approach. We used molecular mechanics (MM) calculations to illustrate and model these conformations. This allowed us to explore the energy surface of conformations corresponding to MK-1 or MK-1(H_2) in either d_5-pyridine, d_3-ACN, or d_6-DMSO determined from the spectral data and provided a means for a visual comparison between conformations (Figure 5). Specific conformations were generated by constraining internuclear distances consistent with the observed 2D NMR spectral data and then energy optimized to calculate an energy value as well as produce realistic bond lengths and angles.

One of the low-energy conformations generated for MK-1 (Figure 5A; 51.8 kcal/mol; H_x−H_y, 4.3 Å) is consistent with the 2D NOESY/ROESY spectral parameters in d_5-pyridine. A lower-energy conformation for MK-1 (Figure 5B; 48.6 kcal/mol; H_x−H_z, 3.9 Å) is consistent with the 2D NOESY/ROESY spectral parameters in d_3-ACN. A slightly lower-energy conformation for MK-1 (Figure 5C; 47.3 kcal/mol; H_x−H_y, 3.2 Å) is consistent with the 2D NOESY/ROESY spectral parameters in d_6-DMSO. One of the low-energy conformations generated for MK-1(H_2) (Figure 5A1; 42.1 kcal/mol; H_x−H_y, 3.6 Å) is consistent with the NOESY/ROESY spectral parameters in d_5-pyridine. A conformation with a slightly higher energy for MK-1(H_2) (Figure 5B1; 43.0 kcal/mol; H_x−H_z, 4.0 Å) is consistent with the 2D NOESY/ROESY spectral parameters in d_3-ACN. A lower-energy conformation for MK-1(H_2) (Figure 5C1; 41.9 kcal/mol; H_x−H_y, 3.4 Å) is consistent with the 2D NOESY/ROESY spectral parameters in d_6-DMSO. All six of these conformations exhibit folding of the isoprenyl side chain upward out of the quinone plane (Figure 5) and can be described as folded−extended conformations. Each conformation for MK-1(H_2) is very similar to that of MK-1 in each organic solvent environment examined based on 2D NMR studies.

For comparison, conformations seen in panels D and D1 of Figure S27 are the lowest-energy conformations we found for MK-1 or MK-1(H_2), where an extended−flat conformation was subjected to a MM simulation using 10000 iterations followed by an energy minimization, which illustrates that folded conformations are easily reached and energetically

DOI: 10.1021/acs.biochem.9b00007
Biochemistry 2019, 58, 1596−1615

Scheme 2. Illustration of the One-Electron Reduction of the Quinone (Q) of MK-1 to the Semiquinone Radical Anion ($Q^{\bullet-}$) and the Second One-Electron Reduction to the Dianion (Q^{2-})

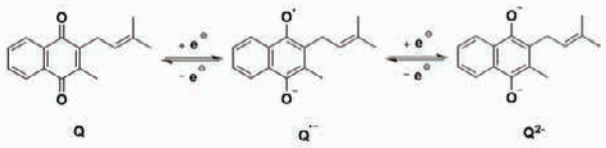

favorable. In addition to the folded conformations shown in Figure 5, a series of alternative flat conformations for MK-1 and MK-1(H_2) (panels E, E1, F, and F1 of Figure S27) were also generated on the basis of what is commonly seen in life science textbooks and literature and then subjected to energy optimization.[12,55,56] These flat−extended conformations are ~11−20 kcal/mol higher than the lowest-energy conformations of MK-1 and MK-1(H_2). A table of selected internuclear distances for conformations seen in Figure 5 and Figure S27 is given in the Supporting Information.

Importantly, the folded−extended conformations for MK-1 determined in an organic solution closely resemble the folded conformation of the first isoprene unit of MK-2 (containing two isoprene units), which we determined previously in the same organic solvent environments.[37]

Reactivity of MK-1 and MK-1(H_2) in Different Organic Solvents: Electrochemistry. To determine the effect of saturation of the MK isoprenyl side chain on the quinone redox potential, we used cyclic voltammetry to measure the redox potentials of MK-1 and MK-1(H_2). Both MK-1 and MK-1(H_2) have two reversible single-electron redox processes; the first is the quinone to semiquinone ($Q/Q^{\bullet-}$) process, and the second the semiquinone to dianion ($Q^{\bullet-}/Q^{2-}$) process (Scheme 2). The half-wave potentials for each redox process $Q/Q^{\bullet-}$ and $Q^{\bullet-}/Q^{2-}$ in each solvent for MK-1 and MK-1(H_2) are listed in Table S9, and cyclic voltammograms are shown in Figure 6. The electrolyte tetrabutylammonium perchlorate (TBAP) was chosen because of its excellent solubility in all organic solvents. Furthermore, the addition of TBAP to MK-1 solutions in each solvent did not affect the observed chemical shifts of the MK-1 hydrogens, and thus, no evidence of ion pairing or association was found (see Figure S28). The water content of the solvents can affect the semiquinone $Q^{\bullet-}/Q^{2-}$ process as acidic hydrogens influence hydroquinone production, which results in potentials that approach the quinone $Q/Q^{\bullet-}$ half-wave potentials, and therefore, we compared only the first redox process, $Q/Q^{\bullet-}$, in our analyses.[57,58] Thus, it was important that we carried out our electrochemical experiments in anhydrous aprotic organic solvents as this issue is then avoided and organic solvents more closely resemble the native MK environment within a cellular membrane compared to aqueous solutions.

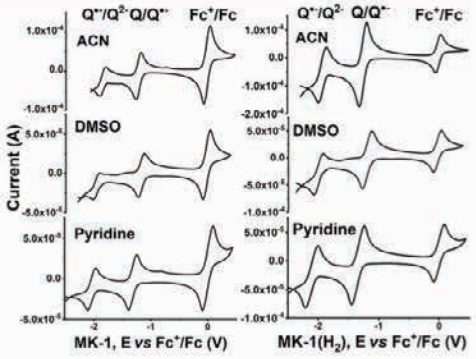

Figure 6. Six cyclic voltammograms of 2 mM MK-1 and MK-1(H_2) in ACN, DMSO, and pyridine. The potentials are referenced to the Fc^+/Fc couple internal standard (2 mM) determined in each solvent. From left to right, redox processes are $Q^{\bullet-}/Q^{2-}$, $Q/Q^{\bullet-}$, and Fc^+/Fc, respectively. Each sample has 0.1 M TBAP and was degassed with argon gas for 10 min at ambient temperature before spectra were recorded. Current sweeps are in the anodic direction from −2 to 1 V and back to −2 V vs Ag/AgCl. A 100 mV/s scan rate was used.

As shown in Figure 6, the ferrocene couple, Fc^+/Fc, was used as an internal reference standard so that the half-wave potentials are set to 0 V versus Fc^+/Fc. The values of $Q/Q^{\bullet-}$ $E_{1/2}$ versus Fc^+/Fc for MK-1 in ACN, DMSO, and pyridine were measured to be −1.227 ± 0.002, −1.158 ± 0.002, and −1.319 ± 0.001 V, respectively. The values of $Q/Q^{\bullet-}$ $E_{1/2}$ versus Fc^+/Fc for MK-1(H_2) in ACN, DMSO, and pyridine were measured to be −1.247 ± 0.007, −1.179 ± 0.002, and −1.343 ± 0.001 V, respectively. The values of $Q/Q^{\bullet-}$ $E_{1/2}$ versus Fc^+/Fc are near those reported for 1,4-naphthoquinone and those previously reported by our group for MK-2.[37,59,60] The values $Q^{\bullet-}/Q^{2-}$ $E_{1/2}$ versus Fc^+/Fc for MK-1 in ACN, DMSO, and pyridine were measured to be −1.882 ± 0.014, −1.949 ± 0.006, and −2.037 ± 0.005 V, respectively. The values of $Q^{\bullet-}/Q^{2-}$ $E_{1/2}$ versus Fc^+/Fc for MK-1(H_2) in ACN, DMSO, and pyridine were measured to be −1.912 ± 0.009, −1.9947 ± 0.0008, and −2.109 ± 0.005 V, respectively. The measured quinone half-wave redox potential differences in these solvents are statistically significant as they are distinctly different from each other at high confidence intervals (see Figure 7 caption and the Supporting Information).

The difference in millivolts between the unsaturated MK-1 and the saturated MK-1(H_2) quinone redox potential in each solvent of the less variable $Q/Q^{\bullet-}$ process is of the same magnitude as ~20 mV with specific values of 20.033 ± 0.007, 21.333 ± 0.002, and 23.917 ± 0.001 mV for ACN, DMSO, and pyridine, respectively (Figure 7). The $Q/Q^{\bullet-}$ process potentials are less variable as the presence of acidic hydrogens and/or water can create the hydroquinone species, which results in the $Q^{\bullet-}/Q^{2-}$ process coalescing onto the first redox potential. Our previous work with MK-2 demonstrated that the isoprenyl side chain folds over toward the naphthoquinone moiety and that the solvent environment can influence the preferred conformation.[37] The mixing of molecular orbitals (MOs) on the naphthoquinone moiety with the isoprenyl side chain may potentially result in different energies of the electrochemical band gap (or HOMO to LUMO gap) needed

DOI: 10.1021/acs.biochem.9b00007
Biochemistry 2019, 58, 1596−1615

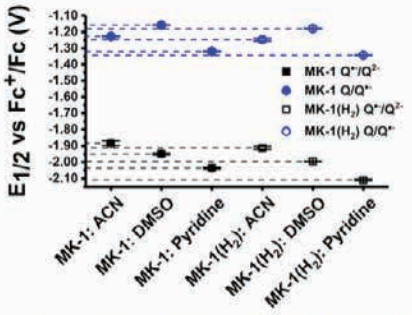

Figure 7. Measured $E_{1/2}$ (vs Fc^+/Fc in volts) of MK-1 and MK-1(H_2) $Q/Q^{\bullet-}$ and $Q^{\bullet-}/Q^{2-}$ redox process vs solvent. Each solvent was run in triplicate, with error bars shown. Added horizontal lines show the distinction between each solvent for each redox process. All solvent comparisons (ACN vs DMSO, etc.) for each redox process half-wave potential for MK-1 or MK-1(H_2) are statistically different with Student's *t* test confidence intervals of 99.9% ($p < 0.0001$), except for that of the ACN vs DMSO $Q/Q^{\bullet-}$ of MK-1, which was 99.5% ($p < 0.0016$) (four degrees of freedom). Comparisons between MK-1 and MK-1(H_2) half-wave potentials of $Q/Q^{\bullet-}$ and $Q^{\bullet-}/Q^{2-}$ for each solvent were at the 99.9% ($p < 0.0001$) confidence level, except for those of ACN, which were 98% ($p < 0.0089$) and 95% ($p < 0.0355$), respectively (four degrees of freedom). See the Supporting Information for data.

to reduce the quinone carbonyl oxygen to an anionic oxygen radical. The electrochemical band gap is suggestive of the potential observed or the energy required to reduce or oxidize an electrochemical process. This difference in the band gap energy results in unique half-wave potentials as the energy (E) and potential difference (V) are directly proportional as shown clearly by the electrostatic equation $E = VQ$, where Q is charge. The saturation or unsaturation of the isoprenyl side chain can therefore potentially influence these MOs and may alter the quinone redox potential in this manner. The semiquinone redox potential difference of ~20 mV between MK-1 and MK-1(H_2) could indicate the band gap energy difference between the saturated and unsaturated double bond in the one-unit isoprenyl side chain. However, the difference of ~20 mV is most likely due to an indirect effect manifested by a through-bond electronic change by the isoprenyl substituent on the quinone. An indirect substituent effect was used to explain a redox potential change for an N-aromatic substituent on a quinone.[1] The conformational differences in MK-1 between solvents were small, and the short isoprenyl side chain has limited spatial reach toward the naphthoquinone. If such an effect existed between conformation and redox potential, it may not be evident in the one-isoprene unit system. However, suitable high-level computational calculations should be carried out to characterize the HOMO–LUMO gap of this system and determine the exact contributions to the observed ~20 mV difference.

We also observed a trend in the data of the potential difference for the $Q/Q^{\bullet-}$ process as compared by solvent versus degree of saturation (Table S10). For MK-1 and MK-1(H_2), the potential differences in the $Q/Q^{\bullet-}$ process between ACN and DMSO are 69.250 ± 0.003 and 67.950 ± 0.008 mV, respectively. The other solvent comparisons also yield values that agree with each other. For MK-1 and MK-1(H_2), the potential differences in the $Q/Q^{\bullet-}$ process between DMSO and pyridine are 161.050 ± 0.002 and 163.633 ± 0.002 mV, respectively. Similarly, the potential differences of MK-1 and MK-1(H_2) of the $Q/Q^{\bullet-}$ process between ACN and pyridine are 91.800 ± 0.003 and 95.683 ± 0.008 mV, respectively. This conserved difference in the $Q/Q^{\bullet-}$ half-wave potentials between MK-1 and MK-1(H_2) in each solvent may signify that how the isoprenyl side chain folds is truly solvent-dependent and/or may suggest that the conformation of the short isoprenyl side chain (five carbons) of MK-1 has little effect on the observed quinone redox potential in the one-isoprene unit system.

In summary, both MK-1 and MK-1(H_2) during the first electrochemical process producing the semiquinone have the most positive potentials in DMSO and the most negative potentials in pyridine, demonstrating MK-1 or MK-1(H_2) is slightly more reducible in DMSO than in ACN or pyridine. Most remarkably, the observation of an ~20 mV change in quinone $Q/Q^{\bullet-}$ $E_{1/2}$ between MK-1 and MK-1(H_2) supports our second hypothesis that saturation of the isoprenyl side chain of MK-1 affects the observed quinone redox potential. This is the first time that these subtle changes have been demonstrated in a quinone/MK system. The difference is presumably mainly due to a through-bond indirect effect, which results in an electronic perturbation of the quinone system upon saturation of the isoprenyl side chain. There was not a large difference between the MK-1 analogue conformations, and therefore, changes in the observed redox potentials are not likely due to conformational differences. However, a potential correlation should be investigated using the appropriate fully unsaturated and partially saturated MK-2 analogues in combination with computational methods to determine if conformational folding of the second isoprene unit can alter the quinone redox potential in MK analogues with an unsaturated versus a partially saturated isoprenyl side chain.

Interaction of Langmuir Phospholipid Monolayers with MK-1 and MK-1(H_2). To understand the interaction and conformation of fundamental MK analogues within a membrane environment, we focused on characterizing the interaction of the most simple, truncated MK analogues, MK-1 and MK-1(H_2), with model membrane interfaces. Model membrane systems, such as Langmuir phospholipid monolayers, liposomes, micelles, and RM microemulsions, have been used to characterize the interaction and location of probe molecules with membranelike interfaces (Figure 8).[44,61−69] Langmuir phospholipid monolayers and RMs are two complementary model membrane systems that together can be used to characterize the interaction, location, placement, and conformation of MKs within a model membrane interface. Using these two model membrane systems together allowed us to determine whether MK-1 analogues interact with model membrane interfaces and if a folded conformation is adopted within the RM model membrane interface.

Surface-pressure compression isotherm experiments using Langmuir monolayers (Figure 8A) have been useful in characterizing interactions among lipids, lipids and fatty acids,[37,40,70−72] and lipids and hydrophilic molecules.[42,61,70] During a surface-pressure compression isotherm experiment, condensing and expanding effects caused by the presence of another lipid (such as MK) can be observed and changes in phase transitions of the lipids can indicate an interaction between the two lipids. To establish that the two MK

DOI: 10.1021/acs.biochem.9b00007
Biochemistry 2019, 58, 1596−1615

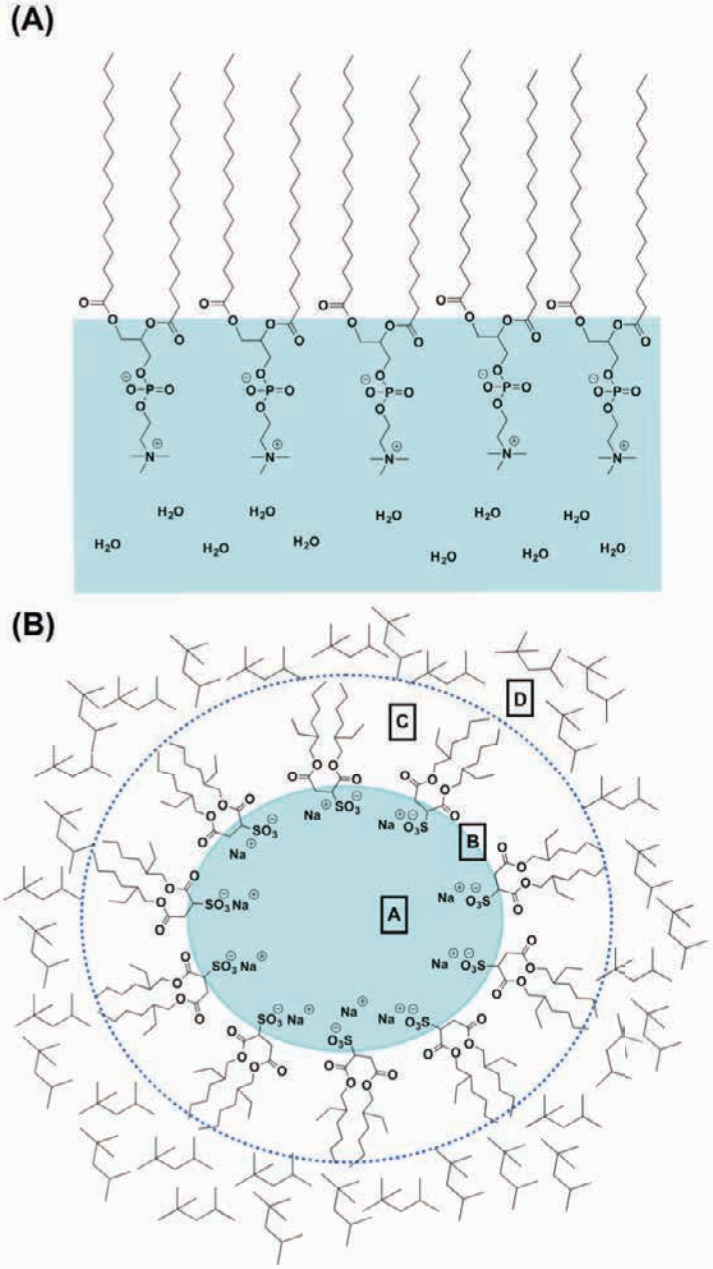

Figure 8. Schematic diagram of (A) a Langmuir phospholipid monolayer (top) and (B) a reverse micelle (bottom) present in a microemulsion with the following labeling: (A) water pool, (B) Stern layer, (C) hydrophobic surfactant tails, and (D) organic solvent isooctane. Adapted with permission from ref 37. Copyright 2018 American Chemical Society.

DOI: 10.1021/acs.biochem.9b00007
Biochemistry 2019, 58, 1596−1615

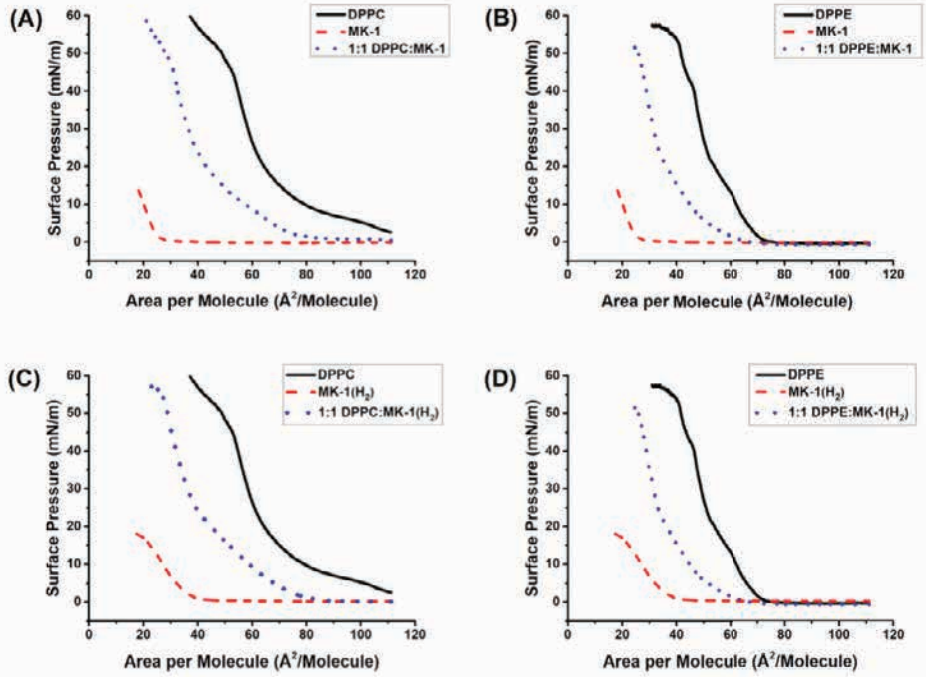

Figure 9. Compression isotherms of MK-1 and MK-1(H_2) films (dashed red lines), DPPC or DPPE phospholipid monolayers (solid black lines), or a 50:50 mixture of MK-1 or MK-1(H_2) and a phospholipid (dotted blue lines): (A) compression isotherms of MK-1 and DPPC, (B) compression isotherms of MK-1 and DPPE, (C) compression isotherms of MK-1(H_2) and DPPC, and (D) compression isotherms of MK-1(H_2) and DPPE.

analogues interact with membrane interfaces, compression isotherms of Langmuir monolayers were used to characterize the interactions of MK-1 and MK-1(H_2) with phospholipid interfaces of common phospholipids found in biological systems such as dipalmitoylphosphatidylcholine (DPPC) or dipalmitoylphosphatidylethanolamine (DPPE).[73−75] Therefore, surface-pressure compression isotherms of Langmuir monolayers consisting of DPPC, DPPE, MK-1, MK-1(H_2), or a mixture of a phospholipid and an MK analogue were performed to determine if the MK analogues had any effect on the packing and compressibility of the phospholipids. The resulting compression isotherms are shown in Figure 9. The control monolayers of DPPC and DPPE are comparable to what has been found in the literature.[40,76] The DPPC monolayers both show a characteristic gas−liquid phase transition at 5 mN/m and collapse at 55 mN/m. The DPPE monolayers also collapsed at 55 mN/m, which aligns well with results in the literature.[40,76]

The MK-1 and MK-1(H_2) pure films were compressed in the same manner as the phospholipid films. Both MK-1 and MK-1(H_2) monolayers did not reach a pressure above 20 mN/m similar to findings reported for ubiquinone-10 (UQ-10) and plastoquinone.[40,71,77] The films were not able to reach a high pressure like other lipoquinones, suggesting that the MK films either slightly soluble in the subphase (similar to UQ-2[40]) as the pressure was increased or aggregation was occurring, which has been shown for lipoquinones with longer isoprenyl side chains.[40,71] Most likely, the MK-1 analogues are aggregating as neither analogue was soluble in D_2O (see 1D ^1H NMR RM Spectroscopic Studies).

When the MKs are mixed with DPPC or DPPE phospholipids, differences in phase transitions and compression moduli indicate that an interaction with the MK analogues and phospholipids can be observed. First, the gas to liquid phase transition for DPPC is nonexistent when either MK-1 or MK-1(H_2) is present. This suggests a condensing effect at low pressures. Within all the compression isotherms of the mixed monolayers, a change in slope occurs at ~20 mN/m [similar to the collapse pressure of MK-1 and MK-1(H_2)], which follows the pattern in the literature with the MK analogues being compressed out of the monolayer to the top of the monolayer similar to UQ.[40,71] To determine if the MK-1 analogues still affected the phospholipid monolayers even at higher surface pressures, the compression moduli of each curve are compared in Figure S29 (see the Supporting Information for compression moduli data and interpretation). In each case, the mixed monolayer exhibited a decrease in its compression modulus (easier to compress) than the pure phospholipid monolayers, indicating that the MK analogues affect the phospholipid monolayer throughout compression even at physiologically relevant surface pressures (~30−35 mN/m).[41]

Overall, the MK analogues do not form stable monolayers at high pressures (>20 mM/m) and have a compressing effect on the phospholipid monolayers, and at higher pressures, the MK

DOI: 10.1021/acs.biochem.9b00007
Biochemistry 2019, 58, 1596−1615

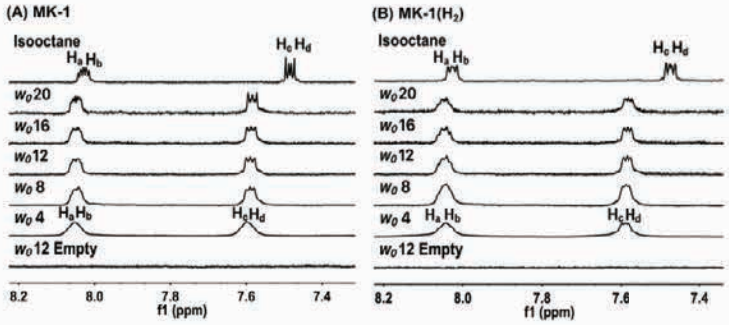

Figure 10. 1D ^{1}H NMR (400 MHz) spectra of (A) MK-1 and (B) MK-1(H_2) aromatic hydrogens H_a, H_b, H_c, and H_d in different sized RMs (w_0 4, 8, 12, 16, and 20) prepared from a 0.50 M AOT/isooctane stock solution. MK-1 or MK-1(H_2) in isooctane is used as a comparison reference spectrum, and w_0 12 Empty is a control spectrum without MK-1 or MK-1(H_2). Peaks are labeled with corresponding hydrogens for MK-1 and MK-1(H_2) (see Figures 3 and 4 for the hydrogen labeling scheme key). Hydrogens, H_a, H_b, H_c, and H_d, undergo a shift upon insertion into the RMs for both MKs. The overall concentrations for the 1.0 mL MK-1 RM samples are as follows: w_0 4, 13.8 mM; w_0 8, 6.5 mM; w_0 12, 3.5 mM; w_0 16, 1.9 mM; w_0 20, 1.3 mM. The overall concentrations for the 1.0 mL MK-1(H_2) RM samples are as follows: w_0 4, 13.8 mM; w_0 8, 6.4 mM; w_0 12, 3.5 mM; w_0 16, 2.0 mM; w_0 20, 1.4 mM.

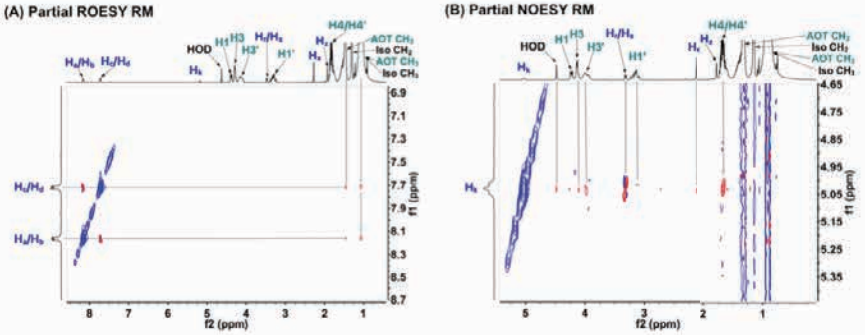

Figure 11. Partial ^{1}H−^{1}H 2D ROESY and ^{1}H−^{1}H 2D NOESY NMR (400 MHz) spectra of MK-1 in a w_0 12 RM. (A) Partial ROESY spectrum illustrating interactions of MK-1 aromatic hydrogens with AOT. (B) Partial NOESY spectrum illustrating interactions of MK-1 H_a hydrogens with AOT. Blue to blue hydrogen text labeling shows MK-1−MK-1 interactions, and blue to teal hydrogen text labeling shows MK-1−AOT interactions. Blue intensity contours represent negative NOEs or ROEs, and red intensity contours represent positive NOEs or ROEs. See Figure 3 for the MK-1 hydrogen labeling scheme key and Figure 13 for the AOT hydrogen labeling scheme key. A standard NOESY pulse sequence consisting of 256 transients with 16 scans in the f1 domain using a 200 ms mixing time and a 1.5 s relaxation delay was used. A standard ROESYAD pulse sequence consisting of 256 transients with 16 scans in the f1 domain using a 200 ms mixing time and a 2.0 s relaxation delay was used.

analogues most likely are compressed out of the monolayer onto the phospholipid tails similar to previously reported lipoquinones with longer isoprenyl side chains.[37,40,71,77] It is important to note that the Langmuir phospholipid monolayers do not provide evidence of a folded MK conformation due to the nature of the experiment; however, they do demonstrate that MK-1 and MK-1(H_2) interact with the phospholipid model membrane interface even at physiological surface pressures like other quinones, and there was not a large difference observed between the unsaturated and saturated MK-1 analogue.[37,40,71,77]

1D ^{1}H NMR Spectroscopic Studies of MK-1 and MK-1(H_2) in RMs. The studies carried out using Langmuir phospholipid monolayers established that the two MKs interacted with the phospholipid interface. However, the placement, orientation, and conformation of the MK-1 analogues within an interface were still uncertain. Therefore, to fully characterize the location, orientation, and conformation of the MKs within a model membrane interface, we used RMs (Figure 8B), which are ternary microemulsion systems in which the surfactant is dissolved in an organic solvent and the addition of water creates nanosized water droplets encased in the surfactant.[44,64−66,78,79] MK-1 or MK-1(H_2) was placed in RMs of various sizes (w_0 4, 8, 12, 16, and 20; where w_0 = [H_2O]/[AOT]), and then 1D ^{1}H NMR spectra were obtained for each RM size as well as a spectrum in isooctane (2,2,4-trimethylpentane) (Figure 10).

The chemical shift difference between MK-1 aromatic hydrogens, H_a/H_b and H_c/H_d, is greater with a value of 0.55 ppm in isooctane versus that of MK-1 in w_0 20 = 0.47 ppm or w_0 4 = 0.45 ppm RMs, which is diagnostic of a change in the environment surrounding MK-1 (Figure 10). Similarly, the chemical shift difference between MK-1(H_2) aromatic hydrogens, H_a/H_b and H_c/H_d, is greater with a value of 0.56 ppm in

DOI: 10.1021/acs.biochem.9b00007
Biochemistry 2019, 58, 1596−1615

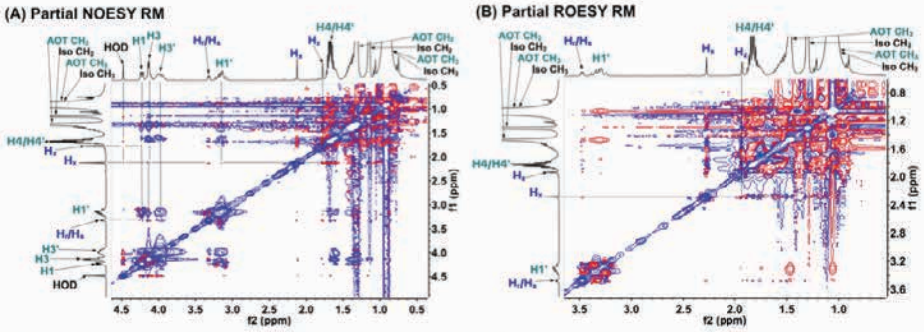

Figure 12. Partial ^{1}H−^{1}H 2D NOESY and ^{1}H−^{1}H 2D ROESY NMR (400 MHz) spectra of MK-1 in a w_0 12 RM. (A) Partial ^{1}H-^{1}H 2D NOESY NMR spectrum in a w_0 12 RM. (B) Partial ^{1}H-^{1}H 2D ROESY NMR spectrum in a w_0 12 RM. Blue to blue hydrogen text labeling shows MK-1−MK-1 interactions, and blue to teal hydrogen text labeling shows MK-1−AOT interactions. Blue intensity contours represent negative NOEs or ROEs, and red intensity contours represent positive NOEs or ROEs. See Figure 3 for the MK-1 hydrogen labeling scheme key and Figure 13 for the AOT hydrogen labeling scheme key. A standard NOESY pulse sequence consisting of 256 transients with 16 scans in the f1 domain using a 200 ms mixing time and a 1.5 s relaxation delay was used. A standard ROESYAD pulse sequence consisting of 256 transients with 16 scans in the f1 domain using a 200 ms mixing time and a 2.0 s relaxation delay was used.

isooctane versus that of MK-1(H_2) in w_0 20 = 0.47 ppm or w_0 4 = 0.45 ppm RMs (Figure 10). The loss of splitting (peak broadening) observed for the aromatic hydrogens as the RM size decreases is attributed to the poorer ability of MK-1 or MK-1(H_2) to tumble freely within the RM interface of smaller sized RMs (e.g., w_0 4). We were unable to obtain a spectrum in D_2O as neither MK was soluble even after extended sonication due to the hydrophobicity of the two MK analogues and it is not likely that either of the MKs are in the water pool due to the very poor water solubility of each compound. Together, the results demonstrated that there was a significant chemical shift difference between the aromatic hydrogens in isooctane and the RMs for both MK-1 analogues. Therefore, we can conclude that neither of the MK-1 analogues are interacting with the isooctane and are residing either at the RM interface or within the AOT alkyl tail region. Furthermore, DLS experiments were carried out and demonstrated that inserting MK-1 or MK-1(H_2) into the RM does not alter the size of the RM or destroy the RMs once inside and the RMs are stable over the course of NMR experiments (see Table S12). Overall, we concluded that MK-1 and MK-1(H_2) interacted with RMs and resided within the RM model membrane interface.

^{1}H−^{1}H 2D NOESY and ^{1}H−^{1}H 2D ROESY NMR Spectroscopic Studies of MK-1 and MK-1(H_2) in a RM Model Membrane System. The 1D ^{1}H NMR spectra of MK-1 and MK-1(H_2) in RMs demonstrated that MK-1 analogues reside within the interface of RMs. However, more information was needed to determine the orientation, position, and conformation while the MK-1 species is residing inside the RM interface. MK-1 was placed inside a w_0 12 RM, and ^{1}H−^{1}H 2D NOESY and ^{1}H−^{1}H 2D ROESY NMR spectra were obtained (Figures 11 and 12 and Figures S12 and S13). NOE/ROE cross peaks between MK-1 and AOT provide evidence for the location, orientation, and conformation within the RM interface. Figure 11A shows ROE cross peaks among all four aromatic hydrogens of MK-1 and the CH_2/CH_3 groups of the AOT alkyl tails. Figure 11B shows cross peaks between MK-1's alkene hydrogen H_k and HOD, H1, H3/H3′, and H4/H4′. Figure 12A also shows cross peaks between hydrogens H_t/H_s and H1, H3, and H3′, which together indicate that MK-1 is located within the RM interface. Panels A and B of Figure 12 show NOE/ROE cross peaks between H_t/H_s and H_y, between H_x and H_y, and between H_x and H1 and H3 and the lack of a cross peak between H_x and H_k, which supports a folded conformation for MK-1 while it is residing in the interface (see Figure S26 for ROE/NOE correlation traces). On the basis of these observations, MK-1 is oriented in a manner in which the naphthoquinone is positioned toward the AOT alkyl tails and the folded isoprenyl side chain is positioned between hydrogens H1/H1′ and H3/H3′ as illustrated in Figure 13. A proposed folded MK-1 conformation that is consistent with the 2D NOESY and ROESY spectral data is illustrated in Figure 14. The phase of the MK-1 to MK-1 cross peaks observed in the NOESY spectrum (Figures 11 and 12) within the RM interface is the opposite phase of the diagonal, indicating MK-1 is behaving as a small molecule within the RM interface and likely tumbling freely but

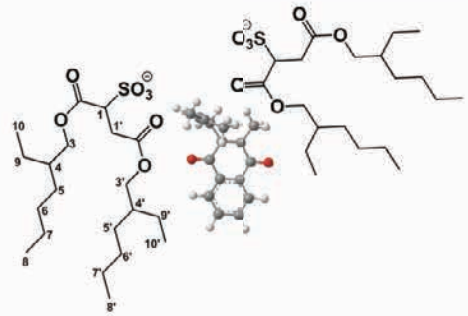

Figure 13. Illustration of the placement and proposed conformation of MK-1 penetrating the RM interface. This arrangement is consistent with the ^{1}H−^{1}H 2D NOESY and ^{1}H−^{1}H 2D ROESY NMR spectral data obtained in a w_0 12 RM. However, MK-1 likely tumbles freely within the interface but maintains interactions with the region of AOT shown in the illustration. The AOT hydrogen labeling scheme key is shown.

DOI: 10.1021/acs.biochem.9b00007
Biochemistry 2019, 58, 1596−1615

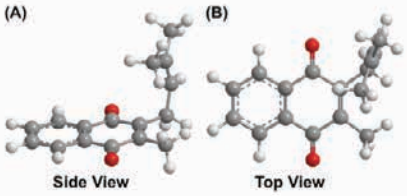

Figure 14. Proposed conformation of MK-1 at an RM interface illustrated using MMFF94 calculations that is consistent with ^{1}H−^{1}H 2D NOESY and ^{1}H−^{1}H 2D ROESY NMR spectral data. (A) Side view of the energy-minimized folded MK-1 conformation (50.3 kcal/mol; H_x−H_x internuclear distance, 2.8 Å). (B) Top view of the energy-minimized proposed MK-1 conformation showing the isoprene methyl groups positioned folded upward.

maintaining interactions with the AOT regions shown in Figure 13.

To determine if saturation of the isoprenyl side chain affects the location and orientation within the RM interface, the same experiment was carried out with MK-1(H_2) (Figure S25). NOE cross peaks are observed between MK-1(H_2) aromatic hydrogens, H_3−H_d, and AOT's CH_2 and CH_3 alkyl tail groups (Figure S25). NOE cross peaks are observed between methylene hydrogens, H_r/H_u, and HOD, H1/H1′, H3/H3′, and H4/H4′. NOE cross peaks are observed between the naphthoquinone methyl, H_q, and HOD, H1/H1′, H3/H3′, and H4/H4′ (Figure S25). The AOT and isooctane hydrogens overlapped with MK-1(H_2)'s terminal methyl hydrogens, H_z and H_y, and the methine hydrogen, H_i, signals in the spectrum for MK-1(H_2) within the RM interface; therefore, we were unable to determine the conformation of MK-1(H_2) within the interface with confidence. Despite this, we would anticipate that MK-1(H_2) adopts a folded conformation similar to that of MK-1 within the RM interface based on similar interactions observed in the 1D and 2D NMR experiments carried out for MK-1. Together, these observations demonstrate that MK-1(H_2) interacted with the interface and has a position and orientation similar to those of MK-1, indicating that saturation of the isoprenyl side chain does induce an observable change in the position and orientation within the RM interface.

Overall, the ^{1}H−^{1}H 2D NOESY and ROESY NMR spectral data of MK-1 inside an RM interface are consistent with MK-1 adopting a folded conformation within an RM model membrane interface. Interestingly, the conformation of MK-1 inside the RM interface remains folded but differs slightly from the folded conformations observed in organic solutions. The observation that MK-1 adopts a folded conformation within the RM model membrane interface is important as understanding the conformational preferences of the first isoprene unit of MK will be crucial in determining and understanding conformations of the naturally occurring longer MK analogues within cellular membranes.

■ CONCLUSIONS

Lipoquinones such as MK, are special types of lipid-quinones and are essential components of the ETS. Partial saturation of MK in these biological systems is necessary for some organisms to survive such as pathogenic *M. tuberculosis*.[7,8,11] The rationale for the observation of partially saturated MK derivatives in various organisms remains unclear. It is intriguing as the double bonds present in the isoprenyl side chain of MK are not conjugated with each other or to the redox active quinone system and therefore would not be expected to affect the redox potential. Interestingly, we recently showed that MK-2 adopts a folded conformation in which the double bond in the second isoprene unit is in the proximity of the quinone carbonyl groups on the naphthoquinone and may potentially have an influence on the reactivity of the quinone.[37] The studies described herein improve our understanding of the chemical, conformational, and biochemical properties on an important class of quinone-containing compounds involved in electron transfer processes. The partially saturated MKs represent an unrecognized group of biologically significant molecules that are essential for pathogenic taxonomic classification.

In this work, we first demonstrated using a semiquantitative 2D NMR spectroscopy approach that the two simplest, most fundamental MK analogues, unsaturated MK-1 and saturated MK-1(H_2), adopt similar folded−extended conformations in each organic solvent but differ slightly between each organic solvent environment. We also observed that the degree of saturation in the isoprenyl side chain of MK-1 only slightly alters the conformation. Importantly, the conformations observed for MK-1 closely resembled the conformation of the first isoprene unit in MK-2, which we previously showed adopted folded conformations in solution and within a model membrane interface.[37] Together, these results support the first hypothesis that MK-1 analogues adopt folded conformations regardless of the degree of saturation in their isoprenyl side chain.

The quinone redox potentials of MK-1 and MK-1(H_2) were measured in various anhydrous organic solvent environments. The organic solvent environments studied more closely resemble the environment of the cellular membrane in which native MKs are located and serve as better comparisons for biological reactivity than those carried out in aqueous solutions. We demonstrated that the measured quinone redox potentials of MK-1 and MK-1(H_2) varied with the solvent environment (presumably mainly due to differences in dielectric constants) where the ease of quinone reduction for the $Q/Q^{\bullet-}$ process follows the trend DMSO > ACN > pyridine. Remarkably, we report for the first time that the degree of saturation in the isoprenyl side chain of MK-1 influences the observed quinone redox potential, where unsaturation in the isoprenyl side chain of MK-1 makes the quinone easier to reduce by ~20 mV and the difference is conserved across several organic solvents (pyridine, ACN, and DMSO). The observed ~20 mV redox potential difference is presumably due mostly to a perturbation of the electronics of the quinone system upon saturation of the double bond by an indirect through-bond effect. The observation of a 20 mV difference in the redox potential between the two MK-1 derivatives with a saturated and unsaturated isoprenyl side chain observed in three different solvents is unexpected and may reflect some important general reactivity pattern of this system. We speculate that if such a difference is also observed for the MKs with longer isoprenyl side chains that it may reflect the biological function of these molecules and provide evidence for the possibility that such a small difference in redox potential may be biologically significant. However, in the simple MK-1 system containing one isoprene unit, the side chain may not have the spatial reach needed present in the MK-9 system, and therefore, more data are needed to properly evaluate the longer MK derivatives. The electrochemical results

DOI: 10.1021/acs.biochem.9b00007
Biochemistry 2019, 58, 1596−1615

confirm our second hypothesis that saturation of the isoprenyl side chain of MK-1 affects the observed quinone redox potential.

Finally, combining results, we found MK-1 and MK-1(H_2) both interacted with Langmuir phospholipid monolayers and RM model membrane interfaces, where MK-1 and MK-1(H_2) had very similar interactions with the Langmuir phospholipid monolayers (DPPC and DPPE phospholipids) and similar placement and location within the RM interface. Importantly, MK-1 also adopted a folded conformation within the RM model membrane interface, further supporting our first hypothesis. The results combined from all the conformational analysis studies presented herein for MK-1 and MK-1(H_2) indicated a folded−extended conformation to be a favorable and stable conformation for MK-1 analogues. Altogether, these results are significant as the conformation and reactivity of these MKs in organic solution and model membrane interfaces provide a first prediction/consideration of the form that exists within the native hydrophobic cellular membrane interface.

Overall, the findings of this study improve our understanding of how the conformation and the degree of saturation in the isoprenyl side chain affect the reactivity and function of biologically relevant molecules. The elucidation of the conformation of MK-1 and MK-1(H_2) in organic solutions and at a model membrane interface is essential and necessary as understanding the conformational preferences of the first isoprene unit of MK is useful for predicting the conformations of the naturally occurring longer MK analogues within solution and cellular membranes. We observed that partial saturation in the isoprenyl side chain only minimally alters the conformation of MK-1 but may potentially affect the reactivity and function within biologically relevant environments because a difference in the redox potential is observed. MK analogues with longer isoprenyl side chains (e.g., MK-9) may also adopt folded conformations, although likely much more complex. Saturation of the double bond in the first isoprene unit of the isoprenyl side chain serves to only minimally alter the preferred conformation but distinctly affects the redox function. The results presented here provide a working model involving the role of structure and redox potential that explains why partial saturation of MK is a virulence factor for pathogenic *M. tuberculosis*, which is responsible for the deaths of ~1.3 million people annually.[7,8,80]

■ ASSOCIATED CONTENT

Supporting Information

The Supporting Information is available free of charge on the ACS Publications website at DOI: 10.1021/acs.biochem.9b00007.

General experimental information, 1D and 2D NMR spectroscopic and structural data for MK-1 and MK-1(H_2), MK-1 and MK-1(H_2) conformations and conformational analysis and tables of relevant internuclear hydrogen distances, energies, and Cartesian coordinates, electrochemistry methods and data and discussion, ^{1}H NMR spectra of MK-1 with TBAP, Langmuir monolayer compression moduli of MK-1 and MK-1(H_2) and interpretation, and DLS data and interpretation (PDF)

■ AUTHOR INFORMATION

Corresponding Author

*E-mail: Debbie.Crans@colostate.edu.

ORCID

Jordan T. Koehn: 0000-0003-3008-6303
Benjamin J. Peters: 0000-0002-6219-4897
Cameron Van Cleave: 0000-0002-0924-1738
Dean C. Crick: 0000-0001-9281-7058
Debbie C. Crans: 0000-0001-7792-3450

Funding

D. C. Crans and D. C. Crick thank the National Institutes of Health (Grant AI119567) and the National Science Foundation (Grant CHE-1709564) for funding. D. C. Crans also thanks the Arthur Cope Foundation administered by the American Chemical Society for partial support.

Notes

The authors declare no competing financial interest.

■ ACKNOWLEDGMENTS

The authors thank Dr. Christopher Rithner for assistance with NMR spectroscopy and Taylor Lucia and Lining Yang for early contributions to this project.

■ REFERENCES

(1) Aguilar-Martínez, M., Macías-Ruvalcaba, N. A., Bautista-Martínez, J. A., Gómez, M., González, F. J., and González, I. (2004) Review: Hydrogen Bond and Protonation as Modifying Factors of the Quinone Reactivity. *Curr. Org. Chem.* 8, 1721−1738.

(2) Astudillo-Sánchez, P. D., Morales-Martínez, D., Sánchez, A., Rocha-Ortiz, G., and Salas-Reyes, M. (2017) Electrochemical Study of the Interactions Between Anionic Species of Menadione and Alkylated Nucleobases in Dimethylsulfoxide. *J. Electroanal. Chem.* 801, 104−113.

(3) Gunner, M. R., Madeo, J., and Zhu, Z. (2008) Modification of Quinone Electrochemistry by the Proteins in the Biological Electron Transfer Chains: Examples from Photosynthetic Reaction Centers. *J. Bioenerg. Biomembr.* 40 (5), 509−519.

(4) Monks, T. J., Hanzlik, R. E., Cohen, G. M., Ross, D., and Graham, D. G. (1992) Quinone Chemistry and Toxicity. *Toxicol. Appl. Pharmacol.* 112 (1), 2−16.

(5) Abraham, I., Joshi, R., Pardasani, P., and Pardasani, R. T. (2011) Recent Advances in 1,4-Benzoquinone Chemistry. *J. Braz. Chem. Soc.* 22 (3), 385−421.

(6) Nowicka, B., and Kruk, J. (2010) Occurrence, Biosynthesis and Function of Isoprenoid Quinones. *Biochim. Biophys. Acta, Bioenerg.* 1797, 1587−1605.

(7) Upadhyay, A., Fontes, F. L., Gonzalez-Juarrero, M., McNeil, M. R., Crans, D. C., Jackson, M., and Crick, D. C. (2015) Partial Saturation of Menaquinone in *Mycobacterium tuberculosis*: Function and Essentiality of a Novel Reductase, MenJ. *ACS Cent. Sci.* 1 (6), 292−302.

(8) Upadhyay, A., Kumar, S., Rocker, S. A., Koehn, J. T., Crans, D. C., McNeil, M. R., Lott, J. S., and Crick, D. C. (2018) Mycobacterial MenJ: An Oxidoreductase Involved in Menaquinone Biosynthesis. *ACS Chem. Biol.* 13, 2498−2507.

(9) da Costa, M. S., Albuquerque, L., Nobre, M. F., and Wait, R. (2011) The Extraction and Identification of Respiratory Lipoquinones of Prokaryotes and Their Use in Taxonomy. In *Methods in Microbiology, Vol 38: Taxonomy of Prokaryotes* (Rainey, F., and Oren, A., Eds.) Vol. 38, pp 197−206, Elsevier Academic Press Inc., San Diego.

(10) Kroppenstedt, R. M., and Mannheim, W. (1989) Lipoquinones in Members of the Family Pasteurellaceae. *Int. J. Syst. Bacteriol.* 39 (3), 304−308.

(11) Collins, M. D., and Jones, D. (1981) Distribution of Isoprenoid Quinone Structural Types in Bacteria and Their Taxonomic Implications. *Microbiol. Rev. 45* (2), 316−354.
(12) Meganathan, R. (2001) Biosynthesis of Menaquinone (Vitamin K_2) and Ubiquinone (Coenzyme Q): A Perspective on Enzymatic Mechanisms. *Vitam. Horm. 61*, 173−218.
(13) Jarchow-Choy, S. K., Koppisch, A. T., and Fox, D. T. (2014) Synthetic Routes to Methylerythritol Phosphate Pathway Intermediates and Downstream Isoprenoids. *Curr. Org. Chem. 18*, 1050−1072.
(14) Collins, M. D., Shah, H. N., and Minnikin, D. E. (1980) A Note on the Separation of Natural Mixtures of Bacterial Menaquinones Using Reverse-phase Thin-layer Chromatography. *J. Appl. Bacteriol. 48* (2), 277−282.
(15) Thomson, R. H. (1971) *Naturally Occurring Quinones*, Academic Press Inc.
(16) Kurosu, M., and Begari, E. (2010) Vitamin K_2 in Electron Transport System: Are Enzymes Involved in Vitamin K_2 Biosynthesis Promising Drug Targets? *Molecules 15* (3), 1531−1553.
(17) Nakagawa, K., Hirota, Y., Sawada, N., Yuge, N., Watanabe, M., Uchino, Y., Okuda, N., Shimomura, Y., Suhara, Y., and Okano, T. (2010) Identification of UBIAD1 as a Novel Human Menaquinone-4 Biosynthetic Enzyme. *Nature 468*, 117−121.
(18) Vos, M., Esposito, G., Edirisinghe, J. N., Vilain, S., Haddad, D. M., Slabbaert, J. R., Van Meensel, S., Schaap, O., De Strooper, B., Meganathan, R., Morais, V. A., and Verstreken, P. (2012) Vitamin K_2 Is a Mitochondrial Electron Carrier That Rescues Pink1 Deficiency. *Science 336*, 1306−1310.
(19) Josey, B. J., Inks, E. S., Wen, X., and Chou, C. J. (2013) Structure−Activity Relationship Study of Vitamin K Derivatives Yields Highly Potent Neuroprotective Agents. *J. Med. Chem. 56*, 1007−1022.
(20) Rahn, J. J., Bestman, J. E., Josey, B. J., Inks, E. S., Stackley, K. D., Rogers, C. E., Chou, C. J., and Chan, S. S. L. (2014) Novel Vitamin K Analogs Suppress Seizures in Zebrafish and Mouse Models of Epilepsy. *Neuroscience 259*, 142−154.
(21) Chadar, D., Camilles, M., Patil, R., Khan, A., Weyhermuller, T., and Salunke-Gawali, S. (2015) Synthesis and Characterization of *n*-alkylamino Derivatives of Vitamin K3: Molecular Structure of 2-propylamino-3-methyl-1,4-naphthoquinone and Antibacterial Activities. *J. Mol. Struct. 1086*, 179−189.
(22) Kathawate, L., Joshi, P. V., Dash, T. K., Pal, S., Nikalje, M., Weyhermuller, T., Puranik, V. G., Konkimalla, V. B., and Salunke-Gawali, S. (2014) Reaction Between Lawsone and Aminophenol Derivatives: Synthesis, Characterization, Molecular Structures and Antiproliferative Activity. *J. Mol. Struct. 1075*, 397−405.
(23) Klauda, J. B., Brooks, B. R., MacKerell, A. D., Venable, R. M., and Pastor, R. W. (2005) An Ab Initio Study on the Torsional Surface of Alkanes and Its Effect on Molecular Simulations of Alkanes and a DPPC Bilayer. *J. Phys. Chem. B 109*, 5300−5311.
(24) Woodward, R. B., and Bloch, K. (1953) The Cyclization of Squalene in Cholesterol Synthesis. *J. Am. Chem. Soc. 75*, 2023−2024.
(25) Chum, S. P., Knight, G. W., Ruiz, J. M., and Phillips, P. J. (1994) Computer Modeling of {110} Adjacent Reentry of Polyethylene Molecules. *Macromolecules 27*, 656−659.
(26) Robertson, M. B., Klein, P. G., Ward, I. M., and Packer, K. J. (2001) NMR Study of the Energy Difference and Population of the *gauche* and *trans* Conformations in Solid Polyethylene. *Polymer 42*, 1261−1264.
(27) Nikki, K., Inakura, H., Wu-Le, Suzuki, N., and Endo, T. (2001) Remarkable Changes in Conformations of *n*-alkanes with thier Carbon Numbers and Aromatic Solvents. *J. Chem. Soc., Perkin Trans. 2*, 2370−2373.
(28) Nikki, K., and Nakagawa, N. (1983) Elucidation of the Structure of Alkane Chains in Solution by Means of ^{1}H NMR. *Org. Magn. Reson. 21* (9), 552−554.
(29) Nikki, K. (1990) ^{1}H and ^{13}C NMR Aromatic Solvent-induced Shifts of *n*-alkanes. *Magn. Reson. Chem. 28* (5), 385−388.
(30) Schramm, M. P., and Rebek, J., Jr. (2006) Moving Targets: Recognition of Alkyl Groups. *Chem. - Eur. J. 12*, 5924−5933.
(31) Choudhury, R., Barman, A., Prabhakar, R., and Ramamurthy, V. (2013) Hydrocarbons Depending on the Chain Length and Head Group Adopt Different Conformations within a Water-Soluble Nanocapsule: ^{1}H NMR and Molecular Dynamics Studies. *J. Phys. Chem. B 117*, 398−407.
(32) Ko, Y. H., Kim, Y., Kim, H., and Kim, K. (2011) U-Shaped Conformation of Alkyl Chains Bound to a Synthetic Receptor Cucurbit[8]uril. *Chem. - Asian J. 6*, 652−657.
(33) Ko, Y. H., Kim, H., Kim, Y., and Kim, K. (2008) U-Shaped Conformation of Alkyl Chain Bound to a Synthetic Host. *Angew. Chem., Int. Ed. 47*, 4106−4109.
(34) Zakharov, A. V., and Vogt, N. (2011) Conformational Analysis of Vitamin K_1 Model Molecule: A Theoretical Study. *Struct. Chem. 22* (2), 305−311.
(35) Tynkkynen, T., Hassinen, T., Tiainen, M., Soininen, P., and Laatikainen, R. (2012) ^{1}H NMR Spectral Analysis and Conformational Behavior of *n*-alkanes in Different Chemical. *Magn. Reson. Chem. 50*, 598−607.
(36) Ishihara, M., and Sakagami, H. (2007) QSAR of Molecular Structure and Cytotoxic Activity of Vitamin K_2 Derivatives with Concept of Absolute Hardness. *Anticancer Res. 27*, 4059−4063.
(37) Koehn, J. T., Magallanes, E. S., Peters, B. J., Beuning, C. N., Haase, A. A., Zhu, M. J., Rithner, C. D., Crick, D. C., and Crans, D. C. (2018) A Synthetic Isoprenoid Lipoquinone, Menaquinone-2, Adopts a Folded Conformation in Solution and at a Model Membrane Interface. *J. Org. Chem. 83*, 275−288.
(38) Stahla, M. L., Baruah, B., James, D. M., Johnson, M. D., Levinger, N. E., and Crans, D. C. (2008) ^{1}H NMR Studies of Aerosol-OT Reverse Micelles with Alkali and Magnesium Counterions: Preparation and Analysis of MAOTs. *Langmuir 24* (12), 6027−6035.
(39) Samart, N., Beuning, C. N., Haller, K. J., Rithner, C. D., and Crans, D. C. (2014) Interaction of a Biguanide Compound with Membrane Model Interface Systems: Probing the Properties of Antimalaria and Antidiabetic Compounds. *Langmuir 30* (29), 8697−8706.
(40) Quinn, P. J., and Esfahani, M. A. (1980) Ubiquinones have Surface-Active Properties Suited to Transport Electrons and Protons Across Membranes. *Biochem. J. 185*, 715−722.
(41) Jones, M. N., and Chapman, D. (1995) *Micelles, Monolayers, and Biomembranes*, Wiley-Liss, New York.
(42) Peters, B. J., Groninger, A. S., Fontes, F. L., Crick, D. C., and Crans, D. C. (2016) Differences in Interactions of Benzoic Acid and Benzoate with Interfaces. *Langmuir 32* (37), 9451−9459.
(43) Peters, B. J., Van Cleave, C., Haase, A. A., Hough, J. P. B., Giffen-Kent, K. A., Cardiff, G. M., Sostarecz, A. G., Crick, D. C., and Crans, D. C. (2018) Structure Dependence of Pyridine and Benzene Derivatives on Interactions with Model Membranes. *Langmuir 34*, 8939−8951.
(44) Maitra, A. (1984) Determination of Size Parameters of Water-aerosol-OT Oil Reverse Micelles From Their Nuclear Magnetic-resonance Data. *J. Phys. Chem. 88* (21), 5122−5125.
(45) Hagiwara, E., Hatanaka, Y., Gohda, K.-i., and Hiyama, T. (1995) Allylation of Quinones with Allyl(trifluoro)silanes: Direct Synthesis of Isoprenoid Quinones. *Tetrahedron Lett. 36* (16), 2773−2776.
(46) Mal, D., Ghosh, K., and Jana, S. (2015) Synthesis of Vitamin K and Related Naphthoquinones via Demethoxycarbonylative Annulations and a Retro-Wittig Rearrangement. *Org. Lett. 17*, 5800−5803.
(47) Teitelbaum, A. M., Scian, M., Nelson, W. L., and Rettie, A. E. (2015) Efficient Syntheses of Vitamin K Chain-Shortened Acid Metabolites. *Synthesis 47*, 944−948.
(48) Yamago, S., Hashidume, M., and Yoshida, J.-i. (2002) A New Synthetic Route to Substituted Quinones by Radical-mediated Coupling of Organotellurium Compounds with Quinones. *Tetrahedron 58*, 6805−6813.
(49) Daines, A. M., Payne, R. J., Humphries, M. E., and Abell, A. D. (2003) The Synthesis of Naturally Occurring Vitamin K and Vitamin K Analogues. *Curr. Org. Chem. 7*, 1625−1634.

DOI: 10.1021/acs.biochem.9b00007
Biochemistry 2019, 58, 1596−1615

(50) Payne, R. J., Daines, A. M., Clark, B. M., and Abell, A. D. (2004) Synthesis and Protein Conjugation Studies of Vitamin K Analogues. *Bioorg. Med. Chem. 12* (22), 5785−5791.
(51) Suhara, Y., Wada, A., Tachibana, Y., Watanabe, M., Nakamura, K., Nakagawa, K., and Okano, T. (2010) Structure-activity Relationships in the Conversion of Vitamin K Analogues into Menaquinone-4. Substrates Essential to the Synthesis of Menaquinone-4 in Cultured Human Cell Lines. *Bioorg. Med. Chem. 18* (9), 3116−3124.
(52) Coppa, F., Fontana, F., Minisci, F., Nogueira Barbosa, M. C., and Vismara, E. (1991) Homolytic Alkylation of Naphthoquinone and Methyl-naphthoquinone. Enthalpic, Steric and Polar Effects. *Tetrahedron 47* (35), 7343−7352.
(53) Koehn, J. T., Crick, D. C., and Crans, D. C. (2018) Synthesis and Characterization of Partially and Fully Saturated Menaquinone Derivatives. *ACS Omega 3*, 14889−14901.
(54) Jones, C. R., Butts, C. P., and Harvey, J. N. (2011) Accuracy in Determining Interproton Distances using Nuclear Overhauser Effect Data from a Flexible Molecule. *Beilstein J. Org. Chem. 7*, 145−150.
(55) Cooper, G. M., and Hausman, R. E. (2009) *The Cell: A Molecular Approach*, 5th ed., p 820, Sinauer Associates, Inc., Sunderland, MA.
(56) Nelson, D. L., and Cox, M. M. (2008) *Lehninger Principles of Biochemistry*, 5th ed., p 1158, W. H. Freeman and Co., New York.
(57) Dryhurst, G., Kadish, K. M., Scheller, F., and Renneberg, R. (1982) *Biological Eletrochemistry*, Academic Press, New York.
(58) Wawzonek, S., Berkey, R., Blaha, E. W., and Runner, M. E. (1956) Polarographic Studies in Acetonitrile and Dimethylformamide: III. Behavior of Quinones and Hydroquinones. *J. Electrochem. Soc. 103* (8), 456−459.
(59) Jaworski, J. S., Leniewska, E., and Kalinowski, M. K. (1979) Solvent Effect on the Redox Potential of Quinone-semiquinone Systems. *J. Electroanal. Chem. Interfacial Electrochem. 105* (2), 329−334.
(60) Prince, R. C., Leslie Dutton, P., and Malcolm Bruce, J. (1983) Electrochemistry of Ubiquinones. *FEBS Lett. 160* (1), 273−276.
(61) Sostarecz, A. G., Gaidamauskas, E., Distin, S., Bonetti, S. J., Levinger, N. E., and Crans, D. C. (2014) Correlation of Insulin-Enhancing Properties of Vanadium-Dipicolinate Complexes in Model Membrane Systems: Phospholipid Langmuir Monolayers and AOT Reverse Micelles. *Chem. - Eur. J. 20* (17), 5149−5159.
(62) Riter, R. E., Kimmel, J. R., Undiks, E. P., and Levinger, N. E. (1997) Novel Reverse Micelles Partitioning Nonaqueous Polar Solvents in a Hydrocarbon Continuous Phase. *J. Phys. Chem. B 101* (41), 8292−8297.
(63) Durantini, A. M., Falcone, R. D., Silber, J. J., and Correa, N. M. (2016) Effect of Confinement on the Properties of Sequestered Mixed Polar Solvents: Enzymatic Catalysis in Nonaqueous 1,4-Bis-2-ethylhexylsulfosuccinate Reverse Micelles. *ChemPhysChem 17* (11), 1678−1685.
(64) Lepori, C. M. O., Correa, N. M., Silber, J. J., and Falcone, R. D. (2016) How the Cation 1-butyl-3-methylimidazolium Impacts the Interaction Between the Entrapped Water and the Reverse Micelle Interface Created with an Ionic Liquid-like Surfactant. *Soft Matter 12* (3), 830−844.
(65) Baruah, B., Roden, J. M., Sedgwick, M., Correa, N. M., Crans, D. C., and Levinger, N. E. (2006) When Is Water Not Water? Exploring Water Confined in Large Reverse Micelles Using a Highly Charged Inorganic Molecular Probe. *J. Am. Chem. Soc. 128*, 12758−12765.
(66) Odella, E., Falcone, R. D., Silber, J. J., and Correa, N. M. (2016) Nanoscale Control Over Interfacial Properties in Mixed Reverse Micelles Formulated by Using Sodium 1,4-bis-2-ethylhexylsulfosuccinate and Tri-n-octyl Phosphine Oxide Surfactants. *ChemPhysChem 17* (15), 2407−2414.
(67) Diaz-Fernandez, Y., Foti, F., Mangano, C., Pallavicini, P., Patroni, S., Perez-Gramatges, A., and Rodriguez-Calvo, S. (2006) Micelles for the Self-Assembly of "Off−On−Off" Fluorescent Sensors for pH Windows. *Chem. - Eur. J. 12*, 921−930.
(68) Pallavicini, P., Diaz-Fernandez, Y., and Pasotti, L. (2009) Micelles as Nanosized Containers for the Self-assembly of Multicomponent Fluorescent Sensors. *Coord. Chem. Rev. 253*, 2226−2240.
(69) Stefaniu, C., Brezesinski, G., and Mohwald, H. (2014) Langmuir Monolayers as Models to Study Processes at Membrane Surfaces. *Adv. Colloid Interface Sci. 208*, 197−213.
(70) Choi, Y., Attwood, S. J., Hoopes, M. I., Drolle, E., Karttunen, M., and Leonenko, Z. (2014) Melatonin Directly Interacts with Cholesterol and Alleviates Cholesterol Effects in Dipalmitoylphosphatidylcholine Monolayers. *Soft Matter 10*, 206−213.
(71) Hoyo, J., Torrent-Burgues, J., and Guaus, E. (2012) Biomimetic Monolayer Films of Monogalactosyldiacylglycerol Incorporating Ubiquinone. *J. Colloid Interface Sci. 384*, 189−197.
(72) Panda, A. K., Nag, K., Harbottle, R. R., Possmayer, F., and Petersen, N. O. (2004) Thermodynamic Studies on Mixed Molecular Langmuir Films: Part 2. Mutual Mixing of DPPC and Bovine Lung Surfactant Extract with Long-chain Fatty Acids. *Colloids Surf., A 247* (1), 9−17.
(73) Veldhuizen, E. J. A., Batenburg, J. J., van Golde, L. M. G., and Haagsman, H. P. (2000) The Role of Surfactant Proteins in DPPC Enrichment of Surface Films. *Biophys. J. 79*, 3164−3171.
(74) Wustneck, R., Perez-Gil, J., Wustneck, N., Cruz, A., Fainerman, V. B., and Pison, U. (2005) Interfacial Properties of Pulmonary Surfactant Layers. *Adv. Colloid Interface Sci. 117* (1), 33−58.
(75) Sohlenkamp, C., and Geiger, O. (2016) Bacterial Membrane Lipids: Diversity in Structures and Pathways. *FEMS Microbiol. Rev. 40* (1), 133−159.
(76) Toimil, P., Prieto, G., Minones, J., Jr, and Sarmiento, F. (2010) A Comparative Study of F-DPPC/DPPC Mixed Monolayers. Influence of Subphase Temperature on F-DPPC and DPPC Monolayers. *Phys. Chem. Chem. Phys. 12*, 13323−13332.
(77) Hoyo, J., Guaus, E., Torrent-Burgues, J., and Sanz, F. (2015) Biomimetic Monolayer Films of Digalactosyldiacylglycerol Incorporating Plastoquinone. *Biochim. Biophys. Acta, Biomembr. 1848* (6), 1341−1351.
(78) Sedgwick, M. A., Trujillo, A. M., Hendricks, N., Levinger, N. E., and Crans, D. C. (2011) Coexisting Aggregates in Mixed Aerosol OT and Cholesterol Microemulsions. *Langmuir 27* (3), 948−954.
(79) Zan, G. T., and Wu, Q. S. (2016) Biomimetic and Bioinspired Synthesis of Nanomaterials/Nanostructures. *Adv. Mater. 28* (11), 2099−2147.
(80) Glaziou, P., Sismanidis, C., Floyd, K., and Raviglione, M. (2015) Global Epidemiology of Tuberculosis. *Cold Spring Harbor Perspect. Med. 5*, a017798.

DOI: 10.1021/acs.biochem.9b00007
Biochemistry 2019, 58, 1596−1615

Appendix IX: Hydrophobicity May Enhance Membrane Affinity and Anti-Cancer Effects of Schiff Base Vanadium(V) Catecholate Complexes

This is the manuscript that corresponds to chapter five and is published in *Dalton Transactions*.[1]

References

1. Crans, D. C.; Koehn, J. T.; Petry, S. M.; Glover, C. M.; Wijetunga, A.; Kaur, R.; Levina, A.; Lay, P. A., Hydrophobicity May Enhance Membrane Affinity and Anti-Cancer Effects of Schiff Base Vanadium(V) Catecholate Complexes. *Dalton Trans.* **2019,** *48*, 6383-6395.

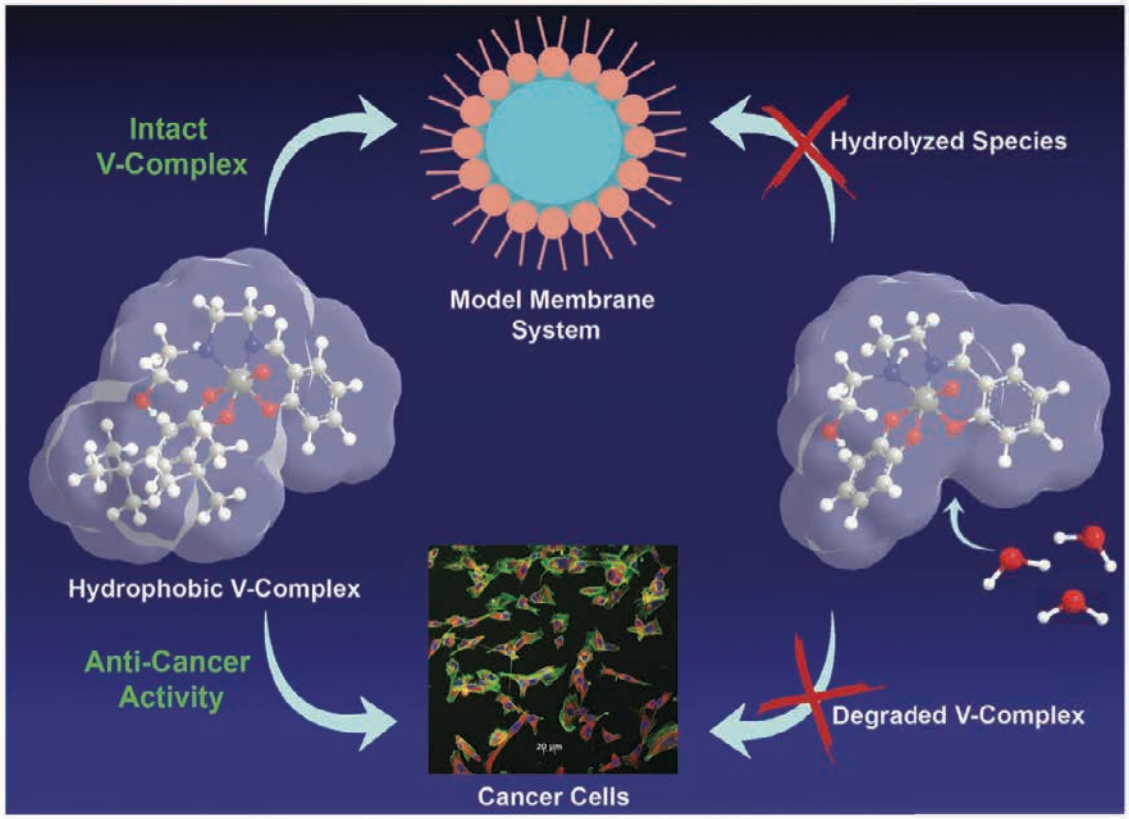

Showcasing research from the Lay and Crans labs at The University of Sydney, Australia and Colorado State University from Colorado, US.

Hydrophobicity may enhance membrane affinity and anti-cancer effects of Schiff base vanadium(v) catecholate complexes

Two hydrophobic V(v) catecholate substituted Schiff bases [VO(Hshed)(cat)] and [VO(Hshed)(dtb)] differing in the catechol, where, (Hshed = *N*-(salicylideneaminato)-*N*'-(2-hydroxyethyl)-1,2-ethanediamine, were examined for their ability to interact with a model membrane system and their anti-cancer effects in human chrondrosarcoma (SW1353) cells.

As featured in:

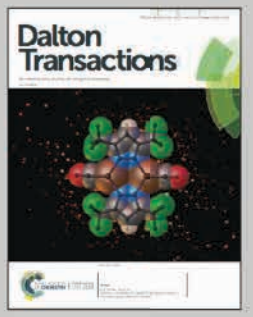

See Debbie C. Crans, Peter A. Lay *et al.*, *Dalton Trans.*, 2019, **48**, 6383.

ROYAL SOCIETY OF CHEMISTRY | Celebrating IYPT 2019

rsc.li/dalton

Registered charity number: 207890

Dalton Transactions

PAPER

View Article Online
View Journal | View Issue

Check for updates

Cite this: *Dalton Trans.*, 2019, **48**, 6383

Published on 14 March 2019. Downloaded on 5/16/2019 4:36:17 PM.

Hydrophobicity may enhance membrane affinity and anti-cancer effects of Schiff base vanadium(v) catecholate complexes†‡

Debbie C. Crans, *[a,b] Jordan T. Koehn,[a] Stephanie M. Petry,[a] Caleb M. Glover,[a] Asanka Wijetunga,[c] Ravinder Kaur,[c] Aviva Levina[c] and Peter A. Lay *[c]

Anti-cancer activities of vanadium compounds have generated recent interest because of a combination of desirable properties for chemotherapy, *i.e.*, strong cytotoxicities, anti-metastatic activities and relatively low systemic toxicities. Certain hydrophobic vanadium(v) Schiff base/catecholate compounds, which as shown herein, have increased stability in aqueous media and affinity for membrane interfaces. Depending on their hydrophobicity, they may be able to enter cells intact. In this manuscript, two hydrophobic V(v) catecholate substituted analogues, [VO(Hshed)(cat)] and [VO(Hshed)(dtb)], (Hshed = *N*-(salicylideneamino)-*N*′-(2-hydroxyethyl)-1,2-ethanediamine, cat = pyrocatechol, and dtb = 3,5-di(*tert*-butyl)catechol and the vanadium(v) precursor $[V(O)_2(Hshed)]$) were synthesized for their ability to interact with membranes and their anti-cancer effects. Using ^{51}V and ^{1}H NMR spectroscopy, the presence and location of the free ligand, H_2shed, and the three V(v) complexes were examined in a model membrane microemulsion system. The stability of the three complexes was measured in aqueous solution, cell media and an inhomogeneous microemulsion system. Our results demonstrated that free ligand H_2shed and the intact V(v) complexes associated with the interface but that the V-complexes hydrolyzed to some extent because oxovanadates were observed by ^{51}V NMR spectroscopy and decreasing complex by absorption spectroscopy in cell media. When determining the effects of V(v) catecholate complexes on bone cancer cells, the strongest effects were observed with the more stable hydrophobic complex [VO(Hshed)(dtb)] that was able to best associate and penetrate the model membrane system intact. These studies are consistent with the membrane permeability studies being a good predictor for *in vitro* cytotoxicity assays because [VO(Hshed)(dtb)] can pass through the cellular membrane intact, which may enhance its anti-cancer activities.

Received 8th February 2019.
Accepted 8th March 2019

DOI: 10.1039/c9dt00601j

rsc.li/dalton

Introduction

Medicinal applications of metal complexes in the past have been dominated by the anti-cancer platinum drugs as well as a range of complexes used for imaging diagnostics and nuclear medicinal applications.[1–7] However, several additional metal-based classes of complexes have been of interest for decades and are increasing in importance. Vitamins and nutritional additives often include metal-ion containing supplements.[8–12] A large number of different formulations for iron and vanadium are testament to the existence of a range of methodologies that can be applied to increase the efficacy of absorption.[13] Furthermore, Lipinski's rules[14] based on an empirical and statistical evaluation of efficacy suggest that statistically successful drugs are of certain size, hydrophobicity, polarity, or reactivity, which thus limits the chemical space to search for available drugs. However, some of the more successful drugs do not follow these empirical rules, such as cisplatin; therefore, drug and supplement design continues to include the entire chemical space. For example, recent investigations have introduced promising hydrophobic titanium and vanadium drugs.[15–19] The water solubility of these compounds and other hydrophobic drugs is very limited, and as a result, the methods for *in vivo* studies with these compounds involves dissolving the com-

[a]*Chemistry Department, Colorado State University, Fort Collins, Colorado 80523, USA. E-mail: debbie.crans@colostate.edu*
[b]*Cell and Molecular Biology Program, Colorado State University, Fort Collins, Colorado 80523, USA*
[c]*School of Chemistry, The University of Sydney, Sydney, NSW 2006, Australia. E-mail: peter.lay@sydney.edu.au*

†This contribution was submitted to the special issue prepared after the 7th EuCheMs Conference on Nitrogen Ligands, Fall 2018.

‡Electronic supplementary information (ESI) available: Fig. S1: 1D ^{1}H NMR spectra of [VO(Hshed)(cat)] in D_2O, DMSO and reverse micelles; Fig. S2: 1D ^{1}H NMR spectra of [VO(Hshed)(dtb)] in D_2O, DMSO, and reverse micelles; dynamic light scattering data. See DOI: 10.1039/c9dt00601j

This journal is © The Royal Society of Chemistry 2019

Published on 14 March 2019. Downloaded on 5/16/2019 4:36:17 PM.

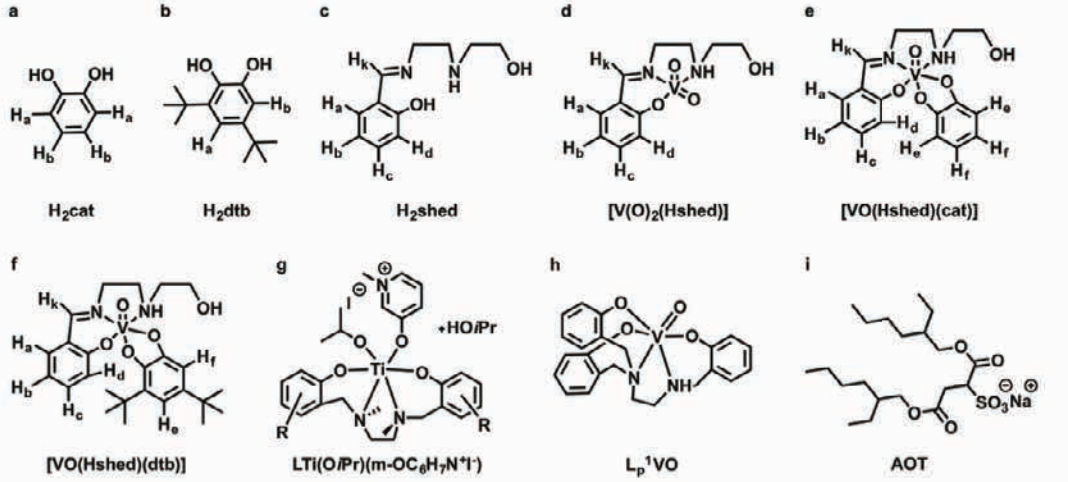

Fig. 1 The structures are labelled as follows: (a) H_2cat; (b) H_2dtb; (c) H_2shed, (d) [V(O)$_2$(Hshed)], (e) [VO(Hshed)(cat)], (f) [VO(Hshed)dtb], (g) example of a hydrolytically stable titanium complex.[26] (h) example of a hydrolytically stable vanadium complex.[25] and (i) AOT.

pounds in methanol, ethanol, or DMSO or dissolution in assays containing surfactants and/or DMSO. In this work, we examine the solubility, stability, and interactions of representative hydrophobic metal complexes (Fig. 1) and free ligand H_2shed with a model membrane interface and their anti-cancer effects.

Identification of inhibitors for signal transduction remains an important target in drug discovery. Phosphatase inhibitors that are particularly potent, or effective in animal studies, include a series of titanium, vanadium, and zinc coordination complexes.[17,20–24] In several studies,[25–28] a series of compounds were tested, and a correlation between hydrophobicity and stability with potency was highlighted, for example, see a representative compound in Fig. 1g.[26] The Tshuva group used this approach with vanadium compounds and prepared a hydrophobic vanadium complex (Fig. 1h), which was found to have anti-cancer properties as well.[25] The high hydrophobicity of these compounds tends to protect the complexes against initial hydrolysis making them more likely to penetrate membranes and extend their lifetime and enter into cells intact. An example of such a compound is shown in Fig. 1h; a vanadium complex that was more effective than cisplatin in growth inhibition of human colon HT-29 and ovarian OVCAR-3 cells.[25] Studies using data mining of vanadium-containing phosphatase complexes[24] and synchrotron studies indicate that most vanadium complexes lose their ligands when binding to phosphatases[24] or transferrin[29] in blood, and in cell medium.[30–37] In contrast, these same complexes interact with human serum albumin and in some cases can form a protein adduct that maintains the ligands.[37–39] It is possible that the complexes containing hydrophobic ligands with steric hindrance preventing substitution reactions may enable the uptake of the intact complex and delivery to the cellular target and thus be particularly potent cytotoxins to breast and pancreatic cancer cells.[40]

To explore how these hydrophobic complexes will interact with membrane interfaces, we have investigated the behavior of V(v) complexes with an ideal representation of a simple microemulsion ternary model membrane system shown in Fig. 2.[41,42] The reverse micelle (RM) is a ternary system, H_2O/AOT/organic solvent, where AOT = sodium bis[2-ethylhexyl]-sulfosuccinate, used as a simple but effective model system to explore the ability of these hydrophobic coordination complexes to penetrate the interface, Fig. 2. These self-assembled structures form in a region of the phase diagram where there

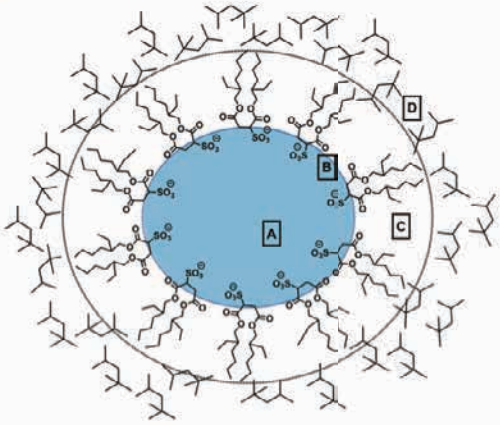

Fig. 2 Schematic diagram of an RM present in a microemulsion. The four distinct locations for potential solutes are labelled as follows: (a) the water pool, (b) the Stern layer, (c) the surfactant hydrophobic layer, and (d) the organic solvent layer, *iso*-octane.

This journal is © The Royal Society of Chemistry 2019

Published on 14 March 2019. Downloaded on 5/16/2019 4:36:17 PM.

is little H_2O, but significant amounts of surfactants and organic solvents.[43–47] The interface system is dynamic, but the overall stability of the system is governed by thermodynamic considerations rather than kinetic ones and, thus, the most thermodynamically stable arrangements are preserved. In the past, we have used mainly *iso*-octane or cyclohexane (or d_{16}-cyclohexane) as the organic solvent,[48] but others have used pentane, benzene, chloroform, and carbon tetrachloride.[49] The microemulsion forms RMs, but the interfacial chemistry enables studies of how such metal complexes will transverse interfaces[50,51] and NMR spectroscopy provides evidence on whether the complexes decompose and where they interact with the interfaces in this simple model system.

Studies with the BMOV/$[VO_2(ma)_2]^-$ system[52] and the V-dipic systems have demonstrated remarkable differences in how even simple compounds interact with model membrane systems. The BMOV/$[VO_2(ma)_2]^-$ compounds hydrolyze as they approach the interface,[52] whereas the V-dipic complexes react differently depending on the oxidation state.[53] The V(v) complex $[VO_2dipic]^-$ is able to penetrate the interface, whereas the V(III) complex $[V(dipic)_2]^-$ is found in the water pool associating with the interface.[53] The V(IV)-dipic system can form two complexes, a neutral 1:2 complex $[VO(dipic)_2]^{2-}$ that is generally prepared upon synthesis as well as a 1:1 complex $[VO(H_2O)_2(dipic)]^-$. The former readily associates with the interface partially penetrating the surface, whereas the 1:1 complex is interacting further up in the hydrophobic part of the interface similarly to the V(v)-dipic complex. These studies demonstrate the versatile modes of actions of these complexes,[54,55] and considering that V-complexes are known to cycle between redox states in the biological systems, this factor is undoubtedly involved in the mode of action of the vanadium complexes.[10,12,19,54–58] Indeed, the redox chemistry of vanadium compounds is likely to be associated with the generation of reactive oxygen species (ROS), which have been implicated in the mode of action of vanadium compounds. This topic is beyond the scope of this manuscript and we refer the reader elsewhere for more information on this important topic.[54,55]

Using this simple model membrane system, the chemistry of the ternary V(v) complex $[V(O)_2(Hshed)]$ and two more hydrophobic analogs prepared from its complexation with catecholate (cat) or di-*tert*-butylcatecholate (dtb) (Fig. 1) ligand were studied. These compounds belong to the family of complexes formed from non-innocent ligands, and as a result, exhibit a broad spectrum of redox chemistry.[59] It is well known that V-compounds redox cycle between V(v) and V(IV) upon administration, and a number of studies have been carried out exploring the details of these processes. Because we focus on V(v) compounds in this study, we refer readers elsewhere on this important topic.[4,10,12,56,71] For the V-catecholate complexes described in this work, the redox chemistry is mainly metal centred.[59] There have only been a few studies with vanadium–catechol complexes exploring their biological activities.[60–63] A recent study demonstrated that these compounds affected cell growth in MDA-MB-231 and PANC-1 cancer cells with varying amounts of effectiveness.[10] Furthermore, a number of vanadium compounds have been reported with naturally occurring non-polar flavonoids including mechanistic studies probing the redox chemistry involved in these processes.[64] It is, therefore, important to investigate how these hydrophobic complexes interact in interface model systems to explore how this may impact their anti-cancer activities.

Results

Synthesis

$[V(O)_2(Hshed)]$, [VO(Hshed)(cat)], and [VO(Hshed)(dtb)] and free ligand H_2shed were synthesized as previously described and the spectroscopic data were found to be consistent with the literature.[65–67] The free ligand, H_2shed, is the condensation product of salicylaldehyde (SalA) and *N*-(2-hydroxyethyl)-1,2-ethanediamine ($NH_2CH_2CH_2NHCH_2CH_2OH$, abbreviated as HyDA).

Solubility of free ligands and V(v) complexes and stability of free ligand H_2shed and $[V(O)_2(Hshed)]$ in RM samples

The three free ligands (H_2shed and cat and dtb catechols) were all dissolved in aqueous solution and *iso*-octane. The three complexes, $[V(O)_2(Hshed)]$, [VO(Hshed)(cat)], and [VO(Hshed)(dtb)], are all soluble in DMSO, dimethylsulfoxide, but have less solubility in aqueous solution and no measurable solubility in *iso*-octane (2,2,4-trimethylpentane) as confirmed by NMR spectroscopy. All three complexes had to be forced into aqueous solvents such as D_2O *via* vortexing and at that point the Schiff base ligand is subject to hydrolysis as shown in eqn (1) and the $[V(O)_2(Hshed)]$ complex as shown in eqn (2).

The stability of the precursor V(v) complex, $[V(O)_2(Hshed)]$, was measured in aqueous solution prior to the addition to the model membrane RM microemulsion system. We observed that the vanadium complexes hydrolyzed as shown in eqn (2) at a faster rate in aqueous solution than in the RM mixture. Due to the presence of the Schiff base in the ligand, once the complex hydrolyzed, the ligand could continue to fragment into salicylaldehyde (SalA) and *N*-(2-hydroxyethyl)-1,2-ethanediamine (HyDA) as shown in eqn (1) below. The equilibrium mixture of both the ligand and $[V(O)_2(Hshed)]$ complex in aqueous solution was obtained as evident by the NMR spectra recorded.

$$Hshed^- + H_3O^+ \rightarrow SalA + HyDA \quad (1)$$

$$2[V(O)_2(Hshed)] + 4HO^- \rightarrow 2H_2VO_4^- + 2Hshed^- \quad (2)$$

Once the equilibrium mixture of the H_2shed ligand had been obtained in aqueous solution, the solution was added to form RMs from two concentrations of AOT/*iso*-octane stock solution (0.200 and 0.750 M). Since the highest resolution ^1H NMR spectra were obtained using 0.750 M AOT stock solution, the rest of the studies were carried out using this stock solution concentration (see below). ^{51}V NMR spectra recorded for the precursor complex $[V(O)_2(Hshed)]$ in D_2O confirmed that it

Published on 14 March 2019. Downloaded on 5/16/2019 4:36:17 PM.

hydrolyzed in aqueous solution, and that equilibrium was reached by 20 min after sample preparation (see below). Compared to the aqueous solution, the equilibrium reaction was slower in RMs and the equilibrium concentration was achieved after 40 min. These studies provided the time-scale of the experiments of the precursor $[V(O)_2(Hshed)]$ complex sample and provided guidelines for the timeframe of the studies with this complex as well as the vanadium complexes with the catechol ligands studied where the lower solubility is problematic, which causes issues in detecting the complex.

^{51}V NMR spectra of the $[V(O)_2(Hshed)]$ complex

In aqueous solutions, the equilibrium concentration of $[V(O)_2(Hshed)]$ is about 60% of the total vanadium. ^{51}V NMR spectra of $[V(O)_2(Hshed)]$ in DMSO, D_2O, and in a series of RMs (w_0 = 6, 8, 12, 16 and 20 prepared from 0.750 M AOT/*iso*-octane stock solution; where w_0 = $[H_2O]/[AOT]$) are given in Fig. 3. Upon placement into the RM, the stability ratio was changed significantly and the amount of the $[V(O)_2(Hshed)]$ complex in the RM environment is much smaller than in D_2O (H_2O), Fig. 3. These studies convincingly show that $[V(O)_2(Hshed)]$ is destabilized by the RM environment more so than in aqueous solution. A slightly greater amount of the $[V(O)_2(Hshed)]$ complex was observed in larger RMs over smaller RMs.

^1H NMR spectra of $[V(O)_2(Hshed)]$ and H_2shed

A series of ^1H NMR spectroscopic studies in RMs were carried out using $[V(O)_2(Hshed)]$, and the corresponding free ligand, H_2shed. The RM studies with the $[V(O)_2(Hshed)]$ complex confirmed that the free H_2shed ligand was formed from the hydrolysis of the complex which, was then followed by subsequent hydrolysis of the H_2shed ligand to SalA and HyDA. The hydrolysis was confirmed in the D_2O spectra by the imine proton

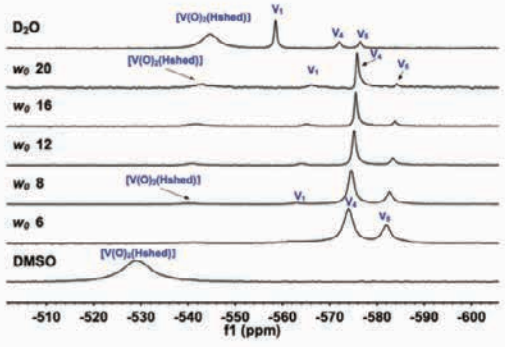

Fig. 3 ^{51}V NMR spectra of $[V(O)_2(Hshed)]$ in D_2O and in a series of RMs (w_0 = 6, 8, 12, 16 and 20 prepared from 0.750 M AOT/*iso*-octane stock solution). The spectra were recorded after equilibration was reached after 20 min for D_2O samples and after 40 min in RM samples. The pH for D_2O and RMs was 6.6 and the pD was 7.0. The total V-concentrations for 1.0 mL $[V(O)_2(Hshed)]$ RM samples are as follows: w_0 20, 2.41 mM; w_0 16, 5.17 mM; w_0 12, 11.05 mM; w_0 8, 23.53 mM; and w_0 6, 36.72 mM.

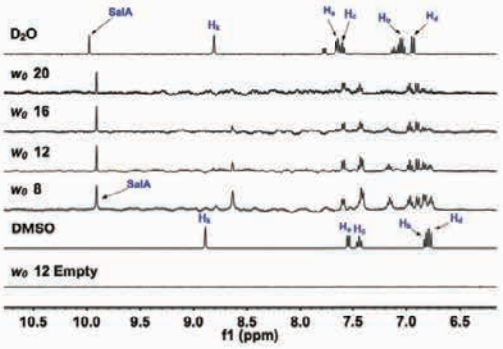

Fig. 4 ^1H NMR spectra of $[V(O)_2(Hshed)]$ in D_2O and in a series of RMs (w_0 = 8, 12, 16, and 20 prepared from 0.750 M AOT/*iso*-octane stock solution). The spectrum in D_2O was recorded after 20 min and the RM spectra were recorded after 40 min once equilibrium had been established. SalA = salicylaldehyde. The pH for D_2O and RMs was 6.6 and the pD was 7.0. The total V-concentrations for 1.0 mL $[V(O)_2(Hshed)]$ RM samples are as follows: w_0 20, 2.41 mM; w_0 16, 5.17 mM; w_0 12, 11.05 mM; w_0 8, 23.53 mM; and w_0 6, 36.72 mM.

signal (HC=N) at 8.81 ppm converting into an aldehyde proton (HC=O) at 9.98 pm (Fig. 4). These peaks are not present in the d_6-DMSO spectrum of $[V(O)_2(Hshed)]$ (Fig. 4). The spectra are shown for RM sizes w_0 8 through w_0 20 and although the ligand hydrolysis is complete, increased reactions are taking place because an increasing SalA:$[V(O)_2(Hshed)]$ (the latter measured by H_k) ratio is observed in the spectra as the RM size continues to increase (see spectrum at w_0 20).

To further confirm the formation of the ligand hydrolysis product, SalA, a study of the non-complexed free ligand, H_2shed, in a series of RMs was carried out (Fig. 5). By monitoring the ^1H NMR chemical shifts, it is apparent that the free ligand is hydrolyzing upon contact with the water pool (Fig. 5). The formation of an aldehyde group signal (HC=O) at 9.90 ppm and a decrease in the imine signal (HC=N) near 8.5 ppm readily shows the formation of one of the starting materials of the Schiff base, SalA, and almost complete conversion is seen after an equilibrium time of 45 min in D_2O. The ^1H NMR spectra demonstrated that the equilibrium mixture was different in the RMs compared to the H_2shed ligand in aqueous solution, and that the Schiff base is more stable in the environment of the smaller RMs in contrast to the $[V(O)_2(Hshed)]$ complex. Combined, these results show that SalA and H_2shed begin to form both in solutions with uncomplexed free ligand H_2shed (Fig. 5) and with the precursor $[V(O)_2(Hshed)]$ complex (Fig. 4).

There is a chemical shift change observed for $[V(O)_2(Hshed)]$ protons H_a, H_b, H_c, H_d, and H_k upon addition to the RM, which showed a change in the chemical environment and supported the interpretation that the $[V(O)_2(Hshed)]$ complex penetrated at least partially into the RM interfacial layer (Fig. 4). The free ligand H_2shed hydrolyzed as evidenced by a peak at 9.94 ppm in D_2O and at 9.89 ppm in w_0 8 RM

This journal is © The Royal Society of Chemistry 2019

Published on 14 March 2019. Downloaded on 5/16/2019 4:36:17 PM.

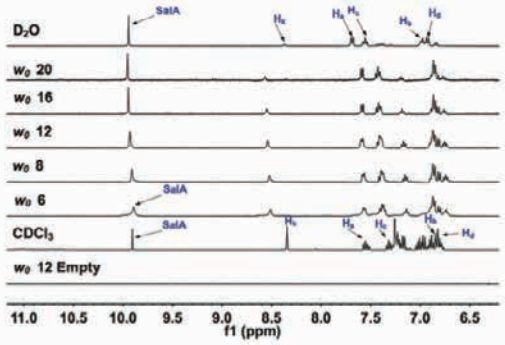

Fig. 5 ^{1}H NMR spectra of H_2shed in D_2O and in a series of RMs (w_0 = 6, 8, 12, 16, and 20 prepared from 0.750 M AOT/*iso*-octane stock solution). The spectrum in D_2O was recorded after 35 min and the spectra in RMs were recorded after 45 min once equilibrium had been established. Proton labelling scheme is found in Fig. 1. SalA = salicylaldehyde. The pH for D_2O and RMs was 6.6 and the pD was 7.0. The overall concentrations for 1.0 mL H_2shed RM samples are as follows: w_0 20, 2.71 mM; w_0 16, 5.65 mM; w_0 12, 11.77 mM; w_0 8, 24.48 mM; and w_0 6, 37.87 mM.

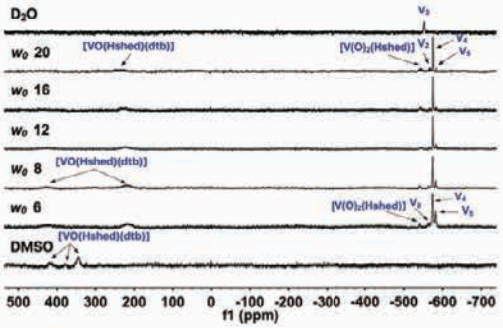

Fig. 6 ^{51}V NMR spectra of [VO(Hshed)(dtb)] in d_6-DMSO, *iso*-octane, and in a series of RMs (w_0 = 6, 8, 12, 16, 20 prepared from 0.750 M AOT/*iso*-octane stock solution). The spectrum in D_2O was recorded after 60 min and the spectra in RMs were recorded after 50 min once equilibrium had been established. The pH for D_2O and RMs was 6.6 and the pD was 7.0. The total V-concentrations for 1.0 mL [VO(Hshed)(dtb)] RM samples are as follows: w_0 20, 2.46 mM; w_0 16, 5.23 mM; w_0 12, 11.09 mM; w_0 8, 23.55 mM; w_0 6, 36.78 mM.

(Fig. 4). There is a chemical shift change observed for H_2shed protons H_a, H_b, H_c, H_d, and H_k, which also showed a change in the chemical environment and supported a significant interaction of the H_2shed ligand with the RM interface (Fig. 5).

NMR spectra of [VO(Hshed)(dtb)] in aqueous solution and in RM samples

^{51}V NMR spectra were recorded to determine if the [VO(Hshed)(dtb)] complex hydrolyzed in aqueous solution and within RMs. This was non-trivial considering the low solubility of the complex in aqueous solution; therefore, these samples were prepared by dissolving the compound into the AOT/*iso*-octane stock solution rather than in the D_2O stock solution. The equilibrium for the hydrolysis products was observed in a saturated [VO(Hshed)(dtb)]/D_2O sample that was sonicated for 5 min, then vortexed for ~1 min, and then allowed to sit for 60 min (Fig. 6). [VO(Hshed)(dtb)] hydrolyzed to form [$V(O)_2$(Hshed)] first and further hydrolysis formed vanadate and the H_2shed ligand according to eqn (3) and (4). The sample in d_6-DMSO (Fig. 6) contained three signals for [VO(Hshed)(dtb)], the major peak signal is consistent with the literature[66] and in addition we also observed two minor peaks, which we attribute to association and concentration phenomena. When placed in RMs, the equilibration was established slightly faster in this system (~50 min) after which time point the spectra no longer changed.

$$[\mathrm{VO(Hshed)(dtb)}] + \mathrm{H_2O} \rightarrow [\mathrm{V(O)_2(Hshed)}] + \mathrm{H_2dtb} \quad (3)$$

$$[\mathrm{V(O)_2(Hshed)}] + 3\mathrm{H_2O} \rightarrow \mathrm{SalA} + \mathrm{HyDAH^+} + \mathrm{H_2VO_4^-} \quad (4)$$

The ^{51}V NMR spectra recorded for [VO(Hshed)(dtb)] in d_6-DMSO, D_2O, and in RMs (RMs (w_0 = 6, 8, 12, 16, and 20)) are shown in Fig. 6. The spectrum in d_6-DMSO shows three signals (see above). No complex is observed in the D_2O spectrum documenting that this compound is not soluble but does form vanadate oligomers when attempting to dissolve the material. In the RM samples, more vanadate oligomers, possibly a little [$V(O)_2$(Hshed)], and two signals, which are attributed to the [VO(Hshed)(dtb)] complex are observed (Fig. 6). Both ^{51}V and ^{1}H NMR spectra confirm that in RMs at a higher concentration of the complex, more [VO(Hshed)(dtb)] is observed than in pure D_2O. When placing [VO(Hshed)(dtb)] in RMs, some of the complex hydrolyzed, and there was a large change in chemical shifts from the d_6-DMSO sample and the distribution of signals varied depending on the size of the RM. This suggests that the [VO(Hshed)(dtb)] complex is in an environment different from aqueous solution. As the size of the RM changed, the chemical shifts did not significantly change, consistent with the possibility that the compound is in similar environments in different sized RMs. These results are consistent with an interpretation that the stability of the [VO(Hshed)(dtb)] complex increases through association or interactions with the interface and although still separated from the water pool, the water reaches the complex, initiating the hydrolysis of [VO(Hshed)(dtb)] and resulting in the formation of vanadate oligomers and [$V(O)_2$(Hshed)] (Fig. 6). As the RM size increases, the extent of hydrolysis increases because the [VO(Hshed)(dtb)] complex signal decreases and an increase in oligomers formed is observed (as evidenced by the changes in the speciation).[68]

The ^{1}H NMR spectra of [VO(Hshed)(dtb)] in D_2O, d_6-DMSO, and various sized RMs were recorded (see ESI Fig. S1‡). The spectrum in D_2O does not show all the proton peaks present in the [VO(Hshed)(dtb)] complex due to limited solubility of the complex; however, the ligand of the complex was also hydrolyzed as evidenced by an aldehyde peak at 10.04 ppm in

Published on 14 March 2019. Downloaded on 5/16/2019 4:36:17 PM.

D_2O and at 9.91 ppm in RMs. These peaks are not present in the d_6-DMSO spectrum. There is a chemical shift change for [VO(Hshed)(dtb)] aromatic protons H_b, H_d, H_e, and H_f, which showed a change in the environment of the complex and supported the interpretation based on the ^{51}V NMR spectra of an association and possible penetration of the complex into the RM interface. Combined, these studies show that the aqueous insoluble [VO(Hshed)(dtb)] complex can solubilize and partition in a heterogeneous environment, but such an environment also facilitates increased hydrolysis of the complex and its Schiff base ligand.

NMR spectra of [VO(Hshed)(cat)] in aqueous solution and in RM samples

^{51}V NMR spectra were recorded as a function of time to determine if the [VO(Hshed)(cat)] complex hydrolyzed after it was dissolved in aqueous solution, as well as in AOT/*iso*-octane RMs (Fig. 7). The solubility of [VO(Hshed)(cat)] was limited in aqueous solution; therefore, ~1 min of vortexing was needed to prepare a saturated sample of [VO(Hshed)(cat)] in D_2O. This system also had the potential of forming $[V(O)_2(Hshed)]$ and the H_2shed ligand according to eqn (5) and (6).

$$[VO(Hshed)(cat)] + H_2O \rightarrow [V(O)_2(Hshed)] + H_2dtb \quad (5)$$

$$[V(O)_2(Hshed)] + 3H_2O \rightarrow SalA + HyDAH^+ + H_2VO_4^- \quad (6)$$

[VO(Hshed)(cat)] was dissolved in d_6-DMSO and in aqueous solution as well as in AOT/*iso*-octane RMs. By ^{51}V NMR, it was found that no [VO(Hshed)(cat)] remained in the D_2O solution or the RM mixture and intact [VO(Hshed)(cat)] was observed only in d_6-DMSO (Fig. 7). These results suggest that the equilibrium favors complex hydrolysis upon dissolution in D_2O and that the energetics are not sufficiently favorable for the complex to reform in RM samples. ^1H NMR spectra show that the H_2shed ligand from the complex does hydrolyze more slowly, because some C=NH signal remains in w_0 8–12 samples (see Fig. S2‡). These studies do confirm that the [VO(Hshed)(cat)] complex has significantly different properties than the [VO(Hshed)(dtb)] complex.

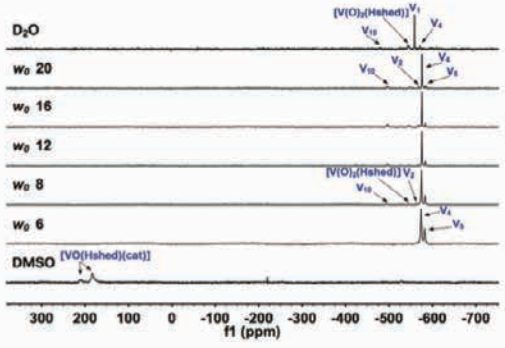

Fig. 7 ^{51}V NMR spectra of [VO(Hshed)(cat)] in D_2O and in a series of RMs (w_0 = 6, 8, 12, 16, and 20 prepared from 0.750 M AOT/*iso*-octane stock solution). The spectra were recorded after equilibration was reached after 50 min for D_2O samples and after 40 min for RM samples. The pH for D_2O and RMs was 6.6 and the pD was 7.0. The total V-concentrations for 1.0 mL [VO(Hshed)(cat)] RM samples are as follows: w_0 20, 2.41 mM; w_0 16, 5.17 mM; w_0 12, 11.05 mM; w_0 8, 23.53 mM; and w_0 6, 36.72 mM.

Examining the AOT/*iso*-octane RMs containing H_2shed, $[V(O)_2(Hshed)]$, [VO(Hshed)(cat)] and [VO(Hshed)(dtb)] using dynamic light scattering

To determine if RMs formed in the AOT/RM samples, w_0 12 and w_0 20 RM samples were investigated using Dynamic Light Scattering (DLS). In Table S1,‡ the RM samples are listed with the no cargo, with H_2shed, with $[V(O)_2(Hshed)]$, with [VO(Hshed)(cat)] or with [VO(Hshed)(dtb)]. The results show that AOT/*iso*-octane RM structures form in all cases and that the sizes are comparative with literature values.[69] Furthermore, there were no significant differences observed between the hydrodynamic radii of the empty RM samples and those containing cargo. This suggests that no significant changes in the structures of the RMs are induced upon placement of any of the probe molecules inside the RMs.

The anticancer effects of V(v) catecholate complexes on bone cancer cells (SW1353 cells)

The hydrophobicity of the [VO(Hshed)(dtb)] complex enhances complex stability to hydrolysis and thus increases the ability of the compound to enter the cells intact. The question whether increased uptake due to hydrophobicity will be reflected in increased cytotoxicity was investigated in human chondrosarcoma cells, SW1353. However, before these studies were carried out, we determined the stability of the compounds in cell culture media (advanced DMEM, supplemented with 2.0 vol% of fetal calf serum and 10 mM of HEPES buffer to maintain pH = 7.4 under an ambient atmosphere)[70] using electronic absorption spectroscopy, because both [VO(Hshed)(cat)] and [VO(Hshed)(dtb)] showed strong absorbance bands in the visible and near-IR range in accord with the literature.[66]

As shown in Fig. 8, the electronic absorption spectra of the [VO(Hshed)(dtb)] complex show an intact complex in DMSO and fresh media (DMSO shown with black lines in Fig. 8; fresh media with red lines). Although the complex is intact in DMSO, the [VO(Hshed)(dtb)] complex is only partially stable over time in cell media where it ultimately undergoes hydrolysis. However, after 24 h the [VO(Hshed)(dtb)] complex had degraded (shown with green lines in Fig. 8). In contrast, the addition of [VO(Hshed)(cat)] (0.10 mM V-complex) to cell culture medium instantly caused the disappearance of the characteristic absorbance bands of the complex at ~530 nm and ~870 nm (red line in Fig. 8a). The [VO(Hshed)(cat)] complex is, therefore, much less stable compared to the [VO(Hshed)(dtb)] complex. These results are consistent with the results by NMR spectroscopic studies described above (Fig. 6

This journal is © The Royal Society of Chemistry 2019

Published on 14 March 2019. Downloaded on 5/16/2019 4:36:17 PM.

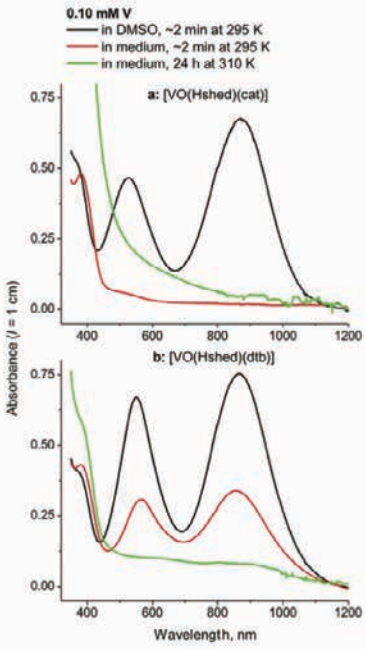

Fig. 8 Representative absorption spectra of fresh (2 min after dissolution) and aged (24 h after dissolution) (a) [VO(Hshed)(cat)] and (b) [VO(Hshed)(dtb)] (0.10 mM V-compound) in DMSO solutions or in cell culture medium (advanced DMEM, containing 2.0 vol% of fetal calf serum and 10 mM HEPES buffer, pH 7.4).

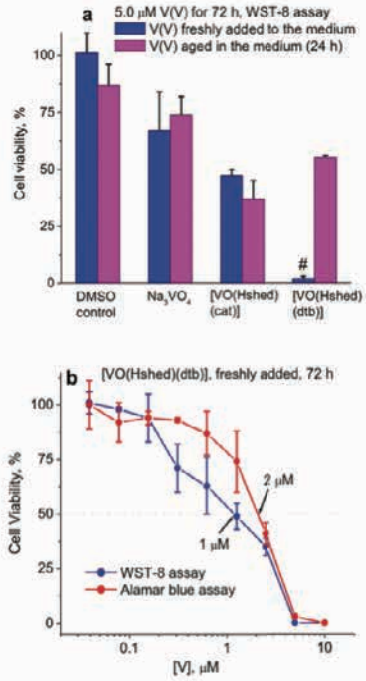

Fig. 9 Anti-proliferative activity of [VO(Hshed)(cat)], [VO(Hshed)(dtb)] and Na_3VO_4 in human chondrosarcoma (SW1353) cells: (a) comparative effects of V(v) complexes at 5.0 μM V; and (b) concentration-dependent effects for fresh solutions of [VO(Hshed)(dtb)]. Treatment media were added to cells either within 1 min after the addition of V(v) complexes (fresh media), or pre-incubated with the V(v) complexes for 24 h at 310 K and 5% CO_2 before the addition to cells (aged media). In both cases, the cells were treated for 72 h (310 K, 5% CO_2) before the determination of cell viability by endpoint colorimetric assays (WST-8 or Alamar Blue). All the treatments, including controls, contained 0.50 vol% DMSO. Error bars represent the mean values and standard deviations of six replicate wells. The # sign shows highly significant difference ($P < 0.001$) in activity between fresh and decomposed solutions of [VO(Hshed)(dtb)].

and 7). Both complexes decomposed after 24 h incubation with the cell culture medium at 310 K. The following cell culture studies were, therefore, carried out with both fresh and aged solutions. This allowed us to compare the effects over time for the two different V(v) Schiff base/catecholate compounds and vanadate in bone cancer cells (human chondrosarcoma, SW1353 cells). This also permitted us to explore when [VO(Hshed)(dtb)] was still intact and when both complexes were hydrolysed.

Initial experiments on the anti-proliferative activities of the [VO(Hshed)(cat)] and [VO(Hshed)(dtb)] complexes in SW1353 cells (Fig. 9a) were carried out with the consideration of their different hydrolysis rates in aqueous solutions, in cell culture media and in artificial membrane systems (Fig. 6–9). Stock solutions of both complexes in DMSO, which were stable for at least 24 h under ambient conditions (verified by electronic absorption spectroscopy, Fig. 8) were added to cell culture medium to the required final concentrations (typically, 5.0 μM V). The resultant medium was either immediately added to the cells within 1 min (fresh medium), or allowed to age for 24 h (310 K, 5% CO_2) prior to addition to the cells.[33,70] Vanadate (Na_3VO_4, either fresh or aged in the medium) was used as a reference compound.[32] Previous studies by XANES spectroscopy[35] and EPR spectroscopy[71] have shown that vanadate converts to a mixture of V(v) (predominantly) and V(iv) complexes with medium components upon aging. As shown in Fig. 9a, [VO(Hshed)(cat)] was moderately active at 5.0 μM V-complex (cell viability after 72 h treatment was 40–50% of control), while Na_3VO_4 added to the media resulted in 70–75% of the control. For [VO(Hshed)(cat)] and vanadate, no significant difference in anti-proliferative activity was observed between fresh and aged solutions in cell culture medium.

The [VO(Hshed)(dtb)] complex showed much stronger anti-proliferative activity when freshly added to the medium (only ~2% of control), compared with the aged solution (50–60% of control) (Fig. 9a). Furthermore, compared to the less hydrophobic [VO(Hshed)(cat)] complex, or the ionic vanadate, the

Published on 14 March 2019. Downloaded on 5/16/2019 4:36:17 PM.

fresh solution of the more hydrophobic and intact [VO(Hshed)(dtb)] complex was significantly more potent. As a result, we were interested in exploring the anti-proliferative activity of [VO(Hshed)(dtb)] further. Concentration-dependent studies of fresh [VO(Hshed)(dtb)] solutions using two different assays for cell viability, WST-8[72] and Alamar Blue,[73] gave consistent results with IC_{50} = 1.3 ± 0.3 μM V-complex and a plateau is seen at high V-concentrations (5–10 μM) (Fig. 9b). This level of activity is similar or higher compared to that of well-established Pt(II) anti-cancer drugs in typical human cancer cell lines (IC_{50} ~1–5 μM Pt).[74] Taken together, data from Fig. 6–8 show that the higher stability of [VO(Hshed)(dtb)] compared with [VO(Hshed)(cat)] in cell culture medium and in the hydrophobic environment of cell membranes is likely to lead to its significant cellular uptake before hydrolysis in aqueous medium is complete.[75] The observed higher cytotoxicity of fresh solutions in cell culture medium compared to aged ones correlates with the greater stability of the [VO(Hshed)(dtb)] complex. High hydrolysis rates of [VO(Hshed)(cat)] in cell culture medium (Fig. 8) are likely to prevent cellular uptake of the intact complex, which means that the anti-proliferative activity is due to decomposition products as has been recognized previously in multiple biological systems.[4,10,32,76–83] A similar relation between aqueous stability, cellular uptake and anti-proliferative activity was observed previously for Ru complexes.[84,85] We conclude that the increased hydrophobicity and steric bulk of the dtb catechol ligand is preventing early hydrolysis leading to the enhanced cellular uptake of the intact [VO(Hshed)(dtb)] complex.

Discussion

Numerous studies were carried out with different V-compounds exploring the mode of action and the identity of the active species when V-compounds were considered for the treatment of diabetes.[4,56,80,86,87] It is well-known that V-compounds are protein tyrosine phosphatase inhibitors,[56,88,89] however, much work has been done on the transport of V-compounds from the administration site to the site of action.[39,90–92] Specifically, studies have been carried out exploring the transport of V-compounds in blood,[37,38,91,93,94] and the speciation of these compounds[13,56,95] has been investigated in detail both in model systems,[38,94] in blood,[37,91,93] in animal model studies[96] and in human studies.[11] The interaction of V-compounds with transferrin, human serum albumin or other blood components has demonstrated that V-compounds can lose one or more of their ligands and remain active.[37,91,93,97] How the vanadium complexes enter cells and what properties dictate the efficacy of transport through cell membranes remain important questions.

These studies have shown that the interface dramatically impacted the stability of the vanadium precursor complex, $[V(O)_2(Hshed)]$, as well as two hydrophobic vanadium complexes, [VO(Hshed)(cat)] and [VO(Hshed)(dtb)]. Both ternary mixed-ligand complexes are soluble in polar organic solvents, such as DMSO, and less soluble in nonpolar organic solvents (*e.g.*, 2,2,4-trimethylpentane). However, the inhomogeneous environment of a microemulsion supports these complexes even if they have been hydrolyzed in the presence of interfacial water. Based on the NMR spectroscopic studies presented in this work, the interaction with the RM interface protects the V-compound against rapid initial hydrolysis. The slow hydrolysis effect was more pronounced for the more sterically-hindered hydrophobic dtb ligand. This effect could be due to sterics or hydrophobicity of the ligand or a combination of both, and studies with additional compounds will shed light on the origin of this observation. Alternatively, it may be possible that pK_a values of the catechols can affect the inherent thermodynamic stability of the coordination complexes. The pK_a value of the parent catechol is higher than that of the *t*-butyl substituted catechol and thus, the coordinated complex of the latter would be more stable. Initial V-complex stability may be important for the anti-cancer activity of the compounds as shown by the study in human bone cancer cells (chondrosarcoma). The anti-cancer effects reduce with decreased hydrophobicity and decreased hydrolytic stability of the V-complexes. Future studies with additional related V-compounds will shed further light on the exact origin of the anti-cancer effects.

The kinetic stability of [VO(Hshed)(dtb)] in water and aqueous media is unusual for a V-complex but in this case provides sufficient stability to enable this complex to enter the cancer cells intact. The hydrophobic environment of the cell membrane is likely to further stabilize this compound.[40] This unusual short-term stability of this highly cytotoxic complex may show considerable promise in cancer treatment, particularly against aggressive cancers such as prostate cancer. Since such hydrophobic complexes are likely to undergo cellular uptake *via* passive diffusion through the cell membrane, it is important to investigate if hydrophobicity or hydrolytic stability of these compounds correlates with uptake in membrane model systems.

The results presented here with two different hydrophobic catecholate complexes based on studies in the AOT-*iso*-octane microemulsion system show that although the [VO(Hshed)(dtb)] complex may be stabilized, the membrane system is not able to completely prevent hydrolysis from the water penetrating the interface. If a complex remains intact for some limited time, this will allow the drug to reach the cellular target intact. Importantly, the current results show that the intact complexes indeed interact with the interface and, hence, the results are consistent with the observation of increased cytotoxicity of fresh *versus* aged drug preparation. That is, the freshly prepared solution contains more intact complex and the hydrolyzed aged solution contains less intact complex. Accordingly, the solution with more intact [VO(Hshed)(dtb)] complex is much more cytotoxic compared to the aged solution with a degraded V-complex towards the bone cancer cells investigated. Importantly, the results with the aged solutions show a dramatically decreased cytotoxic effect for both V-complexes against SW1353 bone cancer cells, consistent with the free

This journal is © The Royal Society of Chemistry 2019

Published on 14 March 2019. Downloaded on 5/16/2019 4:36:17 PM.

ligands having no significant cytotoxicity (free ligands alone are significantly less cytotoxic (unpublished data)).

Given the fact that humans are largely composed of water and cell assay studies generally are carried out using water-based approaches, the administration of hydrophobic drugs remains a challenge. However, there are ways of delivering a drug into the body that does not require water solubility but in the case of these very hydrophobic drugs, cell assays in aqueous solution remains problematic. The studies described herein may imply that hydrophobic metallo-compounds with increased hydrolytic stability will continue to be of interest and suggest that alternative approaches for effective drug delivery that will circumvent significant decomposition should be developed.

Conclusions

The [VO(Hshed)(cat)] complex is found to have lower thermodynamic stabilities in both water and cell culture medium compared to the [VO(Hshed)(dtb)] complex. Although the complexes show limited stability in the presence of membrane model systems, this may be a consequence of the pre-equilibrium that resulted in partial hydrolyzed complex(es). The greater cytotoxic activities are observed in fresh solutions of V-catecholate complexes containing higher amounts of the intact compound in *in vitro* cytotoxicity assays in bone cancer cells and are in line with additional studies in MDA-MB-231 and PANC-1 cells.[40] Importantly, the membrane model results shown here demonstrate that the intact V(v) catecholate complexes will penetrate the membrane, which supports the cell cytotoxicity assays which indicate that the intact complexes are taken up before they are decomposed in the cell medium.

In summary, the hydrophobic V(v) catecholate compounds presented here are found to interact with a model membrane systems and the V-complex with the highest stability is found to have the most potent anti-cancer properties. It is possible that complexes containing hydrophobic ligands with a sterically hindered V-atom preventing substitution reactions may enable the uptake of the intact complex and delivery to the cellular target. Alternatively, similar behavior could arise from different thermodynamic stabilities. Regardless of the origin, the hydrophobic V(v) catecholate complexes were found to be particularly potent cytotoxins to bone cancer cells. These results warrant future studies of these and similarly stable hydrophobic vanadium compounds as potential anti-cancer agents.

Experimental section

Chemicals, biochemicals, and general methods

Most reagents were used without further purification including 2,2,4-trimethyl-pentane (*iso*-octane, Sigma-Aldrich, ≥99.0%), deuterium oxide (D_2O, Cambridge Isotope Laboratories, 99.9%), acetone HPLC grade, *n*-pentane, and argon. Sodium bis(2-ethylhexyl)sulfosuccinate (AOT, Sigma-Aldrich, 99.8%) was purified using activated charcoal and methanol to remove acidic impurities using a modified procedure of that previously reported (see below).[10,98,99] Salicylaldehyde (SalA) was purified *via* vacuum distillation to remove impurities prior to synthesis. [$V(O)_2$(Hshed)], H_2shed, [VO(Hshed)(cat)], and [VO(Hshed)(dtb)] were prepared according to the literature procedures.[65–67] All pH measurements were conducted using a Thermo Orion 2 Star pH meter with a VWR semi-micro pH probe.[86] When samples were prepared for RM or D_2O NMR experiments, deuterium oxide was used instead of H_2O and the pH was adjusted to consider the presence of deuterium (pD = pH + 0.4); therefore, we report values for both pD and pH for clarity.[99,100] Pre-sterilized media and sterile plasticware used in cell culture were purchased from Life Technologies Australia. Human chondrosarcoma SW1353 cells were purchased from the American Type Culture Collection (ATCC, cat. no. HTB-94) and cultured using standard techniques[101,102] in advanced DMEM (where DMEM = Dulbecco's modified Eagle's medium; Thermo Fischer Scientific, cat. no. 12491-015). Abbreviations are as follows: aot, bis(2-ethylhexyl)sulfosuccinate sodium salt; cat, catecholate; dtb, di-*tert*-butylcatecholate; DLS, dynamic light scattering; HEPES, (4-(2-hydroxyethyl)-1-piperazine-ethanesulfonic acid; H_2shed, condensation product of salicylaldehyde and *N*-(2-hydroxyethyl)-1,2-ethanediamine; pdi, polydispersity index; SalA, salicylaldehyde; HyDA, *N*-(2-hydroxyethyl)-1,2-ethanediamine; CCR2, CC chemokine receptor 2; CCL2, CC chemokine ligand 2; CCR5, CC chemokine receptor 5.

Purification of NaAOT

NaAOT was purified by a slightly modified procedure from that reported previously.[43,103] AOT (60.0 g) was dissolved in methanol (150 mL) and the solution was shaken for a period of two weeks in the presence of mesh activated charcoal (15.0 g).[43,103] The suspension was then vacuum filtered through a bed of Celite and then the methanol was removed, first *via* rotary evaporation under reduced pressure at room temperature and then *via* high vacuum (~150 milliTorr) until the desired dryness was achieved. The residual water content ranged from 0.019 to 0.300 waters per AOT and was measured as previously reported.[41]

Preparation of AOT/*iso*-octane stock solution and RM samples

The 750 mM AOT/*iso*-octane stock solution was prepared by dissolving AOT (8.333 g, 18.80 mmol) in *iso*-octane in a volumetric flask (25.00 mL), vortexing until clear, and then diluting to the mark. For all six probe molecules studied, a 52.75 mM stock solution was used to prepare RM containing suspensions. The stock solution was prepared by dissolving the probe molecule (0.5275 mmol) in 750 mM AOT/*iso*-octane stock in a volumetric flask (10.00 mL), mixing until solubilized, and then diluting to the mark. The probe AOT/*iso*-octane stock solutions containing either vanadium or the H_2shed ligand were mixed by hand and not vortexed to have as little outside impact on hydrolysis as possible. Before the preparation of 1 mL RM samples, 2 mL solutions of varying concentrations of probe

Published on 14 March 2019. Downloaded on 5/16/2019 4:36:17 PM.

stock were created by diluting various aliquots of 52.75 mM probe stock with 750 mM AOT/*iso*-octane stock. Then, 1 mL RM samples (w_0 = 6, 8, 12, 16, and 20) were prepared by diluting specific aliquots of 2 mL solutions with various amounts of D_2O (pH = 6.6, pD = 7.0, see general methods for pH measurements). The addition of D_2O resulted in the formation of a white flocculent at the bottom of the samples and, when shaken, a homogeneous solution resulted. For the free H_2cat and H_2dtb ligand RM samples, NMR studies were performed immediately after preparation while the free H_2SHED ligand, [$V(O)_2$(Hshed)], [VO(Hshed)(dtb)], and [VO(Hshed)(cat)] RM samples were allowed to equilibrate before the NMR spectroscopic studies were performed. The total V-concentrations for 1.0 mL [$V(O)_2$(Hshed)] RM samples are as follows: w_0 20, 2.41 mM; w_0 16, 5.17 mM; w_0 12, 11.05 mM; w_0 8, 23.53 mM; and w_0 6, 36.72 mM. The overall concentrations for 1.0 mL H_2shed RM samples are as follows: w_0 20, 2.71 mM; w_0 16, 5.65 mM; w_0 12, 11.77 mM; w_0 8, 24.48 mM; and w_0 6, 37.87 mM. The total V-concentrations for 1.0 mL [VO(Hshed)(dtb)] RM samples are as follows: w_0 20, 2.46 mM; w_0 16, 5.23 mM; w_0 12, 11.09 mM; w_0 8, 23.55 mM; w_0 6, 36.78 mM. The total V-concentrations for 1.0 mL [VO(Hshed)(cat)] RM samples are as follows: w_0 20, 2.41 mM; w_0 16, 5.17 mM; w_0 12, 11.05 mM; w_0 8, 23.53 mM; w_0 6, 36.72 mM.

Stability of the probe in aqueous solution and RMs

The stability of the precursor complex [$V(O)_2$(Hshed)], vanadium(v) catecholates [VO(Hshed)dtb] and [VO(Hshed)cat], and the free ligand H_2shed in aqueous solution was determined by solution NMR spectroscopy. NMR measurements of the hydrolysis of each probe molecule in D_2O (pH = 6.6, pD = 7.0, see general methods for pH measurements) were carried out until the probe molecule had reached equilibrium as evidenced by the NMR peak integrations changing over time. Similar equilibrium stability measurements were carried out for each V-compound in a w_0 = 12 RM. Once the equilibrium had been determined for each probe molecule in a RM system, complete RM studies were performed at the determined equilibrium time point.

^{1}H and ^{51}V NMR spectroscopic studies on RM samples

All ^{51}V solution NMR spectra were recorded on a Varian 400MR NMR spectrometer with a spectral window of −700 ppm to 700 ppm, 4096 scans, RD = 0.001 s, and 90° pulse angle at 26 °C. The ^{1}H NMR spectroscopic experiments on the RMs were performed using a 400 MHz Varian iNova NMR spectrometer or a 400 MHz MR400 spectrometer, using standard parameters at 22 or 26 °C, respectively. The 1D ^{1}H NMR spectra in $CDCl_3$ or d_6-DMSO were referenced to the internal solvent peak at 7.26 ppm and 2.50 ppm, respectively. The 1D ^{1}H NMR spectra in RMs were referenced to the *iso*-octane methyl peak (0.904 ppm) as previously reported.[99] ^{51}V solution chemical shifts in DMSO are determined relative to the external neat liquid $VOCl_3$ reference (0.00 ppm).[104] ^{51}V solution chemical shifts in D_2O or RMs are measured relative to an external 1 M sodium metavanadate reference (pH = 12) which, in aqueous solution, produces two signals at −535.7 ppm (used as auxiliary reference) and −560.4 ppm, relative to $VOCl_3$.[105] Spectral data were processed using MestReNova NMR processing software version 10.0.1.

RM sample preparation for dynamic light scattering (DLS) studies

RMs for DLS studies were prepared in a similar manner to those used for the NMR spectroscopic experiments except that distilled deionized (DDI) H_2O (pH = 6.6) was used as the water pool instead of D_2O, and 0.750 M AOT/RM solution was diluted to a 0.1 M AOT/RM solution with *iso*-octane after the RMs were formed.

DLS measurements

The hydrodynamic radius of w_0 = 12 and w_0 = 20 RMs was determined by DLS measurements performed on a Malvern Zetasizer Nano ZS instrument (Malvern Instruments, Malvern, UK). The DLS cuvette (1 cm × 1 cm, glass) was washed three times with *iso*-octane followed by three washes with the RM sample (prepared at pH 6.6). Then, the cuvette was filled with 1 mL of the RM sample and closed with a Teflon cap. Each experiment was conducted at 25 °C and consisted of a 700 s sample equilibration period followed by 10 measurements each made of 15 scans.[106] Each sample was measured in triplicate, and the diameter and pdi were recorded and compared to those values in the literature.[69] The data were analyzed using Malvern DLS software. See the ESI.‡

Stability studies by electronic absorption spectroscopy

Freshly prepared stock solutions of [VO(Hshed)(cat)] or [VO(Hshed)(dtbc)] (10 mM V-complex in DMSO) were diluted 100-fold either with DMSO or with cell culture medium (advanced DMEM, containing 2.0 vol% of fetal calf serum and 10 mM HEPES buffer, pH 7.4).[30] The spectra in the 350–1200 nm range (resolution, 1 nm; acquisition rate, 600 nm min^{-1}) were acquired on an Agilent Cary 5000 spectrometer at 295 K. The corresponding solvents were used in background scans.

Cytotoxicity experiments

Advanced DMEM medium (Thermo Fisher Scientific cat. no. 12491-015, where DMEM = Dulbecco's modified Eagle's medium) was supplemented with L-glutamine (2.0 mM), antibiotic–antimycotic mixture (100 U mL^{-1} penicillin, 100 mg mL^{-1} streptomycin and 0.25 mg mL^{-1} amphotericin B) and fetal calf serum (FCS; heat-inactivated; 2 vol%). For proliferation experiments, the cells were seeded in 96-well plates at an initial density of 1.0 × 10^3 viable cells per well (counted using Invitrogen Countess device with trypan blue staining)[101,102] in 100 μL medium and left to attach overnight. Freshly prepared 10 mM stock solutions in DMSO ([VO(Hshed)(dtb)] or [VO(Hshed)(cat)]) or in Milli-Q H_2O (Na_3VO_4, 99.98%, Aldrich cat. no. 450243) were used for cell assays. All the cell treatments, including controls, contained 0.50 vol% of DMSO.[107] Stock solutions of the treatment compounds were diluted with fully

This journal is © The Royal Society of Chemistry 2019

Published on 14 March 2019. Downloaded on 5/16/2019 4:36:17 PM.

supplemented cell culture media to the required final concentrations, and the resultant media were either added to the cells within one minute (fresh solutions) or left in the cell culture incubator (310 K, 5% CO_2) for 24 h prior to the cell treatments (aged solutions). For end-point viability assays, the cells were incubated with fresh or aged treatment compounds for 72 h, after which WST-8 reagent (cell counting kit-8, Dojindo Molecular Technologies) or Alamar Blue reagent (Thermo Fisher Scientific cat. no. DAL1025) was added at 10 μL per well. The cells were then further incubated for six hours, and the absorbance at 450 nm (WST-8) or fluorescence at 570/585 nm (Alamar Blue) was measured using a Victor V^3 multiwell plate reader. For each treatment, six replicate cell-containing wells and two background wells (containing all the components except cells) were used, and statistical analysis of the data was performed using Origin software.[108] Preliminary calibration experiments with WST-8 assay have shown that the A_{450} values in the entire working range (0.25–1.5) were linearly dependent on the number of viable SW1353 cells ($\sim 10^2$–10^4 cells per well).

Conflicts of interest

There are no conflicts to declare.

Acknowledgements

DCC and PAL thank the University of Sydney for an International Scholar Award to DCC. SMP and DCC thank the NSF REU (CHE-1461040) for summer support to SMP. DCC also thanks the Arthur Cope Foundation Administered by the American Chemical Society for partial support. Financial support for this work was also provided by the Australian Research Council (ARC) grants to PAL including support for an ARC Senior Research Associate position to AL (DP130103566, DP160104172).

References

1 S. E. Sherman and S. J. Lippard, *Chem. Rev.*, 1987, **87**, 1153–1181.
2 A. M. Evangelou, *Crit. Rev. Oncol. Hematol.*, 2002, **42**, 249–265.
3 N. Farrell, *Met. Ions Biol. Syst.*, 1996, **32**, 603–639.
4 J. C. Pessoa, S. Etcheverry and D. Gambino, *Coord. Chem. Rev.*, 2015, **301**, 24–48.
5 X. Yang and K. Wang, *Curr. Top. Med. Chem.*, 2016, **16**, 675–676.
6 S. Petanidis, E. Kioseoglou, K. Domvri, P. Zarogoulidis, J. M. Carthy, D. Anestakis, A. Moustakas and A. Salifoglou, *Int. J. Biochem. Cell Biol.*, 2016, **74**, 121–134.
7 A. P. Vieira, C. A. Wegermann and A. M. Da Costa Ferreira, *New J. Chem.*, 2018, **42**, 13169–13179.
8 K. Gruzewska, A. Michno, T. Pawelczyk and H. Bielarczyk, *J. Physiol. Pharmacol.*, 2014, **65**, 603–611.
9 D. Rehder, J. C. Pessoa, C. Geraldes, M. Castro, T. Kabanos, T. Kiss, B. Meier, G. Micera, L. Pettersson, M. Rangel, A. Salifoglou, I. Turel and D. R. Wang, *J. Biol. Inorg. Chem.*, 2002, **7**, 384–396.
10 K. H. Thompson, J. Lichter, C. LeBel, M. C. Scaife, J. H. McNeill and C. Orvig, *J. Inorg. Biochem.*, 2009, **103**, 554–558.
11 G. R. Willsky, K. Halvorsen, M. E. Godzala III, L.-H. Chi, M. J. Most, P. Kaszynski, D. C. Crans, A. B. Goldfine and P. J. Kostyniak, *Metallomics*, 2013, **5**, 1491–1502.
12 D. C. Crans, L. Yang, A. A. Haase and X. Yang, *Met. Ions Life Sci.*, 2017, **18**, 251–280.
13 D. C. Crans, K. A. Woll, K. Prusinskas, M. D. Johnson and E. Norkus, *Inorg. Chem.*, 2013, **52**, 12262–12275.
14 C. A. Lipinski, F. Lombardo, B. W. Dominy and P. J. Freeney, *Adv. Drug Delivery Rev.*, 2001, **46**, 3–26.
15 P. Köpf-Maier, *Met. Complexes Cancer Chemother.*, 1993, 259–296.
16 P. Ghosh, O. J. D'Cruz, R. K. Narla and F. M. Uckun, *Clin. Cancer Res.*, 2000, **6**, 1536–1545.
17 I. Kostova, *Anti-Cancer Agents Med. Chem.*, 2009, **9**, 827–842.
18 I. León, N. Butenko, A. Di Virgilio, C. Muglia, E. Baran, I. Cavaco and S. Etcheverry, *J. Inorg. Biochem.*, 2014, **134**, 106–117.
19 I. León, J. Cadavid-Vargas, A. Di Virgilio and S. Etcheverry, *Curr. Med. Chem.*, 2017, **24**, 112–148.
20 B. I. Posner, A. Shaver and I. G. Fantus, in *New Antidiabetic Drugs*, ed. C. J. Bailey and P. R. Flatt, Smith-Gordon, London, 1990, ch. 8, pp. 107–118.
21 M. Li, W. Ding, B. Baruah, D. C. Crans and R. Wang, *J. Inorg. Biochem.*, 2008, **102**, 1846–1853.
22 L. P. Lu and M. L. Zhu, *Anti-Cancer Agents Med. Chem.*, 2011, **11**, 164–171.
23 D. C. Crans, M. L. Tarlton and C. C. McLauchlan, *Eur. J. Inorg. Chem.*, 2014, 4450–4468.
24 C. C. McLauchlan, B. J. Peters, G. R. Willsky and D. C. Crans, *Coord. Chem. Rev.*, 2015, **301–302**, 163–199.
25 L. Reytman, O. Braitbard, J. Hochman and E. Y. Tshuva, *Inorg. Chem.*, 2016, **55**, 610–618.
26 H. Glasner, S. Meker and E. Y. Tshuva, *J. Organomet. Chem.*, 2015, **788**, 33–35.
27 S. Clede, F. Lambert, R. Saint-Fort, M.-A. Plamont, H. Bertrand, A. Vessieres and C. Policar, *Chem. – Eur. J.*, 2014, **20**, 8714–8722.
28 P. Khosravi-Shahi, L. Cabezón-Gutiérrez and S. Custodio-Cabello, *Asia-Pac. J. Clin. Oncol.*, 2018, **14**, 32–39.
29 I. Correia, L. Chorna, I. Cavaco, S. Roy, M. L. Kuznetsov, N. Ribeiro, G. Justino, F. Marques, T. Santos-Silva, M. F. A. Santos, H. M. Santos, J. L. Capelo, J. Doutch and J. C. Pessoa, *Chem. – Asian J.*, 2017, **12**, 2062.
30 A. Levina, D. C. Crans and P. A. Lay, *Coord. Chem. Rev.*, 2017, **325**, 473–498.
31 A. Levina and P. A. Lay, *Dalton Trans.*, 2011, **40**, 11675–11686.

Published on 14 March 2019. Downloaded on 5/16/2019 4:36:17 PM.

32 A. Levina and P. A. Lay, *Chem. – Asian J.*, 2017, **12**, 1692–1699.
33 M. Le, O. Rathje, A. Levina and P. A. Lay, *J. Biol. Inorg. Chem.*, 2017, **22**, 663–672.
34 A. Levina, A. I. McLeod, S. J. Gasparini, A. Nguyen, W. G. M. De Silva, J. B. Aitken, H. H. Harris, C. Glover, B. Johannessen and P. A. Lay, *Inorg. Chem.*, 2015, **54**, 7753–7766.
35 A. Levina, A. I. McLeod, A. Pulte, J. B. Aitken and P. A. Lay, *Inorg. Chem.*, 2015, **54**, 6707–6718.
36 D. Sanna, V. Ugone, M. Serra and E. Garribba, *J. Inorg. Biochem.*, 2017, **173**, 52–65.
37 D. Sanna, V. Ugone, G. Micera, P. Buglyo, L. Biro and E. Garribba, *Dalton Trans.*, 2017, **46**, 8950–8967.
38 D. Sanna, G. Micera and E. Garribba, *Inorg. Chem.*, 2013, **52**, 11975–11985.
39 D. Sanna, V. Ugone, G. Sciortino, P. Buglyo, Z. Bihari, P. L. Parajdi-Losonczi and E. Garribba, *Dalton Trans.*, 2018, **47**, 2164–2182.
40 A. Levina, A. Wijetunga, R. Kaur, J. T. Koehn, D. C. Crans and P. A. Lay, to be submitted.
41 M. L. Stahla, B. Baruah, D. M. James, M. D. Johnson, N. E. Levinger and D. C. Crans, *Langmuir*, 2008, **24**, 6027–6035.
42 D. C. Crans, C. D. Rithner, B. Baruah, B. L. Gourley and N. E. Levinger, *J. Am. Chem. Soc.*, 2006, **128**, 4437–4445.
43 J. Eastoe, B. H. Robinson and R. K. Heenan, *Langmuir*, 1993, **9**, 2820–2824.
44 L. D. Giddings and S. V. Olesik, *Langmuir*, 1994, **10**, 2877–2883.
45 O. Fernando Silva, M. A. Fernandez, J. J. Silber, R. H. de Rossi and N. Mariano Correa, *ChemPhysChem*, 2012, **13**, 124–130.
46 O. F. Silva, R. H. de Rossi and N. M. Correa, *RSC Adv.*, 2015, **5**, 34878–34884.
47 R. D. Falcone, N. M. Correa, M. A. Biasutti and J. J. Silber, *Langmuir*, 2000, **16**, 3070–3076.
48 B. Baruah, J. M. Roden, M. A. Sedgwick, N. M. Correa, D. C. Crans and N. E. Levinger, *J. Am. Chem. Soc.*, 2006, **128**, 12758–12765.
49 N. M. Correa, J. J. Silber, R. E. Riter and N. E. Levinger, *Chem. Rev.*, 2012, **112**, 4569–4602.
50 N. A. Vodolazkaya, N. O. Mchedlov-Petrossyan, N. V. Salamanova, Y. N. Surov and A. O. Doroshenko, *J. Mol. Liq.*, 2010, **157**, 105–112.
51 N. A. Vodolazkaya, Y. A. Kleshchevnikova and N. O. Mchedlov-Petrossyan, *J. Mol. Liq.*, 2013, **187**, 381–388.
52 D. C. Crans, S. Schoeberl, E. Gaidamauskas, B. Baruah and D. A. Roess, *J. Biol. Inorg. Chem.*, 2011, **16**, 961–972.
53 A. G. Sostarecz, E. Gaidamauskas, S. Distin, S. J. Bonetti, N. E. Levinger and D. C. Crans, *Chem. – Eur. J.*, 2014, **20**, 5149–5159.
54 G. R. Willsky, L.-H. Chi, M. Godzala III, P. J. Kostyniak, J. J. Smee, A. M. Trujillo, J. A. Alfano, W. Ding, Z. Hu and D. C. Crans, *Coord. Chem. Rev.*, 2011, **255**, 2258–2269.
55 M. Li, W. Ding, J. J. Smee, B. Baruah, G. R. Willsky and D. C. Crans, *BioMetals*, 2009, **103**, 585–905.
56 D. C. Crans, *J. Org. Chem.*, 2015, **80**, 11899–11915.
57 T. Scior, J. A. Guevara-Garcia, Q.-T. Do, P. Bernard and S. Laufer, *Curr. Med. Chem.*, 2016, **23**, 2874–2891.
58 D. Sanna, J. Palomba, G. Lubinu, P. Buglyo, S. Nagy, F. Perdih and E. Garribba, *J. Med. Chem.*, 2019, **62**, 654–664.
59 C. Milsmann, A. Levina, H. H. Harris, G. J. Foran, P. Turner and P. A. Lay, *Inorg. Chem.*, 2006, **45**, 4743–4754.
60 D. Sanna, V. Ugone, A. Fadda, G. Micera and E. Garribba, *J. Inorg. Biochem.*, 2016, **161**, 18–26.
61 T. Jakusch, E. A. Enyedy, K. Kozma, Z. Paar, A. Benyei and T. Kiss, *Inorg. Chim. Acta*, 2014, **420**, 92–102.
62 Z. Chi, L. Zhu, X. Lu, H. Yu and B. Liu, *Z. Anorg. Allg. Chem.*, 2012, **638**, 1523–1530.
63 Z. Chi, L. Zhu and X. Lu, *J. Mol. Struct.*, 2011, **1001**, 111–117.
64 I. E. Leon, J. F. Cadavid-Vargas, I. Tiscornia, V. Porro, S. Castelli, P. Katkar, A. Desideri, M. Bollati-Fogolin and S. B. Etcheverry, *J. Biol. Inorg. Chem.*, 2015, **20**, 1175–1191.
65 V. Rajendiran, R. Karthik, M. Palaniandavar, H. Stoeckli-Evans, V. S. Periasamy, M. A. Akbarsha, B. S. Srinag and H. Krishnamurthy, *Inorg. Chem.*, 2007, **46**, 8208–8221.
66 C. R. Cornman, G. J. Colpas, J. D. Hoeschele, J. Kampf and V. L. Pecoraro, *J. Am. Chem. Soc.*, 1992, **114**, 9925–9933.
67 X. Li, M. S. Lah and V. L. Pecoraro, *Inorg. Chem.*, 1988, **27**, 4657–4664.
68 D. C. Crans, *Comments Inorg. Chem.*, 1994, **16**, 1–33.
69 A. Maitra, *J. Phys. Chem.*, 1984, **88**, 5122–5125.
70 N. Samart, Z. Arhouma, S. Kumar, H. A. Murakami, D. C. Crick and D. C. Crans, *Front. Chem.*, 2018, **6**, 519.
71 G. R. Willsky, D. A. White and B. C. McCabe, *J. Biol. Chem.*, 1984, **259**, 13273–13281.
72 H. Tominaga, M. Ishiyama, F. Ohseto, K. Sasamoto, T. Hamamoto, K. Suzuki and M. Watanabe, *Anal. Commun.*, 1999, **36**, 47–50.
73 R. Hamid, Y. Rotshteyn, L. Rabadi, R. Parikh and P. Bullock, *Toxicol. in Vitro*, 2004, **18**, 703–710.
74 M. D. Hall, K. A. Telma, K.-E. Chang, T. D. Lee, J. P. Madigan, J. R. Lloyd, I. S. Goldlust, J. D. Hoeschele and M. M. Gottesman, *Cancer Res.*, 2014, **74**, 3913–3922.
75 A. Levina, A. Mitra and P. A. Lay, *Metallomics*, 2009, **1**, 458–470.
76 X. G. Yang, K. Wang, J. F. Lu and D. C. Crans, *Coord. Chem. Rev.*, 2003, **237**, 103–111.
77 D. C. Crans, L. Q. Yang, J. A. Alfano, L. H. Chi, W. Z. Jin, M. Mahroof-Tahir, K. Robbins, M. M. Toloue, L. K. Chan, A. J. Plante, R. Z. Grayson and G. R. Willsky, *Coord. Chem. Rev.*, 2003, **237**, 13–22.
78 D. C. Crans, *J. Inorg. Biochem.*, 2000, **80**, 123–131.
79 X. G. Yang, X. D. Yang, L. Yuan, K. Wang and D. C. Crans, *Pharm. Res.*, 2004, **21**, 1026–1033.
80 K. Thompson and C. Orvig, *J. Inorg. Biochem.*, 2006, **100**, 1925–1935.

This journal is © The Royal Society of Chemistry 2019

Published on 14 March 2019. Downloaded on 5/16/2019 4:36:17 PM.

81 D. Rehder, *Future Med. Chem.*, 2012, **4**, 1823–1837.
82 N. D. Chasteen, *Copper, Molybdenum, and Vanadium in Biological Systems*, Springer, 1983.
83 E. Alessio and L. Messori, in *Metallo-Drugs: Development and Action of Anticancer Agents*, ed. A. Sigel, H. Sigel, E. Freisinger and R. Sigel, 2018, pp. 141–170.
84 A. Levina, J. B. Aitken, Y. Y. Gwee, Z. J. Lim, M. Liu, A. M. Singharay, P. F. Wong and P. A. Lay, *Chem. – Eur. J.*, 2013, **19**, 3609–3619.
85 S. Thota, D. A. Rodrigues, D. C. Crans and E. J. Barreiro, *J. Med. Chem.*, 2018, **61**, 5805–5821.
86 G. R. Willsky, L.-H. Chi, M. Godzala III, P. J. Kostyniak, J. J. Smee, A. M. Trujillo, J. A. Alfano, W. Ding, Z. Hu and D. C. Crans, *Coord. Chem. Rev.*, 2011, **255**, 2258–2269.
87 X. Niu, R. Xiao, N. Wang, Z. Wang, Y. Zhang, Q. Xia and X. Yang, *Curr. Top. Med. Chem.*, 2016, **16**, 811–822.
88 C. C. McLauchlan, B. J. Peters, G. R. Willsky and D. C. Crans, *Coord. Chem. Rev.*, 2015, **301**, 163–199.
89 B. I. Posner, R. Faure, J. W. Burgess, A. P. Bevan, D. Lachance, G. Zhang-Sun, I. G. Fantus, J. B. Ng, D. A. Hall, B. Soo Lum and A. Shaver, *J. Biol. Chem.*, 1994, **269**, 4596–4604.
90 G. Sciortino, D. Sanna, V. Ugone, G. Micera, A. Lledos, J.-D. Marechal and E. Garribba, *Inorg. Chem.*, 2017, **56**, 12938–12951.
91 T. Kiss, T. Jakusch, D. Hollender, Á. Dörnyei, É. A. Enyedya, J. C. Pessoa, H. Sakurai and A. Sanz-Medel, *Coord. Chem. Rev.*, 2008, **252**, 1153–1162.
92 A. Dornyei, S. Marcao, J. C. Pessoa, T. Jakusch and T. Kiss, *Eur. J. Inorg. Chem.*, 2006, **18**, 3614–3621.
93 D. Sanna, V. Ugone, P. Buglyo, S. Nagy, I. Kacsir and E. Garribba, *Inorg. Chim. Acta*, 2018, **472**, 127–138.
94 D. Sanna, M. Serra, G. Micera and E. Garribba, *Inorg. Chem.*, 2014, **53**, 1449–1464.
95 K. A. Doucette, K. N. Hassell and D. C. Crans, *J. Inorg. Biochem.*, 2016, **165**, 56–70.
96 S. A. Dikanov, B. D. Liboiron and C. Orvig, *J. Am. Chem. Soc.*, 2002, **124**, 2969–2978.
97 J. C. Pessoa and I. Tomaz, *Curr. Med. Chem.*, 2010, **17**, 3701–3738.
98 Y. Yoshikawa, H. Sakurai, D. C. Crans, G. Micera and E. Garribba, *Dalton Trans.*, 2014, **43**, 6965–6972.
99 N. Samart, C. N. Beuning, K. J. Haller, C. D. Rithner and D. C. Crans, *Langmuir*, 2014, **30**, 8697–8706.
100 P. K. Glasoe and F. A. Long, *J. Phys. Chem.*, 1960, **64**, 188–190.
101 A. Levina, H. H. Harris and P. A. Lay, *J. Am. Chem. Soc.*, 2007, **129**, 1065–1075.
102 R. I. Freshney, *Culture of Animal Cells: A Manual of Basic Technique and Specialized Applications*, Wiley-Blackwell, Hoboken, NJ, 7th edn, 2016.
103 N. Schweigert, A. J. B. Zehnder and R. I. L. Eggen, *Environ. Microbiol.*, 2001, **3**, 81–91.
104 N. Pooransingh-Margolis, R. Renirie, Z. Hasan, R. Wever, A. J. Vega and T. Polenova, *J. Am. Chem. Soc.*, 2006, **128**, 5190–5208.
105 M. Zizic, Z. Miladinovic, M. Stanic, M. Hadzibrahimovic, M. Zivic and J. Zakrzekska, *Res. Microbiol.*, 2016, **167**, 521–528.
106 B. J. Peters, A. S. Groninger, F. L. Fontes, D. C. Crick and D. C. Crans, *Langmuir*, 2016, **32**, 9451–9459.
107 M. Timm, L. Saaby, L. Moesby and E. W. Hansen, *Cytotechnology*, 2013, **65**, 887–894.
108 Microcal Ltd., *Microcal Origin Version 6.1*, Northampton, MA, USA.

Appendix X: Mycobacterial MenJ: An Oxidoreductase Involved in Menaquinone Biosynthesis

This manuscript concerns the kinetic characterization of Mycobacterial MenJ using menaquinone-1 we synthesized and is published in *ACS Chemical Biology*. [1]

References

1. Upadhyay, A.; Kumar, S.; Rooker, S. A.; Koehn, J. T.; Crans, D. C.; McNeil, M. R.; Lott, J. S.; Crick, D. C., Mycobacterial MenJ: An Oxidoreductase Involved in Menaquinone Biosynthesis. *ACS Chem. Biol.* **2018,** *13*, 2498-2507.

ACS chemical biology

Articles

Cite This: ACS Chem. Biol. 2018, 13, 2498−2507

pubs.acs.org/acschemicalbiology

Mycobacterial MenJ: An Oxidoreductase Involved in Menaquinone Biosynthesis

Ashutosh Upadhyay,[†,⊥] Santosh Kumar,[†,⊥] Steven A. Rooker,[†] Jordan T. Koehn,[‡] Debbie C. Crans,[‡] Michael R. McNeil,[†] J. Shaun Lott,[§] and Dean C. Crick*[,†]

[†]Mycobacteria Research Laboratories, Department of Microbiology, Immunology and Pathology, Colorado State University, Fort Collins, Colorado 80523, United States

[‡]Chemistry Department, Colorado State University, Fort Collins, Colorado 80523, United States

[§]Biological Sciences, The University of Auckland, Auckland 1010, New Zealand

Supporting Information

ABSTRACT: MenJ, annotated as an oxidoreductase, was recently demonstrated to catalyze the reduction (saturation) of a single double bond in the isoprenyl side-chain of mycobacterial menaquinone. This modification was shown to be essential for bacterial survival in J774A.1 macrophage-like cells, suggesting that MenJ may be a conditional drug target in *Mycobacterium tuberculosis* and other pathogenic mycobacteria. Recombinant protein was expressed in a heterologous host, and the activity was characterized. Although highly regiospecific *in vivo*, the activity is not absolutely regiospecific *in vitro*; in addition, the enzyme is not specific for naphthoquinones vs benzoquinones. Coenzyme Q-1 (a benzoquinone, UQ-1) was used as the lipoquinone substrate, and NADH oxidation was followed spectrophotometrically as the activity readout. NADPH could not be substituted for NADH in the reaction mixture. The enzyme contains a FAD binding site that was 72% occupied in the purified recombinant protein. Enzyme activity was maximal at 37 °C and pH 7.0; addition of divalent cations, EDTA, and reducing agents such as dithiothreitol to the reaction mixture had no effect on activity. The addition of detergents did not stimulate activity, and addition of saturating levels of FAD had relatively little effect on the observed kinetic parameters. These properties allowed the development of a facile assay needed to study this potential drug target, which is also amenable to high throughput screening. The K_m values for UQ-1 using recombinant MenJ from *Mycobacterium smegmatis* or *M. tuberculosis* without saturating concentrations of FAD were found to be 52 ± 9.6 and 44 ± 4.8 μM, respectively, while the K_m^{NADH} values were determined to be 59 ± 14 and 64 ± 15 μM. The K_m for MK-1, the menaquinone analogue of UQ-1, using recombinant MenJ from *M. tuberculosis* without saturating concentrations of FAD but in the presence of 0.5% Tween 80 was shown to be 30 ± 2.9 μM. Thus, this is the first report of a kinetic characterization of a member of the geranylgeranyl reductase family of enzymes.

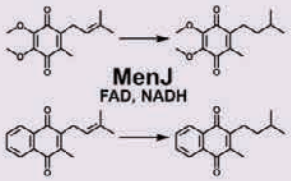

Lipoquinones play key roles in the respiratory electron transport systems (ETS) of both prokaryotes and eukaryotes by shuttling electrons between the membrane-bound electron donors (hydrogenases, dehydrogenases, and oxidoreductases) and acceptors (terminal oxidases in aerobic respiration and terminal reductases in anaerobic respiration).[1,2] These lipids can be divided into two major structural groups: ubiquinones (or benzoquinones, UQ) and menaquinones (or naphthoquinones, MK).[3] UQ and MK are characterized by the presence of an isoprenyl side-chain of varying length and degree of saturation (reduction or hydrogenation of double bonds). The variations in the structures of the lipoquinones have been used to assist taxonomic differentiation of prokaryotes for many decades,[3,4] suggesting conservation of function. Generally Gram-negative bacteria contain UQ, MK, demethylmenaquinone (DMK), or a combination; while strictly aerobic Gram-negative chemotrophs synthesize only UQ, the Gram-positive taxa synthesize MK or DMK.[3] The Gram-negative facultative anaerobe *Escherichia coli*, for example, mainly utilizes UQ-8 (ubiquinone with an isoprenyl side-chain containing eight isoprene units) in its ETS under aerobic conditions but produces increased amounts of menaquinone (MK-8) under anaerobic conditions.[5] However, the Gram-positive pathogen *Mycobacterium tuberculosis* utilizes only MK in its ETS. In mycobacteria, this molecule is predominantly MK-9(II−H_2),[6−8] a molecule that has an isoprenyl side-chain of nine isoprene units with the one in the β-position hydrogenated (saturated, see Figure 1). Many studies have reported varying degrees of regiospecific saturation of the lipoquinone isoprenyl side-chain of MK and in some cases UQ. Hydrogenation of the MK side-chain is widespread in corynebacteria and mycobacteria and is not uncommon in Archaea.

Recently, an enzyme, designated MenJ (Rv0561c), was shown to catalyze the hydrogenation of a single isoprene unit in MK of *M. tuberculosis*,[9] which results in conversion of MK-9 to MK-9(II−H_2) (Figure 1) and is highly conserved

Received: May 2, 2018
Accepted: August 9, 2018
Published: August 9, 2018

ACS Publications © 2018 American Chemical Society

DOI: 10.1021/acschembio.8b00402
ACS Chem. Biol. 2018, 13, 2498−2507

Downloaded via COLORADO STATE UNIV on November 5, 2018 at 20:25:15 (UTC).
See https://pubs.acs.org/sharingguidelines for options on how to legitimately share published articles.

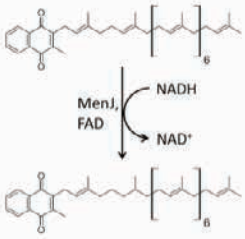

Figure 1. Reaction converting MK-9 to MK-9(II−H_2) catalyzed by $MenJ_{tb}$ (Rv0561c).

throughout both pathogenic and nonpathogenic *Mycobacterium* spp. For example, MenJ from *M. tuberculosis* ($MenJ_{tb}$) and *Mycobacterium smegmatis* ($MenJ_{smeg}$) have 74% amino acid identity with 99% coverage. Based on sequence similarity, MenJ belongs to the geranylgeranyl reductase (GGR) family of enzymes; that is, both $MenJ_{tb}$ and $MenJ_{smeg}$, to date, the only empirically identified MK saturases, were annotated as GGRs.[9] Thus, MenJ appears to represent a previously unreported subclass of GGR, which in Archaea, bacteria and plants are multifunctional enzymes that saturate multiple isoprene units of bacteriochlorophyll, chlorophyll, tocopherol, phylloquinone, and Archaeal phospholipids in a stepwise fashion.[10−12]

Data presented previously[9] indicated that the reduction of a single double bond in the isoprenoid-tail of MK by MenJ increases the efficiency of the mycobacterial ETS system. That is, MenJ deletion mutants had reduced mycobacterial electron transport efficiency, although rates of ATP synthesis and bacterial growth rates in culture were unaltered due to increased levels of total MK per bacillus.[9] Interestingly, MenJ deletion mutants grow as well as the WT bacteria in both aerobic and hypoxic conditions but have severely attenuated survival in macrophages.[9] Thus, MenJ appears to present a testable system for a contextual drug target in *M. tuberculosis*. The first steps in testing the validity of this hypothesis is development of a facile assay and characterization of the enzyme activity. Little is known about the enzymatic properties of this class of enzyme or the classical GGRs, even though crystal structures of GGRs from two of the Archaea have been determined,[13−15] presumably due to the inherent difficulties reported in assaying the activity. Using MK as a substrate in an enzyme assay presents a number of technical hurdles. MK is essentially insoluble in aqueous solutions (MK-9 has a calculated log *P* value 21.1), is sensitive to light,[16] and its absorbance and fluorescence spectra overlap those of NADH,[17,18] precluding use of a simple, sensitive spectrophotometric readout of a NADH consumption assay. Development of a facile assay required structural analysis of UQ-8 biosynthesized in *E. coli* transformed with mycobacterial *menJ* and chemical synthesis of truncated analogues of MK-9. Thus, this manuscript reports the identification of a suitable lipoquinone substrate resulting in the development of a facile, high throughput amenable *in vitro* assay for MenJ activity and the first *in vitro* characterization of the enzymatic properties of a member of the GGR family.

RESULTS AND DISCUSSION

Characterization of Lipids Extracted from *E. coli* Cells Expressing $MenJ_{smeg}$. Mycobacterial MenJ reduces a double bond in MK-8, Table 1, when expressed in *E. coli*.[9] To

Table 1. Structures and Calculated Monoisotopic Masses of Lipoquinones Described in This Study[a]

Quinones	Calculated monoisotopic masses (Da)	Structures
UQ-1	250.12051	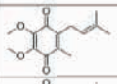
*UQ-1(H_2)	252.13616	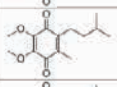
UQ-8	726.55871	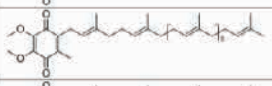
*UQ-8(H_2)	728.57436	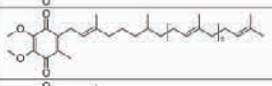
MK-1	240.11503	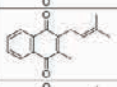
MK-4	444.30283	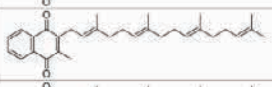
MK-8	716.55323	
*MK-8(H_2)	718.56888	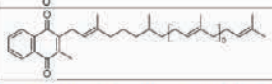

[a]Asterisks (*) indicate lipoquinones witha saturated double bond, which in UQ-8(H_2), and MK-8(H_2) is drawn to be consistent with previous reports for *M. phlei* and various other Gram-positive organisms.[6−8,21] Monoisotopic masses were calculated using ChemDraw Ultra 12.0 software (PerkinElmer Informatics).

determine if UQ is also a substrate of $MenJ_{smeg}$, partially purified neutral lipids from control *E. coli* (transformed with empty vector) or *E. coli* transformed with *pET28a::*$MenJ_{smeg}$ were analyzed by HPLC coupled to mass spectrometry (LCMS) and tandem MS. UQ was identified by observation of protonated $[M + H]^+$ ions and verification by LC MS/MS.

The monoisotopic mass of UQ-8 containing 8 isoprene units, each with a single double bond, is calculated at 726.5587 Da; therefore, the expected *m/z* value for $[M + H]^+$ is 727.5667 or 729.5824 if a single double bond was reduced. Extracted ion chromatograms (EIC) were generated from total ion chromatograms (TIC) by extracting collected data for ions with $[M + H]^+$ at *m/z* 727.6 ± 0.5 or $[M + H]^+$ at *m/z* 729.6 ± 0.5 for UQ-8 and UQ-8(H_2), respectively (Figure 2). The lipids from the control strain contain a molecular feature with an observed *m/z* of 727.5611 at a retention time of 19.4 min consistent with the presence of UQ-8 but did not contain any lipids with *m/z* values that could be attributed to UQ-8(H_2) by LC-MS/MS. The observed peak at *m/z* 729.5722, coincident with *m/z* 727.5611 (Figure 2A), represents an isotope peak. However, lipids extracted from *E. coli* expressing *MenJ* contained a new peak, with a retention time of about 20.2 min and an observed *m/z* value of 729.5722 in addition to the peaks at 19.4 min, indicating a gain of function consistent with the presence of UQ-8(H_2) (Figure 2B). This increase of 2 Da (727.6 to 729.6 Da) could potentially be attributed to

DOI: 10.1021/acschembio.8b00402
ACS Chem. Biol. 2018, 13, 2498−2507

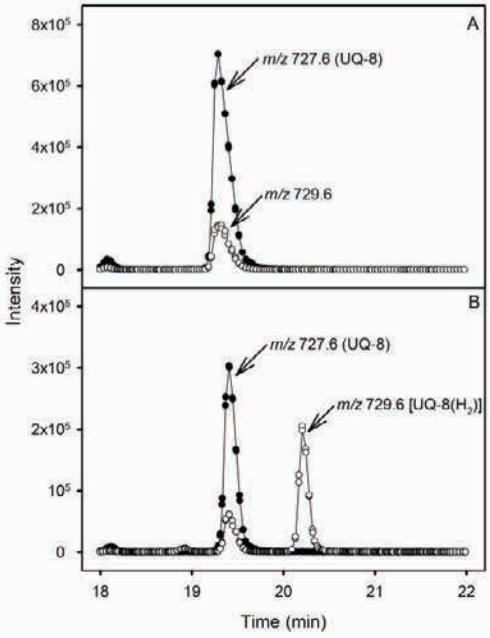

Figure 2. MenJ catalyzes the reduction of UQ-8 when expressed in *E. coli*. EIC derived from Q-TOF LC/MS analysis of partially purified lipids from recombinant *E. coli* containing pET28a empty vector (panel A) or vector containing $menJ_{smeg}$ (*MSMEG1132*) (panel B). EIC were generated from TIC by extracting data for ions with $[M + H]^+$ at m/z 727.6 ± 0.5 or m/z 729.6 ± 0.5 for UQ-8 or UQ-8(H_2), respectively.

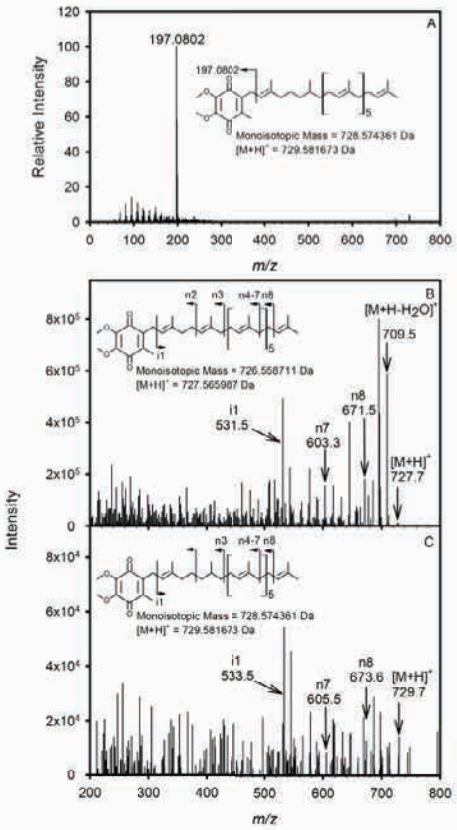

Figure 3. Tandem MS analysis of UQ-8 from recombinant *E. coli* expressing MenJ. Panel A shows a representative Q-TOF LC MS/MS analysis of ions having m/z 729.5744 identified as UQ-8(H_2) in Figure 2B, the inset shows the inferred fragmentation generating the fragment ion at m/z of 197.0802. Panels B and C show LCQ ion-trap tandem MS analysis of isoprenyl side chain of UQ-8 from WT *E. coli* and UQ-8(II−H_2) from recombinant *E. coli* expressing $MenJ_{smeg}$ respectively. The insets show the inferred fragmentation patterns.

reduction of the ketones in the benzoquinone moiety (as seen in the lipoquinone's role in electron transport), a double bond in the benzoquinone moiety, or one of the double bonds in the isoprenyl side-chain.

Tandem MS analysis of UQ molecules generate a major diagnostic fragment ion at m/z = 197.1, likely corresponding to a benzylium ion.[19,20] The molecular features with m/z values of 727.56 and 729.57, tentatively assigned as UQ-8 and UQ-8(H_2), produced major fragment ions at m/z of 197.0802 (Figure 3A) when subjected to tandem MS analysis on a Q-TOF instrument, confirming the assignment as UQ-8 and suggesting that a reduction had occurred in the isoprenoid tail and not in the aromatic ring. This conclusion was supported by LC MS/MS analysis performed on an LCQ ion-trap instrument. The resulting spectra were complex, consisting of several series of ions (Figures 3B and C). However, identification of a series of ions that retain the benzoquinone structure and differ by 68 Da (designated n2−n8) and an ion that retains only the isoprenoid moiety (designated i1) confirm the reduction in the UQ isoprenoid tail (Figure 3C). Thus, the molecular ion (m/z 729.5), $[M + H - H_2O]^+$ (m/z 711.5) and the n-series ions (m/z 605.4 and 673.5) all indicate that the molecule has a single reduced double bond near the benzoquinone ring. The fragments i1 (m/z 533.1) and n2 (calculated m/z 253.1) would identify the location of that reduction in the β-isoprene unit; however, the spectra are very complex and weak in the n2−n5 region, making unambiguous assignment of the position difficult. However, results indicate that, in addition to saturating a single double bond in the isoprenoid tail of MK as seen in mycobacteria,[9] MenJ also saturates a single double bond in the isoprenoid tail of UQ when expressed in *E. coli*. While the precise position of the saturation is difficult to identify using mass spectral methods,[6,7,9] the data point to a position close to the aromatic ring(s) in both MK and UQ. This is in agreement with earlier data that indicate that all hydrogenated MK isolated from Gram-positive eubacteria, including mycobacteria, have the β-isoprene unit from the naphthoquinone system saturated, if only one isoprene unit is saturated.[6−9,21] Thus, mycobacterial MenJ is not specific for MK vs UQ.

Expression and Purification of MenJ. The purified recombinant MenJ proteins had appropriate apparent molec-

DOI: 10.1021/acschembio.8b00402
ACS Chem. Biol. 2018, 13, 2498−2507

ular weights, and the final protein purity was consistently found to be >80−90% as judged by SDS-PAGE. The yield of the purified $MenJ_{tb}$ protein ranged from 0.7 to 1.0 mg per liter of culture.

Although $MenJ_{smeg}$ was cloned and expressed in the heterologous host *E. coli* in active form the MenJ homologue from *M. tuberculosis* is not active when expressed in *E. coli*. However, the $MenJ_{tb}$ protein complements a MenJ KO when expressed in *M. smegmatis*[9] and could be purified from this host. Although the protein is associated with membrane enriched preparations, the His tagged recombinant MenJ could be purified to at least 80% purity, as estimated by SDS-PAGE analysis, after solubilization in buffer containing an appropriate detergent. The purified recombinant protein is yellow in color in keeping with the prediction that it has a FAD binding domain [GxGxxG(x)17/18 D/E,[22] Supporting Information Figure SI1]. Bound FAD could be removed from the protein under denaturating conditions. The molar extinction coefficient of MenJ protein at 280 nm (ε_{280}) was calculated from its amino acid sequence;[23] for His_6-MenJ, ε_{280} = 72 420 M^{-1} cm^{-1},[24] and the molar extinction coefficient for FAD at 450 nm (ε_{450}) was taken to be 11 300 M^{-1} cm^{-1}. These values were used to determine the molar ratio of FAD to protein. $MenJ_{smeg}$ was found to be on average 72 ± 5% saturated with FAD when freshly purified from 3 independent preparations. Similar results were obtained for $MenJ_{tb}$. The presence of non-covalently bound FAD appears to be a characteristic of the GGR family of proteins, which has been demonstrated to be involved in electron transfer from the reducing agent to the substrate.[13] However, FAD was only associated with ~70% of the recombinant MenJ produced in either host species.

MenJ Enzyme Activity Assay. IMAC purified MenJ was used to perform *in vitro* reductase enzyme assays. Initially, commercially available MK-4 and MK-9 (see Table 1 and Figure 1 for structures) were used as potential substrates; however, no enzyme activity could be detected. While inactivation of the enzyme during purification could not be ruled out, the insolubility of MK in aqueous solutions (MK-4 and MK-9 have calculated log *P* values of 10.9 and 21.1, respectively), its sensitivity to light[16] and absorbance/fluorescence spectra presented significant technical problems. Chemically synthesized MK-1, Scheme 1, with a calculated log *P* of 4.84, could be utilized as a lipoquinone substrate.

Scheme 1. Synthesis of MK-1 (3)[a]

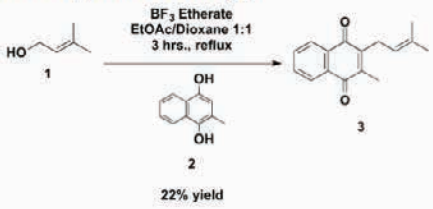

[a]MK-1, previously synthesized by other routes,[45−48] was prepared using a two-step reaction from commercially available menadione via a procedure adapted from literature.[38] Menadiol was synthesized from menadione as previously described.[36−38] Then, menadiol (**2**) was reacted with 3-methyl-2-buten-1-ol (**1**) in the presence of boron trifluoride, a Lewis acid catalyst, to attach the isoprenyl side-chain.[37,38] The coupling reaction to obtain MK-1 (**3**) resulted in a 22% yield.

However, this molecule required 20% Tween-80 for solubilization of the stock material in aqueous buffer and assay mixtures containing a final concentration of 0.5% of the detergent. In addition, overlap of absorption and fluorescence spectra with those of NADH required activity detection at 360 nm, a wavelength where loss of NADH absorbance could be separated from MK-1 absorbance, which is less sensitive than the more typical analysis at 340 nm (Supporting Information Figure SI2).

Because MenJ catalyzes the reduction of an appropriate isoprene unit in UQ-8, the concept of using UQ as MK analogues in *in vitro* assays was pursued. This approach has several advantages, in that UQ-1 is commercially available, of significantly greater solubility in water than available MKs, and allows for the design of a simple spectrophotometric assay. Activity detection, based on the loss of NADH absorbance at 340 nm, was utilized when UQ-1 was present in the reaction mix.

MS Analysis of *In Vitro* MenJ Assay Product. To verify that the enzyme was saturating the isoprenyl moiety rather than reducing the keto groups on the quinone core of UQ-1 *in vitro*, mass spectral analysis of the enzyme reaction product was conducted. In this case, large volume (2 mL) assays containing 1 mM UQ-1, 1.5 mM NADH, and recombinant protein (20 ng) were incubated at 37 °C for 75 min. Lipids were extracted from the reaction mixtures using chloroform/methanol (2/1) as described for the *E. coli* bacteria. After extraction of product lipids from the reaction mix, the identification of extracted lipids was carried out by LC-MS and tandem MS on the Q-TOF instrument as described above.

The monoisotopic mass of UQ-1 containing 1 isoprene unit is calculated at 250.1205 Da; therefore, the expected *m/z* value for $[M + H]^+$ is 251.1205 or 253.1441 if a double bond or the keto groups were reduced. EIC were generated from TIC by extracting collected data for ions with $[M + H]^+$ at *m/z* 251.1 ± 0.5 or $[M + H]^+$ at *m/z* 253.1 ± 0.5 for UQ-1 and UQ-1(H_2), respectively. The lipids extracted from the control assays without protein contain a molecular feature with an observed *m/z* of 251.1248 at a retention time consistent with the presence of UQ-1 but did not contain any lipids with *m/z* values that could be attributed to UQ-1(H_2) by LC-MS/MS. However, lipids extracted from assays containing MenJ contained a new peak with a retention time of about 1.2 min and an observed *m/z* value of 253.1395, indicating a gain of function consistent with the presence of UQ-1(H_2) (data not shown).

Tandem LC-MS analysis of the 251.1248 feature showed the parent ion ($[M + H]^+$), the diagnostic benzylium ion at *m/z* of 197.0802 that is presumably generated by a hydrogen transfer reaction,[19,20] and a fragment ion at *m/z* 219.1023 that is likely a vinyl carbocation generated by the loss of a methoxy group from the parent ion (Figure 4A). Tandem LC-MS analysis of the *m/z* 253.1395 peak in the product lipids also showed the molecular ion ($[M + H]^+$) and the diagnostic protonated fragment ion at *m/z* of 197.0807. However, in this case, the ion corresponding to the vinyl carbocation had an *m/z* value of 221.1167, an increase of ~2 Da. Thus, the tandem MS analysis of the lipid extracts demonstrated that the recombinant MenJ reduced (saturated) the double bond of the isoprenoid moiety of UQ-1, and all subsequent experiments, except those to determine the K_m for MK-1, were conducted using this substrate.

DOI: 10.1021/acschembio.8b00402
ACS Chem. Biol. 2018, 13, 2498−2507

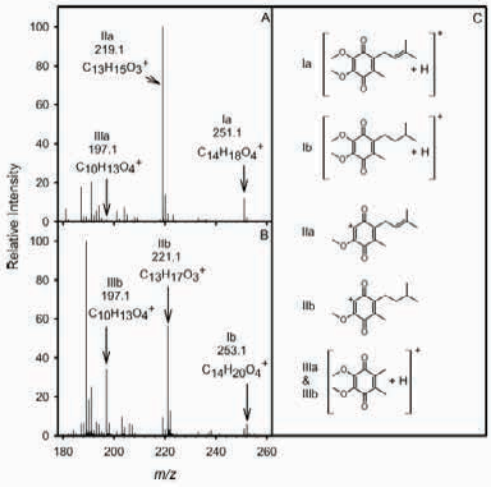

Figure 4. Tandem MS analysis of product from *in vitro* $MenJ_{smeg}$ assays showing saturation of the isoprenyl side-chain of UQ-1. A representative Q-TOF LC tandem MS analysis of MenJ reaction mix extracted with 2:1 chloroform methanol showed characteristic mass peaks for substrate UQ-1 (m/z 251.1, panel A) and product UQ-1(H_2) (m/z 253.1, panel B). The structures of diagnostic ions shown in panel C correspond to the ion peaks indicated in panels A and B. All m/z values indicated are rounded to 1 decimal place for ease of presentation, the corresponding accurate mass values are presented in the text. The 2 Da difference between ions Ia, IIa, and IIIa vs Ib, IIb, and IIIb indicates saturation of the only available isoprene unit in UQ-1.

MenJ's lack of specificity for lipoquinone (MK or UQ) allowed the development of the first facile *in vitro* assay for an enzyme of this class. Previously, kinetic analysis of GGR activity had been hampered by the requirement for complex substrates that are difficult to obtain, long incubation periods (up to 48 h), and difficult readouts based on NMR, MS, or HPLC analysis.[10,11,15,25,26]

The fact that MenJ is able to reduce the single isoprene unit available in UQ-1 indicates that although the enzyme is highly regiospecific *in vivo*[6,7] the specificity is not absolute *in vitro*. The basis of the regiospecificity of the GGR from *Sulfolobus acidocaldarius* and *Methanosarcina acetivorans*[13,27] appears to be based on accessibility of the substrate to the isoalloxazine ring of the required FAD. For example, when substrate is bound to the *S. acidocaldarius* enzyme, it can reduce three of four double bonds but not the one proximal to the phosphates in geranylgeranyl diphosphate; this appears to be because the double bond between C3 and C4 of this molecule is inaccessible to the isoalloxazine ring when the diphosphate is anchored in the anion pocket of the catalytic site.[13] However, the reduction of these double bonds is not processive, as the substrate must dissociate from the enzyme after each reduction.[15] Taken together, these observations suggest that the change from a naphthoquinone to a benzoquinone substrate may allow deeper penetration into the catalytic site of MenJ, assuming that there are geometric similarities to the GGR from *S. acidocaldarius*. However, the fact that MK-1 and UQ-1 are both substrates for the enzyme with similar kinetic constants (see below) suggests that a definitive answer as to what controls the regiospecificity of MenJ *in vivo* will require further experimentation. In that regard, determination of a crystal structure of MenJ is an ongoing a process.

Enzymatic Properties of MenJ. The activity of recombinant MenJ proteins from either source was linear with time of incubation and protein concentration for at least 30 min and up to 6 μg of protein. The enzyme activity was maximal at 37 °C and pH 7.0. Addition of supplements to the reaction mixture, including divalent cations, EDTA, and β-mercaptoethanol, had no effect on activity. The addition of CHAPS at concentrations up to 0.5% had no significant effect on the activity, but the addition of Tween 80 at 0.5% of the reaction mixture reduced the $MenJ_{smeg}$ activity by 50%. Chaps, cholate, and Tween-80 reduced the activity of $MenJ_{tb}$ by about 20%, and Triton X-100 reduced activity by 60%. It is surprising that the addition of detergents did not increase the enzyme activity. This observation is likely related to the use of UQ-1 as a substrate, as MK-1 (with a higher calculated log P) required addition of detergent for solubilization. It is likely that detergents will be required in the assay mixtures for comparison of more natural and hydrophobic (larger) benzoquinones and naphthoquinones as substrates.

Consistent with the observation that the FAD binding site was only 72% occupied in the purified recombinant protein the addition of exogenous FAD to the reaction mixture stimulated activity by approximately 30%, an effect that saturated at 10 μM with a dissociation constant of 1.3 μM.

MenJ requires two cofactors: FAD and NADH. MenJ utilizes NADH as the electron donor in catalysis, and NADPH could not be substituted as a cofactor in the reaction. This specificity seems to be unusual for a member of the GGR family. The *A. fulgidus* GGR enzyme does not appear to utilize either NADH or NADPH; the bound FAD could only be reduced using dithionite under anaerobic conditions *in vitro*.[11] Similarly, only dithionite could be used to reduce the FAD bound to the GGR from *S. acidocaldarius*;[28] however, NADH, NADPH, and dithionite were all reported to be able to sustain activity in the GGR from *T. acidophilum*.[25]

Kinetic Parameters for MenJ. The kinetic parameters for MenJ from *M. smegmatis* and *M. tuberculosis* were determined using Michaelis–Menten assumptions. The effects of UQ-1 concentration on $MenJ_{smeg}$ in the presence and absence of saturating concentrations of FAD and NADH were as shown in Figure 5. The addition of saturating levels of FAD to $MenJ_{smeg}$ had relatively little effect on the kinetic parameters associated with the UQ-1, although K_m values were unchanged, and k_{cat} values were reduced by less than 2-fold (Table 2). The $MenJ_{smeg}$ K_m values for UQ-1 as substrate without and with saturating concentrations of FAD were found to be 52 and 41 μM, respectively, at saturating concentrations of NADH. The K_m^{NADH} was determined to be 59 μM in the presence of saturating levels of UQ-1. Similar K_m values were identified for $MenJ_{tb}$, 44 and 64 μM for K_m^{UQ-1} and K_m^{NADH}, respectively. The K_m^{MK-1} was determined to be 30 μM for $MenJ_{tb}$ in the presence of saturating levels of NADH and 0.5% Tween-80. Surprisingly, V_{max} values for the recombinant $MenJ_{smeg}$ were 3 orders of magnitude greater than those for $MenJ_{tb}$ when normalized for protein used in the assays, and the calculated parameters k_{cat} and k_{cat}/K_m are presented in Table 2. Importantly, the affinities of $MenJ_{tb}$ for UQ-1 and MK-1 were similar at 44 and 30 μM, respectively, strengthening the

DOI: 10.1021/acschembio.8b00402
ACS Chem. Biol. 2018, 13, 2498–2507

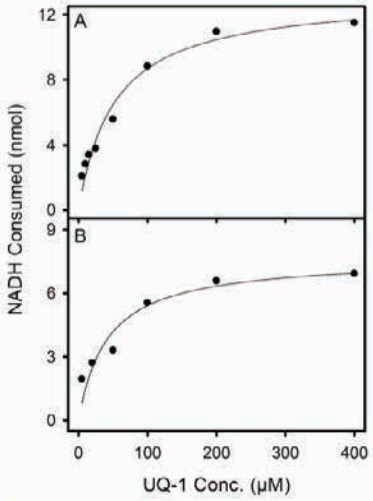

Figure 5. Representative Michaelis–Menten curves for $MenJ_{smeg}$ showing the effect of UQ-1 concentration in assays without exogenous FAD (panel A) or saturating levels (10 μM) of FAD (panel B). Assays also contained 1 ng of $MenJ_{smeg}$, 100 μM NADH, and 0.1 M McIlvaine's buffer (pH 7.0) in a final volume of 200 μL and were incubated at 37 °C for 30 min. Calculated kinetic parameters can be found in Table 2.

Table 2. Kinetic Parameters of Purified $MenJ_{tb}$ and $MenJ_{smeg}$[a]

enzyme	substrate	K_m (μM)	k_{cat} (S^{-1})	k_{cat}/K_m (S^{-1} M^{-1})
$MenJ_{tb}$	UQ-1	44 ± 4.8	0.35	7.9×10^3
	MK-1	30 ± 2.9	0.28	9.3×10^3
	NADH	64 ± 15	0.58	9.1×10^3
$MenJ_{smeg}$	UQ-1	52 ± 9.6	320	6.1×10^6
	UQ-1 + FAD	41 ± 16	180	4.5×10^6
	NADH	59 ± 14	309	5.2×10^6

[a] K_m values for UQ-1 and MK-1were determined in the presence of saturating levels of NADH and vice versa. K_m values for UQ-1 + FAD were determined in the presence of saturating levels of FAD and NADH. K_m values for MK-1 were determined in the presence of 0.5% Tween 80 and saturating levels of NADH. Assays also contained 1 ng of $MenJ_{smeg}$ or 500 ng of $MenJ_{tb}$ and 0.1 M McIlvaine's buffer (pH 7.0) in a final volume of 200 μL and were incubated at 37 °C for 30 min. The reductase activity was measured by monitoring NADH consumption spectrophotometrically by following the decrease in absorbance at 340 nm. See Figure 5 for representative concentration curves.

hypothesis that UQ-1 is an appropriate substrate for analytical purposes.

The K_m values for all of the tested substrates are approximately 2.7-fold below the reported median of 130 μM for enzymes,[29] and it is likely that the K_m for the lipoquinone will decrease as the chain length of the isoprenoid side-chain increases in size, and consequently in hydrophobicity, toward that of the natural product. The addition of saturating levels of FAD to $MenJ_{smeg}$ resulted in unchanged K_m values; however, varying the exogenous FAD concentration resulted in a saturable increase in reaction rates when both NADH and UQ-1 were at saturating concentrations. Both k_{cat} and k_{cat}/K_m values for $MenJ_{tb}$ are 3 orders of magnitude lower than those of $MenJ_{smeg}$, Table 2. Over all, k_{cat}/K_m values for $MenJ_{tb}$ are 2 orders of magnitude below the median value for all proteins,[29] while that of $MenJ_{smeg}$ is about 1.5 orders of magnitude above the median. This suggests that the selection pressure for rapid enzymatic turnover may be higher in the fast growing (3 h doubling time) *M. smegmatis* than in the slow growing (24 h doubling time) *M. tuberculosis*.[29] However, it must be remembered that the enzymes are not identical in terms of amino acid sequence and were expressed from different vectors in different heterologous hosts at different times; thus, an alternate explanation could be that the recombinant enzyme expressed in *E. coli* has a higher specific activity than that expressed in *M. smegmatis*. That is, there may be a higher proportion of active molecules in the $MenJ_{smeg}$ preparation than in the $MenJ_{tb}$ preparation, although analysis using circular dichroism did not indicate that there were significant amounts of unfolded protein in either preparation (data not shown).

Characterization of MenJ Activity from *M. smegmatis* Membranes. Having developed a reliable activity assay, reaction rates were determined in membranes isolated from *M. smegmatis*. In WT *M. smegmatis* membrane enriched preparations, NADH was oxidized independently of the addition of UQ-1 (Figure 6A). Addition of 20 μg/mL of trifluoperazine (TPZ), reported to be a specific inhibitor of mycobacterial type II NADH:menaquinone oxidoreductase,[2] abolished this activity (Figure 6A). Thus, TPZ was routinely added to assays conducted using membrane enriched fractions as the enzyme source. Introduction of UQ-1 to the assay mixture restored activity and specificity to the assay; that is, the oxidation of NADH became dependent on the addition of UQ-1. NADH oxidation was then assayed with equal amounts of protein derived from membrane preparations of WT and $MenJ_{smeg}$ KO strains of *M. smegmatis*. In the presence of TPZ and absence of UQ-1, there was no significant difference ($P \leq 0.05$, see Supporting Information) in the rates of oxidation of NADH by the two protein sources (Figure 6B and Supporting Information). When UQ-1 was added to the reaction mixture, the specific activity of the membrane fraction from the $MenJ_{smeg}$ KO was significantly ($P \leq 0.05$) less than the membrane fraction from the WT *M. smegmatis* strain a difference that can be attributed to the lack of MenJ activity in the KO strain.

Overall, results suggest that the specific activity of type II NADH:menaquinone oxidoreductase (Complex 1 of the ETS) is much greater than that of MenJ in these membrane preparations. The observed UQ-1 independent Complex 1 activity presumably utilizes endogenous MK as an electron acceptor under these conditions. Addition of UQ-1 to reaction mixtures containing TPZ restored NADH oxidation in a concentration dependent manner to membranes isolated from both WT and $\Delta MenJ_{smeg}$ strains of *M. smegmatis*, and it appears that there is little difference in the specific activity of MenJ relative to Complex 1 in membranes harvested at the mid log (OD_{600} = 0.6) or stationary (OD_{600} = 1.1) growth phase (data not shown).

■ CONCLUSIONS

The observations that MenJ lacks specificity for naphthoquinones over benzoquinones and does not have absolute regiospecificity *in vitro* allowed the generation of a facile

DOI: 10.1021/acschembio.8b00402
ACS Chem. Biol. 2018, 13, 2498–2507

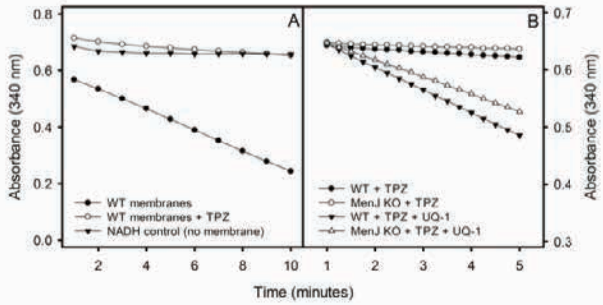

Figure 6. Effect of TPZ on oxidation of NADH by WT *M. smegmatis* membrane (panel A) and $MenJ_{smeg}$ KO membranes (panel B). Enzyme activity was measured by monitoring NADH consumption spectrophotometrically. Assays contained 15 μM NADH, 75 μM UQ-1, and 0.1 M McIlvaine's buffer (pH 7.0) in a final volume of 200 μL. TPZ was added to a final concentration of 20 μg/mL as indicated. See Supporting Information for statistical analysis.

spectrophotometry-based activity assay, more specifically, the first well characterized *in vitro* assay of a MK saturase, and the first kinetic characterization of a member of the GGR family of enzymes. The assay described herein appears to be amenable to high throughput screening (HTS) for inhibitors: it is already in 96 multiwell plate format and can easily be miniaturized to 386 well format, uses recombinant protein, is robust enough to generate reproducible data, utilizes detection of NADH consumption (which can be detected either by absorption or fluorescence changes), and is inexpensive.

MK biosynthesis in general has been proposed to be an attractive drug target in *M. tuberculosis* and potentially other Gram-positive pathogens.[30−32] Based on previous work, it is clear that MenJ is not essential for mycobacterial growth in culture.[9] However, deletion of *menJ* results in a threefold decrease in the efficiency of electron transport and severely impairs *M. tuberculosis* survival in macrophages.[9] The fact that MenJ is not an essential enzyme for bacterial growth in culture would seem to preclude its usefulness as a potential drug target. However, targeting bacterial virulence has been proposed as a paradigm for antimicrobial therapy that may circumvent, or slow, resistance mechanisms.[33−35] Usually, this would mean targeting toxin function or delivery, regulation of virulence expression, or cellular adhesion.[33] The *menJ* KO phenotype does not appear due to inhibition of toxin function or delivery, regulation of virulence expression, or cellular adhesion. It does, however, appear to fall into the proposed category of an *in vivo* essential gene target.[33] That is, MenJ activity is not essential for mycobacterial survival in culture but appears to be contextually essential for survival in host macrophages. Therefore, it is possible that MenJ represents a testable system of a contextual drug target in *M. tuberculosis*. The assay system described herein provides a necessary tool required for a search for an inhibitor of MenJ, which would not be expected to inhibit bacterial growth in culture but would inhibit bacterial growth in host cells.

METHODS

Materials and Methods. High Fidelity Taq polymerase was from Roche Diagnostics, and BCA Protein Assay Kits were purchased from Thermo Scientific Pierce. Kanamycin was from Fisher Scientific; hygromycin was from Calbiochem, and media and supplements (7H9, 7H10, OADC, LB) were from BD Difco. Vitamin K2 (MK-4), UQ-1, NADH, FAD, sodium cholate, sodium deoxycholate, goat antimouse IgG alkaline phosphatase conjugate secondary antibody, BCIP/NBT tablets, acetamide, Complete Protease Inhibitor Cocktail, Ni-NTA beads, menadione (crystalline), sodium hydrosulfite (85.0%), 1,4 dioxane (99.9%), 3-methyl-2-buten-1-ol (99%), and BF_3 etherate (≥46.5%) were purchased from Sigma-Aldrich. d_6-Dimethyl sulfoxide (99.9% + 0.05% v/v tetramethylsilane) was acquired from Cambridge Isotope Laboratories, Inc. All nonaqueous reactions were carried out under an atmosphere of argon in flame-dried glassware and were stirred on a magnetic stir plate using anhydrous solvent unless otherwise noted. All reactions in the synthesis of MK-1 were monitored by thin layer chromatography (TLC) on Whatman Partisil K6F TLC plates (silica gel 60 Å, 0.250 mm thickness) and visualized using a UV lamp (366 or 254 nm). Products were purified by flash chromatography (SiliCycle SiliaFlash F60, 43−60 μm 60 Å). Yields refer to chromatographically and spectroscopically (^{1}H NMR) homogeneous materials unless otherwise noted. Chemical shift values (δ) are reported in ppm and referenced against the internal solvent peaks in ^{1}H NMR (d_6-DMSO, δ at 2.50 ppm) and in ^{13}C NMR (d_6-DMSO, δ at 39.52 ppm). Integral values were determined using standard, uncalibrated NMR experiments and should be viewed accordingly. ^{1}H and ^{13}C spectra were recorded on a 400 MHz Varian Model MR400. NMR Spectra were processed using MestReNova version 10.0.1. High resolution mass spectrometry (HRMS) experiments for characterization of MK-1 were conducted on an Agilent 6220 TOF LC/MS ("OTOF") interfaced to an Agilent 1200 HPLC with Direct Analysis in Real Time (DART) source.

Synthesis of MK-1 [2-Methyl-3-(3-methylbut-2-en-1-yl)-naphthalene-1,4-dione]. Menaciol was synthesized from menadione as previously described,[36−38] and the procedure for the synthesis of MK-1 was adapted from previous publications for preparation of other MK derivatives.[37,38] EtOAc (8 mL) and 1,4 dioxane (8 mL) were added to a dry 50 mL round-bottom Schlenk flask, which was then purged with argon. Crude menadiol (1.50 g, 6.89 mmol, 4:1 menadiol:menadione by NMR integration) was added and stirred at 60 °C. 3-Methyl-2-buten-1-ol (0.641 g, 7.44 mmol) was added followed by dropwise addition of fresh BF_3 diethyl etherate (0.4 mL). The dark orange solution was allowed to reflux at 70 °C for 3 h under argon. The reaction was quenched with ice-water (100 mL) and extracted with diethyl ether (3 × 100 mL). The pooled organic extracts were washed with sat. $NaHCO_3$ (100 mL), followed by brine (100 mL), and dried with anhydrous Na_2SO_4. The yellow solution was then concentrated under reduced pressure at RT to yield 2.07 g of crude orange-red oil, which was subjected to flash chromatography on 230−400 mesh SiO_2 in pentane/EtOAc (20:1). MK-1, as a pure red oil, was further dried under reduced pressure overnight to yield 0.369 g (1.54 mmol) of product in 22.4% yield. ^{1}H NMR (400 MHz, d_6-DMSO) δ: 7.97−8.00 (m, 2H), 7.80−7.85 (m, 2H), 5.00 (t, J = 7 Hz, 1H), 3.29 (d, 2H, J = 7 Hz), 2.11 (s, 3H), 1.74 (s, 3H), 1.64 (s,

DOI: 10.1021/acschembio.8b00402
ACS Chem. Biol. 2018, 13, 2498−2507

3H). ^{13}C NMR (101 MHz, d_6-DMSO) δ: 184.7, 183.9, 145.1, 142.9, 133.8, 133.0, 131.55, 131.51, 125.87, 125.80, 119.4, 25.6, 25.5, 17.9, 12.4. HRMS (DART) m/z: [(M + H)$^+$] Calcd for $C_{16}H_{17}O_2$ 241.1223; Found 241.1225.

PCR Amplification, Cloning, Expression, and Purification of MenJ$_{smeg}$ and MenJ$_{tb}$. PCR amplification of *menJ$_{smeg}$* (*MSMEG1132*) was done from genomic DNA using primers with *NdeI* and *Hind*III restriction sites (underlined) engineered in the forward and reverse primers respectively; Smeg1132F ATTCATATG-AACACCCGAGCGGATGTGGTC and Smeg1132R TATAAGCTTTCAGCTGAACGGCACCCGCTG. *Taq* DNA polymerase was used for PCR amplification, and amplified gene products were cloned into the pET28a+ vector using standard molecular biology techniques.[39] The fidelity of the clone was confirmed by restriction digestion and sequencing. A confirmed clone was used to transform *E. coli* DH5α cells for expansion, purified, and used to transform *E. coli* BL21 (DE3) pLysS for expression. Recombinant protein was expressed by growing transformed bacteria in LB broth supplemented with 50 μg/mL of kanamycin at 37 °C. When the $OD_{600\ nm}$ of the culture reached 0.6, IPTG was added to a final concentration of 1.0 mM. The resulting cultures were incubated overnight; cells were harvested, washed, and disrupted by sonication in buffer A (150 mM NaCl, 1.0 mM DTT, 0.5% Triton X-100, and protease inhibitor cocktail in 50 mM phosphate buffer at pH 7.4). The homogenate was centrifuged at 15 000g for 15 min, and the supernatant was recovered. The supernatant was then incubated at 4 °C with Ni-NTA beads that had previously been equilibrated in lysis buffer. The beads were poured into a column and washed with buffer B (500 mM NaCl, 1.0 mM DTT, 0.5% Triton X-100 in 50 mM phosphate buffer, pH 7.4), and specifically bound proteins were eluted with buffer B containing 100 or 200 mM imidazol.

The *menJ$_{tb}$* (*rv0561c*) gene was PCR amplified from *M. tuberculosis* H37Rv genomic DNA using forward primer 5′-ATTCATATG-AGCGTGGATGACAGTGCCGAC-3′ and reverse primer 5′-TATAAGCTTTCAGCTGAACGGCGGTCGTCG-3′. *NdeI* and *Hind*III restriction sites are underlined. The resulting PCR products were amplified and cloned into pET28a+ vector using standard molecular biology techniques.[39] The fidelity of the clone was confirmed by restriction digestion and sequencing. Due to a lack of protein expression in *E. coli*, the Rv0561c gene was subcloned into pMyNT, an *E. coli*/mycobacteria shuttle/expression vector[40] using *Nco*I and *Hind*III restriction sites. The resulting construct was used to transform *M. smegmatis* MC^{2}155. A single, isolated colony was picked and used to inoculate 10 mL of Middlebrook 7H9 medium, supplemented with 0.2% (v/v) glycerol, 10% ADC, 0.05% Tween-80, and 50 μg/mL hygromycin, which was then incubated at 37 °C for 36 h. The resulting culture was used to inoculate 1000 mL of supplemented Middlebrook 7H9 medium and incubated at 37 °C until the OD_{600} reached 0.5−0.7. The recombinant protein expression was then induced by the addition of acetamide to a final concentration of 0.2% (w/v). The culture was then incubated for another 24−36 h at 37 °C, and cells were harvested by centrifugation, resuspended in buffer containing 50 mM Hepes and 50 mM potassium phosphate at pH 7.4, and stored at −80 °C. The frozen bacteria were thawed on ice and disrupted by sonication (described above) as needed. Sodium cholate and sodium deoxycholate (final concentration 1% each) were added to the suspension and the mixture was incubated on ice for 1 h. with gentle stirring.[41] The detergent solubilized homogenate was centrifuged at 27 000g and 4 °C for 15 min. The supernatant was then incubated with Ni-NTA beads (Sigma) at 4 °C. Bound protein was eluted with the HEPES/phosphate buffer containing imidazole.

Fractions containing the recombinant MenJ$_{smeg}$ or MenJ$_{tb}$, were identified using 12% SDS polyacrylamide gel (SDS-PAGE) visualized with Coomassie brilliant blue 250R and pooled. Imidazole was removed using PD-10 columns, and recombinant protein was concentrated as needed by ultrafiltration. The concentration of protein in the fraction of interest was determined using a BCA Protein Assay Kit with bovine serum albumin (BSA) as a standard. After resolution of proteins by SDS-PAGE, proteins were transferred to a Whatman Protran BA83 Nitrocellulose membrane using a Bis-Tris electrophoresis buffer system. The transfer blot was incubated in Tris-buffered saline pH 7.5 containing 1% BSA in for 1 h at RT. The blot was rinsed and then incubated with mouse monoclonal anti-polyHis primary antibody for 1 h. The membrane was washed three times with Tris-buffered saline pH 7.5 containing 0.1% Tween-20 at 10 min intervals. The blot was then incubated in goat antimouse IgG alkaline phosphatase conjugate secondary antibody for 1 h and developed using BCIP/NBT tablets. Recombinant protein was divided into aliquots and stored at −80 °C.

MenJ Activity Assay. For MenJ$_{smeg}$ activity assays using *M. smegmatis* membranes, cultures were harvested at the log or stationary phase of growth. Cells were washed and disrupted by sonication in buffer C (10% glycerol, 5 mM $MgCl_2$, 5 mM DTT, 50 mM phosphate buffer, pH 7.0). The homogenate was centrifuged at 27 000g for 15 min, and the supernatant was recovered. Membranes were isolated by centrifugation of the supernatant at 70 000g for 1 h, resuspended in a desired amount of buffer C, and quantified for protein content. The MenJ reaction mixtures typically contained 150 μM NADH (<1.0 $OD_{340\ nm}$), 100 μM UQ-1 as substrate and an appropriate amount of membrane protein in 0.1 M McIlvaine's buffer (pH 7.0). The reductase activity was measured by monitoring NADH consumption spectrophotometrically by following the decrease in absorbance at 340 nm in a 200 μL reaction mix at 37 °C. Complex I (NADH:menaquinone oxidoreductase) activity from the membranes was inhibited, as required, by adding 20 μg/mL of trifluoperazine (TPZ). Protein and substrate blanks were run concurrently with each assay. The decrease in absorbance due to NADH consumption was read using a BioTek Synergy HT Multi-Mode Micro Plate Reader in kinetic mode. MenJ activity assays using recombinant MenJ$_{smeg}$ or MenJ$_{tb}$, purified as described above, were performed similarly, but TPZ was omitted from the reaction mix. In cases where MK-1 was used as the lipoquinone substrate, MK-1 was solubilized in 20% Tween-80, which was diluted to a final concentration of 0.5% in the assay mixtures, and activity was monitored by change in absorbance at 360 nm (Figure S12). All assays were conducted under conditions where the reactions were linear with regard to protein concentration and time.

Lipid Extraction and Identification. Lipid extraction from intact WT *E. coli* cells or those expressing recombinant protein was done essentially as described earlier[9,42] using chloroform/methanol (2:1, by vol.). The extracts were washed,[43] solvent was removed under a stream of N_2, lipids were dissolved in chloroform, loaded onto silicic acid columns and eluted with chloroform to effect partial purification of UQ and MK. An aliquot of the partially purified lipids was applied to a reverse-phase hypersil ODS column (Agilent) connected to an Agilent 1200 series high-performance liquid chromatography (HPLC) system. Separation was achieved using a gradient running from water to 90% methanol over 40 min at flow rate of 0.3 mL/min at 40 °C. The eluates were introduced into an Agilent 6250 quadrupole time-of-flight (Q-TOF) mass spectrometer equipped with an Agilent multimode source operated in the simultaneous electrospray ionization and atmospheric pressure chemical ionization mode (APCI). Nebulizing gas temperature was 350 °C and nebulizer pressure was 30 psi. Data obtained were analyzed using Agilent Mass Hunter Workstation software.

Samples were also analyzed using an Agilent Technologies HP1100 series HPLC connected to a Thermo 2000 Finnigan LCQ-Duo ion-trap mass spectrometer. HPLC separation was achieved using a reverse-phase XBridge C18 3.5 μm 2.1 × 150 mm column (Waters) and a gradient running from 100% methanol to methanol/isopropanol (1:1 v/v) over 50 min at 0.4 mL/min and 40 °C. Eluted molecules were subjected to positive ion MS using APCI as the ionization interface. Capillary temperature was 150 °C and APCI vaporizer temperature was 450 °C. Electrospray needle voltage was 4.5 kV. Sheath gas flow was maintained at 40 units. Data acquisition and analysis were performed using Xcaliber software from Thermo Scientific.

DOI: 10.1021/acschembio.8b00402
ACS Chem. Biol. 2018, 13, 2498−2507

In all cases, samples were spiked with known amounts of vitamin K_2 (MK-4) as an internal standard prior to extraction, and peak area[44] was used to quantitate MK.

In some cases, large scale *in vitro* assays containing 1 mM UQ-1, 1.5 mM NADH, and an appropriate amount of protein in total volumes of 2 mL were incubated at 37 °C for 75 min. Reaction products were extracted, purified, and analyzed by tandem MS using the Q-TOF mass spectrometer as described above.

Characterization of MenJ. $MenJ_{smeg}$ and $MenJ_{tb}$ are predicted to have FAD binding domains (the National Center for Biotechnology Information Web site); hence, the ratio of protein to FAD in purified recombinant MenJ was calculated. The protein concentration was first measured by UV spectroscopy followed by denaturation by heating to 100 °C for 10 min to release the bound FAD. The denatured protein was removed from solution by centrifugation at 14 500*g* for 10 min, and the FAD concentration in the supernatant was measured by spectroscopy at 450 nm. The effect of pH on MenJ activity was assayed at 37 °C and McIlvaine's buffer at various pH values under standard assay conditions. The effect of temperature was determined at pH 7 at various temperatures. To determine the effect of detergents on enzyme activity, CHAPS, Triton X-100, cholate, or Tween-80 was added to the standard reaction mix at the indicated concentrations. The effects of divalent cations, EDTA, and exogenous FAD were determined using standard assay conditions. The effect of UQ-1 concentration on MenJ activity was determined with and without exogenous FAD and in the presence of 150 μM NADH. The effect of NADH concentration on the reaction rate was determined at 200 μM UQ-1 in the reaction mix. Initial rates were used to calculate the kinetic properties of the purified enzyme, and K_m and V_{max} values were derived using Sigma Plot software (version 13).

■ ASSOCIATED CONTENT

Supporting Information

The Supporting Information is available free of charge on the ACS Publications website at DOI: 10.1021/acschembio.8b00402.

Figure SI1: Amino acid sequence alignment of the N-terminal amino acids of geranylgeranyl reductases and $MenJ_{tb}$ and $MenJ_{smeg}$; Figure SI2: UV−vis spectra of MK-1 and NADH; Figures SI3 and 4: ^1H and ^{13}C NMR spectra of MK-1; Statistical analysis of data in Figure 6B (PDF)

■ AUTHOR INFORMATION

Corresponding Author

*E-mail: Dean.Crick@colostate.edu; Tel.: (+1) 970 491 3308; Fax: (+1) 970 491 1815.

ORCID

Jordan T. Koehn: 0000-0003-3008-6303

Debbie C. Crans: 0000-0001-7792-3450

Dean C. Crick: 0000-0001-9281-7058

Author Contributions

⊥A.U. and S.K. contributed equally to this research.

Funding

Funded by NIH/NIAID Grants AI049151 and AI119567 to D.C. Crick and NSF Grant CHE-1709564 to D.C. Crans and D.C. Crick

Notes

The authors declare no competing financial interest.

■ REFERENCES

(1) Pandya, K. P., and King, H. K. (1966) Ubiquinone and menaquinone in bacteria: a comparative study of some bacterial respiratory systems. *Arch. Biochem. Biophys. 114*, 154−157.

(2) Weinstein, E. A., Yano, T., Li, L. S., Avarbock, D., Avarbock, A., Helm, D., McColm, A. A., Duncan, K., Lonsdale, J. T., and Rubin, H. (2005) Inhibitors of type II NADH:menaquinone oxidoreductase represent a class of antitubercular drugs. *Proc. Natl. Acad. Sci. U. S. A. 102*, 4548−4553.

(3) Collins, M. D., and Jones, D. (1981) Distribution of isoprenoid quinone structural types in bacteria and their taxonomic implication. *Microbiol. Rev. 45*, 316−354.

(4) Jarosz, Ł., Grądzki, Z., and Kalinowski, M. (2014) Phenotypic properties and virulence factors of *Trueperella pyogenes*. *Medycna Wet 70*, 73−80.

(5) Lin, E. C., and Kuritzkes, D. R. (1987) *Pathways for Anaerobic Electron Transportin Escherichia Coli and Salmonella Typhimurium*, American Society for Microbiology, Washington DC.

(6) Azerad, R., Cyrot, M. O., and Lederer, E. (1967) Structure of the dihydromenaquinone-9 of *Mycobacterium phlei*. *Biochem. Biophys. Res. Commun. 27*, 249−252.

(7) Azerad, R., and Cyrot-Pelletier, M. O. (1973) Structure and configuration of the polyprenoid side chain of dihydromenaquinones from Myco- and Corynebacteria. *Biochimie 55*, 591−603.

(8) Dunphy, P. J., Gutnick, D. L., Phillips, P. G., and Brodie, A. F. (1968) A new natural naphthoquinone in *Mycobacterium phlei*. Cis-dihydromenaquinone-9, structure and function. *J. Biol. Chem. 243*, 398−407.

(9) Upadhyay, A., Fontes, F. L., Gonzalez-Juarrero, M., McNeil, M. R., Crans, D. C., Jackson, M., and Crick, D. C. (2015) Partial saturation of menaquinone in *Mycobacterium tuberculosis*: Function and essentiality of a novel reductase, MenJ. *ACS Cent. Sci. 1*, 292−302.

(10) Keller, Y., Bouvier, F., d'Harlingue, A., and Camara, B. (1998) Metabolic compartmentation of plastid prenyllipid biosynthesis–evidence for the involvement of a multifunctional geranylgeranyl reductase. *Eur. J. Biochem. 251*, 413−417.

(11) Hemmi, H., Takahashi, Y., Shibuya, K., Nakayama, T., and Nishino, T. (2005) Menaquinone-specific prenyl reductase from the hyperthermophilic archaeon *Archaeoglobus fulgidus*. *J. Bacteriol. 187*, 1937−1944.

(12) Addlesee, H. A., and Hunter, C. N. (2002) *Rhodospirillum rubrum* possesses a variant of the *bchP* gene, encoding geranylgeranyl-bacteriopheophytin reductase. *J. Bacteriol. 184*, 1578−1586.

(13) Sasaki, D., Fujihashi, M., Iwata, Y., Murakami, M., Yoshimura, T., Hemmi, H., and Miki, K. (2011) Structure and mutation analysis of archaeal geranylgeranyl reductase. *J. Mol. Biol. 409*, 543−557.

(14) Xu, Q., Eguchi, T., Mathews, II, Rife, C. L., Chiu, H. J., Farr, C. L., Feuerhelm, J., Jaroszewski, L., Klock, H. E., Knuth, M. W., Miller, M. D., Weekes, D., Elsliger, M. A., Deacon, A. M., Godzik, A., Lesley, S. A., and Wilson, I. A. (2010) Insights into substrate specificity of geranylgeranyl reductases revealed by the structure of digeranylgeranylglycerophospholipid reductase, an essential enzyme in the biosynthesis of archaeal membrane lipids. *J. Mol. Biol. 404*, 403−417.

(15) Kung, Y., McAndrew, R. P., Xie, X., Liu, C. C., Pereira, J. H., Adams, P. D., and Keasling, J. D. (2014) Constructing tailored isoprenoid products by structure-guided modification of geranylgeranyl reductase. *Structure 22*, 1028−1036.

(16) Dawson, R. M. C., Elliott, D.C., Elliott, W.H., and Jones, K.M. (1969) *Data for Biochemical Research*, Oxford University Press.

(17) Bondza-Kibangou, P., Millot, C., Dufer, J., and Millot, J. M. (2001) Microspectrofluorometry of autofluorescence emission from human leukemic living cells under oxidative stress. *Biol. Cell 93*, 273−280.

(18) Blacker, T. S., Mann, Z. F., Gale, J. E., Ziegler, M., Bain, A. J., Szabadkai, G., and Duchen, M. R. (2014) Separating NADH and NADPH fluorescence in live cells and tissues using FLIM. *Nat. Commun. 5*, 3936.

(19) Geyer, R., Peacock, A. D., White, D. C., Lytle, C., and Van Berkel, G. J. (2004) Atmospheric pressure chemical ionization and atmospheric pressure photoionization for simultaneous mass spectrometric analysis of microbial respiratory ubiquinones and menaquinones. *J. Mass Spectrom. 39*, 922−929.

(20) Lytle, C. A., Gan, Y. D., Salone, K., and White, D. C. (2001) Sensitive characterization of microbial ubiquinones from biofilms by electrospray/mass spectrometry. *Environ. Microbiol. 3*, 265–272.
(21) Phillips, P. G., Dunphy, P. J., Servis, K. L., and Brodie, A. F. (1969) A new menaquinone series differing in the degree of unsaturation of the side chain. *Biochemistry 8*, 2856–2861.
(22) Dym, O., and Eisenberg, D. (2001) Sequence-structure analysis of FAD-containing proteins. *Protein Sci. 10*, 1712–1728.
(23) Pace, C. N., Vajdos, F., Fee, L., Grimsley, G., and Gray, T. (1995) How to measure and predict the molar absorption coefficient of a protein. *Protein Sci. 4*, 2411–2423.
(24) Aliverti, A., Curti, B., and Vanoni, M. A. (1999) Identifying and quantitating FAD and FMN in simple and in iron-sulfur-containing flavoproteins. *Methods Mol. Biol. 131*, 9–23.
(25) Nishimura, Y., and Eguchi, T. (2006) Biosynthesis of archaeal membrane lipids: digeranylgeranylglycerophospholipid reductase of the thermoacidophilic archaeon *Thermoplasma acidophilum*. *J. Biochem. 139*, 1073–1081.
(26) Addlesee, H. A., and Hunter, C. N. (1999) Physical mapping and functional assignment of the geranylgeranyl-bacteriochlorophyll reductase gene, *bchP*, of *Rhodobacter sphaeroides*. *J. Bacteriol. 181*, 7248–7255.
(27) Ogawa, T., Isobe, K., Mori, T., Asakawa, S., Yoshimura, T., and Hemmi, H. (2014) A novel geranylgeranyl reductase from the methanogenic archaeon *Methanosarcina acetivorans* displays unique regiospecificity. *FEBS J. 281*, 3165–3176.
(28) Sato, S., Murakami, M., Yoshimura, T., and Hemmi, H. (2008) Specific partial reduction of geranylgeranyl diphosphate by an enzyme from the thermoacidophilic archaeon *Sulfolobus acidocaldarius* yields a reactive prenyl donor, not a dead-end product. *J. Bacteriol. 190*, 3923–3929.
(29) Bar-Even, A., Noor, E., Savir, Y., Liebermeister, W., Davidi, D., Tawfik, D. S., and Milo, R. (2011) The moderately efficient enzyme: evolutionary and physicochemical trends shaping enzyme parameters. *Biochemistry 50*, 4402–4410.
(30) Lu, X., Zhou, R., Sharma, I., Li, X., Kumar, G., Swaminathan, S., Tonge, P. J., and Tan, D. S. (2012) Stable analogues of OSB-AMP: potent inhibitors of MenE, the o-succinylbenzoate-CoA synthetase from bacterial menaquinone biosynthesis. *ChemBioChem 13*, 129–136.
(31) Li, X., Liu, N., Zhang, H., Knudson, S. E., Li, H. J., Lai, C. T., Simmerling, C., Slayden, R. A., and Tonge, P. J. (2011) CoA adducts of 4-oxo-4-phenylbut-2-enoates: Inhibitors of MenB from the *Mycobacterium tuberculosis* menaquinone biosynthesis pathway. *ACS Med. Chem. Lett. 2*, 818–823.
(32) Debnath, J., Siricilla, S., Wan, B., Crick, D. C., Lenaerts, A. J., Franzblau, S. G., and Kurosu, M. (2012) Discovery of selective menaquinone biosynthesis inhibitors against *Mycobacterium tuberculosis*. *J. Med. Chem. 55*, 3739–3755.
(33) Clatworthy, A. E., Pierson, E., and Hung, D. T. (2007) Targeting virulence: a new paradigm for antimicrobial therapy. *Nat. Chem. Biol. 3*, 541–548.
(34) Allen, R. C., Popat, R., Diggle, S. P., and Brown, S. P. (2014) Targeting virulence: can we make evolution-proof drugs? *Nat. Rev. Microbiol. 12*, 300–308.
(35) Rasko, D. A., and Sperandio, V. (2010) Anti-virulence strategies to combat bacteria-mediated disease. *Nat. Rev. Drug Discovery 9*, 117–128.
(36) Payne, R. J., Daines, A. M., Clark, B. M., and Abell, A. D. (2004) Synthesis and protein conjugation studies of vitamin K analogues. *Bioorg. Med. Chem. 12*, 5785–5791.
(37) Koehn, J. T., Magallanes, E. S., Peters, B. J., Beuning, C. N., Haase, A. A., Zhu, M. J., Rithner, C. D., Crick, D. C., and Crans, D. C. (2018) A synthetic isoprenoid lipoquinone, menaquinone-2, adopts a folded conformation in solution and at a model membrane interface. *J. Org. Chem. 83*, 275–288.
(38) Suhara, Y., Wada, A., Tachibana, Y., Watanabe, M., Nakamura, K., Nakagawa, K., and Okano, T. (2010) Structure-activity relationships in the conversion of vitamin K analogues into menaquinone-4. Substrates essential to the synthesis of menaquinone-4 in cultured human cell lines. *Bioorg. Med. Chem. 18*, 3116–3124.
(39) Maniatis, T., Fritsch, E. F., and Sambrook, J. (1983) *Molecular Cloning: A Laboratory Manual*, Cold Spring Harbor Laboratory, New York.
(40) Noens, E. E., Williams, C., Anandhakrishnan, M., Poulsen, C., Ehebauer, M. T., and Wilmanns, M. (2011) Improved mycobacterial protein production using a *Mycobacterium smegmatis* groEL1DeltaC expression strain. *BMC Biotechnol. 11*, 27.
(41) Yano, T., Li, L. S., Weinstein, E., Teh, J. S., and Rubin, H. (2006) Steady-state kinetics and inhibitory action of antitubercular phenothiazines on *Mycobacterium tuberculosis* type-II NADH-menaquinone oxidoreductase (NDH-2). *J. Biol. Chem. 281*, 11456–11463.
(42) Dhiman, R. K., Mahapatra, S., Slayden, R. A., Boyne, M. E., Lenaerts, A., Hinshaw, J. C., Angala, S. K., Chatterjee, D., Biswas, K., Narayanasamy, P., Kurosu, M., and Crick, D. C. (2009) Menaquinone synthesis is critical for maintaining mycobacterial viability during exponential growth and recovery from non-replicating persistence. *Mol. Microbiol. 72*, 85–97.
(43) Folch, J., Lees, M., and Sloane Stanley, G. H. (1957) A simple method for the isolation and purification of total lipides from animal tissues. *J. Biol. Chem. 226*, 497–509.
(44) Wasinger, V. C., Zeng, M., and Yau, Y. (2013) Current status and advances in quantitative proteomic mass spectrometry. *Int. J. Proteomics 2013*, 180605.
(45) Hagiwara, E., Hatanaka, Y., Gohda, K., and Hiyama, T. (1995) Allylation of quinones with allyl(trifluoro)silanes - direct synthesis of isoprenoid quinones. *Tetrahedron Lett. 36*, 2773–2776.
(46) Mal, D., Ghosh, K., and Jana, S. (2015) Synthesis of vitamin K and related naphthoquinones via demethoxycarbonylative annulations and a retro-Wittig rearrangement. *Org. Lett. 17*, 5800–5803.
(47) Teitelbaum, A. M., Scian, M., Nelson, W. L., and Rettie, A. E. (2015) Efficient syntheses of vitamin K chain-shortened acid metabolites. *Synthesis 47*, 944–948.
(48) Yamago, S., Hashidume, M., and Yoshida, J. (2002) A new synthetic route to substituted quinones by radical-mediated coupling of organotellurium compounds with quinones. *Tetrahedron 58*, 6805–6813.

DOI: 10.1021/acschembio.8b00402
ACS Chem. Biol. 2018, 13, 2498–2507

List of Abbreviations

ACN	Acetonitrile
AcOH	Acetic acid
AOT	Bis(2-ethylhexyl) sulfosuccinate sodium salt
C_6D_6	Benzene-d_6
Bz	Benzoyl
br	Broad
Calcd	Calculated
cat	catecholate
CCR2	CC chemokine receptor 2
CCR5	CC chemokine receptor 5
CCL2	CC chemokine ligand 2
$CDCl_3$	Chloroform-d
COSY	Correlation spectroscopy
d	Doublet
DCM	Dichloromethane
DDI-H_2O	Distilled Deionized Water
DMF	Dimethylformamide
DMSO	Dimethylsulfoxide
DLS	Dynamic light scattering
DPPC	Dipalmitoylphosphatidylcholine
DPPE	Dipalmitoylphosphatidylethanolamine

dtb	Di-*tert*-butylcatecholate
Et	Ethyl
ETS	Electron transport system
EtOAc	Ethyl acetate
Et_2O	Diethyl ether
EtOH	Ethanol
Equiv.	Equivalent
Fc	Ferrocene
H_2shed	Condensation product of salicylaldehyde and *N*-(2-hydroxyethyl)-1,2-ethanediamine
HEPES	4-(2-hydroxyethyl)-1-piperazine-ethanesulfonic acid
HSQC	Heteronuclear single quantum correlation
HRMS	High resolution mass spectrometry
HyDa	Ethanediamine
Hz	Hertz
m	Multiplet
Me	Methyl
MeOH	Methanol
MHz	Megahertz
MK	Menaquinone
Ms	Methanesulfonyl (mesylate)
MsCl	Methanesulfonyl chloride
Mtb	*Mycobacterium tuberculosis*
M. tuberculosis	*Mycobacterium tuberculosis*

NOESY	Nuclear Overhauser effect spectroscopy
NMR	Nuclear magnetic resonance
pdi	Polydispersity index
PTLC	Preparative thin layer chromatography
i-Pr	Isopropyl
Py. or Pyr	Pyridine
q	Quartet
ROESY	Rotating frame Overhauser effect spectroscopy
R_f	Retention Factor
r.t.	Room temperature
s	Singlet
SalA	Salicylaldehyde
t	Triplet
TB	Tuberculosis
TBAP	Tetrabutylammonium perchlorate
t-BuOK	Potassium *tert*-butoxide
THF	Tetrahydrofuran
TLC	Thin layer chromatography
UQ	Ubiquinone
V	Volts